Final Report

Effects of Chemical and Mineral Admixtures on Performance of Florida Structural Concrete

FDOT Contract Number: BDV25-977-02

Date: June 21, 2016

Submitted to

Research Center (Research.center@dot.state.fl.us)

The Florida Department of Transportation

Research Center

605 Suwannee Street, MS 30

Tallahassee, FL 32399

c/o Dr. Harvey DeFord

Structural Materials Research Specialist

State Materials Office

5007 NE 39th Avenue

Gainesville, FL 32609

Phone: (352)955-6671

Email: Harvey.deford@dot.state.fl.us

Submitted by

Principal Investigator: Dr. A. Zayed

Department of Civil and Environmental Engineering

University of South Florida

4202 E Fowler Avenue; ENB 118

Tampa, FL 33620-5350

Email: zayed@usf.edu

DISCLAIMER

The opinions, findings, and conclusions expressed in this publication are those of the authors and not necessarily those of the State of Florida Department of Transportation (FDOT) or the U.S. Department of Transportation (USDOT) or the Federal Highway Administration (FHWA).

Approximate Conversions to SI Units (from FHWA)				
Symbol	**When You Know**	**Multiply By**	**To Find**	**Symbol**
Length				
in	inches	25.4	millimeters	mm
ft	feet	0.305	meters	m
yd	yards	0.914	meters	m
mi	miles	1.61	kilometers	km
Area				
in^2	square inches	645.2	square millimeters	mm^2
ft^2	square feet	0.093	square meters	m^2
yd^2	square yard	0.836	square meters	m^2
mi^2	square miles	2.59	square kilometers	km^2
Volume				
fl oz	fluid ounces	29.57	milliliters	mL
gal	gallons	3.785	liters	L
ft^3	cubic feet	0.028	cubic meters	m^3
yd^3	cubic yards	0.765	cubic meters	m^3
NOTE: volumes greater than 1000 L shall be shown in m^3				
Mass				
oz	ounces	28.35	grams	g
lb	pounds	0.454	kilograms	kg
Temperature (exact degrees)				
°F	Fahrenheit	5 (F-32)/9 or (F-32)/1.8	Celsius	°C
Illumination				
fc	foot-candles	10.76	lux	lx
fl	foot-Lamberts	3.426	candela/m^2	cd/m^2
Force and Pressure or Stress				
lbf	pound-force	4.45	newtons	N
psi	pound-force per square inch	6.89	kilopascals	kPa

Technical Report Documentation Page

1. Report No.	2. Government Accession No.	3. Recipient's Catalog No.
4. Title and Subtitle Effects of Chemical and Mineral Admixtures on Performance of Florida Structural Concrete		5. Report Date June 21, 2016 6. Performing Organization Code
7. Author(s) A. Zayed, N. Shanahan, V. Tran, A. Markandeya, A. Williams, and A. Elnihum		8. Performing Organization Report No.
9. Performing Organization Name and Address Department of Civil and Environmental Engineering University of South Florida 4202 E Fowler Avenue; ENB 118 Tampa, FL 33620-5350		10. Work Unit No. 11. Contract or Grant No. BDV25-977-02
12. Sponsoring Agency Name and Address US Department of Transportation-Florida Department of Transportation		13. Type of Report and Period Covered Final Report; 5/06/2013 - 7/01/2016 14. Sponsoring Agency Code
15. Supplementary Notes None		

16. Abstract

Several mineral and chemical admixtures, commonly used in Florida structural concrete, were studied here to assess their effect on the fresh and hardened properties of cementitious systems. Pozzolans examined here were Class F fly ash, silica fume, blast furnace slag, and metakaolin, while chemical admixtures were air-entrainer, water reducer/retarder and two superplasticizers. The as-received materials were characterized for their chemical oxide composition, crystalline and amorphous content, density, fineness, specific surface area, and particle size distribution. Several tests were conducted on binary and ternary mixtures to assess the performance of the cementitious system, including heat of hydration using isothermal calorimetry, strength evolution, rheological properties, setting properties of paste and mortar, sulfate durability, semiadiabatic calorimetry and adiabatic temperature rise, and cracking potential. Microstructural evolution was followed by x-ray diffraction studies of the hydration phases, nanoindentation, and characterization of the pore structures using nitrogen adsorption for binary cementitious systems. The effect of chemical admixtures dosages on the pore size distribution was followed using nitrogen adsorption. The cracking potential for binary cementitious concrete mixtures was studied using an imposed temperature profile simulating a 1 m^3 wall. The findings indicated that mineral admixtures, in general, retard setting and the extent was dependent on the amount and type of each pozzolan. Metakaolin mixtures showed the highest early-strength gain. Heat of hydration (HOH) measurements indicated that both metakaolin and slag (14.25% Al_2O_3) affect the sulfate-to-aluminate balance in the cementitious system. Factorial design was successful in predicting potential interaction between different mineral and chemical admixture combinations. Sulfate durability tests indicated that slag cementitious mixtures did not perform better than plain cement mixtures, and silica fume offered superior protection for cementitious mixtures exposed to a sulfate environment. Adiabatic temperature rise was highest for slag mixtures and lowest for Class F fly ash mixtures. High dosages of water reducer/retarder and superplasticizers increased the number of pores in the 2-30 nm range. Metakaolin and slag mixtures increased the number of large gel pores.

17. Keywords.	18. Distribution Statement
Class F fly ash, silica fume, blast-furnace slag, silica fume, metakaolin, air-entrainer, water-reducer, superplasticizers, sulfate durability, heat of hydration, adiabatic temperature rise, cracking potential, Rietveld analysis, rheology, factorial design, nitrogen adsorption, and pore size distribution	No restrictions.

19. Security Classification (this report)	20. Security Classification (this page)	21. Pages	22. Price
Unclassified	Unclassified	359	

Form DOT F 1700.7 (8-72) Reproduction of completed page authorized

ACKNOWLEDGEMENTS

This work has been sponsored by the Florida Department of Transportation (FDOT) and the Federal Highway Administration (FHWA). The Principal Investigator appreciates the valuable discussions with Dr. Harvey DeFord, Project Manager, and Mr. Michael Bergin, PE. The authors would like to thank Mr. Richard DeLorenzo and Mr. Shelby Brothers with the FDOT State Materials Office (SMO) for their assistance with this research. The following participants are acknowledged for their tremendous contributions to this research: Dr. Yuriy Stetsko, Jeremy Castello, Tanya Anisimova, Thomas Meagher, Daniel Buidens, and William Johnson.

EXECUTIVE SUMMARY

E.1 Background

Mineral admixtures (supplemental cementitious materials, SCMs) and chemical admixtures are used extensively in Florida structural concrete elements. The addition of admixtures can have profound effects on concrete performance and durability. Current published literature inadequately covers the possible interactions between different mineral and chemical admixtures and the consequences on the fresh and hardened concrete properties. One concern is the possibility for incompatibility of some portland cement-admixture combinations. New chemical admixtures are continually being developed and the need for new SCMs will continue to increase. The large number of existing admixtures and the proliferation of new chemical and mineral admixtures increase the chances that chemical reactions, for some portland cement-admixture combinations, will occur that are detrimental to the plastic and cured properties of concrete mixtures. Another concern is the potential for thermal cracking due to the heat generated during hydration and adiabatic temperature rise of some cement-admixture combinations. Excessive heat generation could be responsible for higher cracking potential in concrete mixtures incorporating those admixtures.

E.2 Research Objectives

The objectives of the proposed research were 1) to investigate the effects of chemical and mineral admixture combinations on the fresh and hardened properties of cement mixes, 2) to evaluate the compatibility of selected combinations of portland cement and mineral and chemical admixtures, 3) to assess the potential for thermal cracking of cement-admixture combinations, and 4) to assess the effects of cement-admixture combinations on strength and durability. Recommendations would be made, based on the findings, to enhance and ensure a sustainable and durable infrastructure in the state of Florida.

E.3 Main Findings

The main findings from this study are summarized as follows:

- Heat of hydration measurements indicated that high alumina-bearing mineral admixtures, such as slag and metakaolin, affect the sulfate depletion peak intensity and position, while others, such as class F fly ash, do not.
- Incorporation of pozzolanic materials (slag, metakaolin, silica fume, and class F fly ash) affected the setting time, strength evolution, heat generation, pore size distribution, cracking potential, and sulfate durability.
- In general, pozzolanic materials retarded setting in most mixtures, with the degree of retardation dependent on the dosage and type of admixture used. Similar effects were found for water reducer/retarders and superplasticizers.
- Nitrogen adsorption measurements indicated that metakaolin and slag increased pore volume in the 2-30 nm pore size range.
- For chemical admixtures, nitrogen adsorption indicated that increasing the superplasticizer dosage increased substantially the accessible pore structure in the 2-30 nm range.
- The highest adiabatic temperature rise predicted for a 1-m^3 wall concrete element was for concrete mixtures incorporating slag at a 52% replacement level.
- Silica fume offered the highest sulfate resistance in the mixtures studied, while slag at 52% replacement did not improve sulfate resistance when compared to the plain Type I/II cement mixture. X-ray diffraction measurements indicated that monosulfoaluminate and ettringite were present prior to sulfate exposure.
- Nanoindentation measurements showed good correlation with porosity measurements. The slag mixture, at a replacement level of 52% and cured for 7 days, had a low elastic modulus and the highest volume of large gel pores.

E.4 Recommendations

Based on the findings from this study, the following recommendations were made:

- Reconsider the use of high alumina slag in concrete mixtures exposed to an aggressive sulfate environment.
- Require slag suppliers to identify the alumina content of the slag on the slag Mill Certificate.
- Establish a specified range of alumina content that will be used for slag source approval and for slag quality assurance.

- Require successful ASTM C1012 testing, for a period of 18 months, as part of the approval process for a slag to be used in concrete that will be exposed to an environment where sulfate durability is of concern. Each slag concrete mix design tested should include a control mix made from the same mix design, but with portland cement replacing the slag.

E.5 Recommendations for Future Study

Results of the current study indicate that FDOT concrete specifications do not adequately insure the durability of portland cement-slag concrete. The following are recommended to resolve this inadequacy. Initiate an extensive study to:

- Identify the effects of the alumina content of FDOT-approved slags on the sulfate durability of structural concrete containing slag;
- Determine the influence of the C_3A content of portland cements on the sulfate durability of structural concrete containing slag; and
- Establish the impact of alumina content of slags on the concrete cracking potential.

TABLE OF CONTENTS

LIST OF FIGURES

LIST OF TABLES

Introduction

The cement and concrete industry has experienced several drastic changes in the last 100 years. Cement fineness has increased dramatically from typical values of approximately 1600 cm^2/g in 1917 [1] to values of 5000 cm^2/g not being uncommon today. Invention of chemical admixtures was a technological breakthrough that resulted in acceleration of typical construction schedules and production of such "exotic" concrete mixes as high-strength high-performance concrete and self-compacting concrete to name a few. In addition to chemical admixtures, supplementary cementitious materials (SCMs) have gained popularity and are now widely used by the construction industry.

These new advances have not been without problems though. New issues of concern arising from fine cements and low w/c ratios are thermal cracking and autogenous shrinkage. There have also been reports of chemical-mineral admixture interactions, such as the negative effect of Class F fly ash on the air-entraining admixture dosage, and chemical admixture-cement type interactions. With new chemical and mineral admixtures continuously coming to market, there is a need to evaluate different cement-admixture combinations and their effects on the fresh and hardened concrete properties.

ASTM C125 [2] provides the following definition of admixture: "a material other than water, aggregates, hydraulic cementitious material, and fiber reinforcement that is used as an ingredient of a cementitious mixture to modify its freshly mixed, setting, or hardening properties and that is added to the batch before or during its mixing." Chemical and mineral admixtures can significantly improve concrete performance, from accelerated strength gain to increased durability. However, each admixture needs to be evaluated prior to use not only in terms of its intended effect, but also with respect to its "side effects" which may range from increased heat of hydration to delayed setting time. Additionally, interaction of each admixture with cement components as well as other admixtures in the mix design has to be considered.

Since the introduction of chemical admixtures on the market, a number of cases of negative interactions between chemical admixtures and cement/mineral admixtures have been reported. Tuthill et al. [3] reported an extreme delay in final setting of concrete used in railroad tunnel lining that caused the concrete to come down with the formwork when the formwork was removed after 10 hours. In 2007, Roberts and Taylor [4] reported the arrested hydration of a bridge deck concrete

after water-reducing admixture addition at hot temperatures. Although such extreme examples are rare, it is not uncommon to encounter undesirable cement-admixture interactions, such as rapid slump loss or delayed setting in construction practice. In order to better understand the causes of these interactions, it is necessary to understand how the admixtures affect the cement hydration process.

Cement Hydration

Bullard et al. [5]stated that cement hydration "involves a collection of coupled chemical processes, each of which occurs at a rate that is determined both by the nature of the process and by the state of the system at that instant." The reaction kinetics of cement hydration are very complex and the composite behavior is typically demonstrated using a typical heat flow versus hydration time curve obtained from isothermal calorimetry. The curve is usually divided into 5 regions with indistinct boundaries: initial hydrolysis (1), induction (dormant) period or period of slow reaction (2), acceleration period (3), post-acceleration period which can be split into deceleration period (4) and steady state period (5) as depicted in Figure 1-1. Figure 1-1 shows the heat flow for a portland cement-water mixture (paste) at 30°C over a period of 7 days and the typical stages of the hydration process. A recent article by Scrivener et al. [6]presents a comprehensive review of the current state of knowledge concerning the processes occurring in the various hydration stages.

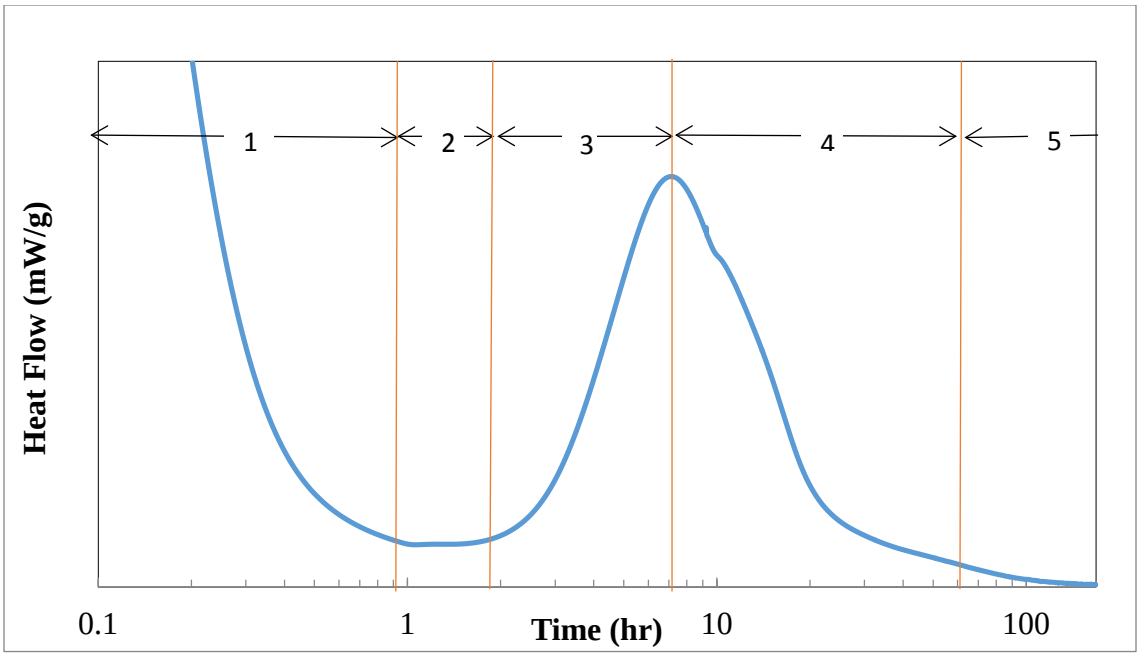

Figure 1-1: Typical Stages of the Hydration Process

The initial high rate of heat evolution in Stage 1 is produced by exothermic wetting and dissolution of the cement particle surfaces, followed by formation of hydrated cement phases. After contact with water, sodium and potassium sulfates dissolve almost instantly and calcium sulfates dissolve until saturation. At the same time, tricalcium silicate (alite, C_3S) and tricalcium aluminate (C_3A) begin to dissolve, and calcium silicate hydrate, the cementitious binding phase (C-S-H), and ettringite deposit on the surface of C_3S and C_3A grains respectively. Since the CaO/SiO_2 ratio of C-S-H is lower than in C_3S, alite dissolution contributes Ca^{2+} and OH^- ions to the solution increasing the pH [7], [8]. It is believed that the reaction kinetics, up to the end of the induction (dormant) period (Stage 2), are dissolution-controlled and driven by the degree of undersaturation of the reactants [6]. The causes of the rapid decrease in the rate heat evolution (hydration) after the first few minutes of hydration (Stage 1) and the very low rate of hydration during the induction period (Stage 2) have not been conclusively determined. Stage 2 typically lasts several hours, which permits the placing and handling of portland cement since the mixture is still in a plastic state.

For normal concrete, initial set occurs shortly after the end of the dormant period and during the early part of the acceleration period (Stage 3). This is where the hydration reactions are

accelerating, which reduces the free water and increases the content of interlocking C-S-H, resulting in stiffening of the mix and initial set. Final set occurs when enough interlocking C-S-H has been produced to form a rigid skeleton. The time range for final set typically corresponds to the upper region of the ascending portion of the main heat flow curve, prior to the occurrence of the maximum heat flow. During Stage 3, the rate of C_3S reaction increases to a maximum, which corresponds to the maximum rate of heat generation. Calcium hydroxide begins to precipitate out of solution, which had become saturated with respect to Ca^{2+} and OH^- ions by the end of stage 2, and "second stage C-S-H" begins to form. The concentration of sulfate ions decreases due to complete dissolution of calcium sulfates and the formation of ettringite.

The rate-controlling mechanisms for Stages 3-5 have not been conclusively determined due to the complexity of processes occurring during hydration. The acceleration period (Stage 3) for the main hydration peak corresponds to the rapid growth of C-S-H. However, whether the growth is controlled by dissolution or precipitation has not been determined. In Stage 4, the rate of growth of C-S-H decreases, eventually reaching a steady state. Continued hydration eventually leads to (1) a reduction in the surface area of exposed, unreacted cementitious phases available for reaction; (2) a reduction in the volume of water in the pore network that is available for hydration; and (3) a decrease in transport of reactants (permeability) caused by a reduction in the cross section and volume of interconnected, water-filled capillaries necessary for fluid transport of reactants. These conditions can reduce the rate of C-S-H growth by limiting the dissolution of cement phases and precipitation of C-S-H. It was stated by Scrivener et al. [2015] that the filling of space by hydration products becomes the limiting factor in long-term hydration.

Lerch [9] has shown that calcium sulfate plays a critical role in the rate of hydration of C_3A. In the absence of sulfates, tricalcium aluminate quickly reacts with water to form calcium aluminate hydrate resulting in a flash set. The presence of sulfates slows down the reaction of aluminates as ettringite crystals form around the C_3A grains. Calcium sulfates are added to clinker during grinding to control setting and can be present as either gypsum, bassanite, or soluble anhydrite. Roberts and Taylor state that "reactions between the sulfates and aluminates are the basis of most incompatibility problems" [4]. It has been reported that some admixtures lower the solubility of calcium aluminates [10]. Some supplementary cementitious materials can place additional demand on the sulfate ions [4]. Rapid hydration of C_3A retards the hydration of calcium

silicates severely delaying setting time [11]. Although Cheung et al. state that the "exact mechanism whereby the aluminate reaction slows down or shuts off silicate reaction has not been described" [12], it may be due to the decreased solubility of silicates in the presence of aluminum ions. Chappex [13] demonstrated that the presence of aluminum ions in solution inhibits dissolution of amorphous silica. Additionally, $Al(OH)_4^-$ has been shown to decrease the dissolution rate of quartz [14].

It should be noted that solubility of all three of the calcium sulfate phases is affected by temperature in a similar manner: solubility of calcium sulfates decreases as the temperature increases [15], while solubility of cement compounds increases with temperature [16]. Combinations of admixtures such as set accelerators, which increase fresh concrete temperature, and water-reducers, which lower calcium sulfate solubility, can dramatically increase concrete's sensitivity to admixture dosage, especially at elevated temperatures.

Chemical Admixtures

An admixture is defined as "a material other than water, aggregates, hydraulic cementitious material, and fiber reinforcement that is used as an ingredient of a cementitious mixture to modify its freshly mixed, setting, or hardened properties and that is added to the batch before or during its mixing," and a chemical admixture is defined as "an admixture in the form of a liquid, suspension, or water-soluble solid" [2]. ASTM C494 [17] separates chemical admixtures into eight different types. The first seven types are based on water-reducing and set-accelerating or retarding characteristics, and the eighth covers specific performance admixtures. Specifications for air-entraining admixtures are provided in ASTM C260 [18].

Formulations for chemical admixtures are numerous, and it is impossible to cover all the possible combinations. Additionally, manufacturers rarely disclose the chemical composition of their admixtures, and information that can be obtained from the material safety data sheets (MSDS) is limited. Interactions of chemical admixtures with anhydrous cement and hydration products are not well understood, and research in this area is hampered by the lack of complete compositional data for the chemical admixtures. Therefore, this literature review will focus on the active ingredients that are known to be most commonly used in each type of chemical admixture.

Many chemical admixtures, such as air-entraining agents, water-reducing admixtures, and shrinkage-reducing admixtures, belong to a class of chemicals called surfactants. Surfactants are organic molecules that are amphiphilic, which means that one end of the molecule is polar and is able to attract water molecules (hydrophilic) and the other end is non-polar, making it hydrophobic. These hydrophobic tails repel water enabling surfactants to be adsorbed at the solid-water and air-water interfaces [19], [20]. Anionic surfactants (containing a negatively charged group on the polar end) are most common in concrete technology [19]. Carboxylates ($-COO^-$), sulfonates ($-SO_3^-$), and sulfate ethers ($-SO_4^-$) are common examples of anionic surfactants. When the polar head contains a positively charged ion, like ammonium ion (NH_3^+), the surfactant is termed cationic. When the polar portion does not have a charge, the surfactant is nonionic. For example, polyoxyethylenated compounds are nonionic surfactants used as chemical admixtures [20].

Depending on the nature of the polar head (anionic, cationic, or nonionic), surfactants may exhibit different adsorptive behavior. After testing adsorption of four different surfactants on portland cement particles, Zhang et al. concluded that while anionic and cationic surfactants show adsorption to the portland cement/hydration products surfaces, nonionic surfactants are not adsorbed [21]. Merlin et al. [22] also concluded that nonionic surfactants of the alkyl-phenol-poly(ethylene oxide) family did not adsorb to the surface of C_3S or hydration products due to the inability of these mineral phases to form hydrogen bonds with these surfactants.

For a given admixture, adsorption also depends on the type of cement and the presence of supplementary cementitious materials (SCMs). Uchikawa et al. [23] determined the degree of adsorption of β-naphthalene sulfonic acid condensate admixtures and lignosulfonate admixtures on eight different cements including blended cements containing slag and fly ash. The adsorption of both admixtures varied with the type of cement. They also observed that admixtures were adsorbed preferentially to the interstitial phase and free lime.

When several chemical admixtures are present in cement, admixtures with similar chemical structures may compete for adsorption. In this case, admixtures with high anionic charge density will adsorb preferentially, preventing adsorption of low anionic charge density admixtures [24].

Shrinkage-Reducing Admixtures

Shrinkage-reducing admixtures (SRAs), a category of Type S admixtures, are commonly used to prevent concrete shrinkage cracking, although Bentz [25] has suggested that they can also be used as a curing compound. Concrete responds to a loss of moisture by a reduction in volume (shrinkage). When this volume change is restrained and the shrinkage stresses generated exceed the concrete tensile strength, concrete cracks. If this volume change occurs while concrete is still in the plastic state, it is referred to as plastic shrinkage. After hardening, the volume change due to loss of moisture to the external environment is termed drying shrinkage, and the bulk volume change due to the loss of moisture in the capillary pores to the hydration reactions is called autogenous shrinkage. SRAs have been shown to be effective in reducing plastic, drying [26], and autogenous shrinkage [27].

There are a number of different SRA chemical formulations on the market, but all are chemical surfactants that are amphiphilic. They are organic chain molecules that contain one hydrophilic end and one hydrophobic end [28]. The main mechanism of shrinkage reduction is due to the reduction of the pore fluid surface tension [28]–[30] . When water is lost from the capillary pores, either due to hydration or due to exposure to low relative humidity (RH) environments, air-water menisci are created in the partially empty pores, which produce tensile stresses on the pore walls. These capillary stresses can be calculated according to the Kelvin-Laplace equation:

$$\sigma_{cap} = \frac{2\gamma \cos\alpha}{r} = \frac{-\ln(RH)RT}{V_m} \qquad \text{Equation 1-1}$$

where σ_{cap} is the capillary tension (Pa), γ is the pore solution surface tension (N/m), α is the angle between the pore solution and the pore walls, r is the meniscus radius (m), V_m is the molar volume of the pore solution (m^3/mol), R is the universal gas constant (8.314 J/(mol K)) and T is the temperature (K) [31] . By reducing the surface tension (γ), SRAs reduce the capillary stresses and consequently the concrete shrinkage. Additionally, SRAs increase RH inside the concrete pores[29], [32] , which also reduces capillary stresses. This effect increases with increasing temperature [27].

The reduction in the surface tension of the pore solution is most pronounced at low concentrations of SRA. As the admixture concentration increases, its effectiveness decreases and

eventually plateaus until a "critical SRA concentration" is reached beyond which addition of SRA does not lead to further reduction in the surface tension [29], [30].

Addition of SRA also changes the early-age drying mechanism of concrete. While it has been observed that in plain paste and mortar, moisture is removed uniformly throughout the cross-section of the specimen [31], [33], [34], addition of SRA creates a drying front that advances from the top of the specimen [32]. As a result, less water is lost due to drying in mixtures containing SRA.

The effectiveness of SRA in preventing cracking depends on the curing temperature. Sant observed that addition of SRA resulted in significant reduction of tensile stresses due to drying shrinkage in concretes cured at 10 and 23°C. However, stress development in SRA-containing concrete cured at 36°C was similar to that of the plain mixture. Cracking was observed in both concretes shortly after the placement: after 14 hours in a plain mixture and 29 hours in the mixture containing the SRA. Similarly, a significant reduction in autogenous shrinkage strain has been observed for concretes cured at 10 and 23°C. Stresses observed in concretes cured at 36°C, however, were similar for both plain and SRA-containing mixtures [27].

A delay in setting time with addition of SRAs has been reported by a number of researchers [28], [30], [35]. It has been recently suggested that this may be due to the decreased solubility of alkali sulfates with SRA addition [30]. Brooks et al. observed that the delay in setting time with addition of SRA for normal concrete was relatively minor (less than 10%); however, for high-strength concrete the delay was significant. This was attributed to the interaction of SRA with superplasticizer [36].

Rajabipour et al. [30] observed that the concentration of hydroxide ions in the pore solution containing SRA begins to decrease after 10 hours, compared to the pore solution of the plain paste, and the concentration of calcium ions in the SRA-containing pore solution is always higher than in the pore solution of the plain paste. It is clear that SRA changes the solubility of calcium hydroxide, although the reported results seem to be contradictory. Sant et al. [35] observed that at 11 hours SEM images of plain paste show fewer calcium hydroxide crystals than the images of paste containing SRA. The phase saturation index for the two pore solutions indicates oversaturation with portlandite in the SRA-containing pore solution. This contradicts the quantitative x-ray diffraction (QXRD) and thermogravimetric analysis (TGA) results obtained in

this study. QXRD showed similar portlandite content in both plain paste and paste containing SRA. TGA consistently showed higher portlandite content for SRA-containing paste from the age of 10 to 50 hours.

Addition of SRA does not result in significant changes in the cement activation energy. Sant reported activation energies of 37.8 kJ/mol and 36.2 kJ/mol for mixtures with and without the SRA respectively [27]. SRA does reduce the maximum heat flow [35]. SRAs have also been reported to decrease the entrained air content [26], [28], [37], although other researchers have observed this to be true only for some SRAs. Naik et al. [38] compared three different SRAs and found that the effect on air entrainment and compressive strength varied with the chemical formulation of the admixture as well as with the type of air-entraining and water-reducing admixture combinations.

Similarly, the magnitude of compressive strength reduction appears to be dependent on the SRA formulation. Although all the SRA seem to decrease early compressive strength, Ribeiro et al. [39] reported 28-day compressive strength for a high molecular weight polyglycol SRA comparable to that of the control mix, while an alkyl-ether SRA showed the expected lower compressive strength. It has been indicated that addition of SRA may be beneficial for increasing concrete durability. Reduced surface tension of the pore solution containing SRA leads to reduced sorptivity and moisture diffusivity of concrete [40]. Concretes containing SRA have been reported to be more resistant to chloride ion ingress [40], [41].

Air-Entraining Admixtures

Air-entrainment admixtures (AEs) are added to concrete for the purpose of entraining additional air voids in the hardened concrete. Air bubbles are continuously introduced into concrete during the mixing process by the mixer action. However, these air bubbles are not stable. Small bubbles formed in this manner have high internal pressure due to the high surface tension of water and will tend to coalesce to form larger bubbles that can escape more easily [42]. The air that is trapped in the concrete by the mixing process is routinely called entrapped air.

Air-entraining admixtures are surfactants usually consisting of a hydrocarbon chain and a polar anionic head, although some other compounds have been proposed as well. The hydrophilic polar head of the AE molecule is adsorbed at the air-water interface of a bubble, while the non-

polar tail (hydrophobic) points towards the center of the bubble. The surface tension of water at the interface is lowered, decreasing the internal pressure and ensuring a more stable bubble. Additionally, since each bubble is surrounded by negatively charged anionic groups, bubbles cannot coalesce due to electrostatic repulsion [43]. Due to their negative charges, the anionic heads are attracted to cement grains, resulting in a coating of hydration products around each bubble [42]. Addition of AEs creates nearly-spherical discrete bubbles that are not connected to the rest of the void system and never become filled with hydration products [44]. The active compounds most commonly used in AEs are salts, wood resins, fatty-acid salts, proteinaceous materials, alkyl-aryl sulfonates, and alkyl sulfates. Phenol ethoxylates are nonionic AEs, although they are not widely used [28], [45]. The effectiveness of nonionic AEs in creating a stable air-void system is questionable [45].

AEs are mostly used to protect concrete from freeze-thaw damage. The adequacy of the air void system in terms of freeze-thaw resistance is determined not only by the total air content, but also by the specific surface area of the bubbles and the spacing factor. The typical diameter of the entrained-air voids is 50 microns and their recommended spacing factor for effective freeze thaw resistance is 200 microns [44]. In addition to air-entrainment, small quantities of AE can be used to reduce bleeding and prevent segregation of concrete mixtures containing aggregates with low fines [28].

Very limited data is available on the effect of AEs on the hydration process. Kreijger, cited by Edmeades and Hewlett [43], observed that certain admixtures can affect cement hydration at high dosages. Vinsol resin had a retarding effect on C_3S hydration while accelerating the C_3A hydration. Sodium oleate accelerated C_3A hydration, but had no effect on the C_3S. AEs reduce bleeding. Use of AEs with water-reducing admixtures that delay setting time increases the risk of premature drying of the concrete surface and consequent plastic shrinkage cracking, especially in hot and dry weather [46].

As AEs increase porosity, the compressive and tensile strengths of concrete will be reduced. Mindess [16] states that generally concrete strength is reduced by 5% for every 1% of entrained air, decreasing the concrete's ability to resist stresses.

AEs can interact with a number of materials in the concrete mixture. The presence of soluble alkalis in cement can aid in the production of a stable air void system [10]. Less air-

entraining admixture is required to achieve a given air content for a high-alkali content cement than for a low-alkali-content cement [47], [48]. Rixom and Mailvaganam [28] cite the results obtained by Greening that when the alkali content of the mixing water "reaches 0.8% by weight of water, the amount of air-entraining agent is minimized." It appears that the governing factor is the amount of dissolved alkalis, not necessarily their source, as Greening observed the same affect for alkalis added as part of admixture formulation. The extent of the alkali-admixture interaction depends on the specific AE composition.

Increase in cement fineness decreases the amount of entrained air for a given admixture dosage. Since AE molecules can be adsorbed not only at the air-water interfaces, but the surface of cement particles as well, increase in cement fineness increases the amount of cement surface area that adsorbs AE molecules, reducing their availability for bubble adsorption [45].

Use of water-reducing admixtures can generally lower the demand of AE to entrain a given amount of air [47]. However, some WRs can increase the diameter of the entrained air voids and their spacing factor, making the air-void system inadequate for protection against freeze-thaw damage. When used in conjunction with $CaCl_2$ accelerator, a given dosage of AE entrains slightly more air[47].

Mixing and placing temperatures affect the efficiency of the AEs. At higher temperatures, more admixture is needed to achieve the required air content [45], [47]. This may be due to the higher viscosity of water at lower temperatures and a reduced amount of hydration products. Du and Folliard [45] also hypothesized that the effectiveness of AEs is higher when the concentration of calcium ions in the mixing water is lower (due to slower hydration at lower temperatures).

Water-Reducing Admixtures

A water-reducing admixture (WR) is defined as an admixture that "either increases the slump of freshly mixed mortar or concrete without increasing the water content or that maintains the slump with a reduced amount of water due to factors other than air entrainment" [49]. Water-reducing admixtures are able to decrease water demand in concrete mixtures by improving dispersion of cement particles. WRs adsorb to the surface of cement particles imparting a negative charge to each particle. Electrostatic repulsion forces prevent particles from flocculating and ensure that each cement particle is surrounded by water. This improves workability allowing a

lower quantity of water to be used to achieve the same slump [44]. Van Dam et al. observed that the use of water reducers results in a finer capillary pore system with uniformly distributed pores [50].

ASTM C494 [17] defines five different types of water-reducing admixtures: Type A – water-reducing admixtures; Type D – water-reducing and retarding; Type E – water-reducing and accelerating; Type F – water-reducing, high range; and Type G – water-reducing, high range, and retarding admixtures. This literature review is limited to the Type D admixtures.

Although there are a number of different formulations on the market, most Type D WRs contain either lignosulfonate salts or salts of hydroxycarboxylic acid [44]. Most admixtures containing lignosulfonates contain sugars as well. The type and concentration of the sugars depend on the source and the processing of the lignosulfonates. Both sugars and lignosulfonates delay the setting time of concrete. Lignosulfonates also tend to entrain air, although the quality and stability of these air voids are not sufficient to provide resistance to freezing and thawing. Air-detraining agents are added to some admixtures to avoid this undesirable effect [28].

Salts of hydroxycarboxylic acid do not affect setting time at normal dosages, but become retarding at high dosages. Sodium salts are used most often, although some admixtures are based on ammonia or triethanolamine salts. Hydroxycarboxylic acid admixtures can have an air-detraining agent as well [28].

WRs allow the use of lower w/c ratios by improving the dispersion of cement particles. Soroka and Ravina [51] observed that the use of Type D admixtures (water reducer with retarder) under hot weather conditions accelerates the rate of slump loss in the ready-mix concrete as well as decreases early tensile strength and increases the risk of plastic shrinkage cracking. Increased drying shrinkage and creep with the use of WRs have also been observed, particularly with lignosulfoaluminate-based admixtures [16].

It has been reported that the stability of the air void system is affected when a lignosulfonate water-reducing admixture is added to concrete in combination with an AE. Even though a lignosulfonate WR increases the total air content, it decreases the specific surface area of air voids. This effect is attributed to the presence of contaminants such as sugars in the WR [46].

Addition of chemical admixtures containing calcium lignosulfonate (CLS), salts of hydroxylated carboxylic acids, or carbohydrates lowers the rate of dissolution of calcium sulfates. In cements containing soluble anhydrite, this can result in a flash set as it has the lowest solubility out of the calcium sulfate compounds [10]. Sandberg and Roberts [52] showed the acceleration of C_3A hydration and retardation of C_3S hydration with addition of lignosulfonate WRs through isothermal heat evolution curves. The effect increased with increasing WR dosage. As additional doses of WR can be added on site to restore workability, excessive quantities of WR can lead not only to segregation, but also to delay in setting time. The admixture saturation point varies for different cements depending on their C_3A content and fineness. Lower C_3A cements require lower admixture dosages. Addition of higher dosages of WRs containing calcium lignosulfonates to low C_3A cement can result in a significant delay in setting time and, in extreme cases, cessation of hydration [10]. The crystal structure of tricalcium aluminate may be of significance as well. Cheung et al. [12] reported that addition of sodium gluconate had a significantly more pronounced retarding effect on the hydration of cubic C_3A than on orthorhombic C_3A in cements with adequate sulfate contents. In undersulfated cements, retardation of orthorhombic C_3A was much more significant.

It has been reported that some organic admixtures can be incorporated into the tricalcium aluminate hydration products resulting in severe retardation of setting time. This may be due to the deposition of these organomineral products on the surfaces of C_3S resulting in a delay of C_3S hydration [12].

Wang et al. [53] observed that addition of water-reducing and retarding admixtures to binary blends of portland cement and fly ash resulted in severe retardation of hydration. This effect was much greater for Type II cement compared to Type I cement. Blends of Type II cement with Class F and Class C fly ashes did not reach final set within 24 hours. It is clear that cement phase composition plays an important role in determining admixture interactions. Type II cements used by Wang et al. [53] had slightly lower C_3A content (7% vs. 10% for Type I), and the SO_3/C_3A ratio of the Type II cement was higher than that of the Type I cement. The major difference between the cements used in this study appears to be in the C_3S content, with the Type I cement containing much more alite. Unfortunately, the researchers did not test the combinations of each cement with admixtures without fly ash so the effect of cement composition on cement/admixture

interaction could be clarified. The brand of admixtures used or their chemical formulation was not reported either. As discussed previously, the mode of action of a particular admixture depends on its chemical composition, and generalizations to broad admixture classes should be avoided.

Accelerating Admixtures

A number of accelerating admixtures are currently available on the market containing a number of active ingredients. Depending on the chemical compounds used in their production, accelerating admixtures can generally be grouped into two categories: soluble inorganic salts (most commonly used are calcium chloride, calcium nitrate, calcium formate and calcium thiocyanate) and soluble organic compounds (triethanolamine and triisopropanolamine) [12], [28]. The action of the accelerating admixtures, again depending on their formulation, can be to shorten the induction period thus accelerating initial and final setting, or to increase the rate of hydration and the rate of strength gain, or both.

Calcium chloride ($CaCl_2$) accelerator is the most commonly used inorganic accelerator. It is perhaps the cheapest and the most effective among the accelerating compounds [28]. Addition of $CaCl_2$ results in faster setting time and increased early compressive strength. This effect has been attributed to the increased reaction rate of C_3S with the addition of $CaCl_2$, although the mechanism of acceleration of C_3S hydration is not well understood [54]. Juenger et al. [55] proposed that $CaCl_2$ promotes the formation of inner-product calcium silicate hydrate (C-S-H) thus increasing the rate of ion diffusion through the C-S-H layer and accelerating the rate of C_3S hydration. In the absence of $CaCl_2$, surface area per mole of C-S-H decreases with time, while the surface area per mole of C-S-H formed in the presence of $CaCl_2$ remains fairly constant [56].

The rate of heat evolution is also increased as well as the maximum concrete temperature [54]. This is the case with most accelerators. In addition, the occurrence of the maximum temperature shifts to an earlier age [57], which is consistent with accelerated silicate hydration. However, the total heat of hydration is not affected [47].

At equal dosages, $CaCl_2$ is more effective in cements containing sufficient quantities of sulfate ions. Chloride ions will remain in solution until the sulfate has been consumed by reaction with the aluminates, after which the aluminates will react with the chloride ions, and the conversion of ettringite to monosulfoaluminate will not occur until all the chlorides have been consumed [12].

The use $CaCl_2$ results in concrete that is more susceptible to sulfate attack and alkali-silica reaction (ASR). Drying shrinkage and creep are also increased with the use of $CaCl_2$ [57]. Hope and Manning also observed an increase in creep with addition of $CaCl_2$ [58].

The major disadvantage of $CaCl_2$ is the presence of chloride ions, which can make reinforcement more susceptible to chloride-induced corrosion. For this reason, the use of calcium chloride in reinforced concrete is prohibited by most codes, standards, and specifications. A number of "non-chloride" accelerators containing combinations of other inorganic salts, such as calcium nitrate, calcium and sodium nitrite, and sodium thiocyanate, are commercially available for reinforced concrete applications. The reactions of these inorganic salts are believed to be similar to those of calcium chloride, although they have not been studied as well [28]. Care should be taken in using admixtures containing sodium as they may increase the likelihood of alkali-aggregate reaction [44].

Triethanolamine (TEA) is commonly incorporated into other admixtures, such as WRs, to compensate for their retarding effect [28]. It is also included in some accelerating admixture formulations together with $CaCl_2$ (MSDS). Additionally, TEA is used as a grinding aid during cement production [59]. The effect of TEA on concrete is dosage-dependent. At lower dosages, TEA acts as an accelerator, while at higher dosages it has a retarding effect [28]. It has been shown that the accelerated setting with TEA addition is due to the acceleration of the reactions of aluminates with calcium sulfates and accelerated formation of ettringite [11], [28]. A delay in the C_3S hydration has been reported by several authors [11], [28], [60]. Ramachandran attributed this effect to the formation of a TEA complex on the surface of the calcium silicates [60]. Although addition of low dosages of TEA can dramatically increase early-age strength, it results in a lower ultimate concrete strength. Cheung et al. reported that with addition of 0.02% TEA, 1-day concrete strength was increased to 115% of that of the control mix. However, the rate of concrete strength gain began to decline immediately. At 2 days compressive strength of concrete containing TEA was 105% of the control mixture and at 28 days it was below the compressive strength of the control mixture [12]. Hope and Manning reported that addition of TEA in combination with a lignosulfonate admixture significantly increased early-age creep and decreased the ultimate strength of concrete [58].

Unlike TEA, triisopropanolamine (TIPA) does not affect early strength, but it is very effective in increasing later-age strength (beyond 3 days) in cements with high C_4AF composition and lower fineness. It is believed that the strength increase with TIPA addition is due to the increased dissolution of C_4AF, more specifically due to the interaction of TIPA with the iron ions, since TIPA does not affect the rate of dissolution of C_3A [12].

ACI report 212.3R-91 cautions that the use of accelerators may have a negative impact on the entrained air-void system with respect to freezing and thawing resistance. Although less air-entraining admixture is generally required to obtain a given air content when used in conjunction with an accelerating admixture, in some cases increases in bubble size and spacing factors have been observed [47].

Mineral Admixtures

There are three general types of mineral admixtures: filler materials, pozzolans, and latent hydraulic materials. Filler materials are non-hydraulic materials, such as finely ground limestone or quartz. Finely-ground filler materials added to concrete can accelerate hydration reactions by providing nucleation sites for the early-age hydration products [61]. Although filler materials are not included in this report, it is important to note that addition of any fine materials, such as pozzolans, to cement can affect hydration reactions due to the filler effect, even before the commencement of pozzolanic reaction[62].

A pozzolan is defined in ASTM C125 [2] as a "siliceous or siliceous and aluminous material that in itself possesses little or no cementitious value but will, in finely divided form and in the presence of water, chemically react with calcium hydroxide at ordinary temperatures to form compounds possessing cementitious properties". Pozzolans require calcium hydroxide as well as water to form cementitious products. In cement-pozzolan mixtures, pozzolans react with calcium hydroxide (CH) produced during cement hydration. C-S-H produced during cement hydration has an approximate composition of $(CaO)_{1.5\text{-}1.9}\cdot SiO_2\cdot(H_2O)_x$, where the number of water molecules (n) depends on the temperature and internal relative humidity [62][63]. Unlike pozzolans, latent hydraulic materials, such as slag, do not require CH to form cementing compounds. However, the hydration reactions of the self-cementing compounds are slow and do not produce enough cementitious products for them to be used on their own [19]. In addition to cost-reduction benefits,

addition of mineral admixtures can decrease concrete permeability, increase ultimate strength, and provide improved resistance to aggressive environments.

Metakaolin

Metakaolin (MK) is a pozzolanic material obtained by subjecting kaolin clay to heat treatment (calcination) at 500-800°C. Upon heating, kaolinite ($Al_2O_3 \cdot 2SiO_2 \cdot 2H_2O$) is dehydroxylated and is transformed into a more disordered metakaolin phase [64]. Metakaolin generally consists of about 53% SiO_2 and 40% Al_2O_3, although the exact composition varies depending on the source of kaolin [64]–[67].

Cabrera and Rojas [68] concluded that the initial reaction of MK (during the first 50 hours) is very rapid and is diffusion-controlled. The rate of reaction depends on curing temperature and increases with increasing temperature [69]. The reactivity of metakaolin is related to its amorphous content [64], [66], which Kakali et al. [66] found to be related to the amorphous content of the original kaolinite. When added to cement paste, metakaolin reacts with calcium hydroxide (CH) to produce additional calcium silicate hydrate (C-S-H) as well as aluminosilicate hydrates and aluminate hydrates [70], [71]. At replacement rates of up to 30% by weight of cement, metakaolin has an accelerating effect on cement hydration. Additions of metakaolin above 30% can delay the final setting [70]. Increased formation of C-S-H results in increasing the compressive strength, while the consumption of CH results in a lower pH of the pore solution. Ambroise et al. [70] reported that the highest compressive strengths are achieved at 10% cement replacement level. At a 20% replacement level pastes have similar compressive strengths to that of an ordinary portland cement (OPC) paste. Similar results were obtained for mortars. Other researchers have similarly reported 10% replacement to be optimal for maximizing compressive strength [72], [73].

An increase of tensile strength in addition to compressive strength has been reported in the literature for appropriate MK additions [74], [75]. However, Qian and Li [75] observed only a slight increase in the elastic modulus, and the ratio of tensile to compressive strength decreased with increased MK content indicating increased brittleness of concrete.

Wild and Khatib [76] reported a 50% decrease in CH after one year for pastes with 15% cement replacement by metakaolin. Ramlochan et al. [67] showed that at 20% cement replacement, there is a consistent reduction in the OH^- ions in the pore solution up to 2 years. At

10% replacement levels, OH^- ion concentration decreased up to 7 days and increased after 7 days, presumably due to the consumption of metakaolin during the first 7 days. However, paste containing metakaolin had lower OH^- concentrations at all ages compared to the control mixtures, regardless of the cement replacement level. Coleman and Page [77] reported a consistent reduction in pH up to 100 days at both 10 and 20 % cement replacement with metakaolin.

MK has been shown to be effective in reducing concrete expansion due to alkali-aggregate reaction [67], [78] as well as due to external sulfate attack [79], [80]. In terms of chloride-induced corrosion, it has been shown that addition of metakaolin results in a lower concentration of Cl^- ions in the pore solution, thus counteracting the negative effect of the reduction of pH on the passivation of steel [77]. Batis et al. [72] reported that corrosion resistance of mortars was improved by addition of 10% metakaolin, although at higher replacement levels addition of metakaolin had a negative effect on corrosion resistance. Courard et al. [80] reported a significant decrease in chloride ion diffusion through mortars containing MK. It is interesting to note that they did not observe any diffusion after 1 year through the samples containing 20% metakaolin.

Similar to silica fume, concretes containing MK show an increase in the depth of carbonation with increased cement replacement levels. This is attributed to the consumption of CH [74]. It has been proposed that C-S-H created during metakaolin hydration differs from the C-S-H produced in the reaction of cement with water. Ambroise et al. [70] found the Ca/Si molar ratio of metakaolin-produced C-S-H to be 1.0-1.6.

Addition of MK results in smaller pores. Ambroise et al. [70] reported an increased amount of micropores with 20-30% MK addition in spite of increased w/cm ratio for the blended cements. Poon et al. [73] also reported that addition of metakaolin at a constant w/cm ratio decreases the average pore diameter for any age and at any cement replacement level up to 20%.

Addition of up to 20% MK increases the maximum temperature rise during hydration [70]. Frias et al. [81] also noted that addition of MK results in a slight increase in the heat of hydration compared to OPC. On the other hand, Kim et al. reported a slight decrease in the maximum adiabatic temperature with addition of 10% MK [74]. It appears that the change in the heat of hydration with MK addition is determined by two factors: MK fineness and cement composition. Cumulative heat of hydration increases with the increase in surface area of MK. Increased alkali content of cement appears to increase the rate of reaction of MK, also increasing the heat of

hydration [82]. MK is more reactive at early ages than SF. Consequently, it produces higher early-age strengths and smaller pore radii at early ages [73].

Addition of MK reduces workability [75], [80], [83], requiring addition of high-range water reducers or increasing the water content. Ding and Li [84] compared the slump of MK-modified concretes to those of SF-modified concretes and concluded that addition of MK resulted in a slight decrease in workability with increased replacement levels compared to SF.

The literature on the effect of MK on autogenous shrinkage is scarce and contradictory. Brooks and Johari reported that long-term autogenous shrinkage measured from the age of 24 hours is increased. However, when long-term shrinkage was measured from the time of initial set, only the mixture with 5% MK had higher autogenous shrinkage than the OPC mixture, and autogenous shrinkage decreased with increased replacement level [85]. On the contrary, Gleize et al. [86] reported a decrease in autogenous shrinkage at all replacement levels.

With respect to drying shrinkage, a number of researchers have reported a reduction in shrinkage with additions of MK [84], [85]. This is attributed to the fast reaction of MK at early ages and a higher percentage of water that is used up in the hydration process, compared to the OPC concrete, leaving less water that can be lost due to evaporation.

Inclusion of MK results in significant reduction of creep [85]. This is attributed to the improved interfacial transition zone (ITZ) between the paste and aggregate [87], higher strength and the filler effect suggested by Wild et al. [83].

Silica Fume

Silica fume (SF), also referred to as microsilica, is a pozzolanic by-product of silicon metal production. It consists of small spherical particles of amorphous silica with an average particle size of 0.1 microns and a surface area of 15,000-25,000 m^2/kg. Silica fume resulting from ferrosilicon alloy production contains only 50% silica and is not suitable for use as a pozzolanic material [19], [44].

There is no clear agreement in the literature regarding the process of silica fume hydration. Lilkov et al. [88] demonstrated that hydration reactions involving SF begin during the first hour after contact with water. Acceleration of the alite hydration by SF has been reported earlier by Wu and Young [89]. They observed that the presence of SF increases the duration of stage 1

(initial hydrolysis) of alite and decreases the induction period. Feldman and Cheng-yi [90] concluded that in addition to C_3S, C_3A hydration is also accelerated by the presence of SF. Langan et al. [91] confirmed the accelerating effect of SF on cement hydration, but only at high w/cm ratios. They reported a retarding effect at low w/cm ratios. This effect was attributed to the adsorption of water by silica fume, which at low w/cm ratios would reduce the water available for reaction with cement particles. On the contrary, Kadri and Duval [92] observed acceleration of hydration with addition of silica fume at low w/cm ratios. Zelic et al. [93] concluded that the acceleration of early-age cement hydration by SF is strictly due to the filler effect and contribution from the pozzolanic reaction could only occur after 3 days. With respect to the total heat of hydration (HOH), they observed an increase in HOH with 10% cement replacement by SF. However, at 30% replacement level, the HOH was decreased [92].

Larbi et al. [94] examined the pore solution concentrations during cement hydration with silica fume. They observed that the concentration of calcium ions decreased much more rapidly in the cement-silica fume pastes than in the control pastes. Hydroxide ion concentration, although initially higher in pastes containing silica fume, decreased sharply after 1 day, while OH^- ion concentration in plain pastes continued to increase. Similarly, concentration of Na^+ and K^+ ions declined drastically after 1 day. The researchers concluded that the changes in the pore solution were independent of the w/cm ratio.

The early onset of the pozzolanic reaction explains the increased early-age concrete strength with SF addition [95]. Later-age strength, up to 90 days, is also increased [95]–[97]. The increase in strength is even more significant when concrete is cured at elevated temperatures [97]. After 90 days, however, the strength of concrete with and without silica fume is the same [95]. Flexural and tensile strength at 28 days is improved by SF addition [98]. Elastic modulus of silica fume concretes is higher as well [97].

Since SF essentially contains no calcium, it is very efficient at consuming calcium hydroxide (CH) produced during cement hydration. At the same replacement levels, CH content in paste containing silica fume is significantly lower than that of paste containing slag or fly ash [99]. This reduction in CH may be beneficial in reducing thermal stresses generated upon heating or cooling. Schulson et al. reported existence of a thermal mismatch between CH and C-S-H that

can generate significant internal stresses in the hardened cement paste[100]. Reducing the amount of CH also reduces the overall coefficient of thermal expansion of paste [99].

While most mineral additions tend to refine the pore size, incorporation of silica fume reduces also the total porosity [99]. Since silica fume particles are on average 100 times smaller than cement particles, they are able to significantly improve the packing between cement grains as well as at the aggregate interfaces [44]. This decrease in porosity significantly reduces permeability of silica fume concretes, increasing their durability in aggressive environments [93], [96], [101].

Similarly to metakaolin, consumption of CH by SF reduces the pH of the pore solution [94]. However, since SF reduces permeability, resistance to corrosion due to chloride ion ingress is improved in silica fume concretes [96].

Due to its fine particle size, use of silica fume requires addition of superplasticizer even at high w/c ratios [102]. The superplasticizer demand increases with increasing SF content [95]. Neville [44] states that there are "no reports of incompatibility of silica fume with admixtures in general." The retarding effect of lignosulfonate admixtures is reduced when used in conjunction with silica fume. Larger amounts of AE are required to obtain a given air content due to admixture adsorption onto the large surface area of SF. However, the quality of the air-void system is not affected.

Silica fume increases cohesion and reduces bleeding. However, the risk of drying shrinkage cracking is increased [44]. Addition of SF increases autogenous shrinkage; drying shrinkage, however, is reduced. Creep is also reduced with increasing SF content [95].

Class F Fly Ash

Fly ash (FA) is a pozzolanic material that is a by-product of coal combustion. FA mostly consists of solid spherical glass particles. Hollow empty spheres (cenospheres) and hollow spheres packed with small spheres (plerospheres) may also be present. Diameter of these spheres typically varies between 1 to 100 microns; however, most particles are less than 20 microns. Particle size distribution plays an important role in the reactivity of fly ash. Mehta and Monteiro [19] state that "particles of less than 10 μm contribute to early strength of concrete up to 28 days; particles of 10 to 45 μm contribute to later strength, and particles coarser than 45 μm are difficult to hydrate".

Based on the chemical composition, fly ashes are divided into two categories: Class F fly ash and Class C fly ash [103]. The main difference between these two fly ash classes is their CaO content. Class C fly ash has a high CaO content and contains some crystalline compounds including C_3A. Class F fly ash consists mainly of amorphous aluminosilicates and usually contains less than 10% CaO [19]. Only Class F fly ash is discussed in this report.

Addition of Class F fly ash reduces the total heat released during hydration due to the dilution effect. It does not affect sulfate consumption rate or the onset of the acceleration period [48]. Neville [44] states that addition of fly ash results in a slight retardation. The pozzolanic reaction of Class F fly ash is slow; the rate of reaction is significantly lower compared to the reaction rates of silica fume and metakaolin. Dissolution of fly ash begins only when the pH of the pore solution has reached 13.2 [44]. FA reaction rate can be increased by addition of TEA. Heinz et al. [104] observed that TEA increases the dissolution of iron, calcium and aluminum from fly ash, thus increasing its rate of hydration. An extended induction period and an increase in the maximum heat evolution were observed in isothermal calorimetry testing. Total heat of hydration was slightly increased as well. It is interesting to note that TEA increased 1-day strengths of fly ash mixtures, but only at low dosages of TEA. FA reactivity increases also with temperature [44].

With respect to fresh concrete properties, fly ash improves workability of concrete mixtures and reduces water demand. Fine FA particles are adsorbed onto the surface of cement grains resulting in deflocculation [44]. Bleeding and segregation are reduced as well [105]. A number of reports have been published regarding the negative effect of fly ash addition on air entrainment [48], [106]. Higher dosages of AE are required to compensate for adsorption of AE molecules to the surface of unburned carbon particles. Additionally, variation in entrained air content is not uncommon in hardened concrete due to variations in fly ash.

It is generally accepted that Class F fly ash does not contribute significantly to compressive strength development until 56 days. Early-age compressive strengths of concrete containing fly ash are lower than those of the plain concrete; later-age strength is increased. Creep and shrinkage are not affected by fly ash [44]. Chan et al. [107] reported that addition of Class F fly ash reduced autogenous shrinkage, although the drying shrinkage was increased.

Improvement to sulfate resistance is generally reported with incorporation of Class F fly ash [108]. However, Mehta [109] reported that some Class F fly ashes display poor performance

in sulfate environment. For two out of five Class F fly ashes tested, monosulfate was observed prior to sulfate exposure, which upon introduction of samples into a sulfate environment, was converted to ettringite. He concluded that the high content of amorphous alumina and iron oxide was responsible for the poor performance of these fly ashes. Durability in terms of resistance to chloride ion penetration is also improved due to decreased permeability [110].

Slag

Slag is a by-product of the manufacturing process of cast iron. Slag is a latent hydraulic material. Unlike the previously discussed mineral admixtures, it does not require the presence of portland cement to develop cementing properties and can be used on its own in the presence of an alkali activator [44]. However, this literature review is limited to the use of slag as an addition to ordinary portland cement.

ASTM C989 [111] divides slag proposed for use in concrete and mortar into three grades based on their activity index: grade 80, 100 and 120. Grade 120 possesses the highest compressive strengths at 7 and 28 days. Most commonly used grades are 100 and 120 [105].

Slag is mainly composed of lime, silica, alumina, and magnesia. The exact composition varies; however, lime and silica are the predominant phases [44]. In order to produce a useful cementing material, slag has to be quenched in either water or air, which results in a material with high amorphous content. Slag that is allowed to cool slowly forms crystalline compounds that are not reactive. Slag that is quenched in water is referred to as granulated slag, and quenching in air produces pelletized slag. Slag is normally ground to a Blaine fineness of 400-500 m^2/kg [19]. Grinding results in smooth angular particles [105] in contrast to silica fume and fly ash which have spherical particles.

Reactivity of slag depends on its amorphous content, temperature history, fineness, chemical composition, and alkali content. Higher temperatures and faster quenching rates produce higher amorphous content in the slag, making it more reactive. Higher alkali content can increase the reactivity of slag through alkali activation [19], [105]. Slag reacts with CH produced during cement hydration to form additional C-S-H [44]. The initial reaction of slag is slow, although it reacts at a faster rate than fly ash. The reaction of slag depends on the dissolution of silica in a

high pH environment [56]. Dissolution of slag releases alkalis into the pore solution, ensuring a continuous reaction of slag into the later ages [44].

Substitution of cement with slag results in a lower heat of hydration [19], [112]. Hydration of slag becomes very slow at low temperature, and use of slag in cold-weather concreting is not recommended [44]. At normal temperatures, addition of slag results in a slight delay of setting time, approximately one hour compared to the control mixture [113].

Addition of slag has been reported to improve workability and cohesion of the mix [114]. Since slag fineness is higher than that of cement, smaller slag particles improve packing and the smooth particle surface results in minimal water adsorption [44]. Slag addition also increases the bleed capacity of concrete with a minor increase in the bleed rate [114].

As slow, early-age hydration of slag results in increased capillary porosity compared to concrete with no slag, concretes containing slag may be more susceptible to drying shrinkage cracking [44]. Improvement in later-age compressive strength, as well as in modulus of elasticity, has been observed with addition of slag [115], [116]. Darquennes et al. [116] compared compressive strength and elastic modulus development of concretes prepared with 42% and 71% cement replacement by slag to that of a control mix. It is interesting to note that between 3 days and 28 days the elastic modulus was unaffected by the level of slag replacement. The only difference was observed at 1 day for the 71% slag mixture, which had a lower modulus of elasticity compared to the control mixture and the 42% slag blend. Compressive strength of the slag-containing concretes was lower at early ages, but began to exceed the strength of the control mix at 28 days.

Slag has been reported to have a negative impact on the entrained air-void system. Giergiczny et al. [117] reported decreased specific surface area and increased spacing factor between the air voids in concretes containing slag. Another undesirable consequence of incorporating slag in the concrete mixtures is increased autogenous shrinkage. Lim and Wee [118] observed that the amount of autogenous shrinkage increases with both the cement replacement level and slag fineness.

Concrete durability is improved with slag addition. Although chloride concentration near the surface is higher in slag concretes, it quickly diminishes, and virtually no chlorides are detected

at 30 mm below the surface [119]. The higher porosity of the slag concretes at early ages, before the onset of slag hydration, allows the ingress of chloride ions near the surface; however, since the diffusion coefficient is significantly reduced due to pore refinement at later ages, their progress towards reinforcement is impeded. ASTM C989 [111] indicates that the alumina content of slag has significant implications on the sulfate durability of binary mixtures incorporating high alumina slags. Slags with alumina content less than 11% have shown better performance in sulfate durability tests.

Ternary and Quaternary Blends

It is clear from the previous discussion that each of these mineral additions has its own advantages and disadvantages. Several investigations have been conducted into binary and ternary blends of these materials with portland cement in order to optimize concrete fresh and hardened properties.

Alexander and Magee [102] evaluated blends of OPC/slag/SF. They concluded that compressive strength and durability (in terms of oxygen permeability, chloride conductivity, and water sorptivity) of slag concrete was improved by addition of 10% silica fume. Additionally, they found that the superplasticizer dosage for the ternary mixture was reduced compared to the binary PC/10% SF mixture. As silica fume consists of very fine particles, and high superplasticizer dosages are generally held accountable for negative admixture-cement interactions, addition of a second coarser SCM, such as slag, may be beneficial to avoid potential problems.

Similarly, Li and Ding [120] observed that addition of slag to OPC/MK blends reduces water demand and superplasticizer dosage of the mixtures. However, addition of slag delayed setting time compared to OPC and OPC/MK mixtures. Compressive strengths were improved by the MK/slag addition due to the increased consumption of CH as evidenced by x-ray diffraction scans.

Khatib and Hibbert [115] also investigated blends of slag and metakaolin with OPC. They confirmed additions of MK to the slag/OPC blends increase early-age compressive strength, and determined that flexural strength and elastic modulus are increased as well. The OPC/MK/slag blend did not show a decrease in later-age compressive strength characteristic of MK/OPC binary blends. However, these studies did not address the effect of MK/slag blends on carbonation and

chloride-induced corrosion. Since both slag and MK lower the pH of the pore solution, increased probability of reinforcement corrosion may be of concern.

Mixtures with silica fume and fly ash have also been evaluated. Addition of SF to cement in combination with fly ash retards cement hydration and decreases the heat of hydration [91]. Inclusion of SF compensates for decreased early strength resulting from fly ash addition and reduces oxygen permeability [121].

Codina et al. [122] investigated a number of blends: OPC/SF, OPC/SF/FA, OPC/SF/slag, and clinker/SF/slag/FA. The total heats of hydration of all the ternary blends and of the quaternary blend was lower than that of the portland cement mixture. At the same level of cement replacement, the ternary blend containing fly ash had a lower heat of hydration than the blend with slag. Examination of the mineralogical composition of the pastes at 6 months revealed the presence of CH only in the OPC/SF/slag blend. Unhydrated C_3S and C_2S were present in all the samples. Unfortunately, the relative amounts of the phases in each sample are not reported. The total porosity of the pastes did not change over the course of 3 months; however, all the blends displayed pore-system refinement with time: the number of pores greater than 20 nm decreased, while the number of pores less than 20 nm increased. It should be noted that pores smaller than 20 nm are C-S-H gel pores, and the increase in porosity in this range indicates an increase in the C-S-H amount. The pH and alkali contents of the pore solution were decreased compared to OPC. The greatest reduction in the pore solution pH after 1 year was observed for the OPC/SF/FA blend.

Güneyisi et al. [123] evaluated ternary and quaternary blends of OPC with FA, SF, slag, and MK in terms of compressive strength and drying shrinkage. Similarly to Khan and Lynsdale [121], they reported that the use of other SCMs with FA reduces the strength decrease associated with the use of fly ash. They determined that the contribution of slag to compressive strength in these mixtures was not statistically significant. With respect to drying shrinkage, the negative effect of silica fume was eliminated when used in combination with other mineral admixtures.

Basheer et al. [119] reported that slump and compressive strength of OPC/FA blends was decreased when MK or SF were added to the mixture. Both MK and SF additions to the OPC/FA system decrease the Cl^- ion concentration at 10 mm depth, while the addition of slag resulted in a slight increase of Cl^- at 10 mm.

Jones et al. [124] evaluated ternary blends of OPC, slag, fly ash, and silica fume with respect to chloride ion penetration resistance and depth of carbonation. Even though the chloride resistance is improved, the carbonation rates for ternary blends are significantly higher compared to those of the OPC/FA mixtures.

Gesoğlu , et al. [125] reported that the delay in setting time with the use of FA and slag can be overcome by using ternary blends of these materials with silica fume. They further observed that quaternary blends of these materials with OPC resulted in an earlier setting time compared to the control mixture. Incorporating slag or FA in conjunction with SF and OPC resulted in improved rheology.

Due to its fine particle size, SF requires high dosages of superplasticizer to achieve desired workability. Addition of fly ash to silica fume mixtures allows the dosage of superplasticizer to be reduced significantly. Contrary to Gesoğlu, et al. [125], Bouzoubaâ et al. [126] concluded that addition of SF to FA mixtures does not have an appreciable effect on setting time. Maximum temperature rise of the OPC/FA blends was also unaffected by addition of SF. They confirmed the improved performance of ternary blends in terms of chloride ion penetrability. In addition to chloride ingress resistance, ternary blends of slag and SF show improved resistance to ASR [127]. Ternary blends of OPC/SF/FA offer improved sulfate resistance as well [128].

Erdem and Kırca [129] observed that compressive strengths of ternary blends of OPC/SF/slag and OPC/SF/Class F FA were higher than those of the binary OPC/SF mixture. The improvement was more significant at 7 and 28 days compared to 3 days. Addition of slag to the OPC/SF blends resulted in higher compressive strengths than addition of Class F fly ash.

In terms of autogenous shrinkage, addition of Class F fly ash to slag/OPC blends does not result in significant improvement. Ternary blends of OPC/slag/Class F FA show similar autogenous shrinkage to those of the binary OPC/slag blends [107].

[redacted] Materials Characterization

[redacted] Introduction

[redacted] Oxide Chemical Analysis and Density Measurements of As-Received Cement and Mineral Admixtures

Oxide chemical analysis of the as-received cement and mineral admixtures was conducted using x-ray fluorescence spectroscopy (XRF) according to ASTM C114-11b [130]. Free calcium oxide was also determined in accordance with ASTM C114-11b [130]. X-Ray fluorescence (XRF) was used for elemental oxide quantification. ASTM C150-12 was used to determine the potential compound compositions of cements [131]. The density measurements for all of the as-received materials were conducted in accordance to ASTM C188-09 [132].

One cement (SW) and four mineral admixtures, Class F fly ash (FA), metakaolin (MK), blast furnace slag (SL) and silica fume (SF), were obtained for the purpose of this study. Oxide chemical composition of the as-received cement is presented in Table 2-1. Potential phase composition calculated using the Bogue equations per ASTM C150-12 is listed in Table 2-2 [131]. The table includes potential phase composition both with and without the adjustment for the limestone addition. Information regarding the percent limestone added to the cement was obtained from the Mill Certificate. Results of cement and mineral admixtures density measurements are presented in Table 2-3. Oxide chemical composition of mineral admixtures is presented in Table 2-4.

Mineral admixture densities are in agreement with those published in the literature [105], except for metakaolin. The metakaolin density of 2.23 Mg/m^3 is below the typical values reported in the literature, which were generally around 2.50 Mg/m^3 [105], [133], [134]. This could be attributed to the lower Fe_2O_3 content of metakaolin used in this study compared to the published values [105], [133], [134]. The oxide chemical composition of the rest of the mineral admixtures is in agreement with the published values [105]. Fly ash used in the study complies with the ASTM C618-12 [135] Class F classification, while metakaolin meets the requirements of Class N pozzolan.

Table 2-1: Oxide Chemical Analysis for As-Received Cement

Analyte	**SW cement (wt%)**
SiO_2	20.40
Al_2O_3	5.20
Fe_2O_3	3.20
CaO	63.10
MgO	0.80
SO_3	3.60
Na_2O	0.10
K_2O	0.38
TiO_2	0.28
P_2O_5	0.12
Mn_2O_3	0.03
SrO	0.08
Cr_2O_3	0.01
ZnO	<0.01
L.O.I(950°C)	2.80
Total	100.10
Na_2O_{eq}	0.35
Free CaO	2.23
SO_3/Al_2O_3	0.69

Table 2-2: Bogue-Calculated Potential Compound Content for As-Received Cements

Phase	**Without Limestone Correction**	**With Limestone Correction**
C_3S	52	50
C_2S	19	19
C_3A	8	8
C_4AF	10	9
C_4AF+2C_3A	26	26
$C_3S+4.75C_3A$	92	89

Table 2-3: Calculated Cement and Mineral Admixture Density

Material	**Density (Mg/m^3)**
SW	3.14
Class F fly ash (FA)	2.25
Metakaolin (MK)	2.23
Slag (SL)	2.91
Silica Fume (SF)	2.22

Table 2-4: Oxide Chemical Analysis for Mineral Admixtures

Analyte	**MK (wt%)**	**SF (wt%)**	**SL (wt%)**	**FA (wt%)**
SiO_2	51.29	92.90	35.15	55.48
Al_2O_3	44.16	0.31	14.25	27.46
Fe_2O_3	0.49	0.10	0.48	6.70
CaO	<0.01	0.78	41.45	0.99
MgO	0.14	0.18	5.21	0.88
SO_3	<0.01	<0.01	1.86	0.05
Na_2O	0.26	0.10	0.22	0.29
K_2O	0.27	0.52	0.32	2.28
TiO_2	1.12	<0.01	0.50	1.47
P_2O_5	0.06	0.09	0.01	0.21
Mn_2O_3	<0.01	0.04	0.22	0.02
SrO	0.01	0.01	0.05	0.09
Cr_2O_3	0.01	<0.01	<0.01	0.03
ZnO	<0.01	0.05	<0.01	0.01
BaO	<0.01	<0.01	0.07	0.15
Total	99.22	99.63	99.83	99.93
Na_2O_{eq}	0.44	0.44	0.43	1.80
Moisture	0.13	0.28	N/A	0.10
SiO_2+ Al_2O_3+ Fe_2O_3	95.94	N/A	N/A	89.6
L.O.I(750°C)	N/A	4.51	N/A	3.87
L.O.I(950°C)	1.40	4.55	0.04	3.83

Mineralogical Analysis of Cement and Mineral Admixtures

Apart from the bulk elemental oxide analysis, phase content of portland cement is of great significance. It is understood that different cement phases have different contributions to concrete properties. Stutzman [136] suggested that the application of accurate measurement techniques for

cement phase quantification would improve the knowledge of their influences on cement hydration characteristics, concrete strength development, and durability of structures. Additionally, it renders concrete a more predictable construction material. For mineral admixtures, amorphous content, rather than mineral phases present, are of importance with respect to reactivity. It has been shown that reactivity of mineral admixtures considered in this study increases with increasing amorphous content [64], [66], [105], [137], while crystalline phases act as filler material.

X-ray diffraction (XRD) is a direct method of identification and quantification of the crystalline compounds in portland cements [138]–[140]. In this study, quantitative x-ray diffraction was adopted in identifying and quantifying crystalline phases present in the cement. XRD was also used for identification and quantification of crystalline phases in mineral admixtures. Although amorphous materials cannot be identified with this technique, XRD can be used to quantify the total amorphous content.

XRD scans of the as-received cement were collected in accordance with ASTM C1365-06 "Standard Test Method for Determination of the Proportion of Phases in Portland Cement and Portland-Cement Clinker Using X-ray Powder Diffraction Analysis" [141]. Mixtures of cement and ethanol 200 (99.5% pure) were prepared and wet-ground in a McCrone micronizing mill to a particle size between 1 and 10 μm. The wet grinding method was used to avoid the effect of temperature on gypsum and its possible phase transformation to hemihydrate or anhydrite. The samples were then dried in an oven at 43°C. Mineral admixtures, except metakaolin, were also ground following this procedure. Metakaolin was not ground since most of the metakaolin particles were already below 10 μm. After drying, cement samples were placed in a sample holder using a back-loading technique with frosted glass in order to minimize preferred orientation [142].

Since mineral admixtures are known to contain large amounts of amorphous material, ground mineral admixture samples were mixed with 10% titanium dioxide (TiO_2) to enable quantification of amorphous content. TiO_2 was obtained from the National Institute of Standards and Technology (NIST) as part of the Standard Reference Material (SRM) 674b set. Samples were mixed in the McCrone micronizing mill for 10 minutes with 5 mL of ethanol per every gram of sample as recommended by ASTM C1365-06 [141]. This was done to achieve homogeneous dispersion of the internal standard throughout the sample. After mixing, the samples were dried

in an oven at 40 °C in order to evaporate the ethanol. Samples were loaded into the sample holder using the back-loading technique.

X-ray diffraction scans were collected using a Phillips X'Pert PW3040 Pro diffractometer with Cu Kα radiation. The samples were scanned with a step size of 0.02 degrees per step and counting time of 4 seconds per step. The tension and current were set at 45 kV and 40 mA. Divergence slit was fixed at 1°, receiving slit had a height of 0.2 mm, and anti-scatter slit was fixed at 1°.

After collecting the x-ray scans of the as-received cement, phase identification was performed using HighScore Plus software. In order to aid the identification of the minor phases as well as the C_3S and C_3A crystal structures, selective dissolutions of the major phases (extractions) were performed.

Salicylic acid/methanol (SAM) extraction dissolves the silicates and free lime leaving a residue of aluminates, ferrites, and minor phases, such as periclase, carbonates, alkali sulfates and double alkali sulfates [138], [143]. In addition to minor phase identification, SAM residues were used to determine the presence of the C_3A polymorph. Tricalcium aluminate can be present in cement either in cubic or orthorhombic form or as a combination of both. Although the XRD patterns of cubic and orthorhombic C_3A are very similar, orthorhombic C_3A does not have a peak at 2θ of 21.8˚. In addition, cubic C_3A has only one peak at 2θ of 33.3˚, while orthorhombic C_3A has two peaks in this angular range, one at 2θ of 32.9˚ and another at 2θ of 33.2˚ [138], [144].

Potassium hydroxide/sucrose extraction dissolves aluminates and ferrites, thus leaving a residue of C_3S, C_2S, alkali sulfates and MgO [138]. Potassium hydroxide/sucrose extraction residues were used to identify the alite polymorph present in cements. Although alite has a number of polymorphs, triclinic, monoclinic, and rhombohedral [145], only monoclinic polymorphs are generally present in cements. Monoclinic alite has three polymorphs: M1, M2, and M3 [146], although it is generally accepted that only M1 and M3 polymorphs exist in commercial clinkers [144], [147]. X-ray diffraction scans were collected for the 5 angular windows recommended by Courtial et al. for alite polymorph identification [147].

Cement phase quantification was performed using the Rietveld refinement. Rietveld refinement is a well-established technique used for quantitative x-ray diffraction (QXRD) analysis.

It is based on fitting the whole pattern, which allows overlapped peaks to be resolved. A simulated pattern based on theoretical crystal structures input by the user is iteratively compared to the collected x-ray pattern and refined based on a number of parameters, which describe the crystal structure of the phases and their amount in the sample, and equipment characteristics. Two scans were collected and two Rietveld refinements were performed for the cement, and their average is reported here.

In addition to Rietveld refinement, the amount of alite was verified using the internal standard calibration curve. Internal standard analysis is based on the principle that the peak intensity of a phase, determined either as peak height or peak area, is directly proportional to the amount of this phase in the sample, as described by the following equation:

$$\frac{I_{ij}}{I_{ks}} = K\frac{x_j}{x_s} \qquad \text{Equation 2-1}$$

Where I_{ij} is the intensity of peak i of phase j, I_{ks} is the intensity of peak k of the internal standard, x_j and x_s are the weight fraction of the phase j and the internal standard respectively, and K is a constant [148]. The advantage of the single-peak internal standard analysis is that quantification of the phase of interest is not affected by any other phases present in the sample, meaning that unlike Rietveld analysis it is not affected by unidentified or amorphous content.

The alite calibration curve was prepared by mixing samples of known C_3S content with 10% of internal standard by total weight of sample following the general procedures described by Klug and Alexander [148]. TiO_2 was selected as an internal standard for two reasons: it has a mass absorption coefficient (MAC) close to that of cements and most of the TiO_2 diffraction peaks do not interfere with the major peaks of portland cement.

Standard reference clinkers SRM 2686a, SRM 2687, and SRM 2688 were obtained from NIST and were used as a source of C_3S for the standardization mixtures. These clinkers have certified phase compositions and are representative of the modern-day clinkers produced by the cement industry. The clinkers were first ground with a mortar and pestle to reduce the particle size to below 45 microns and then ground in the McCrone micronizing mill for 10 minutes with ethanol prior to collecting x-ray diffraction scans.

After observing 5 angular alite windows for these clinkers as described previously, it was determined that SRM 2688 contained the M1 alite polymorph and was suitable for the preparation

of the M1-C_3S calibration curve. SRM 2688 contains 64.95% of alite. Ground SRM 2688 was mixed with 10% TiO_2 to produce the 65% point on the calibration curve. In order to produce the 40 and 50% points for the calibration curve, SRM 2688 was diluted with C_3A in order to achieve the required alite content. Alite content of the sample was calculated for the SRM 2688/C_3A mixture excluding the TiO_2 addition.

The samples were mixed in the McCrone micronizing mill for 10 minutes with 5 mL of ethanol per every gram of sample as recommended by ASTM C1365. This was done to achieve homogeneous dispersion of the internal standard throughout the sample. After mixing, the sample was dried in an oven at 40 °C in order to evaporate the ethanol. Samples were loaded into the sample holder using the back-loading technique and scanned using the settings described previously. Three samples were analyzed for each point on the calibration curve.

The diffraction pattern collected for each sample was analyzed with HighScore Plus software in order to determine the areas of 51.8° 2θ peak of alite and the 54.3° 2θ peak of TiO_2. The area ratios of the alite peak to the TiO_2 peak were plotted against the alite content of the sample fraction excluding TiO_2 as shown in Figure 2-1. Subsequently, ground cements were mixed with 10 % TiO_2 to determine the area ratios in the as-received cements.

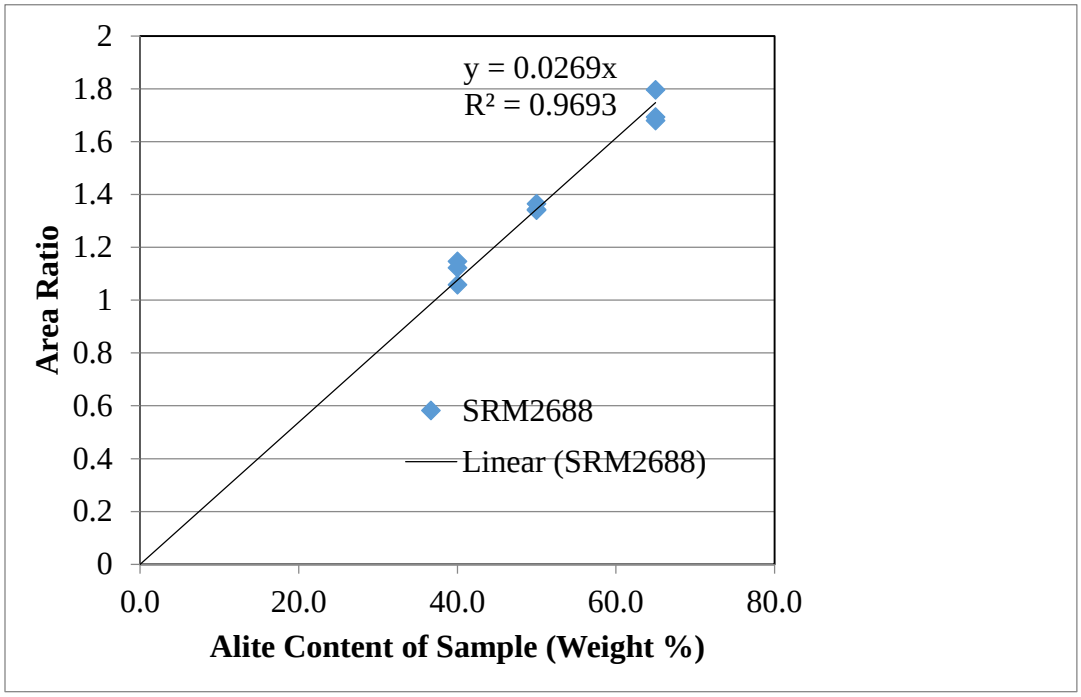

Figure 2-1: Internal Standard Calibration Curve for M1 Alite Polymorph

Mineral admixture phase identification was performed using the HighScore software. Since all the mineral admixtures were expected to contain large amounts of amorphous material, mineral admixtures were mixed with an internal standard as described previously to allow for indirect quantification of amorphous content using Rietveld refinement together with the quantification of the mineral phases. Rietveld refinement performed on samples containing an amorphous fraction is expected to overestimate the percentage of internal standard in the sample. However, when the amount of internal standard is known, the weight fractions of the crystalline phases can be calculated using the equation below:

$$\boldsymbol{Corr(W_\alpha) = W_\alpha \frac{STD_{known}}{STD_{measured}}} \qquad \text{Equation 2-2}$$

Where $Corr(W_\alpha)$ is the corrected weight fraction of the crystalline phase, W_α is the weight fraction of the crystalline phase α, STD_{known} is the weighed concentration of internal standard present in the sample, and $STD_{measured}$ is the concentration of internal standard determined by Rietveld refinement [149]. The weight fraction of amorphous material can then be determined by subtracting the sum of the corrected weight fractions from unity. Results of quantitative x-ray diffraction (QXRD) analysis for as-received cement and mineral admixtures are depicted in Table 2-5 and Table 2-6. As discussed previously, mineralogical phase composition of the cement was quantified with Rietveld analysis. The alite amount was also calculated based on the internal standard calibration curve. Based on observing the five angular windows recommended by Courtial et al. [147], it was determined that alite was present in the as-received cements as the M1 polymorph. Table 2-5 shows that the results obtained for alite, based on Rietveld refinement and the calibration curve methods, are in general agreement. The disagreement between the phase content determined through XRD and potential phase content determined through ASTM C150-12 was expected as indicated in the published literature [136], [138], [144].

For mineral admixtures, the results indicate that they are predominately amorphous in nature. Class F fly ash appears to have the lowest amorphous content at 72%, while metakaolin, slag and silica fume have significantly higher contents in the 96-98% range.

Table 2-5: Cement Phase Content Using QXRD

Cement Phase	**Source**	**SW**
C_3S (%)	Rietveld	46.9
C_3S (%)	Calibration curve	49
C_2S (%)	Rietveld	25.2
C_3A (%)	Rietveld	9.6
C_4AF (%)	Rietveld	8.0
Gypsum	Rietveld	2.8
Hemihydrate	Rietveld	1.8
Anhydrite	Rietveld	0.5
Calcite	Rietveld	2.0
Portlandite	Rietveld	2.5
Quartz	Rietveld	0.8

Table 2-6: Mineral Admixtures Phase Content Using QXRD

Mineral Admixture	**Mineral Phase**	**Amount (wt %)**
FA	Mullite	16.1
	Hematite	1.6
	Magnetite	1.1
	Quartz	9.0
	Amorphous	72.2
MK	Mullite	1.0
	Illite	0.7
	Quartz	0.3
	Amorphous	98.0
SL	Melilite	1.3
	Merwinite	0.1
	Quartz	1.4
	CaO	0.1
	Calcite	0.4
	Amorphous	96.7
SF	Silicon Carbide	2.0
	Crystobalite	0.3
	Quartz	1.9
	Amorphous	95.8

Particle Size Analysis and Fineness for Portland Cement and Mineral Admixtures

The last step in manufacturing portland cement involves grinding of portland cement clinker with calcium sulfate or one of its hydrates. The product of this grinding stage is known as portland cement. The fineness to which cement is ground has a significant effect on the behavior of cement, especially during the early stages of hydration [16]. For cements, there are two basic measures of fineness; namely, Blaine (air permeability) and Turbidimetry. Blaine fineness was used in this study. It is an indirect measure of the total surface area of each cement sample and can be determined by the air permeability apparatus according to ASTM C204-11 "Standard Test Method for Fineness of Hydraulic Cement by Air Permeability Apparatus" [150].

Prior to conducting Blaine fineness measurements on the as-received cement, the air-permeability apparatus was calibrated in accordance with ASTM C204 section 4. A sample bed of standard cement SRM 114q obtained from the National Institute of Standards and Technology (NIST) was used. The calibration was run at 21.8°C (71°F) and a relative humidity of 59%. Using the same settings, Blaine fineness was determined for the as-received cements. While the method is widely used in the cement industry for quality control, it has some drawbacks. For example, a single averaged value may be given to two cements with different proportion of fines; that is, two different cements having the same surface area will give the same Blaine value even though they have very different particle size distributions (PSD) [19], [151]. In contrast, particle size distribution measurements provide more accurate insight on the quality and grading of the cement [151].

PSD measurement describes the frequency and size of particles contained in a sample [152]. Typical particle sizes in portland cement vary from <1 μm to 100 μm in diameter [19]. Particle size influences the hydration rate and strength; it is also a valuable indicator for predicting cement quality and performance [153], [154]. The characterization of the particles of the as-received cements was conducted using the principle of laser diffraction. That is, a particle will scatter light at an angle determined by its particle size. The angle of diffraction increases as the particle size decreases; this method is particularly effective in the particle size range of 0.1 to 3,000 μm [152]. An LA-950 laser scattering particle size analyzer manufactured by HORIBA Instruments was used to analyze the particle size distribution of the cements. The instrument has the capacity to measure wet and dry samples in the range of 10 nm to 3 mm.

Sample preparation was conducted per manufacturer procedures using the dry method. An adequate amount of dry cement was homogenized by mechanical agitation through the flow cell of the instrument at the start of measurement [153]. Figure 2-2 and Figure 2-3 depict examples of data collected for the as-received cement. It is worth noting that the results presented in Figure 2-2 and Figure 2-3 are for 3 runs conducted on the same cement. The obvious overlap is indicative of the accuracy and precision of the testing technique.

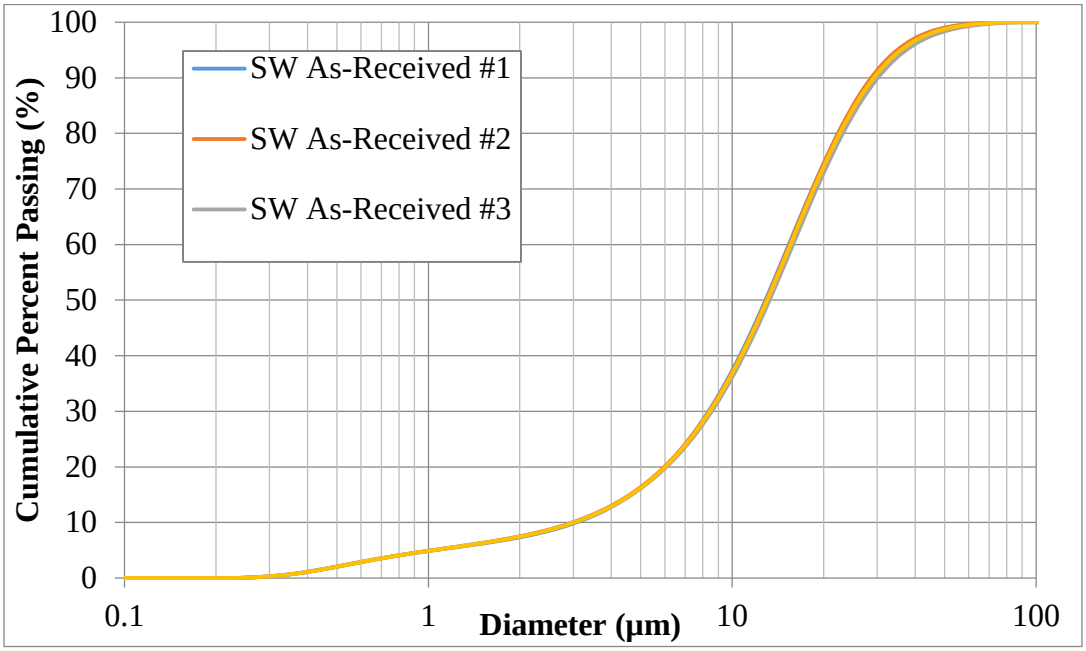

Figure 2-2: Cumulative Particle Size Distribution for SW Cement

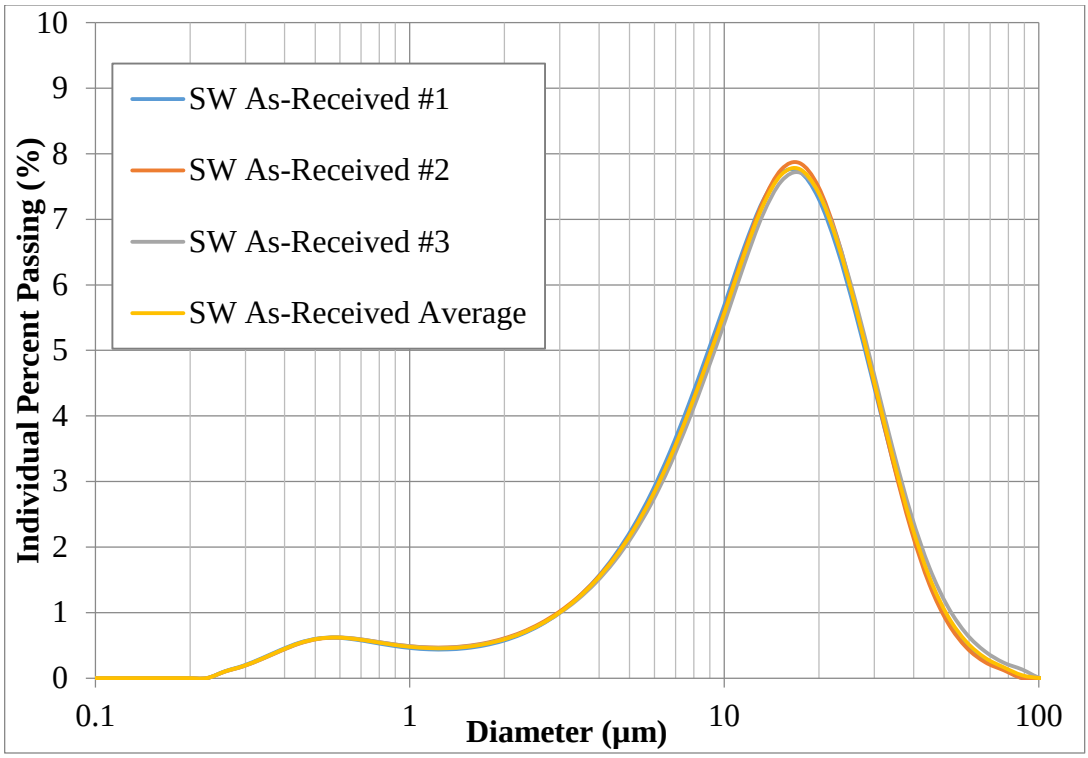

Figure 2-3: Differential Particle Size Distribution for SW Cement

The expressions of PSD results are based on a volume distribution using measures of D_{10}, D_{50}, and D_{90} (under size %) which identify the 10th, 50th, and 90th percentiles below a given particle diameter [155]. D_{50} is also defined as the median size; that is, the size that splits the size distribution with half above and half below the specified diameter. Similar to the concept of average, the mean size or mean particle size (MPS) expresses the volume mean as an average of D_{10}, D_{50}, and D_{90} [154]. In other words, MPS provides an approximation of the central point of the particle size distribution of an entire sample on volume basis [153]–[155]. Triplicate tests were conducted on the as-received cement and all the mineral admixtures and averages of the 3 tests were reported. Fineness of mineral admixtures was determined by nitrogen adsorption using an Autosorb-1 analyzer by Quantachrome Instruments. The samples degassed under vacuum at 80°C immediately prior to analysis in order to remove any moisture or contaminants from the sample surface. The Brunauer-Emmett-Teller (BET) method was used for surface area calculation. Multipoint BET was selected over the single point BET for greater accuracy [156].

Two methods were used in characterizing cement particle size; namely, cement Blaine fineness and particle size distribution. In the first, the total specific surface area of particles is

quantified, while in the second the mass fraction or volume fraction is quantified for specific particle diameters. For mineral admixtures, particle size distribution and multipoint BET specific surface area were determined. The results of the particle size analyses for all the materials used in this study are presented in Table 2-7, Figure 2-4, and Figure 2-5. As expected, metakaolin was finer than cement, and fly ash and slag had fineness values that were similar to that of cement. MPS of slag, fly ash, and cement were also comparable. However, the particle size distribution for silica fume as well as its MPS were significantly coarser than that of the other materials. This was unexpected, since over 95% of the silica fume particles are reported to be finer than 1 μm [105]. Since the silica fume used in this study is densified, it appears that the dry process of particle size analysis was unable to provide sufficient dispersion of the silica fume particles, and a wet method with a dispersing agent should be used to obtain a true particle size distribution. The fact that the true fineness of silica fume is significantly higher than what was indicated by the particle size analysis was supported by the BET results. Since the BET method is based on the physical adsorption of nitrogen gas molecules on the sample surface, it is not affected by agglomeration and is able to measure the true fineness [157].

Table 2-7: Particle Size Analysis of As-Received Cement and Mineral Admixtures

Physical Properties	**SW**	**FA**	**MK**	**SL**	**SF**
D_{10} (μm)	3.0105	5.1220	1.7189	3.3053	14.6222
D_{50} (μm)	13.0177	9.943	5.4822	10.8598	50.5237
D_{90} (μm)	29.3028	22.0212	11.6546	23.4001	190.2104
Median size (μm)	13.01767	9.94296	5.48219	10.85981	50.52368
Mean size (MPS) (μm)	15.08836	14.06485	6.24684	12.55918	79.37632
ASTM C204-Blaine Fineness (m^2/kg)	442	N/A	N/A	N/A	N/A
Multipoint BET Fineness (m^2/kg)	2,140	2,270	14,970	3,700	21,410

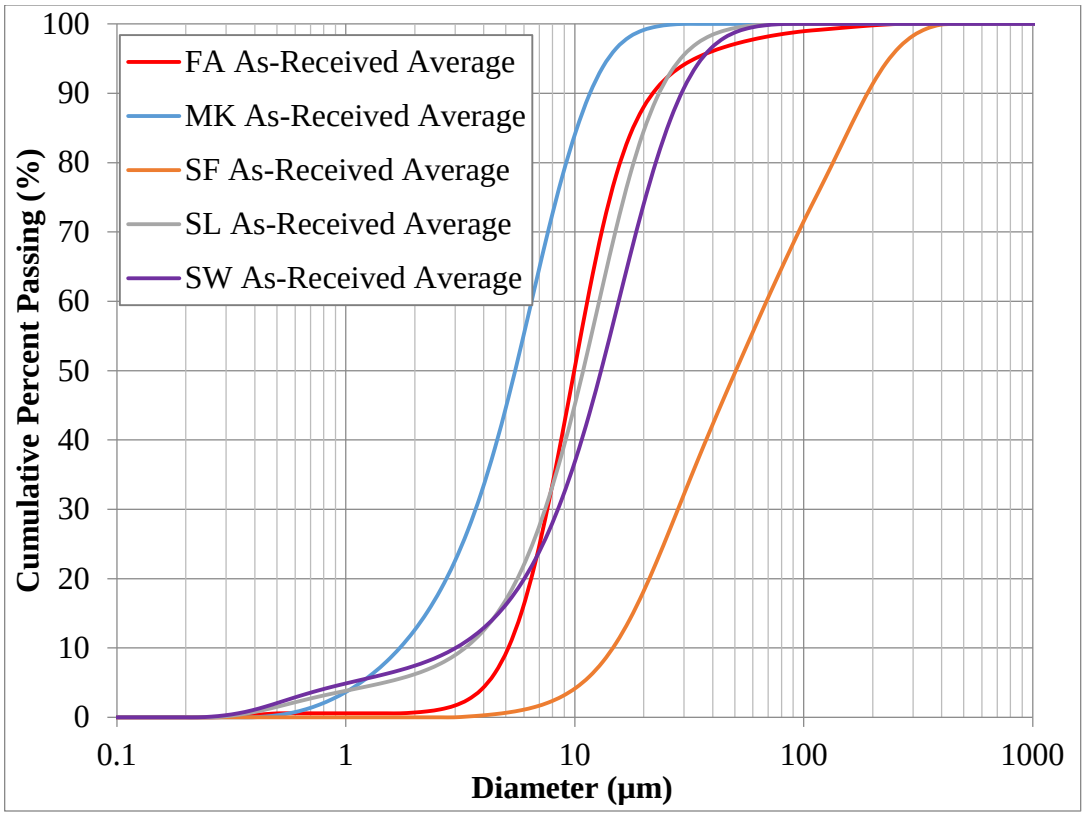

Figure 2-4: Cumulative Particle Size Distribution for SW Cement and Admixtures

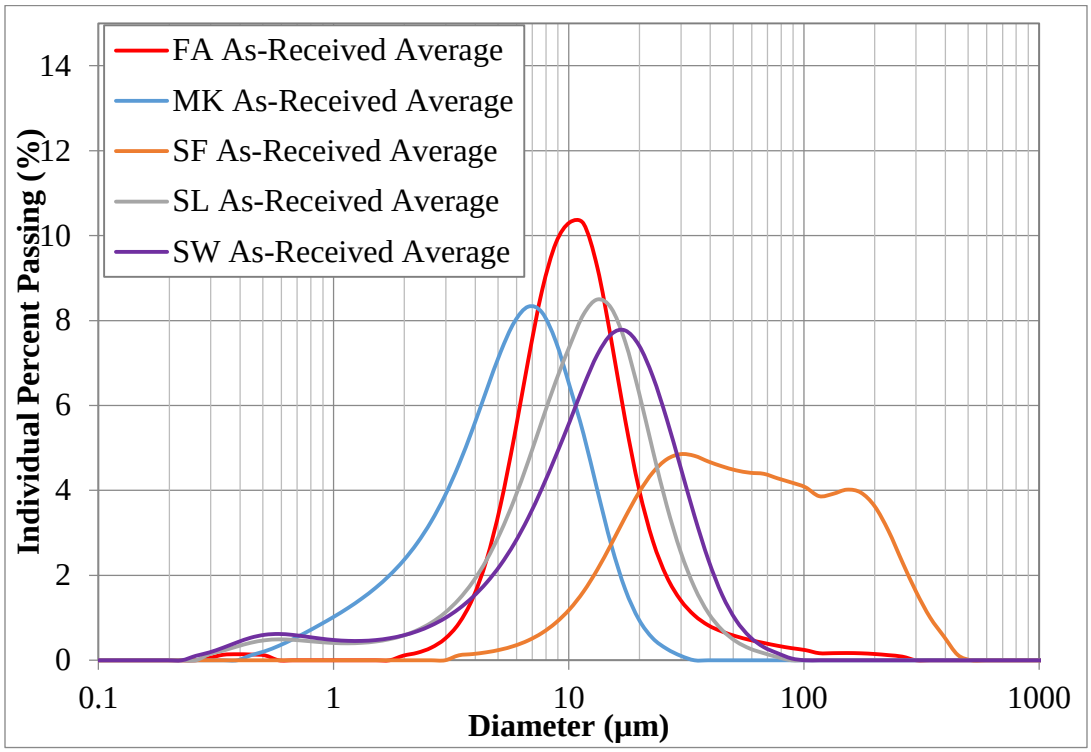

Figure 2-5: Differential Particle Size Distribution for SW Cement and Admixtures

Conclusions

Chemical and mineralogical analysis of the as-received cement indicates that it can be classified as Type I/II according to ASTM C150-12**.** The fly ash used satisfied ASTM C618 requirements for Class F ash while the metakaolin met the requirements for a Class N pozzolan. Silica fume analysis indicated that it is in compliance with ASTM C1240 while slag satisfied ASTM C989. The alumina content for slag was reported at 14.25%.

[redacted] Heat of Hydration (HOH) Measurements for Cementitious Materials (CM)

[redacted] Introduction

Cement hydration is an exothermic reaction. The total amount of heat evolved can be related to the degree of hydration and correlated to mechanical properties. Isothermal calorimetry, if internal mixing protocol is followed, is able to capture the heat of reaction from the moment of contact between water and cement. As most chemical and mineral admixtures are expected to affect cement hydration, internal mixing was employed, in order to capture the reaction process from the beginning.

Five stages of cement hydration, comprised of the initial reaction (dissolution), induction (dormant), acceleration, deceleration, and diffusion (steady state) stages, can be identified from the plot of heat flow versus time, as illustrated in Figure 3-1. The first peak (P1) occurring during the first 15 minutes corresponds to the dissolution of cement phases, which is accompanied by a large release of heat. Beginning of the induction period is indicated by a sharp drop in thermal power, which typically lasts for approximately 2 hours, after which heat flow increases signaling the beginning of the acceleration period. The peak that follows (P2) is referred to as the main hydration peak and, for properly-sulfated cements, is associated with C_3S hydration. This peak is indicative of early strength gain and the peak maximum occurs after final set. After the maximum, hydration enters the deceleration stage. Sulfate depletion point is generally indicated by a shoulder (P3) on the right-hand side of the main peak, again, for a properly-sulfated cement. The heat flow decreases until reaching a constant value as the hydration process enters steady state. A fourth peak (P4) can sometimes be observed as well, although its nature has not been established conclusively. The presence of this peak has been previously attributed to C_4AF hydration [82], [144] although others suggested that it may be due to the second growth of ettringite [158], [8] or conversion of ettringite to monosulfoaluminate [144], [159].

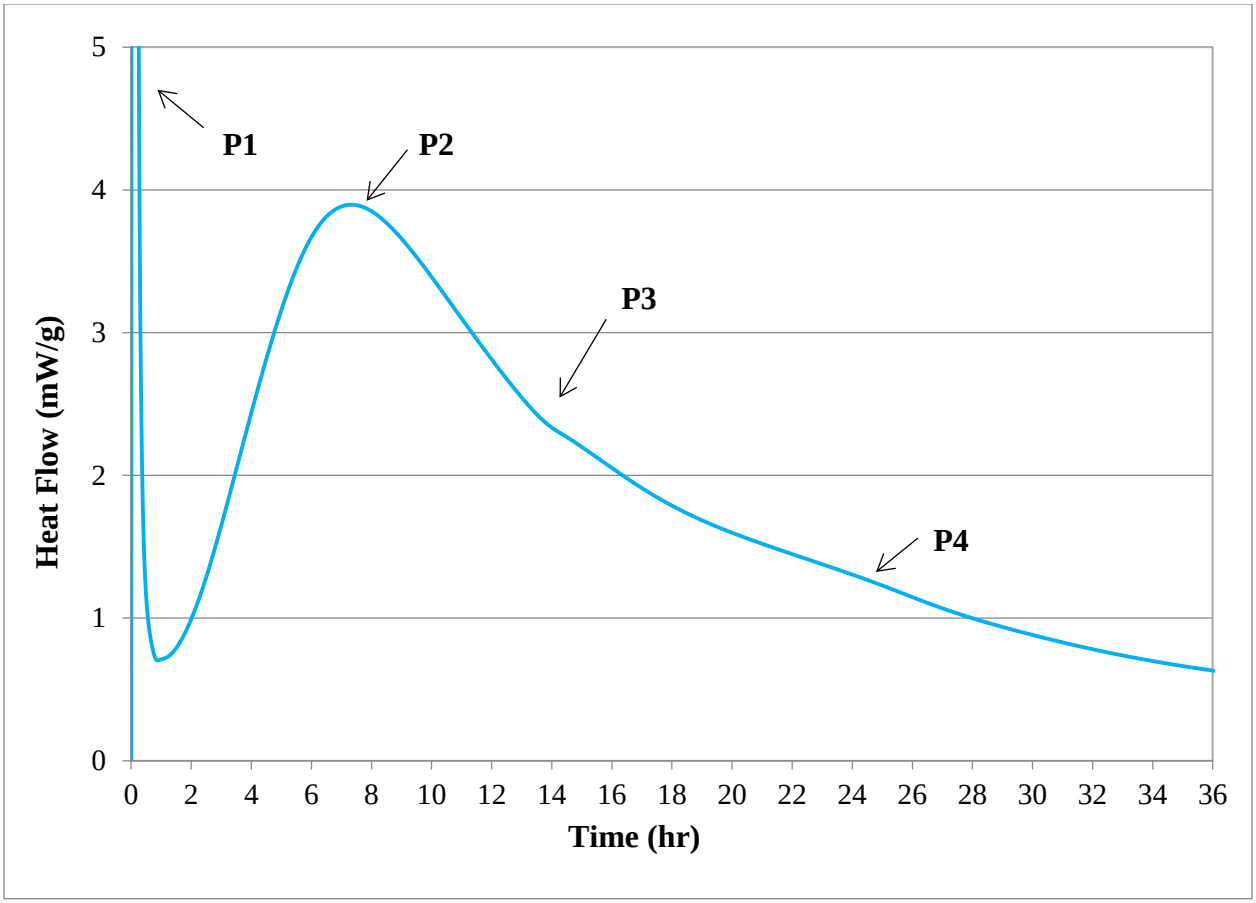

Figure 3-1: Typical Heat Flow Plot for the OPC Cement

As several researchers have pointed out, the study of the effect of mineral admixtures on cement presents several challenges: separating the degree of hydration of cement from the degree of hydration of pozzolanic/cementitious material, distinguishing between cement hydration, pozzolanic/cementitious material hydration, interaction of the two hydration processes, and the physical effects of mineral additions [62], [160]. These challenges are magnified with addition of chemical admixtures as well as using combinations of several mineral admixtures. Binary cement-admixture combinations were first assessed in this study in order to evaluate the effect of each admixture separately on cement hydration.

Additions of mineral admixtures affect cement both physically and, in the case of reactive materials, chemically. The main physical effects identified in the literature are dilution and heterogeneous nucleation [161]. The term, “filler effect” has also been used by different authors to refer to either or both of these effects. Addition of nonreactive or low-reactivity admixtures

effectively increases the w/c of the mixture. This is referred to as a dilution effect. Bentz [162] illustrated the impact of dilution by comparing the heat flow of two OPC pastes with no mineral additions prepared with the same cement at w/c ratios of 0.3 and 0.6. He observed a 1-hour delay in the occurrence of the main hydration peak maximum as well as a decrease in peak intensity with the increase in w/c ratio. The rate of heat flow also decreased. The dilution effect has commonly been invoked by researchers to explain the changes in cement hydration with addition of SCMs, such as Class F fly ash [62], [162]–[164].

The term heterogeneous nucleation refers to the addition of nucleation sites through the addition of fine mineral powders. Lawrence et al. [161] state that addition of nucleation sites leads to a "chemical activation of the hydration process." Lothenbach et al. [62] state that addition of nucleation sites has a much greater effect on C_3A hydration than on C_3S hydration. The authors cite a study by Le Saout and Scrivener that showed an increase in the intensity of the aluminate peak with addition of nonreactive fillers. Peak intensity increased with the increase in filler fineness. There was a slight increase in the intensity of the C_3S peak as well, but the peak position did not change. A material's ability to provide nucleation sites for precipitation of hydration products is determined by its specific surface area (SSA). Coarse mineral admixtures (with SSA below 50-100 m^2/kg) cannot provide acceleration due to heterogeneous nucleation [86]. As most mineral admixtures have SSAs well above this range, heterogeneous nucleation should definitely be considered in analyzing the effect of mineral admixture additions on cement hydration.

While for mineral admixtures both chemical composition and physical properties are of significance, only chemical composition is of interest in the case of chemical admixtures. However, commercial chemical admixtures are proprietary formulations, and manufacturers rarely disclose their composition. A number of published studies identify admixtures used only by their type, which explains often contradictory results. While admixture type provides information about its intended use, of greater importance in understanding its effect on cement hydration are the chemical compounds included in the admixture.

Methodology

Four different chemical admixtures were selected for this project; namely, an air-entrainer (AE), a water-reducer and retarder (WR), and two high-range water-reducers (SP). Additionally, four SCMs were studied here: Class F fly ash, slag, silica fume and metakaolin, The selected

mineral and chemical admixtures were identified based on mutual agreement between the Project Manager (PM) and the Principal Investigator (PI). The selected materials represent the most commonly used admixtures on current FDOT structural concrete projects. The selected chemical admixtures are listed in Table 3-1.

Table 3-1: Chemical Admixtures

Admixture Class	**ASTM Type**	**Active Component**
AE	ASTM C260	Sodium dodecylbenzenesulfonate
WR	ASTM C494 Type D	Sulfite liquors, molasses, triethanolamine
SP1	ASTM C494 Type F	Polyacrylate
SP2	ASTM C494 Type F	Polyacrylate

Heat of hydration measurements of the as-received cement as well as the mixtures of cement with mineral and chemical admixtures were performed in accordance with ASTM C1702-09a Method A, internal mixing [165]. Heat flow measurements were performed using a TAM Air isothermal calorimeter produced by TA instruments. All measurements were performed at the isothermal temperature of 23°C. The reference cells contained 12.33 g of Ottawa sand during all the measurements. Two runs were performed for each mixture, and average values are reported here.

Paste samples for as-received cement were prepared with 3.3750 g of cement and 1.6370 g of water at a water-to-cement (w/c) ratio of 0.485. Mineral and chemical admixture addition rates are listed in Table 3-2. For cement-mineral admixture combinations, a portion of the cement mass was substituted by an equal mass of mineral admixture. A constant water-to-binder (w/b) ratio of 0.485 was maintained for all the mixtures. For chemical admixtures, solutions of required concentrations were prepared volumetrically in order to minimize errors in measuring small amounts of admixture. Chemical admixtures were added to cement together with the mixing water. Very limited data is available regarding the composition of chemical admixtures. Material safety data sheets (MSDS) were used to ascertain the active compounds of each admixture.

Table 3-2: Admixtures Addition Rates

Mineral Admixture	Cement Replacement (w/o)	Chemical Admixture	Addition Rate (ml/100 kg cement)
21FA	21	AE	46
10MK	10	WR	300
8SF	8	SP2	397
52SL	52		

After measuring out the required amount of dry cementitious materials and water or chemical admixture solutions, the ampules were placed in the calorimeter, and the system was allowed to reach thermal equilibrium. Then, water or solution was injected into the vial, and the paste was mixed constantly for 60 seconds. Heat flow measurements were collected for 7 days.

Additionally, there were concerns that manual mixing was not sufficient to disperse SF and MK appropriately; therefore, heat of hydration measurements were also performed following Method B, external mixing, of ASTM C1702 [165]. Heat flow measurements with external mixing protocol were performed using an iCal-8000 calorimeter produced by Calmetrix. As with internal mixing, all the measurements were performed at the isothermal temperature of 23°C, and heat evolution was recorded for 72 hours. The water-to-binder ratio was maintained constant at 0.485, except for 8SF, 52SL, 21FA and 10MK mixtures, for which it was 0.42.

The mixing of the cement paste followed the mixing procedure described in [166] with the IKA WERKE mixer using the kitchen blade accessory for a total of 7 min. WR was added to the mixing water. After combining water and cementitious materials, paste was mixed for 1 minute prior to addition of AE, after which it was mixed for an additional 2 minutes (elapsed time: 3 min). The mixture was then rested for 2 minutes (Elapsed time: 5 min). After the rest period, superplasticizer was added to the mixture, and the sample was mixed for an additional 2 minutes (elapsed time: 7 min) at 1200 rpm rather than the stated 2000 rpm as reported by Muller et al. [166].

Results and Discussion

Internal Mixing

Mineral Admixtures

Figure 3-2 and Figure 3-3 present the heat flow and total heat plots for all the mineral admixture and as-received cement samples normalized by the total mass of cementitious materials (CM). Cement replacement with mineral admixtures decreased the magnitude of the main hydration peak. The smallest decrease was observed for SF and MK, which were added at 8 and 10% cement replacement levels respectively, while the largest decrease was achieved with 52% cement replacement by slag. Additionally, a slight retardation of the main hydration peak was observed with addition of FA or SL, which indicates a possible delay in setting time with 21% cement replacement by FA or 52% cement replacement by SL.

Isothermal calorimetry measurements demonstrated that the cement used in this study was properly sulfated, as the sulfate depletion point occurred after the main hydration peak. Addition of SF and FA did not affect the time of occurrence of the sulfate depletion point. However, addition of Al_2O_3 containing mineral admixtures, MK and SL, shifted the occurrence of this peak to an earlier time and increased the magnitude of the aluminate peak relative to the main hydration peak. This indicates that these mixtures may become undersulfated at higher temperatures, when the solubility of gypsum decreases [4], [15] and the solubility of clinker phases increases [16], or when in combination with other mineral or chemical admixtures that also accelerate sulfate depletion. Lack of sulfate ions in solution under these circumstances is likely to lead to reduced control of the aluminate reaction and increase in concrete temperature.

The slope of the heat flow curve during the acceleration period, which is indicative of the rate of hydration reactions during this stage, was slightly reduced by incorporation of MK and SF. This reduction was greater in the case of FA, and the largest reduction in slope was observed for the 52SL mixture.

As for the rate of heat evolution after the first 24 hours, it was the highest for SL and MK blends, followed by the control paste with no chemical admixtures (CN), and then by SF and FA mixtures. The high rate of heat evolution of the MK and SL mixtures compared to the control indicate that this test should be continued for these mixtures beyond 7 days. However, the signal-

to-noise ratio of the instrument may not be adequate to capture statistically meaningful data beyond 7 days.

The total heat evolved at 7 days was identical for the control sample and the 10MK paste. Cement replacement by 8% SF reduced the total heat by approximately 30 J/g of cementitious materials, by 60 J/g in the case of 21% FA, and by 70J/g in the case of 52% slag. Total heat can be related to the temperature rise in concrete. Under isothermal conditions of 23˚C the control paste with no mineral admixtures is expected to have the highest temperature rise, while 52% slag blend is expected to have the lowest temperature rise. However, typical curing conditions are not isothermal due to self-insulation of the concrete, and for very large structures (mass concrete) the conditions approach adiabatic, for which the trend observed above may not hold true. Increasing temperature is likely to accelerate the reaction of aluminates in the slag and metakaolin mixtures, as discussed previously, leading to a further increase in temperature. Additionally, the higher rate of total heat evolution of these mixtures indicates that they may continue to generate heat for a longer period of time.

Based on the total heat values up to 7 days, compressive strength is expected to be lowest for the 52SL mixture and highest for the control mixture. At 7 days, the CN (control) and 10MK mixtures are expected to have about the same compressive strength (same total heat). While the 1-day 10MK and 8SF mixtures should have about the same strength, the 10MK strength gain is expected to be higher after 24 hours and its compressive strength should exceed that of the 8SF mix at 3 and 7 days. As for 21FA, its strength should be between that of 52SL and CN at 1 day, and only slightly higher than that of the 52SL by 7 days.

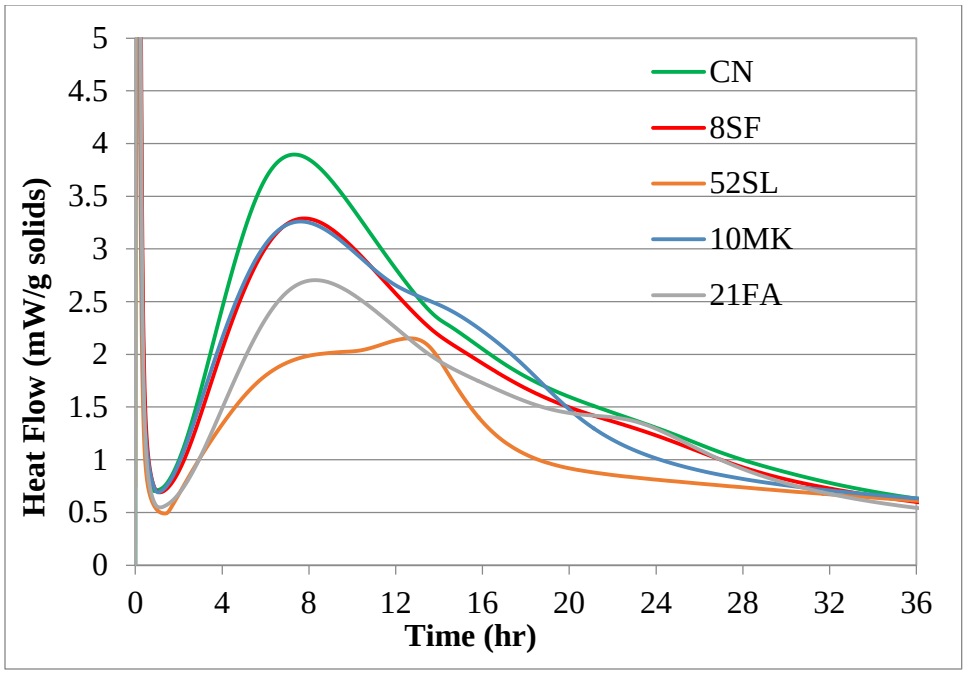

Figure 3-2: Heat Flow for Mixtures Prepared with Mineral Admixtures Normalized by Mass of Cementitious Materials

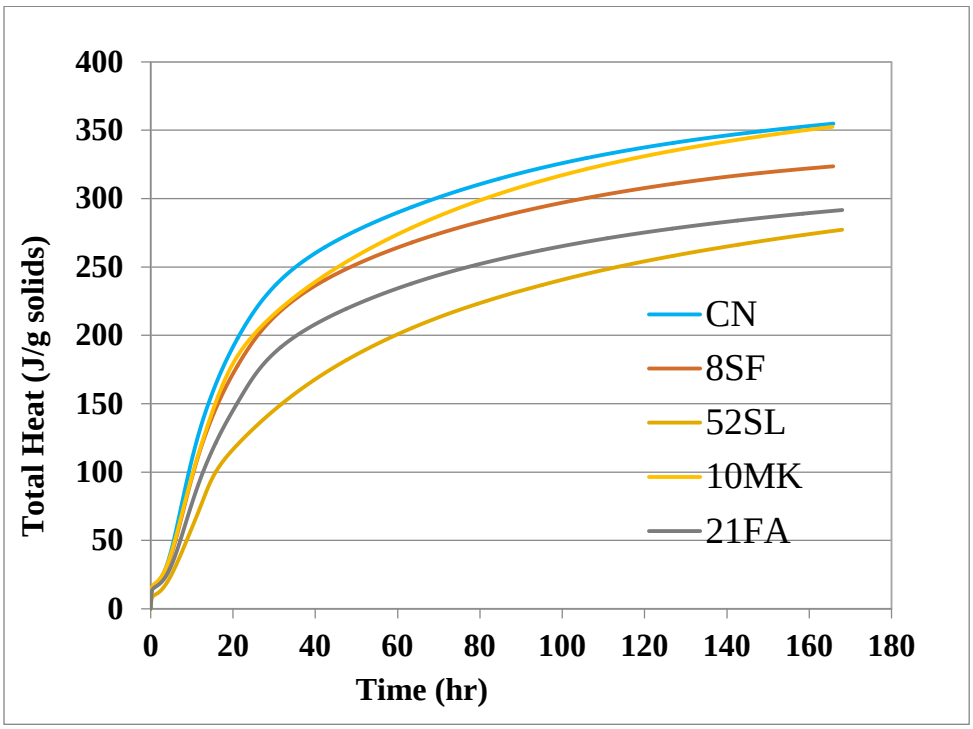

Figure 3-3: Total Heat for Mixtures Prepared with Mineral Admixtures Normalized by Mass of Cementitious Materials

While Figure 3-2 and Figure 3-3 are useful to predict compressive strength of the mixtures, they do not allow direct comparison between admixtures since each was used at a different replacement level. It has been recognized that normalizing heat flow and total heat by the mass of cement alone is more appropriate for evaluating the effect of mineral admixtures on cement hydration kinetics [162]. This normalization procedure has been applied to the data presented in Figure 3-4 to Figure 3-9 as well as Table 3-3.

As can be seen in Figure 3-4, addition of Class F fly ash did not have a significant effect on the length of the induction period, as expected [53]. The rate of reaction in the acceleration period, however, was decreased as indicated by a lower slope of the 21FA paste. It has been demonstrated that the effect of fly ash on the length of the induction period depends on the cement replacement level. High-volume fly ash mixes (Class F) experience significant retardation [162], [167], while at lower replacement levels (20%) there is no significant increase of the induction period [53].

Addition of fly ash also resulted in a slight retardation of the main hydration peak: in the CN paste, the maximum occurred at 7 hours, while with addition of fly ash it shifted to 8 hours. This retardation can be attributed to the dilution effect [62], [162]–[164], since Class F fly ash has very low reactivity during early ages. In this study, the addition of 21% fly ash changed the effective w/c ratio from 0.485 (plain OPC paste) to 0.614. The sulfate depletion point is not affected by the fly ash addition as it occurs at the same time in both OPC paste and the paste prepared with fly ash. Again, this was expected as Class F fly ash does not affect sulfate consumption rate [53].

It appears that addition of fly ash itself, excluding the dilution effect, did not impact the hydration kinetics of portland cement. This is in line with the conclusions made by others where it was indicated that Class F fly ash does not have a significant effect on the hydration of cement [164], [168]. However, a definite statement to that effect would require calorimetry measurement of a cement-fly ash sample for which the effective w/c ratio is corrected to 0.485 to allow for proper comparison with OPC paste.

A fourth peak occurs around 24 hours. This peak has been observed by Quennoz and Scrivener [158] in C_3S-C_3A-gypsum systems, although they were not able to explain it by XRD or microscopy analysis. They observed that the intensity and timing of this peak was dependent

on the water/solid (w/s) ratio. As the w/s increased, the intensity of the peak decreased and it occurred at later time. This is the opposite of what was observed in this study. Although the effective w/c ratio of the fly ash sample is higher, the fourth peak in this sample is more pronounced. Since the cement content in the OPC/FA sample was reduced by fly ash addition, it does appear likely that the increased intensity of this peak is due to C_4AF hydration as suggested by others [82], [144]. The fly ash used in this study had a moderate amorphous content (72%). Frias et al. [81] showed that although its reactivity is very low, fly ash does show some pozzolanic activity at 1 day. XRD and SEM analysis would be required to confirm this hypothesis.

Based on the heat flow plot presented in Figure 3-4, a delay in the final setting time of the fly ash sample is expected. When total heat normalized by the mass of cementitious material (CM) is considered (Figure 3-3), compressive strength of the fly ash samples is expected to be lower than that of CN at all ages up to 7 days as indicated by the lower total heat evolution in the FA mixture.

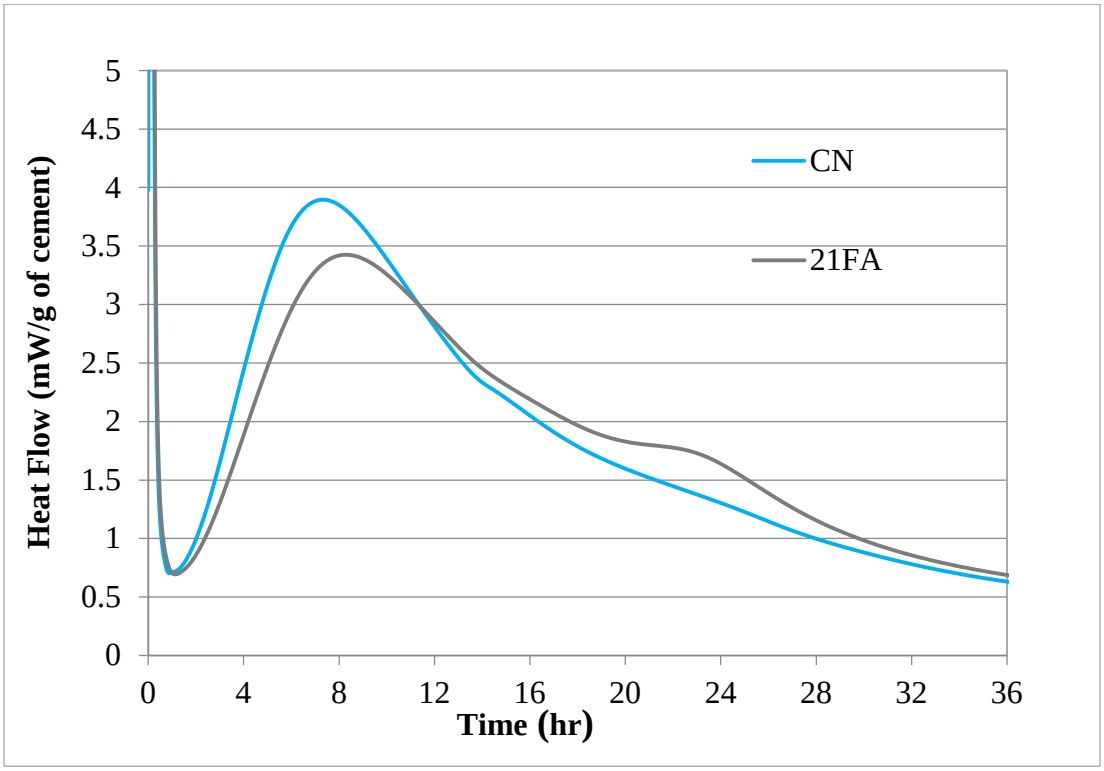

Figure 3-4: Measured Heat Flow of the OPC/FA Sample Compared to the Control OPC Sample Normalized by the Mass of Cement

There is no clear agreement in the literature regarding the kinetics of silica fume (SF) hydration. Lilkov et al. [88] demonstrated that SF begins to hydrate during the first hour after contact with water. Frias et al. [81] reported that the pozzolanic activity of SF was double that of metakaolin (MK) at 2 hours. Acceleration of the alite hydration by SF has been reported earlier by Wu and Young [89]. Wu and Young observed that the presence of SF increases the duration of stage 1 (initial hydrolysis) of alite and decreases the induction period. Cheng-Yi and Feldman [90] concluded that in addition to C_3S, C_3A hydration is also accelerated by the presence of SF. Langan et al. [91] confirmed the accelerating effect of SF on cement hydration, but only at high w/cm ratios. They reported a retarding effect at low w/cm ratios. This effect was attributed to the adsorption of water by silica fume, which at low w/cm ratios would reduce the water available for the reaction with cement particles [91]. On the contrary, Kadri and Duval [92] observed acceleration of the hydration process with addition of silica fume at low w/cm ratios. With respect to the total heat of hydration (HOH), they observed an increase in HOH with 10% cement replacement by SF. However, at 30% replacement level, HOH was decreased. Zelić et al. [93] concluded that the acceleration of early-age cement hydration by SF is strictly due to the filler effect, and contributions from the pozzolanic reaction could only occur after 3 days. Lothenbach et al. [62] state that there is "almost no reaction of silica fume" at 1 day, and the improvement of compressive strength is merely due to the filler effect.

Neither an accelerating nor a retarding effect was observed with silica fume addition in this study, as illustrated in Figure 3-5. Apart from a slight decrease in the intensity of the main hydration peak, both the heat flow and the total heat plot of the silica fume sample followed that of the OPC control paste. It has been reported that, due to its fine particle size, silica fume requires addition of superplasticizer, even at high w/c ratios for proper dispersion [102]. As discussed in Chapter 2 large agglomerations were observed in the silica fume sample during particle size determination, ranging from 14 to 190 μm, with a mean size of approximately 80 μm. Manual mixing inside the calorimeter, even at w/c ratio of 0.485, was not sufficient to disperse these agglomerates, which most likely were too large to accelerate hydration through heterogeneous nucleation. It appears that the dilution effect, which would have resulted in retardation, was offset by the pozzolanic reaction of silica fume. The degree of silica fume reaction was most likely reduced by its agglomeration. Gapinski and Scanlon [167] indicate that it takes a 600-watt

ultrasonic homogenizer eleven minutes to sufficiently disperse the weak-bonded silica fume agglomerates.

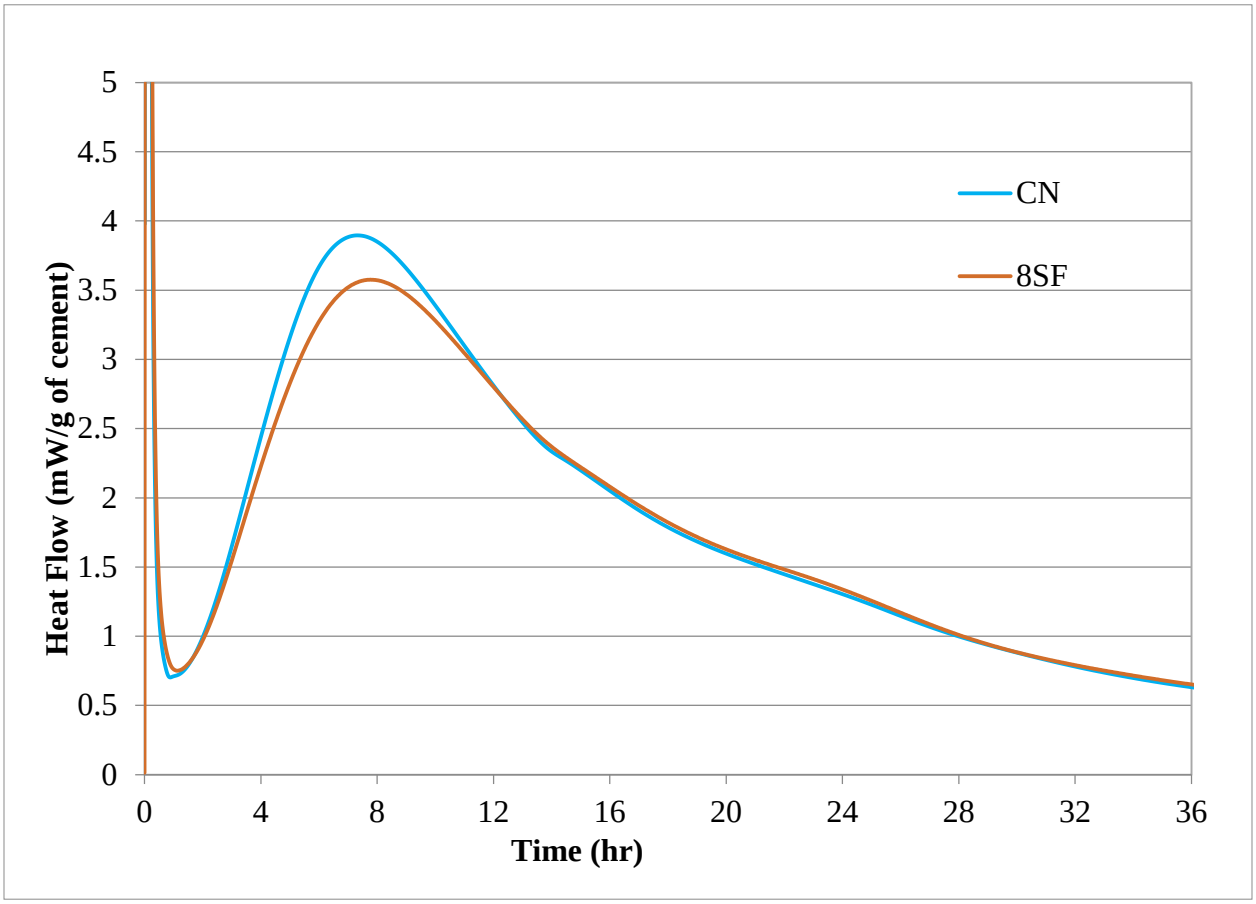

Figure 3-5: Measured Heat Flow of OPC and OPC/SF Pastes Normalized by Mass of Cement

Addition of metakaolin (MK) was expected to have a measurable effect on cement hydration. Initial reaction of MK (during the first 50 hours) is very rapid [68], with measurable pozzolanic activity reported as early as after 2 hours of hydration [81]. Since the reactivity of metakaolin is related to its amorphous content [64], [66], MK used in the current study was expected to be highly reactive due to its high amorphous content (98%).

However, the hydration rate observed for the OPC/MK sample, up to the end of the acceleration stage, was very similar to that of the OPC sample (Figure 3-6). Addition of MK did not have an effect on the timing of the main hydration peak, although its intensity was reduced slightly. Many researchers have reported an accelerating effect of metakaolin on cement hydration both in terms of intensity and timing of the main peak [80], [124], [168], [169] which is contrary

to what was observed here. Lagier and Kurtis [82] have shown that this accelerating effect is strongly dependent on the fineness of metakaolin: as fineness increases, so does acceleration of cement hydration. The metakaolin used here had similar fineness (14.97 m^2/g) to the low-fineness metakaolin (11.1 m^2/g) used by Lagier and Kurtis [82], which did not show a significant accelerating effect on the main hydration peak. They also concluded that the accelerating effect of metakaolin is much more pronounced on the C_3A hydration, while C_3S hydration is only slightly affected. In this light, the decrease in the main peak intensity may be attributed to the dilution effect, as discussed earlier. The presence of agglomerates that were not sufficiently dispersed by manual mixing is very likely, which would have affected the hydration behavior.

The sulfate depletion peak shifted from 14 hours in the OPC paste to 12 hours in the OPC/MK sample and the intensity of the peak increased, indicating acceleration of C_3A hydration, as reported by Lagier and Kurtis [82]. The mechanism of the C_3A acceleration is not well understood. It is generally proposed that hydration is accelerated because metakaolin provides additional nucleation sites [82], [171]. It is interesting to note that the fourth peak disappears with addition of metakaolin. Antoni et al. [171] suggested that it merged with the third peak; however, the researchers were not able to determine whether the aluminates contained in metakaolin participated in the reaction with sulfates at this point. If they did, then the shift in the sulfate depletion point can be attributed to the lower SO_3/Al_2O_3 ratio in the cementitious system. Since the metakaolin contained 44.16 % Al_2O_3 and no sulfates, 10% cement replacement by metakaolin effectively reduced the SO_3/Al_2O_3 ratio in the paste from 0.69 (OPC) to 0.40 (OPC/MK-90/10). Since sulfate balance has been identified as one of the main reasons for admixture incompatibility [4], [12], the addition of other admixtures that accelerate the aluminate-sulfate reaction in the OPC/MK mixture, or an increase in the ambient temperature may result in an undersulfated condition. Further investigation is needed to determine if such conditions will lead to abnormal setting, or excessive temperature rise in the OPC/MK mixtures.

The 10MK mixture appeared to reach steady state faster than the CN sample, and its heat flow at this stage was higher as well. This can be explained by the reaction of metakaolin with CH to produce additional C-S-H. Comparing the total heat normalized by the mass of cementitious materials, compressive strength of the OPC/MK mixture is expected to be lower at earlier ages due to the relatively low acceleration of the early C_3S reactions by metakaolin.

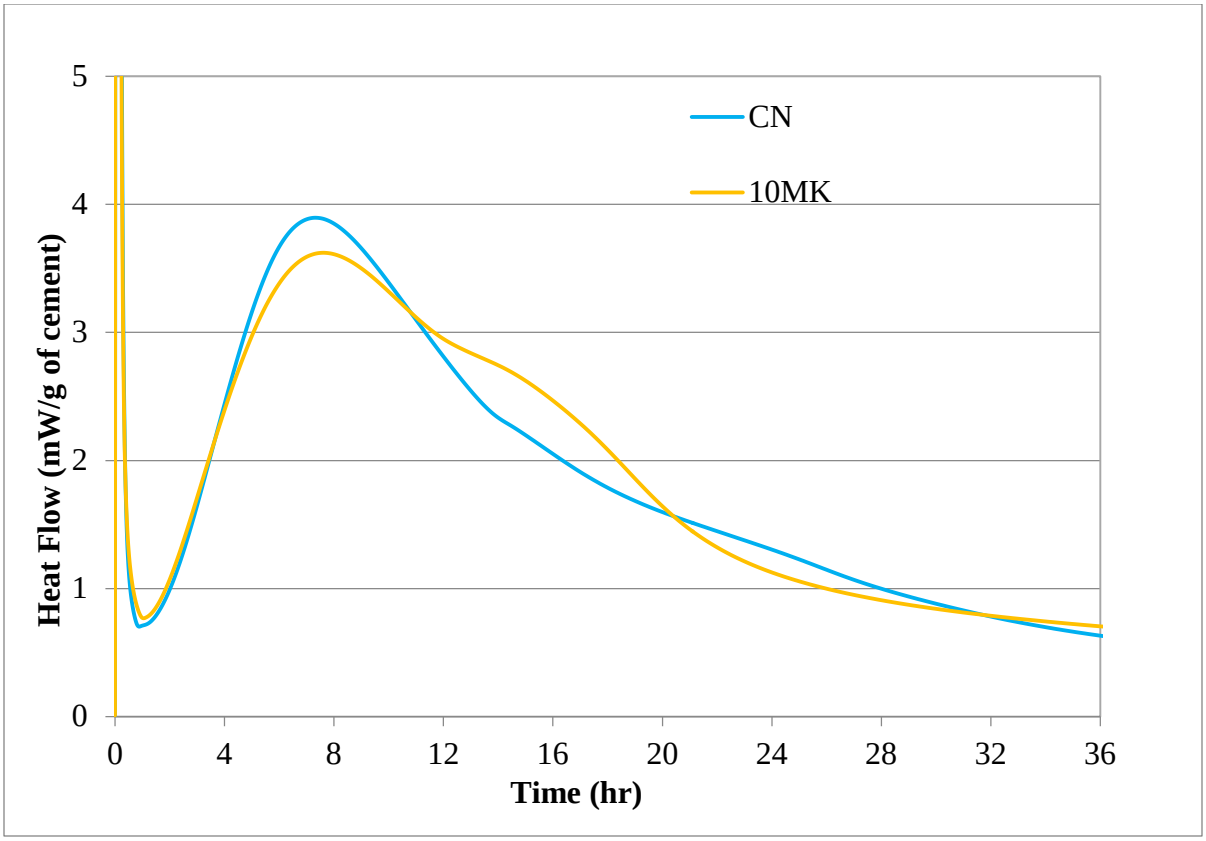

Figure 3-6: Measured Heat Flow of OPC and OPC/MK Pastes Normalized by Mass of Cement

There is little data available for the early-age reactivity of slag. It has been reported that reactivity of slag depends on its amorphous content, temperature history, with higher temperature and faster quenching rates producing more reactive materials, fineness, chemical composition, and alkali concentration in the mixture, as hydration of slag is alkali- and sulfate-activated [19], [105]. Dissolution of slag releases alkalis into the pore solution, ensuring a continuous reaction of slag into the later ages [44]. Escalante et al. [137] determined, through selective dissolution, that reactivity of slag increases with increasing amorphous content. The first measurements were performed at 3 days. Feng et al. [172] also observed an accelerating effect of slag addition on cement hydration. The degree of hydration was determined via SEM point-counting technique. Again, the first measurement was conducted at 3 days. The authors also compared degree of reaction of slag and Class F fly ash, and determined that the reactivity of slag was much higher than that of fly ash.

Since it was determined previously, using x-ray diffraction, that the slag used in this project had an amorphous content of approximately 97 %, it was expected to be highly reactive. Addition of slag resulted in a significant increase in heat evolution compared to the OPC sample. In terms of the silicate reaction, Figure 3-7 shows a reduced induction period for the 52SL sample, increased intensity of the main hydration peak, as well as a shift of the peak maximum to the right by approximately 1 hour. Kocaba [159] showed that the effect of slag on OPC hydration depends on the mineralogical composition of the cement. She reported acceleration of the C_3S reaction, based on isothermal calorimetry, with addition of 40% slag for one cement, and retardation of the C_3S reaction for two other cements, although the degree of alite hydration was determined to be the same for all three of these systems. No explanation was offered for this phenomenon.

As for the aluminate reaction, the sulfate depletion peak was shifted to the left, its intensity was significantly increased, and the rate of deceleration was decreased as well. Brunet et al. [173] reported that aluminates in slag had higher reactivity compared to the silicates, which can explain the observed shift in the sulfate depletion peak to an earlier time. Kocaba [159] attributed the acceleration of the aluminate reaction to the filler effect (heterogeneous nucleation). At steady state, the heat flow of the OPC-slag remained consistently higher than that of the OPC control sample, which points to a continuous reaction of slag.

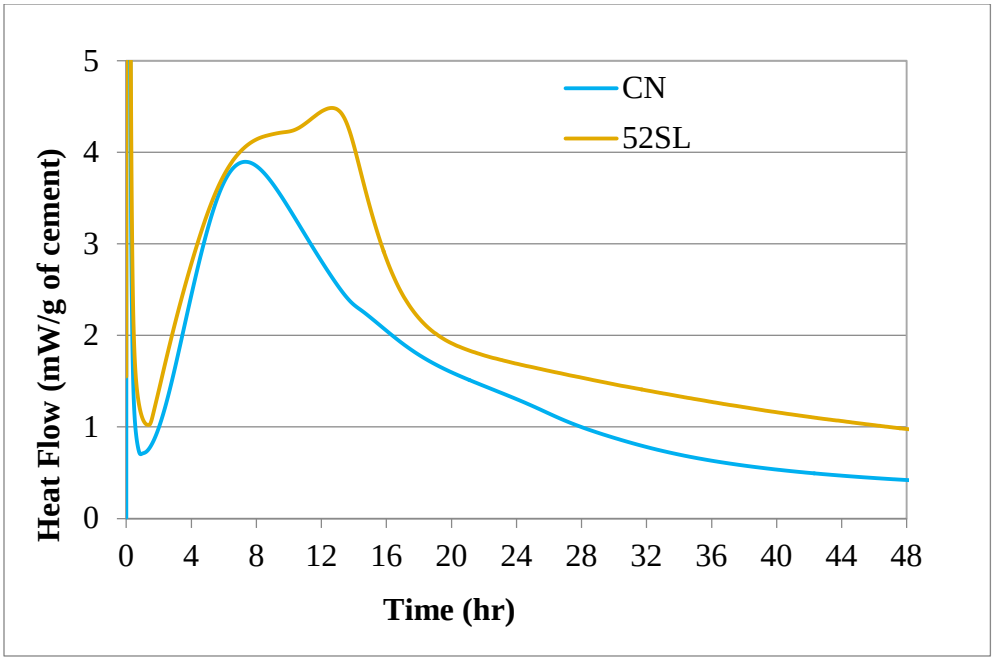

Figure 3-7: Measured Heat Flow of OPC and OPC/Slag Pastes Normalized by Mass of Cement

Table 3-3 and Figure 3-8 and Figure 3-9 present the heat measurements for all the OPC-mineral admixtures combinations. Addition of slag resulted in both the highest heat flow and the highest total heat among all samples, including OPC control paste. There is a significant increase in the total heat in the 52SL mixture followed by 10MK at 7 days. The total heat of the 21FA, at 7 days, was slightly higher than that of the OPC sample, while no difference was observed between CN and 8SF, most likely due to particle agglomeration as discussed previously.

Table 3-3: Heat of Hydration for Cement-Mineral Admixture Combinations (Internal Mixing)

Mix ID	**Mineral Admixture**	**w/o Cement Replacement**	**1-Day HOH (J/g cement)**	**3-Day HOH (J/g cement)**	**7-Day HOH (J/g cement)**
CN	None	0	211	302	354
10MK	Metakaolin	10	217	320	393
8SF	Silica fume	8	210	302	353
21FA	Class F Fly Ash	21	214	340	370
52SL	Slag	52	269	450	578

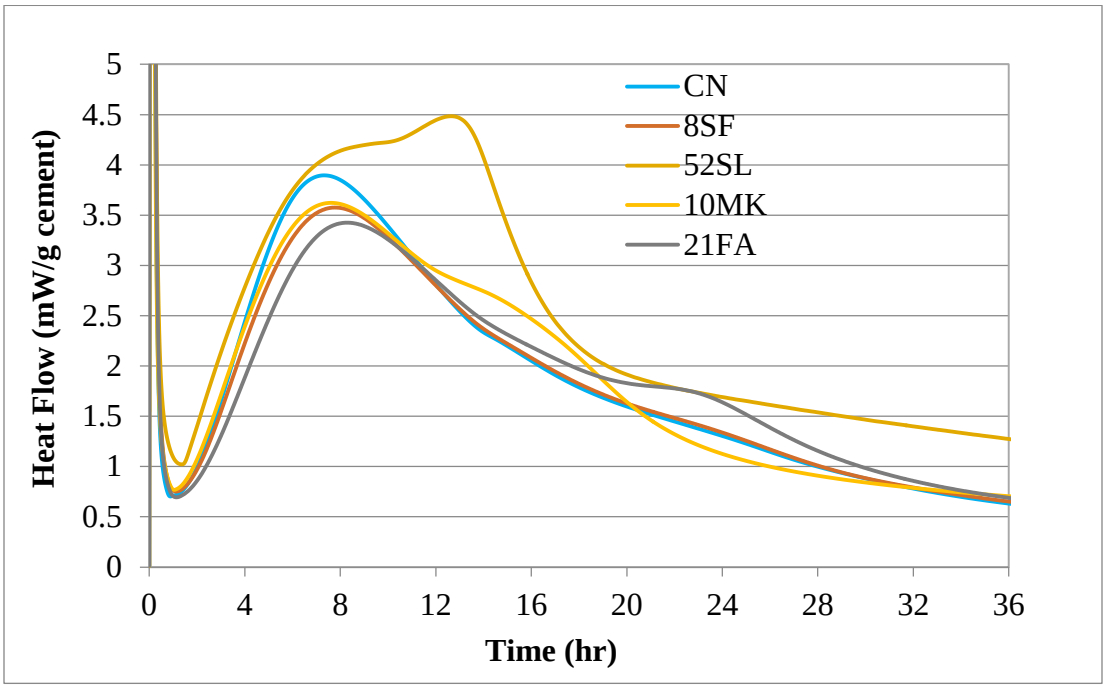

Figure 3-8: Measured Heat Flow of OPC and OPC/SCM Pastes Normalized by Mass of Cement

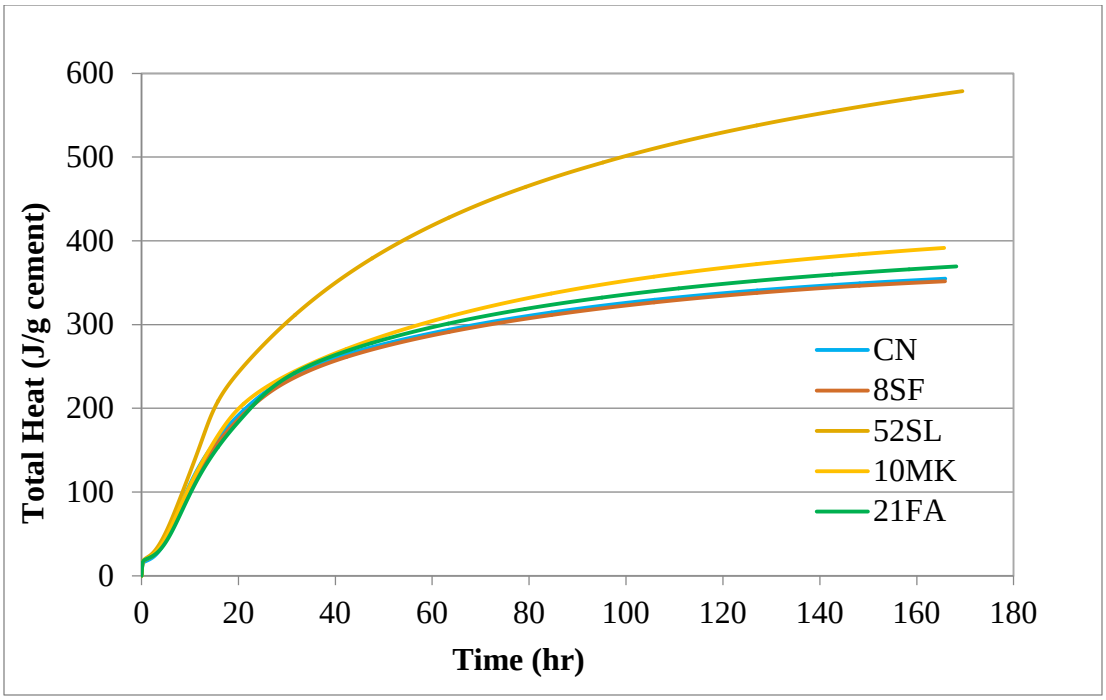

Figure 3-9: Total Heat of Cement and Mineral Admixture Samples Normalized by Mass of Cement

Chemical Admixtures

The WR used in this project is classified as a Type D water-reducing and retarding admixture. This admixture contained sulfite liquors, molasses, and triethanolamine (TEA) [174]. Since sulfite liquors are a by-product of the pulp industry, it can be presumed that this admixture contain lignosulfonates, which are derived from wood pulp waste liquors [175]. In addition to lignosulfonates, pulp liquors commonly contain sugars, which are present in molasses as well. The effect of the WR on cement hydration was considered in terms of these three main compounds: lignosulfonate, sugar, and TEA.

Considering the heat flow data presented in Figure 3-10, the retarding effect of WR addition on C_3S hydration can be seen both in the reduced rate of heat flow in the acceleration period as well as in the position of the main hydration peak. For the paste containing WR, the position of the silicate peak maximum was shifted by 2 hours, from 7 hours in plain cement paste to 9 hours. The peak height decreased as well by the addition of the water reducer. This points

out the retarding effect of lignosulfonate on C_3S hydration, which has been reported in several studies [52], [175], [176].

Addition of sugar has been reported to have a retarding effect on C_3S hydration as well [177], [178]. However, it should be noted that the magnitude of this retardation effect is dependent on the crystal structure of C_3S; while triclinic C_3S can be retarded with small dosages, a retardation of monoclinic C_3S requires higher sugar content [179]. Since the cement used in this study only contained monoclinic C_3S and no increase in the initial dissolution peak was observed, it is concluded that sugar likely did not have a measurable effect on cement hydration.

Triethanolamine (TEA) is commonly incorporated into admixtures, such as WRs, to compensate for their retarding effect. The effect of TEA on concrete is dosage-dependent. At lower dosages, TEA acts as an accelerator, while at higher dosages it has a retarding effect [28]. It is not clear if, and to what extent, TEA contributed to, or compensated for, this retardation.

The timing of the sulfate depletion peak was not affected by WR addition, but its intensity was higher for the WR paste sample than the control CN paste. The time of occurrence of the fourth peak did not change, and its intensity increased. This could possibly point to increased hydration of C_3A; however, it is impossible to separate the effect of lignosulfonate from that of TEA in the case of commercial WR, as both have been reported to accelerate C_3A hydration [11], [28], [52], [176]. Studies with pure lignosulfonate and pure TEA would be required to separate such an effect.

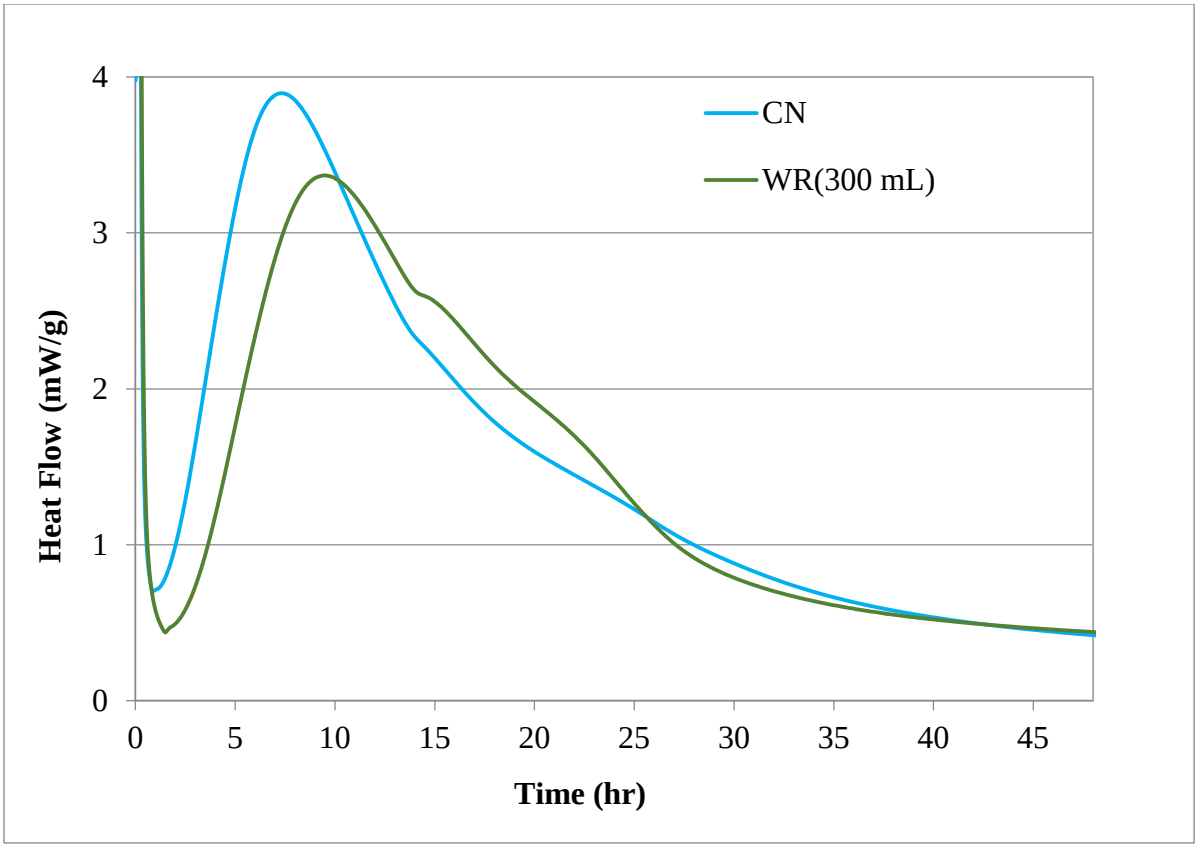

Figure 3-10: Measured Heat Flow of OPC and OPC/WR Pastes Normalized by Mass of Cement

The superplasticizers (SP) used in this study contained a polyacrylate aqueous solution [180] that belongs to the polycarboxylate-polyether (PCE) family of superplasticizers. As can be seen in Figure 3-11, significant retardation of the acceleration stage was observed with SP2 addition: the length of the induction period increased from 1 hour in the OPC paste, to approximately 7 hours in the SP2 sample. The rate of heat flow and the intensity of the main hydration peak also were significantly decreased. The timing of the main hydration peak maximum was also delayed from 7 to 14 hours with addition of SP2. Although there was a corresponding delay in the occurrence of the sulfate depletion peak (from 14 to 19 hours), its intensity did not appear to be affected. Heat flows of approximately 2.2 mW/g were recorded for both samples at the peak maximum.

Cheung et al. [12] state that most WRs and SPs have a retarding effect. The retarding effect of PCEs observed by isothermal calorimetry [181]–[183] and by setting time measurements [184] has been reported in the literature. This is consistent with the delay of the main hydration peak

observed in this study. Lothenbach et al. [183] showed through XRD measurements that the C_3S reactions are retarded in the presence of PCE. However, Winnefeld et al. [182] also reported that the timing between the silicate peak and the sulfate depletion shoulder increased with addition of PCE, while in this study the time between the occurrence of these two peaks actually decreased. Winnefeld et al. [182] pointed out that the extent of retardation depends on the side chain length of the polymers present in the admixture. They observed that the retarding effect increased as the side chain length decreased. The mechanism of this retardation is not well understood. Lothenbach et al. [183] did not observe any changes in the pore solution chemistry with addition of PCE and concluded that PCE complexes, with calcium or other ions, are absent. Winnefeld et al. [182] proposed that adsorption of PCEs to the surfaces of cement particles is responsible for a delay in cement hydration.

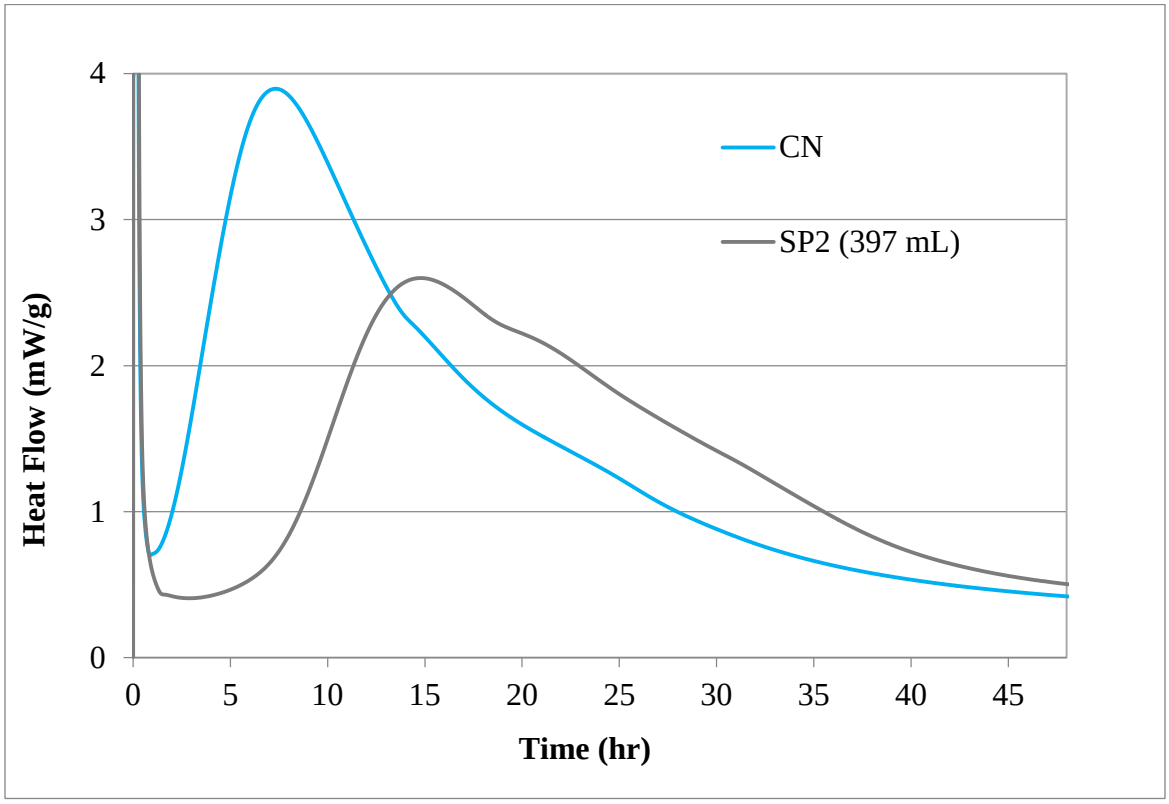

Figure 3-11: Measured Heat Flow of OPC and OPC/SP2 Pastes Normalized by Mass of Cement

Addition of AE had a minor retarding effect on cement hydration (Figure 3-12). As can be seen in Figure 3-12, addition of AE extended the induction period slightly, and reduced the rate of

heat flow in the accelerating stage. The intensity of the main hydration peak was reduced and the timing of its maximum was delayed by approximately 1 hour. After that, the heat flow curve for AE closely followed the curve for the OPC control sample.

It is difficult to compare the above findings to the published literature, as the data on the effect of AEs on the hydration process is very limited. Dolch [20] states that AEs "have no appreciable effect of the rate of hydration of cement or on the heat evolved by that process." He further asserts that even if some of these admixtures did have a retarding effect, the dosages at which AEs are typically added to concrete would not be sufficient to produce a discernable effect. Ma and Wang [185] did not observe any effects from AE addition on cement hydration through isothermal calorimetry; however, the chemistry of the admixture used in this study was not identified. Kreijger, cited by Edmeades and Hewlett [43], observed that certain admixtures can affect cement hydration at high dosages. Vinsol resin had a retarding effect on C_3S hydration while accelerating the C_3A hydration. Sodium oleate accelerated C_3A hydration, but had no effect on C_3S. Rixom and Mailvaganam [28] state that ethoxylates and other non-ionic AEs do not affect OPC heat of hydration, while addition of high dosages of wood resins, sulfates and sulfonates, such as sodium dodecylbenzenesulfonate used in this study, has a retarding effect on C_3S hydration and an accelerating effect on C_3A. Although no accelerating effect was observed for the sulfate depletion peak, C_3S hydration did appear slightly retarded by AE addition, even though the admixture dosage used in this study was at the low end of the range recommended by the manufacturer [186].

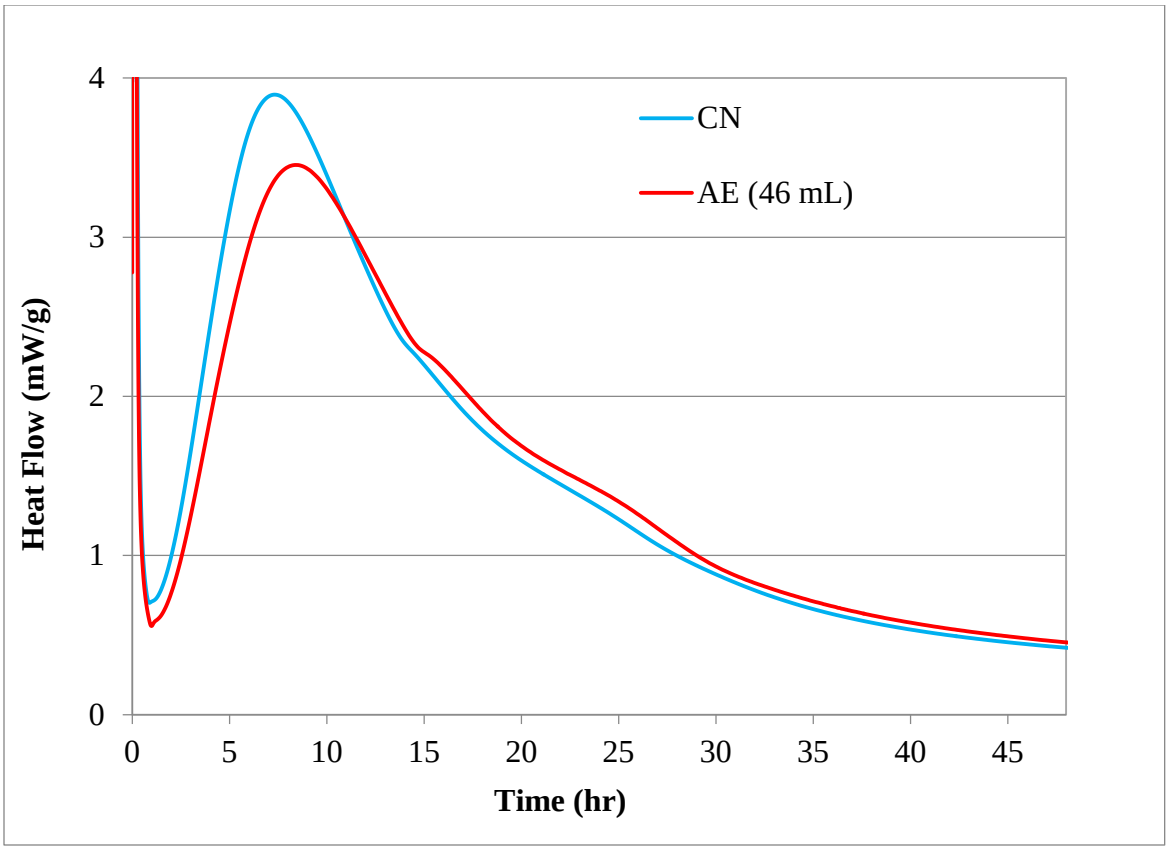

Figure 3-12: Measured Heat Flow of OPC and OPC/AE Pastes Normalized by Mass of Cement

Table 3-4, Figure 3-13, and Figure 3-14 present heat measurements for all the OPC-chemical admixture combinations. Addition of water-reducing and air-entraining admixtures had a negligible effect on cement hydration kinetics after 1 day. Addition of these admixtures resulted in a retardation of the main hydration peak by 2 and 1 hours, respectively, indicating an expected delay in setting time compared to the control OPC paste. Addition of SP2 significantly delayed the timing of the main hydration peak and resulted in lower total heat measurements, although by 7 days the difference between CN and SP2 samples is negligible.

Table 3-4: Heat of Hydration for Binary Cement-Chemical Admixture Combinations

Mix ID	Dosage (ml/100 kg)	1-Day HOH (J/g)	3-Day HOH (J/g)	7-Day HOH (J/g)
CN	0	211	302	354
SP2 (397 mL)	397	163	285	351
WR (300 mL)	300	205	295	356
AE (46 mL)	46	202	299	355

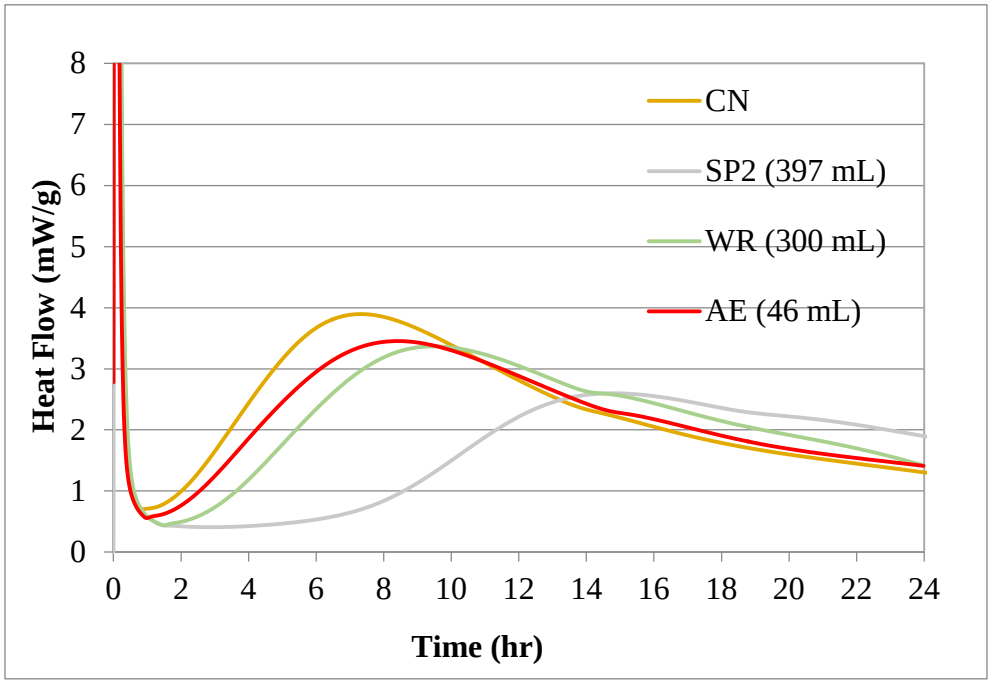

Figure 3-13: Measured Heat Flow of CN and OPC/ Chemical Admixture Pastes Normalized by Mass of Cement

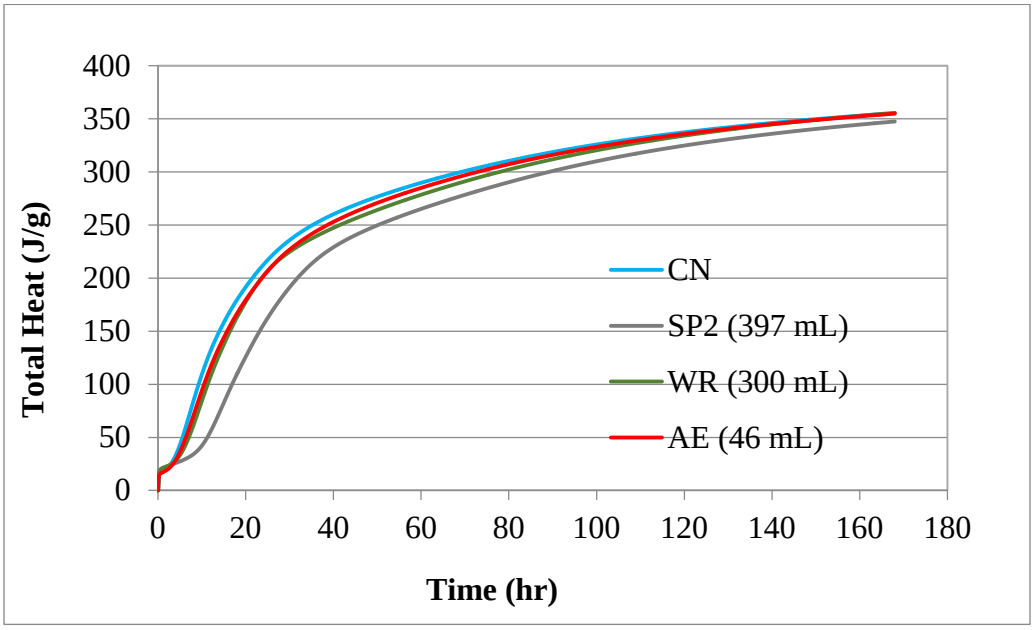

Figure 3-14: Measured Total Heat of CN and OPC/Chemical Admixture Pastes Normalized by Mass of Cement

External Mixing

Mineral Admixtures

External mixing of the cement-mineral admixture binary mixtures (Figure 3-15) showed slightly different heat flow trends from those tested following the internal mixing protocol (Figure 3-8). With external mixing, the main hydration peak of all cement-mineral admixture combinations occurred earlier and had higher intensity compared to internal mixing. This is attributed to better dispersion of mineral admixtures with the external mixing procedure. As for the total heat, both external (Figure 3-16) and internal (Figure 3-9) mixing protocols produced the same trends. Addition of slag resulted in the highest total heat at 72 hours when normalized per gram of cement, addition of metakaolin slightly increased the total heat compared to that of cement, and fly ash and silica fume additions did not have any effect.

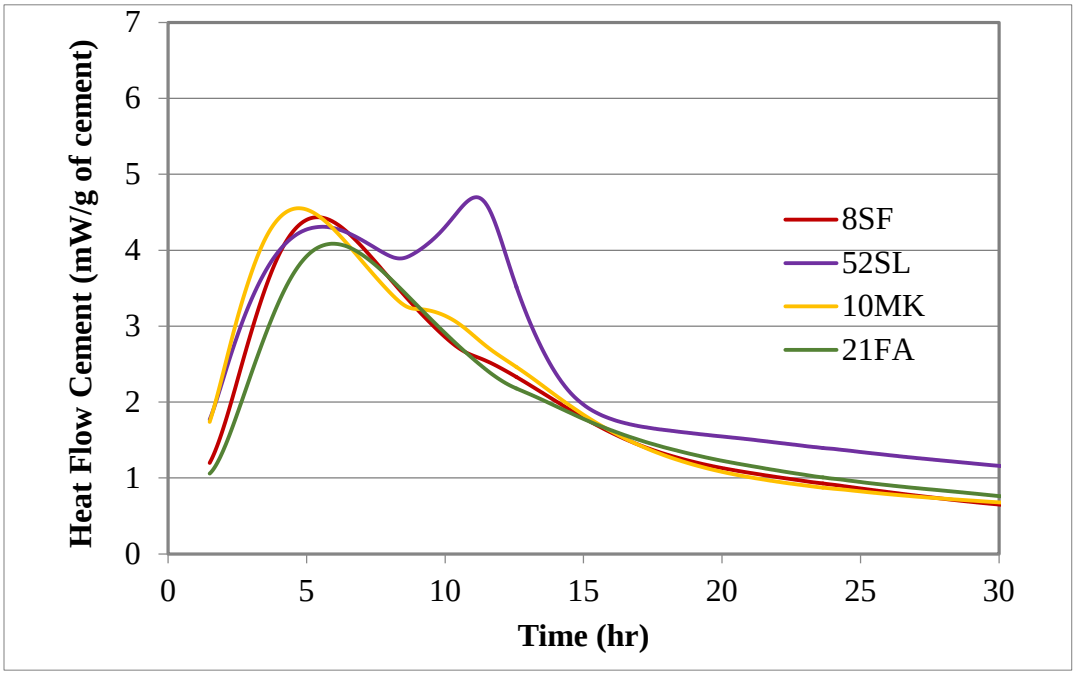

Figure 3-15: Measured Heat Flow (External Mixing) of OPC and OPC/Mineral Admixture Pastes Normalized by Mass of Cement

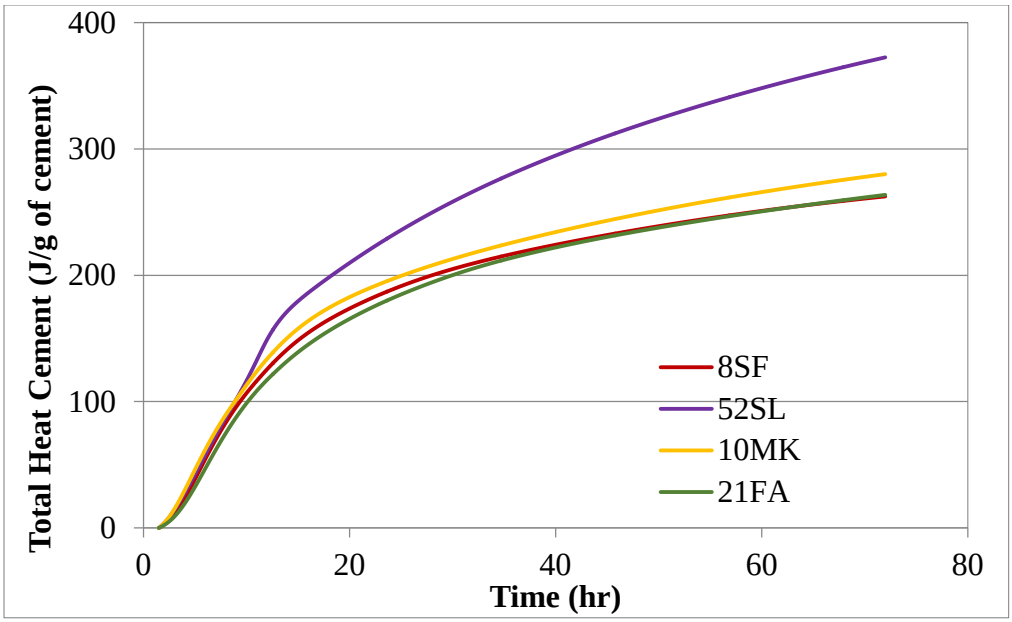

Figure 3-16: Total Heat of Cement and Mineral Admixture Samples (External Mixing) Normalized by Mass of Cement

These conclusions are only valid for the specific cement replacement rates that were tested. In order to evaluate the dosage effect of each mineral admixture on cement hydration, mixtures with four different cement replacement levels were prepared for each mineral admixture. Figure 3-17 and Figure 3-18 illustrate the effect of Class F fly ash dosage on heat flow and total heat, respectively, normalized per gram of cement. It is clear that at cement replacement levels below 30%, there is no effect on cement hydration. This is not surprising, as Class F fly ash is expected to be non-reactive during the first week of hydration [44]. Even at 30% replacement, the timing and magnitude of the silicate and aluminate hydration peaks remains unaffected as reported in the literature [53], [164], [168]. The only difference observed at 30% replacement level was the presence of the fourth peak, which was observed with internal mixing at 21% fly ash replacement. As discussed previously, the nature of this peak remains undetermined. When normalized by the mass of total cementitious content, both the heat flow (Figure 3-19) and total heat (Figure 3-20) decreased with increasing cement replacement level. Since fly ash is not reactive at such early ages, the decreased heat was due to the reduction of cement content.

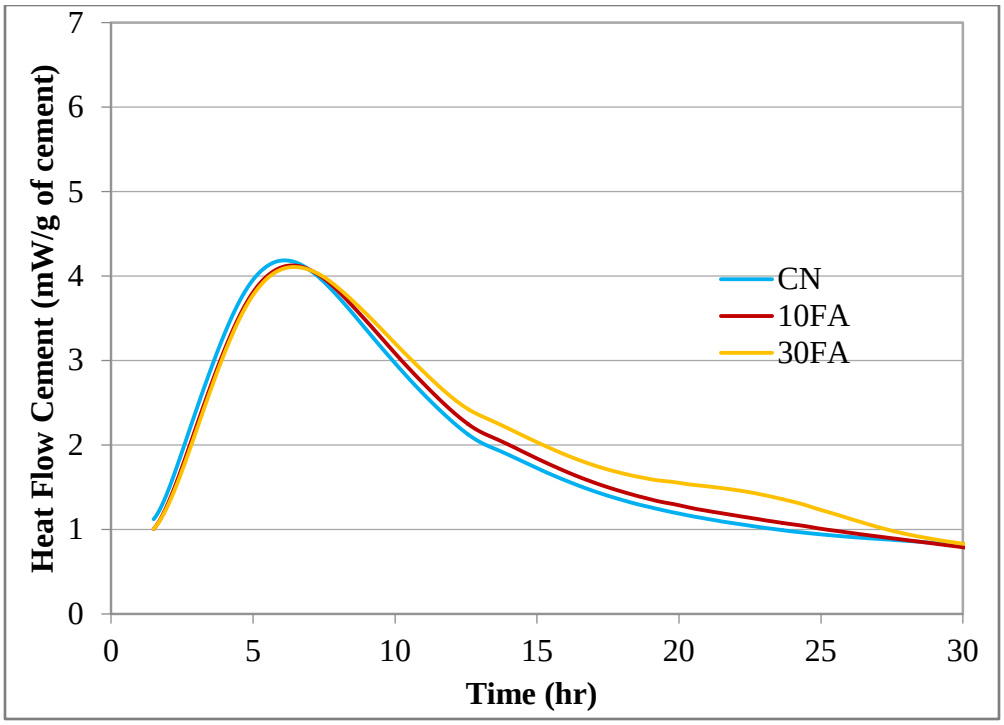

Figure 3-17: Measured Heat Flow of Cement/Fly Ash Pastes Normalized by Mass of Cement

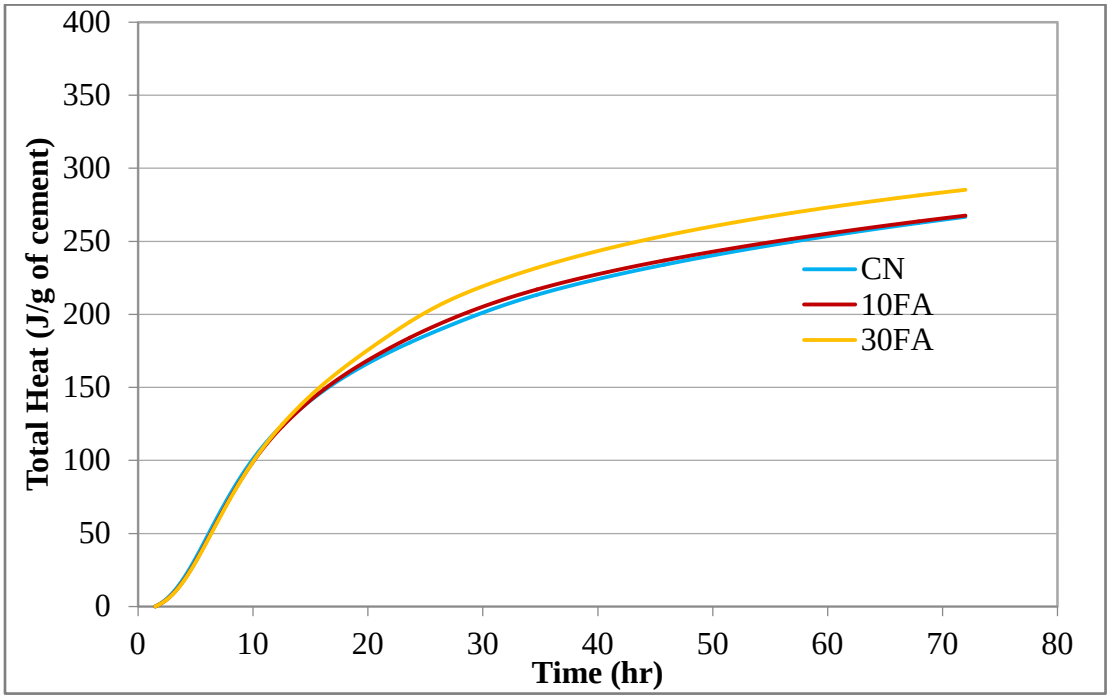

Figure 3-18: Total Heat of Cement/Fly Ash Pastes Normalized by Mass of Cement

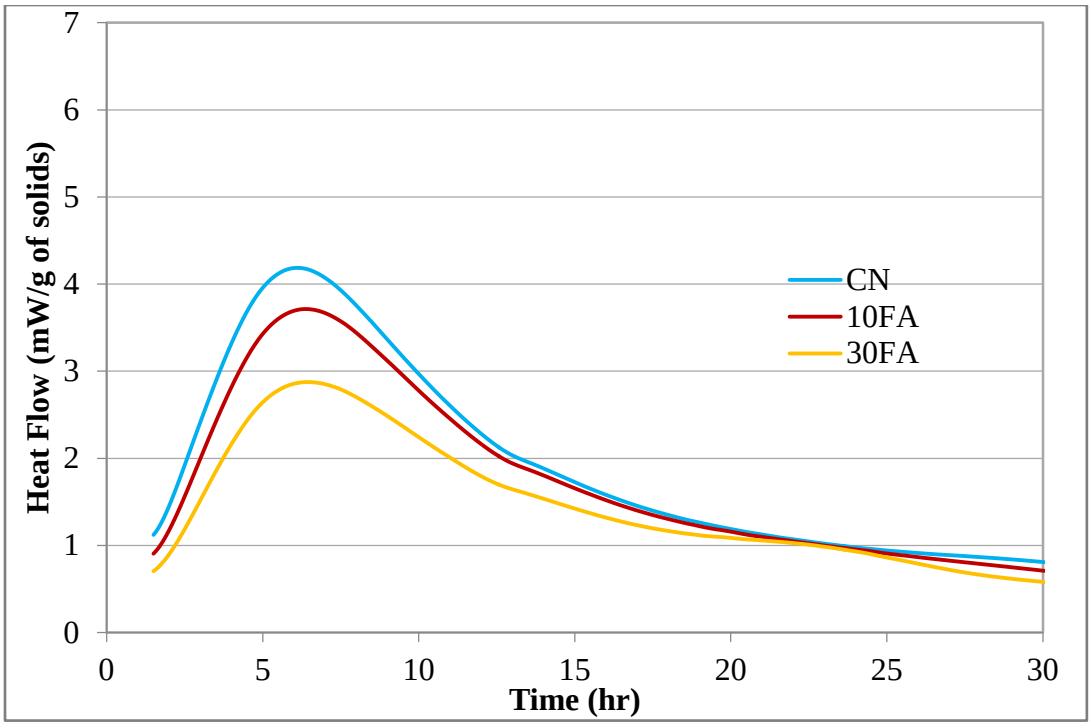

Figure 3-19: Measured Heat Flow of Cement/Fly Ash Pastes Normalized by Mass of Cementitious Materials

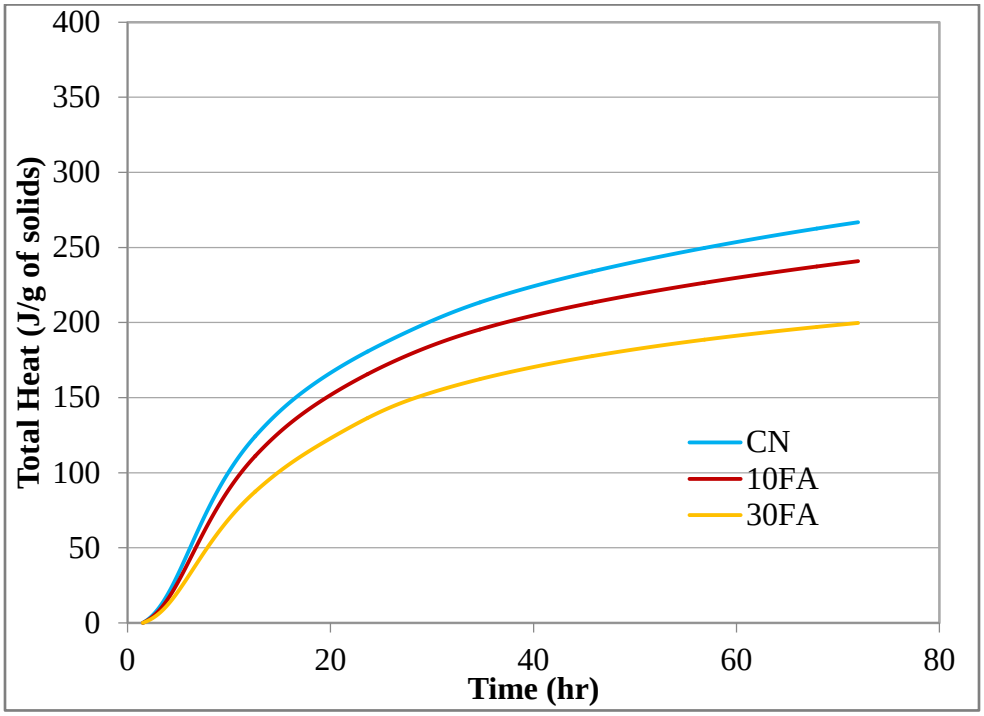

Figure 3-20: Total Heat of Cement/Fly Ash Pastes Normalized by Mass of Cementitious Materials

Unlike fly ash, the effect of slag on cement heat flow was observed to be dosage-dependent (Figure 3-21). The effect on silicate hydration only became visible at 52% cement replacement, while the aluminate hydration peak was affected at all replacement levels. There was an increase in the magnitude of the aluminate peak with increasing slag dosage, possibly due to the reaction of amorphous alumina from slag. Although the reactivity of different slags varies [19], [105], reactivity of slag activated by portland cement has been generally compared to that of C_2S [16]. Brunet et al. [173] reported that in slags, the reactivity of alumina is higher than that of silica. This can explain the greater effect of slag addition on the aluminate hydration compared to silicate hydration. Increased slag content increased the heat flow and increased the total heat, when normalized by mass of cement (Figure 3-22).

Normalizing heat flow by mass of cementitious materials revealed that both heat flow (Figure 3-23) and total heat (Figure 3-24) generally decreased with increasing slag content due to decreased cement content. It is interesting to note that at 10% replacement of cement with slag, the total heat curve was very similar to that of the plain cement mix. It appears that at 10% replacement, there is sufficient acceleration in cement hydration by slag (possibly coupled with the reaction of slag itself) to offset the effect of decreased cement content in terms of heat generation. Also, heat flow and total heat curves (normalized by mass of cementitious materials) for 21% and 30% slag were very similar despite variable cement replacement levels. Comparing Figure 3-21 and Figure 3-23 reveals that although the sulfate depletion point in the two samples occurred at the same time, it occurred at a higher heat flow value for the 30% slag paste (Figure 3-21), which indicates a higher reactivity of the aluminates.

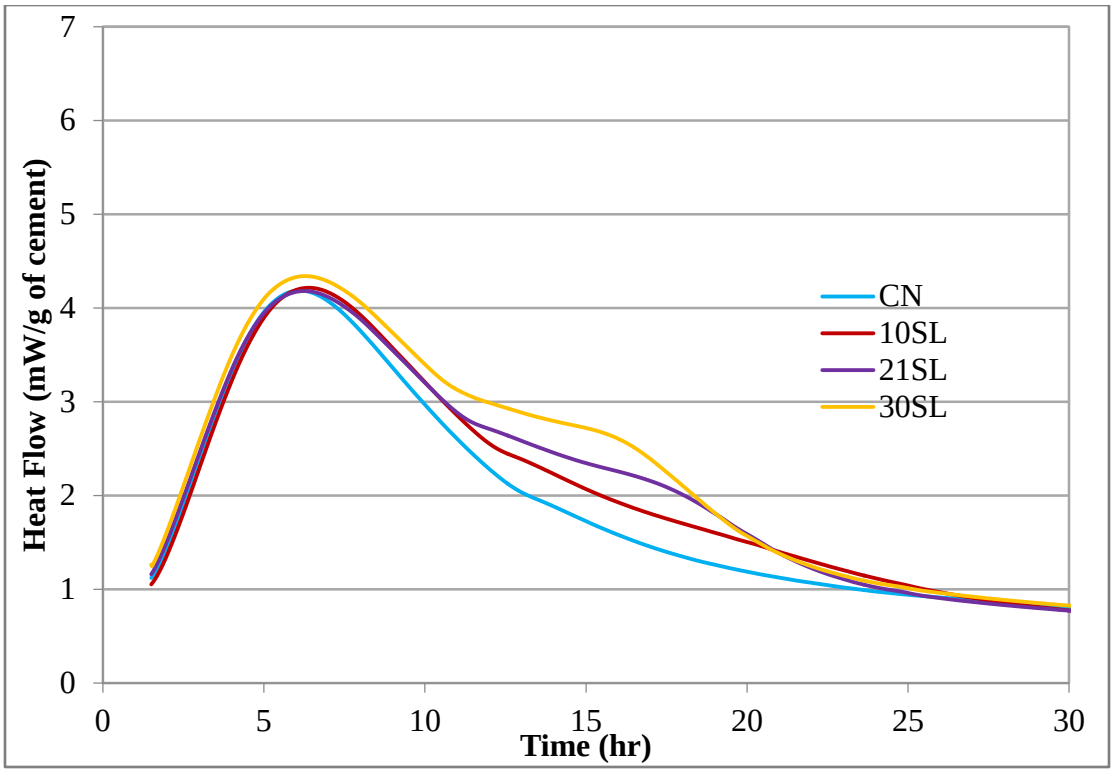

Figure 3-21: Measured Heat Flow of Cement/Slag Pastes Normalized by Mass of Cement

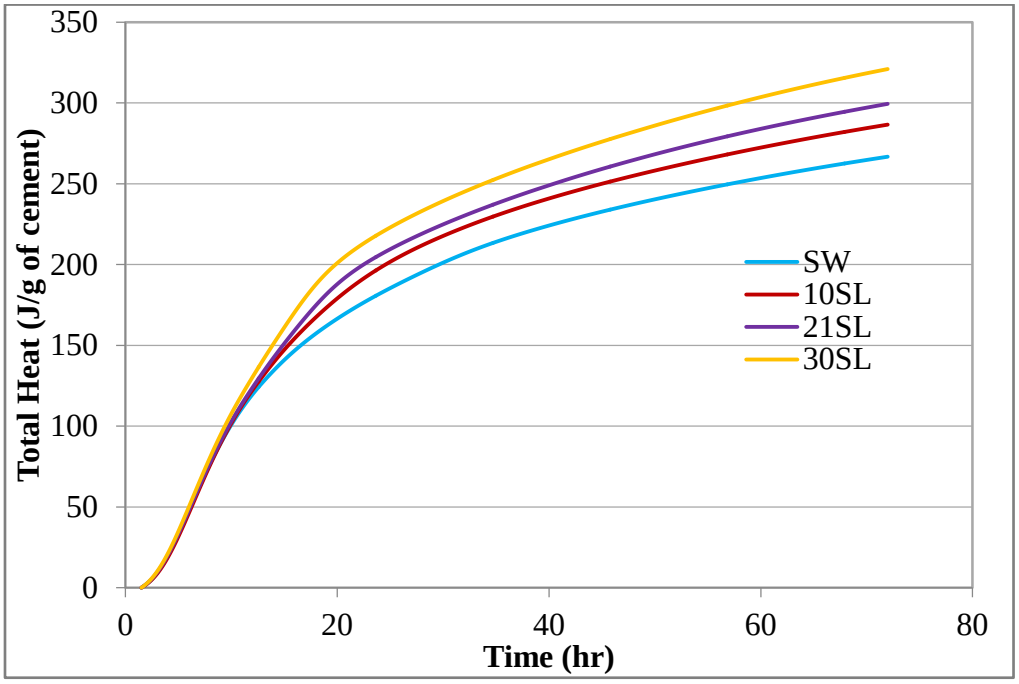

Figure 3-22: Total Heat of Cement/Slag Pastes Normalized by Mass of Cement

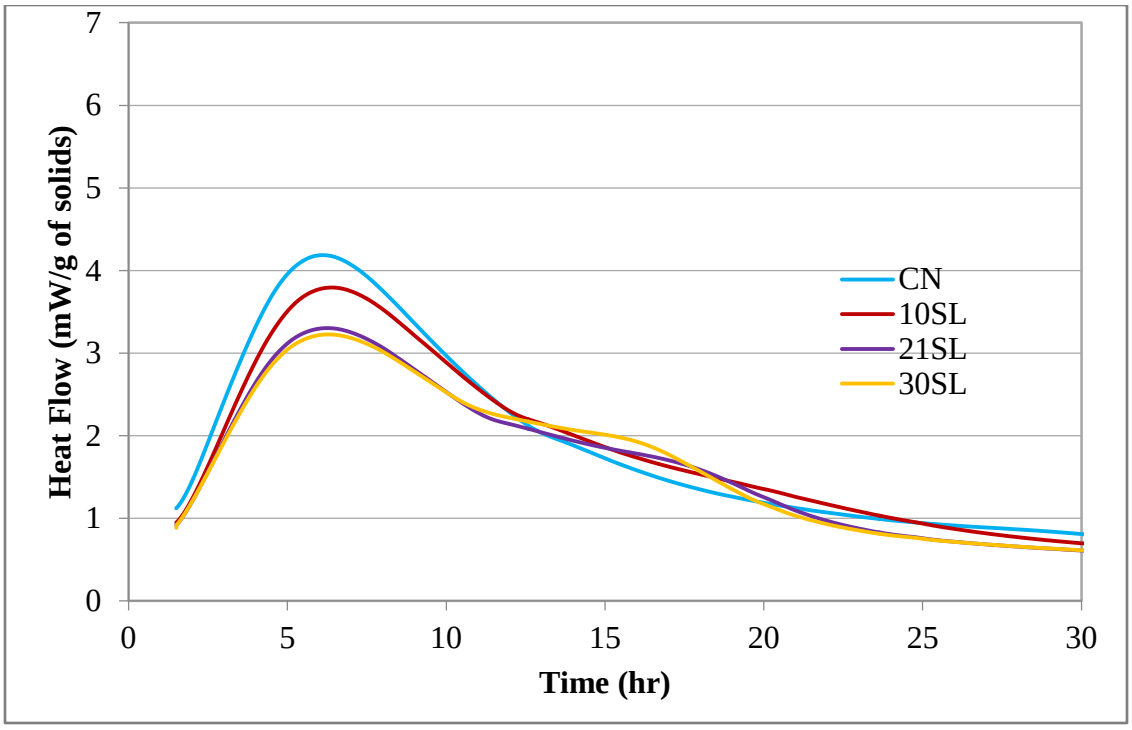

Figure 3-23: Measured Heat Flow Normalized by Mass of Cementitious Materials

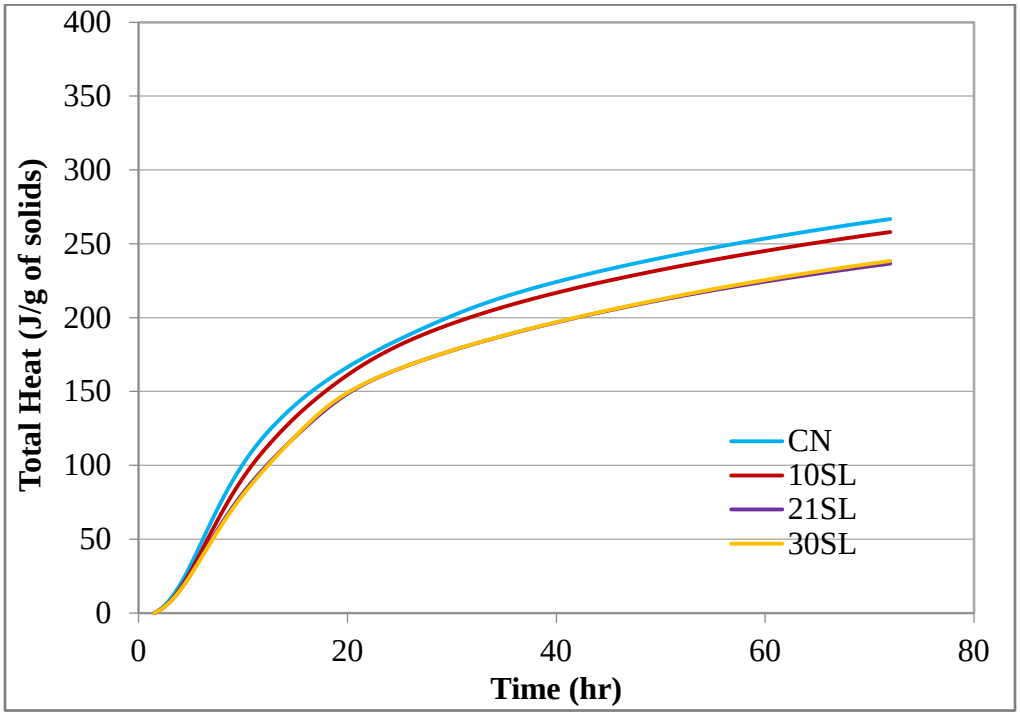

Figure 3-24: Total Heat Normalized by Mass of Cementitious Materials

In terms of cement reactivity, silica fume addition affected both the silicate and aluminate peaks at all replacement levels (Figure 3-25). There was an increase in the main hydration peak, with a slight shift to the left, with increasing SF addition. As for the sulfate depletion peak, both its magnitude and timing were accelerated by increasing silica fume replacement levels. Several researchers have discounted the possibility of silica fume reaction during the first 24 hours [62], [93]; therefore, the accelerating effect was most likely due to heterogeneous nucleation. It is interesting that the cement heat flow continued to increase with increasing silica fume content up to 30%, indicating that the saturation limit, where addition of extra nucleation sites does not result in increased hydration rate, had not been reached. Total heat also increased with increasing SF dosages, when normalized by mass of cement (Figure 3-26), which is somewhat contrary to the findings of Zelić et al. [93], who observed a decrease in total heat at 30% SF replacement.

Normalizing by total cementitious content showed that heat flow (Figure 3-27) and total heat (Figure 3-28) decreased as silica fume content increased. The same effect was observed for the fly ash; however, in the case of silica fume this decrease is significantly lower. While the total heat at 3 days for fly ash at 30% cement replacement level was approximately 70 J/g of cementitious materials lower than that of the plain cement paste, for silica fume it was lower by 42 J/g. This points to significant acceleration of cement hydration.

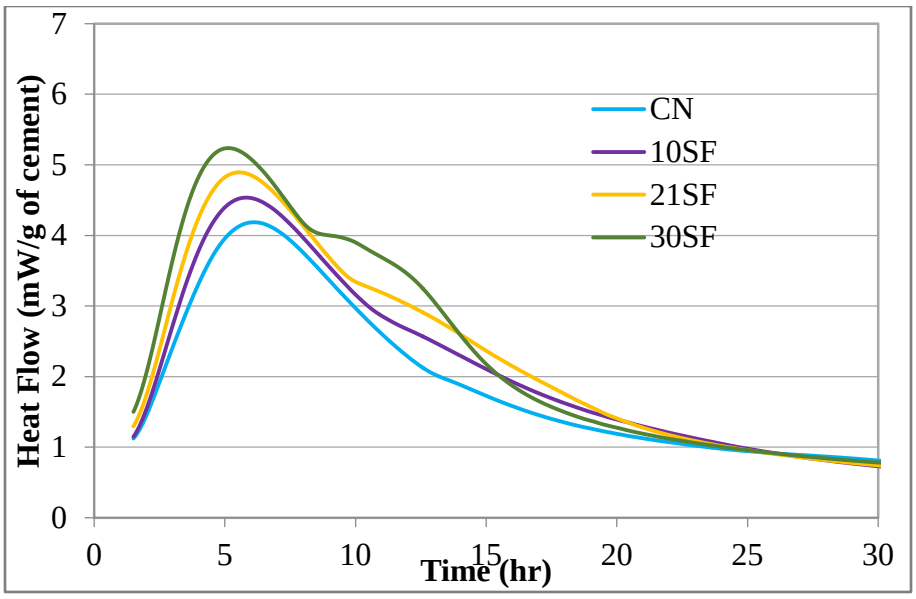

Figure 3-25: Measured Heat Flow of Cement/Silica Fume Pastes Normalized by Mass of Cement

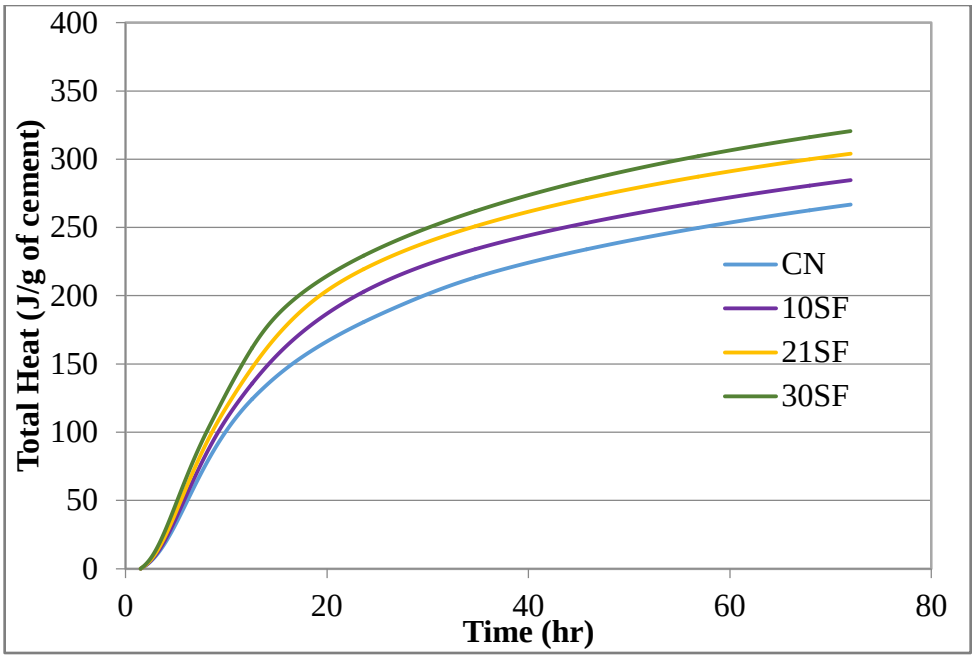

Figure 3-26: Total Heat of SF Normalized by Mass of Cement

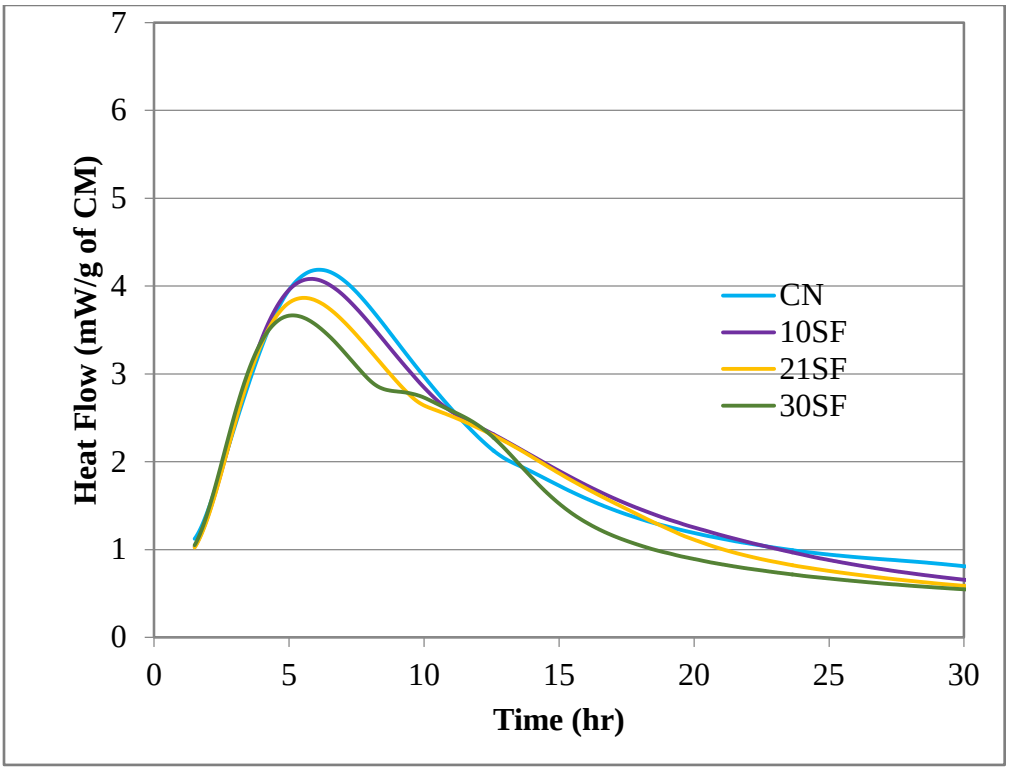

Figure 3-27: Measured Heat for SF Flow Normalized by Mass of Cementitious Materials

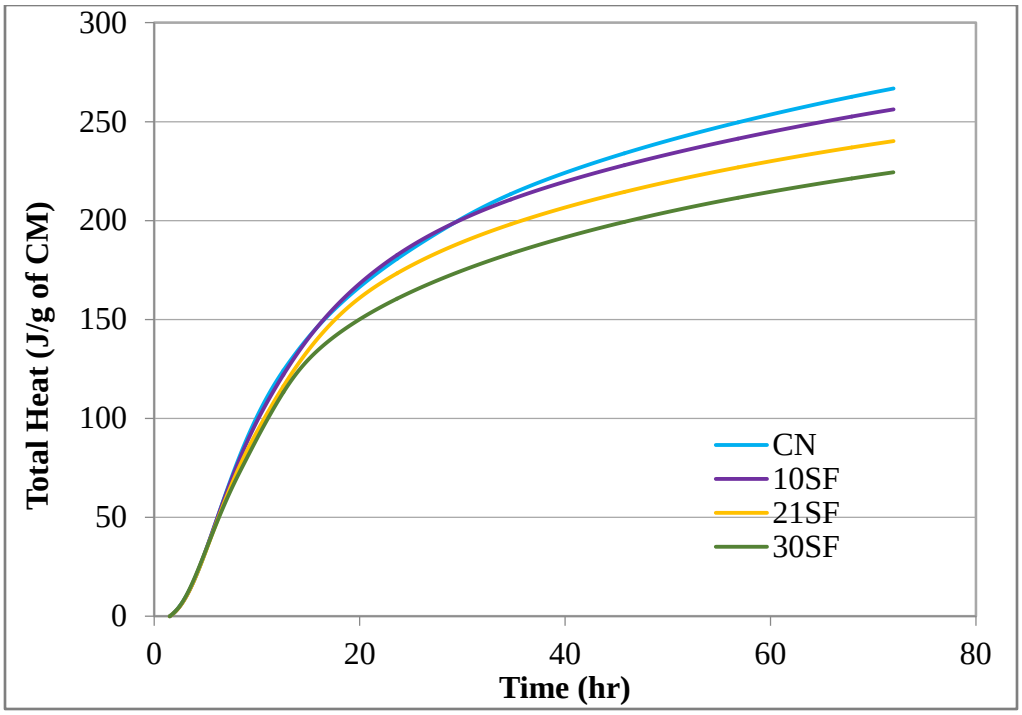

Figure 3-28: Total Heat for SF Normalized by Mass of Cementitious Materials

Similar to silica fume, initial addition of metakaolin shifted the main hydration peak to the left; however, subsequent MK addition did not affect the timing of the main hydration peak (Figure 3-29). The intensity of the main hydration peak increased with 21% MK addition, although further increase of replacement level to 30% did not affect its magnitude. If silicate hydration is accelerated by MK through heterogeneous nucleation, it may be possible that at 21% MK, the maximum effective number of nucleation seeds had been reached and further increase did not affect silicate reactivity. Unlike the silicate peak, both the timing and magnitude of the aluminate peak were accelerated by increasing MK dosage. It appears that the reaction of aluminates supplied by MK may have contributed to this acceleration. MK is known to be reactive at early ages [68], [81]; Frias et al. [81] reported measureable pozzolanic activity as early as 2 hours. As for the total heat, there was an increase with 21 and 30% MK addition, although the total heat of these mixtures was very similar (Figure 3-30).

Figure 3-31 and Figure 3-32 show the heat flow and total heat curves for pastes with metakaolin normalized by the mass of total cementitious materials. The maximum heat flow remained unaffected at 21% replacement and was attributed to the main hydration peak, while at

30%, the maximum heat flow was due to the reaction of aluminates and was increased compared to the control and 21MK samples. Figure 3-32 shows that all the pastes, regardless of cement replacement levels, had the same total heat up to 10 hours, after which the sample with 30% MK started to show lower total heat. Total heat of the 21MK sample continued to be the same as that of the control up to 15 hours, after which total heat was higher in the plain cement mix.

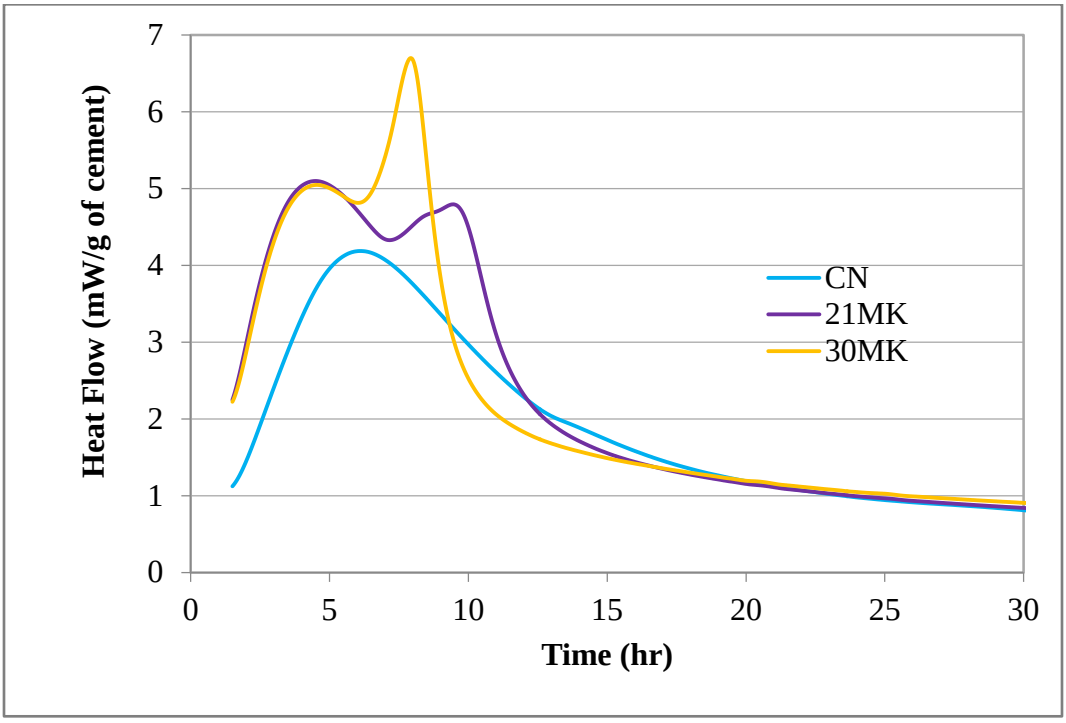

Figure 3-29: Measured Heat Flow of Cement/Metakaolin Pastes Normalized by Mass of Cement

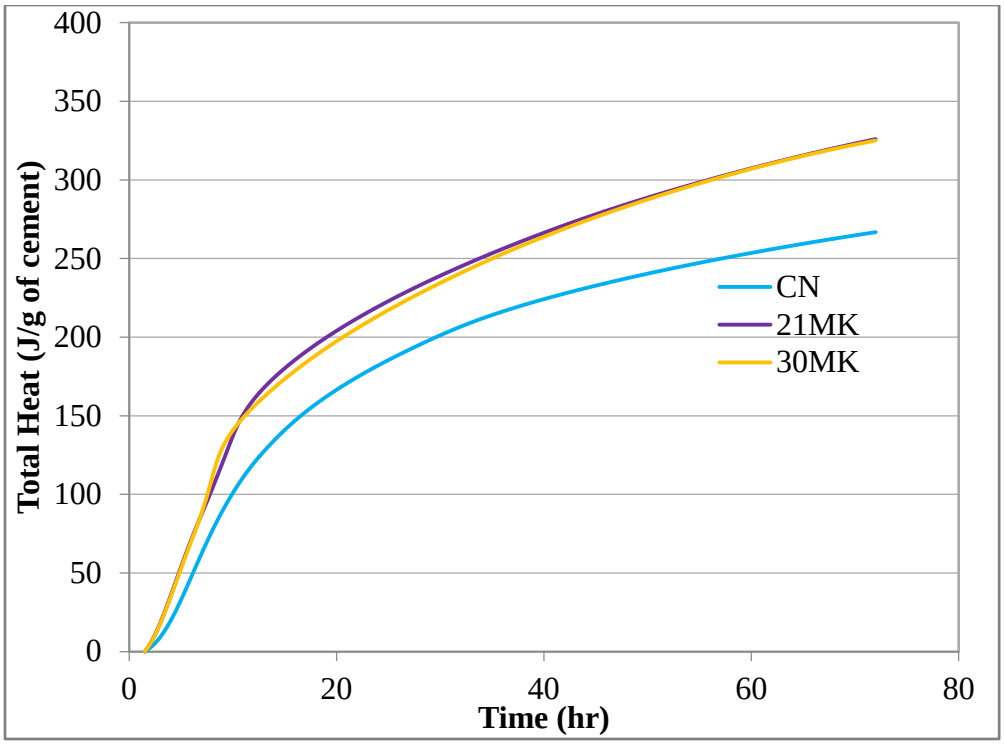

Figure 3-30: Total Heat of Cement/Metakaolin Pastes Normalized by Mass of Cement

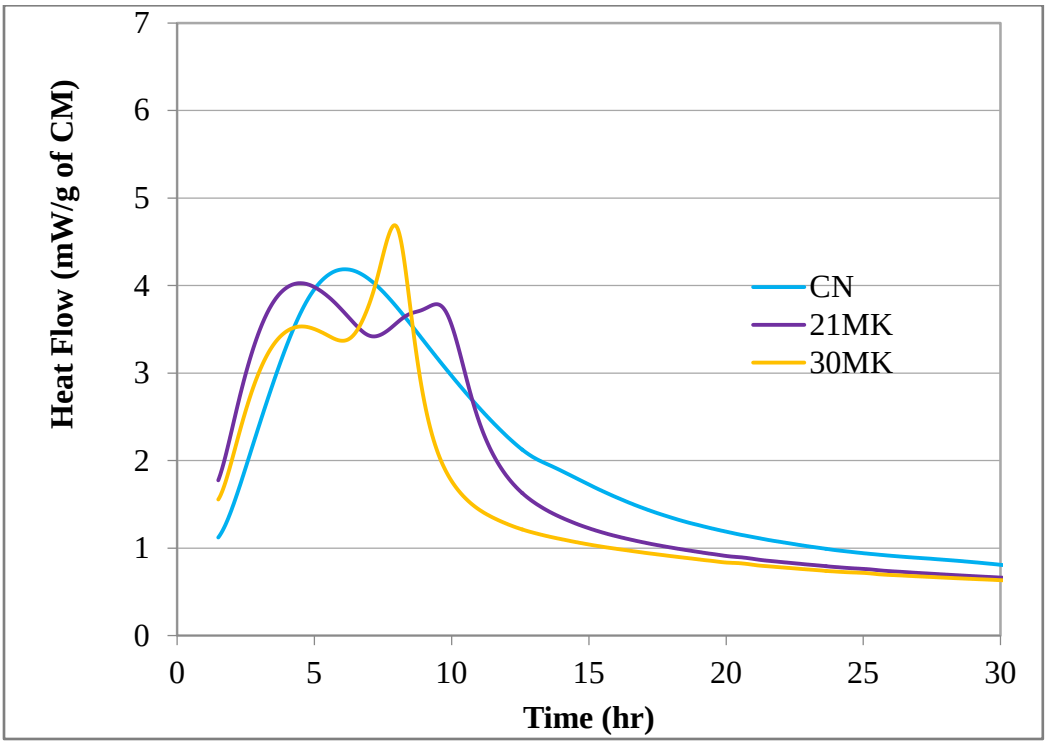

Figure 3-31: Measured Heat Flow of MK Normalized by Mass of Cementitious Materials

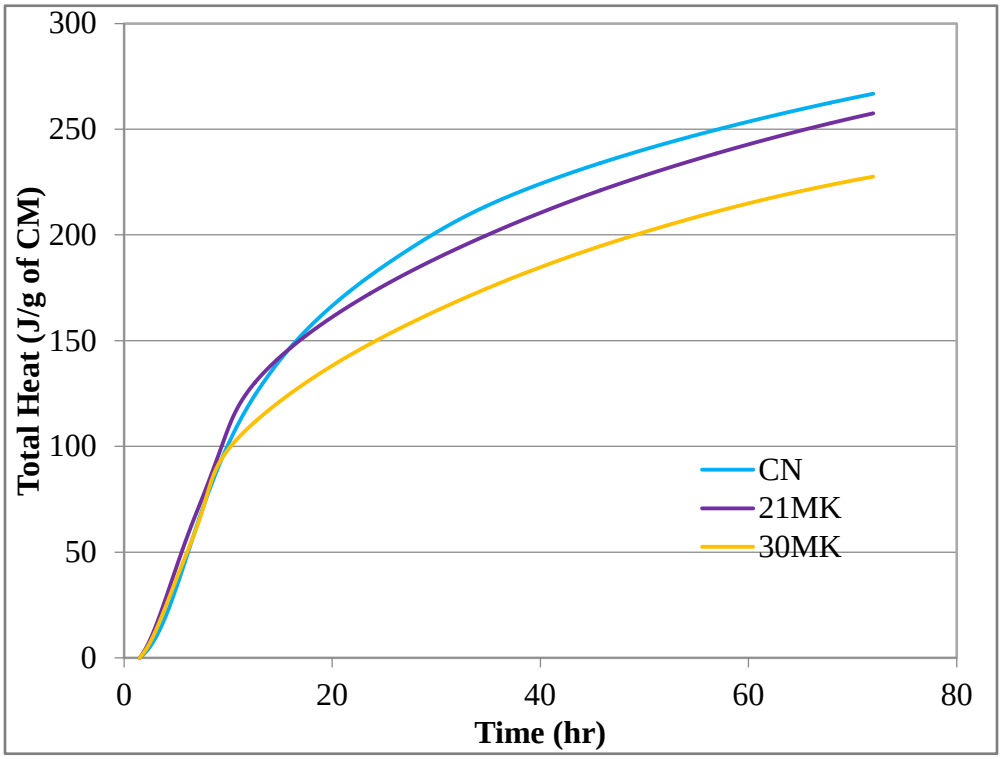

Figure 3-32: Total Heat of MK Normalized by Mass of Cementitious Materials

[redacted]Chemical Admixtures

In the case of cement-chemical admixture combinations, the retarding effect of all the chemical admixtures observed with internal mixing was reduced when external mixing protocol was used (Figure 3-33). As a result, AE addition had no effect on cement hydration, while the largest retardation of the main hydration peak was observed in the case of SP1. The greater effect of SP1 compared to SP2 was not surprising as SP1 is more concentrated than SP2. The magnitude of the main hydration peak was the same for all mixtures, which was not the case when internal mixing was used. In addition to retarding the main hydration peak, WR, SP1, and SP2 accelerated the sulfate depletion point.

In terms of the total heat (Figure 3-34), the trends are the same with both internal and external mixing. AE and WR did not have a significant effect on the total heat of hydration up to 7 days; however, additions of SP1 or SP2 decreased the total heat compared to the rest of the mixes up to approximately 15 hours, after which the total heat generated exceeded the other mixes. At 7 days, the heat evolved by SP1 and SP2 mixtures was higher by approximately 17 J/g of cement.

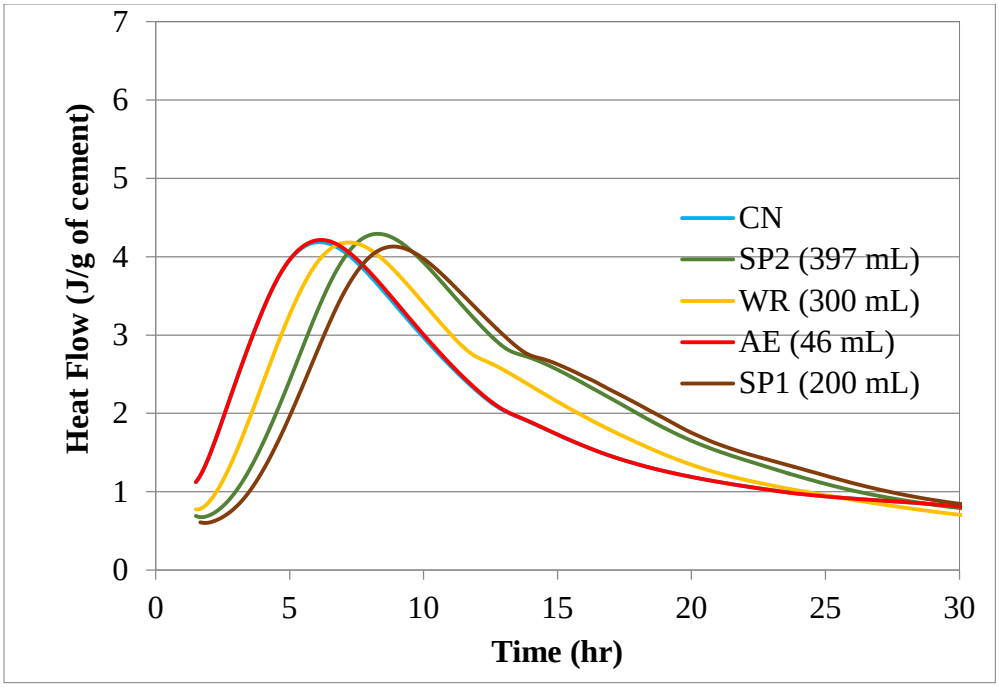

Figure 3-33: Heat Flow (External Mixing) of Chemical Admixture Pastes Normalized by Mass of Cement

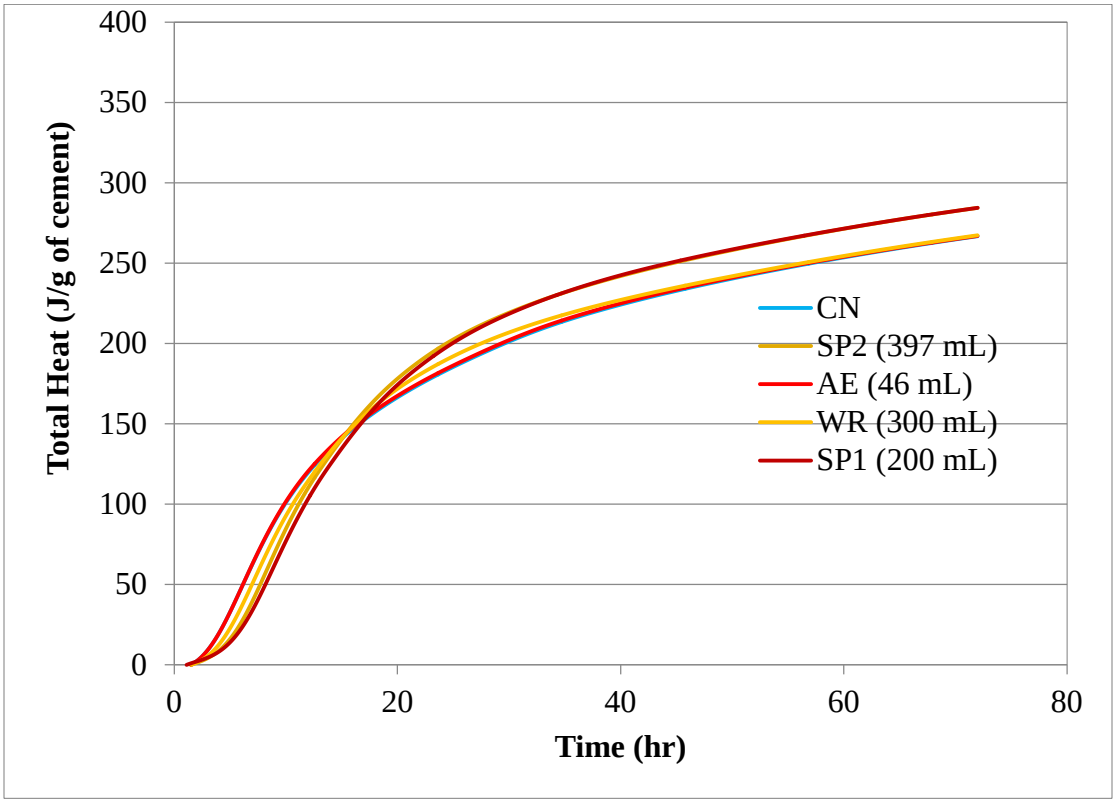

Figure 3-34: Measured Total Heat (External Mixing) of OPC and OPC/Chemical Admixture Pastes Normalized by Mass of Cement

In addition, the combination of all chemical admixtures was evaluated for cement pastes with no mineral admixtures. It is interesting to note that when WR and AE, or WR, AE and SP1 (A1) or WR, AE and SP2 (A2) are combined together, the heat flow of the system is very similar to that of cement and WR alone as can be seen in Figure 3-35. This suggests that the effect of WR dominates over the other admixtures.

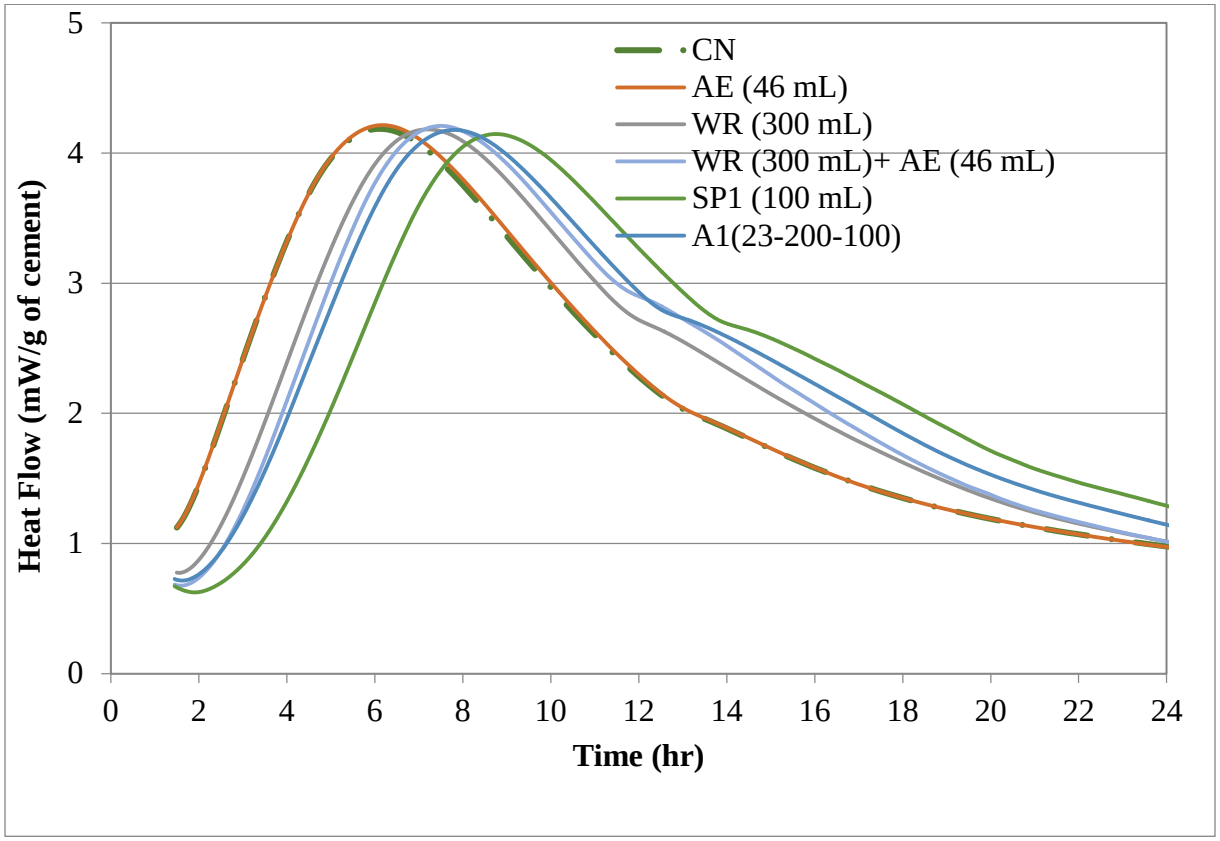

Figure 3-35: Effect of Chemical Admixtures and Their Combinations on Measured Heat Flow Normalized by Mass of Cement

Conclusions

Based on the observed heat flow and total heat trends from isothermal calorimetry, it can be concluded that addition of FA or SL resulted in a slight retardation of the main hydration peak, which could indicate a delay in setting time. No delay in setting time was noted with additions of SF or MK. Since both SL and MK accelerated the occurrence of the sulfate depletion point and increased the magnitude of the aluminate peak, these mixtures may become undersulfated at higher temperatures or in combination with other mineral or chemical admixtures that also accelerate

sulfate depletion. External mixing showed that addition of SF, above 10%, also affected the sulfate depletion point, accelerating both its timing and magnitude.

From the heat flow measurements, the slope of the total heat curve, beyond 6 days, was highest for MK and SL mixtures, indicating that their contribution to heat generation will continue to rise beyond 7 days. This, together with the increase in the aluminate reaction with SL and MK addition, can lead to higher temperatures in concrete mixtures subjected to adiabatic conditions.

Additions of chemical admixtures are likely to delay the setting time, as indicated by initial retardation of cement hydration. The longest setting time retardation is expected with SP1 addition, and the shortest retardation, if any, with addition of AE. WR, SP1, and SP2 additions affected the sulfate depletion point. Combinations of WR, SP1, or SP2 with MK or SL may further affect the sulfate balance and increase the temperature sensitivity of the hydrating system. It should be noted that trends obtained from internal and external mixing were not always the same, especially in the case of chemical admixtures. Therefore, caution should be taken with respect to drawing conclusions on concrete compressive strength from isothermal calorimetry tests.

[redacted] HOH of Ternary Combinations of Portland Cement with Chemical and Mineral Admixtures

[redacted] Introduction

One of the objectives of this study was to evaluate the effect chemical and mineral admixture combinations on cement hydration through monitoring heat evolution data obtained from isothermal calorimetry. Since it was not possible to evaluate all possible mineral and chemical admixture combinations that are used in the field, admixture interactions were evaluated through the use of factorial experimental deign. Factorial designs are commonly used to identify significant factors and factor interactions using the smallest number of experiments [187]. In concrete research, factorial designs have been previously used for mix design optimization [188]–[196], prediction of shrinkage cracking [197], and compressive strength modeling [194], [198], [199]. In a factorial design experiment, all the factors are varied together, which enables the researcher to identify factor (in this case admixture) combinations that fail to "produce the same effect on the response at different levels of another factor" [187]. In other words, if two admixtures added to cement do not interact with each other, their effect on cement hydration and heat evolution is expected to be additive, while an admixture interaction will produce an effect on heat flow that cannot be predicted by adding the effects of individual components of the mixture.

[redacted] Methodology

[redacted] Heat of Hydration Measurements

Heat of hydration measurements were performed following Method B, external mixing, of ASTM C1702 [165]. Heat flow measurements with external mixing protocol were performed using iCal-8000 calorimeter produced by Calmetrix. All the measurements were performed at the isothermal temperature of 23°C for 72 hours. Water-to-binder (w/b) ratio was maintained at 0.485 for all the mixtures.

The paste was mixed, following the procedure described by Muller et al. [166] with an IKA WERKE mixer using the kitchen blade accessory, for a total of 7 min. WR was added to the mixing water. After combining water and cementitious materials, the paste was mixed for 1 minute prior to addition of AE, after which it was mixed for an additional 2 minutes (elapsed time: 3 min). The mixture was then rested for 2 minutes (Elapsed time: 5 min). After the rest period,

superplasticizer was added to the mixture, and the sample was mixed for an additional 2 minutes (elapsed time: 7 min) at 1200 rpm, rather than the 2000 rpm reported by Muller et al. [166].

Factorial Design

Factorial design was used to identify admixture combinations that do not have an additive effect on hydration measured via isothermal calorimetry. Seven admixtures (factors) were identified for this study: Class F fly ash, silica fume, metakaolin, slag, AE, WR and SP1. The dosages of each chemical and mineral admixture are listed in Table 4-1. SP1 was selected over SP2 because SP1 has a higher concentration of the active chemical. Initially, a fractional factorial design was used to evaluate the effects of admixture combinations, at two dosages or levels (α=1 where α is the distance from the center point of the design to the closest factorial point), on heat of hydration. The fractional factorial design matrix is listed in Table 4-2. This was a resolution III design, which means that the effect of each factor could not be separated from the effect of two-factor interactions. In order to improve the resolution, axial points and a center point were added to create a central composite design (CCD) with α=2 (Table 4-4). One run was performed for each mixture, except for the center point, where two runs were performed to assess the error associated with experimental results. The CCD was a resolution IV design, in which the main effects were not compounded with any two-factor interactions, but the two-factor interactions were compounded with each other. Additionally, since the CCD uses three levels of each factor, it can be used to assess whether or not the response changes linearly with changing the factor level. All the experimental designs were created using JMP software from SAS.

Table 4-1: Experimental Design Addition Levels

Design Level	**2**	**1**	**0**	**-1**	**-2**
FA (weight %)	40%	30%	20%	10%	0%
SF (weight %)	20%	15%	10%	5%	0%
MK (weight %)	20%	15%	10%	5%	0%
SL (weight %)	40%	30%	20%	10%	0%
AE (ml/100 kg cement)	46	34.5	23	11.5	0
WR (ml/100 kg cement)	400	300	200	100	0
SP1 (ml/100 kg cement)	200	150	100	50	0

Table 4-2: Mix Designs for the Fractional Factorial Design Matrix

Mix #	FA	SF	MK	SL	AE	WR	SP1
1	30%	5%	5%	10%	11.5	300	150
2	10%	5%	15%	10%	34.5	300	50
3	30%	15%	5%	10%	34.5	300	50
4	10%	15%	5%	10%	34.5	100	150
5	10%	15%	15%	30%	34.5	100	50
6	10%	5%	5%	10%	11.5	100	50
7	30%	5%	15%	10%	34.5	100	150
8	30%	15%	15%	10%	11.5	100	50
9	30%	5%	5%	30%	34.5	100	50
10	10%	5%	5%	30%	34.5	300	150
11	10%	15%	5%	30%	11.5	300	50
12	30%	15%	5%	30%	11.5	100	150
13	30%	15%	15%	30%	34.5	300	150
14	10%	5%	15%	30%	11.5	100	150
15	30%	5%	15%	30%	11.5	300	50
16	10%	15%	15%	10%	11.5	300	150

Table 4-3: Fractional Factorial Design Matrix

Mix #	FA	SF	MK	SL	AE	WR	SP1
1	1	-1	-1	-1	-1	1	1
2	-1	-1	1	-1	1	1	-1
3	1	1	-1	-1	1	1	-1
4	-1	1	-1	-1	1	-1	1
5	-1	1	1	1	1	-1	-1
6	-1	-1	-1	-1	-1	-1	-1
7	1	-1	1	-1	1	-1	1
8	1	1	1	-1	-1	-1	-1
9	1	-1	-1	1	1	-1	-1
10	-1	-1	-1	1	1	1	1
11	-1	1	-1	1	-1	1	-1
12	1	1	-1	1	-1	-1	1
13	1	1	1	1	1	1	1
14	-1	-1	1	1	-1	-1	1
15	1	-1	1	1	-1	1	-1
16	-1	1	1	-1	-1	1	1

Table 4-4: Mix Designs for the Additional Axial Points Design Matrix

Mix #	FA	SF	MK	SL	AE	WR	SP1
17	40%	10%	10%	20%	23	200	100
18	0%	10%	10%	20%	23	200	100
19	20%	20%	10%	20%	23	200	100
20	20%	0%	10%	20%	23	200	100
21	20%	10%	20%	20%	23	200	100
22	20%	10%	0%	20%	23	200	100
23	20%	10%	10%	40%	23	200	100
24	20%	10%	10%	0%	23	200	100
25	20%	10%	10%	20%	46	200	100
26	20%	10%	10%	20%	0	200	100
27	20%	10%	10%	20%	23	400	100
28	20%	10%	10%	20%	23	0	100
29	20%	10%	10%	20%	23	200	200
30	20%	10%	10%	20%	23	200	0
31	20%	10%	10%	20%	23	200	100
32	20%	10%	10%	20%	23	200	100

Table 4-5: Additional Axial Points Design Matrix

Mix #	FA	SF	MK	SL	AE	WR	SP1
17	2	0	0	0	0	0	0
18	-2	0	0	0	0	0	0
19	0	2	0	0	0	0	0
20	0	-2	0	0	0	0	0
21	0	0	2	0	0	0	0
22	0	0	-2	0	0	0	0
23	0	0	0	2	0	0	0
24	0	0	0	-2	0	0	0
25	0	0	0	0	2	0	0
26	0	0	0	0	-2	0	0
27	0	0	0	0	0	2	0
28	0	0	0	0	0	-2	0
29	0	0	0	0	0	0	2
30	0	0	0	0	0	0	-2
31	0	0	0	0	0	0	0
32	0	0	0	0	0	0	0

After isothermal calorimetry measurements were performed for all the mixtures listed in Table 4-2 and Table 4-4, the heat flow data was analyzed by JMP software in order to identify significant factor combinations; that is, admixture combinations for which the effect of heat evolution is not additive. After that, several admixture combinations were selected from the list of significant factor combinations and isothermal calorimetry measurements were performed, varying the admixture levels in these combinations in order to verify the results of the factorial design analysis.

Results and Discussion

Interactions of Portland Cement-Admixture Combinations Identified by the Factorial Design

Heat flow curves for axial points representing the high, medium, and low levels of each admixture are presented in Figure 4-1 through Figure 4-14. To illustrate the effect of admixture combinations, heat flow curves for binary combinations of cement and each respective admixture are included in the plots as well.

Portland Cement with SP1

The disadvantage of the "one factor at a time" approach can be clearly be seen in the results obtained for SP1 paste (Figure 4-1). While addition of SP1 to plain cement at the dosage of 200 ml/kg resulted in almost a 3-hour retardation of the main hydration peak and enhancement of the magnitude of the aluminate peak, these effects were not observed in the presence of the mineral and chemical admixtures. Varying the dosage of SP1 did not have a significant effect on cement hydration in the presence of other chemical and mineral admixtures, as evidenced by the heat flow curves for a mix with 200 ml of SP1 (Mix 29) and for a mix without any SP1 (Mix 30). The same effect was observed for the heat flow normalized by the total cementitious material (CM) content (Figure 4-2).

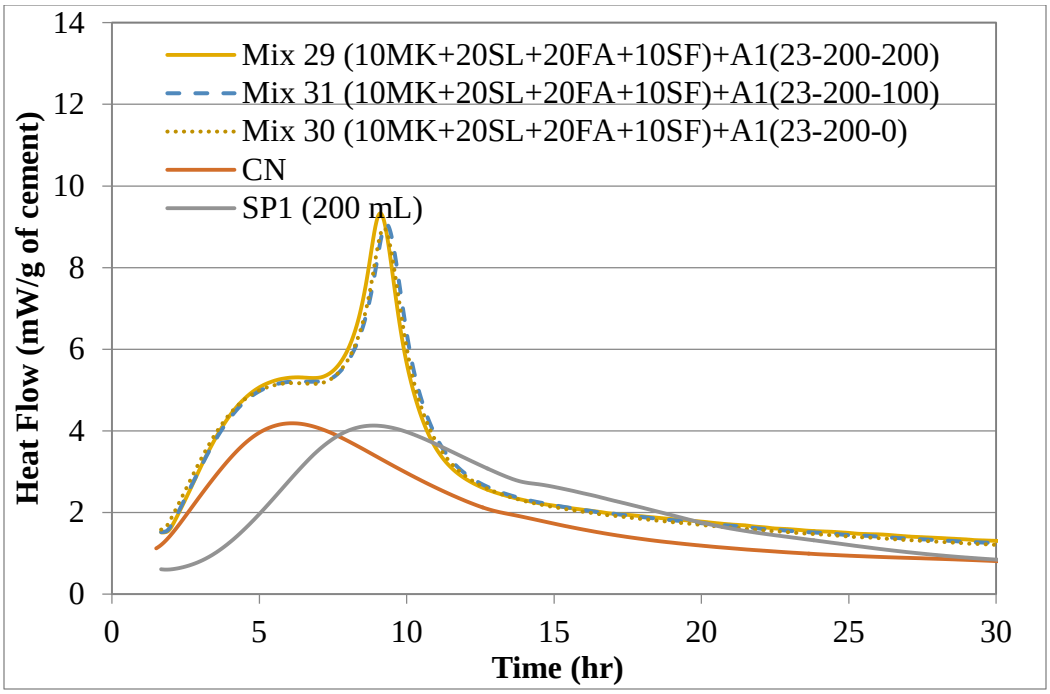

Figure 4-1: Effect of SP1 on Measured Heat Flow Normalized by Mass of Cement, where A1 is the combination of AE, WR and SP1

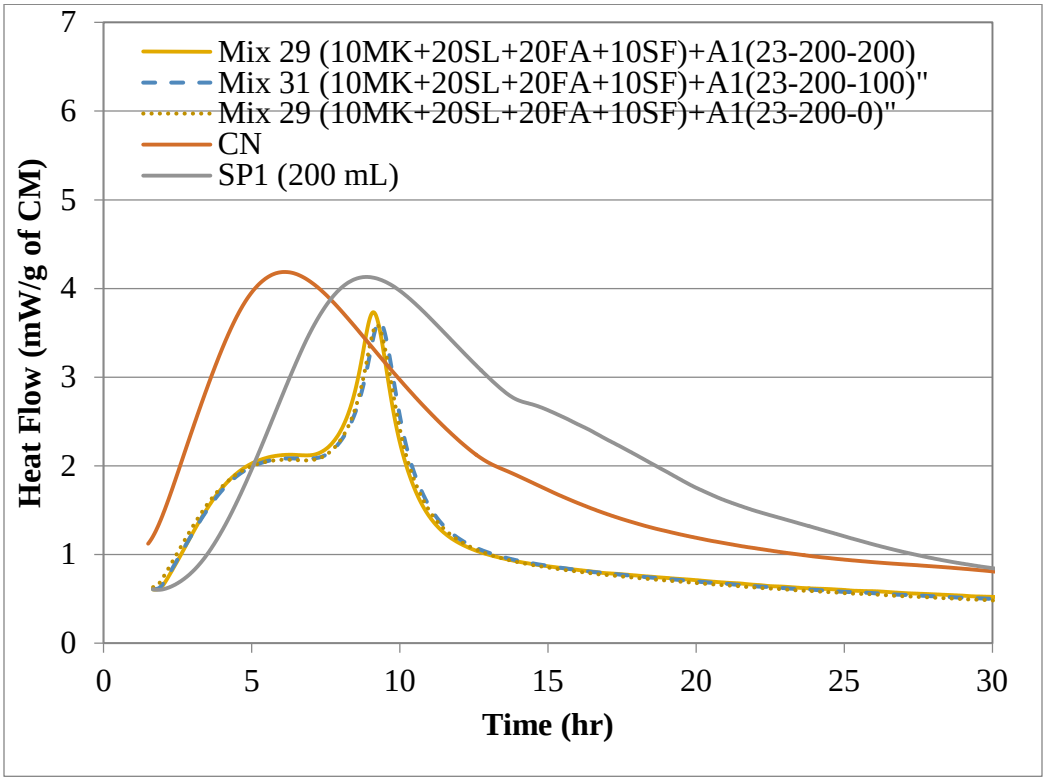

Figure 4-2: Effect of SP1 on Heat Flow Normalized by Mass of Cementitious Materials

[redacted] Portland Cement with AE

As can be seen from Figure 4-3, AE did not have any effect on cement hydration. The heat flow curves for mixes with and without the air entrainer are identical (Mixes 25, 26, 31). This behavior was also observed in the AE paste.

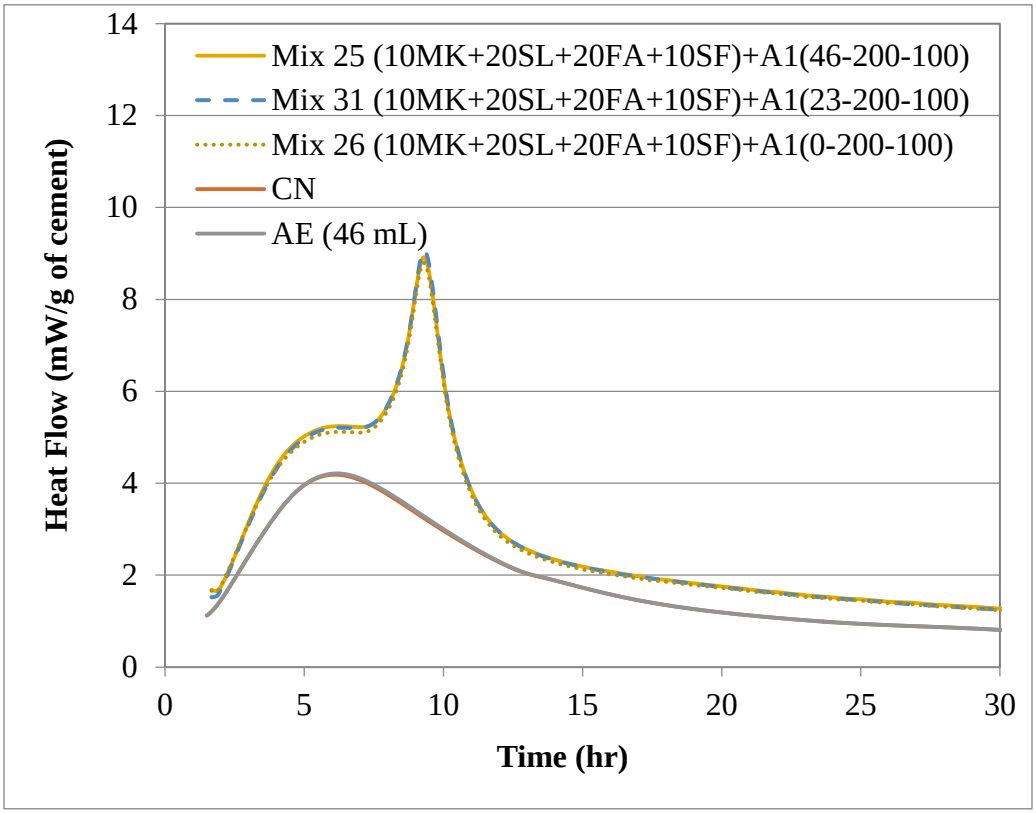

Figure 4-3: Effect of AE on Measured Heat Flow Normalized by Mass of Cement

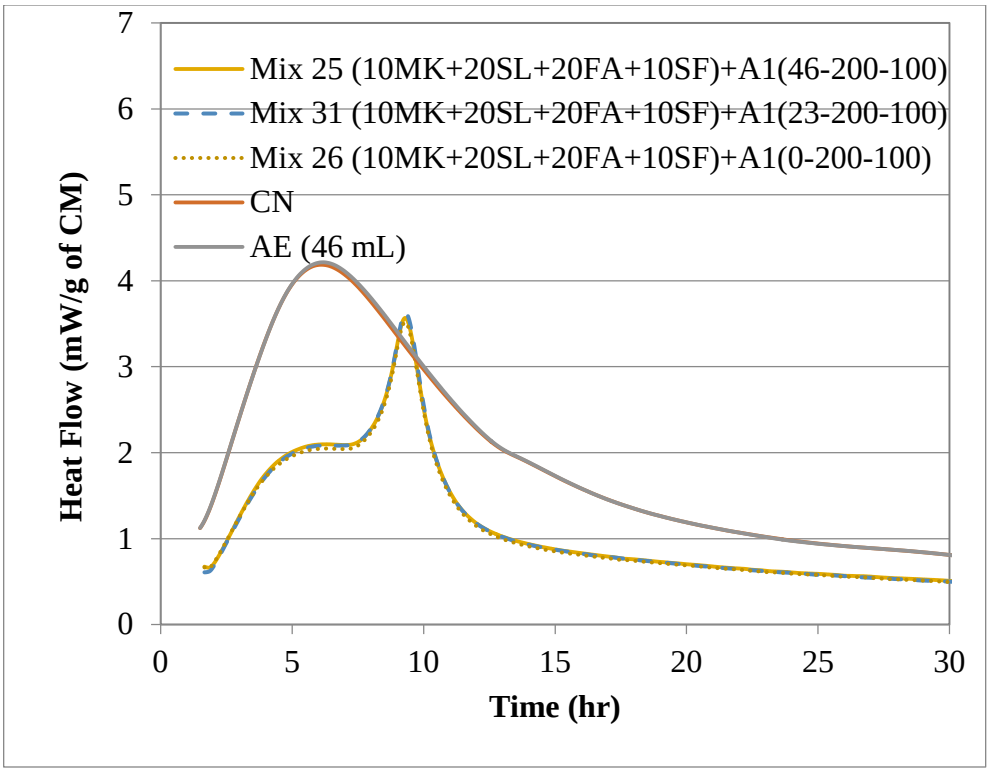

Figure 4-4: Effect of AE on Normalized by Mass of Cementitious Materials

Portland Cement with WR

Addition of WR had a retarding effect on cement hydration both in the binary system (cement and WR alone) and in the presence of other chemical and mineral admixtures (Figure 4-5). It is interesting to note that while addition of WR delayed the occurrence of the silicate hydration peak in both pure cement and cementitious systems, the magnitude of the peak in the pure cement system was not affected, while in the cementitious mixtures the main hydration peak was slightly reduced. The aluminate reaction was enhanced by addition of WR, and this effect was dosage-dependent as can be observed from Mixes 27, 28 and 31. Although an increase in the magnitude of the aluminate peak was also observed for the binary combination of cement and WR, this increase was greater in the presence of other chemical and mineral admixtures.

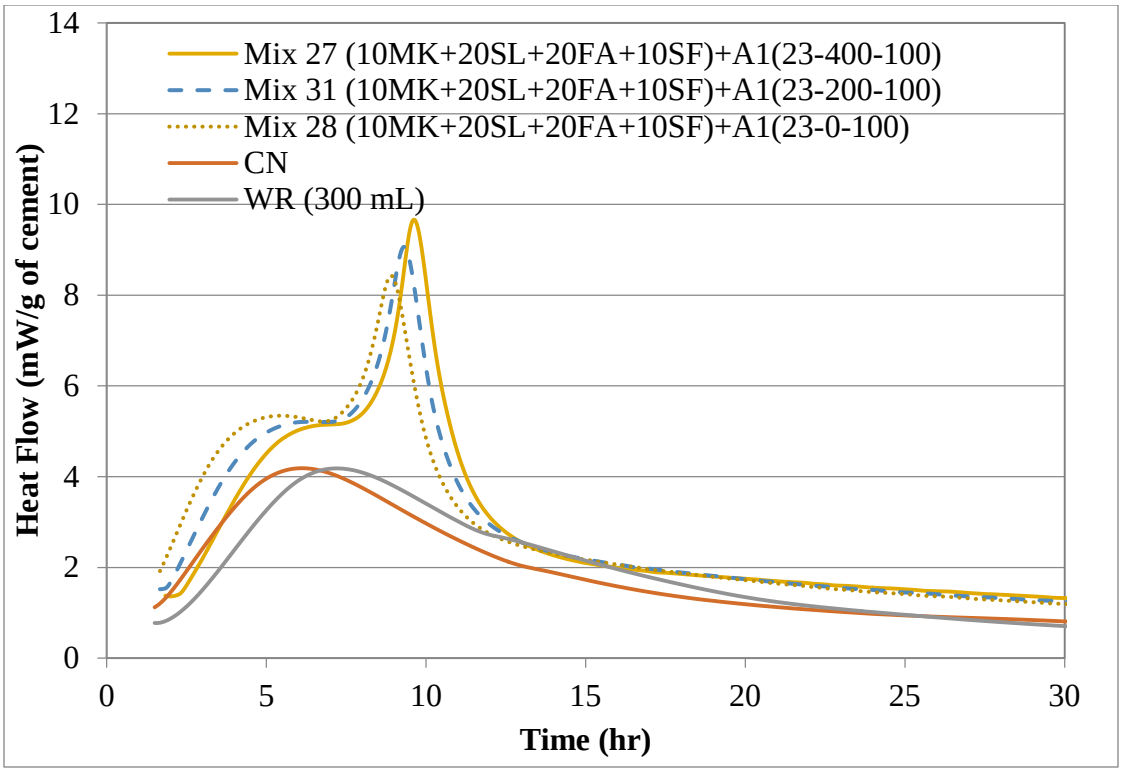

Figure 4-5: Effect of WR on Measured Heat Flow Normalized by Mass of Cement

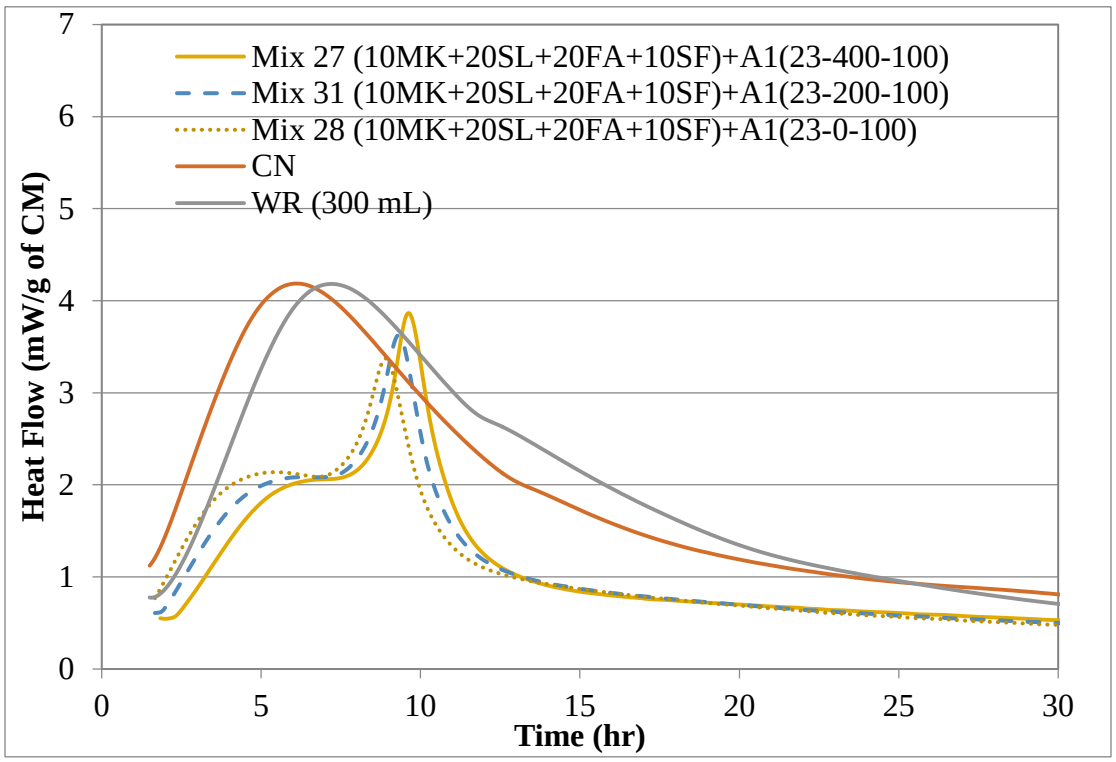

Figure 4-6: Effect of WR on Heat Flow Normalized by Mass of Cementitious Materials

Portland Cement with Fly Ash

In the binary systems, addition of fly ash had minimal effect on both silicate and aluminate hydration. In the presence of other mineral and chemical admixtures, there was a slight acceleration in the hydration of silicates with addition of fly ash (Figure 4-7), although this effect was not dosage dependent and the timing of the main hydration peak was not affected. However, the effect on the aluminate hydration was quite different. Although there was a shift in the aluminate peak to an earlier time, its magnitude increased linearly with fly ash dosage from 5.5 mW/g for cement at 0% FA (Mix 18) to 8.9 mW/g at 20% FA (Mix 31) to 12.2 mW/g at 40 % FA (Mix 17) (Figure 4-7). The acceleration of the aluminate hydration is in line with observations by Dittrich et al. [167] who reported that a 50% FA replacement accelerated C_3A dissolution in OPC.

The fly ash used in this study had a high Al_2O_3 content of 27.46% as determined by XRF. It also had 16.1% mullite ($Al_6Si_2O_{13}$) as determined by XRD, which is known to be non-reactive. However, only 4 % of Al_2O_3 are accounted for by mullite; the rest, most likely, exist in the amorphous form. Although fly ash is expected to be non-reactive at early ages as discussed previously, there is a clear contribution from its presence to the aluminate reaction suggesting that a portion of the aluminates contributed by the fly ash may be participating in the hydration reactions. Heinz et al. [104] reported that addition of triethanolamine (TEA) increases fly ash reactivity by increasing the dissolution rates of iron, calcium and aluminum, which could then explain the observed increase in the aluminate peak. The only admixture containing TEA (based on MSDS sheets) was WR. Possible interaction of WR and fly ash is discussed later.

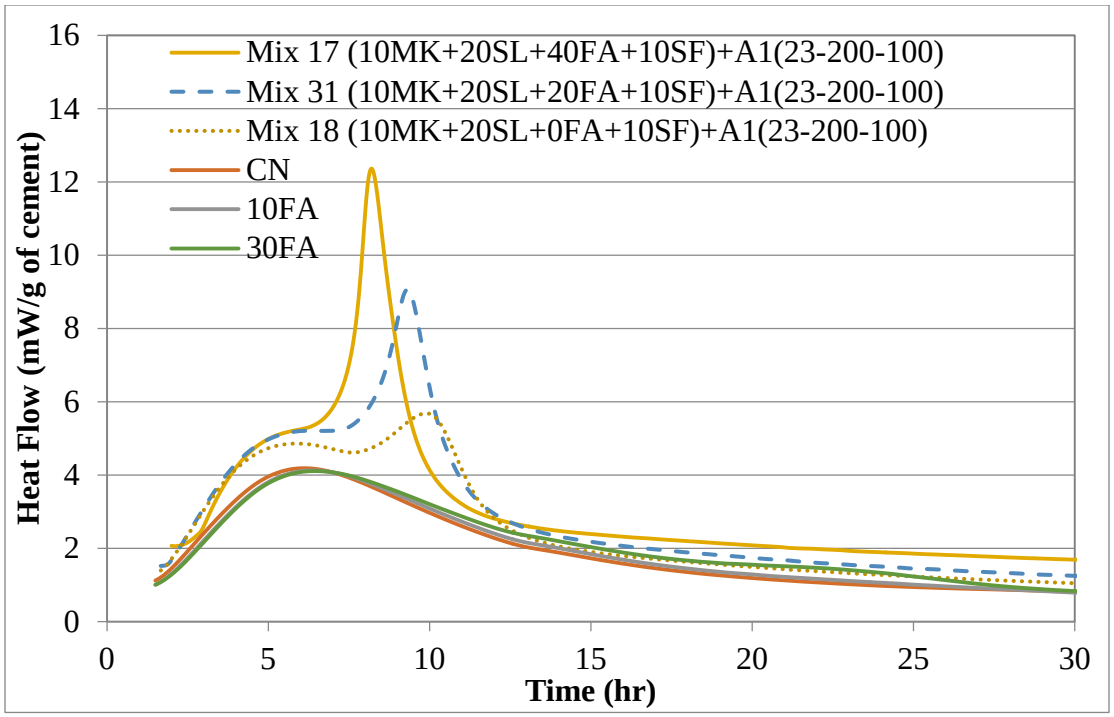

Figure 4-7: Effect of Fly Ash on Measured Heat Flow Normalized by Mass of Cement

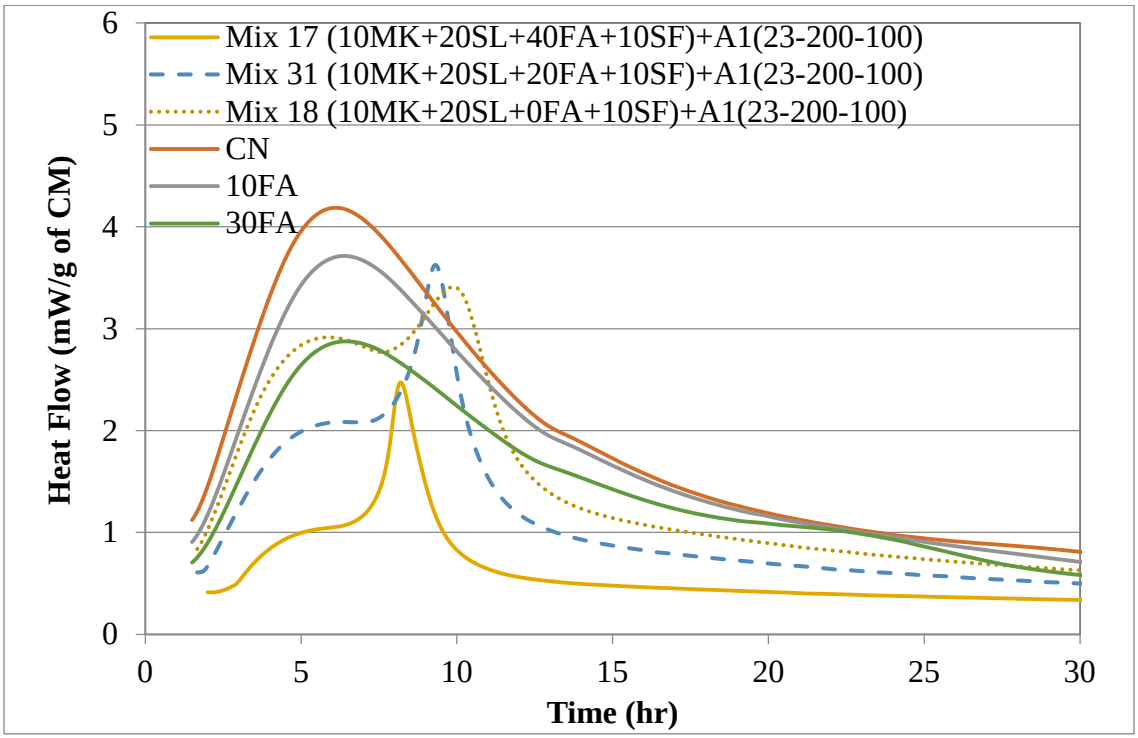

Figure 4-8: Effect of Fly Ash on Measured Heat Flow Normalized by Mass of Cementitious Materials

Portland Cement with Slag

The effect of slag on cement hydration, specifically the aluminate peak, was not linear (Figure 4-9). With increase in the slag content, the magnitude of the peak increased from 4.6 mW/g for cement at 10.5 hours (Mix 24 - 0% slag) to 9 mW/g at 9 hours (Mix 31 - 20% slag), and 11.5 mW/g at 7 hours (Mix 23 - 40% slag). Comparing the heat flow at a specified time, for example at 7 hours, the differences were even more pronounced: heat flow was 4.3 mW/g for mix 24, 5.2 mW/g for mix 31, and 11.5 mW/g for mix 23. As for the silicate peak, addition of slag in the presence of other mineral and chemical admixtures affected its magnitude, but not its timing. Comparing the sample with 20% slag (Mix 31) to the sample with no slag (Mix 24), the magnitude of the main hydration peak was increased by slag addition by 1 mW/g cement, although its timing was not affected. At 40% slag addition, the height of the silicate peak decreased, as it was almost completely overlapped by the aluminate peak. The increase in the aluminate peak is consistent with the results reported by Whittaker et al. [200], who observed acceleration of C_3A hydration with slag addition. Additionally, Brunet et al. [173] observed that silicates and aluminates in slag react at different rates, with aluminates being more reactive. The decrease in the main hydration peak was also not surprising. Lerch [9] established that uncontrolled aluminate reaction slows down C_3S hydration, which was observed in the case of Mix 23. However, it should be reiterated that although the increase in the aluminate peak was observed in the binary systems, its magnitude was significantly lower.

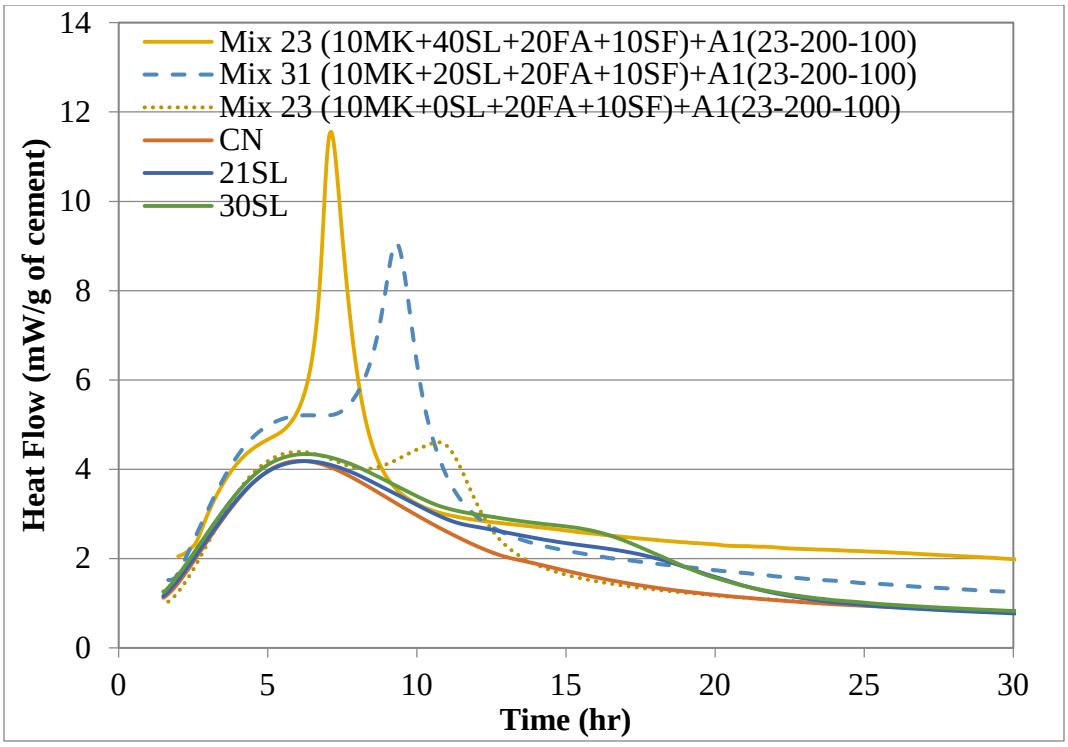

Figure 4-9: Effect of Slag on Measured Heat Flow Normalized by Mass of Cement

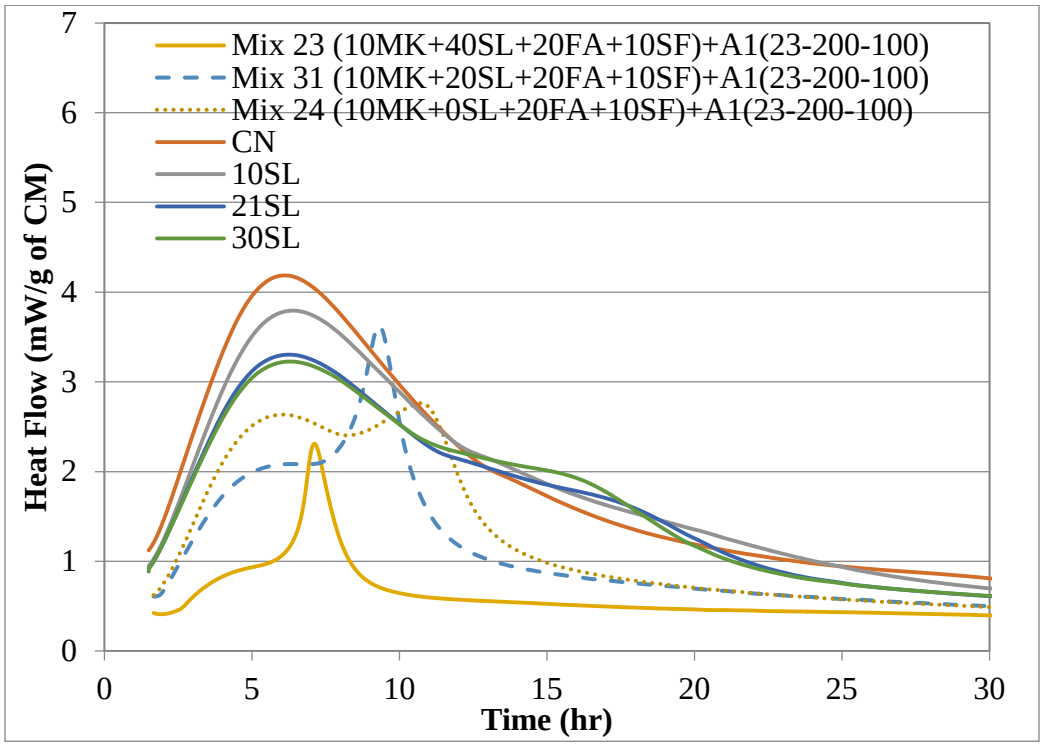

Figure 4-10: Effect of Slag on Measured Heat Flow Normalized by Mass of Cementitious Materials

Portland Cement with Metakaolin

Figure 4-11 shows the influence of MK dosage on heat evolution per gram of cement. An increase in MK dosage from 0% (Mix 22) to 10% (Mix 31) and 20% (Mix 21) resulted in acceleration of C_3S hydration, as evidenced by the monotonic increase in the magnitude of the main hydration peak. The timing of the peak was also accelerated from approximately 6.3 hours with no MK to 5.3 hours with 15% MK, and 4 hours with 30% MK. This behavior is different from that observed in the binary OPC+MK systems. Addition of 21% MK to the control paste accelerated the time of occurrence of the main hydration peak and increased its magnitude; however, further increase of MK content to 30% did not affect the main hydration peak any further.

MK accelerated the time of occurrence of the sulfate depletion point both in the presence of other admixtures and in binary systems, and the magnitude of the aluminate peak was increased. Increasing MK from 0 to 20% (Mixes 22 and 21 and the binary mixes) resulted in 4 to 5 mW/g increase in the magnitude of the sulfate depletion peak.

The alumina-containing crystalline phases in MK were found to be in small amounts (1% mullite and 0.7% illite), leading to the conclusion that the majority of aluminate was amorphous. Talero and Rahhal [201] state that pozzolanic activity of MK depends largely on its amorphous content and on the amount of reactive alumina. As these parameters increase, so does the heat flow generated per gram of cement. Therefore, the increase in the aluminate peak was not surprising.

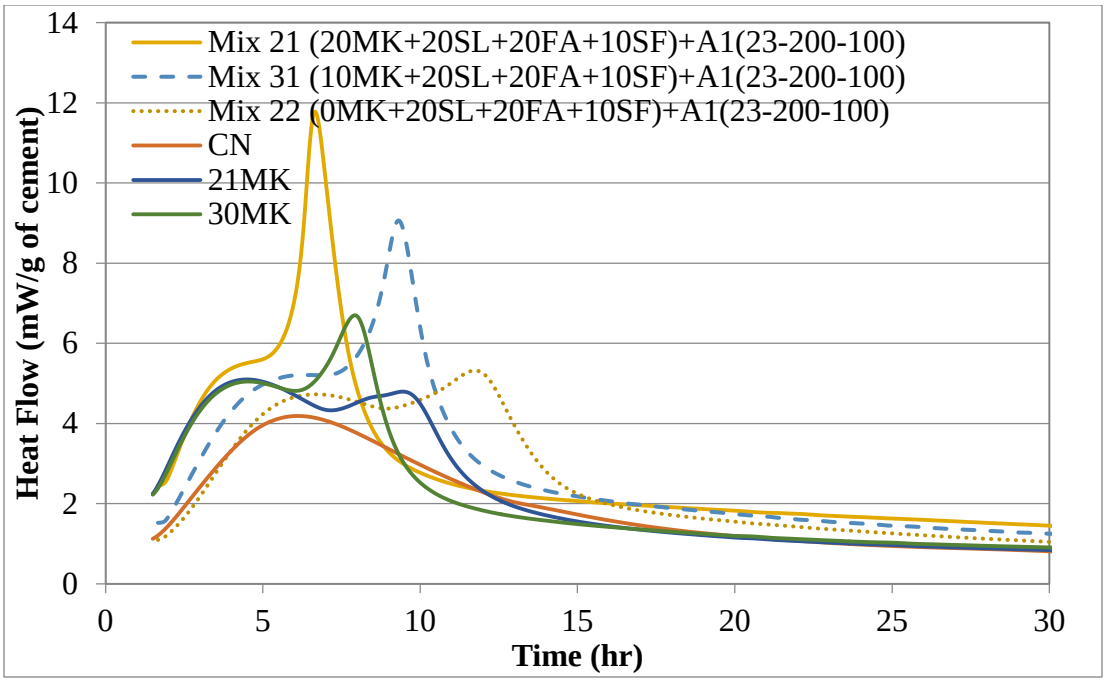

Figure 4-11: Effect of Metakaolin on Measured Heat Flow Normalized by Mass of Cement

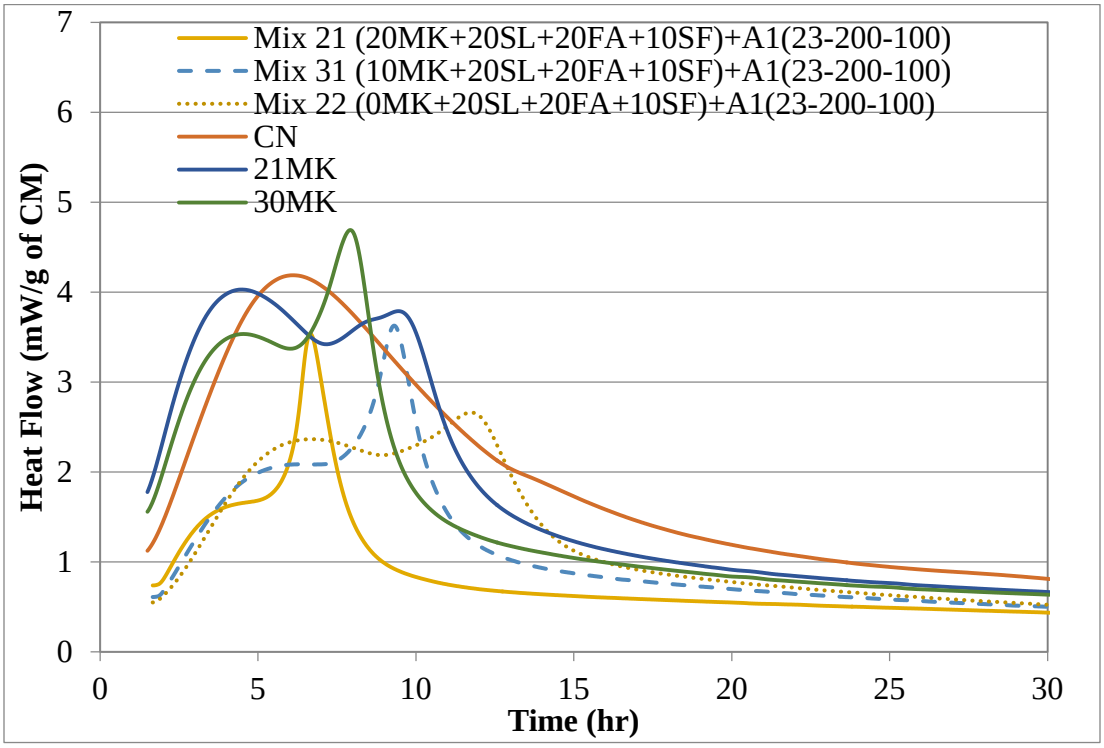

Figure 4-12: Effect of Metakaolin on Measured Heat Flow Normalized by Mass of Cementitious Materials

Portland Cement with Silica fume

Addition of SF slightly increased the magnitude of the silicate peak, and slightly decreased the time of its occurrence (Figure 4-13). This is consistent with the effect observed in the binary OPC+SF mixtures. The acceleration of the aluminate reaction, however, was more pronounced in the presence of other mineral and chemical admixtures. Although there was only a slight shift to the left in the timing of the peak, there was a notable increase in its magnitude, and the effect of the dosage was non-linear. In the absence of SF (Mix 20), the aluminate peak intensity was approximately 6 mW/g, which increased to 9 mW/g when 10% SF was added (Mix 31). With addition of another 10% SF (Mix 19) the peak increase was much smaller, only 1 mW/g. Acceleration of C_3S and C_3A hydration has been demonstrated in the literature [89], [90]; however, it is still unclear whether this is due to the "filler" effect [93] or reaction of SF itself at very early ages [88].

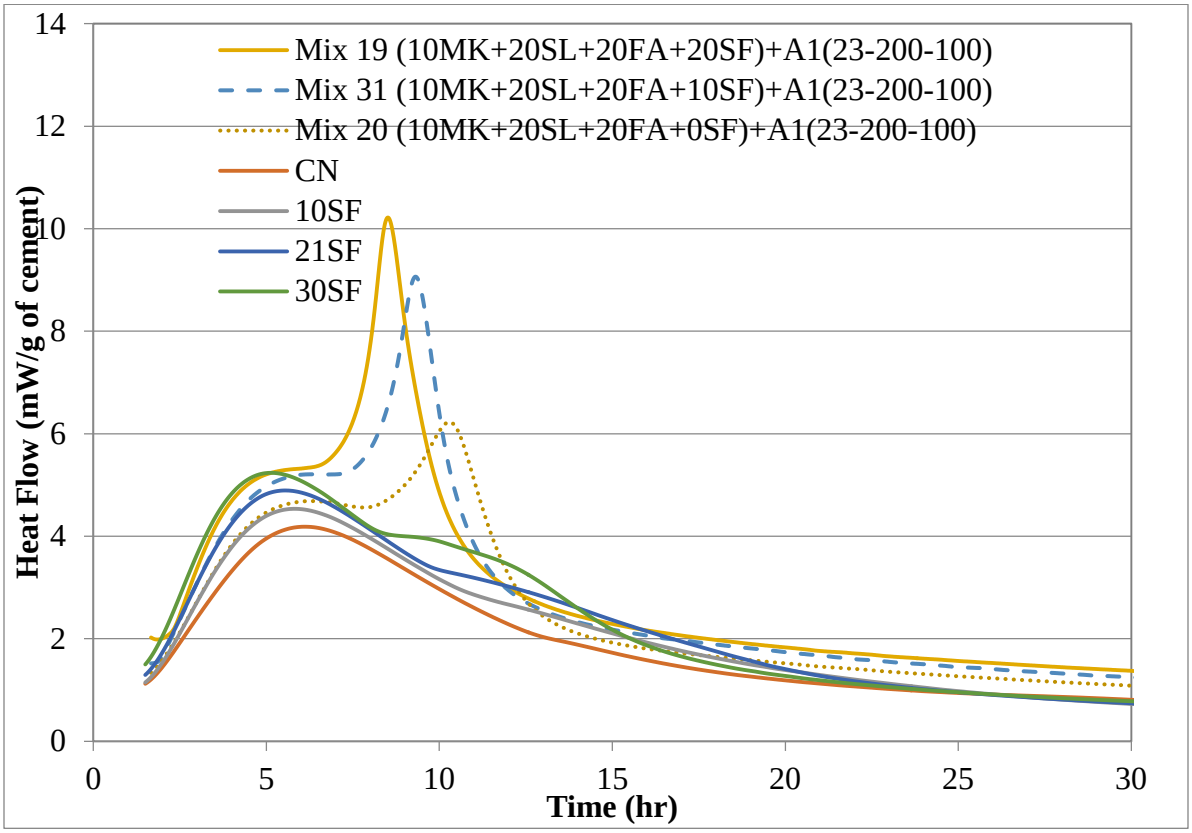

Figure 4-13: Effect of Silica Fume on Measured Heat Flow Normalized by Mass of Cement

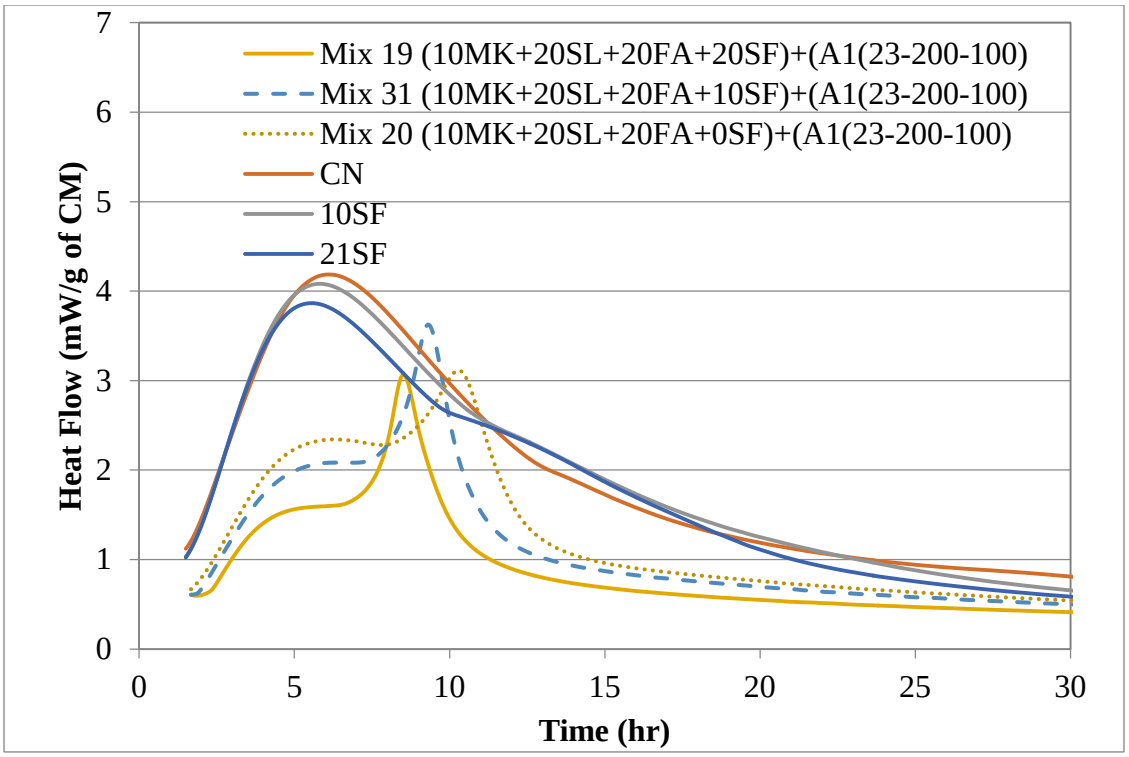

Figure 4-14: Effect of Silica Fume on Measured Heat Flow Normalized by Mass of Cementitious Materials

Identification of Two-Factor Interactions Exhibiting Non-Additive Behavior

The results illustrate that the effect of different admixture combinations, with exception of AE, on cement hydration and heat flow, changes depending on the nature of the constituents of the mixture combination. In general, significant changes observed in the heat flow, especially in the aluminate peak, point to the existence of non-additive admixture interactions.

Heat flow measurements, normalized by mass of cement and by mass of total cementitious materials for the 32 mixtures measured in the factorial design, were analyzed to identify significant two-factor interactions (admixture combinations) that exhibited this non-additive behavior. The results are listed in Table 4-6.

Table 4-6: Significant Two-Factor Interactions Identified by Factorial Design

Response variable	99% probability	95% probability	90% probability
Heat flow (mW/g cement)	MK*SL FA*SL SF*SL FA*SP1 MK*WR FA*SF MK^2*AE SL*WR WR*AE	FA*WR MK*SF	SF*WR SF*AE FA*AE SL*AE MK*FA WR*SP1
Heat flow (mW/g cementitious)	MK*SL FA*SL FA*SF MK*SP1	MK*SF SL*AE SF*WR SF*SL MK*FA	

[redacted] Verification of Factorial Design Results – Admixture Combinations

Several admixture combinations identified in Table 4-6 were selected for further study in order to verify the results of the factorial design analysis. The following combinations were selected: fly ash and slag, fly ash and metakaolin, fly ash and silica fume, metakaolin and slag, and fly ash and WR. These combinations are frequently used by the FDOT in structural concrete mixes and they have all been identified by the factorial design analysis as significant at the confidence level of either 95 or 99%.

[redacted]Fly Ash and Slag

Figure 4-15 shows the effect of cement replacement with FA-SL combinations. While the main hydration peak remained largely unaffected with varying percentages of fly ash and slag, except in the case of the 30FA+52SL combination, the magnitude of the aluminate peak increased with increase in slag and fly ash contents. This also accelerated the timing of its occurrence. When 20% FA was added to the 20% SL mixture, the aluminate peak became clearly defined, with its maximum occurring at approximately 16 hours. When an additional 20% was added (40FA+20SL mixture), the aluminate peak shifted further to the left by 2 hours and its magnitude increased by 1 mW/g of cement. The same result was achieved by a 10% increase in the slag content of the 20FA+20SL mixture. When the slag content was further increased to 52%, at a fly ash replacement

level of 30%, the aluminate peak shifted further to the left, almost overlapping the silicate peak, and its magnitude increased to 9 mW/g. Clearly, there is inadequate amount of sulfate ions in this system for the proper control of the aluminate reaction. Based on Lerch's work [9], this mix can be expected to have reduced compressive strength. The increase in the aluminate peak was not surprising, as both slag and fly ash contain alumina (14.25 and 27.46% respectively). As discussed previously, most of the alumina in the fly ash can be assumed to be amorphous. The same assumption can be made for slag since the only alumina-containing crystalline phase (melilite) was quantified by XRD to be at 1.3%.

Addition of chemical admixtures did not have a significant effect on the magnitudes of the silicate and aluminate hydration peaks. There was a slight delay in the main hydration peak, which is consistent with the retarding effect of WR observed in cement pastes. The acceleration of the aluminate peak may be due to increased fly ash dissolution caused by WR addition. Since the fly ash used in this project had a high alkali content, accelerated dissolution of fly ash by WR would release more alkalis into solution, which in turn would accelerate slag hydration.

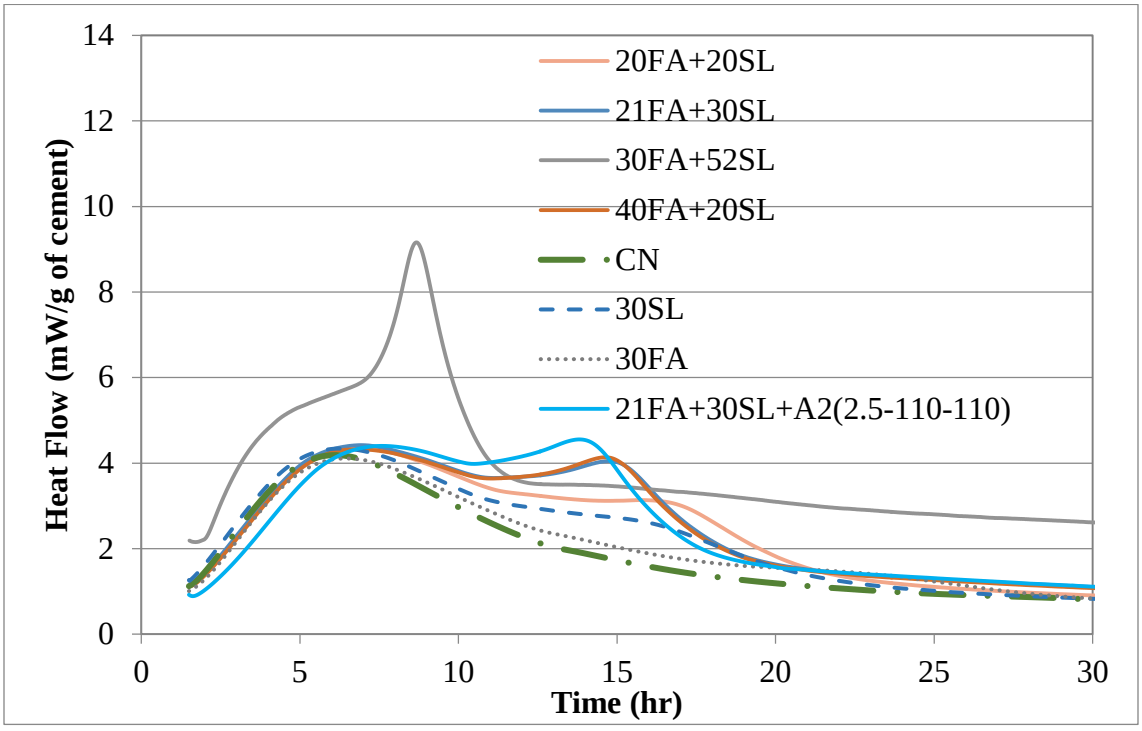

Figure 4-15: Effect of Fly Ash and Slag Interaction on Measured Heat Flow Normalized by Mass of Cement

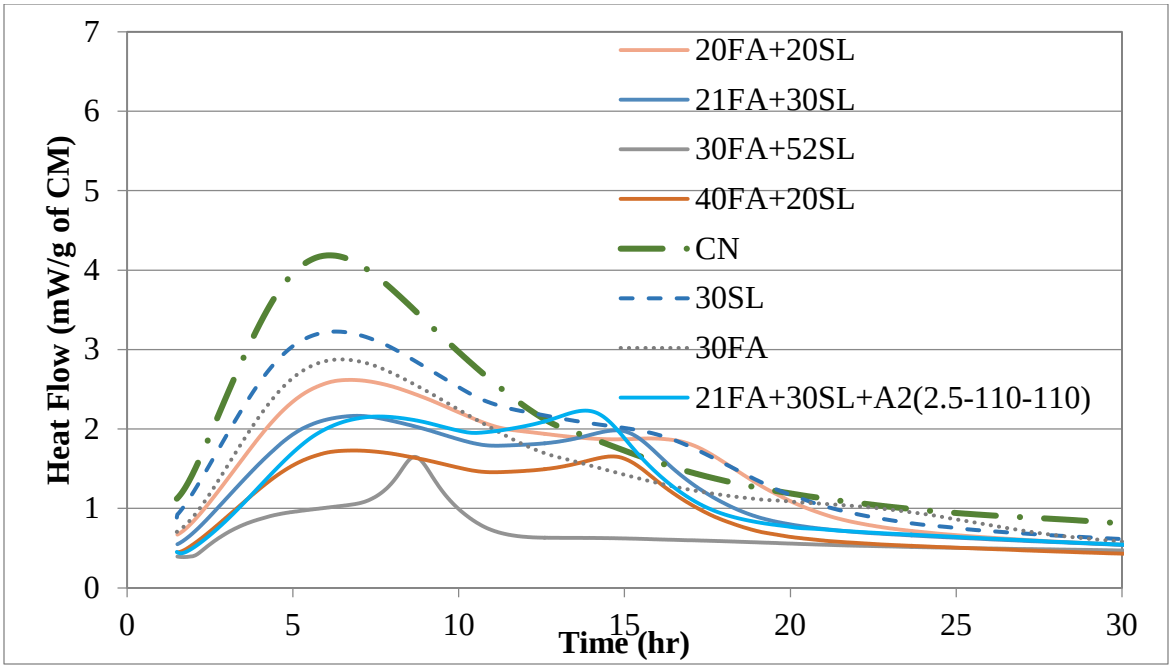

Figure 4-16: Effect of Fly Ash and Slag Interaction on Measured Heat Flow Normalized by Mass of Cementitious Materials

[redacted]Fly Ash and Metakaolin

As can be seen from Figure 4-17, the combination of FA and MK had a significant effect on the magnitude and timing of the aluminate peak. An increase in FA to 40% did not affect the silicate peak, although the aluminate peak increased to 5 mW/g, so an increase of 20% in the FA content of this ternary mixture resulted in a 1 mW/g increase in the magnitude of the aluminate peak. An increase in MK content (20%) dramatically accelerated the aluminate hydration as can be evidenced by the increase in the magnitude and decrease in the timing of the aluminate peak. A 10% increase in MK content shifted the aluminate peak to the left by 4 hours and increased the peak height by 4 mW/g of cement.

Addition of chemical admixtures to fly ash/metakaolin/cement mixtures retarded the main hydration peak and accelerated the aluminate peak, same as in the fly ash/slag/cement systems (Figure 4-15). Both the retarding and accelerating peak shifts are approximately 1 hour forward.

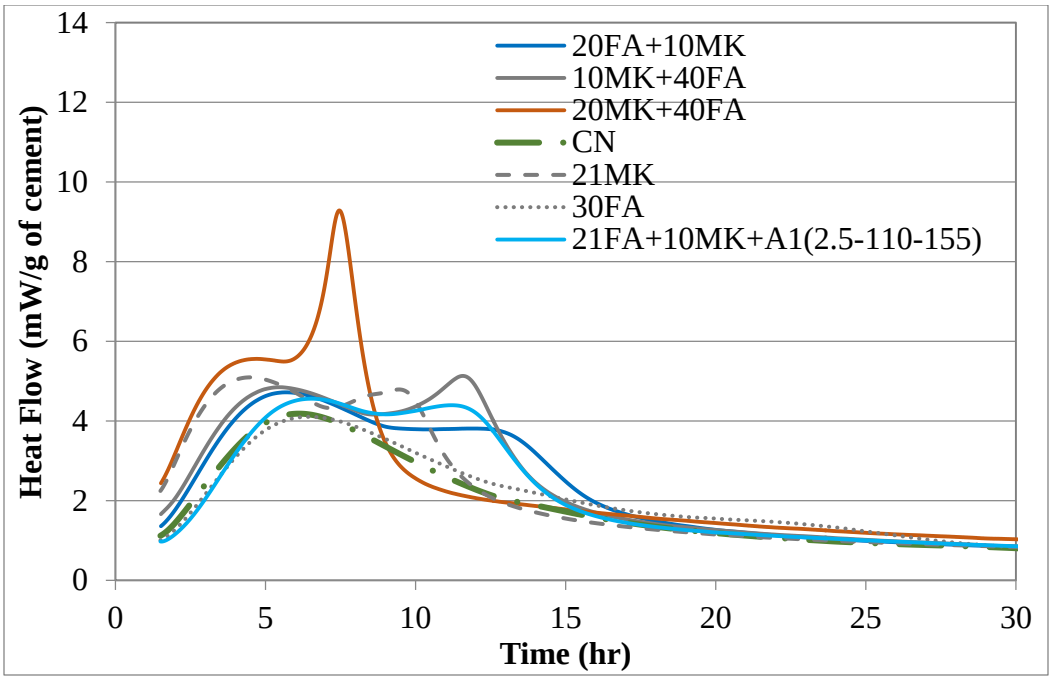

Figure 4-17: Effect of Fly Ash and Metakaolin Interaction on Measured Heat Flow Normalized by Mass of Cement

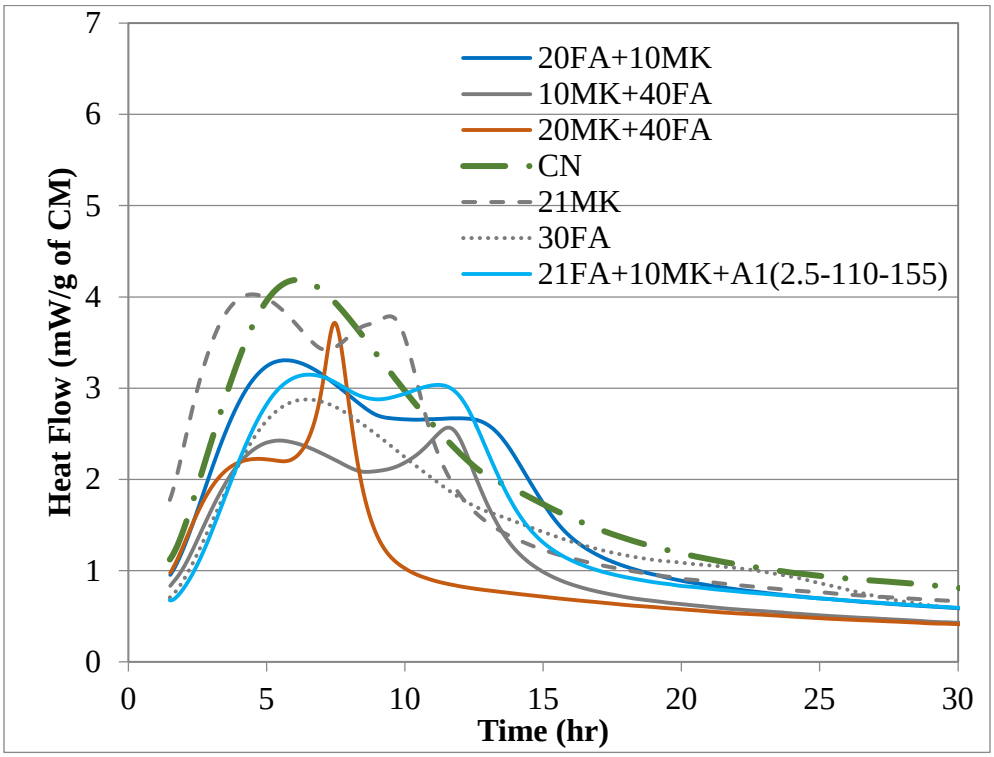

Figure 4-18: Effect of Fly Ash and Metakaolin Interaction on Measured Heat Flow Normalized by Mass of Cementitious Materials

[redacted]Fly Ash and Silica Fume

When a small quantity of silica fume (8%) was added to cement with 21% fly ash replacement, the heat flow showed a slight enhancement of the silicate hydration peak (peak broadening), with a greater effect on the aluminate reaction (Figure 4-19). Effect of admixtures in the fly ash/silica fume/cement systems on silicate hydration was less pronounced than in the ternary systems considered previously. There was no significant delay in the occurrence of the main hydration peak, most likely due to better dispersion of silica fume particles, which would accelerate silicate hydration through nucleation seeding. As in the previous ternary systems, the aluminate reaction was accelerated, and the sulfate depletion point shifted to the left by approximately 1 hour.

With addition of equal quantities of FA and SF, silica fume had a dominant effect on silicate hydration. The main hydration peaks for 20FA+20SF and 30FA+20SF mixes were almost identical to those of the binary 21SF mix. The magnitude of the aluminate peak, however, increased with increasing FA content. A 10% increase in fly ash increased the aluminate peak height by approximately 0.5 mW/g of cement.

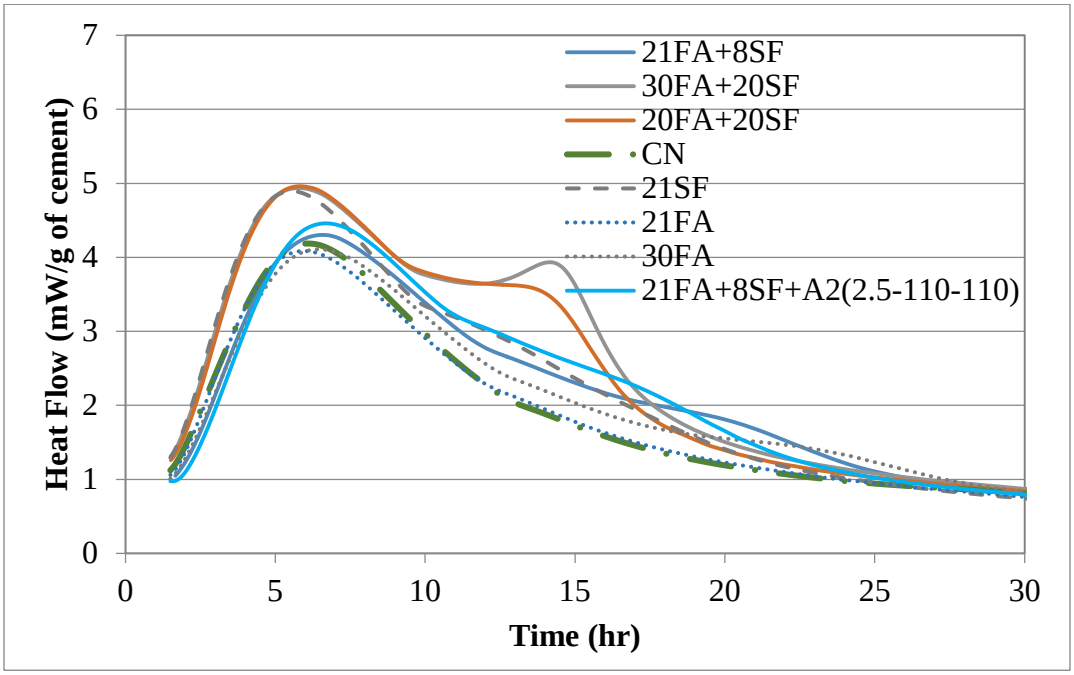

Figure 4-19: Effect of Fly Ash and Silica Fume Interaction on Measured Heat Flow Normalized by Mass of Cement

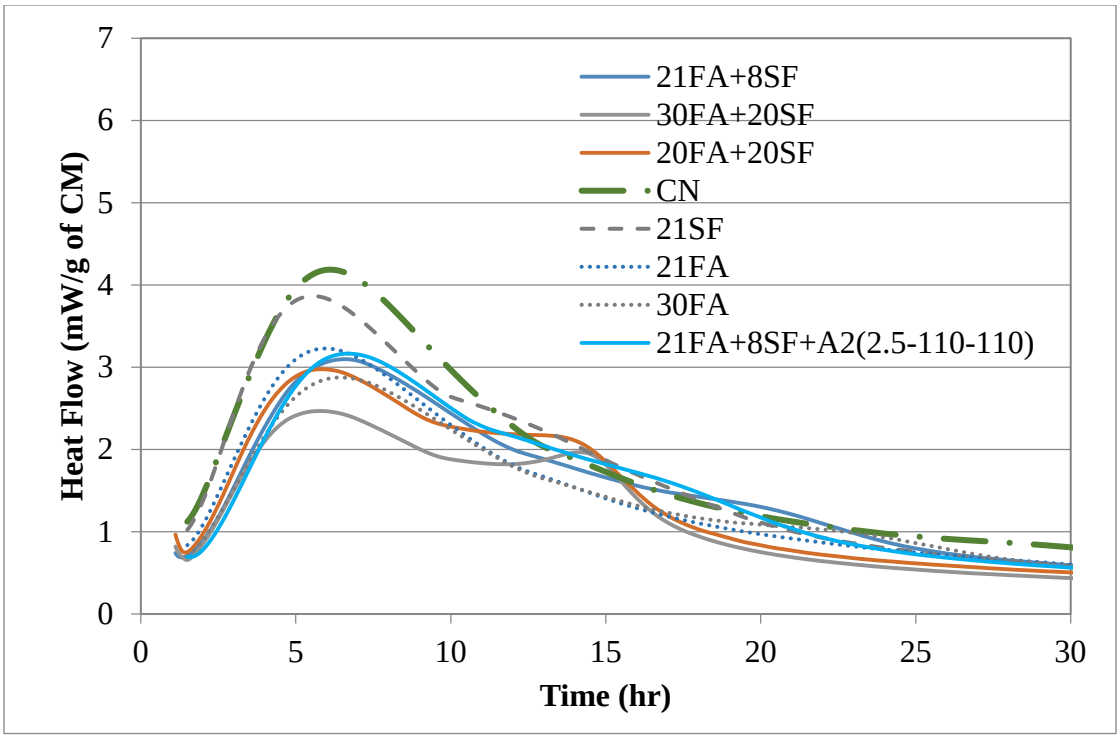

Figure 4-20: Effect of Fly Ash and Silica Fume Interaction on Measured Heat Flow Normalized by Mass of Cementitious Materials

[redacted]Slag and Metakaolin

Unlike preceding ternary combinations, metakaolin/slag interaction had a significant effect on the aluminate and the silicate hydration peaks (Figure 4-21). At a 10% MK dosage, the timing and magnitude of the main hydration peak did not appear to depend on the amount of slag replacement. However, at 20% MK, both the timing and the magnitude of the main hydration peak were accelerated with increasing slag dosage. As for the aluminate peak, its timing and magnitude were affected by both slag and metakaolin dosage. As can be seen from Figure 4-23 and Figure 4-24, there is a linear relationship between slag content and peak height, as well as timing of occurrence.

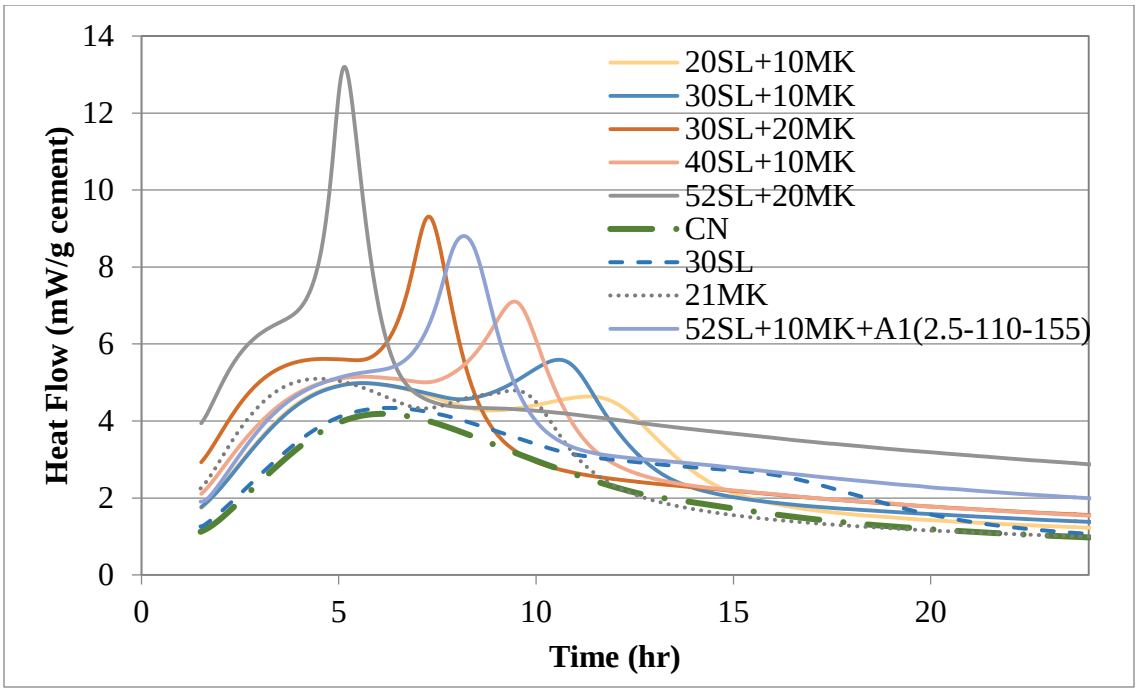

Figure 4-21: Effect of SL and MK on Measured Heat Flow Normalized by Mass of Cement

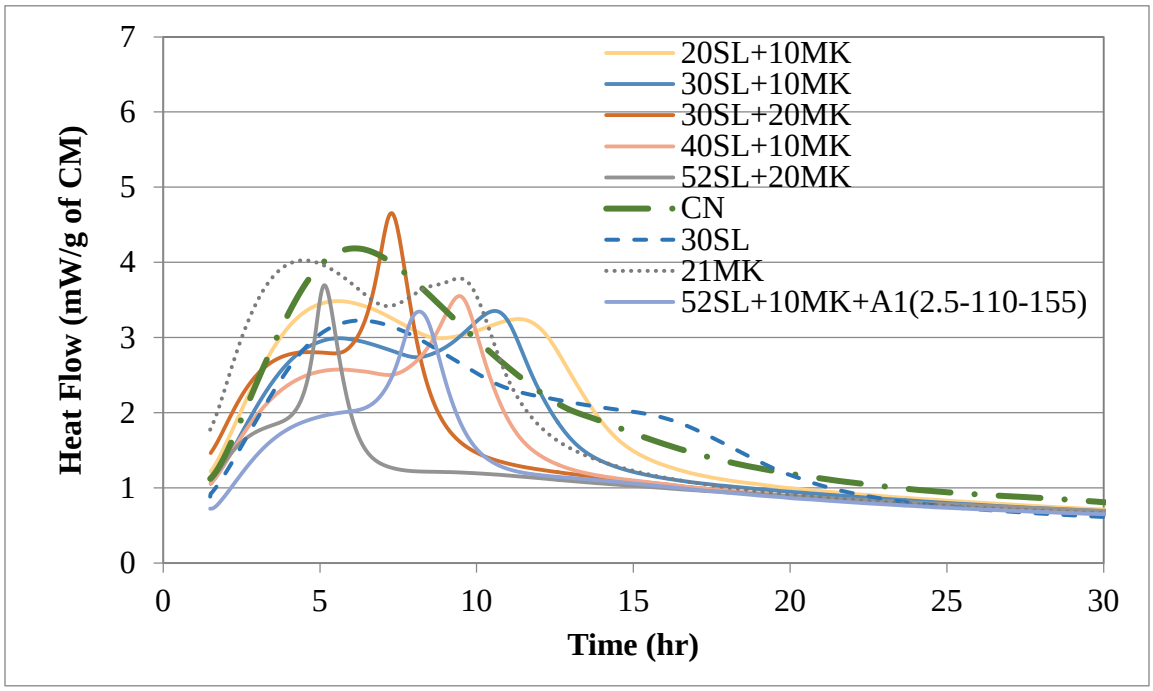

Figure 4-22: Effect of Slag and Metakaolin Interaction on Measured Heat Flow Normalized by Mass of Cementitious Materials

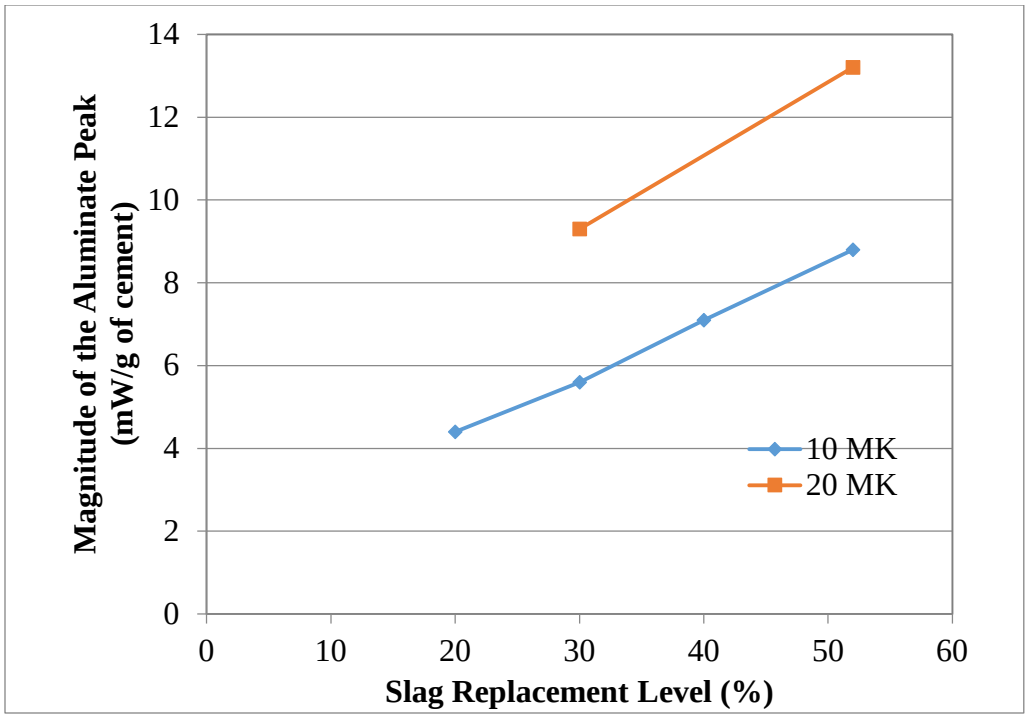

Figure 4-23: Effect of Metakaolin and Slag Dosages on the Magnitude of the Aluminate Peak

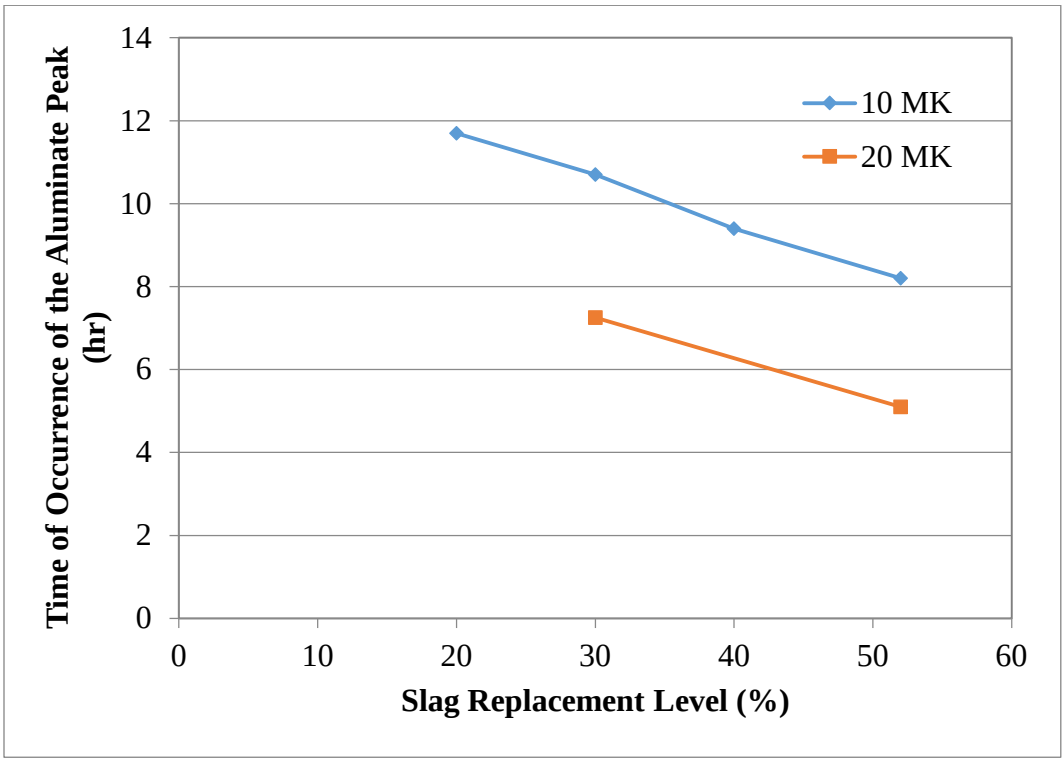

Figure 4-24: Effect of Metakaolin and Slag Dosages on the Timing of the Aluminate Peak

Fly Ash and WR

Interaction of FA and WR has been identified as significant by factorial design. In order to confirm the hypothesis that WR may be increasing fly ash reactivity as reported by Heinz et al. [104], two mixes were prepared with WR at the dosage of 300 ml/kg of cementitious materials and 10 and 20% fly ash (Figure 4-25 and Figure 4-26, respectively). It can be seen from Figure 4-25 that at 10% FA, the magnitude of both the silicate and aluminate peaks were increased, while the onset of the acceleration period was delayed, consistent with the WR mix. The effect of WR on the 20% FA mix was less, most likely due to a decreased TEA-to-FA ratio. In both cases, there was a slight increase in the induction period with addition of WR, which was reported by Heinz et al. [104] for pastes with 25% FA. However, they did not offer an explanation for this increase in the induction period.

TEA can form complexes with Al and Fe ions from the fly ash making them available for hydration. In addition, TEA may facilitate fly ash dissolution by increasing the pH of the pore water at early ages. Fraay et al. [202] have reported that dissolution of Class F fly ash occurs only after the pore solution reaches a pH of approximately 13.2. In the absence of chemical and mineral admixtures, pore solution pH depends on cement alkali content; however, even for low-alkali cements, pH values at early ages are expected to be around 13 [16]. Addition of fly ash is expected to lower the pH [203], [204]. Pietersen [204] observed that with incorporation of fly ash, it takes approximately 1 week to achieve the pH that is high enough for fly ash dissolution. Since TEA is a base, its addition may increase the pH of the pore solution to promote fly ash reaction at early ages. Pore solution analysis, with and without TEA addition, would be required to confirm this hypothesis.

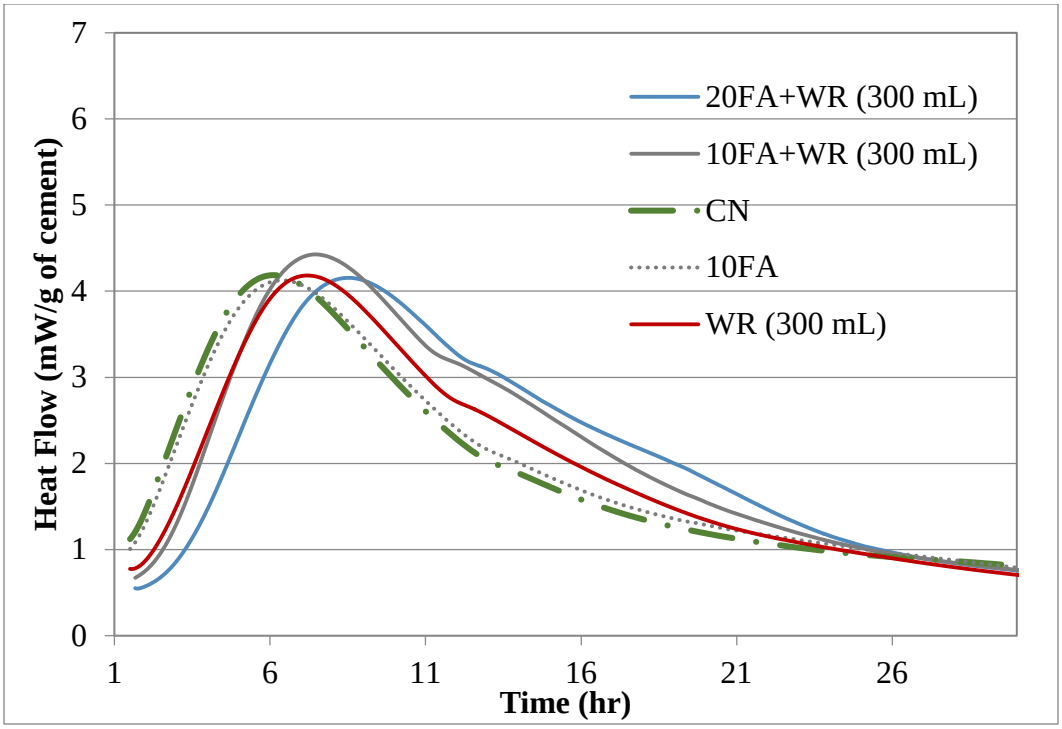

Figure 4-25: Effect of Fly Ash and WR Interaction on Measured Heat Flow Normalized by Mass of Cement

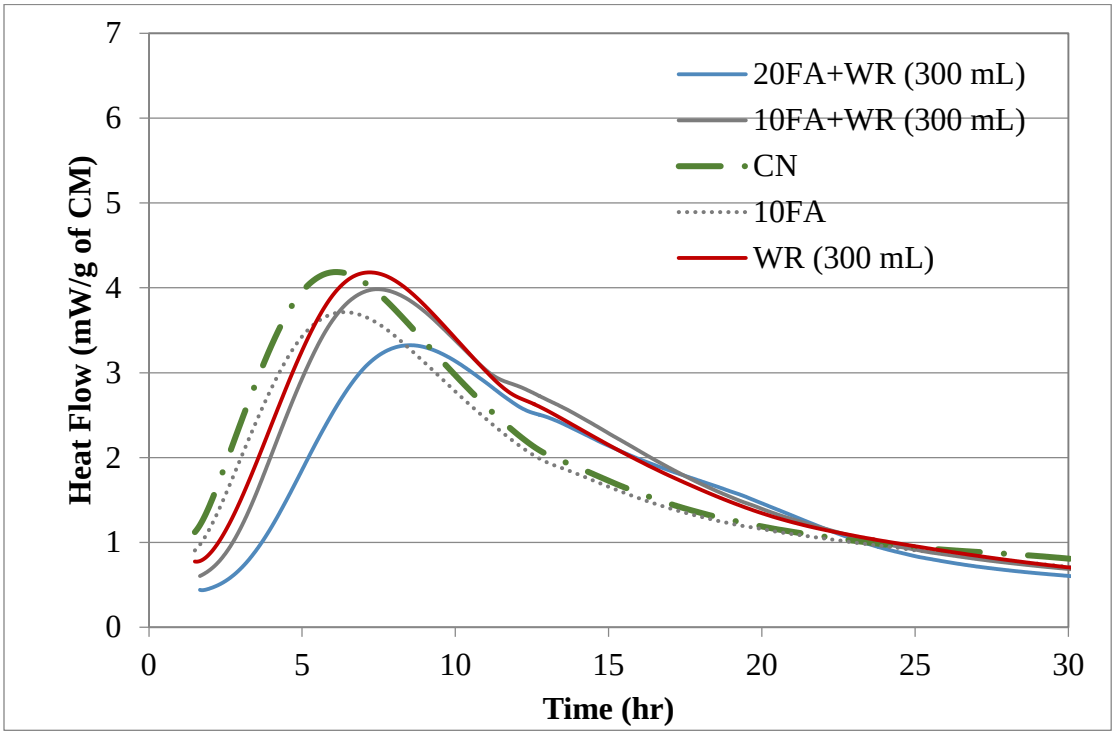

Figure 4-26: Effect of FA and WR on Measured Heat Flow Normalized by Mass of Solids

The results for the validation mixes indicate that factorial design was successful in identifying admixture combinations that may produce a non-additive effect on cement hydration and heat flow. Since it was not possible to test all the combinations identified by the factorial design, the untested combinations require further study.

Conclusions

It is clear that, for most of the mineral and chemical admixtures, their effect on heat of hydration differs, in the presence of other admixtures, from that observed in binary cement+admixture systems. The use of factorial design was successful in identifying admixture combinations that have a non-additive effect on heat evolution. Separate tests on ternary combinations confirmed the interaction of fly ash and slag, fly ash and metakaolin, fly ash and silica fume, slag and metakaolin, and fly ash and WR.

Plastic Properties of Cementitious Systems

Introduction

With respect to fresh concrete properties, the parameters that are of most importance during construction are adequate workability, which allows the concrete to be properly placed and consolidated, and a setting time that occurs during the expected period of time. Loss of workability and rapid or prolonged setting can be indicative of admixture incompatibilities. Typical tests used to assess the compatibility of different chemical and mineral admixtures, besides isothermal calorimetry, establish the setting time and rheological properties of the mix. It is recommended to perform setting time measurements on cement paste at normal consistency to "avoid errors due to incomplete consolidation in samples with a very stiff consistency, and errors due to bleeding in samples with a very fluid consistency" [205].

Addition of mineral admixtures is known to modify flow and workability of cement pastes. Although some mineral admixtures can improve workability, it is not clear what specifically is responsible for this improvement. As Ferraris et al. [206] point out, testing is the only way to evaluate the effect of mineral admixtures on concrete workability. Since concrete is subjected to various shearing conditions between mixing and placement, no single test can characterize all the rheological properties of cement paste [207]. Strain rate sweep is typically used to measure cement paste properties under the conditions that concrete is subjected to during mixing and transport to the site, while dynamic oscillatory shear tests measure rheological properties under stationary conditions.

Strain rate sweep was used in this study to assess the effect of mineral and chemical admixtures on rheological properties in the first several minutes after mixing. A helical ribbon geometry was selected, as it simulates the mixing action of a commercial impeller, and is, therefore, most suitable to evaluate rheological changes during the mixing process. Helical ribbon impellers have also been recognized as one of the best systems for homogenizing non-Newtonian fluids [208].

Yield stress is one of the most common parameters extracted from cement paste rheology experiments, as it has been shown that yield stress can be used as an indication of concrete slump, which increases with decreasing yield stress [209]–[211]. Although there are a number of

equations that can be used to obtain the yield stress from rheology data, cement pastes are often analyzed using the Bingham model [212]:

$$\boldsymbol{\tau = \tau_0 + \mu \gamma} \qquad \text{Equation 5-1}$$

Where, τ is the shear stress, τ_0 is the yield stress, μ is plastic viscosity and γ is the shear rate.

Equation 5-1 describes rheological behavior of viscoplastic fluids with a yield response [213]. A yield stress τ_0 has to be applied to initiate flow. Below the yield stress value, an ideal Bingham fluid behaves as an elastic solid, but once the yield stress is exceeded, it behaves as a Newtonian fluid. Typically, cement pastes do not behave as ideal Bingham fluids, as the shear stress response exhibited at low shear rates is not linear. Therefore, they can be better described as non-ideal Bingham fluids with an apparent yield stress τ_0^*, which can be obtained by finding an intersection of the extrapolated linear portion of the stress-strain curve observed at high shear rates with the shear stress axis [213]. Figure 5-1 illustrates the typical stress-strain behavior of Newtonian, Bingham, and non-ideal Bingham fluids. Plastic viscosity μ for all of these fluids is the slope of the linear portion of the curve. The use of the Bingham equation to determine the yield stress of fluids with nonlinear behavior at low shear rates has been criticized in the literature [214]. Dzuy and Boger [214] state that yield stresses calculated by the linear Bingham equation are approximately twice as high as those calculated by nonlinear equations, such as Casson and Herschel-Bulkley. At the same time, the authors point out that for comparison purposes the choice of model is not particularly important. Since all the models provide the same trends and since the purpose of this study was to compare the effects of different admixtures, rather than determine the true yield stress of each mixture, yield stresses were calculated using the Bingham equation. The Bingham equation has been extensively used in cement and concrete research. From this point forward, the term "yield stress" in this report will be used to refer to the apparent yield stress τ_0^*.

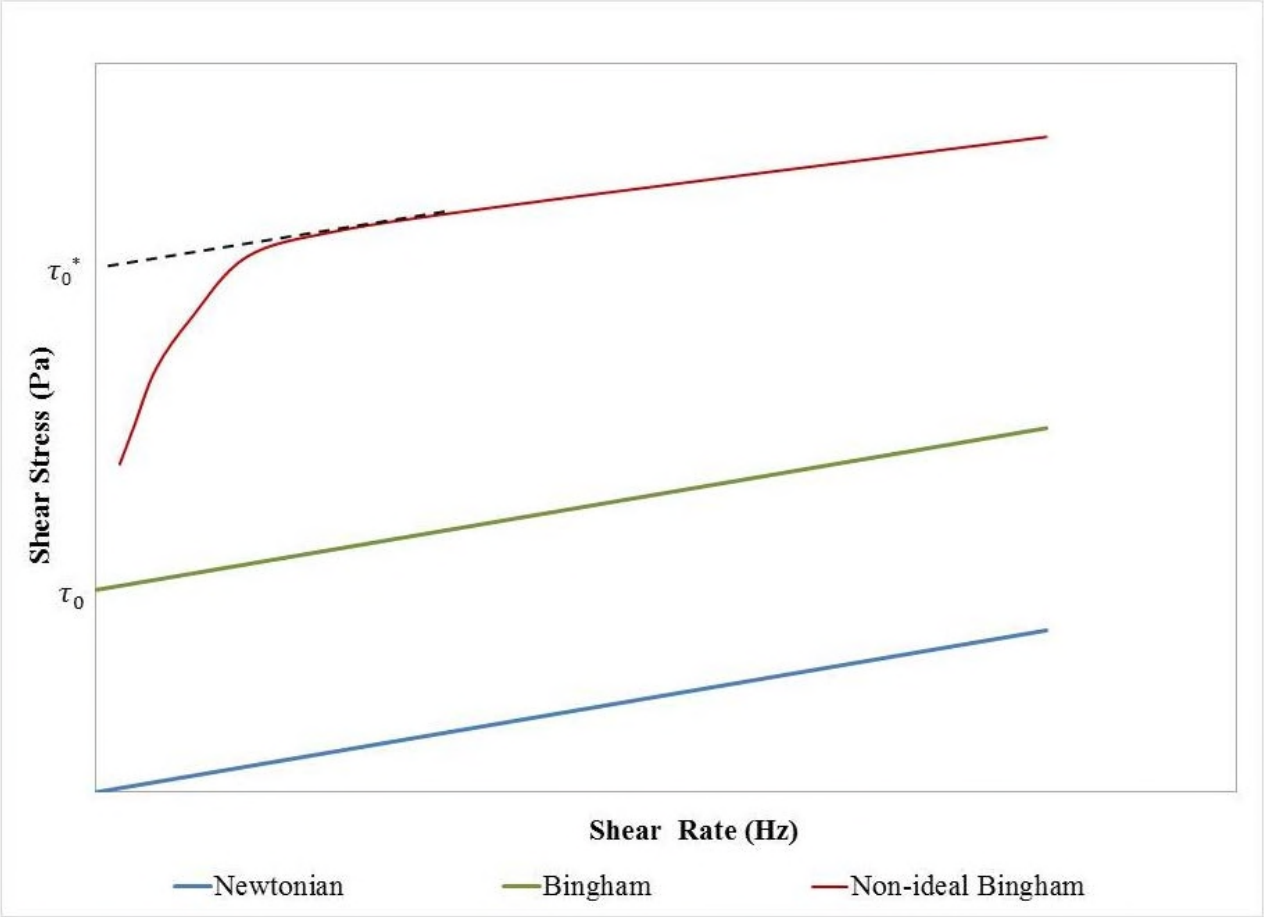

Figure 5-1: Typical Flow Curves for Newtonian, Bingham, and Non-Ideal Bingham Fluids

Methodology

Rheology Measurements

Rheology of binary, ternary, and quaternary cement-mineral admixture combinations prepared with chemical admixtures was determined by measuring the shear stress and viscosity of freshly mixed pastes in an AR 2000ex rheometer manufactured by TA Instruments. Binary OPC/SCM combinations were tested with and without chemical admixtures. A fixed w/cm ratio of 0.485 was used for all pastes, taking into account the water present in the chemical admixtures. Chemical admixture dosages were maintained constant, when included in mixtures, and are listed in Table 5-1. The selected chemical admixture dosages are the average dosages used by FDOT based on the Ternary Mix Log spreadsheet provided by the PM. As for the mineral admixture amounts, the replacement levels used in Chapter 3 (Table 5-1) were taken as a starting point, after

which replacement levels were varied to obtain measurements at 10, 21 and 30 % cement replacement. Additionally, ternary combinations were prepared using combinations of mineral admixtures at these replacement levels, which closely resemble the ternary mixtures used by the FDOT. A quaternary mixture was also created, not currently in use by the FDOT to the best of the authors' knowledge, using a combination of metakaolin, silica fume, and slag. The ternary and quaternary mixtures are listed in Table 5-2. SP1 HRWR was used in all the mixtures containing metakaolin, while the rest of the mixtures contained SP2, as was the case for the mixtures listed in the FDOT Ternary Mix Log spreadsheet.

All measurements were performed at an isothermal temperature of 23°C. Pastes were mixed in the IKA-Werke RW16 low shear mixer manufactured by IKA Werke for 3 minutes, after which they were transferred into a rheometer cup. Pastes were sheared in the rheometer for 2 minutes at a constant shear rate of 50 Hz, which was followed by a 2-minute equilibration period. After the equilibration period, a shear rate sweep was performed from 0.5 to 50 Hz. Shear rate sweep was performed under steady state flow conditions, which means that the flow field was allowed to stabilize for 30 seconds and that measurements were recorded when 3 consecutive readings were within 10% of each other. If the readings could not stabilize during 60 seconds, the measurement obtained at 60 seconds was recorded.

Table 5-1: Chemical and Mineral Admixture Addition Rates

Admixture	**Addition Rate**
AE	2.5 (ml/100 kg cement)
WR	110 (ml/100 kg cement)
SP2	110 (ml/100 kg cement)
SP1	155 (ml/100 kg cement)
FA	21 (% cement replacement)
MK	10 (% cement replacement)
SF	8 (% cement replacement)
SL	52 (% cement replacement)

Table 5-2: Cement Replacement Levels by SCMs for Ternary and Quaternary Mixtures

FA	SL	SF	MK
Ternary Mixtures (% Cement Replacement)			
21	21	-	-
21	30	-	-
21	40	-	-
21	-	10	-
10	-	-	10
40	-	-	10
-	52	-	10
Quaternary Mixture (% Cement Replacement)			
-	20	10	10

Setting Time and Normal Consistency

In addition to rheology, normal consistency and Vicat setting time were measured for all the combinations described previously. Normal consistency for all mixes was determined following ASTM C 187. Normal consistency refers to the amount of water needed to make a standard paste of similar workability. The paste is at normal consistency when the paste sample settles after the dropping of the rod at 10±1 mm below the original surface. The paste was mixed using the procedure in ASTM C 305 [215].

The setting time was determined following ASTM C 191. The initial set of cement paste is determined as the time it takes for the Vicat needle to penetrate the sample by 25 mm. The final set of cement paste is determined as the time it takes for the needle to have a penetration of 0 mm into the sample.

Results and Discussion

Rheological Measurements

Figure 5-2 presents the flow curves for the binary cement/chemical admixture combinations as well as the combinations of AE, WR, and HRWR. Table 5-3 lists the apparent yield stress and plastic viscosity values extracted from the linear portion of each curve. As can be

seen from Table 5-3 and Figure 5-2, addition of AE and WR used in this study had no significant effect on the yield stress and shear stress behavior of paste compared to that of the control mixture. Addition of both HRWRs, however, resulted in significant reduction in both the yield stress and shear stresses at any given shear rate up to 50 Hz. The effect of SP1 was much more pronounced.

Ferraris [216] observed that addition of HRWR decreased the yield stress and viscosity, however, the effect on plastic viscosity was not dosage-dependent. While yield stress continued to decrease with increasing dosage of SP, plastic viscosity remained unchanged. Hot [217] suggested that the decrease in plastic viscosity with superplasticizer addition is due to unadsorbed superplasticizer molecules. In this case, if the smallest addition of SP is sufficient to allow some of the HRWR molecules to remain in solution; further increase in SP dosage would not result in further decrease in viscosity.

Table 5-3: Apparent Yield Stress and Viscosity for Cement-Chemical Admixture Combinations

Mix ID	**Chemical Admixture Dosage (ml/100 kg cementitious)**	**Apparent Yield Stress (Pa)**	**Plastic Viscosity (Pa·s)**
CN	0	29	0.6
AE	2.5	29	0.5
WR	110	30	0.5
SP2	110	14	0.3
A2	110/2.5/110	14	0.2
SP1	155	3	0.2
A1	110/2.5/155	4	0.2

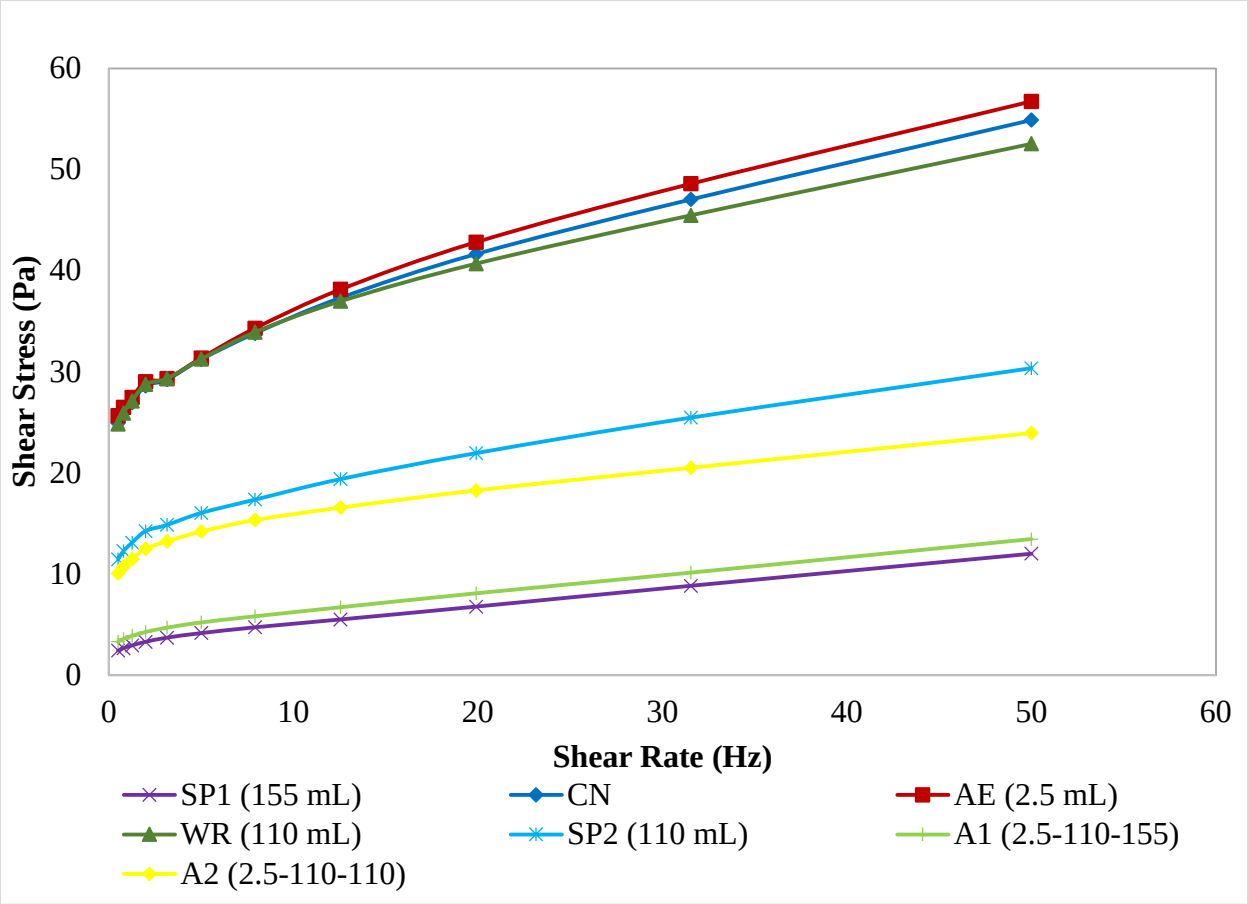

Figure 5-2: Effect of Chemical Admixtures on Paste Flow

Cement replacement with fly ash in this study did not have a significant effect on rheological properties of paste. Addition of up to 30% FA to pastes without chemical admixtures resulted in a slight reduction of apparent yield stress compared to the control paste (Table 5-4). This effect was not dosage dependent; no further yield stress reduction was observed when FA content was increased from 10 up to 30%. Plastic viscosity remained unchanged compared to the control mix. In the presence of WR, AE and SP, plastic viscosity also remained unaffected by fly ash addition; however, a reduction in yield stress was observed. Again, the stress reduction was not dependent on fly ash content. The stress reduction in plasticized mixes was approximately 10 Pa, which is double that observed in the non-plasticized pastes (4 Pa). It appears that the spherical nature of fly ash particles is more effective at improving workability in the presence of chemical admixtures.

Addition of fly ash is well known to improve workability due to the spherical shape of fly ash particles, the so-called "ball bearing effect" [44]. Typically, a decrease in the yield stress with increasing fly ash content is reported [218], [219]. As for plastic viscosity, some researchers observed no change with fly ash incorporation [218], while others reported a decrease in viscosity [219]. Park et al. [220] observed an initial decrease in yield stress and viscosity upon introduction of fly ash compared to control mix, but the values increased, although slightly, with increasing fly ash content. The authors attributed this effect to adsorption of superplasticizer to the unburned carbon particles in fly ash. At a constant superplasticizer dosage, increasing FA content would have reduced the effective superplasticizer dosage. An increase in both shear stress and viscosity with introduction of fly ash is reported [221], as well as an increase in viscosity with a decrease in yield stress with increasing fly ash content [105]. It has been suggested that the effect of fly ash is only discernable when replacement is done on the volume rather than mass basis [218], [222].

Table 5-4: Apparent Yield Stress and Viscosity for Cement-Fly Ash Pastes

Mix ID	**Chemical Admixture Dosage (ml/100 kg cementitious)**	**Apparent Yield Stress (Pa)**	**Plastic Viscosity (Pa·s)**
CN	0	29	0.6
10FA	0	25	0.5
21FA	0	25	0.6
30FA	0	25	0.6
A2	110/2.5/110	14	0.2
10FA +A2	110/2.5/110	1	0.1
21FA+A2	110/2.5/110	5	0.2
30FA+A2	110/2.5/110	4	0.1

Similar to fly ash, cement replacement with slag in the absence of chemical admixtures did not have any effect on shear stresses or plastic viscosity of paste (Table 5-5). In the presence of chemical admixtures, cement replacement with 10% slag resulted in a slight decrease in yield stress; a further decrease by 5 Pa is achieved by increasing slag replacement dosage to 21%.

Beyond 21%, however, slag dosage did not have an effect on yield stress up to 52% slag replacement. Plastic viscosity remained unchanged. Similar to the findings of this study, Zhang and Han [223] did not observe changes in yield stress with slag addition. Palacios et al. [224], on the other hand, report an increase in yield stress with increasing slag content above 10%. However, similar to this study, they did not observe an effect on plastic viscosity.

In addition to binary cement-slag mixes, ternary cement-slag-fly ash combinations were also tested (Table 5-5). Addition of 21% fly ash to plasticized mixes at slag replacement levels of 20-40% did not have a notable effect on yield stress or plastic viscosity.

Table 5-5: Apparent Yield Stress and Viscosity for Cement-Slag Pastes

Mix ID	**Chemical Dosage (ml/100 kg cementitious)**	**Apparent Yield Stress (Pa)**	**Plastic Viscosity (Pa·s)**
CN	0	29	0.6
10SL	0	28	0.5
21SL	0	29	0.6
30SL	0	29	0.6
52Slag	0	30	0.6
A2	110/2.5/110	14	0.2
10SL+A2	110/2.5/110	11	0.2
21SL+A2	110/2.5/110	6	0.1
30SL+A2	110/2.5/110	6	0.1
52SL+A2	110/2.5/110	5	0.1
21SL+21FA+A2	110/2.5/110	4	0.1
30SL+21FA+A2	110/2.5/110	4	0.2
40SL+21FA+A2	110/2.5/110	4	0.2

Addition of silica fume had no effect on viscosity, but it did increase the apparent yield stress for both plasticized and non-plasticized mixes (Table 5-6). This increase in the yield stress was more pronounced in non-plasticized mixes, although in both cases yield stresses increased linearly with silica fume dosage. It should be noted that the mixture containing 30% SF and no chemical

admixtures was too stiff to be measured with a helical ribbon. Increased yield stress with silica fume addition has been observed previously and is commonly attributed to increased water demand, as SF has a high surface area [206]. Shi et al. [225] observed a decrease in yield stress compared to the control mix with addition of up to 9% silica fume. However, yield stress increased with increasing SF content and exceeded that of the control mix at 12% SF.

Addition of 21% FA to a plasticized mix containing 10% SF considerably reduced the yield stress, from 32 Pa for the 10% SF mix to 2 Pa for the 21FA+10SF+A2 mix, and slightly reduced plastic viscosity. The yield stress of the ternary mixture was very similar to that of the plasticized binary mixture of cement with 21% fly ash Table 5-4. It appears that at these replacement levels fly ash had a dominant effect on rheological properties.

Table 5-6: Apparent Yield Stress and Viscosity for Cement-Silica Fume Pastes

Mix ID	**Chemical Dosage (ml/100 kg cementitious)**	**Apparent Yield Stress (Pa)**	**Plastic Viscosity (Pa·s)**
CN	0	29	0.6
8SF	0	40	0.6
10SF	0	41	0.6
21SF	0	80	0.7
A2	110/2.5/110	14	0.2
10SF+A2	110/2.5/110	32	0.3
21SF+A2	110/2.5/110	43	0.3
30SF+A2	110/2.5/110	71	0.3
21FA+10SF+A2	110/2.5/110	2	0.1

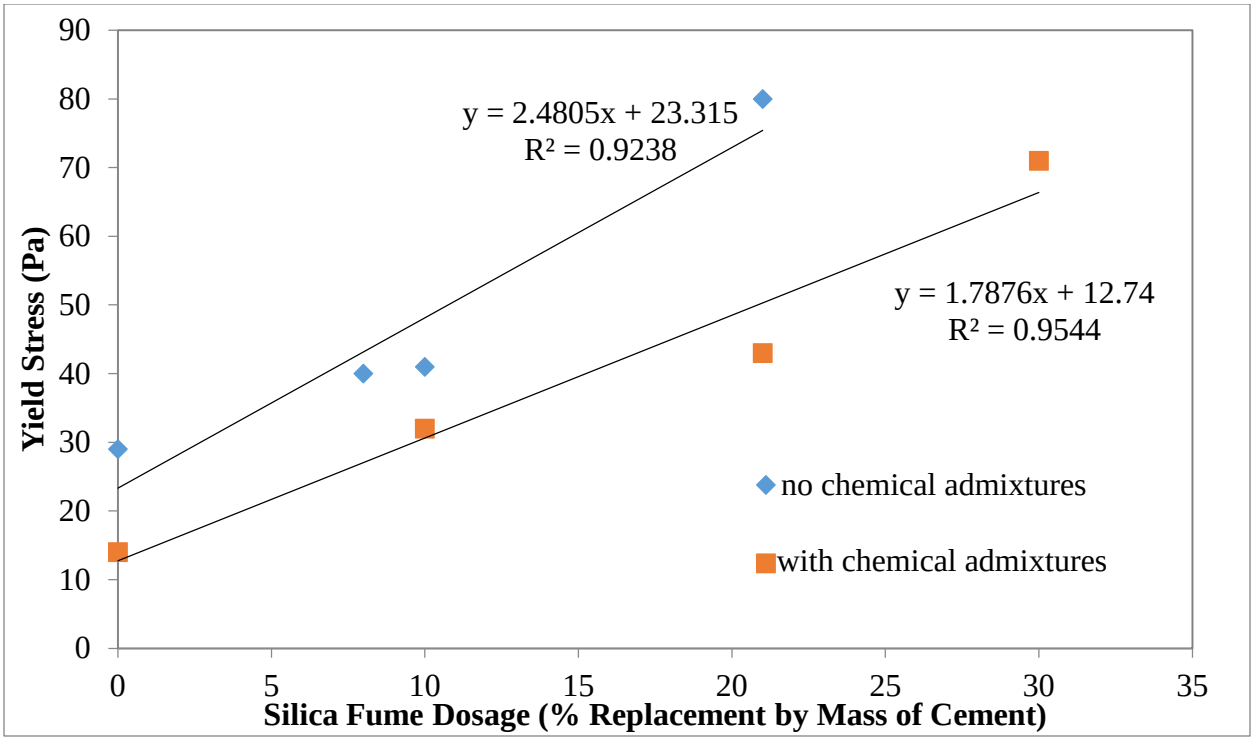

Figure 5-3: Yield Stress Development with Increasing Silica Fume Content

Cement replacement by 10% MK resulted in a drastic increase in apparent yield stress, 29 Pa for the control mix and 129 Pa for 10% MK paste, with only a slight increase in viscosity (Table 5-7). Mixtures with 21 and 30% MK and no chemical admixtures were too stiff and could not be measured. Addition of chemical admixtures to the SW+10%MK decreased both the yield stress and viscosity. Viscosity was identical to that of the plain cement mix with chemical admixtures, and yield stress was only slightly higher. Further increase in MK content of the plasticized mixture did not affect plastic viscosity; the yield stress, however, increased by approximately 150 Pa. Since the viscosity did not change with the increase in MK content, HRWR molecules were still likely to be present in the pore solution, as suggested by Hot [217]. The increase in the yield stress pointed to a change in SP1 adsorption and a consequent change in the flocculation of particles in the system. The SP1 dosage used may not have been sufficient to achieve proper particle dispersion. An increase in the MK content increased the solid surface area since metakaolin is much finer than cement (Table 5-9), and a higher SP1 dosage would have been required to maintain workability.

Table 5-7: Apparent Yield Stress and Viscosity for Cement-Metakaolin Pastes

Mix ID	Chemical Admixture Dosage (ml/100 kg cementitious)	Apparent Yield Stress (Pa)	Plastic Viscosity (Pa·s)
CN	0	29	0.6
10MK	0	129	0.7
A1	110/2.5/155	4	0.2
10MK+A1	110/2.5/155	11	0.2
21MK+A1	110/2.5/155	162	0.2
10MK+10FA+A1	110/2.5/155	25	0.4
10MK+40FA+A1	110/2.5/155	25	0.5
10MK+52SL+A1	110/2.5/155	17	0.3
10MK+10SF+20SL+A1	110/2.5/155	57	0.5
10SF+A2	110/2.5/110	32	0.3
21SL+A2	110/2.5/110	6	0.1

It is interesting to note that dramatic reduction in yield stress can be achieved by replacing 10% MK in the 21MK+A1 mixture with 10% FA. This substitution reduced the yield stress from 162 Pa to 25 Pa, but slightly increased plastic viscosity from 0.2 to 0.4 Pa·s. When compared to the 10MK+A1 mixture, addition of 10% FA slightly increased the yield stress, from 11 Pa to 25 Pa, and viscosity, from 0.2 to 0.4 Pa·s. Further increase in fly ash content to 40% did not have an effect on yield stress and viscosity.

A quaternary combination of cement, metakaolin, silica fume, and slag was also investigated. Compared to the binary combinations, both the yield stress and viscosity of this quaternary combination are higher. While the viscosity for the binary combinations of cement with metakaolin or slag or silica fume ranged from 0.1 to 0.3 Pa·s, the viscosity of the quaternary mixture was 0.5 Pa·s. The yield stress ranged from 6 (21SL+A2) to 32 Pa (10SF+A2) for the binary component mixtures, and was 17 Pa for the ternary mixture 10MK+52SL+A1. A significant increase in the yield stress to 57 Pa for the quaternary mixture was attributable to the addition of 10% SF. Although the amount of slag in the ternary and quaternary mixtures was

different, it was shown in Table 5-5 that slag dosage between 21 and 52% did not have an effect on yield stress or plastic viscosity. Therefore, it appears that the increase in yield stress and viscosity may be predominantly due to silica fume addition.

Based on the results obtained in this study, addition of mineral admixtures, at the same w/cm ratio and chemical admixture dosage, can affect the yield stress of the mixture, but have no effect on plastic viscosity. Chemical admixtures, on the other hand, consistently decreased both the yield stress and plastic viscosity. As can be seen in Table 5-8, only slight variation in plastic viscosity (0.5-0.7 Pa·s) was observed in pastes containing 10% of a mineral admixture without any chemical admixtures. With addition of AE, WR, and HRWR, plastic viscosity decreased to 0.1-0.3 Pa·s.

Table 5-8: All Mineral Admixtures at 10%

Mix ID	**Chemical Admixture Dosage (ml/100 kg cementitious)**	**Apparent Yield Stress (Pa)**	**Plastic Viscosity (Pa·s)**
CN	0	29	0.6
10FA	0	25	0.5
10SL	0	28	0.5
10SF	0	41	0.6
10MK	0	129	0.7
A2	110/2.5/110	14	0.2
10FA+A2	110/2.5/110	1	0.1
10SL+A2	110/2.5/110	11	0.2
10SF+A2	110/2.5/110	32	0.3
A1	110/2.5/155	4	0.2
10MK+A1	110/2.5/155	11	0.2

Based on the results of this study, it appears that, in the absence of chemical admixtures, rheology is related more to the particle size distribution than particle shape. As can be seen from Figure 5-4, particle size distributions of cement and slag are almost identical, and so was their viscosity (Table 5-8). The particle size distribution of fly ash was also very similar (Figure 5-4, Figure 5-5). Its viscosity was slightly lower, possibly due to its spherical shape. At 10%

replacement level, all three of these mineral admixtures produced pastes with similar rheological characteristics. Despite the high surface area measured by BET nitrogen adsorption (Table 5-9), silica fume had a very large mean particle size, which was attributed to agglomeration. Based on viscosity measurements, it appears that some, but not all, of these agglomerates were broken down during the mixing process. Cement replacement with silica fume increased paste viscosity compared to the control, but not as much as metakaolin, even though metakaolin fineness was lower than that of silica fume and, therefore, its particle size should be larger than that of silica fume. The spherical particle size of silica fume likely offsets some of the negative effects of its high surface area on the viscosity of the mix.

Addition of chemical admixtures notably decreased the yield stress and viscosity, indicating a change in the inter-particle interactions. While in the absence of chemical admixtures electrostatic forces most likely dominate, addition of chemical admixtures changes the dominant forces to steric repulsion. This is consistent with observations reported in the literature [224], [226].

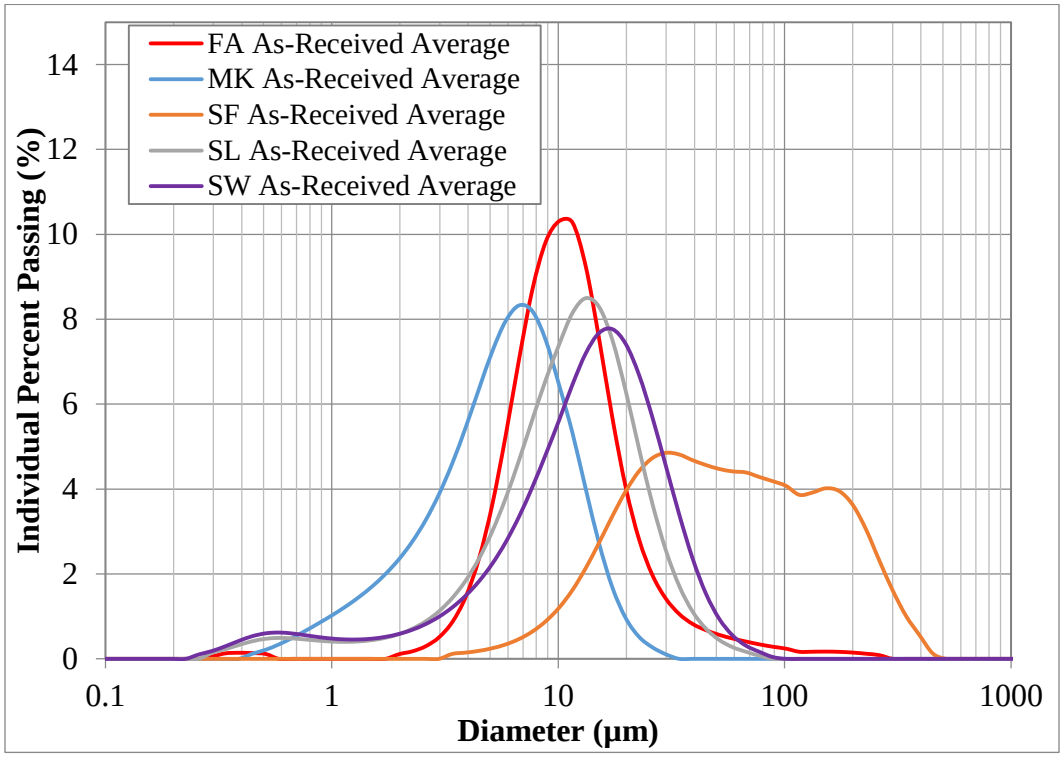

Figure 5-4: Individual Particle Size Distribution of Cement and Mineral Admixtures

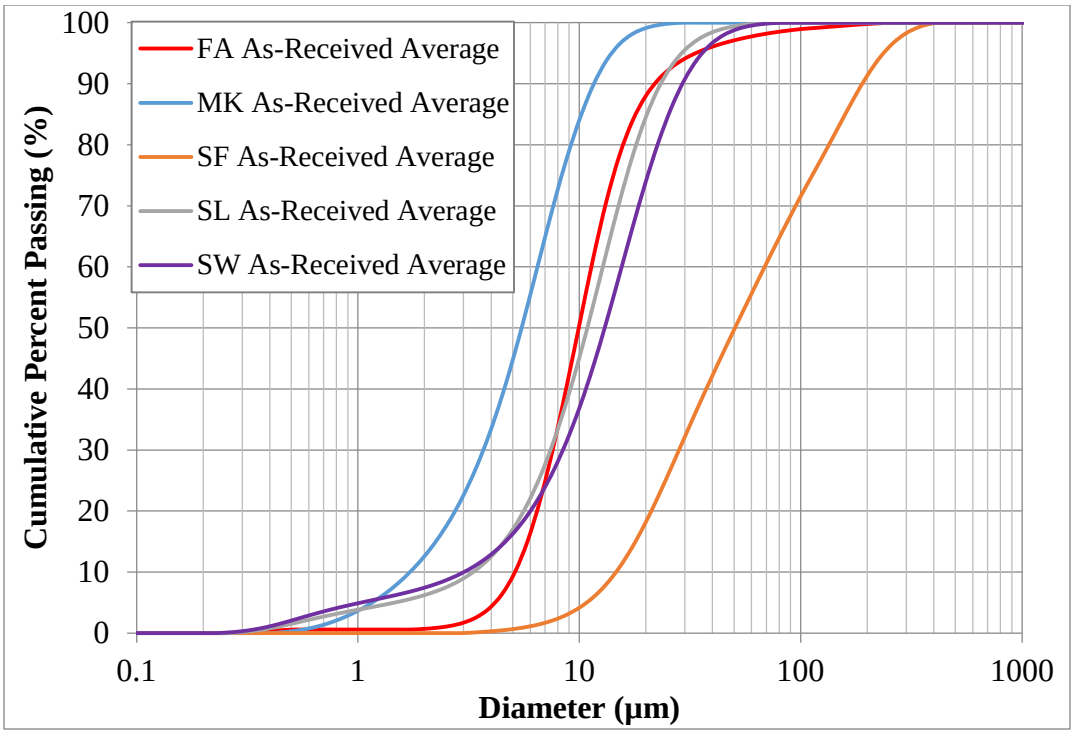

Figure 5-5: Cumulative Particle Size Distribution of Cement and Mineral Admixtures

Table 5-9: Particle Size Analysis of As-Received Cement and Mineral Admixtures

Physical Properties	**SW**	**FA**	**MK**	**SL**	**SF**
Mean size (MPS) (µm)	15.1	14.1	6.2	12.6	79.4
Multipoint BET Fineness (m^2/g)	2.14	2.27	14.97	3.70	21.41

Koehler and Fowler [218] caution against drawing conclusions on the effects of various mineral admixtures on rheology when only a single source of material is used. As they point out, a change in material source may result in a change in chemical composition and physical characteristics of the mineral admixture. A change in these parameters may in turn affect the rheological behavior of the admixture. Each mineral admixture investigated in this study was obtained from a single source. Admixtures were obtained from the sources approved by the FDOT for use in structural concrete. Therefore, conclusions drawn in this study are applicable only to the admixtures obtained from these specific sources. Further research would be required prior to broader application of the observed trends.

Setting Time

Binary Combinations

Unlike rheology, setting time measurements were performed on pastes with the same workability, rather than a fixed w/cm ratio. Since the chemical admixture dosages were maintained constant, their effect on normal consistency and setting time was assessed first. As can be seen in Table 5-10, all the chemical admixtures reduced the water demand compared to the control mix. The largest decrease resulted from a combination of the three admixture types used in this study. Of the two HRWR used, SP1 was slightly more effective at decreasing water demand than SP2.

Setting times remained largely unaffected by addition of AE and WR. There was a slight increase in both the initial and setting times with addition of either HRWR; combinations of the three admixture types further increased final setting times. An increase in setting times with HRWR addition has been previously reported in the literature [227], [228].

The time it takes for a hydrating cementitious material to set is determined both by physical (particle spacing) and chemical (degree of hydration) parameters [227]. The greater the particle spacing, the higher the degree of hydration required to connect the particles by hydration products and, consequently, the longer the setting time. Bentz has observed that addition of HRWRs increases setting times [227]. He explained that improved dispersion of cement particles increases their inter-particle distances, thus increasing setting time. This is consistent with the observation that coarse cements have longer setting times than fine cements [229]. Although both of these previous studies concerning setting time were conducted at constant w/c ratios, while setting times in this study were determined at the w/c ratios needed to attain a normal consistency, the differences in w/c ratios between cement-HRWR mixes and the control were minor. Increased inter-particle distance may be responsible for the slight delay in setting times with HRWR addition observed in this study.

Table 5-10: Normal Consistency and Setting Times for Chemical Admixtures

Mixture	Normal Consistency	Initial Set (min)	Final Set (min)
CN	27.0%	69	90
AE	26.0%	76	95
WR	25.5%	80	95
SP1	25.5%	93	105
SP2	26.0%	84	105
A2	23.5%	84	110
A1	24.5%	95	135

It can be seen from Table 5-11 that water demand increased with increasing fly ash content. This increase was more pronounced in the absence of chemical admixtures (Figure 5-6). Both initial and final set times increased with increasing cement replacement levels. This was expected, since fly ash is not reactive at these early ages and cannot contribute to establishing inter-particle connections by hydration products. As fly ash content is increased, a higher degree of cement hydration would be required to achieve contact between the particles.

Table 5-11: Normal Consistency and Setting Times for Cement-Fly Ash Combinations

Mixture	Normal Consistency	Initial Set (min)	Final Set (min)
CN	27.0%	69	90
10FA	27.0%	94	110
21FA	28.0%	105	140
30FA	29.0%	121	140
10FA+A2	26.0%	101	125
21FA+A2	27.0%	112	140
30FA+A2	27.5%	120	145

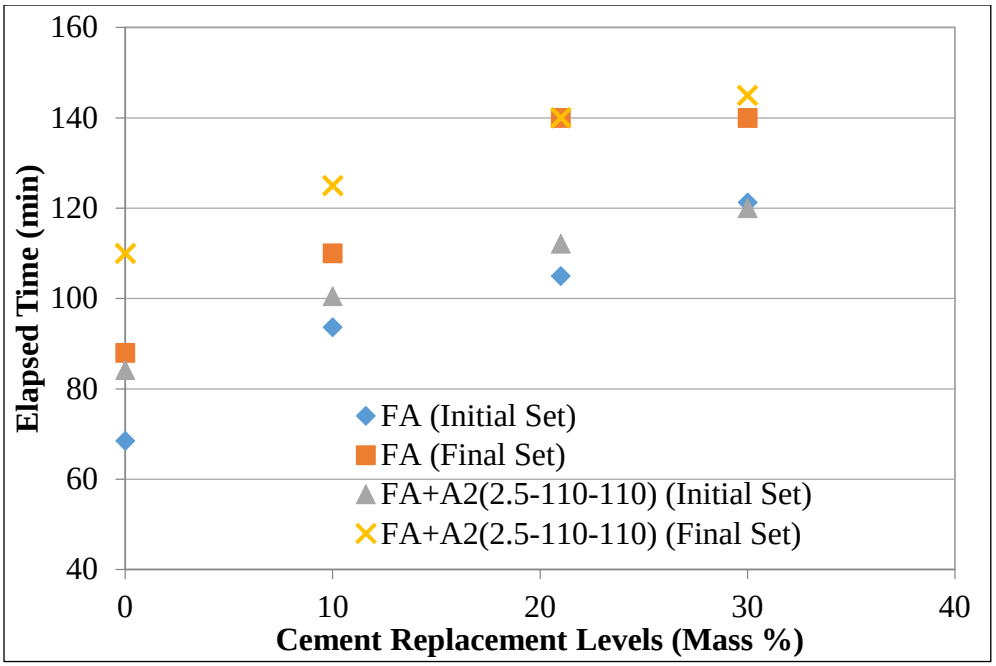

Figure 5-6: Initial and Final Setting Times as a Function of Fly Ash Content

The water requirement for normal consistency of cement-slag pastes increased slightly with slag content, with a corresponding increase in setting time (Table 5-12, Figure 5-7). Similar to fly ash, slag is not reactive at such early ages and is not expected to contribute to formation of hydration products.

Table 5-12: Normal Consistency and Setting Times for Cement-Slag Combinations

Mixture	Normal Consistency	Initial Set (min)	Final Set (min)
CN	27.0%	69	90
10SL	26.5%	89	100
21SL	27.5%	93	110
30SL	28.5%	106	120
52SL	28.0%	108	150
21SL+A2	27.0%	99	125
30SL+A2	26.0%	111	135
52 SL+A2	27.0%	137	170

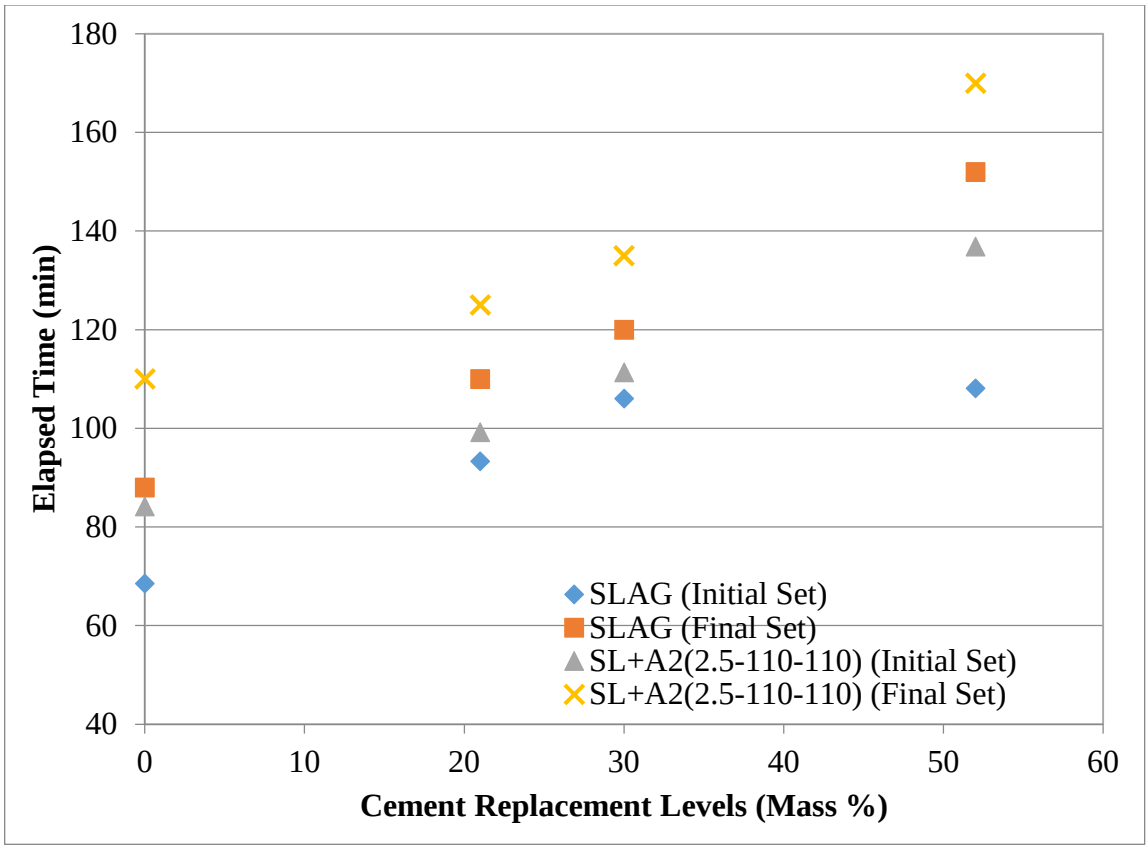

Figure 5-7: Initial and Final Setting Times as a Function of Slag Content

An increase in silica fume content increased the amount of water required to achieve normal consistency, although this increase was only notable at values above 10% (Table 5-13). Only 10% cement replacement by SF was tested with addition of chemical admixtures, since higher replacement levels are not used by the FDOT. For mixes without chemical admixtures, addition of SF increased both initial and final setting times (Figure 5-8). As discussed previously, silica fume forms agglomerates due to its small particles size that cannot be dispersed in water by mixing alone. Silica fume is believed to be non-reactive during the first day [62], [93], so addition of SF to unplasticized mixes increases the degree of cement hydration required to form inter-particle connections to achieve setting, and the same holds for fly ash and slag. With addition of chemical admixtures, there was no significant difference between the control and 10% SF mixes. It appears that dispersion of SF with additions of chemical admixtures accelerated cement hydration through heterogeneous nucleation, and that this acceleration is sufficient to compensate for the effect of decreased cement content.

Table 5-13: Normal Consistency and Setting Times for Cement-Silica Fume Combinations

Mixture	Normal Consistency	Initial Set (min)	Final Set (min)
CN	27.0%	69	90
10SF	28.5%	93	105
21SF	32.0%	95	110
30SF	35.0%	107	120
10SF+A2	26.0%	75	105

Figure 5-8: Initial and Final Setting Times as a Function of Silica Fume Content

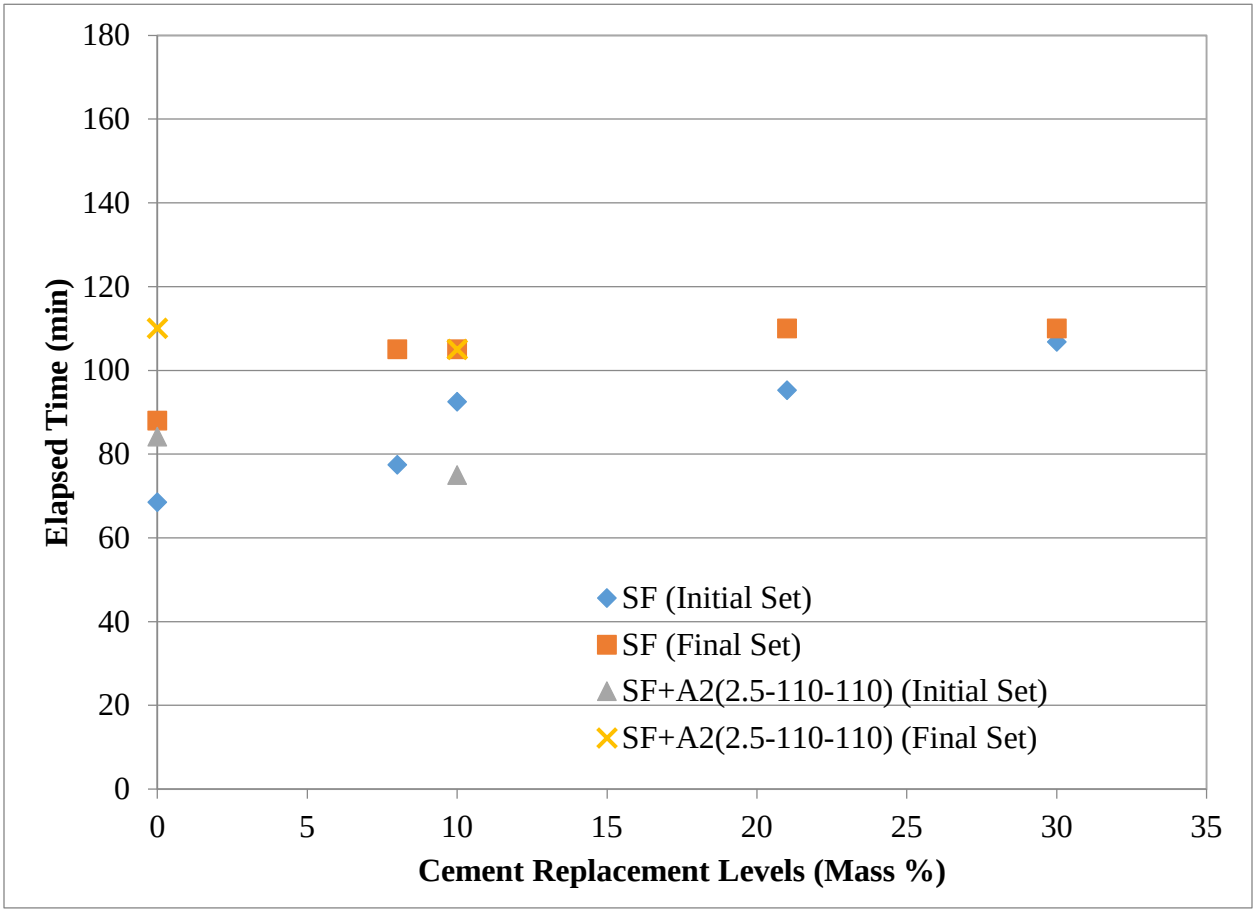

There was a notable increase in the amount of water required to achieve normal consistency with MK additions due to its high surface area (Table 5-14). Increase in normal consistency with addition of calcined clay has been previously reported [230]. Without chemical admixtures, addition of MK increased both initial and final setting times (Figure 5-9). Without chemical admixtures, MK was most likely agglomerated. Although MK has been reported to be reactive at

early ages [68], [81], in the agglomerated state the surface area of MK available for reaction would be significantly decreased, and metakaolin would be unlikely able to contribute significantly to formation of hydration products. In the presence of chemical admixtures, initial and final setting times were decreased by 10% MK addition. Further increase in MK content to 21% had no effect on setting time, while at 30% final setting was increased. In plasticized mixes, metakaolin was dispersed into individual particles, allowing MK to contribute to formation of hydration products in addition to accelerating cement hydration through nucleation seeding. This can offset the set-retarding effect of the chemical admixture combination, and the effect of cement content reduction at 10 and 21% MK replacement.

It can be concluded that in binary combinations incorporating mineral admixtures with particle sizes similar to that of cement, such as Class F fly ash and slag, results in increasing the initial and final setting times. This can be explained by the decreased cement content and the corresponding higher degree of hydration required for hydration products to form connections between particles for setting to occur. Addition of materials with finer particle sizes, such as metakaolin and silica fume, together with chemical admixtures that allow proper dispersion, does not affect initial and final setting times when tested at normal consistency. It is hypothesized that the effect of decreased cement content and increased w/cm ratio (in the case of metakaolin) is offset by acceleration of cement hydration due to heterogeneous nucleation and possibly, in the case of metakaolin, an early-age pozzolanic reaction.

Table 5-14: Normal Consistency and Setting Times for Cement-Metakaolin Combinations

Mixture	Normal Consistency	Initial Set (min)	Final Set (min)
CN	27.0%	69	90
10MK	34.0%	85	105
21MK	41.0%	85	115
30MK	49.0%	100	130
10MK+A1	32.5%	83	110
21MK+A1	40.0%	85	110
30MK+A1	50.0%	87	125

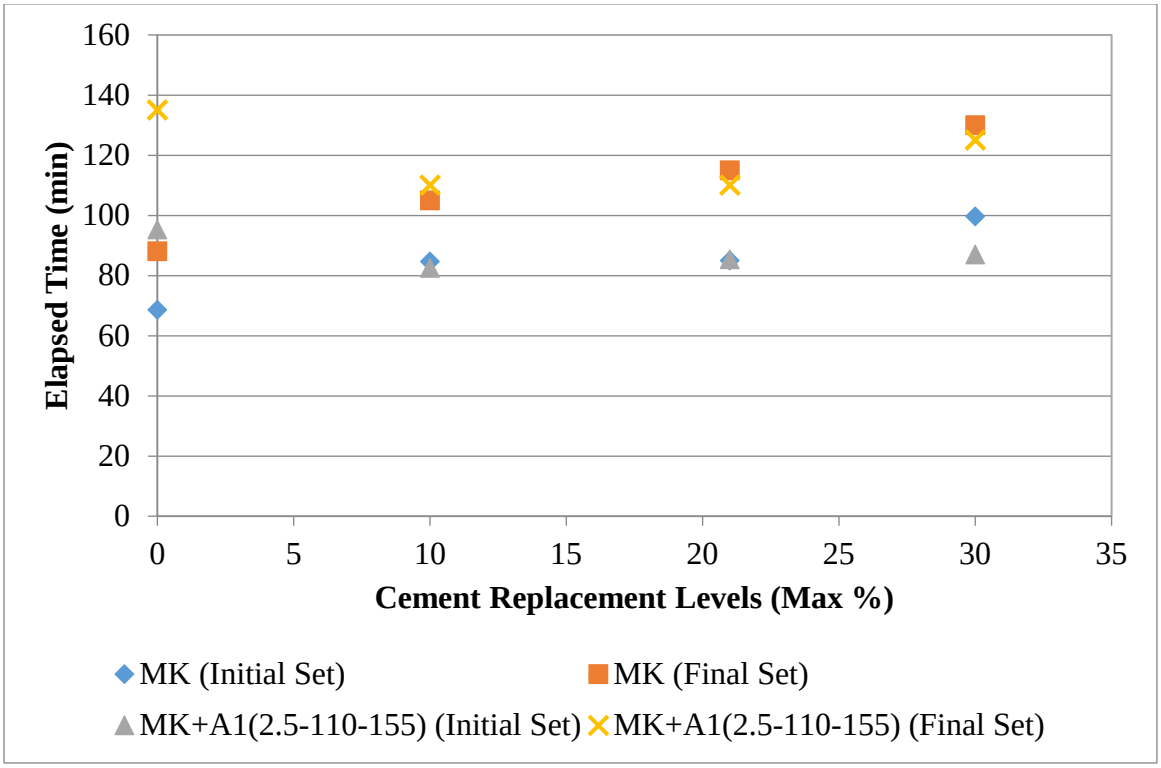

Figure 5-9: Initial and Final Setting Times as a Function of Metakaolin Content

[redacted]Ternary Combinations

Normal consistency and setting times of ternary combinations of cement and mineral admixtures were evaluated. Addition of 10% MK to the plasticized cement+10% FA mixture reduced both initial and final setting times, even though the amount of water required to achieve

normal consistency was increased (Table 5-15). The decrease in setting times with MK addition is expected to be even greater at a fixed w/cm ratio. Setting times were unaffected compared to the cement+10% MK mixture, and normal consistency was slightly decreased. However, a further increase in fly ash content to 40% significantly increased initial and final setting times.

Addition of 10% MK to the plasticized cement+52% slag mixture also reduced the setting times despite an increase in the water content for normal consistency. Compared to the cement+10% MK mixture, initial and final setting times of this ternary blend were increased by additions of slag.

Addition of 10% silica fume to the plasticized cement+21% fly ash mixture did not have an effect on initial and final setting times, while normal consistency was increased slightly. Compared to the cement+10% SF mixture, the setting times of the ternary combination were increased by addition of fly ash.

Ternary combinations of cement, Class F fly ash, and slag were also investigated at three different slag contents. Although normal consistency was not significantly affected, initial and final setting times were increased by increasing slag content. The setting times of the ternary mixtures were also higher than those of the corresponding binary mixtures.

Normal consistency of the quaternary blend (cement/MK/SF/slag) was similar to that of all the mixtures containing MK. The setting times were similar to that of the plasticized cement+21% slag mixture. The reduction in setting time expected with addition of MK and SF was most likely obscured by the increased water content due to a significant increase in the amount of water required to obtain normal consistency compared to the cement-slag mixture.

It can be concluded that in the ternary combinations, the behavior of the mineral admixtures studied was the same as in the binary combinations: silica fume addition did not have a significant effect on setting time, while addition of metakaolin decreased it; addition of fly ash and slag increased setting time.

Table 5-15: Normal Consistency and Setting Times for Ternary and Quaternary Cement-Mineral Admixture Combinations

Mixture	Normal Consistency	Initial Set (min)	Final Set (min)
10FA+A2	26.0%	101	125
10MK+A1	32.5%	83	110
10FA+10MK+A1	31.5%	90	110
40FA+10MK+A1	33.5%	167	200
52SL+A2	27.0%	137	170
52SL+10MK+A1	34.0%	122	140
21FA+A2	27.0%	112	140
10SF+A2	26.0%	75	105
21FA+10SF+A2	27.5%	109	135
21SL+A2	27.0%	99	125
30SL+A2	26.0%	111	135
21FA+20SL+A2	27.0%	128	150
21FA+30SL+A2	27.5%	150	185
21FA+40SL+A2	27.5%	156	190
10MK+10SF+20SL+A1	32.5%	107	135

Conclusions

The following conclusions can be drawn based on the findings:

1. Plastic viscosity of fresh pastes is largely unaffected by addition of mineral admixtures, but is reduced by chemical admixtures.
2. Yield stress, on the other hand, is affected by both mineral and chemical admixtures. Chemical admixtures consistently reduced yield stress, while additions of mineral admixtures had a variable effect. In the absence of chemical admixtures, yield stress was increased by addition of mineral admixtures with particle sizes finer than that of cement (silica fume, metakaolin), while admixtures with similar particle sizes (slag and fly ash) did not have a significant effect. Addition of fly ash reduced yield stresses in the mixtures containing silica fume, while it had no effect on the yield stress of cement-slag mixtures.

For the mixtures containing metakaolin, addition of 10% fly ash to a 10% MK mixture increased yield stress compared to 10% MK mixture; however, the stress was reduced compared to the 21% MK paste.

3. Addition of mineral admixtures always increased setting times of non-plasticized mixes. With addition of chemical admixtures, metakaolin addition decreased setting time compared to the control, silica fume did not appear to affect setting times at cement replacement levels of 10%, and addition of Class F fly ash and slag increased setting times compared to the control. The same behavior was observed in mixes containing combinations of mineral admixtures.

Effects of Mineral and Chemical Admixtures on Strength Evolution and Setting Properties

Introduction

Strength evolution and setting properties of cementitious mixtures are important to assess as both properties will affect concrete workability and strength. In this chapter, the compressive strength and setting time of cementitious mixtures are presented. The mixtures studied here included binary, ternary, and quaternary combinations of chemical and mineral admixtures most commonly used in current FDOT construction projects.

Methodology

Setting Time and Normal Consistency

Setting time for mortar mixes was determined following ASTM C807 [231] using a modified Vicat apparatus. For all mixtures, the amount of cementitious material was at 750 g, and the water-to-cementitious material (w/cm) ratio of 0.5 was maintained constant. Additionally, chemical admixtures amounts were fixed (Table 6-1 and Table 6-2) to allow meaningful comparison. Normal consistency was determined by using various amounts of silica sand to achieve a penetration target of 20 ± 4 mm. Once normal consistency was determined, setting times were determined as the time when a penetration of 10 mm was achieved.

Compressive Strength

Mortar cubes were prepared and tested following ASTM C109 [232]. The admixture dosages were selected following the most commonly used FDOT admixture dosages, and the mixture proportions are presented in Table 6-3 and Table 6-4. Compressive strength tests were conducted on 2-in cube specimens. Testing ages were 1, 7, and 28 days, and after the 1-day test, the mortar cubes were submerged in a saturated lime solution. Mortar cubes were prepared following ASTM C305 [233]. Each mix was prepared using the proportions for 9 cube samples: 740 g of cementitious materials, 2035 g of Ottawa sand, and a w/cm ratio of 0.485. Chemical admixtures were also incorporated into each mix. The amount of water in each chemical admixture was taken into account to maintain a constant w/cm ratio. Chemical admixture dosages were as follows: 2.5 ml per 100 kg of cementitious material for the air-entraining admixture, 110 ml per

100 kg of cementitious material for the water-reducing admixture, and 110 or 115 ml per 100 kg of cementitious material for the superplasticizer, depending on the superplasticizer used.

Table 6-1: Binary Systems Setting Time Mix Design

Mix Design	Cement (g)	MK (g)	FA (g)	SF (g)	Slag (g)	Sand (g)	AE Solution (g)	WR (g)	SP1 (g)	SP2 (g)	AE	WR	SP1	SP2	DI Water (g)
											(ml/100 kg cementitious)				
CN+A1	750					2,235	3.7	0.95	1.25		2.5	110	155		370
CN+A2	750					2,150	3.7	0.95		0.89	2.5	110		110	370
10MK+A1	675	75				1,985	3.7	0.95	1.25		2.5	110	155		370
20MK+A1	600	150				1,435	3.7	0.95	1.25		2.5	110	155		370
10SF+A2	675			75		2,100	3.7	0.95		0.89	2.5	110		110	370
10FA+A2	675		75			2,175	3.7	0.95		0.89	2.5	110		110	370
21FA+A2	592.5		157.5			2,100	3.7	0.95		0.89	2.5	110		110	370
30FA+A2	525		225			2,100	3.7	0.95		0.89	2.5	110		110	370
21SL+A2	592.5				157.5	2,175	3.7	0.95		0.89	2.5	110		110	370
30SL+A2	525				225	2,175	3.7	0.95		0.89	2.5	110		110	370
52SL+A2	360				390	2225	3.7	0.95		0.89	2.5	110		110	370

Table 6-2: Ternary and Quaternary Systems Setting Time Mix Design

Mix Design	Cement (g)	MK (g)	FA (g)	SF (g)	Slag (g)	Sand (g)	AE Solution (g)	WR (g)	SP1 (g)	SP2 (g)	AE	WR	SP1	SP2	DI Water (g)
											(ml/100 kg cementitious)				
10FA+10MK+A1	600	75	75			2,000	3.7	0.95	1.25		2.5	110	155		370
40FA+10MK+A	375	75	300			1,950	3.7	0.95	1.25		2.5	110	155		370
10FA+20MK+A1	525	150	75			1,600	3.7	0.95	1.25		2.5	110	155		370
21FA+10SF+A2	517.5		157.5	75		2,100	3.7	0.95		0.89	2.5	110		110	370
21FA+20SL+A2	442.5		157.5		150	2,175	3.7	0.95		0.89	2.5	110		110	370
21FA+30SL+A2	367.5		157.5		225	2,100	3.7	0.95		0.89	2.5	110		110	370
52SL+10MK+A1	285	75			390	2,075	3.7	0.95	1.25		2.5	110	155		370
10MK+10SF+20SL+A1	450	75		75	150	1,900	3.7	0.95	1.25		2.5	110	155		370

Table 6-3: Binary System Compressive Strength Mix Design

Mix Design	Cement (g)	MK (g)	FA (g)	SF (g)	Slag (g)	Sand (g)	AE Solution (g)	WR (g)	SP1 (g)	SP2 (g)	AE	WR	SP1	SP2	Water (g)
											(ml/100 kg cementitious)				
CN+A1	740.0	-	-	-	-	2,035	3.7	0.94	1.23	-	2.5	110	155		353.9
CN+A2	740.0	-	-	-	-	2,035	3.7	0.94	-	0.88	2.5	110		110	353.9
10MK+A1	666.0	74.0	-	-	-	2,035	3.7	0.94	1.23	-	2.5	110	155		353.9
21MK+A1	584.6	155.4	-	-	-	2,035	3.7	0.94	1.23	-	2.5	110	155		353.9
10SF+A2	666.0	-	-	74.0	-	2,035	3.7	0.94	-	0.88	2.5	110		110	353.9
10FA+A2	666.0	-	74.0	-	-	2,035	3.7	0.94	-	0.88	2.5	110		110	353.9
21FA+A2	584.6	-	155.4	-	-	2,035	3.7	0.94	-	0.88	2.5	110		110	353.9
30FA+A2	518.0	-	222.0	-	-	2,035	3.7	0.94	-	0.88	2.5	110		110	353.9
21SL+A2	584.6	-	-	-	155.4	2,035	3.7	0.94	-	0.88	2.5	110		110	353.9
30SL+A2	518.0	-	-	-	222.0	2,035	3.7	0.94	-	0.88	2.5	110		110	353.9
52SL+A2	355.2	-	-	-	384.8	2,035	3.7	0.94	-	0.88	2.5	110		110	353.9

Table 6-4: Ternary and Quaternary System Compressive Strength Mix Design

Mix Design	Cement (g)	MK (g)	FA (g)	SF (g)	Slag (g)	Sand (g)	AE Solution (g)	WR (g)	SP1 (g)	SP2 (g)	AE	WR	SP1	SP2	Water (g)
											(ml/100 kg cementitious)				
10FA+10MK+A1	592.0	74.0	74.0	-	-	2,035	3.7	0.94	1.23	-	2.5	110	155		353.9
40FA+10MK+A1	370.0	74.0	296.0	-	-	2,035	3.7	0.94	1.23	-	2.5	110	155		353.9
10FA+20MK+A1	518.0	148.0	74.0	-	-	2,035	3.7	0.94	1.23	-	2.5	110	155		353.9
21FA+10SF+A2	510.6	-	155.4	74.0	-	2,035	3.7	0.94	-	0.88	2.5	110		110	353.9
21FA+20SL+A2	436.6	-	155.4	-	148.0	2,035	3.7	0.94	-	0.88	2.5	110		110	353.9
21FA+30SL+A2	362.6	-	155.4	-	222.0	2,035	3.7	0.94	-	0.88	2.5	110		110	353.9
52SL+10MK+A1	281.2	74.0	-	-	384.8	2,035	3.7	0.94	1.23	-	2.5	110	155		353.9
10MK+10SF+20SL+A1	444.0	74.0	-	74.0	148.0	2,035	3.7	0.94	1.23	-	2.5	110	155		353.9

Mortar Setting Time

Binary Combinations

Mortar setting time was determined on mortar mixes of the same consistency. Following ASTM C807 [231], the amount of sand was varied to achieve the same consistency. The amount of cementitious materials and chemical admixtures, and the w/cm ratios were maintained constant.

Binary Mix: Metakaolin

Figure 6-1 shows the data results for the mortar setting time for metakaolin mixes. It is observed from Table 6-1 that the amount of sand decreased as the metakaolin content increased. This is due to its high surface area. The mortar setting time decreased with increasing cement replacement levels. This finding is in agreement with the literature. Brooks et al. [234] investigated the effect of metakaolin replacement on concrete setting time at 5, 10 and 15% replacement levels. While maintaining the chemical admixture dosage fixed and a constant w/cm ratio, it was found that the final setting time decreased when replacement level increased from 10 to 15%.

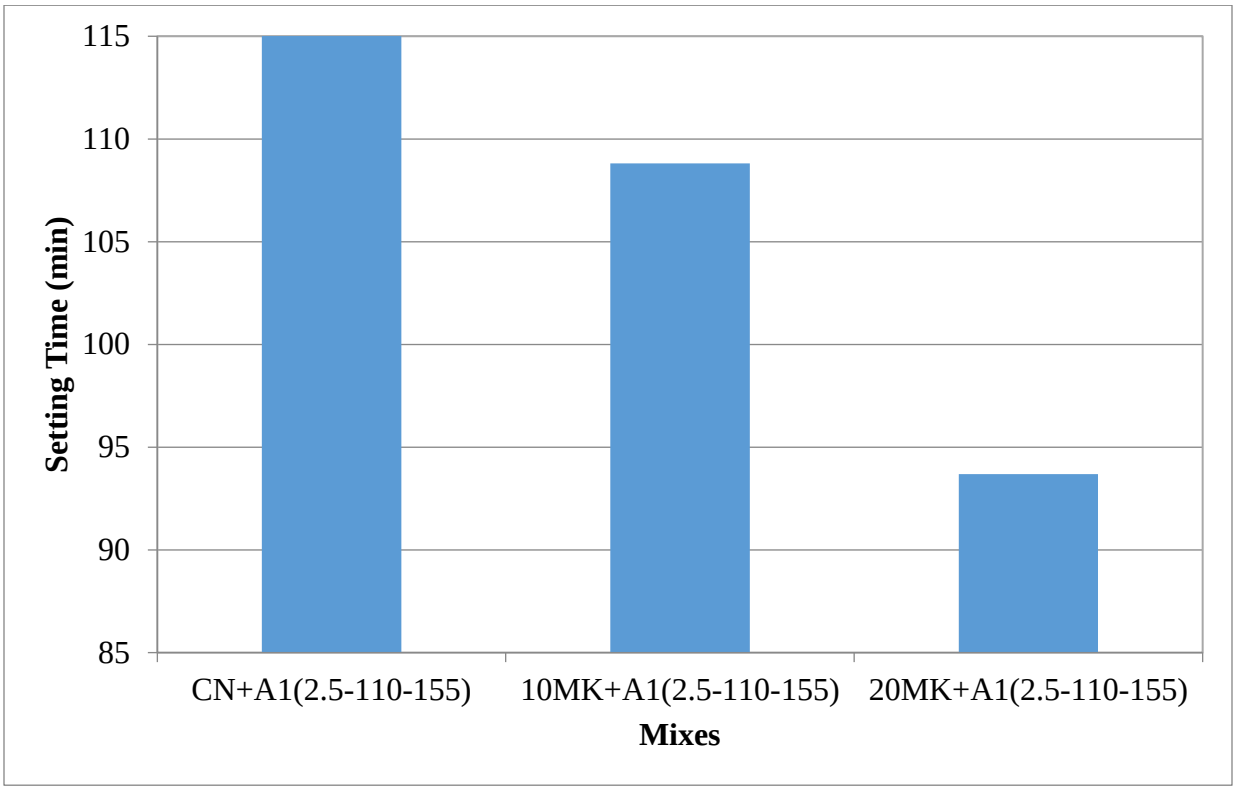

Figure 6-1: Mortar Setting Time for Metakaolin Mixes

Binary Mix: Silica Fume

Figure 6-2 shows the results for the mortar setting time for the silica fume mixes. It is observed from Table 6-1 that the addition of 10% silica fume had little effect on the amount of sand needed to achieve normal consistency, as the difference between the mix and the control was 50 g of silica sand. There appears to have been no significant impact of the addition of 10% silica fume on mortar setting time.

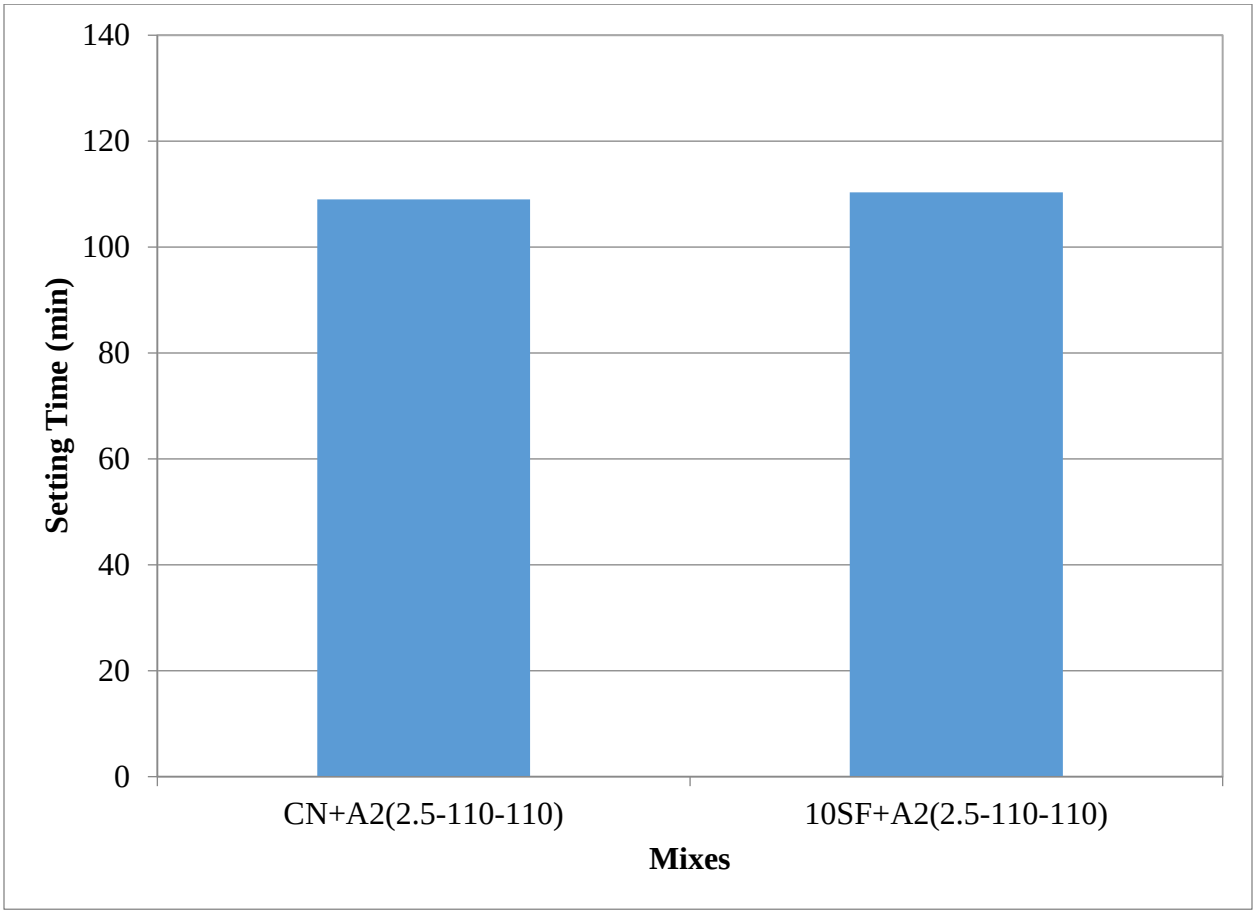

Figure 6-2: Mortar Setting Time for Silica Fume Mixes

Binary Mix: Fly Ash

Figure 6-3 shows the data results for the mortar setting time for fly ash mixes. It is observed from Table 6-1 that the addition of fly ash had little effect on the amount of sand needed to achieve normal consistency, as the difference was only 75 g of silica sand for a replacement level of 30%. From Figure 6-3, it can be observed that a 10% replacement level appears to have had limited

effect on mortar setting time. As the replacement level of FA increased, there was a corresponding increase in setting time. Since fly ash has similar particle size to cement, the results correspond to a decrease in cement content. This is consistent with the results of Kocak and Nas [235], where the addition of fly ash increased the setting times of paste.

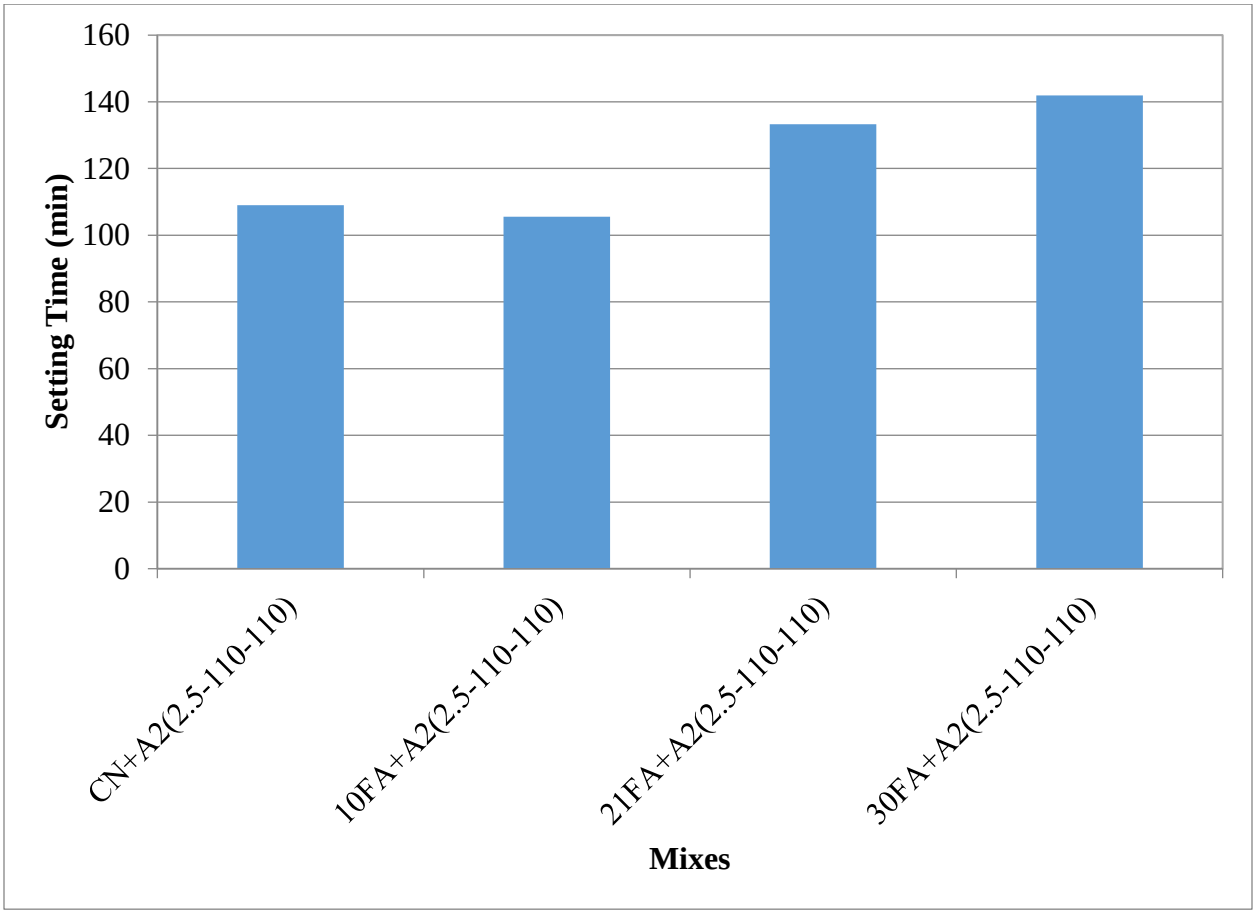

Figure 6-3: Mortar Setting Time for Fly Ash Mixes

Binary Mix: Slag

Figure 6-4 shows the effect of slag replacement on mortar setting time. It is observed from Table 6-1 that the addition of slag had little effect on the amount of sand needed to achieve normal consistency for slag mixes of 21 and 30% mass replacement, as the difference was 25 g of silica sand. For a higher replacement level of 52% slag, an increase in sand content of 75 g was necessary to achieve normal consistency. However, for all replacement levels of slag studied here, there appears to have been no significant impact on mortar setting times, as the difference was under 5

min, for 21, 30, and 52% slag content. The findings of this study are not in agreement with Kourounis et al.[236], where the setting time of the slag paste was found to increase with slag replacement level.

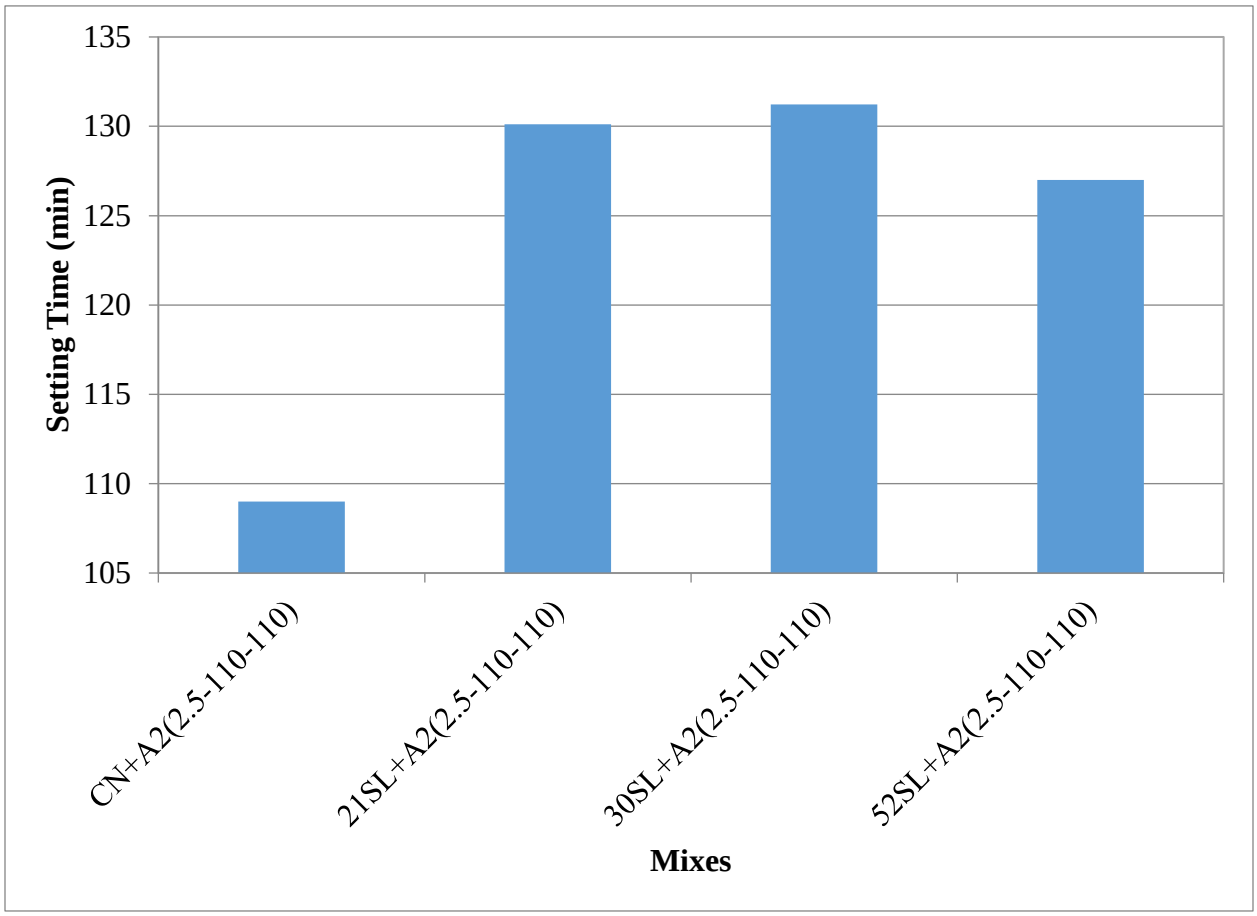

Figure 6-4: Mortar Setting Time for Slag Mixes

Ternary Combinations

In addition to binary mixture combinations, mortar setting times were also evaluated on ternary combinations of cement and mineral admixtures most commonly used in FDOT projects.

Ternary Mix: Metakaolin and Fly Ash

Figure 6-5 shows the data results for the mortar setting time for metakaolin and fly ash mixes. The mortar setting time of the mix containing 10FA+10MK+A1 appears to have been about v\the same compared to the control and to the binary mix of 10FA+A2 or 10MK+A1. The amount of sand needed to achieve normal consistency was similar to the metakaolin mix, showing that

metakaolin had a significant effect on the amount of sand needed versus the control (difference of 150 g for SP2 and 235 g for SP1) mix or fly ash mix (difference of 175 g). The mix containing 40FA+10MK+A1 had a lower amount of sand and a longer setting time. This is similar to the results of the binary mixes for which increasing the fly ash content increased the setting time. The mix containing 10FA+20MK+A1 was similar to the binary mix of 20MK+A1, which shows that the addition of 10% fly ash had little effect on setting times.

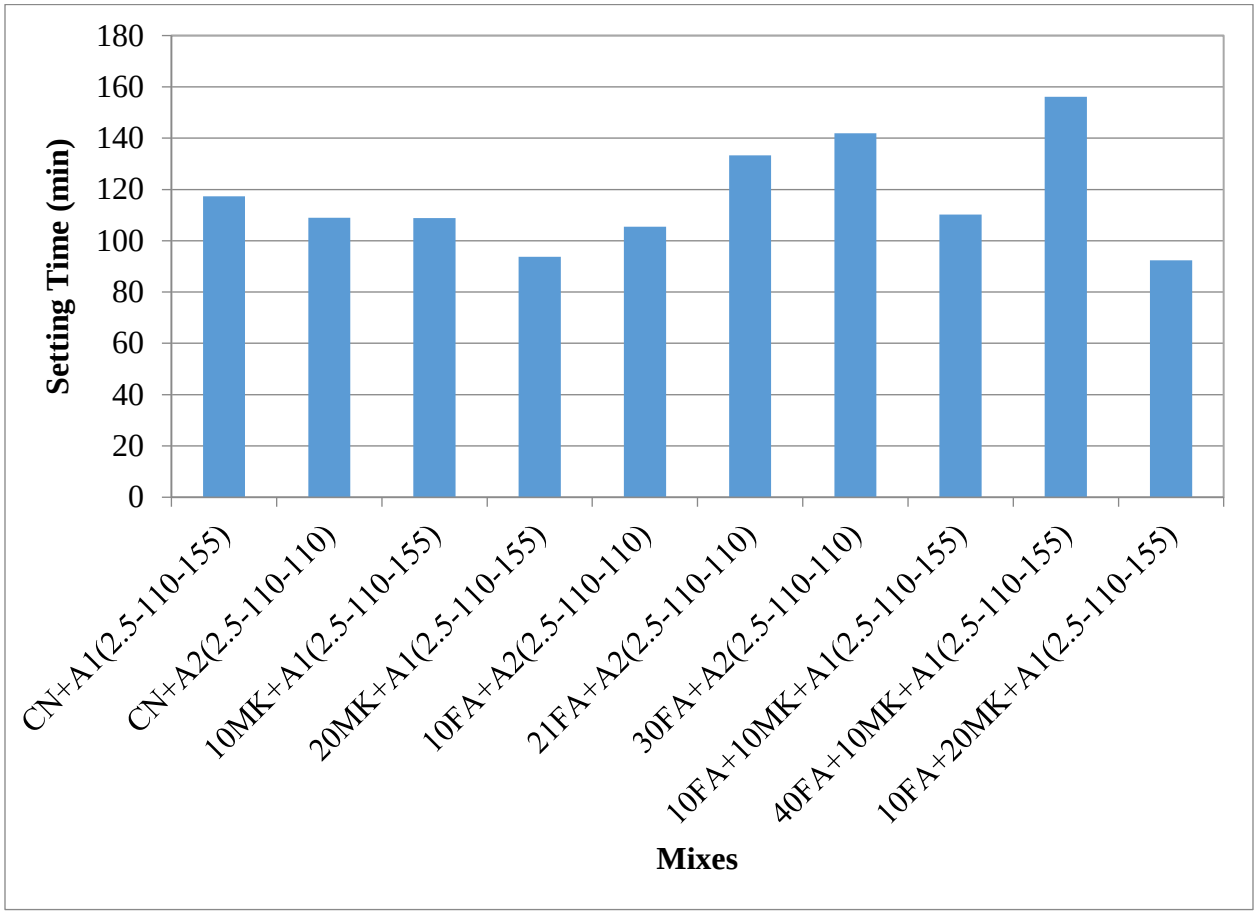

Figure 6-5: Mortar Setting Time for Metakaolin and Fly Ash Mixes

Ternary Mix: Fly Ash and Silica Fume

Figure 6-6 shows the results for the mortar setting time of cement-silica fume, cement-fly ash, and cement-fly ash-silica fume combinations. The ternary mixture of fly ash and silica fume (21FA+10SF+A2) had no impact on the amount of sand needed to achieve normal consistency.

While 21% FA increased setting time, incorporation of 10% silica fume decreased slightly the setting time when compared to the binary mixture of 21FA+A2.

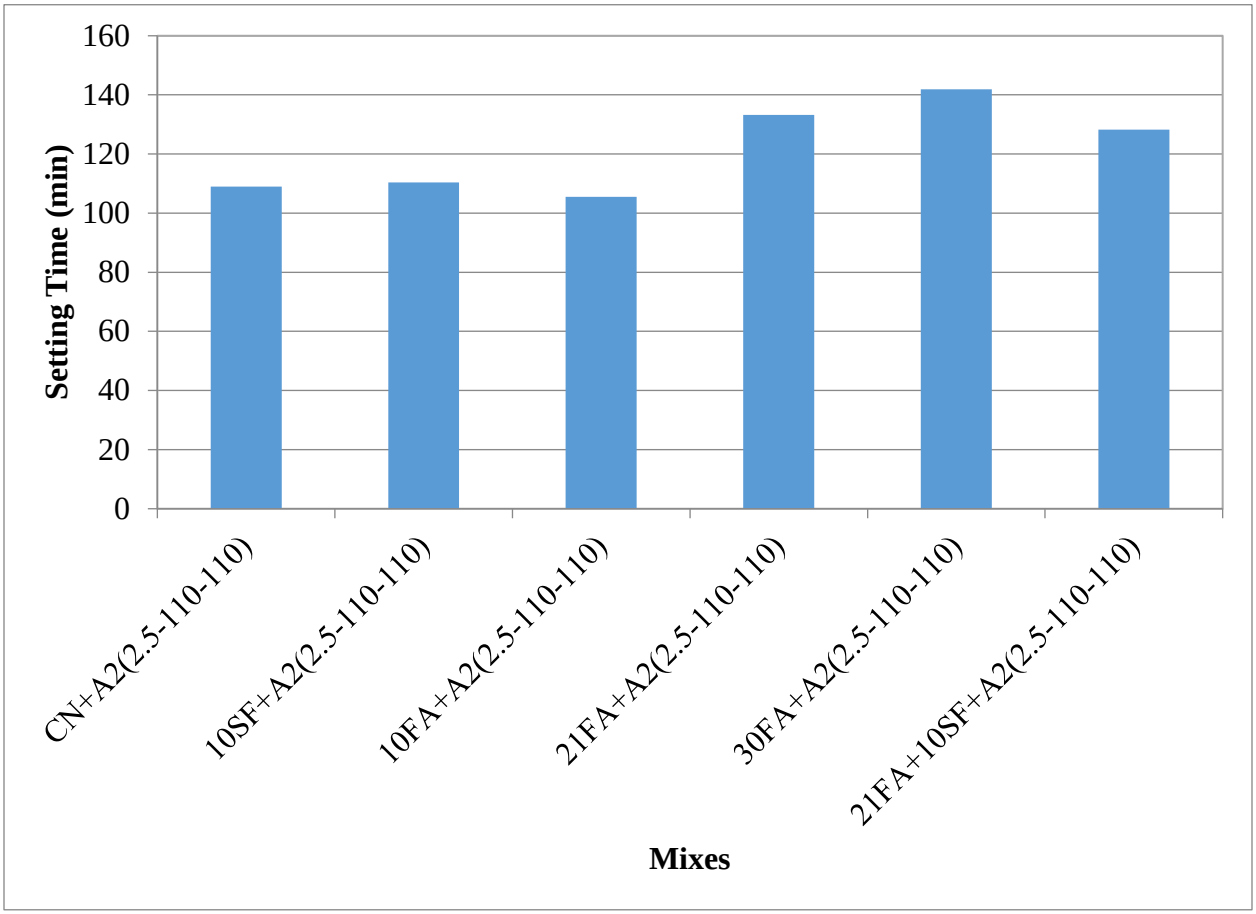

Figure 6-6: Mortar Setting Time for Fly Ash and Silica Fume Mixes

Ternary Mix: Fly Ash and Slag

Figure 6-7 shows the results for the mortar setting time for cement-fly ash-slag mixes. The ternary mixes of fly ash and slag had no significant effect on the amount of sand needed to achieve normal consistency. The mortar setting times were higher than the individual binary mixes. Increasing slag content to 30% in the ternary mix increased the mortar setting time compared to 21% slag. Though the use of FA as a replacement to cement at a level of 21% increased setting time, incorporating slag at 21% increased the setting time to a value similar to the binary cement-30% FA mix. It appears in this mix combination that slag increased the setting time, similar to increasing the replacement level in the FA binary system. Increasing the replacement in the ternary

system by increasing slag content to 30% had the most significant effect on increasing the mixture setting time. When comparing the cement-21% FA-30% slag mixture to the 52% slag mixture, it can be observed that though both mixtures had about the same mineral admixture content, the type of mineral admixture in the combination had a significant effect on the setting properties of the mixture.

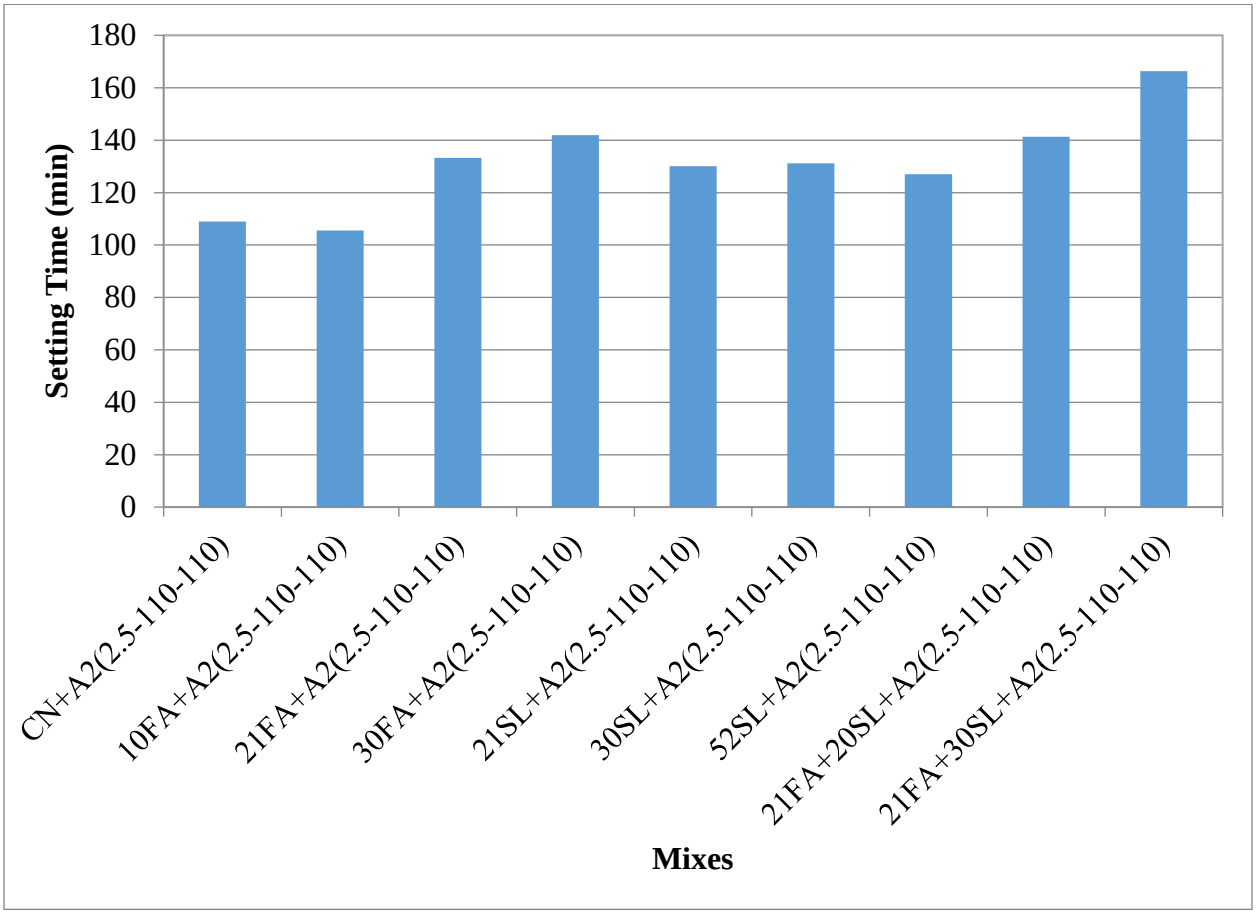

Figure 6-7: Mortar Setting Time for Fly Ash and Slag Mixes

Ternary Mix: Metakaolin and Slag

Figure 6-8 shows the setting time results for cement-metakaolin-slag mixtures. For this ternary metakaolin-slag system, the chemical admixture used for the binary metakaolin mix was adopted. The maximum total cement replacement level (62%) exceeded all binary systems studied here. The setting time was highest but is comparable to the 52% binary slag system.

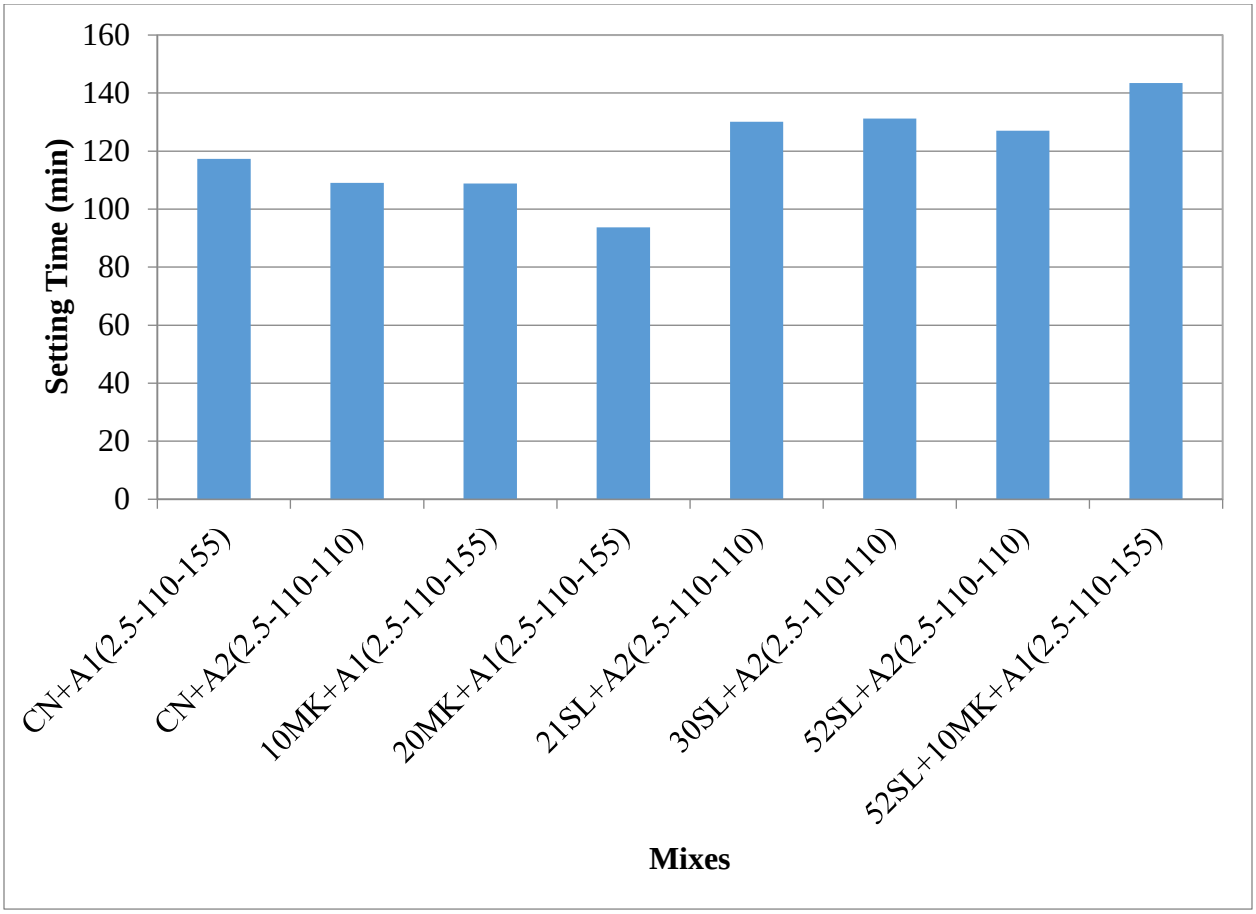

Figure 6-8: Mortar Setting Time for Metakaolin and Slag Mixes

Quaternary Combinations

Mortar setting times were also evaluated on quaternary combinations of cement and mineral admixtures.

Quaternary Mix: Metakaolin, Silica Fume, and Slag

Figure 6-9 shows the results for the mortar setting time of metakaolin, silica fume, and slag quaternary mixtures. The quaternary mix containing 10MK+10SF+20SL+A1 showed a normal consistency similar to the 10MK+A1 mix, having 1,900 g compared to 1,985 g of silica sand. The mortar setting times were close to those of the binary mixes containing metakaolin or silica fume.

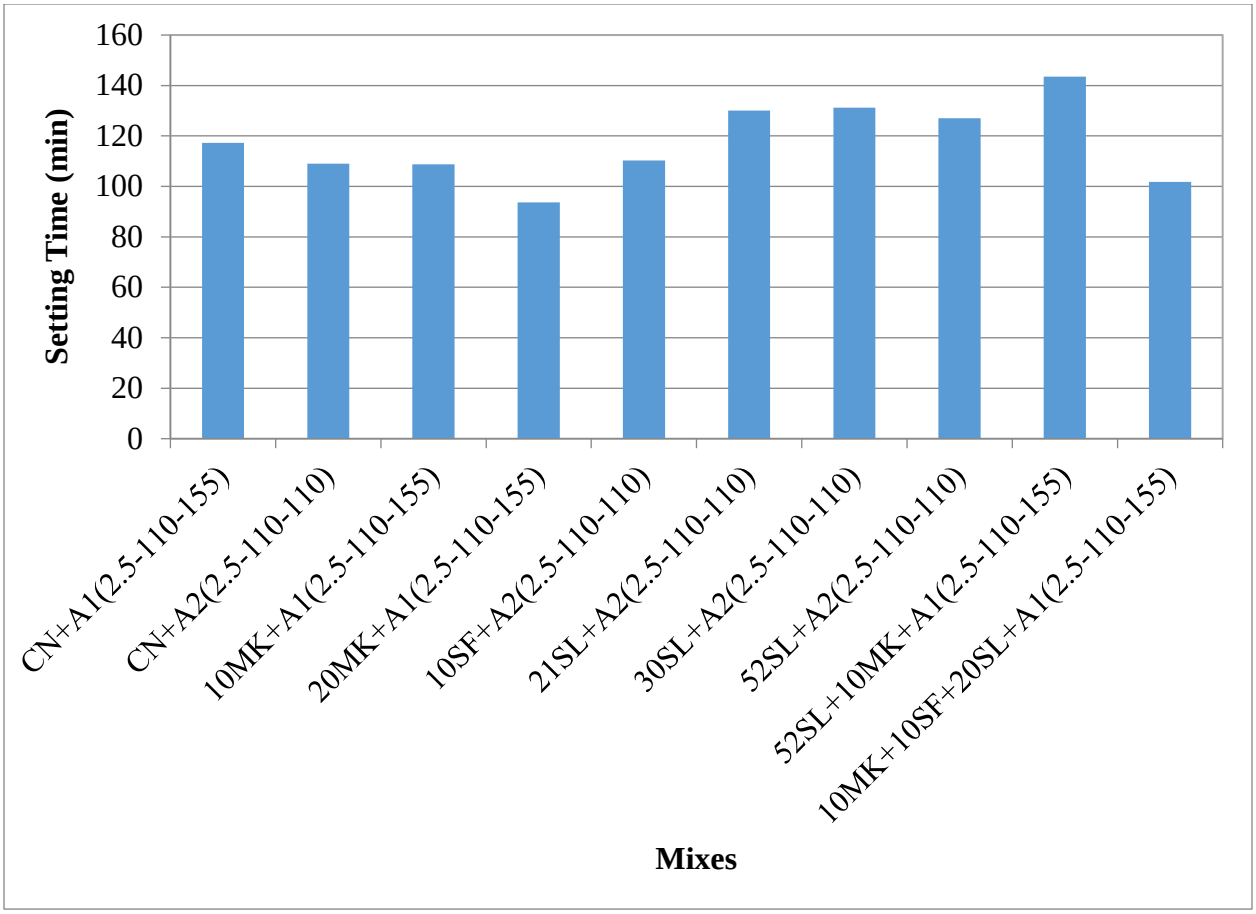

Figure 6-9: Mortar Setting Time for Metakaolin, Silica Fume, and Slag Mixes

Compressive Strength

Binary Combinations

Compressive strength measurements were conducted on mortar cubes prepared with a fixed w/cm ratio. Figure 6-10 shows the results for all of the compressive strength tests. From the results, it appears that at earlier ages the incorporation of metakaolin in mixes resulted in the highest compressive strength. This is consistent with the results from Poon et al. [237], which showed a higher strength development for metakaolin than silica fume at early ages and up to 28 days.

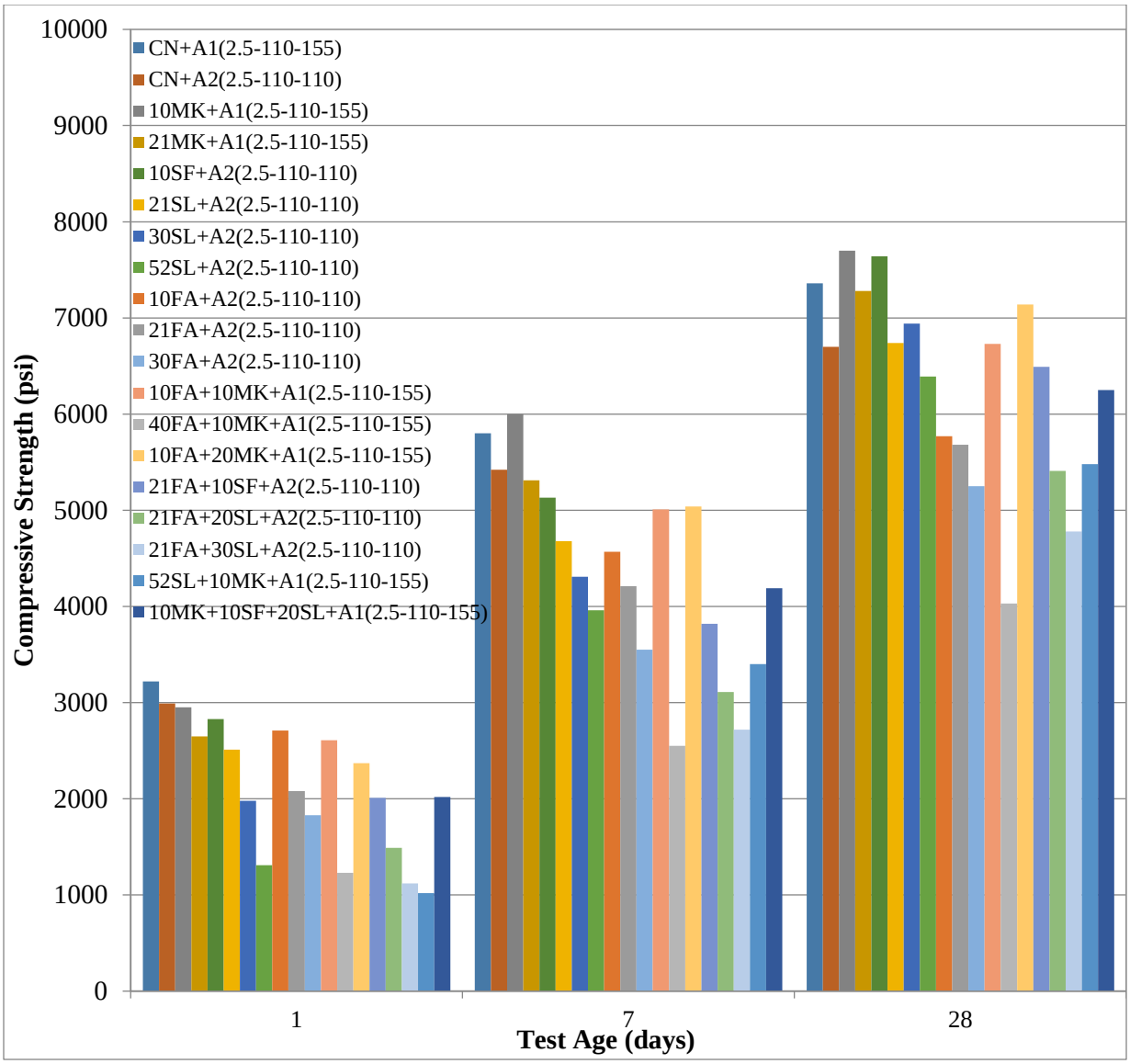

Figure 6-10: Summary of Compressive Strength Tests

[redacted]Binary Mix: Metakaolin

Metakaolin was evaluated at two different replacement levels: 10 and 21%. Figure 6-11 shows the results for the compressive strength gain for metakaolin mixtures. It appears that as the replacement level of metakaolin increased, the 28-day compressive strength decreased. At all ages, the increase in replacement levels of metakaolin decreased the compressive strength. This is consistent with the results of Poon et al. [237], who also found that as the dosage of metakaolin increased from replacement levels of 10% to 20 %, the compressive strength of concrete decreased.

There is higher early strength development at a 10% replacement level, whereas the 20% replacement level had a lower strength than the control. The same results were found for the 28-day compressive strength. Wild et al. [238], however, found that the optimum level of metakaolin for concrete was 20% at a w/cm ratio of 0.45. According to Wild et al., the factors that metakaolin contributes to concrete strength are: the filler effect, the acceleration of OPC hydration, and the pozzolanic reaction of metakaolin with CH. Kadri et al. [239] investigated two metakaolins with different surface area (19 m^2/g and 17 m^2/g) and average particle size (about 1.4 µm and 13 µm, respectively) at 10% replacement levels. They found that the mortars containing the metakaolin with the significantly smaller particle size had a relative strength gain (compared to the control) of about 17% at 7 days and about 21% at 28 days. Li and Ding [120] investigated 10% replacement by metakaolin and found an increase in strength of 8 MPa following the same replacement level as Kadri.

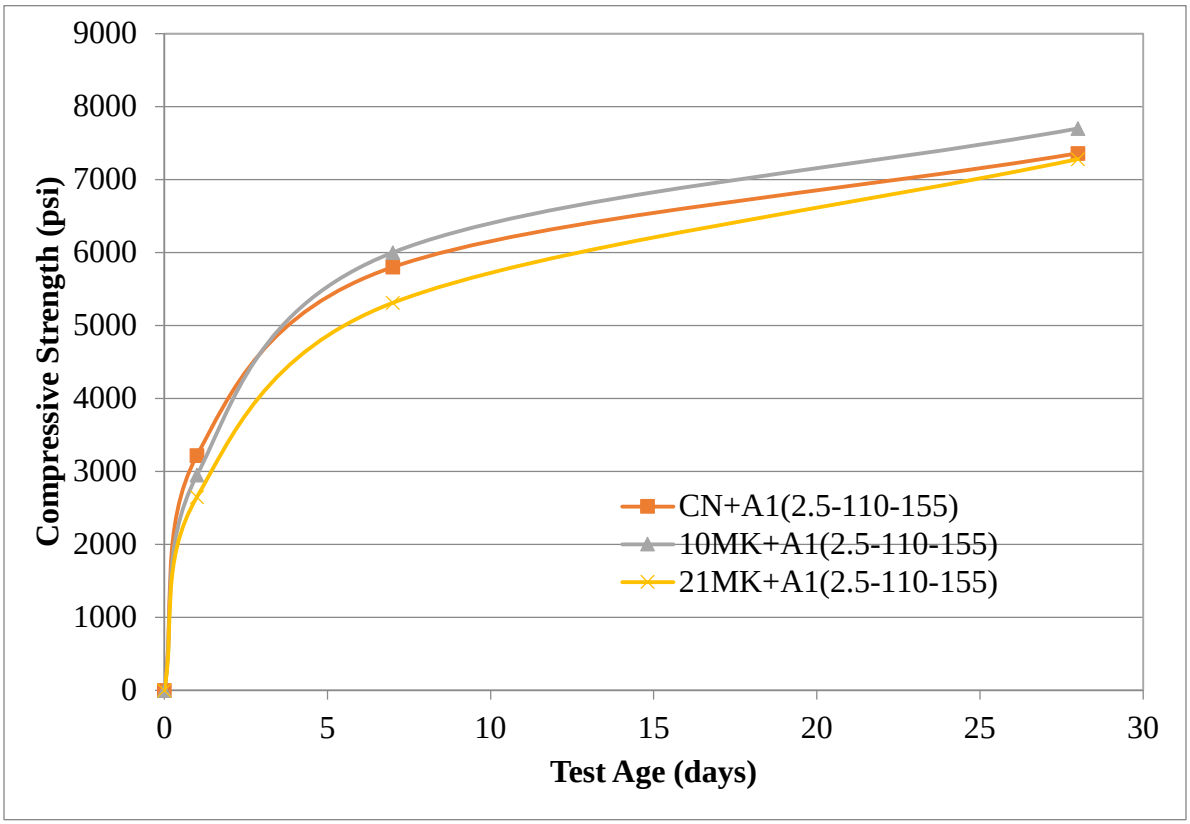

Figure 6-11: Compressive Strength of Metakaolin Mixes

Binary Mix: Silica Fume

Silica Fume was only evaluated at 10% mass replacement of cement because higher replacement levels are not used by the FDOT (3-9%). Figure 6-12 shows the results for the compressive strength data for the silica fume mixes. It appears that the addition of silica fume increased the later-age strength, whereas the control mix had the highest early-age compressive strength. This is consistent with the findings of Toutanji et al. [240], where additions of silica fume increased the mortar strength. Rao [241] investigated the effect of silica fume on compressive strength and found that the optimum silica fume replacement level was within the range of 17.5 and 22.5%. Mohamed [242] investigated the compressive strength of silica fume and found that the optimum level of replacement was 15%. Erdem and Kirca [129] found that for a binder content of 500, 550, 650, and 700 kg/m^3, the optimum replacement level of silica fume was 15%, and for a binder content of 600 kg/m^3, the optimum level was 10%. According to Erdem and Kirca [129], improvements in compressive strength of mixes containing silica fume can be explained by the chemical and physical effects of silica fume. The pozzolanic reaction between the amorphous silica and calcium hydroxide forms more calcium-silicate-hydrate gel. The silica fume particles improve the packing at the interfacial transition zone, thus reducing the size of the pores and forming a denser microstructure.

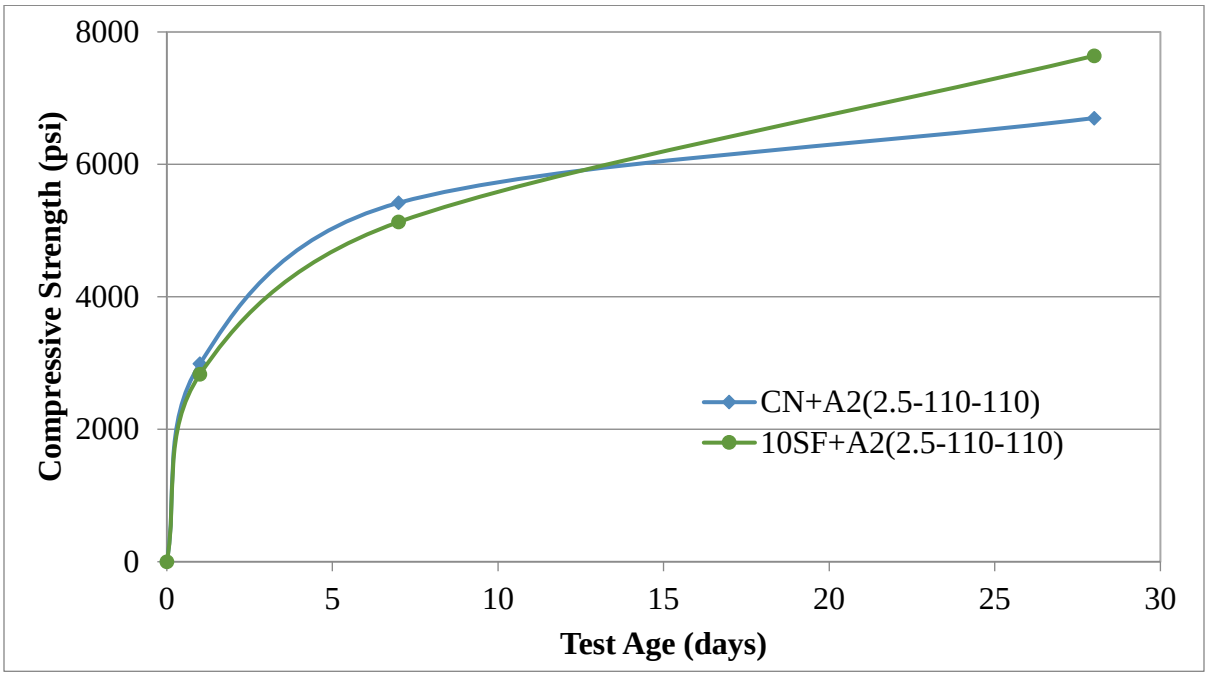

Figure 6-12: Compressive Strength of Silica Fume Mixes

Binary Mix: Fly Ash

Fly Ash was evaluated at 3 different replacement levels: 10, 21, and 30%. Figure 6-13 depicts the variation in compressive strength for the fly ash mixes. The 30% fly ash mix had the lowest early-age compressive strength, while the control had the highest. It appears that as the replacement level increased, there was a corresponding decrease in the compressive strength for all ages tested here. This is consistent with the results from Fan et al. [243] and Kocak and Nas [235], where it was found that as the replacement level of fly ash increased, the compressive strength decreased. From the results by Fan et al., there is a minimal change in compressive strength from the 5% to 15% replacement level. Liu et al. [244] noted that the decrease in strength is due to fly ash having little effect on the chemical activity for early ages. A study by Poon et al. [245] indicated that additions of fly ash to concrete at 25% fly ash replacement showed the highest compressive strength at 28-days. The FA used in this current study had an amorphous content of approximately 72%, which is substantially lower than for typical fly ashes, and may account for its reduced level of performance.

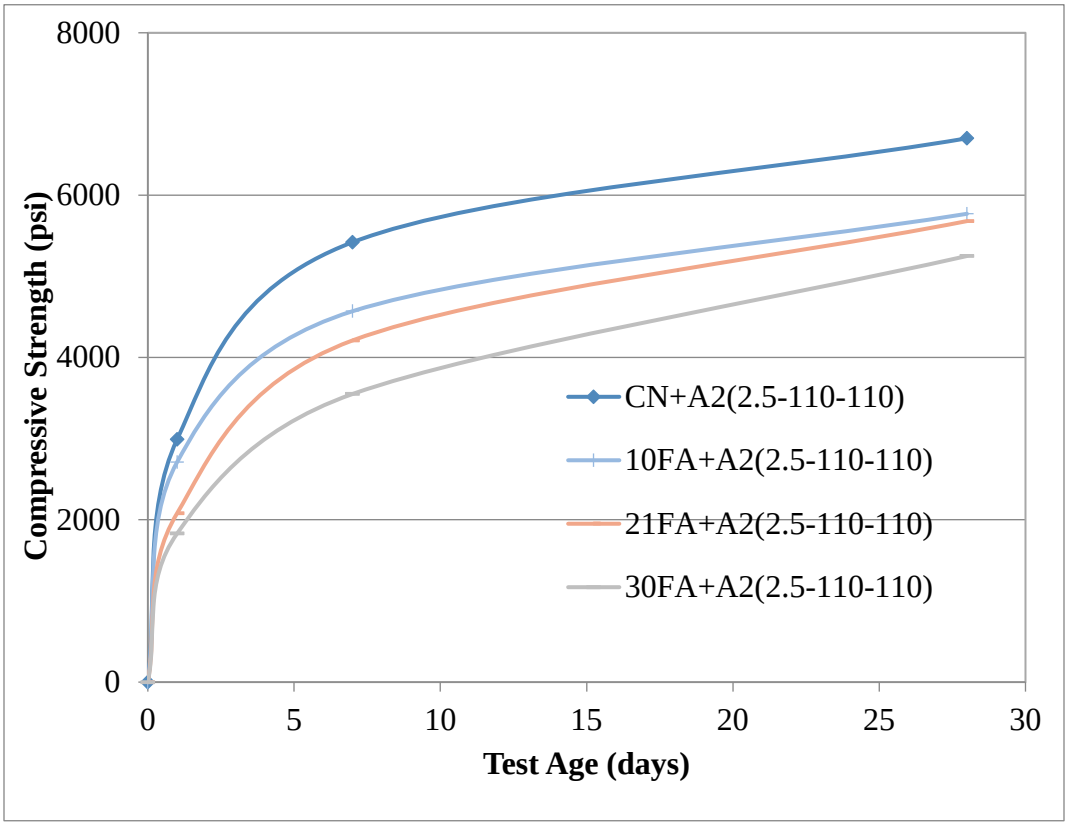

Figure 6-13: Compressive Strength of Fly Ash Mixes

Binary Mix: Slag

Slag was evaluated at 3 different replacement levels: 21, 30, and 52%. Figure 6-14 shows the compressive strength results for slag mixtures. The 52% slag mix had the lowest early-age compressive strength, while the control had the highest. It appears that the early-age strength decreased as the replacement level increased. This is consistent with the results from Menendez et al. [246], where it was found that as the replacement level of slag is increased, the compressive strength decreased. Work by Menendez indicates a minimal change in compressive strength at 10% to 35% replacement levels; that is, at 28 days the strength was the same (42.4 MPa). A study by Aldea et al. [247] found that at a replacement level of 25% slag, concrete showed an optimal compressive strength. At 28 days, the 30% slag mixture in this study showed the highest compressive strength.

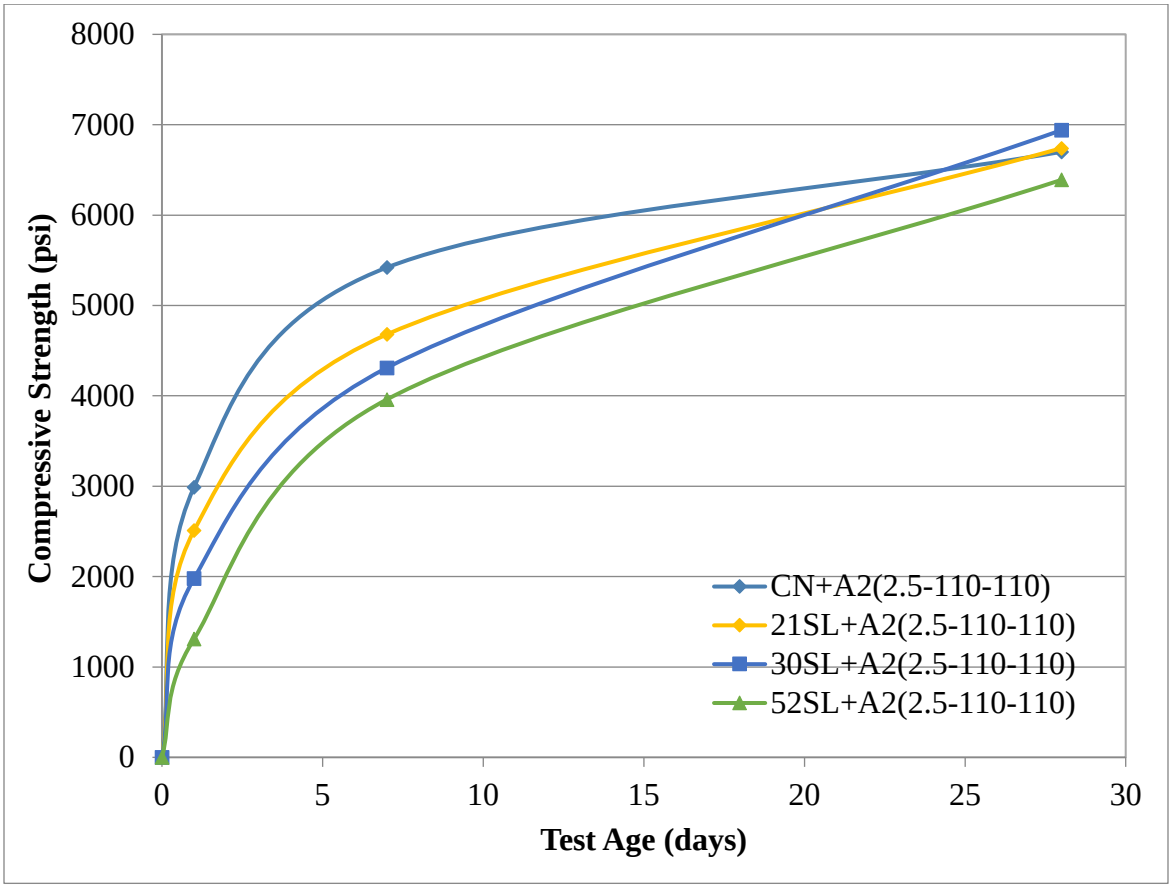

Figure 6-14: Compressive Strength of Slag Mixes

Ternary Combinations

In addition to binary combinations, the compressive strength was also evaluated for ternary combinations of cement and mineral admixtures.

Ternary Mix: Metakaolin and Fly Ash

Figure 6-15 shows the compressive strength results for metakaolin and fly ash mixes. The 40% fly ash with 10% metakaolin mix had the lowest early-age compressive strength, while the 10% metakaolin mix had the highest strength. Incorporation of 10% metakaolin showed the highest early-age compressive strength. Comparing metakaolin and fly ash, metakaolin showed a higher compressive strength at all ages. This is consistent with the results from Roy et al. [248], where it was shown that metakaolin mixtures showed a higher compressive strength than fly ash mixtures. The ternary mixes containing both metakaolin and fly ash showed that the addition of fly ash produced a lower 28-day strength compared to 10% metakaolin. This is not necessarily indicative of the mixture effect, but perhaps the quality of the ash. Comparing the total replacement levels of 21% metakaolin, 21% fly ash, and 10% fly ash+10% metakaolin, the 7-day compressive strengths were 5310 psi, 4210 psi, and 5010 psi, respectively. The 28-day compressive strengths were 7280 psi, 5680 psi, and 6730 psi, respectively. Incorporating 10% metakaolin to a 10% FA mixture resulted in an improvement of the compressive strength as early as 7 days.

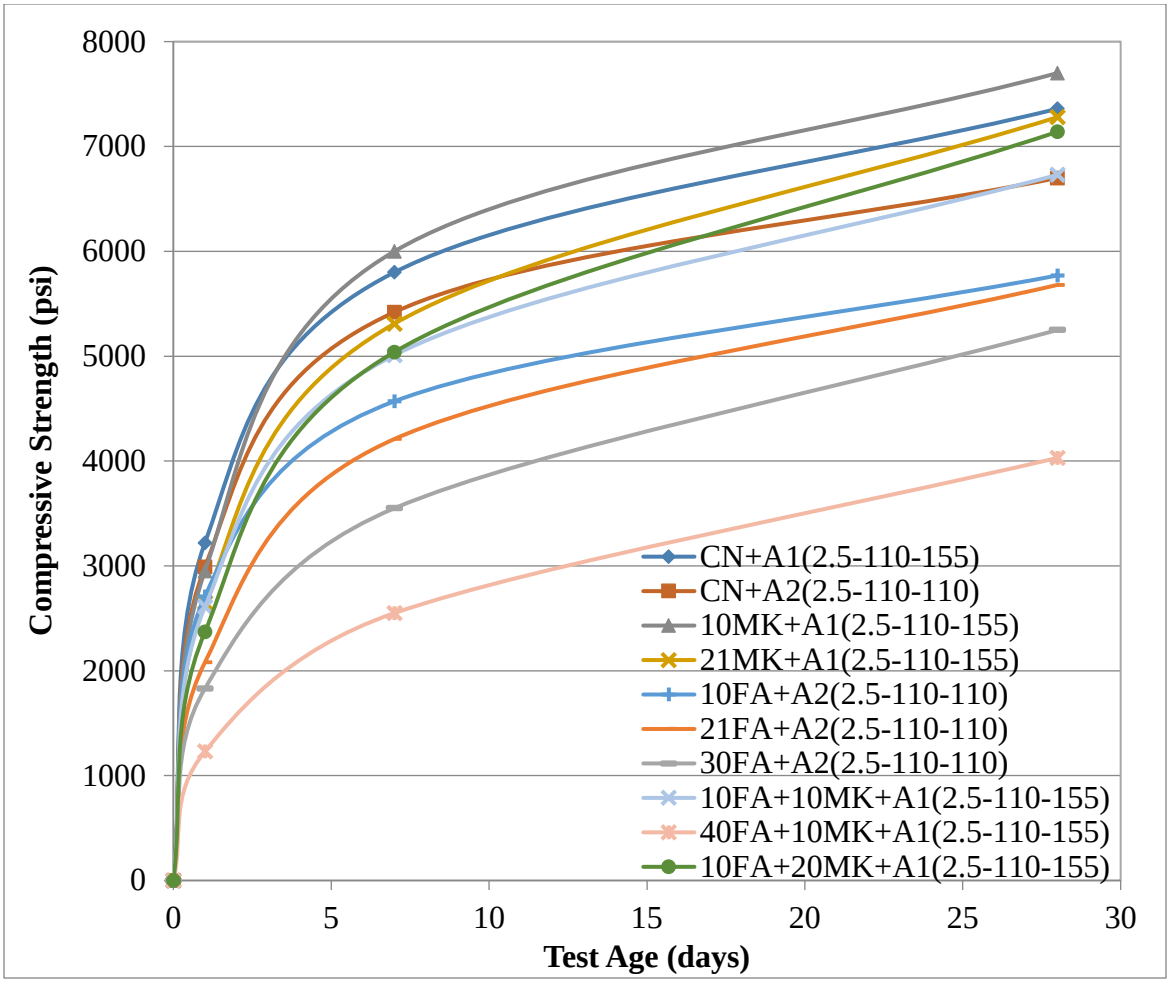

Figure 6-15: Compressive Strength of Metakaolin and Fly Ash Mixes

[redacted]Ternary Mix: Fly Ash and Silica Fume

Figure 6-16 shows the compressive strength results for fly ash and silica fume mixes. The 30% fly ash mix produced the lowest compressive strength at all ages. At 1 and 7 days, the control had the highest strength, though at 7 days the 10% silica fume was almost as strong as the control mixture. The data for the ternary blend of fly ash and silica fume show that the addition of silica fume to the 21% replacement level of fly ash increased the strength at 28 days. Liu et al. [244] and Wongkeo et al. [249] noted that the addition of silica fume to fly ash would increase the strength. Liu et al. found that when the cement replacement levels of fly ash and silica fume were between 10% to 30% and 2% to 8%, respectively, the compressive strength increased. Wongkeo et al. also found that the addition of silica fume to ternary and quaternary mixes would increase strength and

noted that the increase is due to a higher pozzolanic reaction and greater fineness. Again, it is believed that the observed trends will be significantly affected by the amorphous content of FA.

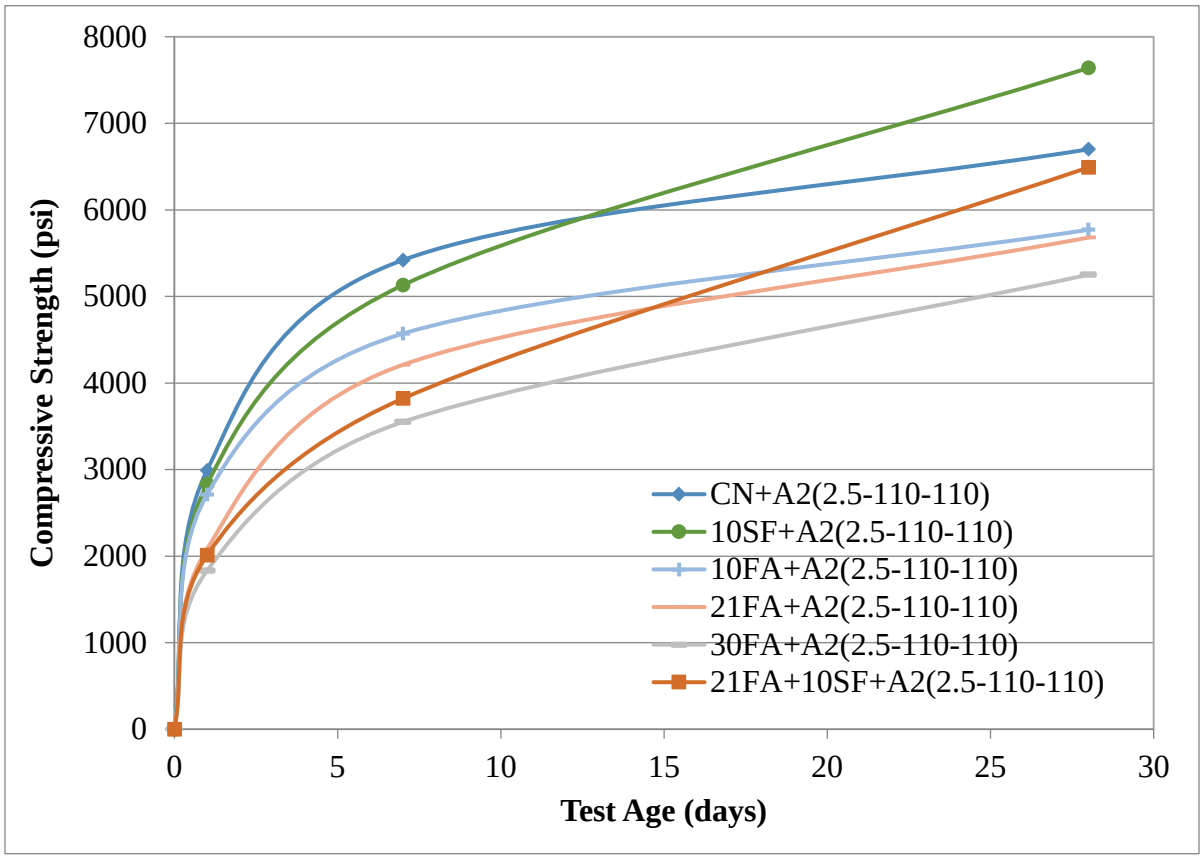

Figure 6-16: Compressive Strength of Fly Ash and Silica Fume Mixes

Ternary Mix: Fly Ash and Slag

Figure 6-16 shows the compressive strength of fly ash and slag mixtures. The combination of 21% fly ash and 30% slag produced the lowest early-age compressive strength, while the control had the highest strength. At all levels of replacement with fly ash, the compressive strength decreased at all ages compared to the control mixture. It appears that the addition of fly ash decreased the early-age strength. Gesoğlu et al. [250] found that the combination of 10% fly ash and 10% slag had the highest compressive strength out of the 22 mixtures that were tested. The mixtures containing 21% or 30% slag showed almost no difference from the control mixture for the 28-day strength.

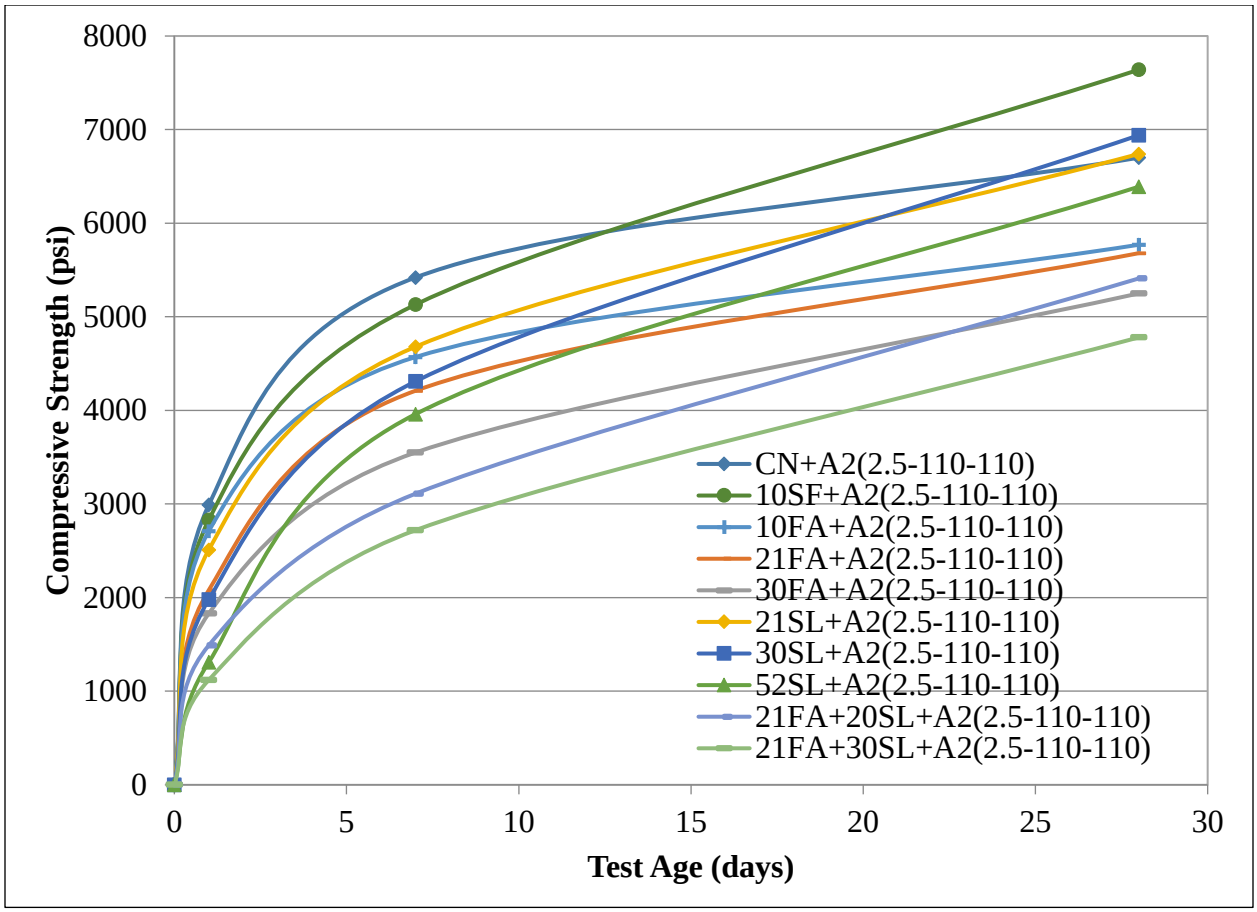

Figure 6-17: Compressive Strength of Fly Ash and Slag Mixes

Ternary Mix: Metakaolin and Slag

Figure 6-18 shows the compressive strength of metakaolin and slag mixes. The 52% slag with 10% metakaolin mix had the lowest early-age strength, while 10% metakaolin had the highest. Addition of slag to metakaolin decreased the early-age strength. This is consistent with Li and Ding [120] who found that at early age, the mix with both metakaolin and slag had a lower compressive strength than the control. According to Li and Ding, slag hydrates slower than the alite, meaning a slow strength development. The mixture of 10% metakaolin had the highest 28-day compressive strength. Li and Ding also found that the mixtures containing 10% metakaolin with 20% slag, and 10% metakaolin with 30% slag, have a higher 28-day compressive strength than the control.

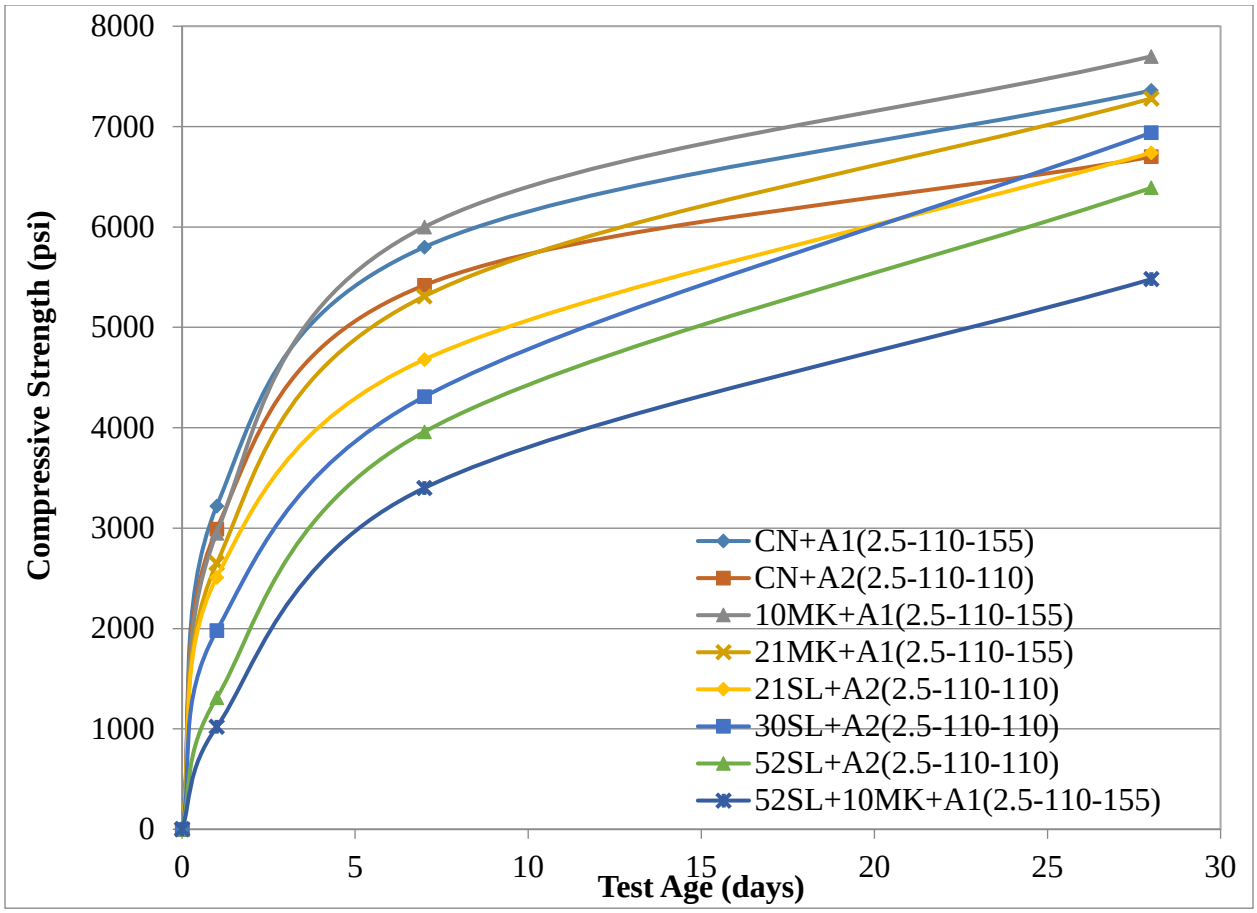

Figure 6-18: Compressive Strength of Metakaolin and Slag Mixes

Quaternary Combinations

Compressive strength was also evaluated on quaternary combinations of cement and mineral admixtures.

Quaternary Mix: Metakaolin, Silica Fume, and Slag

Figure 6-19 shows the compressive strength of metakaolin, silica fume, and slag mixes. The 52% slag mix had the lowest early-age compressive strength while the 10% metakaolin mix had the highest. The 10% metakaolin mix with 10% silica fume and 20% slag mix had the second lowest early-age compressive strength. The 10% metakaolin mix had the highest compressive strength at all ages studied here among pozzolan-containing mixtures.

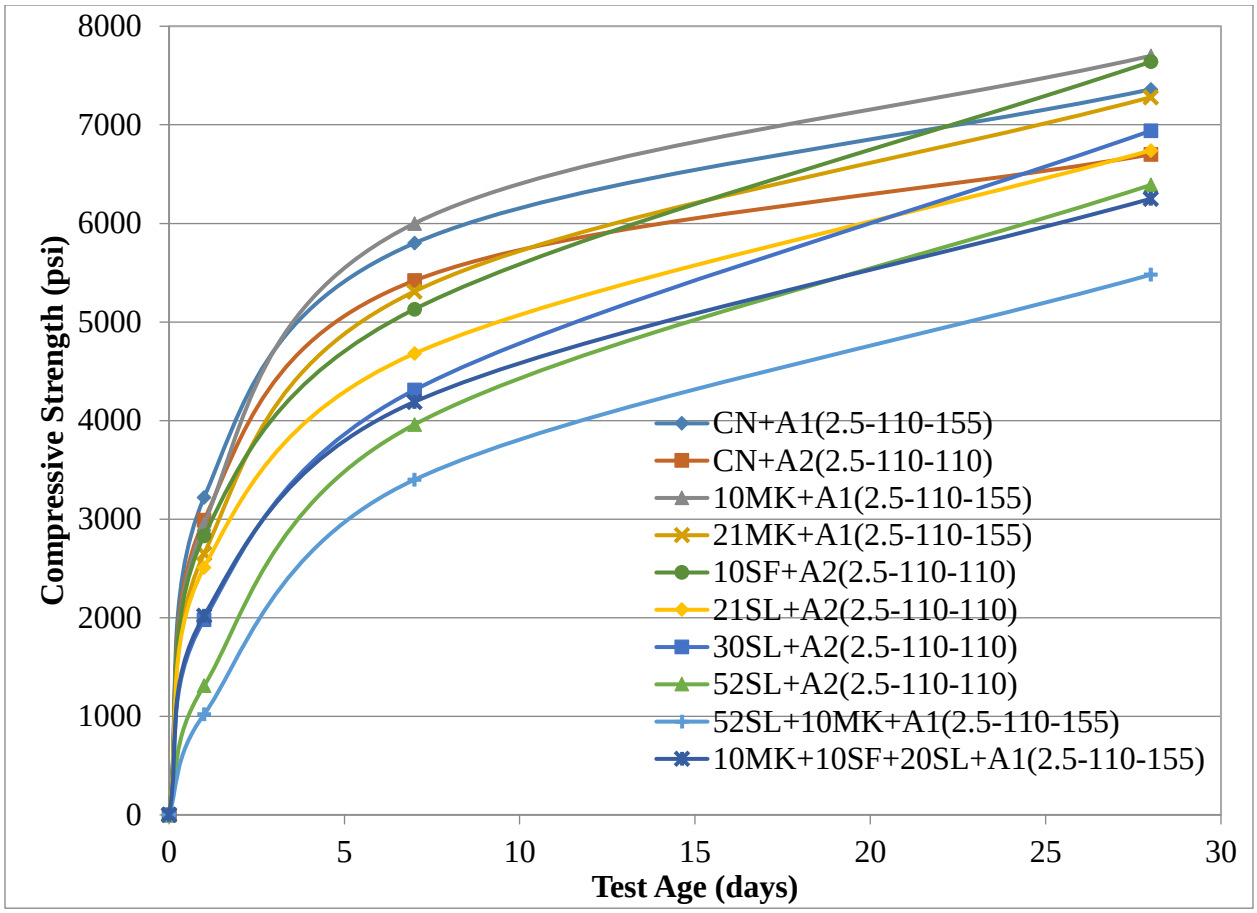

Figure 6-19: Compressive Strength of Metakaolin, Silica Fume, and Slag Mixes

Conclusion

In general, it can be concluded that incorporation of metakaolin, at a replacement level of 10%, gave the highest 7-day compressive strength among all mixtures studied here. Additionally, at 10% replacement level, FA and SF had similar setting times compared to the control paste, while incorporating slag increased the setting time and incorporating metakaolin decreased the setting time when compared to the control mixture.

Effect of Chemical Admixtures Dosage on Cured Properties

Introduction

This chapter addresses the effects of chemical admixture types and dosages on setting time and compressive strength gain of cementitious mixtures. The same as-received materials used in earlier chapters were used here; namely, SF, SL, MK FA, WR, SP1, SP2 and AE. For reference, the chemical composition of each mineral admixture is shown again in Table 7-1. The focus is to study specifically the effects of high-range water-reducer (superplasticizer) dosage on setting properties and strength gain. The superplasticizers, SP1 and SP2, are both polyacrylate-based high-range water-reducing admixtures meeting the requirements of ASTM C494 Type A and F, and ASTM C1017 Type I. Both were selected as they are most commonly used in approved FDOT mixtures.

Table 7-1: Chemical Oxide Composition of Mineral Admixtures

Analyze	SL	MK	SF	FA
SiO_2	35.15	51.29	92.9	55.48
Al_2O_3	14.25	44.16	0.31	27.46
Fe_2O_3	0.48	0.49	0.1	6.7
CaO	41.45	<0.01	0.78	0.99
MgO	5.21	0.14	0.18	0.88
SO_3	1.86	<0.01	<0.01	0.05
Na_2O	0.22	0.26	0.1	0.29
K_2O	0.32	0.27	0.52	2.28
TiO_2	0.5	1.12	<0.01	1.47
P_2O_5	0.01	0.06	0.09	0.21
Mn_2O_3	0.22	<0.01	0.04	0.02
SrO	0.05	0.01	0.01	0.09
Cr_2O_3	<0.01	0.01	<0.01	0.03
ZnO	<0.01	<0.01	0.05	0.01
BaO	0.07	<0.01	<0.01	0.15
L.O.I.	0.04	1.4	4.55	3.83
Total	99.83	99.2	99.63	99.93

Methodology

Setting Time and Normal Consistency

Setting time for mortar mixes was determined following ASTM C807 [231] and using a modified Vicat apparatus. For all mixtures, the amount of cementitious material (750 g) and the water-to-cementitious material ratio (w/cm = 0.5) were maintained constant. Dosages of air entrainer (2.5 ml per 100 kg cementitious material) and water reducer (200 ml per 100 kg cementitious material) were maintained constant. Superplasticizer dosage was either 100 ml per 100 kg cementitious material or 170 ml per 100 kg cementitious material for both types (0.108 and 0.184 weight percent (wt%), respectively). Normal consistency was determined by using various amounts of silica sand to achieve a penetration target of 20 ± 4 mm. Once normal consistency was determined, setting time was determined as the time when a penetration of 10 mm or less was achieved. The mixture proportions are presented in Table 7-2 and Table 7-3. Normal consistency determinations are presented in Table 7-6.

Compressive Strength

Mortar cubes were prepared and tested following ASTM C109 [232]. The mixture proportions are presented in Table 7-4 and Table 7-5. Compressive strength tests were conducted on 2-in cube specimens. Testing ages were 1, 7, and 28 days. After the 1-day test, the mortar cubes were submerged in a saturated lime solution. The mortar was mixed following ASTM C305 [251]. Each mixture was made following the proportions for a 9-cube mix: 740 g of cementitious materials, 2035 g of Ottawa sand, and a water-to-cementitious material ratio (w/cm) of 0.485. Chemical admixtures were also incorporated into each mix. The amount of water in each chemical admixture was taken into account to maintain a constant w/cm ratio. The air-entrainer and water-reducer were kept constant for all mixes at 2.5 ml per 100 kg cementitious material (CM) and 200 ml per 100 kg cementitious material, respectively. Superplasticizer additions were 100 ml per 100 kg cementitious material or 170 ml per 100 kg cementitious material for both types.

Table 7-2: Binary Setting Time Mix Design

Mix Design	Cement (g)	MK (g)	FA (g)	SF (g)	Slag (g)	Sand (g)	AE Solution (g)	WR (g)	SP1 (g)	SP2 (g)	AE (ml/ 100 kg CM)	WR (ml/ 100 kg CM)	SP1 (ml/ 100 kg CM)	SP2 (ml/ 100 kg CM)	Water (g)
CN+A1(2.5-200-170)	750					2,255	3.7	1.7	1.35		2.5	200	170		369.4
CN+A2(2.5-200-170)	750					2,150	3.7	1.7		1.36	2.5	200		170	369.2
10MK+A1(2.5-200-170)	675	75				2,050	3.7	1.7	1.35		2.5	200	170		369.4
10SF+A2(2.5-200-170)	675			75		2,175	3.7	1.7		1.36	2.5	200		170	369.2
21FA+A2(2.5-200-170)	592.5		157.5			2,175	3.7	1.7		1.36	2.5	200		170	369.2
52SL+A2(2.5-200-170)	360				390	2,275	3.7	1.7		1.36	2.5	200		170	369.2
CN+A1(2.5-200-100)	750					2,235	3.7	1.7	0.8		2.5	200	100		369.7
CN+A2(2.5-200-100)	750					2,150	3.7	1.7		0.8	2.5	200		100	369.6
10MK+A1(2.5-200-100)	675	75				2,000	3.7	1.7	0.8		2.5	200	100		369.7
10SF+A2(2.5-200-100)	675			75		2,125	3.7	1.7		0.8	2.5	200		100	369.6
21FA+A2(2.5-200-100)	592.5		157.5			2,175	3.7	1.7		0.8	2.5	200		100	369.6
52SL+A2(2.5-200-100)	360				390	2,250	3.7	1.7		0.8	2.5	200		100	369.6

Table 7-3: Ternary and Quaternary Setting Time Mix Design

Mix Design	Cement (g)	MK (g)	FA (g)	SF (g)	Slag (g)	Sand (g)	AE Solution (g)	WR (g)	SP1 (g)	SP2 (g)	AE (ml/ 100 kg CM)	WR (ml/ 100 kg CM)	SP1 (ml/ 100 kg CM)	SP2 (ml/ 100 kg CM)	Water (g)
10FA+10MK+A1(2.5-200-170)	600	75	75			2,150	3.7	1.7	1.35		2.5	200	170		369.4
21FA+10SF+A2(2.5-200-170)	517.5		157.5	75		2,175	3.7	1.7		1.36	2.5	200		170	369.2
21FA+30SL+ A2(2.5-200-170)	367.5		157.5		225	2,325	3.7	1.7		1.36	2.5	200		170	369.2
52SL+10MK+A1(2.5-200-170)	285	75			390	2,200	3.7	1.7	1.35		2.5	200	170		369.4
10FA+10MK+A1(2.5-200-100)	600	75	75			2,025	3.7	1.7	0.8		2.5	200	100		369.7
21FA+10SF+ A2(2.5-200-100)	517.5		157.5	75		2,100	3.7	1.7		0.8	2.5	200		100	369.6
21FA+30SL+ A2(2.5-200-100)	367.5		157.5		225	2,225	3.7	1.7		0.8	2.5	200		100	369.6
52SL+10MK+A1(2.5-200-100)	285	75			390	1,975	3.7	1.7	0.8		2.5	200	100		369.7
10MK+10SF+20SL+A1(2.5-200-170)	450	75		75	150	2,050	3.7	1.7	1.35		2.5	200	170		369.4
10MK+10SF+20SL+A1(2.5-200-100)	450	75		75	150	1,925	3.7	1.7	0.8		2.5	200	100		369.7

Table 7-4: Binary Compressive Strength Mix Design

Mix Design	Cement (g)	MK (g)	FA (g)	SF (g)	Slag (g)	Sand (g)	AE Solution (g)	WR (g)	SP1 (g)	SP2 (g)	AE (ml/ 100 kg CM)	WR (ml/ 100 kg CM)	SP1 (ml/ 100 kg CM)	SP2 (ml/ 100 kg CM)	Water (g)
CN+A1(2.5-200-170)	740					2,035	3.7	1.7	1.35		2.5	200	170		353.3
CN+A2(2.5-200-170)	740					2,035	3.7	1.7		1.36	2.5	200		170	353.1
10MK+A1(2.5-200-170)	666	74				2,035	3.7	1.7	1.35		2.5	200	170		353.3
10SF+A2(2.5-200-170)	666			74		2,035	3.7	1.7		1.36	2.5	200		170	353.1
21FA+A2(2.5-200-170)	584.6		155.4			2,035	3.7	1.7		1.36	2.5	200		170	353.1
52SL+A2(2.5-200-170)	355.2				384.8	2,035	3.7	1.7		1.36	2.5	200		170	353.1
CN+A1(2.5-200-100)	740					2,035	3.7	1.7	0.8		2.5	200	100		353.6
CN+A2(2.5-200-100)	740					2,035	3.7	1.7		0.8	2.5	200		100	353.5
10MK+A1(2.5-200-100)	666	74				2,035	3.7	1.7	0.8		2.5	200	100		353.6
10SF+A2(2.5-200-100)	666			74		2,035	3.7	1.7		0.8	2.5	200		100	353.5
21FA+A2(2.5-200-100)	584.6		155.4			2,035	3.7	1.7		0.8	2.5	200		100	353.5
52SL+A2(2.5-200-100)	355.2				384.8	2,035	3.7	1.7		0.8	2.5	200		100	353.5

Table 7-5: Ternary and Quaternary Compressive Strength Mix Design

Mix Design	Cement (g)	MK (g)	FA (g)	SF (g)	Slag (g)	Sand (g)	AE Solution (g)	WR (g)	SP1 (g)	SP2 (g)	AE (ml/ 100 kg CM)	WR (ml/ 100 kg CM)	SP1 (ml/ 100 kg CM)	SP2 (ml/ 100 kg CM)	Water (g)
10FA+10MK+A1(2.5-200-170)	592	74	74			2,035	3.7	1.7	1.35		2.5	200	170		353.3
21FA+10SF+A2(2.5-200-170)	510.6		155.4	74		2,035	3.7	1.7		1.36	2.5	200		170	353.1
21FA+30SL+ A2(2.5-200-170)	362.6		155.4		222	2,035	3.7	1.7		1.36	2.5	200		170	353.1
52SL+10MK+A1(2.5-200-170)	281.2	74			384.8	2,035	3.7	1.7	1.35		2.5	200	170		353.3
10FA+10MK+A1(2.5-200-100)	592	74	74			2,035	3.7	1.7	0.8		2.5	200	100		353.6
21FA+10SF+ A2(2.5-200-100)	510.6		155.4	74		2,035	3.7	1.7		0.8	2.5	200		100	353.5
21FA+30SL+ A2(2.5-200-100)	362.6		155.4		222	2,035	3.7	1.7		0.8	2.5	200		100	353.5
52SL+10MK+A1(2.5-200-100)	281.2	74			384.8	2,035	3.7	1.7	0.8		2.5	200	100		353.6
10MK+10SF+20SL+A1(2.5-200-170)	444	74		74	148	2,035	3.7	1.7	1.35		2.5	200	170		353.3
10MK+10SF+20SL+A1(2.5-200-100)	444	74		74	148	2,035	3.7	1.7	0.8		2.5	200	100		353.6

Results and Discussions

Mortar Setting Time

Setting time was determined on mortar mixes of normal consistency. Following ASTM C807 [231], the amount of sand was varied to achieve normal consistency. The amount of sand determined for normal consistency was then used for setting time determination. Sand content for normal consistency and setting time measurements are presented in Table 7-6.

Table 7-6: Amount of Sand for Normal Consistency

Mix	Sand (g)
CN+A1(2.5-200-170)	2,255
CN+A2(2.5-200-170)	2,150
10MK+A1(2.5-200-170)	2,050
10SF+A2(2.5-200-170)	2,175
21FA+A2(2.5-200-170)	2,175
52SL+A2(2.5-200-170)	2,275
CN+A1(2.5-200-100)	2,235
CN+A2(2.5-200-100)	2,150
10MK+A1(2.5-200-100)	2,000
10SF+A2(2.5-200-100)	2,125
21FA+A2(2.5-200-100)	2,175
52SL+A2(2.5-200-100)	2,250
10FA+10MK+A1(2.5-200-170)	2,150
21FA+10SF+A2(2.5-200-170)	2,175
21FA+30SL+ A2(2.5-200-170)	2,325
52SL+10MK+A1(2.5-200-170)	2,200
10FA+10MK+A1(2.5-200-100)	2,025
21FA+10SF+ A2(2.5-200-100)	2,100
21FA+30SL+ A2(2.5-200-100)	2,225
52SL+10MK+A1(2.5-200-100)	1,975
10MK+10SF+20SL+A1(2.5-200-170)	2,050
10MK+10SF+20SL+A1(2.5-200-100)	1,925

As indicated previously, mixture proportions adopted here and presented in Table 7-2 and Table 7-3 have a constant w/cm. According to Alsadey [252], for mixtures where w/cm is maintained constant, there is a tendency for superplasticizers to increase setting time because there is more water available to lubricate particles.

Binary Combinations: SP1 Mixes

Figure 7-1 shows the mortar setting times for varying dosages of SP1 with no mineral admixture replacement. For these mixes, the amount of cement, the dosages of air-entrainer and water-reducer, and the w/cm were maintained constant. The amount of superplasticizer was 100 ml per 100 kg cementitious material or 170 ml per 100 kg cementitious material. For the CN+A1(2.5-200-170), the amount of sand needed for normal consistency was 2,255 g. For the CN+A1(2.5-200-100), the amount of sand needed for normal consistency was 2,235 g. This indicates that varying the amount of SP1 had minimal effects on the sand required for normal consistency. As for the setting time, the results indicate that increasing SP1 increased the setting time from 124 to 140 minutes. This is consistent with Heikal et al. [253], where it was found that increasing polycarboxylate superplasticizer dosage increased the initial setting time of the paste. Heikal et al. measured the initial set times using electrical conductivity-time curves. The cementitious material additions were kept constant but the water was adjusted to achieve normal consistency following ASTM C187 [254] for each superplasticizer dosage. Setting times were also reported to increase with superplasticizer dosage on pastes prepared with a fixed cementitious content and constant w/cm of 0.4 [255]. Yamada and Takahashi [256] also investigated the effect of superplasticizer dosage on setting time of paste and found that as the dosages increased so did the setting time. The setting time was determined using an automated setting tester. The cementitious content and w/cm of 0.3 were maintained constant for all mixes. Xiao et al. [257] investigated the effect of superplasticizer dosage on setting time of paste and found that at a dosage of 0.15 to 0.35 wt%, the final setting time increased from a factor of 101 to 256%, respectively.

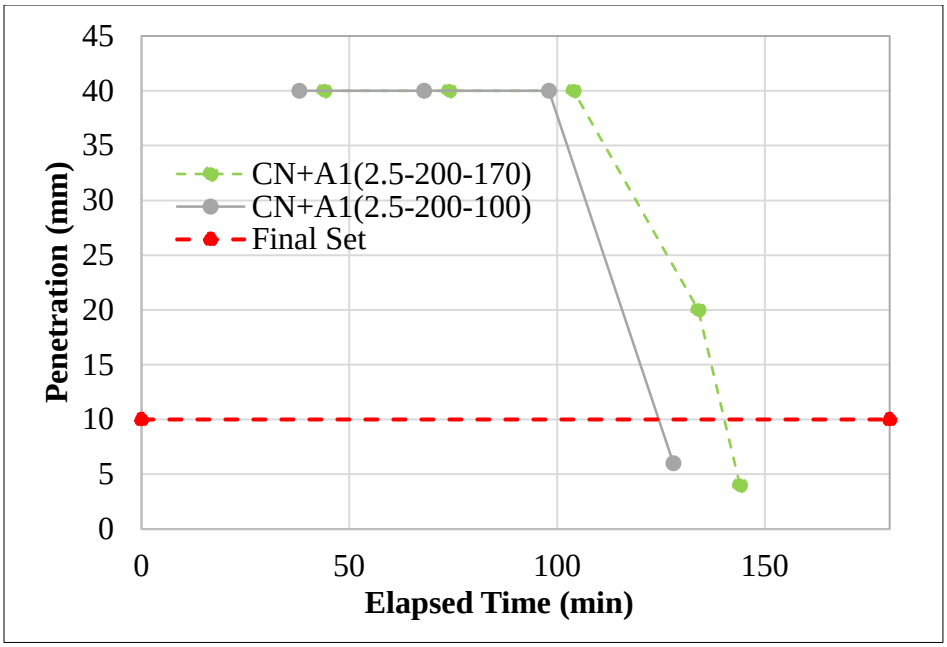

Figure 7-1: Mortar Setting Times for SW with Varied SP1 Dosages

Figure 7-2 shows the mortar setting time for SP1 dosages of 100 and 170 ml per 100 kg of cementitious material with 10% metakaolin replacement. The amount of sand needed for normal consistency was 2,050 g and 2,000 g for 10MK+A1(2.5-200-170) and 10MK+A1(2.5-200-100), respectively. This shows that the superplasticizer had minimal effect on normal consistency for the metakaolin mixes, as the difference was 50 g. The final set times for 10MK+A1(2.5-200-170) and 10MK+A1(2.5-200-100)were 124 min. and 105 min, respectively, for a difference of 19 min. The same results were found previously for plain mixtures with no mineral admixture replacement; that is, a higher dosage of superplasticizer increased the final set time.

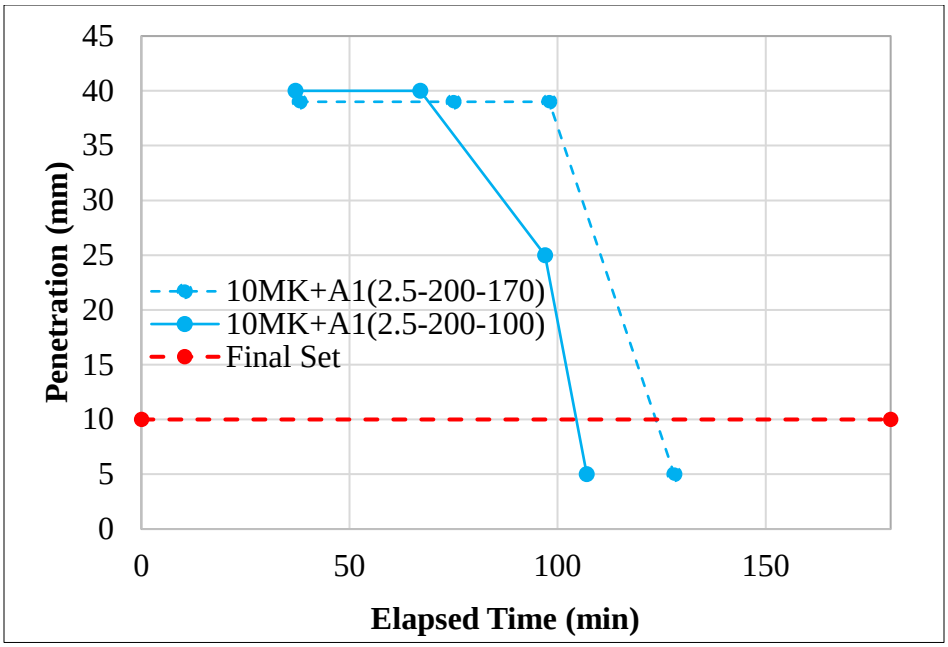

Figure 7-2: Mortar Setting Times for 10MK with Varied SP1 Dosages

Binary Combinations: SP2 Mixes

Figure 7-3 shows the mortar setting times for SP2 dosages of 100 and 170 ml per 100 kg of cementitious material. For these mixes, the amount of cement, the dosages of air-entrainer and water-reducer, and the w/cm were maintained constant. The amount of superplasticizer was either 100 or 170 ml per 100 kg cementitious material. The amount of sand used was determined from the normal consistency experiments. For CN+A2(2.5-200-170) and CN+A2(2.5-200-100) , the amount of sand needed for normal consistency was the same, 2150 g. The final set times for CN+A2(2.5-200-170) and CN+A2(2.5-200-100) were 134 min. and 124 min., respectively. The difference between the two of 10 min. was consistent with the trends observed on plain mixes when varying SP1 dosage; that is, a higher dosage of superplasticizer marginally increased the final set time.

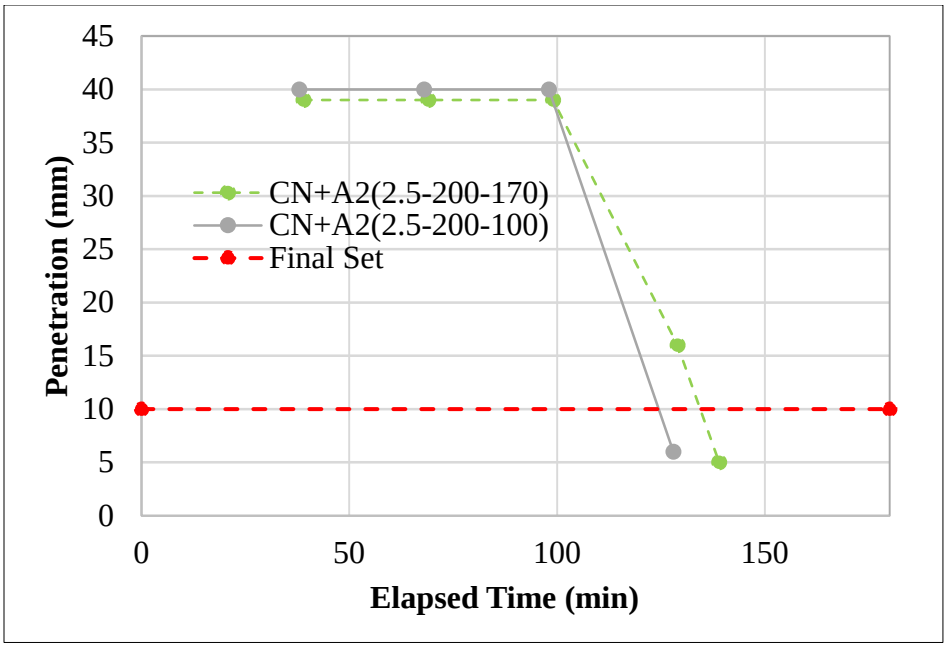

Figure 7-3: Mortar Setting Times for SW with Varied SP2 Dosages

Figure 7-4 shows the mortar setting time for SP2 dosages of 100 and 170 ml per 100 kg of cementitious material with 10% silica fume replacement. The amount of sand needed for normal consistency was 2,175 g for 10SF+A2(2.5-200-170) and 2,125 g for 10SF+A2(2.5-200-100), respectively. The final set times were 133 and 116 min. for 10SF+A2(2.5-200-170) and 10SF+A2(2.5-200-170), respectively. The difference between the two setting times was 17 min, which shows that a higher dosage increased setting time. Heikal et al. [253] investigated the effect of polycarboxylate superplasticizer on initial setting time of 10% silica fume replacement paste and found that the addition of superplasticizer increased the initial setting time up to an addition of 0.75 %, after which the initial setting time decreased. The cementitious content was maintained constant, but the water addition was adjusted for normal consistency following ASTM C308 [254] for each superplasticizer dosage.

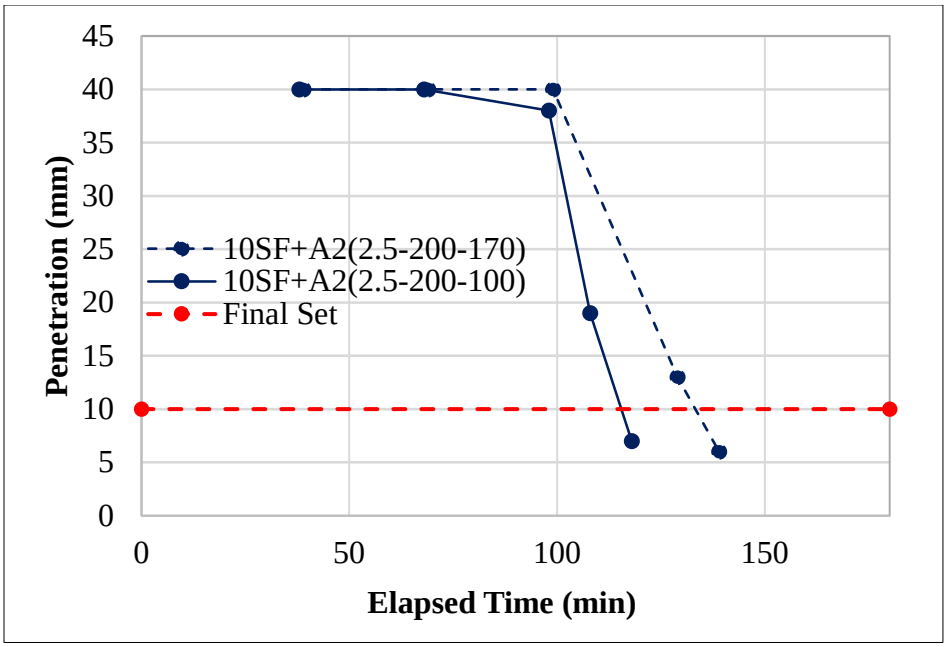

Figure 7-4: Mortar Setting Times for 10SF with Varied SP2 Dosages

Figure 7-5 shows the mortar setting time for SP2 dosages of 100 and 170 ml per 100 kg of cementitious material with 21% fly ash replacement. For 21FA+170SP2 and 21FA+100SP2, the amount of sand needed for normal consistency was 2,175 g, which showed little effect from the superplasticizer. The final set times were 151 min. and 138 min. for 21FA+A2(2.5-200-170) and 21FA+A2(2.5-200-170), respectively. The difference between the two is 13 min, which showed that an increase in superplasticizer increased setting time slightly. The findings are in agreement with Toledano-Prados et al. [258] who investigated the effect of polycarboxylate superplasticizer on fly ash cement and found that increasing the levels of superplasticizer dosage leads to an increase in setting time. The setting time results were determined using a Vicat needle following standard UNE-EN 196-3. The amount of cementitious material and the w/cm of 0.37 were kept constant for all mixes.

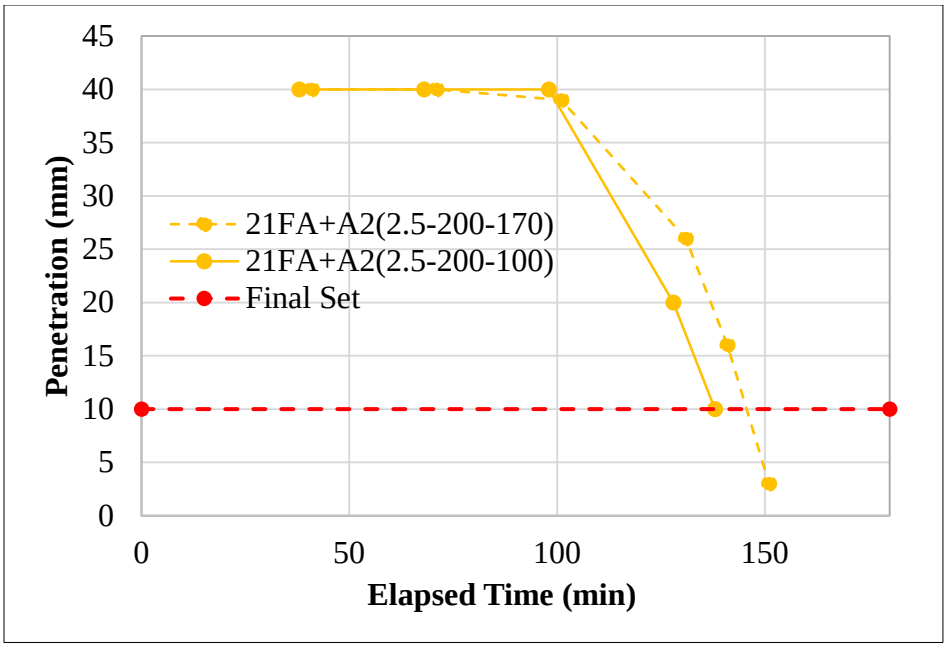

Figure 7-5: Mortar Setting Times for 21FA with Varied SP2 Dosages

Figure 7-6 shows the mortar setting time for SP2 dosages of 100 and 170 ml per 100 kg of cementitious material with 52% slag replacement. The amounts of sand needed for normal consistency were 2,275 g and 2,250 g for 52SL+A2(2.5-200-170) and 52SL+A2(2.5-200-100), respectively. The difference between the two is 25 g of sand, which shows that the superplasticizer had little effect on normal consistency. The final set times were 168 min. and 147 min. for 52SL+A2(2.5-200-170) and 52SL+A2(2.5-200-100), respectively. The difference between the two is 21 min, which shows that the increase in dosage of superplasticizer increased setting time.

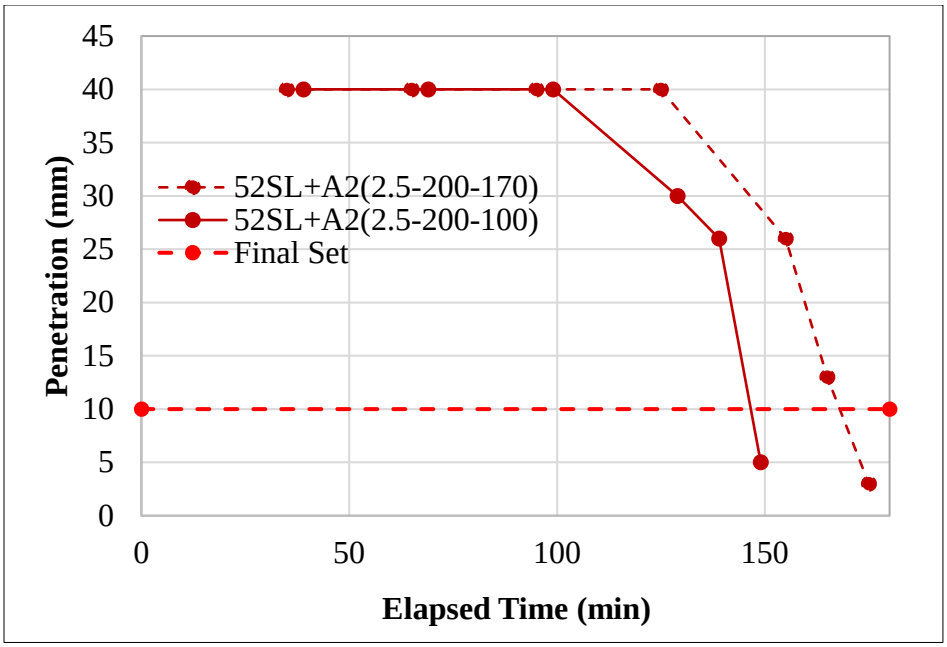

Figure 7-6: Mortar Setting Times for 52Slag with Varied SP2 Dosages

[redacted]Ternary Combinations: SP1 Mixes

Figure 7-7 shows the mortar setting time for SP1 dosages of 100 and 170 ml per 100 kg of cementitious material for the ternary combination of 10% fly ash and 10% metakaolin., The amount of sand needed for normal consistencies were 2,150 g and 2,025 g for 10FA+10MK+A1(2.5-200-170) and 10FA+10MK+A1(2.5-200-100), respectively. The difference between the two is 125 g of sand, which shows that the addition of fly ash to the mixes affected the normal consistency. This can be attributed to the particle size of fly ash and its effectiveness in reducing water demand making the increase in sand necessary to obtain the same normal consistency. The final set times were 115 min. and 112 min. for 10FA+10MK+A1(2.5-200-170) and 10FA+10MK+A1(2.5-200-100), respectively. The difference between the two is 3 min, which shows that for this combination, the increase in superplasticizer dosage had minimal effect on setting time.

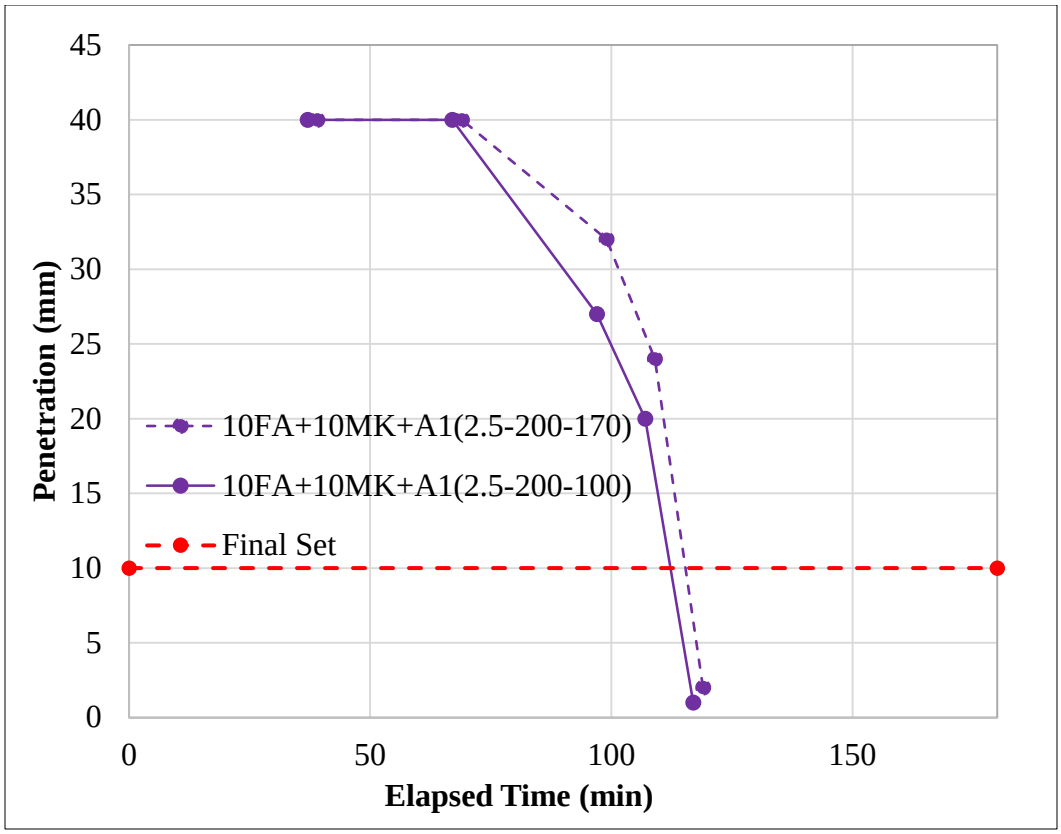

Figure 7-7: Mortar Setting Times for 10FA+10MK with Varied SP1 Dosages

Figure 7-8 shows the mortar setting time for SP1 dosages of 100 and 170 ml per 100 kg of cementitious material for the ternary combination of 52% slag and 10% metakaolin. The amounts of sand needed for normal consistency were 2,200 g and 1,975 g for 52SL+10MK+A1(2.5-200-170) and 52SL+10MK+A1(2.5-200-100), respectively. The difference between the two is 225 g of sand, which shows that the addition of slag affected the normal consistency. This can be attributed to the particle size and morphology of slag and their effect on mixture workability. However, there was no significant effect on the setting time within the range studied here. The final set times were 145 min. and 140 min. for 52SL+10MK+A1(2.5-200-170) and 52SL+10MK+A1(2.5-200-170), respectively.

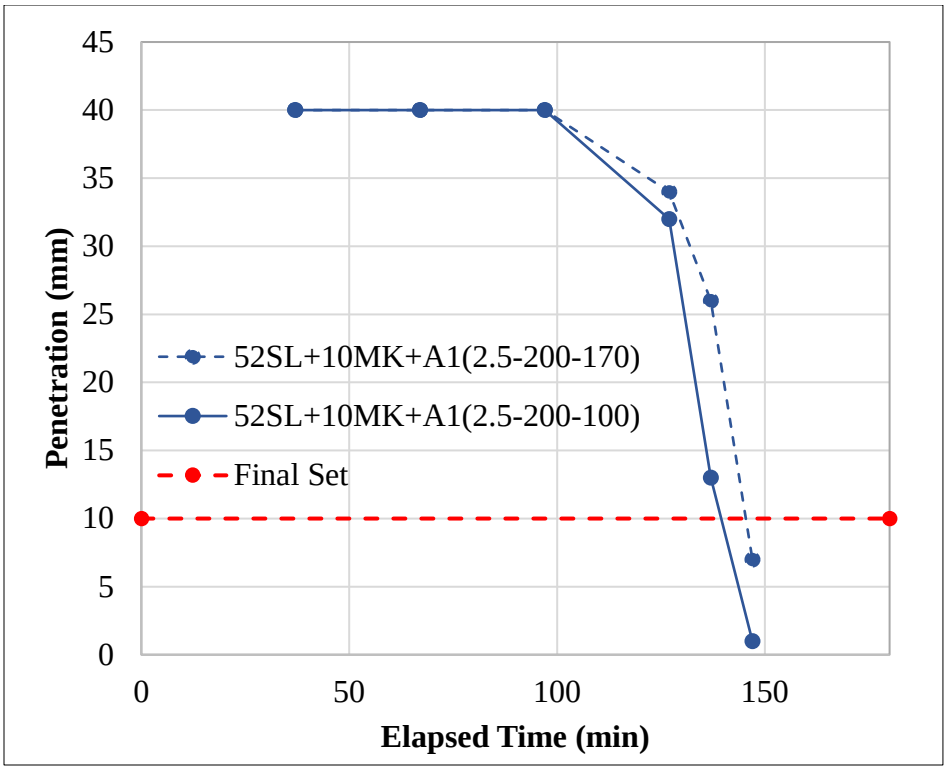

Figure 7-8: Mortar Setting Times for 52Slag+10MK with Varied SP1 Dosages

[redacted]Ternary Combinations: SP2 Mixes

Figure 7-9 shows the mortar setting time for SP2 dosages of 100 and 170 ml per 100 kg of cementitious material for the ternary combination of 21% fly ash and 10% silica fume. The amounts of sand needed for normal consistency were 2,175 g. and 2,100 g for 21FA+10SF+A2(2.5-200-170) and 21FA+10SF+A2(2.5-200-100), respectively. The difference between the two is 75 g of sand, which shows that the superplasticizer had some effect on normal consistency for this combination. The final set times were 147 min. and 136 min. for 21FA+10SF+A2(2.5-200-170)and 21FA+10SF+A2(2.5-200-100), respectively. The difference between the two is 11 min, which is less than the setting time noted earlier for the binary combination of each individual mineral admixture.

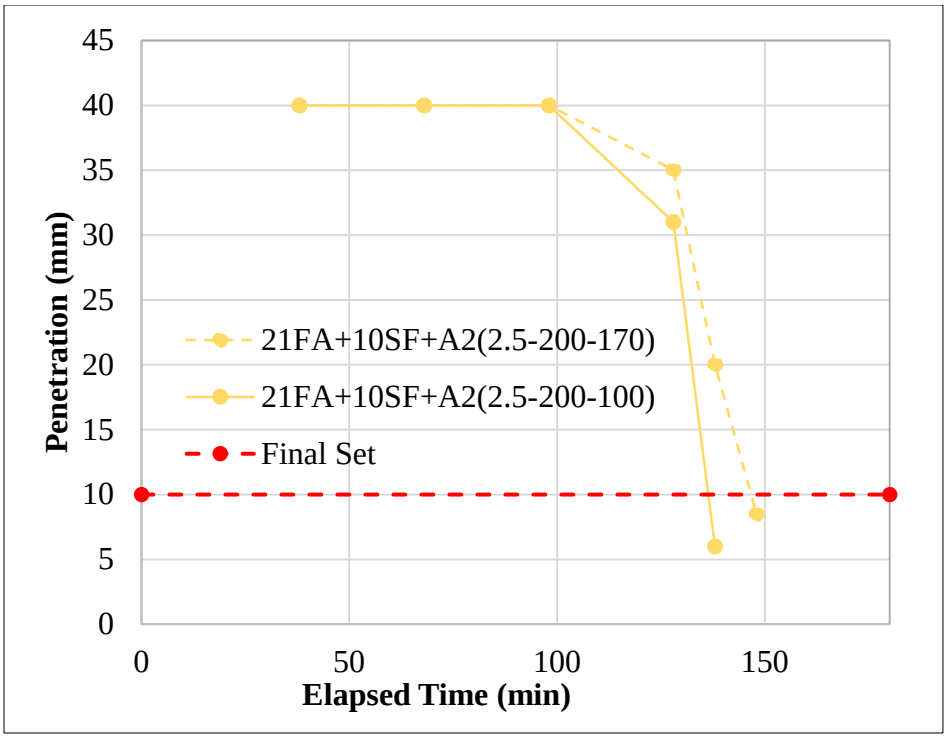

Figure 7-9: Mortar Setting Times for 21FA+10SF with Varied SP2 Dosages

Figure 7-10 shows the mortar setting time for SP2 dosages of 100 and 170 ml per 100 kg of cementitious material for the ternary combination of 21% fly ash and 30% slag. The amounts of sand needed for normal consistency were 2,325 g and 2,225 g for 21FA+30SL+A2(2.5-200-170) and 21FA+30SL+A2(2.5-200-100), respectively. The difference between the two is 100 g of sand, which shows that the superplasticizer had an effect on normal consistency. The final set times were 167 min. and 157 min. for 21FA+30SL+A2(2.5-200-170) and 21FA+30SL+A1(2.5-200-100), respectively. The difference between the two is 10 min., which is similar to the results for the binary combination of fly ash; however, there was a difference in the amount of sand, which could have had an effect on setting time. Jang et al. [259] investigated the effect of a polycarboxylate-based superplasticizer on setting time of a 50% slag and 50% fly ash paste, and found that increasing levels of superplasticizer dosage increased setting time. The 4% superplasticizer mixture increased the overall final setting time by 70 min. Cementitious material and water content were maintained constant for all mixes with superplasticizer dosages varying from 0 to 4 wt%. The setting times were measured using a Vicat needle following ASTM C191 [260] .

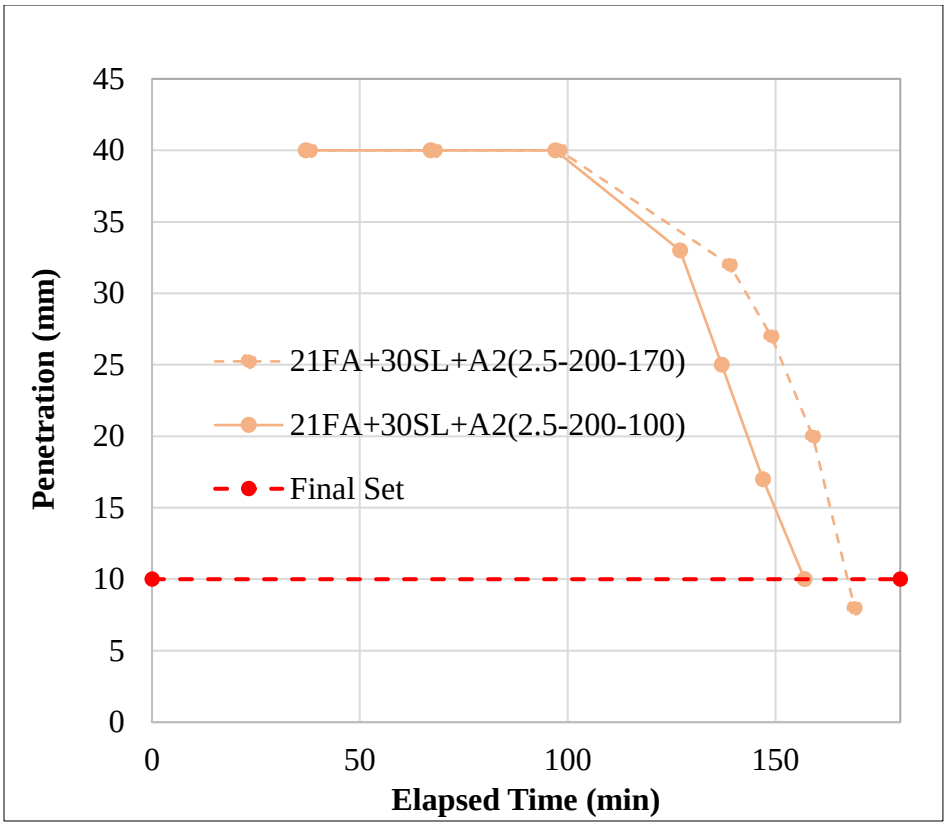

Figure 7-10: Mortar Setting Times for 21FA+30Slag with Varied SP2 Dosages

[redacted]Quaternary Combinations: SP1 Mixes

Figure 7-11 shows the mortar setting time for SP1 dosages of 100 and 170 ml per 100 kg of cementitious material for the quaternary combination of 10% metakaolin, 10% silica fume, and 20% slag. The amounts of sand needed for normal consistency were 2,050 g. and 1,925 g for 10MK+10SF+20SL+A1(2.5-200-170) and 10MK+10SF+20SL+A1(2.5-200-100), respectively. The difference between the two is 125 g of sand, which shows that the superplasticizer had an effect on normal consistency for this mixture. The final set times were 105 min. and 107 min. for 10MK+10SF+20SL+A1(2.5-200-170) and 10MK+10SF+20SL+A1(2.5-200-100), respectively. The difference between the two is 2 min., which shows that for this quaternary combination, the superplasticizer dosage had little effect; however, the difference in sand content could have played a role in affecting setting time.

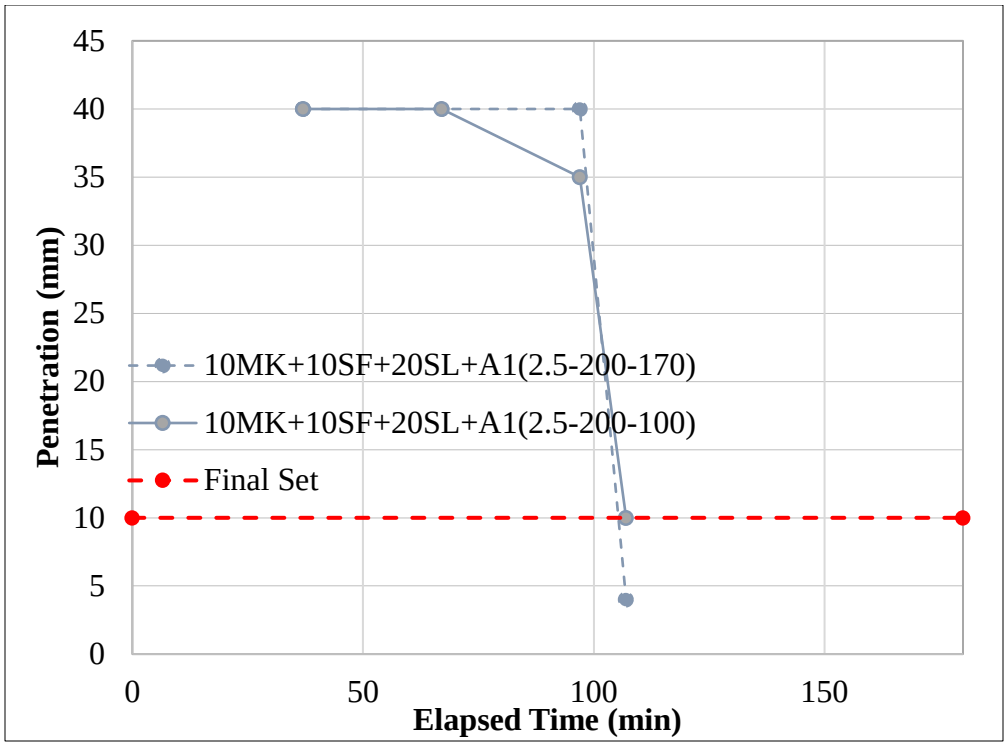

Figure 7-11: Mortar Setting Times for 10MK+10SF+20Slag with Varied SP1 Dosages

[redacted] Compressive Strength

Unlike mortar setting time, compressive strength testing was performed on mortar cubes with a fixed w/cm, and fixed contents of sand, air-entrainer, and water-reducer. The superplasticizer dosage was either 100 or 170 ml per 100 kg cementitious material, which corresponds to 0.108 and 0.184 wt%, respectively. The mix designs are shown in Table 7-4 and Table 7-5. According to Alsadey [252], the use of superplasticizer, in general, increases the compressive strength by producing denser concrete mixtures.

[redacted] Binary Combinations: SP1 Mixes

Figure 7-12 shows the compressive strength for SP1 dosages of 100 and 170 ml per 100 kg of cementitious material in mixtures with no mineral admixture replacement. For these mixes, the increase in dosage of superplasticizer led to a higher compressive strength. The trend was seen for all test ages. It was more noticeable at the 7-day test age, as the higher dosage of superplasticizer resulted in an increase of 1150 psi compared to the 1-day and 28-day strength increases of 420 psi and 580 psi, respectively. The results by Puertas et al. [255] showed that the

dosage of superplasticizer did not have a significant effect on the compressive strength of paste. The strength was measured on paste samples having a constant w/cm of 0.4 for all mixes. Xiao et al. [257] also investigated the effect of superplasticizer dosage on compressive strength and found that the increase in dosage led to an increase in compressive strength until a superplasticizer dosage of 0.35%. The same cementitious material amount and a w/cm of 0.3 were used for all mixes.

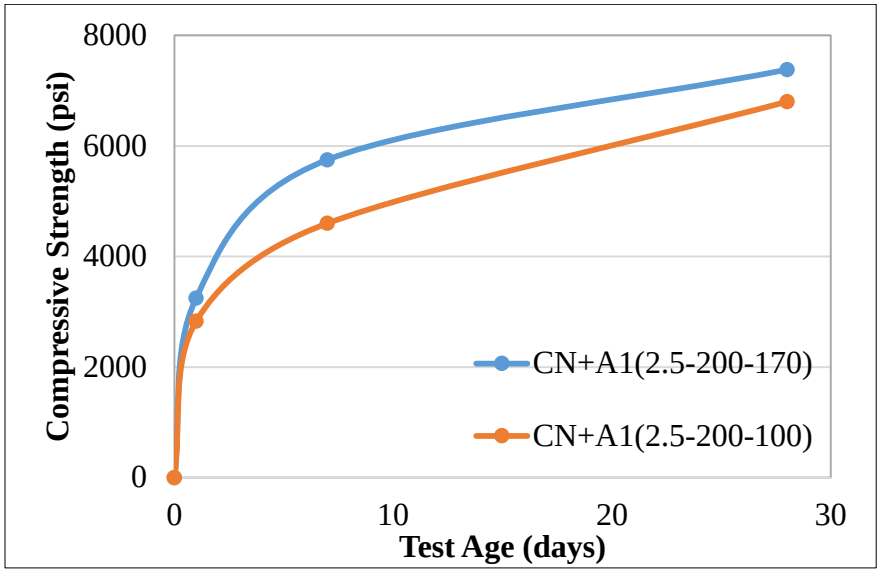

Figure 7-12: Compressive Strength for CN with Varied SP1 Dosages

Figure 7-13 shows the compressive strength for two dosages of SP1, 100 and 170 ml per 100 kg of cementitious material, with 10% metakaolin replacement. From the results, it appears that the SP1 dosage had little effect on early-age strength, as the difference between the mixes was about 30 psi. The results showed a noticeable effect at the 7-day test age, where the difference between the mixes was 1030 psi. The later-age strength showed that the increase in superplasticizer dosage resulted in an increase of 360 psi. The 7-day and 28-day compressive strength followed the same trend as the mixes containing no mineral admixture replacement.

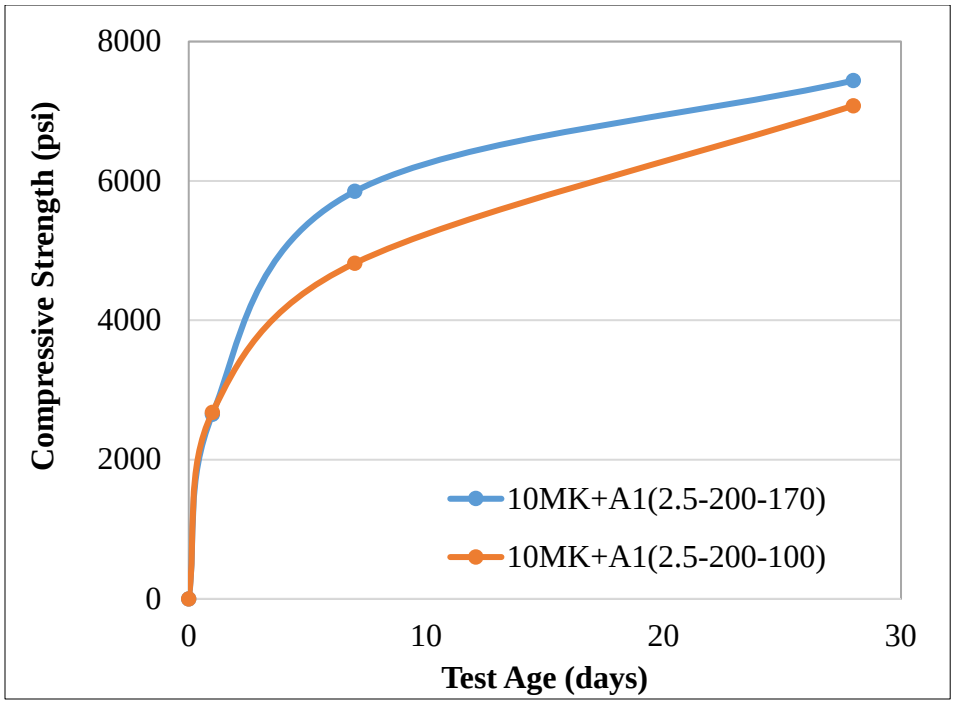

Figure 7-13: Compressive Strength for 10MK with Varied SP1 Dosages

[redacted]Binary Combinations: SP2 Mixes

Figure 7-14 shows the compressive strength for two SP2 dosages, 100 and 170 ml per 100 kg of cementitious material, with no mineral admixture replacement. For these mixes, it appears that the superplasticizer had little effect on early-age strength as the difference between the two is 30 psi. The 7-day and 28-day compressive strengths showed similar trends; that is, increasing superplasticizer dose resulted in increasing the compressive strength by 430 psi and 350 psi, respectively. This shows that for these mixes, the superplasticizer had a minor effect on later-age strength.

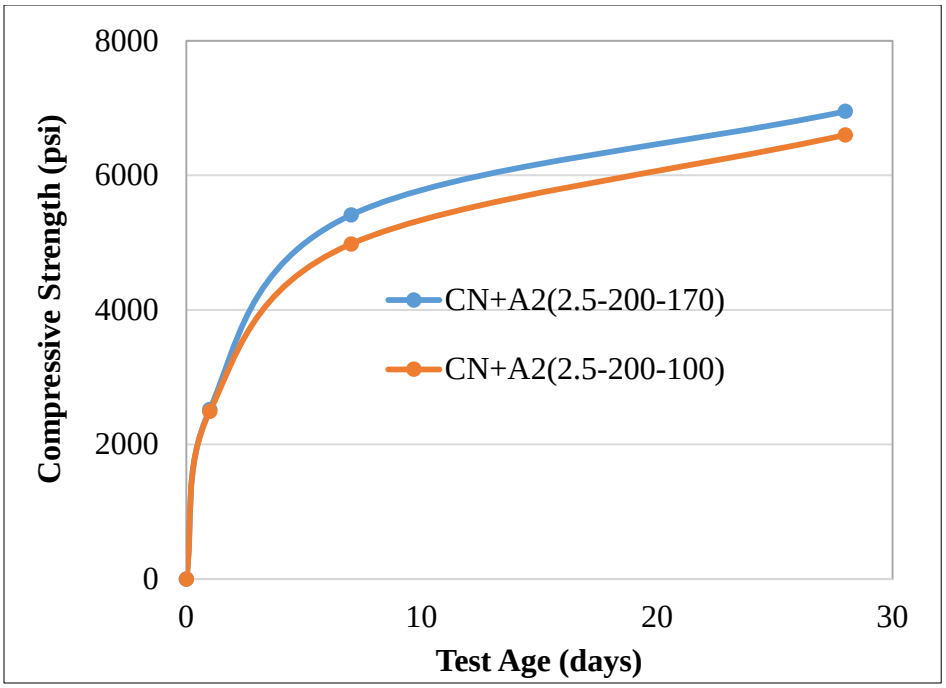

Figure 7-14: Compressive Strength for SW with Varied SP2 Dosages

Figure 7-15 shows the compressive strength for two SP2 dosages, 100 and 170 ml per 100 kg of cementitious material, with 10% silica fume replacement. For these mixes, it appears that the increase in dosage of superplasticizer had little effect on the 1-day strength. For the 7-day compressive strength, however, the lower dosage of superplasticizer showed an increase in strength of 430 psi compared to the higher dosage. For the 28-day compressive strength, the higher dosage of superplasticizer resulted in an increase in strength of about 400 psi compared to the lower dosage. This shows that for this combination, the higher dosage of superplasticizer had a beneficial effect on later-age strength, but not the 7-day strength.

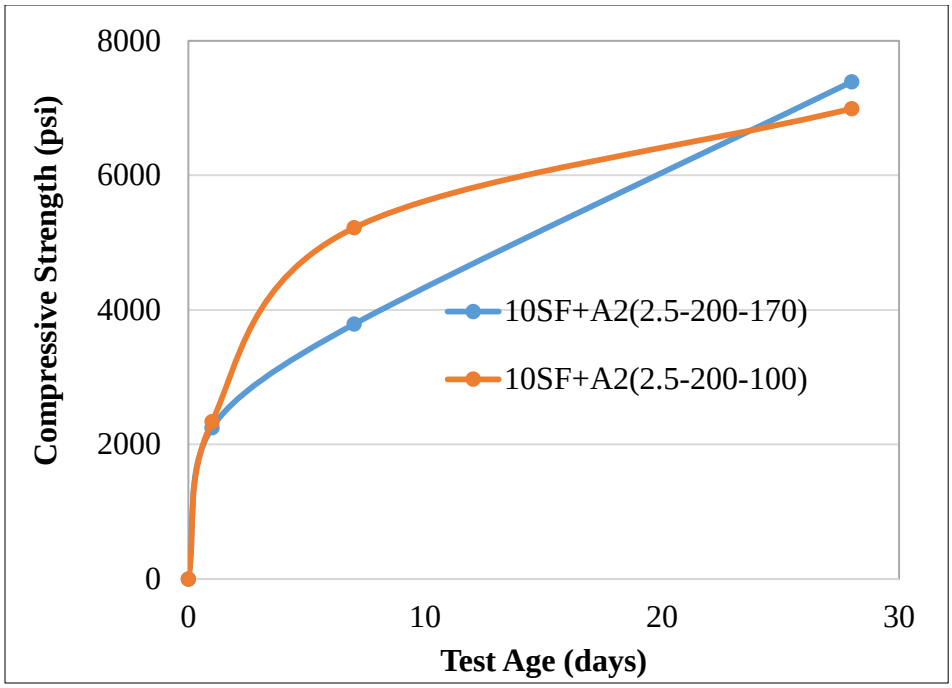

Figure 7-15: Compressive Strength for 10SF with Varied SP2 Dosages

Figure 7-16 shows the compressive strength for two SP2 dosages, 100 and 170 ml per 100 kg of cementitious material, with 21% fly ash replacement. For these mixes, a lower dosage of superplasticizer resulted in a higher compressive strength for early ages. For the 1-day and 7-day test ages, the compressive strength was higher by 340 psi and 260 psi, respectively, for the lower dosage of superplasticizer. For the later age, the results show that the higher dosage of superplasticizer resulted in a marginal increase in compressive strength. The difference between the two was 470 psi. Toledano-Prados et al. [258] investigated the effect of a solid polycarboxylate on compressive strength of fly ash mortars. The results showed that the increase in superplasticizer dosage led to an increase in early-age compressive strength. At 28 days, the dosage of superplasticizer produced no difference in compressive strength compared to the reference mortar. Only at a superplasticizer content of 0.15% was the compressive strength higher than the reference mortar. The cementitious amount and w/cm (0.5) were maintained constant for all mixes.

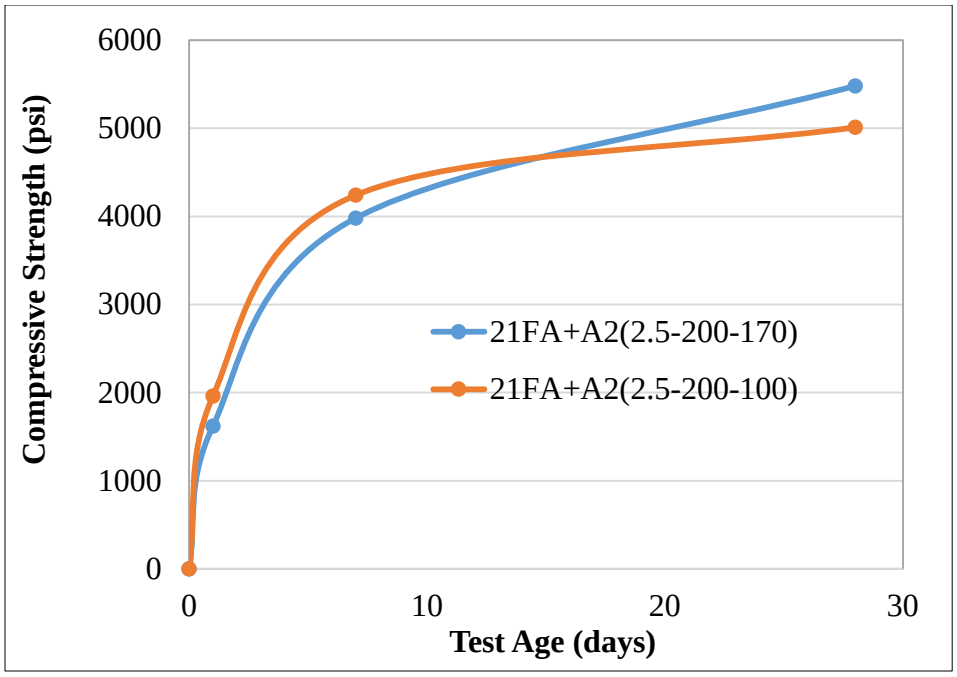

Figure 7-16: Compressive Strength for 21FA with Varied SP2 Dosages

Figure 7-17 shows the compressive strength for two SP2 dosages, 100 and 170 ml per 100 kg of cementitious material, with 52% slag replacement. For these mixes, the higher dosage of superplasticizer resulted in an increase in compressive strength for all test ages. For the 1-day, 7-day, and 28-day test ages, the increase in compressive strength was 180, 420, and 600 psi, respectively.

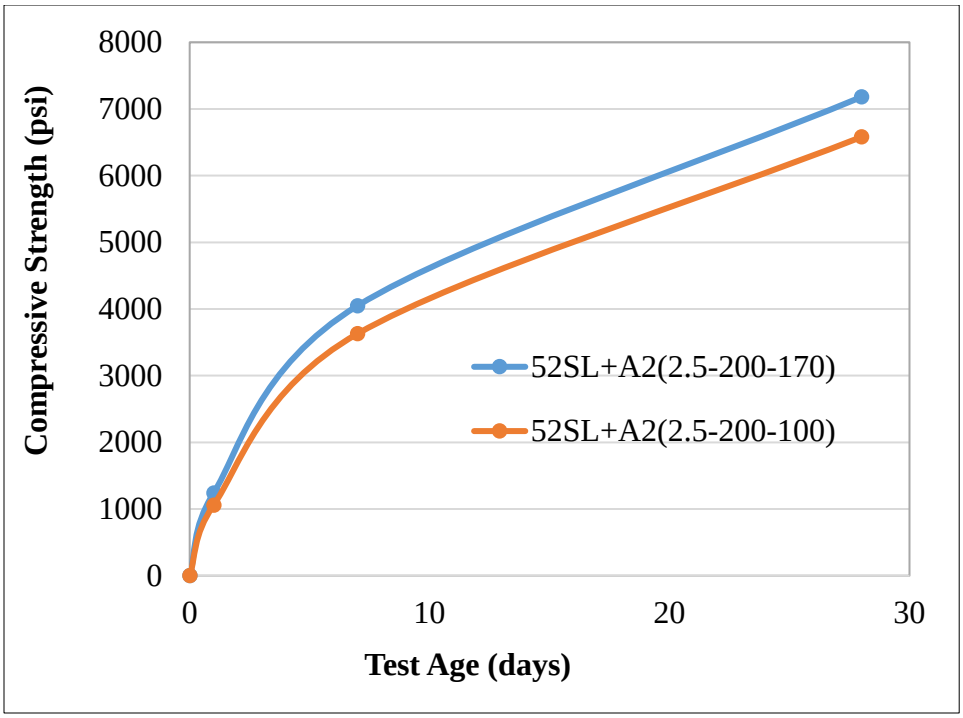

Figure 7-17: Compressive Strength for 52Slag with Varied SP2 Dosages

[redacted]Ternary Combinations: SP1 Mixes

Figure 7-18 shows the compressive strength for two SP1 dosages, 100 and 170 ml per 100 kg of cementitious material, with 10% fly ash and 10% metakaolin replacement. For these mixes, the lower dosage of superplasticizer resulted in a higher compressive strength. The 1-day and 7-day test samples had respective compressive strengths of 110 and 130 psi higher than the higher dosage mixes, which were not significant. For the later age, the higher dosage of superplasticizer resulted in a higher compressive strength of 380 psi. It appears that increasing the superplasticizer dosage did not generate a significant effect on this mixture with the variation of superplasticizer content studied here.

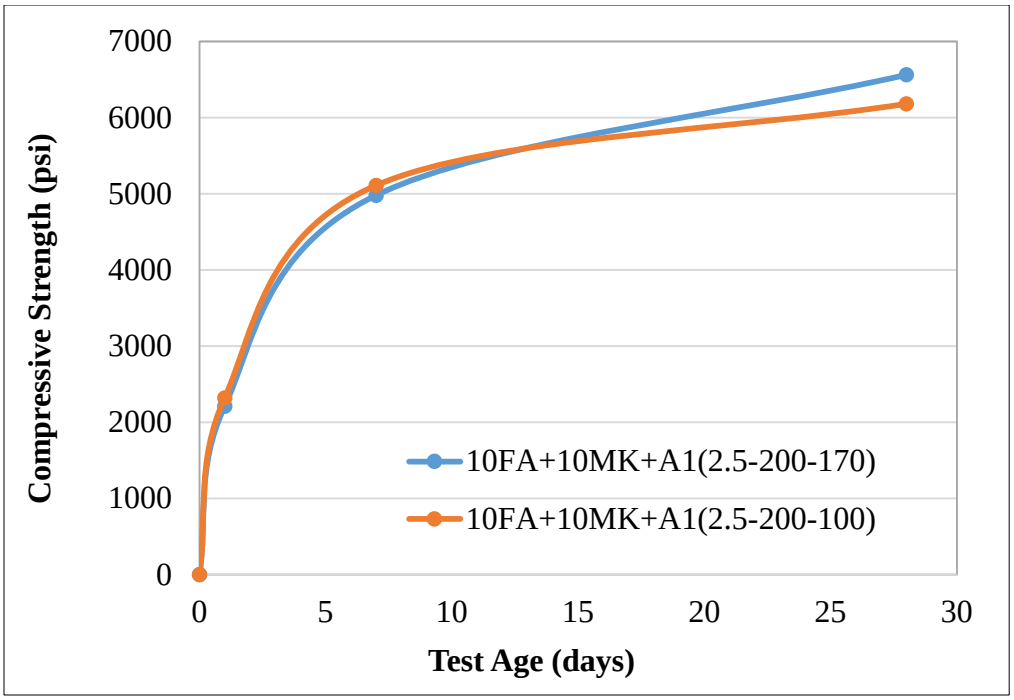

Figure 7-18: Compressive Strength for 10FA+10MK with Varied SP1 Dosages

Figure 7-19 shows the compressive strength with two SP2 dosages, 100 and 170 ml per 100 kg of cementitious material, with 52% slag and 10% metakaolin replacement. It appears that at an early age, the superplasticizer had little effect on compressive strength, as the difference noted here was only 60 psi. At the 7-day test age, the lower dosage of superplasticizer had a slightly higher compressive strength, a 190 psi difference. For the later age, the lower dosage of superplasticizer resulted in a significant outcome, as the compressive strength was 1,080 psi higher. Higher superplasticizer dosages, in this mixture, had a negative effect on the 28-day compressive strength.

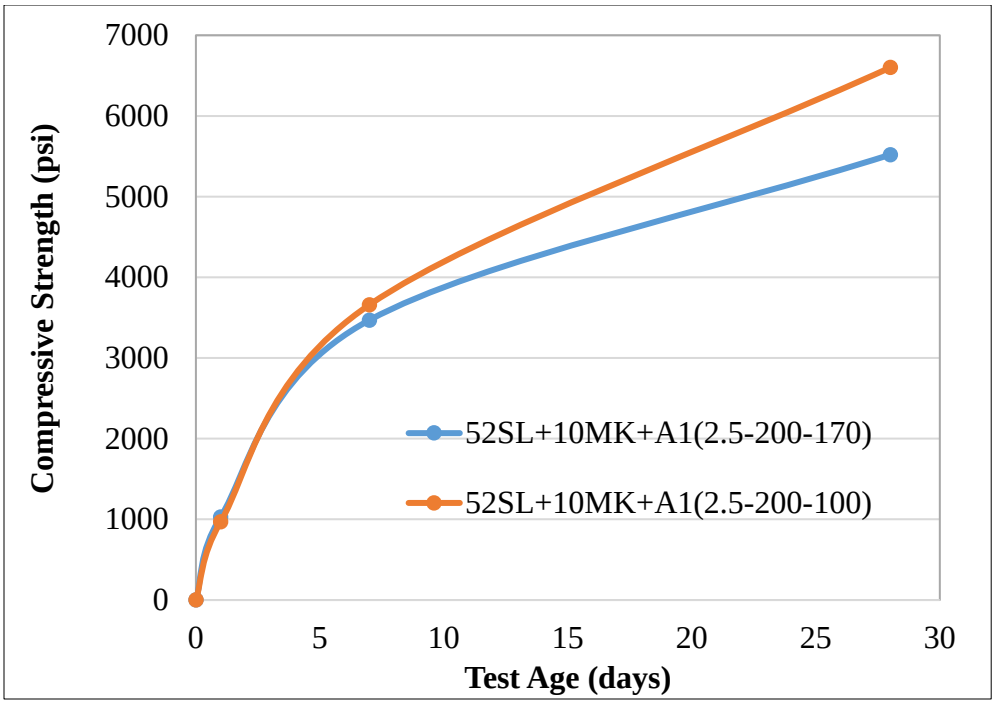

Figure 7-19: Compressive Strength for 52Slag+10MK with Varied SP1 Dosages

[redacted]Ternary Combinations: SP2 Mixes

Figure 7-20 shows the compressive strength for two SP2 dosages, 100 and 170 ml per 100 kg of cementitious material, with 21% fly ash and 10% silica fume replacement. From the results, it appears that the superplasticizer had little effect on early-age compressive strength, as the difference was below 100 psi for 1-day and 7-day samples. For the later age, the higher dosage of superplasticizer resulted in a higher compressive strength, with a 490-psi difference.

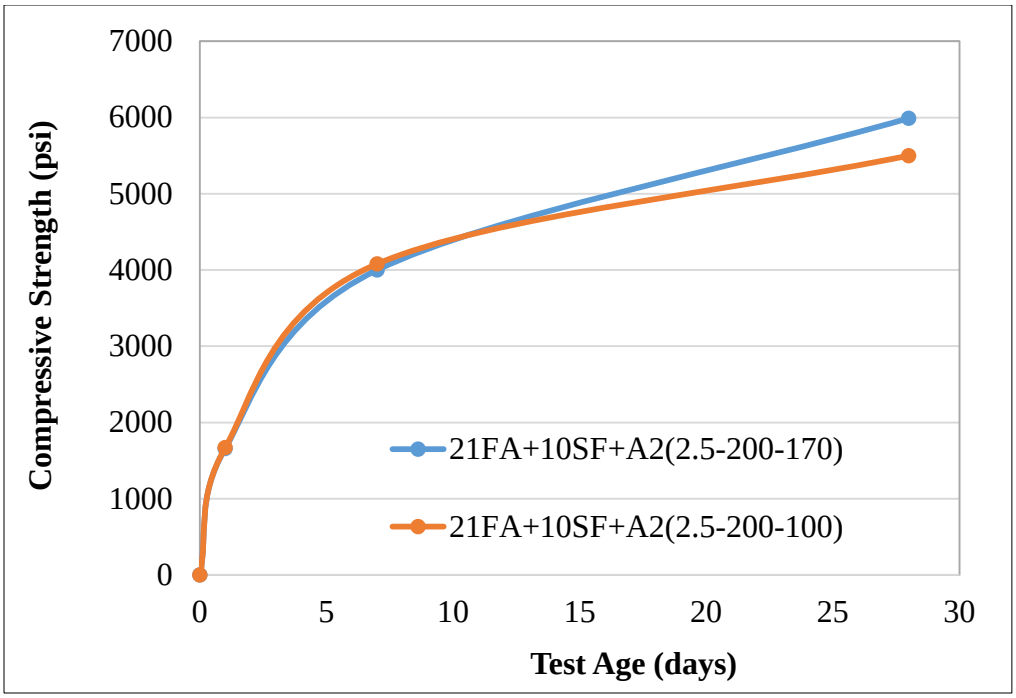

Figure 7-20: Compressive Strength for 21FA+10SF with Varied SP2 Dosages

Figure 7-21 shows the compressive strength for two SP2 dosages, 100 and 170 ml per 100 kg of cementitious material, with 21% fly ash and 30% slag replacement. For all test ages, the lower dosage of superplasticizer resulted in a higher compressive strength. The 7-day test age showed a slightly higher compressive strength, by 200 psi; however, for the 1-day and 28-day test ages, the results showed little effect, as the difference was 20 and 70 psi, respectively. Jang et al. [259] investigated the effect of superplasticizer dosage on the compressive strength of 50% fly ash and 50% slag paste. Jang et al. found that the addition of superplasticizer beyond 2 wt. % increased compressive strength before 7 days, but had an adverse effect after. The cementitious material and water amounts were maintained constant for all mixes. The compressive strengths were measured following ASTM C109 [232]. Jang et al. noted that the results could be explained due to conflicting effects of the superplasticizer on the properties of pastes: the improvement in strength at early age due to adsorption, and in the case of a large amount of superplasticizer, the decrease in long-term strength due to increasing the entrained air content.

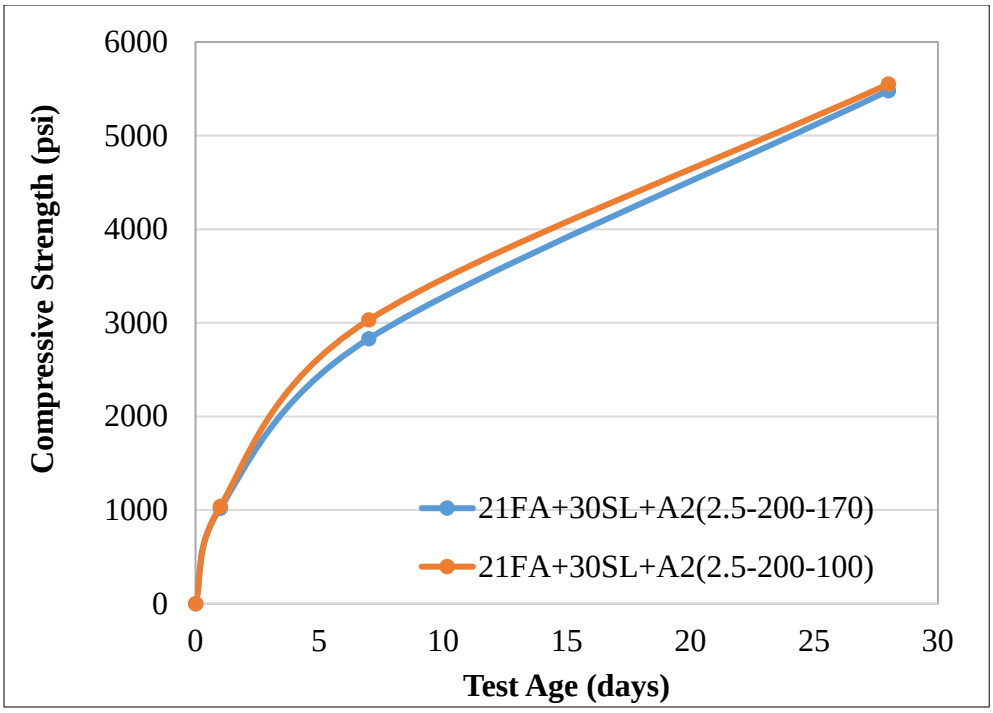

Figure 7-21: Compressive Strength for 21FA+30Slag with Varied SP2 Dosages

[redacted]Quaternary Combinations: SP1 Mixes

Figure 7-22 shows the compressive strength for two SP1 dosages, 100 and 170 ml per 100 kg of cementitious material, with 10% metakaolin, 10% silica fume, and 20% slag replacement. For these mixes, the dosage of superplasticizer studied here had little effect on compressive strength gain.

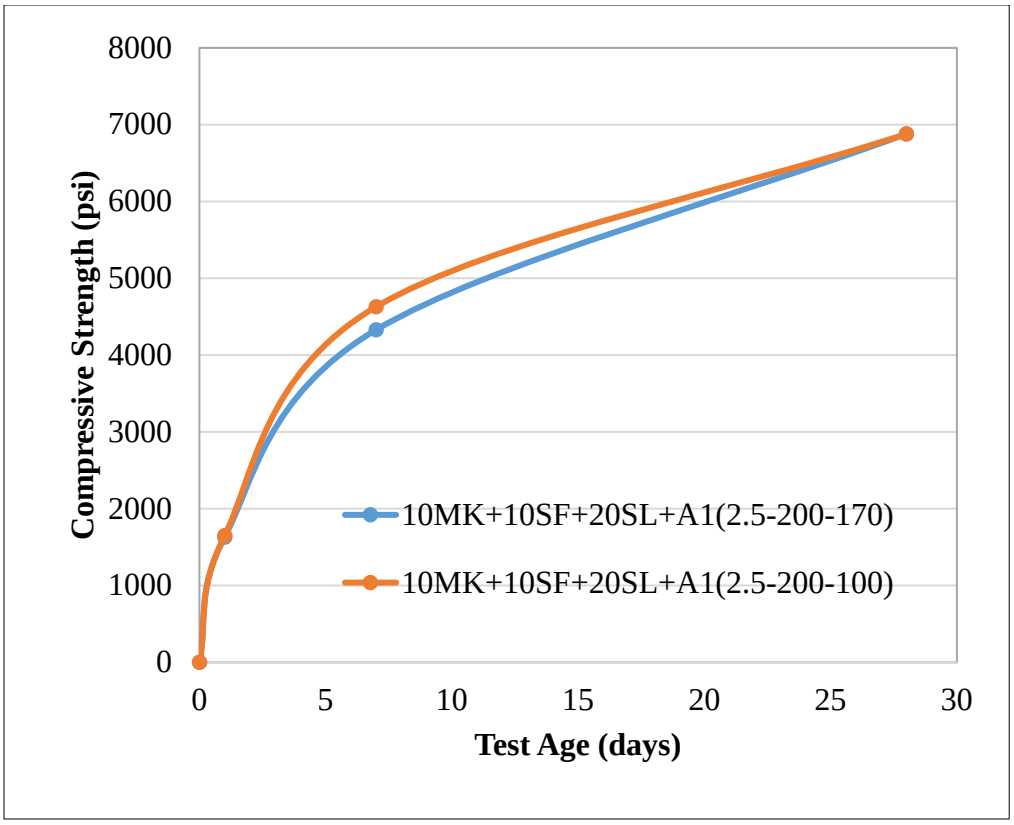

Figure 7-22: Compressive Strength for 10MK+10SF+20Slag with Varied SP1 Dosages

Conclusions

The effect of increasing the superplasticizer dosage, within the range studied here, was a modest increase in setting time for all binary mixtures and the control. The effect was not as pronounced for the control and FA mixtures. As for strength evolution, increasing superplasticizer dosage increased the 28-day strength for all binary mixtures. However, early-age strength measurements showed variation, depending on the binary system studied. For example, the control mixture showed an increase in 1- and 7-day strengths, while SF and FA the 1- and 7-day strengths were not improved by increasing SP dosage.

[redacted] Effects of Mineral and Chemical Admixtures on Sulfate Durability

[redacted] Introduction

Pozzolans are used as supplementary cementitious materials in structural concrete to enhance durability due to their positive effect on the microstructure of the cementitious paste bulk and the interfacial transition zone (region between the cementitious paste bulk and aggregates or reinforcing steel). In addition to the dilution effect, mineral admixtures typically enhance durability through pore size refinement, thus lowering concrete permeability and diffusivity of aggressive ions. The pozzolanic reaction lowers the calcium hydroxide content, a product of hydration of the cement's calcium silicate phases, in the cementitious matrix while enhancing the formation of more C-S-H. The reduction in permeability and consumption of calcium hydroxide to form more C-S-H, in addition to the dilution effects, are effective in enhancing concrete sulfate durability.

In the current study, supplementary cementitious materials were secured from the list of approved suppliers in the state of Florida. The chemical compositions of the mineral admixtures used in the study are shown in Table 2-4, and their mineralogical composition is presented in Table 2-6. One of the objectives of this study is to ensure that the materials used in structural concrete applications in the state of Florida are of a quality that renders structural concrete durable and sustainable. As many of the concrete elements are subjected to sulfate exposure, sulfate durability of the cementitious systems will be assessed through testing according to ASTM C1012 [261], where the criteria of evaluating the effectiveness of a particular mixture is specified by expansion values at 180 days. Other specifications indicate the necessity of extending measurements to 18 months, especially in sulfate environment exposures that are classified as extremely aggressive. However, due to the limited time of the project, expansion experiments are reported here for a period of 6 months.

[redacted] Methodology

[redacted] Length Change Determination

Mortar bars were prepared and tested following ASTM C1012 [261]. The mixture designs are presented in Table 8-1 and Table 8-2. Mortar was mixed following ASTM C305 [233] and molded following ASTM C157 [262]. All mixtures were made following the proportion for a 9-cube mix: 740 g of cementitious, 2,035 g of Ottawa sand, and a water-to-cementitious ratio (w/cm)

of 0.485. Chemical admixtures were also incorporated into each mixture, with the exception of the control (CN). The amount of water in each chemical admixture was taken into account to maintain a constant w/cm ratio. The admixture dosages were selected following typical FDOT concrete admixture dosages. The air entrainer and water reducer were kept constant for all mixes at 2.5 ml/100 kg cementitious and 155 ml/100 kg cementitious, respectively. High-Range Water-Reducing admixture (HRWR, SP1 and SP2) additions were either 110 ml/100 kg cementitious or 155 ml/100 kg cementitious, depending on the type of mineral admixture being used. For all mineral admixtures used here, HRWR (SP2) has been used, except for metakaolin where SP1 was used. SP1 and SP2 are both polycarboxylate-based high-range water-reducing admixtures. Both are classified as ASTM C494 [17]Type A and F, and ASTM C1017 [263] Type I.

Mortar cubes were mixed along with mortar bars, placed in an oven at 35ºC for 23.5 h (+/- 30 minutes) after which the specimens were demolded and placed in saturated lime solution, and 2 cubes were tested for compressive strength. Per specification, a compressive strength of 20 MPa (2,850 psi) or higher is required for the initial comparator readings. The mortar bars and cubes were stored in saturated lime solution until the necessary strength was attained. After the initial readings, the mortars bars were stored in a 5% sodium sulfate solution. Measurements were taken at 1, 2, 3, 4, 8, 13, and 15 weeks, as well as at 4 and 6 months. After each set of readings, the used solution was discarded and a freshly prepared solution was used.

Phase Transformation

Selected phase transformation studies were conducted on paste and mortar specimens to investigate the mechanism of deterioration for mixtures that showed disintegration. A Panalytical x-ray diffractometer was used for data collection and the scans were analyzed using Highscore plus software.

Table 8-1: Binary Mix Design

Mix Design	Cement (g)	MK (g)	FA (g)	SF (g)	Slag (g)	Sand (g)	AE Solution (g)	WR (g)	SP1 (g)	SP2 (g)	Water (g)
CN	740					2,035					359
10SF	666			74		2,035	3.7	0.94		0.88	353.9
52SL	355.2				384.8	2,035	3.7	0.94		0.88	353.9
10MK	666	74				2,035	3.7	0.94	1.23		353.9
20MK	592	148				2,035	3.7	0.94	1.23		353.9
21FA	584.6		155			2,035	3.7	0.94		0.88	353.9
30SL	518				222	2,035	3.7	0.94		0.88	353.9
40SL	444				296	2,035	3.7	0.94		0.88	353.9

Table 8-2: Ternary and Quaternary Mix Design

Mix Design	Cement (g)	MK (g)	FA (g)	SF (g)	Slag (g)	Sand (g)	AE Solution (g)	WR (g)	SP1 (g)	SP2 (g)	Water (g)
10FA+10MK	592	74	74			2,035	3.7	0.94	1.23		353.9
10FA+20MK	518	148	74			2,035	3.7	0.94	1.23		353.9
21FA+30SL	363		155		222	2,035	3.7	0.94		0.88	353.9
21FA+10SF	511		155	74		2,035	3.7	0.94		0.88	353.9
52SL+10MK	281.2	74			384.8	2,035	3.7	0.94	1.23		353.9
10MK+10SF+20SL	444	74		74	148	2,035	3.7	0.94	1.23		353.9

Results and Discussions

Control Mixture

Figure 8-1 shows the sulfate expansion behavior for the control mixture, where it can be seen that the expansion was 0.06% at 6 months. According to ASTM C1157 [264], if the cement experiences expansion of less than or equal to 0.1% at the 6-month mark, the cement sulfate durability can be classified as moderate sulfate resistance.

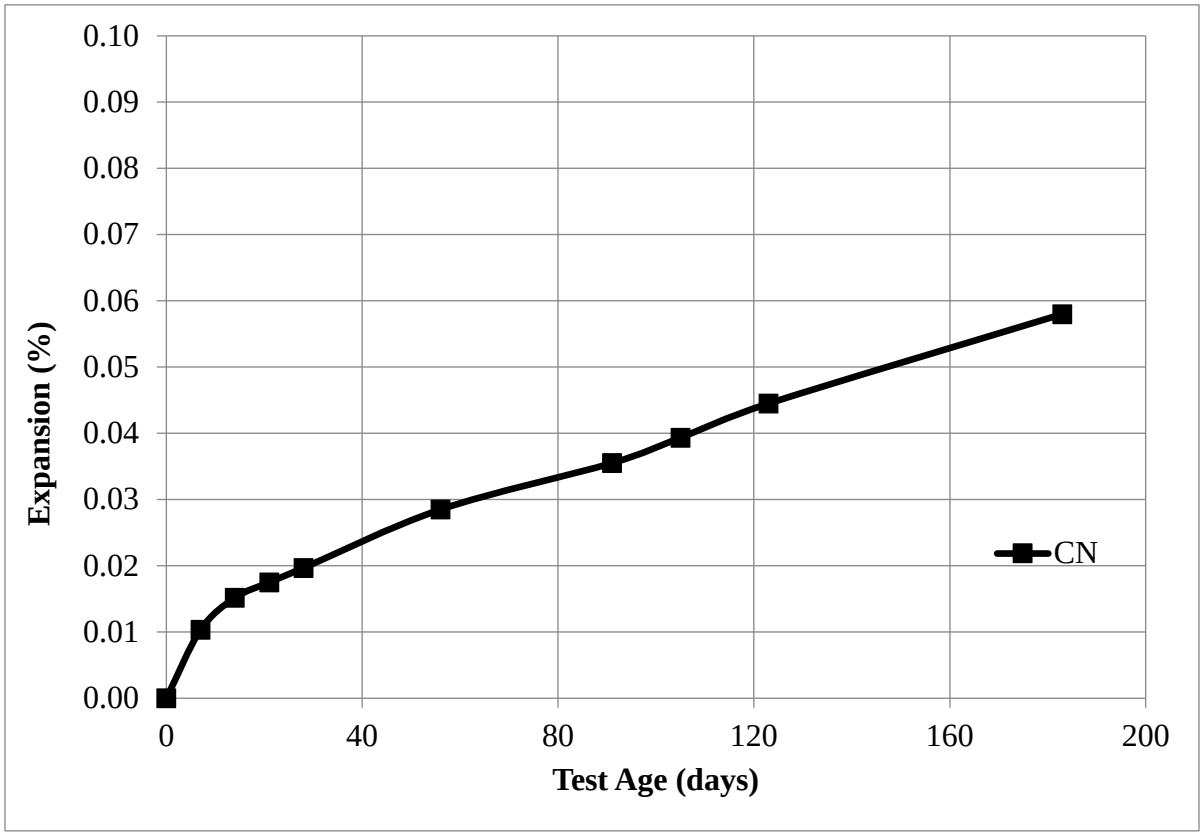

Figure 8-1: Expansion Behavior for CN Mixture in 5% Sodium Sulfate Solution

Binary Combinations

Metakaolin

Figure 8-2 shows the effect of metakaolin on sulfate durability of the cementitious mixture in sodium sulfate solution. Incorporating metakaolin on a 10% replacement basis resulted in an expansion of 0.04% at 180 days versus 0.06% noted for the CN mixture at the same age. Increasing the replacement level to 20% showed marginal change at 180 days (0.03%). While the expansion

data for the short exposure time of 180 days appears to be promising, longer exposure times are necessary to warrant scientific conclusions on the effectiveness of metakaolin on sulfate durability of cementitious mixtures.

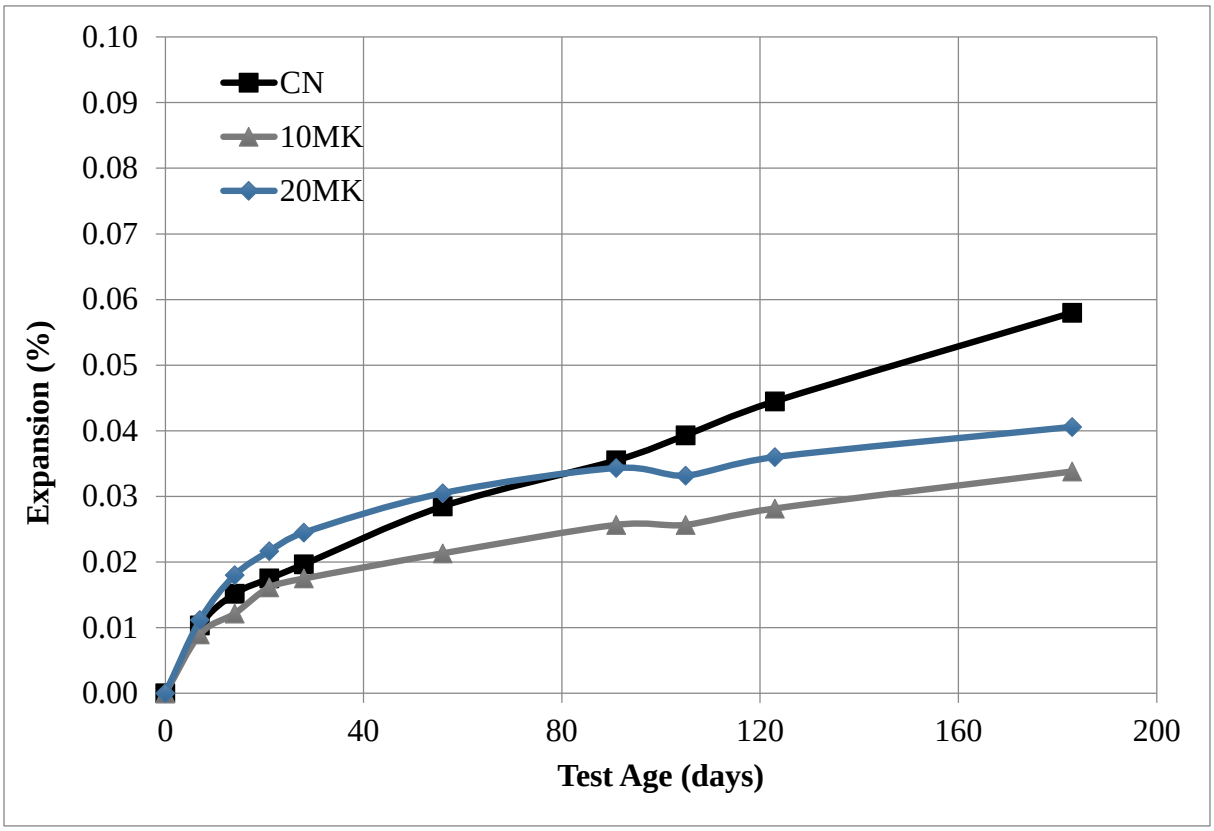

Figure 8-2: Expansion Behavior for MK Mixtures in 5% Sodium Sulfate Solution

Al-Akhras [79] investigated the effect of metakaolin on sulfate durability of the cementitious system, where metakaolin was used at different substitution levels and w/cm ratios (0.5 and 0.6). The results showed that increasing replacement levels led to less expansion for both w/cm ratios. The 10% and 15% metakaolin mixes reached maximum expansion after 18 months of 0.1% and 0.07%, respectively, for a w/cm ratio of 0.5, and 0.13% and 0.1%, respectively, for a w/cm of 0.6. The initial cracking times due to the expansion produced by sulfate attack for the 10% and 15% metakaolin substitutions, at a w/c ratio of 0.5, were 300 and 360 days, respectively. The initial cracking times for the 10% and 15% metakaolin substitutions, at a w/c ratio of 0.6, were 260 and 310 days, respectively. The 5% metakaolin mix showed less improvement in sulfate durability compared to the 10% and 15% mixes, reaching expansions of 0.17% and 0.2% at w/c

ratios of 0.5 and 0.6, respectively. The initial cracking occurred at 240 and 200 days for the w/c ratios of 0.5 and 0.6, respectively. According to Al-Akhras, the increase in sulfate durability can be attributed to the replacement of cement with metakaolin (dilution effect), the pozzolanic reaction, and the filler effect. The replacement of cement with metakaolin reduces the amount of C_3A in the cement. When cement reacts with water, the C_3S and C_2S react to form C-S-H and CH, and as hydration proceeds there is a decrease in the permeability of the system due to the precipitation of hydration products on the walls of the open pores and capillaries that reduces the connectivity of the pore system. Since CH is quite soluble, it can dissolve when in contact with water, thus increasing the porosity and permeability of the system. The dilution effect refers to the use of pozzolans to reduce the cement tricalcium aluminate content as well as the CH, which is consumed in pozzolanic reactions. The pozzolans will then react and consume CH to form secondary C-S-H (of higher volume) and lower the permeability of concrete by filling the network of pores. The filler effect of metakaolin also plays a role in that its finer particle size can fill in the gaps between the bigger cement particles. This allows for a dense pore structure that lowers the permeability of the mix.

Courard et al. [80] investigated the effect of 0, 5, 10, 15, and 20% replacement of metakaolin on the sulfate durability of mortar. The reported findings indicate that for all replacement levels of metakaolin, a relatively lower expansion than the control mixture was noted. After 50 weeks, all metakaolin mixtures showed less than 1 mm/m of variation in length, while the control mixture had about 5 mm/m. According to Courard et al., metakaolin has a positive effect on sulfate durability because of the consumption of $Ca(OH)_2$. Mardani-Aghabaglou et al. [265] compared fly ash, metakaolin, and silica fume at a 10% replacement level and a w/c ratio of 0.485. Mardani-Aghabaglou found that the metakaolin mixture showed sulfate durability intermediate between silica fume and fly ash, with silica fume showing the best performance. Scanning electron microscopy showed the formation of ettringite in all mixtures, though the formations had different distinctive morphologies. Ettringite morphologies were categorized as ball-ettringite or needle-like ettringite. It was also noted that neither the ball-ettringite nor the needle-like ettringite was observed in the metakaolin mixture, but another type was present that showed no expansive effect. For the metakaolin mixes, it was also observed that ettringite formed only inside existing pores.

Khatib and Wild [266] studied the effect of metakaolin on sulfate durability using 2 different types of cements having high and intermediate C_3A contents of 11.7 and 7.8%, respectively. The results showed that for both cements, the increase in metakaolin replacement level led to a decrease in expansion. The results showed that for the high C_3A cement, the control as well as the 5 and 10% metakaolin mixes showed disintegration between 40 and 70 days of sulfate exposure. The 15 and 20% metakaolin showed a sharp increase in expansion between 40 and 70 days, but stabilized afterwards. The 15% metakaolin disintegrated after 290 days, but by 520 days, the 20 and 25% metakaolin showed no apparent changes in length. The metakaolin mixes with intermediate C_3A cement content showed a slower but similar trend to that of the high C_3A cement, but with no disintegration, even after 550 days.

Silica Fume

Figure 8-3 shows the expansion behavior for the cementitious system incorporating 10% silica fume, where it can be seen that at 180 days, the silica fume mixture had an expansion of 0.02% compared to the control mixture at 0.06%. The 10SF mixture satisfies the criteria of high sulfate resistance according to ASTM specifications.

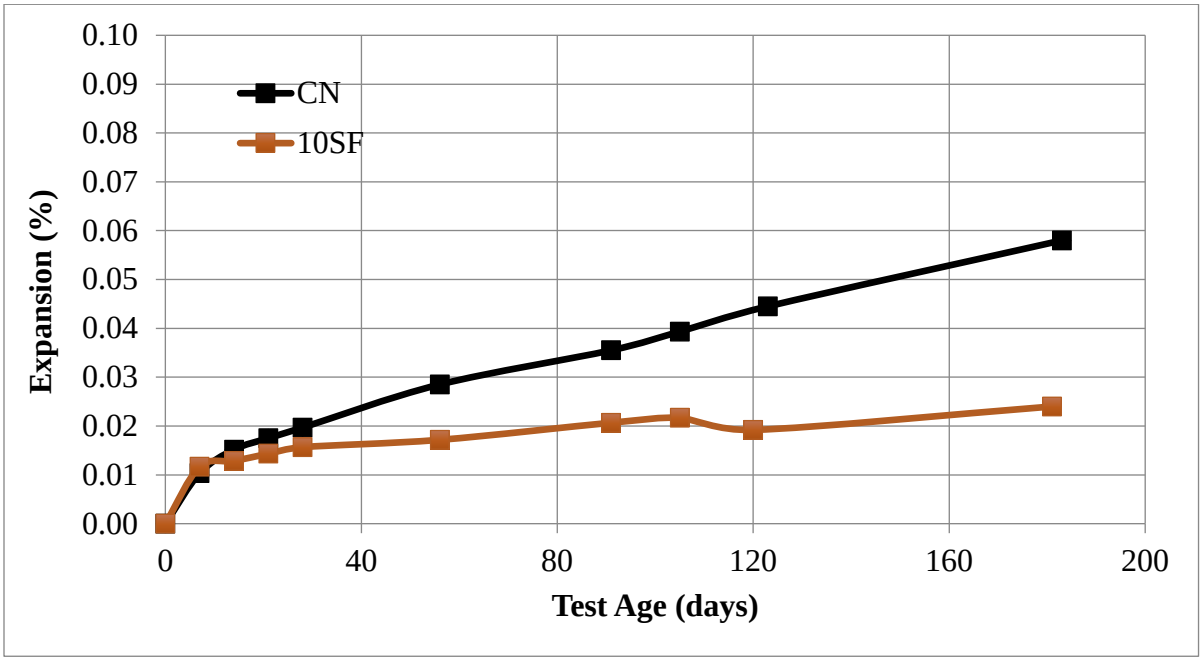

Figure 8-3: Effect of SF on Mortar Expansion in 5% Sodium Sulfate Solution

Hooton [267] investigated the effect of silica fume on sulfate durability. It was observed that the silica fume mixes expanded less than a sulfate-resisting portland cement (SRPC). The SRPC and all silica fume mixes showed expansion of less than 0.1% at 1 year. After 1.7 years, the SRPC failed the 0.1% criteria while the silica fume mixes did not in 5 years of exposure. In their work [6], mortar bars were prepared according to ASTM C1012 and immersed in a 5% Na_2SO_4 solution. Similarly, the findings of Mardani-Aghabaglou et al. [265] indicate the superior performance of silica fume mixtures, when compared to fly ash and metakaolin, at a constant replacement level of 10%. At 180 days, the silica fume mixture showed an expansion of less than 0.05%. Ettringite morphology was categorized as ball-like ettringite for the silica fume mixture and it was localized only inside the pore structure. In all mixtures reported by Mardani-Aghabaglou et al., a w/c ratio and sand/binder ratio were maintained constant at 0.485 and 2.75, respectively. Sulfate tests were performed following ASTM C1012, where samples were immersed in a 5% Na_2SO_4 solution. Length changes were measured every 30 days for 300 days.

In another study conducted by Kunther et al. [268], the effect of 6 and 12% silica fume substitution on sulfate durability was reported. It was shown that the increase in the level of substitution decreased length changes and was attributed to the C/S ratio. Cohen and Bentur [269] investigated the effect of silica fume paste for sulfate durability. It was observed that the mixes containing silica fume showed improvement in expansion using both Type I and V cements.

Fly Ash

Figure 8-4 shows the effect of fly ash replacement on the expansion behavior in the sodium sulfate solution up to 180 days of exposure. According to the results, it appears that the 21% replacement of Class F fly ash improves the sulfate resistance of the mixture compared to the control. An expansion of $\leq 0.05\%$ at 180 days indicates that the mix can be classified as a high sulfate resistant mixture. At 270 days, the fly ash continued to show resistance to sulfate expansion, with an expansion of 0.06%, which is an increase of 0.01% from 180 days. Though the amorphous content of the ash was low (72%), it limited expansion to slightly below the control mixture at 180 days of exposure, but more than double the expansion reported for the silica fume mixture.

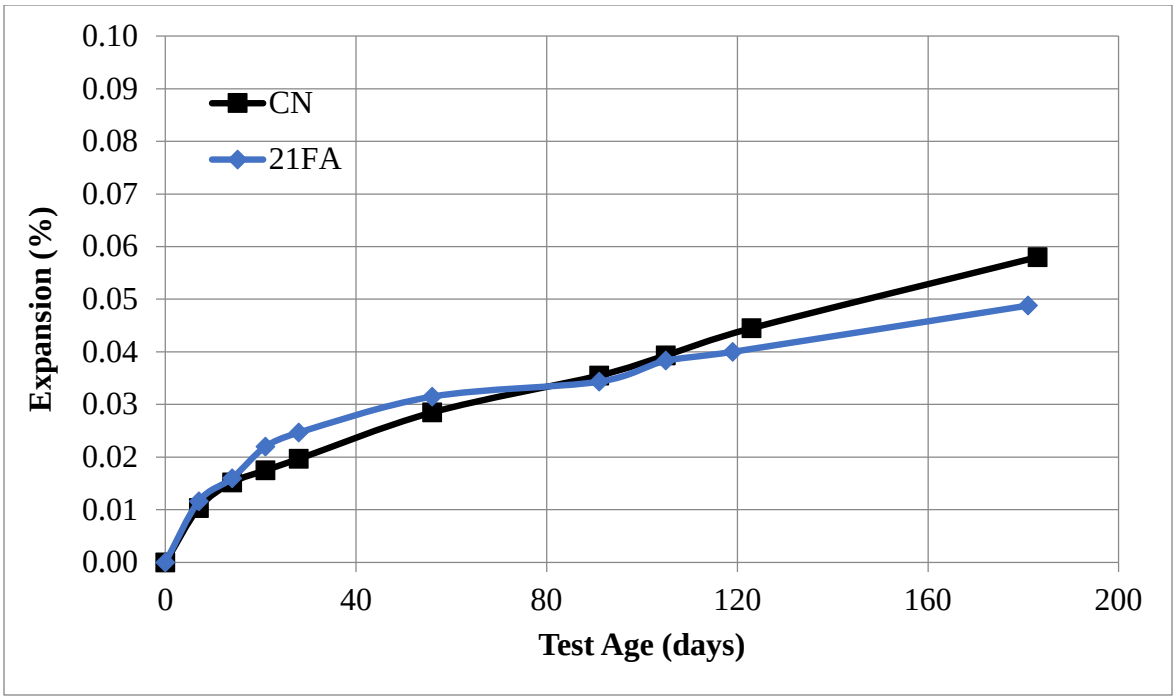

Figure 8-4: Effect of FA on Mortar Expansion in 5% Sodium Sulfate Solution

Mardani-Aghabaglou et al. [265] compared the results of fly ash, metakaolin, and silica fume at a 10% replacement level, where it was noted throughout the testing that the order of effectiveness against sulfate exposure was silica fume, metakaolin, fly ash, and the control, in descending order. Kandasamy and Shehata [270] investigated the effect of high calcium fly ash on sulfate durability. It was shown that the mixes containing 40% fly ash failed before the 4-month measurement, while the 20% fly ash mix failed slightly later than 4 months. According to Kandasamy and Shehata, this can be attributed to the reactive alumina content as well as the free lime contained in the fly ash. Ghafoori et al. [271] investigated the effect of fly ash on sulfate durability of Type V cement and indicated that fly ash performance enhances sulfate durability due to lime consumption and reducing the tricalcium aluminate content of the mixture.

Slag

Figure 8-5 shows the effect of slag on the sulfate durability of cementitious systems. At all replacement levels studied here, slag blends did not result in improving sulfate durability when compared to the control mixture for the period reported here of 180 days. Several mixtures showed cracking and disintegration between 180 and 274 days. It is well established in the literature that

sulfate durability of slags depends on its alumina content, especially if the slag is used at a replacement level of 50 % or less. It also depends on the tricalcium aluminate of the cement.

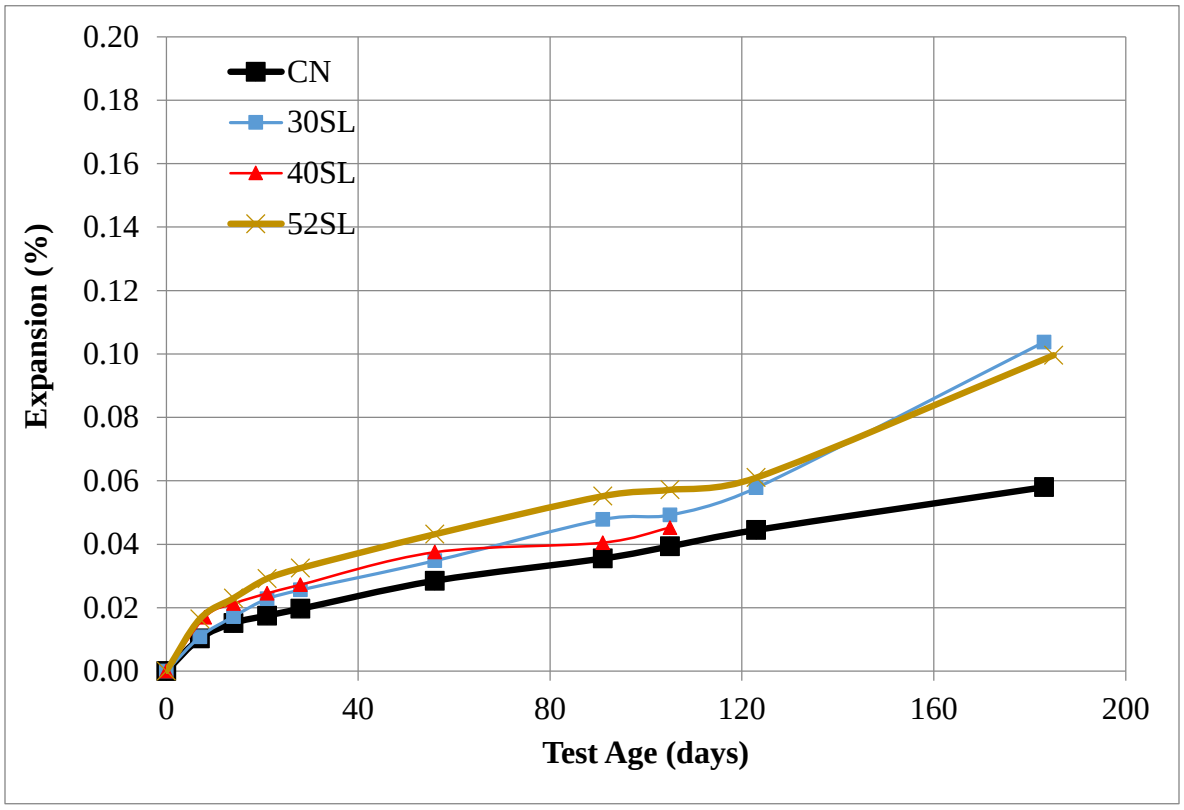

Figure 8-5: Effect of SL on Mortar Expansion in 5% Sodium Sulfate Solution

Between 180 and 274 days, some of the mortar bars disintegrated. The 30% and 52% slag mixtures showed an expansion of 0.10% at 180 days, higher than the CN control, which had an expansion of 0.06%. Gollop and Taylor [272] and Ekolu et al. [273] investigated the effect of slag on sulfate durability of blends and concluded that the blends' susceptibility to sulfate attack increases with the alumina content of the slag and that slag blends made with high alumina slag performed poorly compared to plain portland cement mixes or sulfate resisting cements. Resistance to sulfate attack improved through reducing the slag's alumina content ($\leq$ 11% Al_2O_3), use of high slag proportions (65% or more), or the use of sulfate resisting cements. Failure mechanisms due to sodium sulfate exposure are primarily due to ettringite formation and decalcification of C-S-H. It was also indicated that for blends of portland cement and 69% slag, decreasing sulfate resistance was noted with increasing the alumina content of the slag. This is in agreement with the current observed trends where 30%, 40% and 52% slag-portland cement blends

did not perform better than the control mixtures. Osborne [274] and Yu et al. [275] concluded that the main parameters that influence sulfate durability for portland cement-slag combination are the tricalcium aluminate of the cement and the alumina content of the slag. Low tricalcium aluminate cements, classified as sulfate-resisting cements, or cements with medium and high tricalcium aluminate content when blended with low alumina slag, can render concrete highly resistant to sulfate attack when the level of replacement was 70 to 80%. López et al. [276] investigated the effect of two slags of the same alumina content, but of variable fineness and determined that slag fineness has an effect on sulfate expansion. Ogawa et al. [277] investigated the effect of slag on sulfate durability where 40% blends of unmodified slag (15% Al_2O_3), as well as a novel slag, were used with cement containing 5.3% C_3A. The novel slag had a higher calcium oxide, magnesia and sulfur trioxide but lower alumina content. The unmodified slag showed expansion after 25 weeks and failed at 38 weeks. The modified slag showed excellent results even after 104 weeks. Sulfate tests were conducted on mortar bars immersed in a 5% Na_2SO_4 solution following ASTM C1012. Ogawa et al. [278] proposed improvement to the sulfate durability of slag-cement blends through limestone additions and optimizing the calcium sulfate content of the blend.

Binary Combination Overview

Figure 8-6 shows the effect of different mineral admixtures on sulfate durability in 5% sodium sulfate solution for commonly used cement replacement levels in structural concrete in Florida. It is observed that substitution of cement by 10% silica fume provided the best sulfate resistance among all mixtures studied here. The observed expansion at 180 days was 0.02%, thus resulting in a high sulfate resistance classification for the 10% silica fume mix. Substitutions of 21% Class F Fly ash (21FA) or 10% metakaolin (10MK) provided better sulfate resistance than the control (CN) mixture with 10MK showing lower expansion than 21FA.

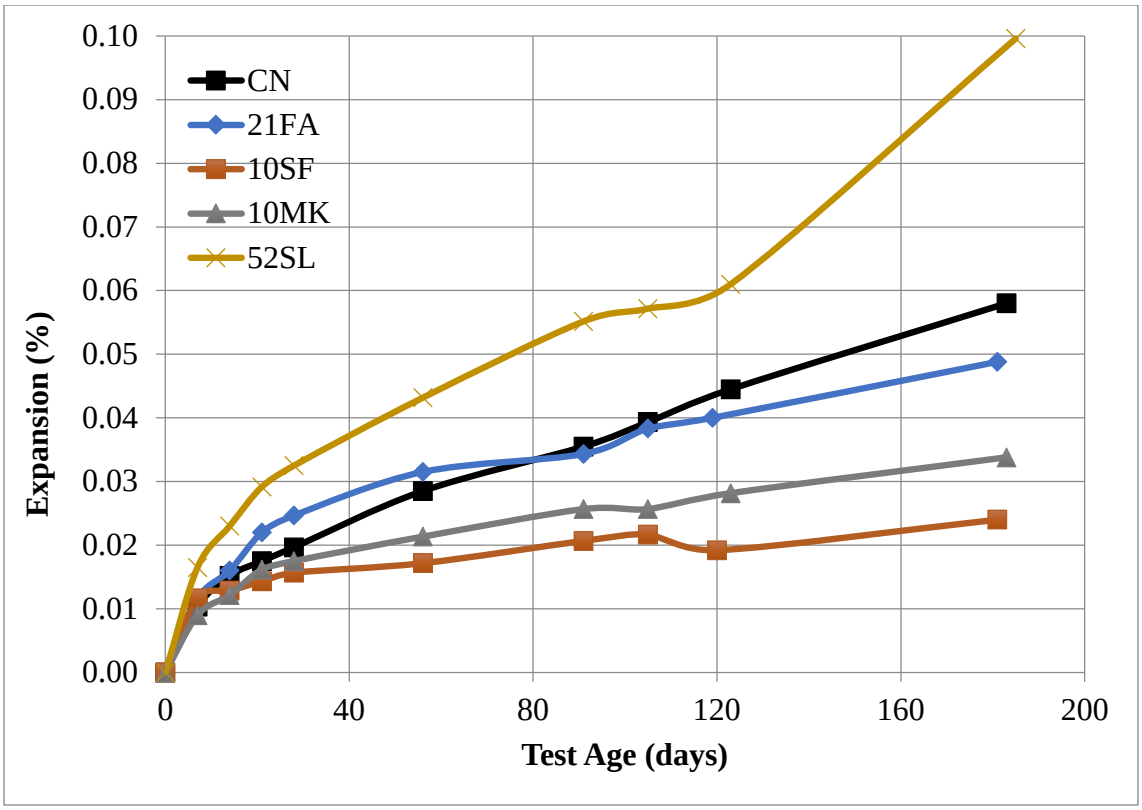

Figure 8-6: Effect of Binary Cementitious Systems on Sulfate Durability

Cement-52% Slag (52SL) samples had higher expansions than the control samples at 180 days. The oxide chemical analysis for the slag, presented in Table 2-4, indicates that the alumina content of this slag was 14.25%. Mortar bars disintegrated between the 180-day and 274-day measurements. In order to assess the mechanism of failure, specimens were studied by x-ray diffraction using external and internal standard techniques. Paste specimens for the 52SL mixture were prepared using the same mixture proportions as for the mortar bars, and were cured at the same temperature imposed for curing of the 52SL mortar bars used for sulfate expansion measurements. A companion CN paste was also prepared and examined. The scans indicated the presence of monosulfoaluminates (C_4ASH_{12}) and ettringite ($C_6AS_3H_{32}$) in the 52SL paste at 3 days (which corresponds to the age at which the mortar specimens reached the required compressive strength, and is also the age when mortar bars were exposed to the sodium sulfate solution in accordance with ASTM C1012). The CN paste did not show the presence of monosulfoaluminate and only ettringite was present. Scans for 52SL mortar specimens at about 180 days were conducted on the inner core and the outer surface of the bar. The inner and outer layers showed

differences in their phases' constituents. While the inner core showed presence of monosulfoaluminates as well as ettringite, the outer layer showed only ettringite. This is not surprising as the sulfate content should be higher at the specimen surface in direct contact with the sulfate solution. Additionally, gypsum was present in the outer surface as well as the inner core, though its amount was higher in the former. Higher amounts of gypsum were accompanied by lower content of portlandite, which is consumed in the formation of secondary gypsum. It was also noted that portlandite was absent in the outer layer, potentially indicating decalcification of C-S-H. This is plausible as the outer layers of the mortar bars were easily separated from the inner core. The findings indicate that the expansion and disintegration of the 52SL mortar bars noted around 180 days of exposure to sodium sulfate solution was due to the formation ettringite and secondary gypsum, in addition to possible decalcification of C-S-H.

Ternary Combinations

Ternary Combination: Fly Ash and Silica Fume

Figure 8-7 shows the effect of fly ash and silica fume combinations on sulfate durability. The ternary combination of fly ash and silica fume showed expansion trends between the binary combinations of fly ash and silica fume: at 180 days, the silica fume mix showed an expansion of 0.02%, the ternary combination had an expansion of 0.04%, while the fly ash mix showed an expansion of 0.05%. The ternary combination of fly ash and silica fume met the criteria for high sulfate resistance. The ternary combination continued to show better resistance to sulfate expansion at 270 days, with an expansion of 0.04%.

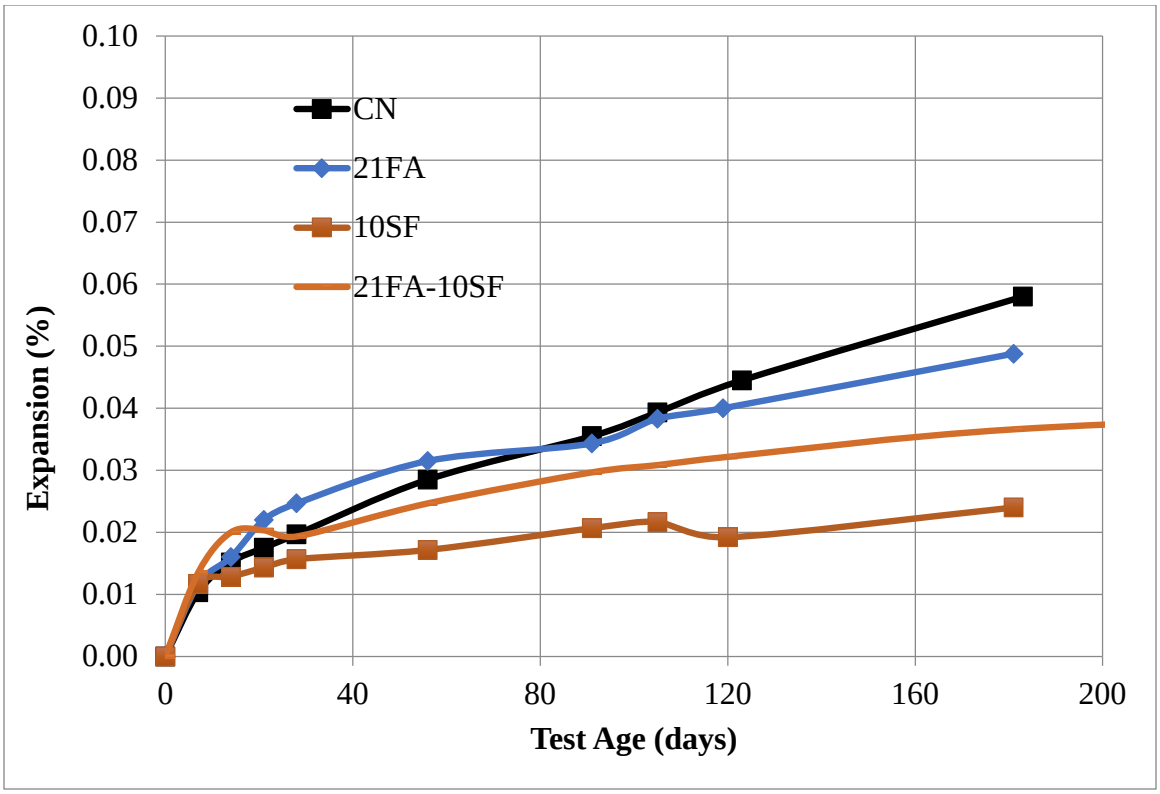

Figure 8-7: Effect of FA and SF on Length Change of Mortar Samples in 5% Na_2SO_4 Solution

[redacted]Ternary Combination: Metakaolin and Fly Ash

Figure 8-8 shows the effect of metakaolin and fly ash on length change of mortar samples in 5% sodium sulfate solution. It appears that the ternary blends of MK and FA did not enhance sulfate durability of the system at the proportions studied here.

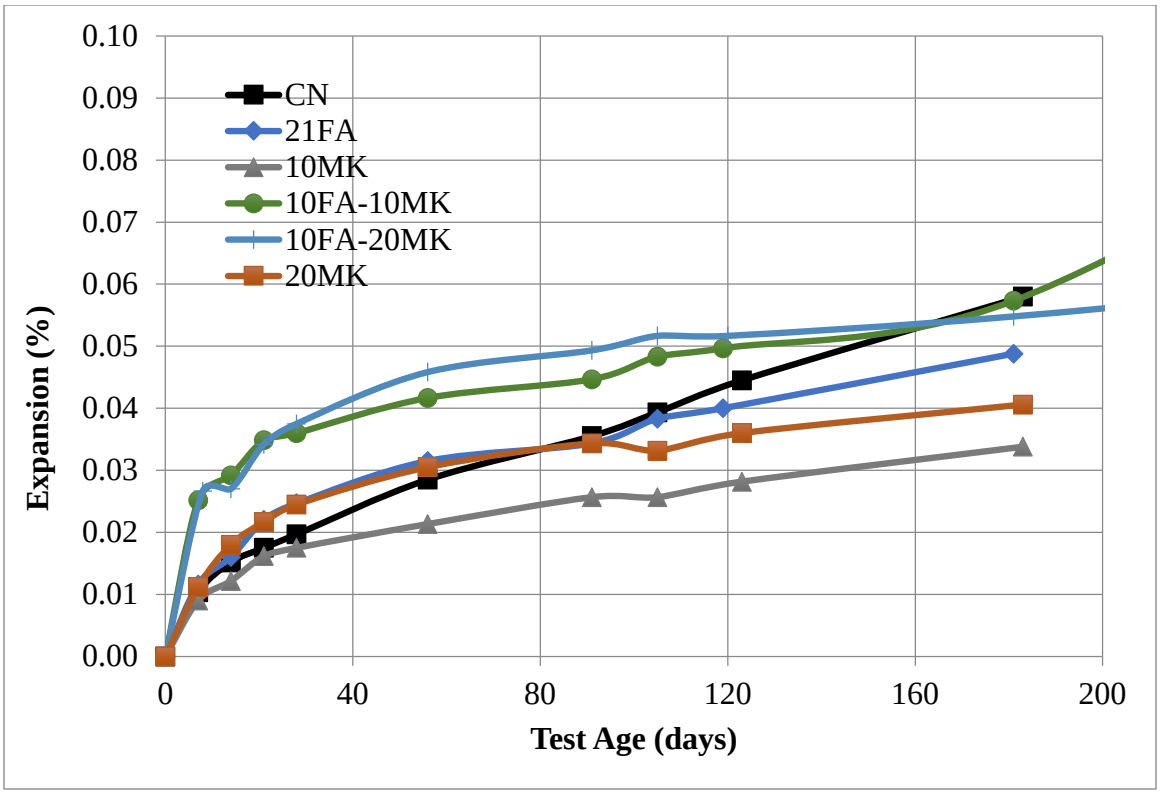

Figure 8-8: Effect of MK and FA Combinations on Expansion Behavior

Ternary Combination: Slag and Fly Ash

Figure 8-9 shows the effect of ternary blends of Class F fly ash and blast-furnace slag. The results show that the ternary combination of Class F fly ash (low lime ash) and slag did not pass the criteria for moderate sulfate resistance. It is therefore concluded that additions of slag of alumina content of 14.25% to Class F fly ash of low amorphous content did not have positive contribution on the blends' sulfate durability. Kandasamy and Shehata [270] investigated the combination of high lime fly ash and slag blends on sulfate durability. The slag used in their study had an alumina content of 7.4%, and showed the best sulfate resistance among all blends studied. The investigation was on the expansion of mortar bars containing fly ash with increasing levels of slag from 20 to 40%. The results reveal that increasing levels of slag increased the sulfate resistance, with the lowest expansion reported for the 40% slag blend with the high lime ash.

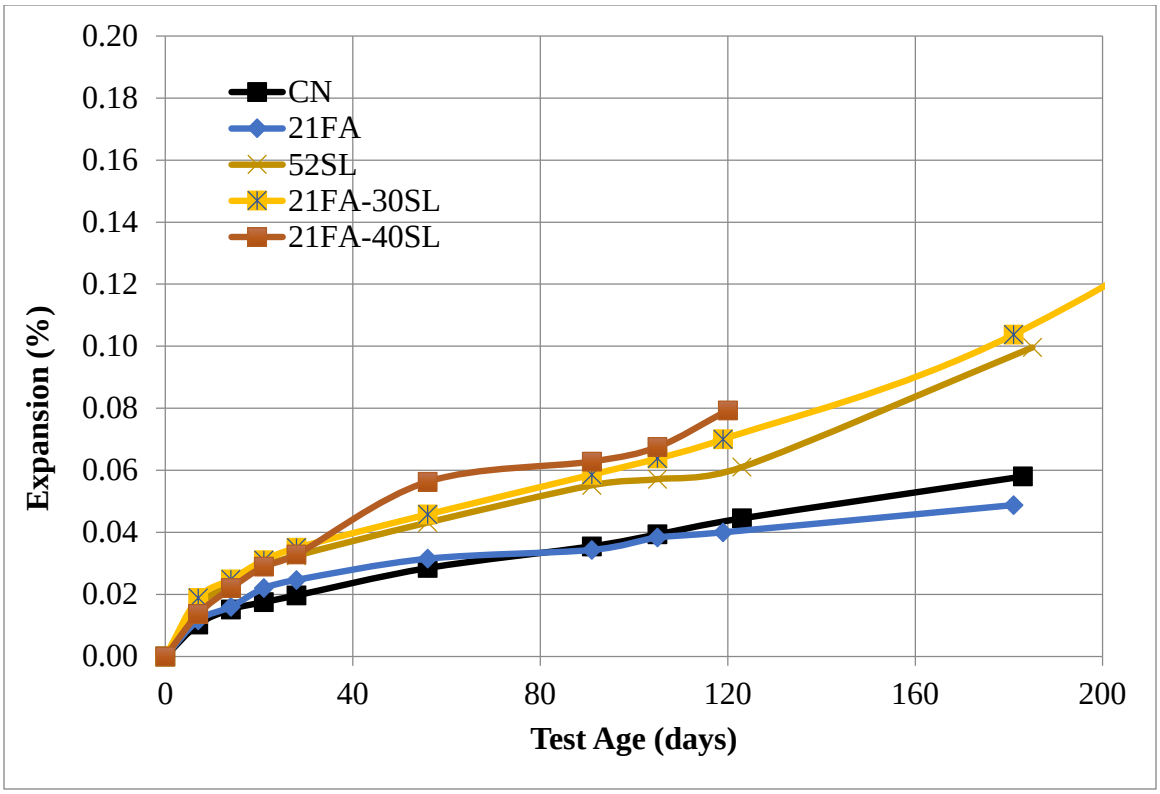

Figure 8-9: Effect of FA and SL Combinations on Expansion Behavior

Ternary Combination: Metakaolin and Slag

Figure 8-10 shows the effect of blends of metakaolin and slag on length change of mortar samples in 5% sodium sulfate solution. From the results, it can be seen that the addition of metakaolin to the mix containing slag improved the sulfate resistance of the 52% blast furnace slag blends. The binary 52SL blend had an expansion of 0.1% at 180 days while the binary mix of 10MK expanded 0.03% at the same age. For the ternary combination of metakaolin and slag mixture, the level of expansion was at 0.05% by 180 days, which is at the limit of being considered a high sulfate resistance mixture. The addition of 10% MK to the 52% SL mixture had a positive effect on sulfate durability. However, longer exposure times are necessary to be able to confirm the early trends.

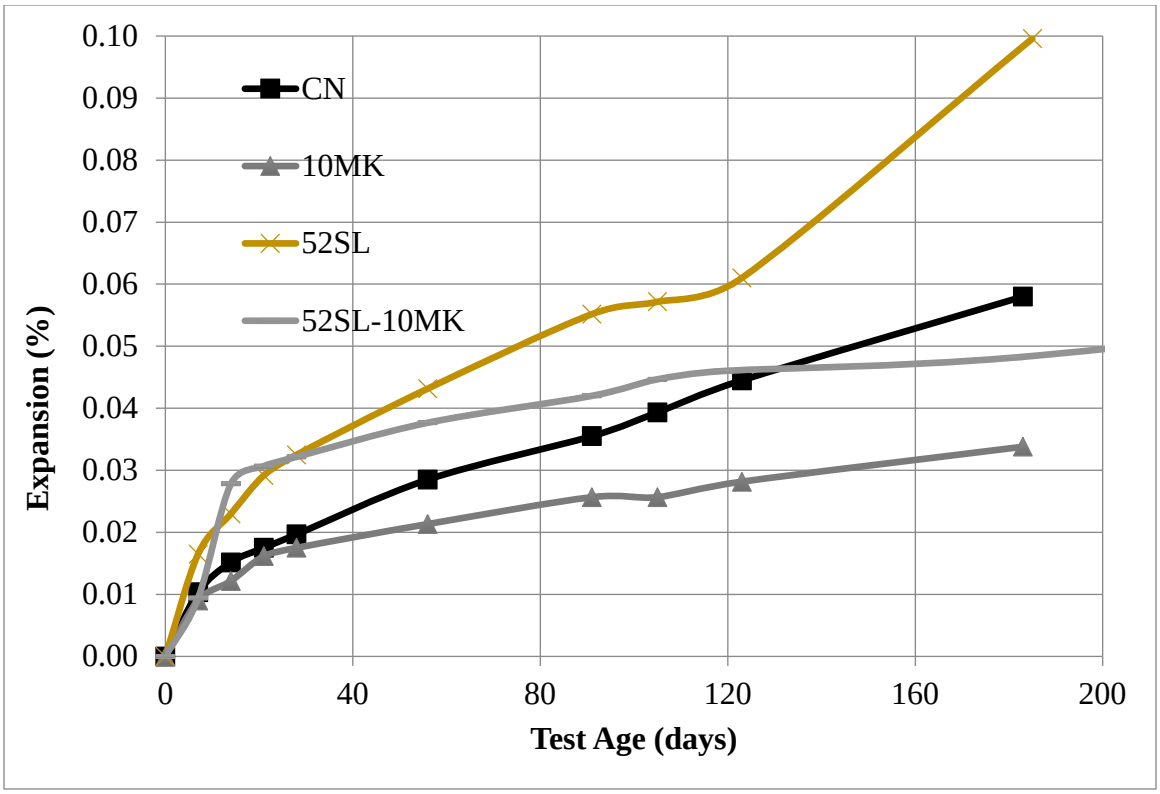

Figure 8-10: Effect of MK and SL on Expansion Behavior of Mortar

Quaternary Combination: Metakaolin, Silica Fume, and Slag

Figure 8-11 shows the effect of the metakaolin, silica fume, and slag combination on sulfate durability. The results indicate quaternary combination of metakaolin, silica fume, and slag passed the criteria of high sulfate resistance, having an expansion of 0.04% at 180 days. It is to be noted that the limited exposure time of 180 days is not adequate to render a conclusion on the benefit of such mixture. Longer exposure times of a minimum of 18 months are necessary for such conclusions. Nevertheless, at 180 days of exposure, the quaternary mixture studied here appears to be promising, especially with mitigation of the expansion due to slag, in its performance in a sulfate environment.

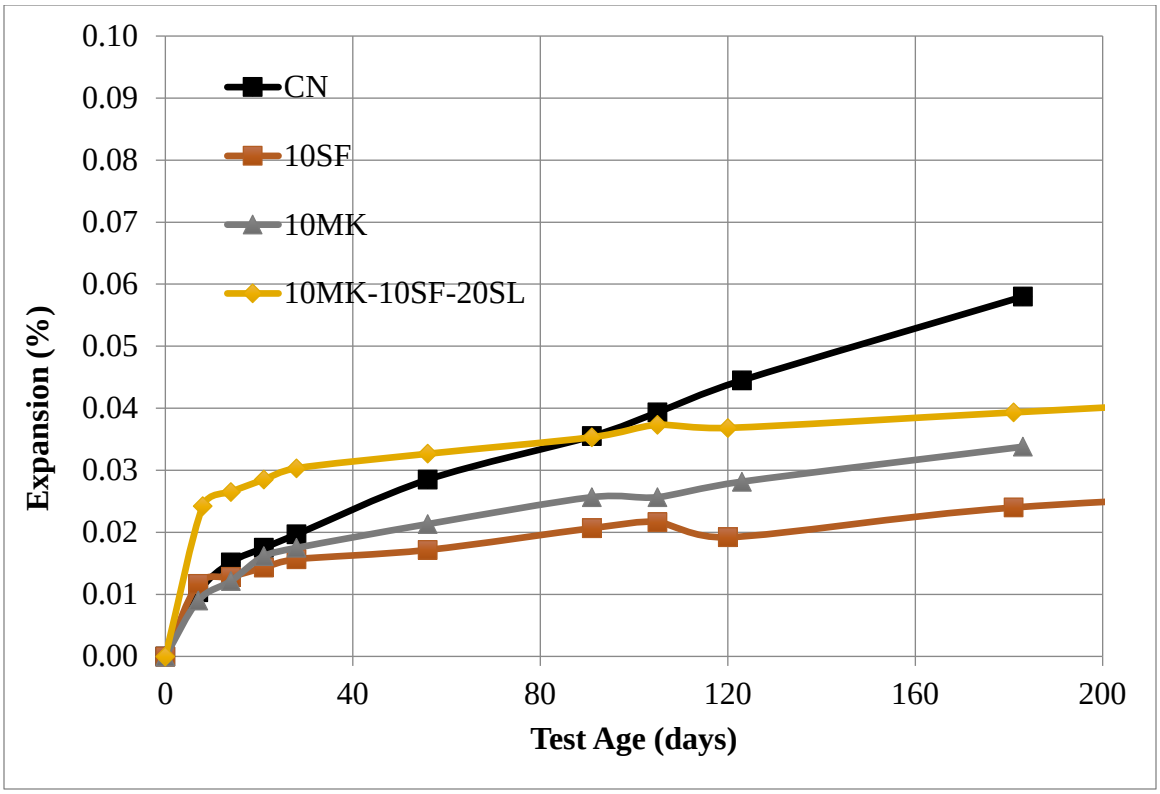

Figure 8-11: Effect of MK, SF, and SL Combination on Expansion Behavior

Conclusions

Sulfate durability studies on binary and ternary mixtures indicate that silica fume outperformed all mixtures studied here. While all mixtures showed expansion at 0.10% or below, using high alumina slag (14.35%) did not offer any beneficial contribution towards enhancing the sulfate durability of cementitious mixtures using a Type I/II portland cement.

Effect of Mineral and Chemical Admixtures on Concrete Cracking Potential

Introduction

In this report the effects of different mineral admixtures on temperature rise and cracking tendencies in concrete mixtures are addressed. A time-temperature profile, simulating temperature rise at the center of a thick element, was generated for different hydrating concrete mixtures incorporating supplementary cementitious materials., and imposed while testing in a rigid cracking frame [279]. In order to generate the temperature profile for each mixture, semi-adiabatic calorimetry was first conducted on all mixtures in order to determine the adiabatic temperature rise and the hydration parameters.

Methodology

Semi-adiabatic Calorimetry

The current study, assessing the cracking potential of different concrete mixtures incorporating mineral and chemical admixtures commonly used in concrete for Florida FDOT projects, was conducted through using a rigid cracking frame. Rigid cracking frame testing was conducted using a simulated temperature profile for a 1 m thick wall. The first step in modeling required inputs, including the hydration parameters, for each mixture. The hydration parameters, α_u, β, and τ were first determined through semi-adiabatic calorimetry, which was also used to determine the adiabatic temperature rise. Semi-adiabatic calorimetry measurements were conducted using a calorimeter constructed at the University of South Florida. The construction, operation, calibration, and procedures for data analyses can be found in Zayed et al. [280]. Activation energy values generated from ConcreteWorks [281] software for the heat-of-hydration-based activation energy for all mixtures studied here, Table 9-1.

Table 9-1: Activation Energies for Concrete Mixtures

Property	**52BFS**	**30BFS**	**21FA**	**10FA**	**21SF**	**10SF**	**SP2**
E_a (kJ/mol)	40.79	38.46	34.30	35.16	25.00	29.97	36.03

In addition to the control mixture, 3 mineral admixtures most commonly used in FDOT construction projects were studied; namely, blast furnace slag (30%, 50%), silica fume (10%) and

Class F fly ash (10% and 21%). Mixing procedures followed ASTM C192 guidelines and mixture details are provided in Table 9-2.

Table 9-2: Mixtures Design

Mixture Name	**CN**	**30SL**	**52SL**	**10FA**	**21FA**	**10SF**	**21SF**
Materials	Wt. (lbs)	Wt. (lbs)	Wt. (lbs)	Wt. (lbs)	Wt. (lbs)	Wt. (lbs)	Wt. (lbs)
Cement	750	525	360	675	592.5	675	592.5
MK	0	0	0	0	0	0	0
FA	0	0	0	75	157.5	0	0
SF	0	0	0	0	0	75	157.5
SL	0	225	390	0	0	0	0
Coarse (SSD)	1600	1600	1600	1600	1600	1600	1600
Fine (SSD)	1051	1036	1026	1026	999	1025	997
Mix Water	260	260	260	260	260	260	260
AE	0.053	0.053	0.053	0.053	0.053	0.053	0.053
SP2	0.682	0.682	0.682	0.682	0.682	1.867	2.764
WR	2.618	2.618	2.618	2.618	2.618	2.618	2.618
W/C	0.35	0.35	0.35	0.35	0.35	0.35	0.35

Temperature Profile

The temperature profile for operating the rigid cracking frame was generated using the Cracking Frame Temperature Profile Program software that predicts the early-age temperature development in concrete members [282]. It was used to replicate the temperature at the center of a 1m thick concrete wall. The temperature profile consists of one heating and cooling cycle that steadily cools after 96 hours by 1°C/ hr. This steady decrease in temperature is imposed to force concrete cracking under thermally induced stresses.

Although there is an option to manually input the CTE value, the value calculated by the program, based on mixture proportions, was used for all the experiments conducted here. A placement temperature and surface temperature of 23° C were used. All input parameters used in generating the temperature profiles imposed when testing concrete in the rigid cracking frame are presented in Table 9-1, Table 9-2, and Table 9-3. The hydration parameters determined from semi-adiabatic calorimetry were used in generating the imposed temperature profile.

Rigid Cracking Frame

A rigid cracking frame, the details of which are presented in Buidens, 2014 [279], was used to study the effects of mineral admixtures on the early-age induced tensile stresses, due to temperature and shrinkage, that are generated under restraint. Modulus development and stress relaxation are accounted for during this test. As the temperature of the restrained sample is increased, compressive stresses develop in the concrete. This pre-compression can be reduced due to stress relaxation. As concrete stiffness increases with time, and stress relaxation is reduced, high tensile stresses start to develop as the concrete temperature starts to decrease. Although the cracking frame test can be conducted with the system insulated, it was preferred to simulate temperatures experienced in a selected structural element, a 1 m thick wall. The tests were conducted with an imposed temperature profile to simulate actual field conditions or applications.

Results and Discussion

Semi-adiabatic

Semi-adiabatic calorimetry measurements for all mixtures are depicted in Figure 9-1 through Figure 9-7. The modeled and the experimentally measured semi-adiabatic data show excellent agreement for all mixtures studied here. The temperature variations under semi-adiabatic conditions indicate that the maxima occur at similar times for all mixtures except BFS, where its occurrence appears to be significantly delayed because of the lower early rate of hydration of slag.

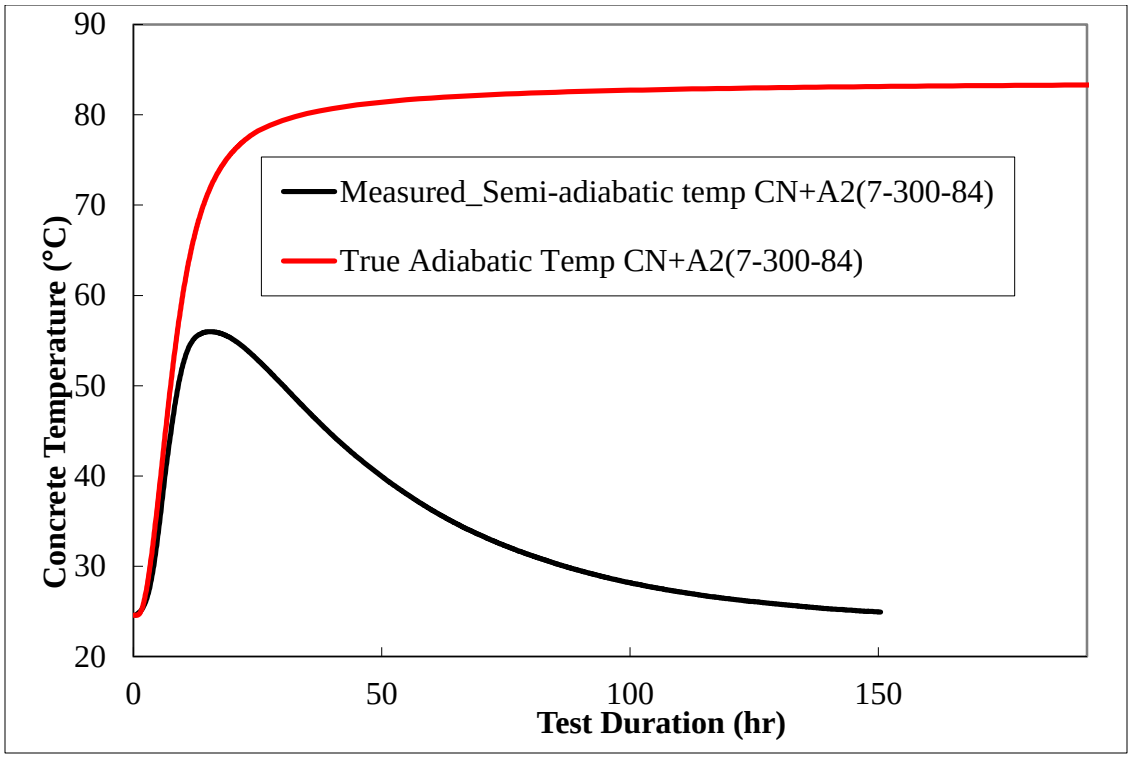

Figure 9-1: Adiabatic Temperature for Control Mixture

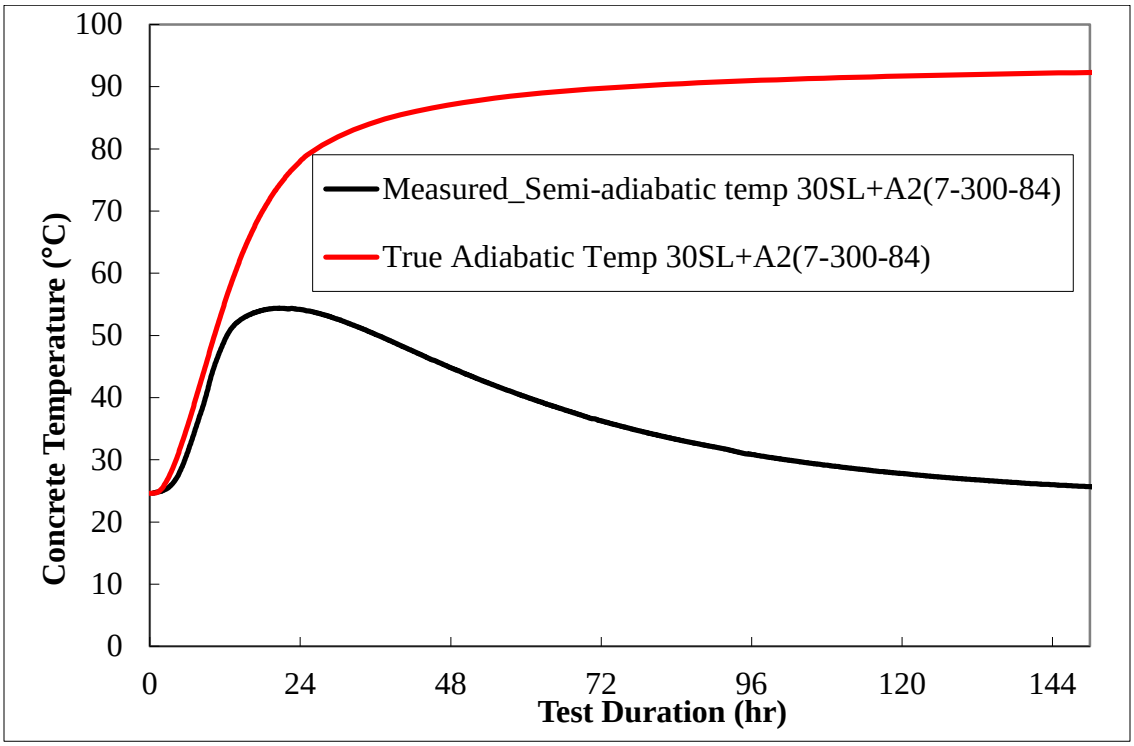

Figure 9-2: Adiabatic Temperature for 30SL Concrete

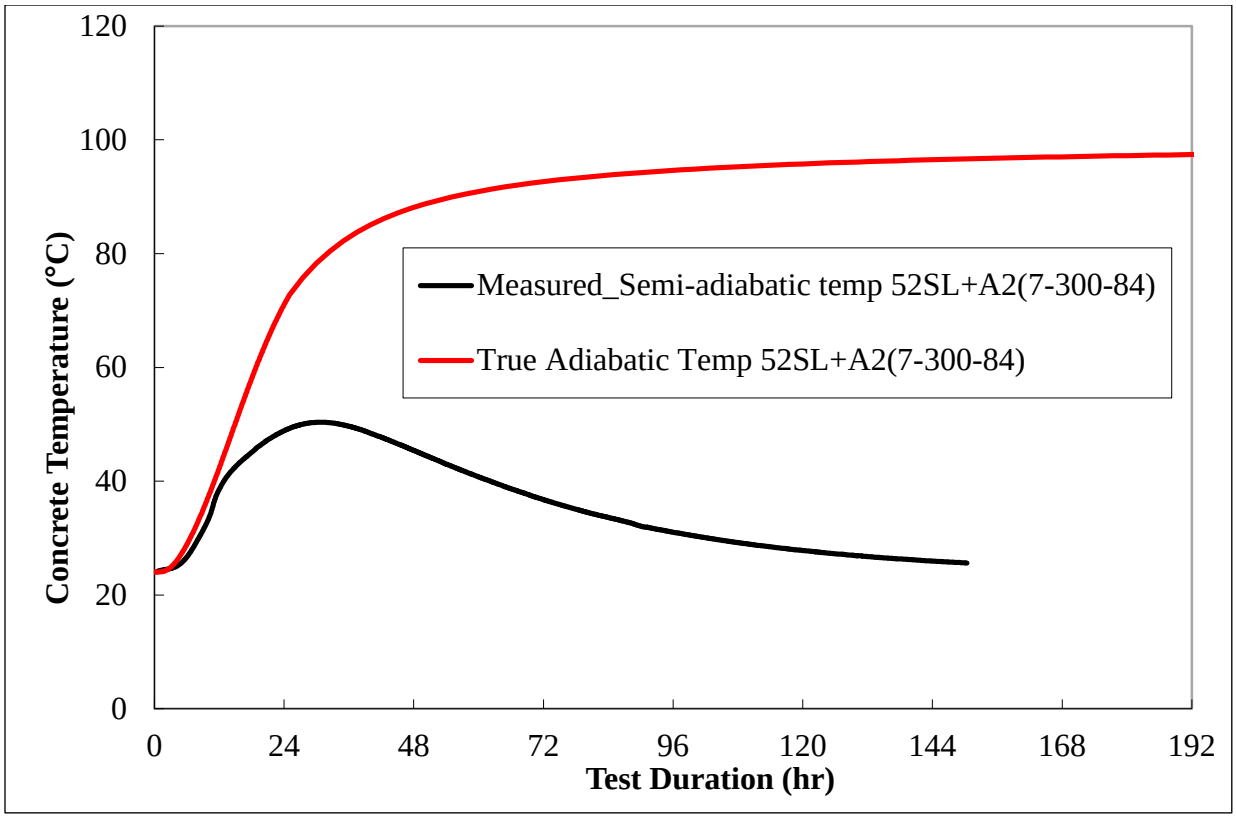

Figure 9-3: Adiabatic Temperature Rise for 52SL Concrete

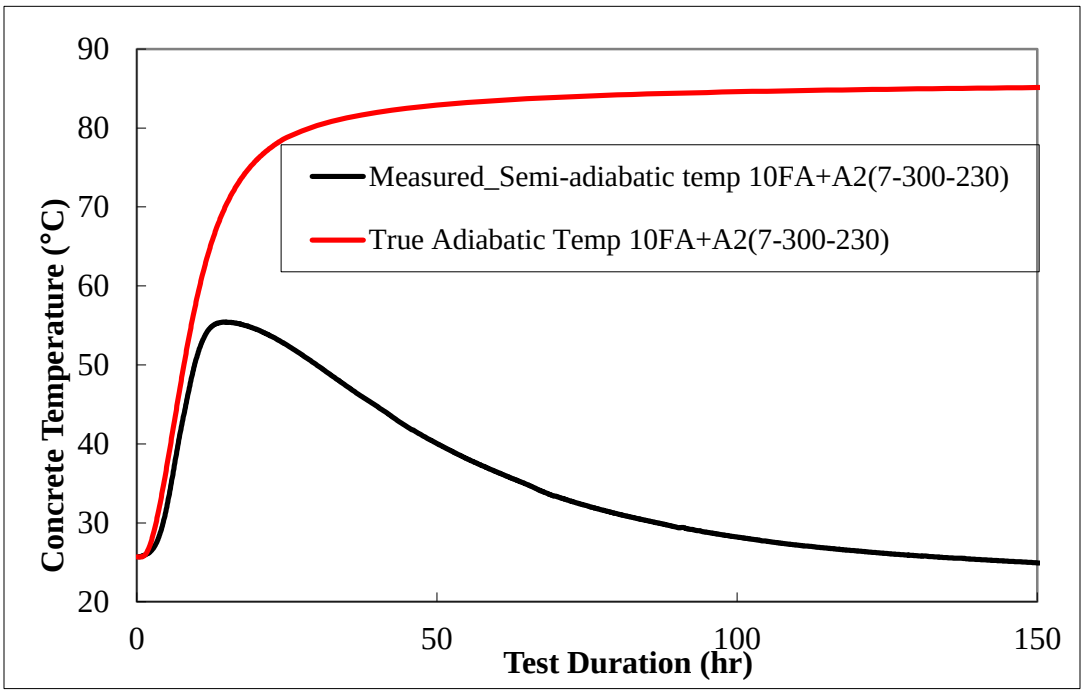

Figure 9-4: Adiabatic Temperature Rise for 10FA Concrete

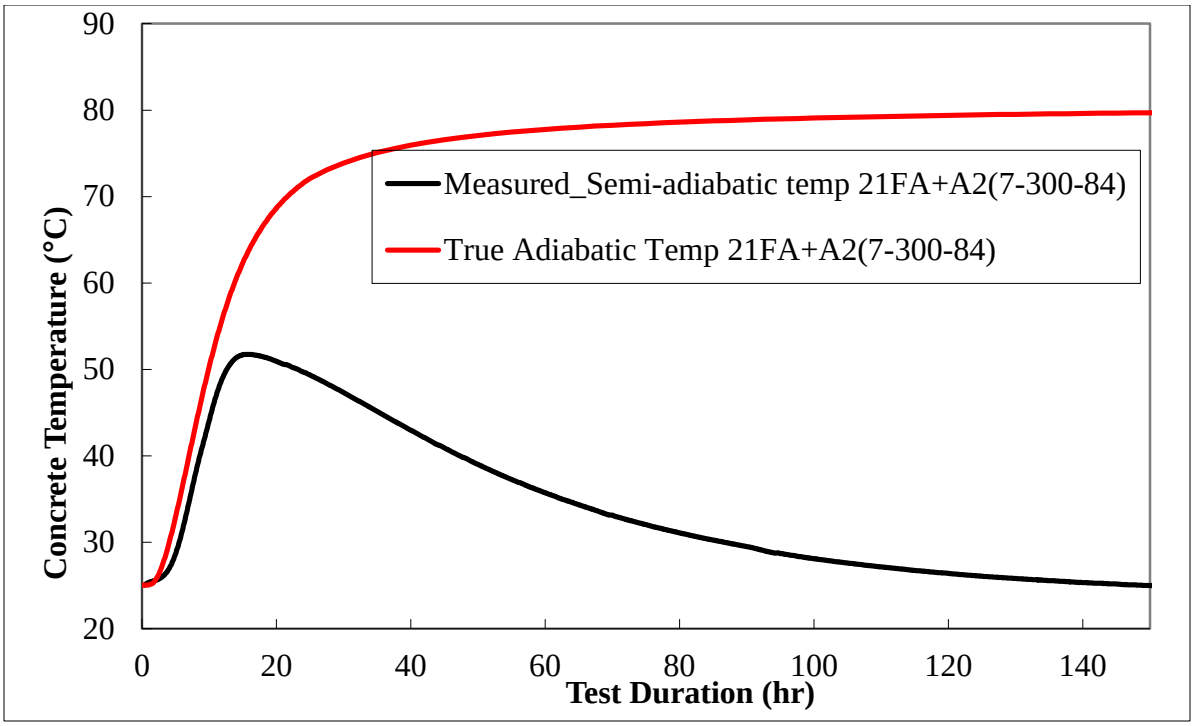

Figure 9-5: Adiabatic Temperature Rise in 21FA Concrete

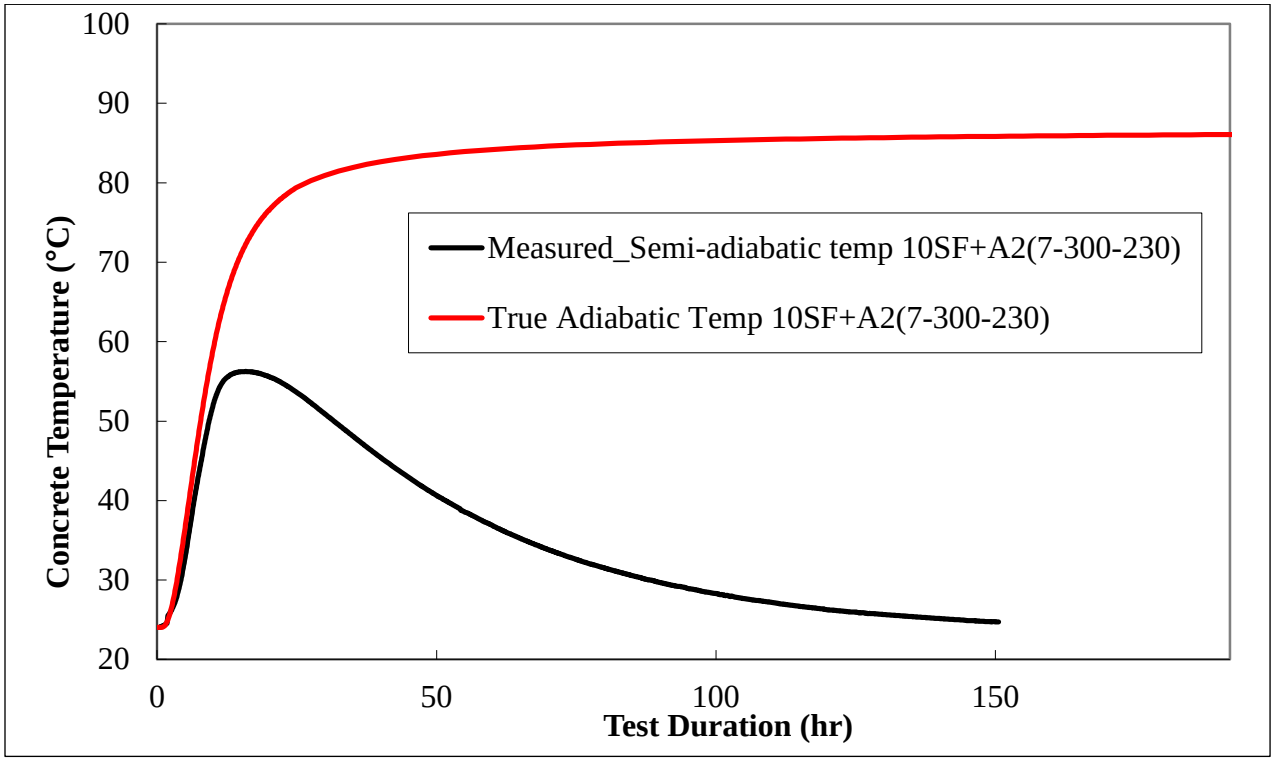

Figure 9-6: Adiabatic Temperature Rise in 10SF Concrete

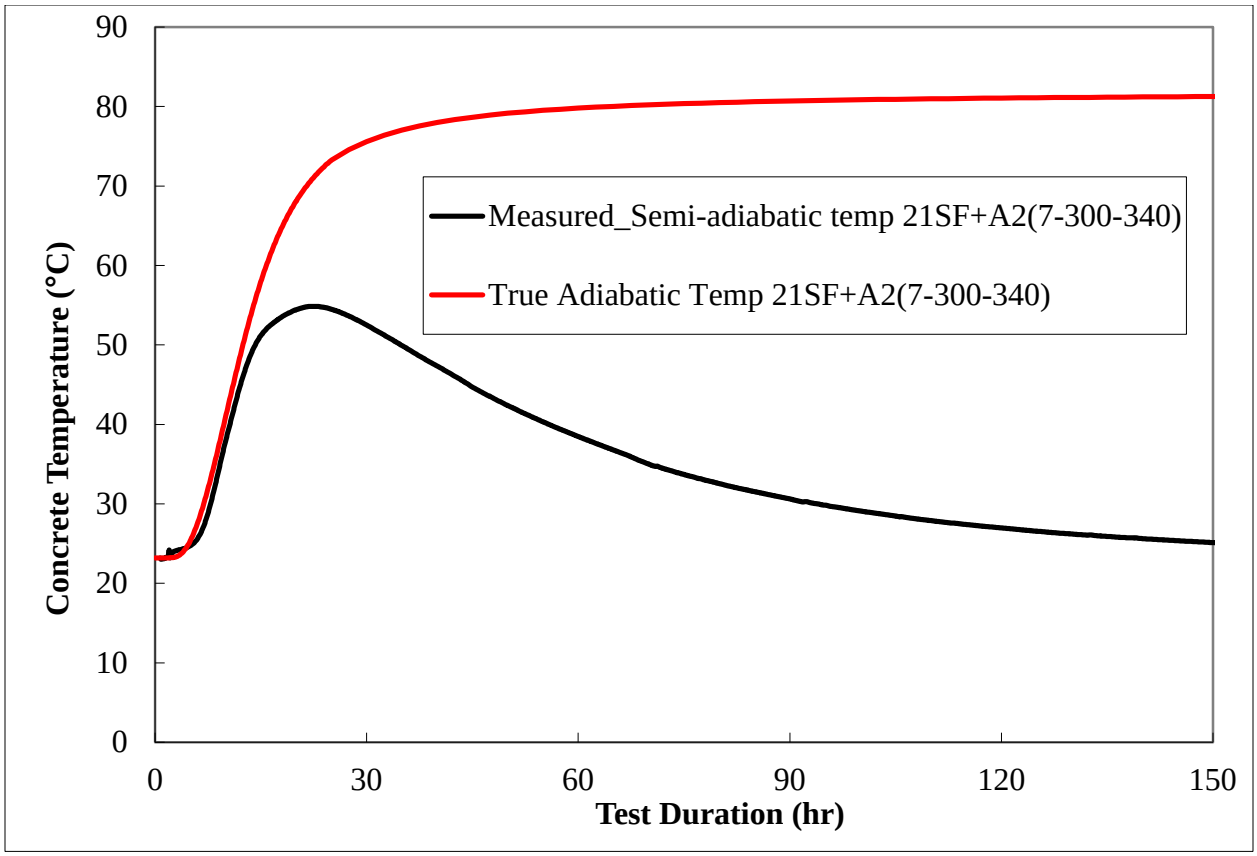

Figure 9-7: Adiabatic Temperature Rise in 21SF Concrete

The results from semi-adiabatic calorimetry indicate that blast furnace slag decreased the peak height and shifted the maximum peak position to longer times. The effect increased as the slag replacement level increased from 30% to 52%. The hydration parameters determined from semi-adiabatic testing are presented in Table 9-3. Table 9-3 also shows the calculated adiabatic temperature rise for each mixture tested. The shape parameter (β) of the hydration curve is higher for silica fume substitutions, but lower for slag and fly ash mixtures when compared to the control. The time parameter (τ) shows an upward trend for all mixtures studied here except for silica fume. These trends indicate that, with the exception of silica fume, the Class F fly ash and slag cement used here decreased the rate of early strength development, increased the setting time, or both.

The adiabatic temperature rise, modeled using the best-fit hydration parameters, indicates that slag incorporation results in the highest adiabatic temperature rises for all mixtures studied here. However, this has to be considered in conjunction with the time parameter (τ), which for

30BFS, was almost double the value of the control mixture, and the 52BFS value was triple the control value. It is anticipated that modulus development and stress relaxation would be of great importance for mixtures incorporating blast furnace slag.

Table 9-3: Hydration Parameters and Adiabatic Temperature Rise

Parameters	**52SL**	**30SL**	**21FA**	**10FA**	**21SF**	**10SF**	**CN**
β	0.654	0.671	0.844	0.825	1.192	0.870	0.851
τ (hrs)	34.541	21.265	14.097	13.038	14.34	10.976	11.247
α_u	0.809	0.818	0.655	0.723	0.687	0.754	0.729
Adiabatic Temp Rise (°C)	76.3	70.3	55.8	60.5	58.6	62.8	59.4

Temperature Profile

As described previously, the Cracking Frame Temperature Profile program was used to generate temperature profiles that were imposed during testing of individual mixtures in the cracking frame. The program simulates temperature rise at the center of a 1-m thick concrete wall with a constant surface temperature for the concrete element. The generated profiles are presented in Figure 9-8 through Figure 9-10.

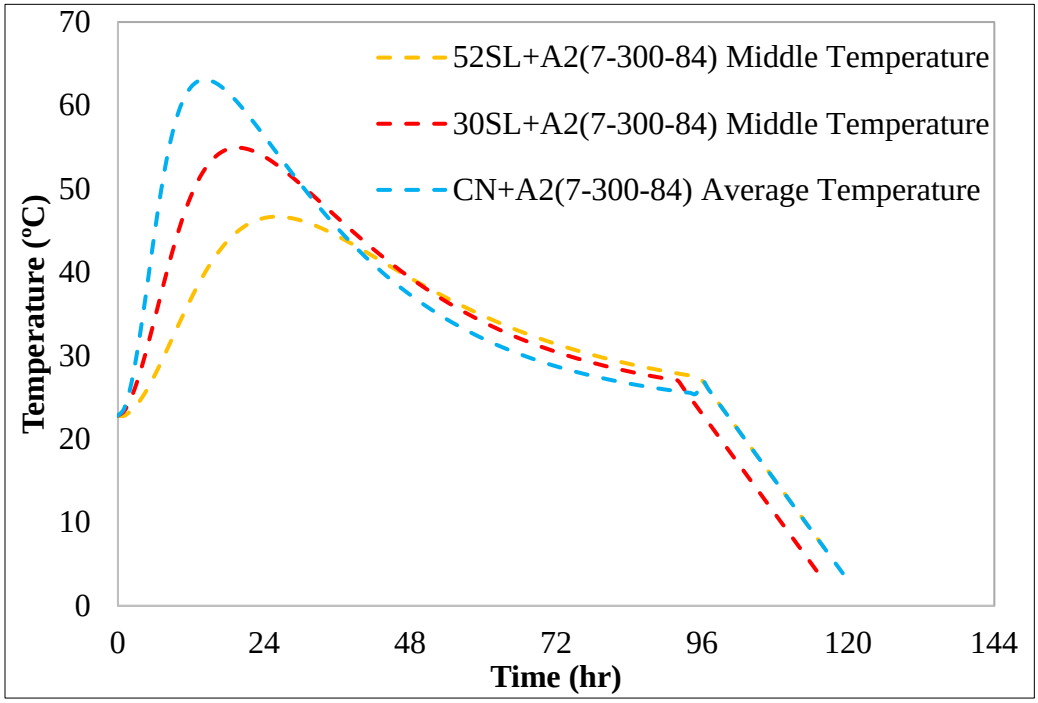

Figure 9-8: Temperature Profile for Slag and Control Mixture

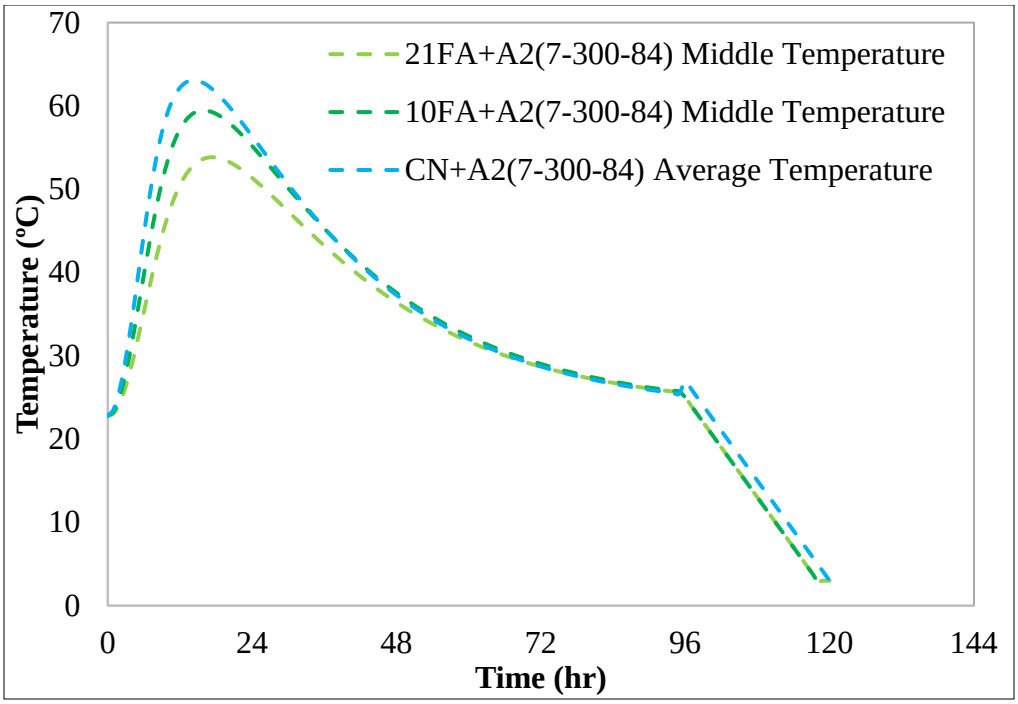

Figure 9-9: Average Temperature for Class F Fly Ash Mixtures and Control

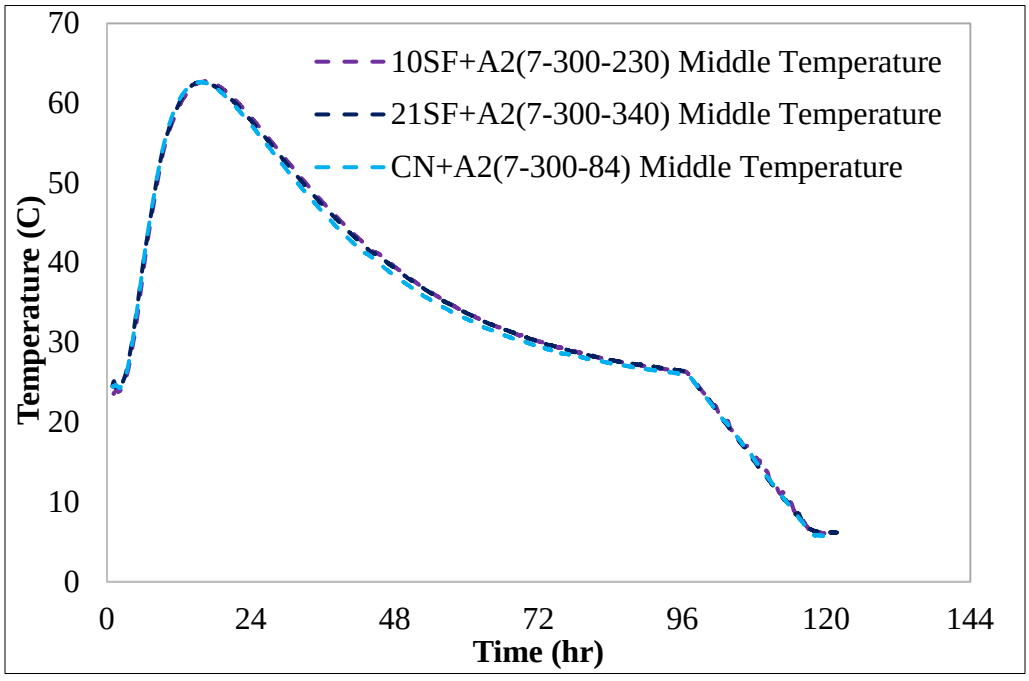

Figure 9-10: Temperature Profile Silica Fume and Control

It can be noted from Figure 9-8 that incorporating slag decreases the maximum temperature magnitude and delays its position. The effect is more pronounced with increasing slag cement

replacement level. The tradeoff for this temperature reduction comes at the cost of lower strain capacity and strength during the early stages of strength development[283]. Figure 9-11 shows that the maximum compressive stresses induced in the mixtures were 246 psi at 14.7 hours, 198 psi at 20.9 hours, and 141 psi at 25.9 hours for the control, 30BFS, and 52BFS, respectively, indicating higher expansion in the control mixture compared to the slag mixes. The stress development due to integrating slag into concrete can be attributed to thermal effects and autogenous shrinkage [284]. Although the rate of tensile stress development in the control and 30BFS mixtures appears to be similar initially, the trend seems to change at about 51 hours, where the 30BFS mixture shows a higher rate. Once cooling is induced, the 52BFS mixture develops the highest stress rate. Other researchers reported that using slag cement does not always reduce the cracking tendency[285]. Higher stresses are typically found in cement pastes containing slag cement due to increased capillary action from pore size refinement. The cracking tendency of slag cement mixtures is partially due to greater long-term autogenous shrinkage [284].

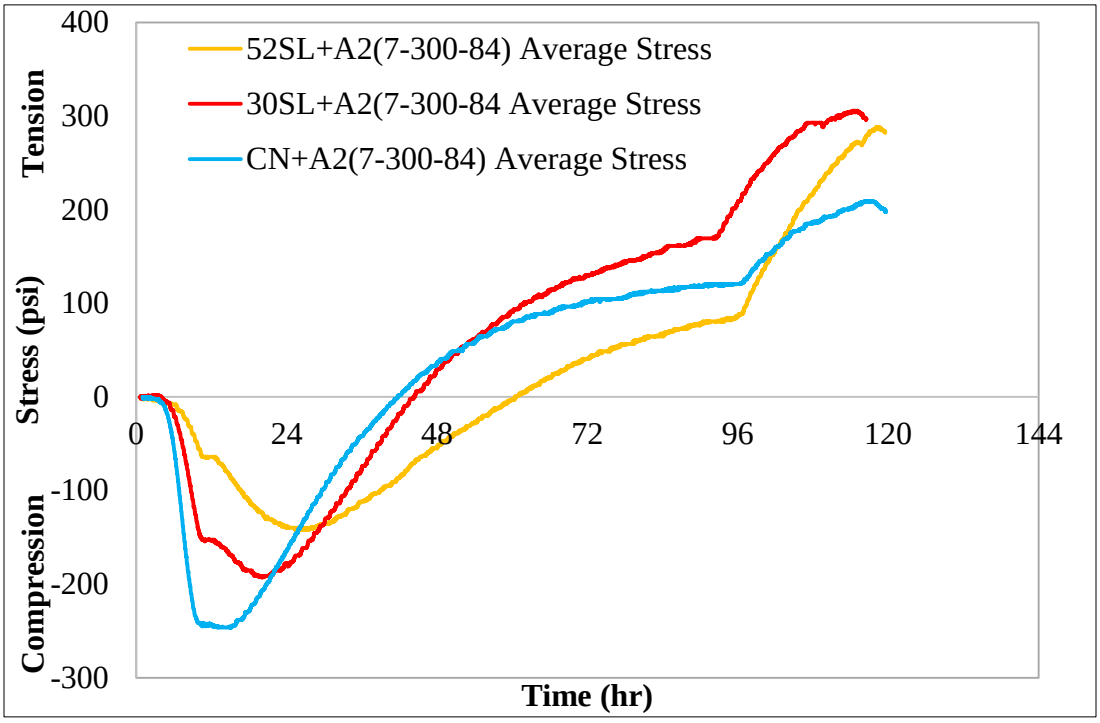

Figure 9-11: Stress Evolution in Slag and Control Mixtures

Figure 9-12 shows that increasing replacement levels of cement with fly ash reduced the induced tensile stresses in concrete prior to initiating cooling at approximately 96 hours. This

decrease in tensile stress can be attributed to the high creep exhibited by fly ash replacement, allowing the concrete to relax [286]. Similar results have been found by other groups regarding lower stresses than the control mix from using fly ash at different replacement levels [287][288]. A slight delay of the crossover at zero stress occurs on incorporating fly ash, but increasing the quantity of fly ash used within the range studied here did not seem to affect the time of crossover. The maximum tensile stresses experienced by the concrete, prior to cooling at 96 hrs, were similar, with a slight reduction in stress in the mixture with 21% Class F fly ash. Lower temperatures were exhibited by all concrete mixtures containing fly ash, due to the dilution effect, as seen from Figure 9-9. Other researchers have found a significant drop in temperature from the introduction of fly ash [4].

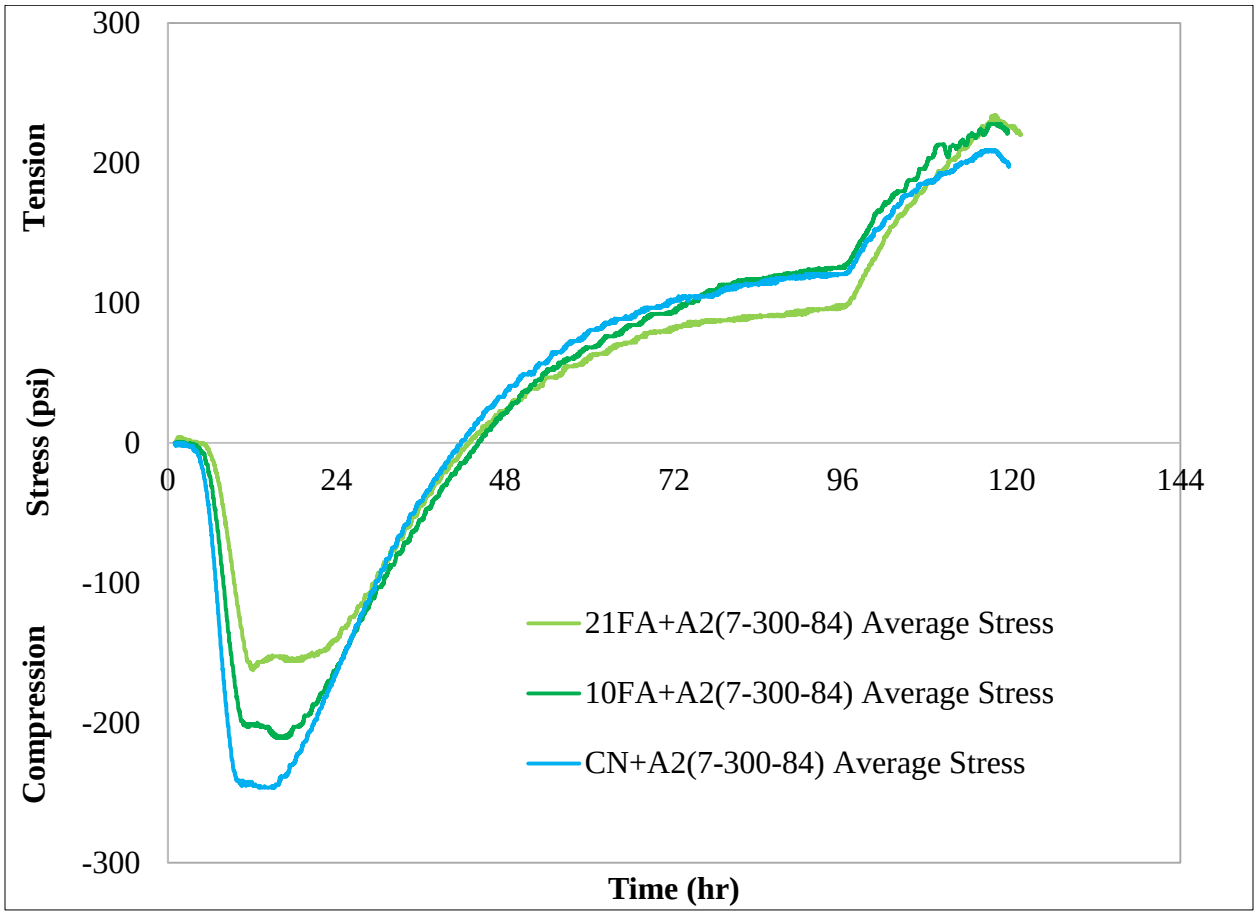

Figure 9-12: Stress Evolution in Fly Ash and Control Concrete Mixtures

Almost identical temperature profiles were generated for the control and 10SF mixtures using the Cracking Frame Temperature Profile program as can be seen from Figure 9-10. Although the modeled and imposed temperature profiles for the control and silica fume mixtures were very similar, the response of both mixtures in the cracking frame was significantly different. The induced compressive stresses were slightly higher in the control mixture, and the rate of tensile stress development was lower when compared to the silica fume mixture (Figure 9-13). Additionally, incorporating silica fume at a 10% replacement level greatly accelerated the timing of the zero stress crossover. The higher induced tensile stress in the 10SF could have been due to higher chemical shrinkage and self-desiccation [289].

The 21% silica fume mixture was also tested in the cracking frame using the modeled temperature profile for 10SF. This exposed the silica fume at 21% replacement level to higher temperatures than it would have had with its own temperature profile At later ages, silica fume specimen underwent higher stresses with higher replacement content. According to Whigham [290], silica fume inclusion increases early-age cracking potential. The higher cracking tendency in the silica fume mixture stems from higher induced tensile stress due to a higher autogenous shrinkage from higher capillary pressures exerted as a result of pore size refinement. Incorporating silica fume in concrete mixtures yields finer pores and an overall reduction in concrete porosity. Increased pore size refinement results in lower stress relaxation, [237][291]. These smaller pores cause the meniscus that forms between the capillary pores to extend further out and cause tensile stresses that pull the pore walls closer together [292].

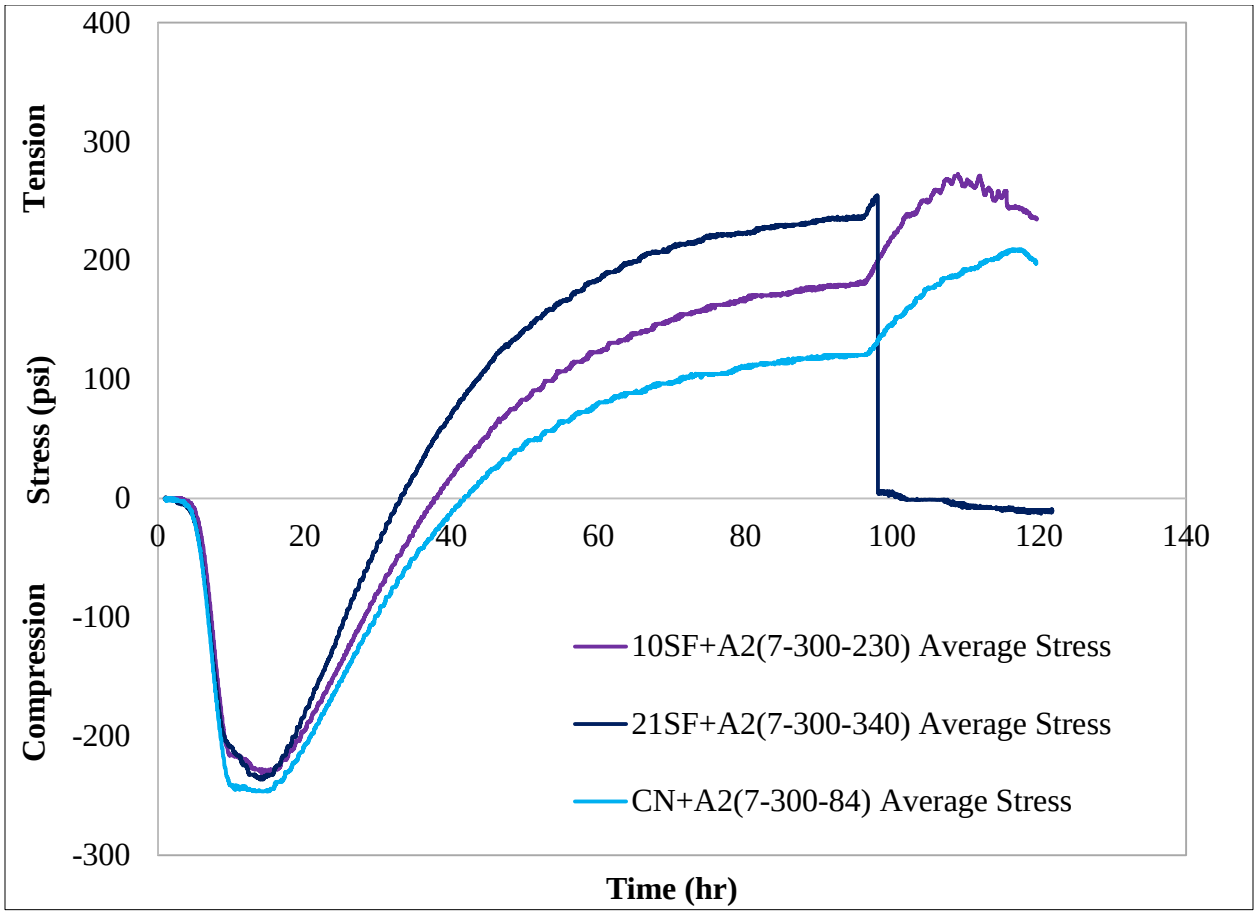

Figure 9-13: Stress Evolution in Silica Fume and Control Mixtures

Conclusion

Semi-adiabatic calorimetry testing of several concrete mixtures incorporating silica fume, blast furnace slag, and Class F fly ash indicate that SL delays setting and strength evolution and generates the highest adiabatic temperature rise. Modeling concrete temperatures and imposing the modeled temperature profiles during testing in the cracking frame identified the higher cracking risk of silica fume mixtures. Further study of blast furnace slag mixtures is needed to identify the effects of variable slag composition on cracking potential.

[redacted] Effects of Mineral Admixtures on the Microstructure Evolution in Cementitious Systems

[redacted] Introduction

Addition of mineral admixtures can result in chemical and physical changes to the concrete microstructure, which can affect macroscopic properties. For example, strength and durability are determined by the phases formed during hydration and their distribution throughout the concrete matrix. A study of microstructure can help to evaluate potential durability issues of a particular mixture that can negatively impact service life of concrete structures. The primary focus of this chapter is to address the effects of supplementary materials on the microstructural characteristics of the hydrating pastes. The materials used were chosen based on the findings from the previously conducted experiments on characterization, kinetics, and durability. This is imperative to explain the process by which mineral admixtures affect durability of concrete. The work entailed identifying and quantifying hydration products formed by using x-ray diffraction and Rietveld analysis. The impact of chemical and mineral admixtures on the microstructure was assessed by measuring porosity through nitrogen adsorption. Nano-indentation was used on selected mixes to identify the direct effects of supplementary cementitious materials on the strength of the binder. Additionally, optical and scanning electron microscopy, coupled with energy dispersive analysis, was used to characterize the microstructure.

[redacted] Methodology

[redacted] Procedure for mixing paste samples

Paste samples were prepared for x-ray diffraction (XRD) analysis, nanoindentation analysis (NA), scanning electron microscopy (SEM), and porosity measurement by nitrogen adsorption. Mix designs for XRD samples are listed in Table 10-1 and Table 10-2. While XRD measurements were performed on all the samples, only selected mixes from Chapter 6 were tested with nanoindentation and SEM.

Table 10-1: Mixture Proportions for XRD, Nanoindentation, SEM and NA Samples

Sample	Mineral Admixture	Mineral Admixture (% Cement Replacement)	WR Dosage	AE Dosage	SP2 Dosage	SP1 Dosage
			(ml/100 kg Cementitious)			
CN	None	0	0	0	0	0
A2	None	0	110	2.5	110	0
21FA+A2	Class F Fly Ash	21	110	2.5	110	0
10SF+A2	Silica Fume	10	110	2.5	110	0
52SL+A2	Slag	52	110	2.5	110	0
A1	None	0	110	2.5	0	155
10MK+A1	Metakaolin	10	110	2.5	0	155

Table 10-2: Mixture Proportions for XRD Samples at Higher Chemical Admixture Dosage

Sample	Mineral Admixture	Mineral Admixture (% Cement Replacement)	WR Dosage	AE Dosage	SP2 Dosage	SP1 Dosage
			(ml/100 kg Cementitious)			
CN	None	0	0	0	0	0
A2	None	0	200	2.5	170	0
21FA+A2	Class F Fly Ash	21	200	2.5	170	0
10SF+A2	Silica Fume	10	200	2.5	170	0
52SL+A2	Slag	52	200	2.5	170	0
A1	None	0	200	2.5	0	170
10MK+A1	Metakaolin	10	200	2.5	0	170

Samples were mixed using the IKA WERKE mixer. The water-reducing admixture (WR) was added to the mixing water; air-entraining admixture (AE) was introduced after mixing for 1 minute at 300 rpm, followed by 30 seconds of mixing at 600 rpm. Superplasticizer (SP1 or SP2) was added after a 90-second rest period, after which the paste was mixed at 600 rpm for 60 seconds. After mixing, paste samples were sealed and cured under isothermal conditions at 23°C. For XRD measurements, samples were demolded at 1, 3, and 7 days. Porosity, nanoindentation, and SEM samples were demolded at 7 days.

[redacted] X-Ray Diffraction

For x-ray diffraction, demolded samples were ground by hand with an agate mortar and pestle to a particle size of less than 45 μm. It should be noted that particle size can be reduced to the point where XRD cannot resolve the crystalline structure (microcrystalline or nanocrystalline) of the constituent materials. Therefore, based on XRD analysis, the material would be considered

amorphous. However, to distinguish this type of material from truly amorphous (or glassy) material, it is termed "x-ray amorphous." Since formation of additional x-ray-amorphous content during grinding is a concern [293]–[295], hand grinding was selected over using a micronizing mill. Paste samples were mixed with a standard reference material (SRM) 676a obtained from the National Institute of Standards and Technology (NIST). SRM 676a is a corundum (α-Al_2O_3) powder of high purity and high crystallinity (99.02% crystalline) [296] and is considered to be the best material for use as an internal standard as it introduces a negligible amount of additional amorphous content to the test sample [297]. Corundum was used as an internal standard (IS) in order to determine the amorphous/unidentified content of each sample [149], [298]. Corundum was mixed with the paste by hand with the mortar and pestle again to in order to avoid increasing the amorphous content. The 20% rate of sample replacement with the IS was small enough to avoid obscuring the peaks from the hydration phases, but large enough to minimize the error in amorphous content determination [299]. No specific technique was used to stop the hydration, as samples were prepared immediately after demolding and loaded into the diffractometer.

XRD measurements were performed using a Phillips X'Pert PW3040 Pro diffractometer equipped with the X'Celerator Scientific detector and a CuKα x-ray source. Tension and current were set to 45 kV and 40 mA, respectively. Scans were performed in the range of 7 - 70° 2θ, with a step size of 0.0167° 2θ. Samples were loaded into the sample holder using a back-loading technique in order to minimize preferred orientation, and placed onto a spinner stage that was rotating at 30 rpm in order to improve counting statistics [142]. Mineralogical analyses of the collected diffraction patterns were carried out using Panalytical HighScore Plus 3.0 software. Quantification was performed using the Rietveld refinement functionality built into the software.

[redacted]Phase Consumption Calculations

The amount of clinker phases reacted at various times is of interest as addition of chemical and mineral admixtures can affect the reactivity of cement, and therefore the degree of hydration, as indicated by isothermal calorimetry. Tracking phase consumption over time can identify the specific clinker phases, if any, affected by admixtures addition. Phase consumption was calculated as follows:

$$\frac{w}{cm} = 0.485 \qquad \text{Equation 10-1}$$

where *w* is the water content and *cm* is the amount of cementitious materials in the mixture. For 1 gram of paste, it follows that

$$0.485cm + cm = 1 \quad \text{Equation 10-2}$$

From here,

$$cm = 0.673 \quad \text{Equation 10-3}$$

The amount of a clinker phase (y_i) in a paste at the time of mixing, also time zero, can be calculated as:

$$y_i = 0.673\, y_0 p_{cm} \quad \text{Equation 10-4}$$

where y_0 is the phase amount in anhydrous cement and p_{cm} is the cement fraction of the total cementitious materials. The phase consumption can then be calculated as a fraction of y_i that has reacted at the time of interest.

$$Phase\ consumption = \frac{y_i - y_R}{y_i} = 1 - \frac{y_R}{0.673\, y_0 p_{cm}} \quad \text{Equation 10-5}$$

where y_R is the phase amount in a paste at the age of interest as determined from Rietveld refinement.

[redacted] Nitrogen Adsorption

Although nitrogen adsorption cannot measure the whole range of concrete porosity, as pore sizes in concrete vary from nm to mm, it can provide information on micro- and mesoporosity [300]. Measurement of porosity by gas adsorption is based on the principle of physisorption, or physical adsorption, where the molecules of gas (adsorbate) attach to the surface of a solid (adsorbent) by weak van der Waals forces [156], [301], [302]. Adsorption occurs when the adsorbent is exposed to a specific volume of adsorbate under finite pressure. Adsorption of gas molecules results in an increase in the mass of solid and decrease in the pressure of gas. These parameters can be measured experimentally and adsorption isotherms are obtained by first exposing the adsorbent to a small volume of gas under very low relative pressure (p/p_0), which relates the pressure of the gas to atmospheric pressure, and then slowly increasing the gas volume

until a relative pressure $p/p_0=1$ is attained. The isotherm obtained from increasing p/p_0 from small values to 1 is the adsorption branch of the isotherm. After $p/p_0=1$ is reached, the process is reversed, and p/p_0 is slowly decreased causing gas molecules to desorb from the solid surface increasing the gas pressure and decreasing the mass of solid. The isotherm obtained in the direction of decreasing p/p_0 is called a desorption branch. The isotherm as a whole is still referred to as an adsorption isotherm. A number of different gases have been used as adsorbents, including nitrogen, argon, water vapor, methanol, and others [156]. Nitrogen gas is probably the most commonly used adsorbate for porosity measurements on cement paste. A typical nitrogen adsorption isotherm for cement paste is shown in Figure 10-1.

Aligizaki [156] states that cement pastes have Type IV adsorption isotherms, which are attributed to materials with meso- and macropores, according to the classification proposed by the International Union of Pure and Applied Chemistry (IUPAC). Rouquerol et al. [301], who proposed three additional isotherm types, state that cement paste isotherms belong to their proposed Type IIb classification. According to Aligizaki [156], Type II isotherms are typical of non-porous materials and represent multilayer adsorption on a solid surface. He also states that the Type IV isotherm is a modification of Type II. Although Aligizaki's classification follows the widely-accepted IUPAC classification, there are slight variations in a typical cement paste isotherm from the Type IV isotherm described by IUPAC, and Rouquerol's proposed Type IIb may be more on point.

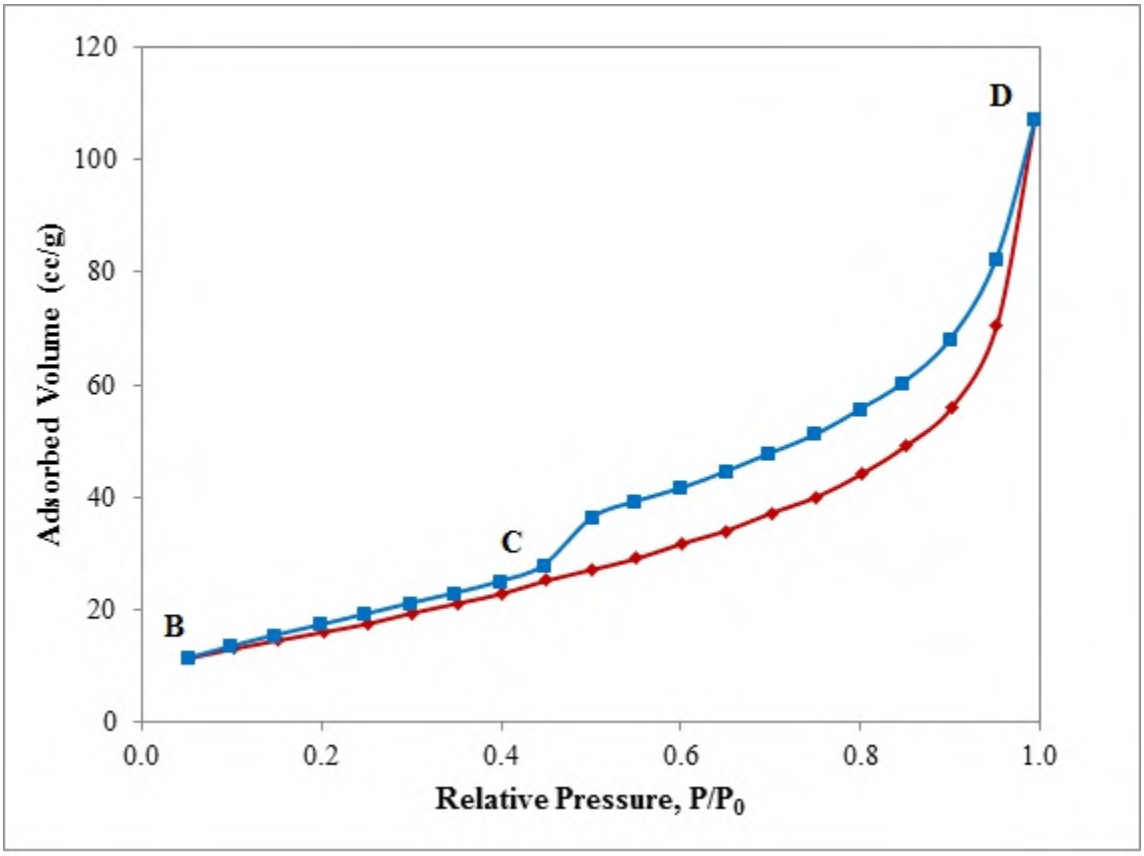

Figure 10-1: Typical Nitrogen Sorption Isotherm

However, regardless of the type, all isotherms exhibiting hysteresis share some common features. Although typical Type IV isotherms exhibit a knee before point B (Figure 10-1), this knee is usually absent in Type II isotherms. Point B represents completion of monolayer formation and the beginning of multilayer adsorption, which proceeds up to point C, after which capillary condensation begins in small pores. As the relative pressure (p/p_0) is increased, capillary condensation fills progressively larger pores producing the adsorption branch of the isotherm indicated by the red line in Figure 10-1 [156]. As p/p_0 is decreased, the larger pores begin to empty first, followed by the smaller pores. Cement pastes, like many other materials, produce isotherms with a hysteresis loop, where the desorption branch of the isotherm, indicated by a blue line in Figure 10-1, does not follow the adsorption branch. Existence of the hysteresis loop in cement pastes has been attributed to the presence of ink-bottle pores [303]. Bodor et al. [303] suggest that the width of the hysteresis loop is determined by the size of the neck of the pore, with a narrower neck for the same size pore resulting in a larger hysteresis loop. This suggestion was later

confirmed by Thommes et al. [304], although the authors caution that this is only true if the pores are emptied by percolation rather than cavitation. Zeng et al. [305] showed that evaporation through cavitation can occur not only in closed pores, but also in ink-bottle pores with long narrow necks. Both percolation and cavitation result in delayed evaporation from a pore, producing a hysteresis loop. The closure of the hysteresis loop is dependent on the adsorbate, and for nitrogen occurs at p/p_0 of approximately 0.4 [156], [306]. Occasionally, the hysteresis loop does not close completely at point C. Mikhail et al. [307] observed this in cement pastes at various w/c ratios from 0.35 to 0.70. The authors postulated that during nitrogen adsorption "an expansion in the pore system is produced, which is not fully reversible; consequently, the hysteresis loop remains open."

Samples for porosity measurement by nitrogen adsorption were mixed as described in section 2.1. One of the challenges in applying this technique to cement pastes is that water, except for chemically bound water, needs to be removed from the pores to allow for nitrogen adsorption. Immediately after demolding, the samples were crushed and sieved to separate the particles in the range of 1-3 mm, and dried at 105°C under vacuum for 2 hours using the outgasser built into Autosorb-1 analyzer manufactured by Quantachrome Instruments. This drying procedure was selected as drying below this temperature may accelerate the hydration process [308] and is not suitable at early ages. Slow removal of water by procedures such as D-drying does not quickly arrest the hydration [156] and these procedures were deemed unsuitable for the same reason. Drying at 105°C was limited to 2 hours to avoid damaging the C-S-H microstructure, which is typically a concern with drying at this temperature for 24 hours [309]. Beaudoin [310] suggests that limiting oven-drying at 105°C to 2-3 hours results in a microstructure that is similar to D-drying, which would be most suitable for nitrogen adsorption. In this work, samples were dried for 2 hours, after which nitrogen isotherms were collected using Autosorb-1.

Pore size distribution calculations were performed using Autosorb-1 software by selecting the Barrett, Joyner, Halenda (BJH) method [311], for the adsorption branch. Both adsorption [307], [312] and desorption [313], [314] branches of the nitrogen adsorption isotherm have been used for BJH analysis of cement pastes. The adsorption branch was selected in this study since it measures the size of the interior of the pore, while the desorption branch measures the pore entry size [303], [315]. Since pores in cement paste are expected to be bottlenecked, and most concrete properties are affected by the size of the pore, not the size of the pore entry, the adsorption branch

was selected. Additionally, the adsorption branch is not influenced by the pore network to the same degree as the desorption branch [303], [316]. The Brunauer, Emmett, Teller (BET) method [317] was used to calculate specific surface area, which is typically attributed to C-S-H [318]. The BET method is valid only in the range of p/p_0 of 0.05-0.35 for the linear portion of the isotherm [156], [319].

Nanoindentation

Concrete mechanical properties are typically measured on a macro scale, where the measured property is a composite response affected not only by the hydration phases, but also by coarse and fine aggregate, porosity, and any defects such as microcracks that may be present in the sample. Nanoindentation, on the other hand, allows the user to measure the mechanical response of the individual hydration phases, most interesting of which is the C-S-H since it occupies the largest volume fraction of a typical ordinary portland cement (OPC) paste and is primarily responsible for its strength.

Nanoindentation testing consists of pressing a very small tip into a material to obtain the load and depth of penetration measurements. Most nanoindentation systems are load-driven, which means that a specified load is applied to the sample and the depth of penetration of the tip into the sample at each indent is measured. The applied load and depth of penetration are continuously recorded, and the test produces a force (P) versus depth (h) plot. A typical P-h plot is shown in Figure 10-2. The unloading portion of the curve is used for analysis [320]–[322].

As can be seen from Figure 10-2, the maximum load (P_{max}) prior to unloading corresponds to a maximum penetration depth (h_{max}). The intersection of the unloading curve with the x-axis is the final penetration depth (h_f). S is the contact stiffness evaluated at P_{max}, which is later used to determine the elastic modulus of the sample/phase [322]. S is used to calculate the contact depth (h_c).

$$S = \left(\frac{dP}{dh}\right) \qquad \text{Equation 10-6}$$

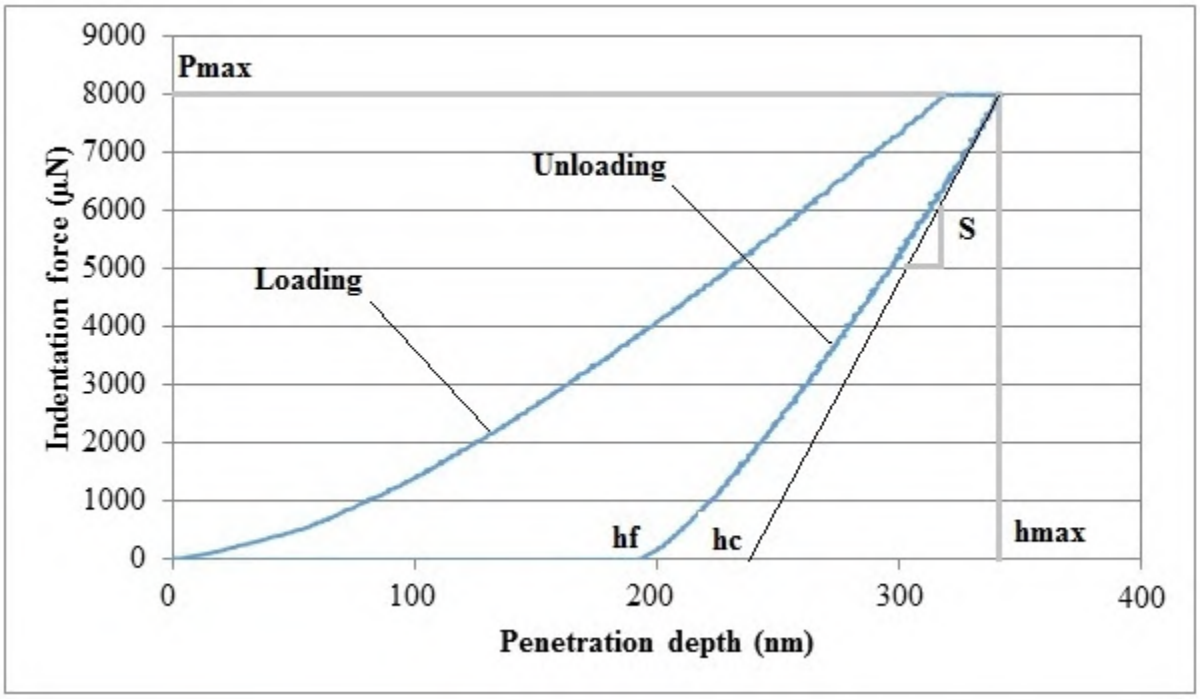

Figure 10-2: Typical Nanoindentation Load versus Depth Curve

Two material properties can be determined from nanoindentation testing: hardness (H) and reduced modulus (E_r) [321], [322].

$$\boldsymbol{H = \frac{P_{max}}{A\,(h_c)}} \qquad \text{Equation 10-7}$$

$$\boldsymbol{E_r = \frac{\sqrt{\pi}}{2\sqrt{A(h_c)}}\,S} \qquad \text{Equation 10-8}$$

where P_{max} is the maximum indentation load and $A(h_c)$ is the indenter's projected contact area, which is a function of h_c.

The reduced modulus (E_r) measured during nanoindentation is affected by the elastic modulus (E) and Poisson's ratio (v) of the sample as well as of the indenter itself, which is illustrated by the following equation:

$$\boldsymbol{\frac{1}{E_r} = \left(\frac{1-\nu^2}{E}\right)_{specimen} + \left(\frac{1-\nu^2}{E}\right)_{indenter}} \qquad \text{Equation 10-9}$$

The Berkovich indenter used in the nanoindentation measurements had an elastic modulus of 1140 GPa and Poisson's ratio of 0.170, so the indenter contribution in Equation 10-9 can be considered approximately equal to zero, therefore $E_r \approx E_{specimen}$.

For nanoindentation and SEM samples, a solvent exchange method was used to stop the hydration. After demolding, samples were crushed and placed in isopropanol for 48 hours. After 48 hours, the samples were dried under vacuum and cast in SPECIFIX-40 two-part epoxy from Struers. Samples were polished using MD-Piano series polishing discs #200, 500, 1200, followed by diamond suspensions of 3, 1, and 0.25 μm. The diamond suspensions were used with MD-Dur polishing cloths. As a final step, the samples were polished with 0.5 alumina powder suspension on an MD-Nap polishing cloth. Samples were washed in ethanol in an ultrasonic bath for 10 minutes between each polishing step.

Indentation measurements were performed using the Hysitron Ti 900 Triboindenter with a Berkovich tip. The Berkovich indenter was selected to minimize the pile-up phenomena [323] and is a common choice for cement pastes [323]–[326]. The data were analyzed based on the Oliver and Pharr method [322] using the TriboScan 6.0 software. Instrument compliance and tip-area-function calibrations were performed using a fused quartz standard prior to sample measurements. Air indent calibration was performed prior to testing each sample.

Since most nanoindenters are equipped with an optical camera, indentation experiments can be carried out by indenting a specific point/phase observed in the camera view or by grid indentation technique. Randall et al. [327] criticized indentation of a specific phase based on optical image observation because "another phase may be present just below the surface resulting in a composite response to the measured indentation." When the indenter is pressed into the sample, the mechanical response of the material is determined not only by the surface of the sample directly in contact with the indenter, but by a sample volume surrounding the indenter, which is referred to as the interaction volume [328], [329]. In a grid indentation technique, a large number of indents are performed in a grid pattern, after which the data is deconvoluted to obtain the modulus of individual phases. As long as the indents are randomly located and the indentation depth does not exceed 10% of the characteristic size of the phase, statistical grid indentation will produce a frequency histogram with peaks representing the mean of the property of interest for each phase [320], [327]. The deconvolution procedure consists of fitting several probability distribution functions (PDF) to the normalized experimental data plot to find the mean and standard deviation for the property of interest for each phase. This procedure is based on the assumption that the data is normally distributed around each mean. Ideally, only sharp peaks should be observed with no spread in the data. However, even with the grid indentations, some

measurements will produce a composite response when, for example, the indent is located at the boundary between two phases. Additionally, variability in the composition of each phase will also result in the spread of the data around a mean value [327]. Constantinides et al. [320] state that volume fractions of each phase can potentially be extracted from the deconvolution analysis. For a sample consisting of *n* phases, the overall distribution of the property *x* follows the theoretical PDF [320]:

$$\boldsymbol{P(x) = \sum_1^n f_n \; p_n(x)} \qquad \text{Equation 10-10}$$

where f_n is the volume fraction of phase *n* and where

$$\boldsymbol{\sum_1^n f_n = 1} \qquad \text{Equation 10-11}$$

A total of 100 points were indented for each sample. Some points had to be excluded due to an irregular response associated with fracture or surface preparation [330]. Points were indented in a grid of 10x10 points, spaced 20 μm apart. The interaction volume was approximated as 3-4 [328] or 3-5 [329] times h_{max}. Given a typical indentation depth of C-S-H of 200-400 nm, Hu et al. [329], [331] estimated the size of the interaction volume in C-S-H as 1-2 μm^3, which means that the spacing of 20 μm is more than sufficient to avoid any overlap in interaction volumes of neighboring indentations. A trapezoidal loading function was used with a 5-second loading time, 3-second hold period and a 5-second unloading period. According to Ulm et al. [332], indentation depths in clinker phases are less than 100 nm, while in C-S-H they are in the order of 200-300 nm. A maximum load (P_{max}) of 2 mN was selected based on the work of Vandamme [333], who found that this load corresponds to an average penetration depth of 200 nm. Miller et al. [324] also reported that a P_{max} of 2 mN typically produced 100-400 nm indentation depths in cement paste.

Degree of Hydration Calculations

Since mineral admixtures investigated in this study had variable reactivity, it was useful to compare them not only based on age, but also based on their degree of hydration. In order to calculate the degree of hydration *α(t)*, the total heat *H(t)* released by each mixture, obtained from isothermal calorimetry for the age of interest, was divided by the total available heat H_u that can be generated by the cementitious components of the mixture:

$$\boldsymbol{\alpha\,(t) = \frac{H(t)}{H_u}} \qquad \text{Equation 10-12}$$

H_u is quantified as a function of cement composition, the amount of each phase, and type of supplementary cementing materials present in the system [168], [334]. The effects of chemical admixtures were not included in previous models for calculating H_u; therefore, it was assumed in this study that chemical admixtures do not affect the ultimate heat of hydration.

$$H_u = H_{cem} P_{cem} + 461 P_{slag} + 1800 P_{FA\text{-}CaO} P_{FA} \quad \text{Equation 10-13}$$

where

P_{slag} = Slag mass-to-total-cementitious-material-content ratio,

P_{FA} = Fly ash mass-to-total-cementitious-material-content ratio,

$P_{FA\text{-}CaO}$ = Fly ash-CaO mass to total fly ash mass-to-total-fly ash-content ratio,

P_{cem} = Cement mass-to-total-cementitious-material-content ratio,

H_{cem} = Heat of hydration of the cement (J/gram).

Gajda [335] states that heat of hydration of metakaolin can be approximated as "100% to 125% that of Portland cement." Since Equation 10-2 does not account for metakaolin addition, the upper level (125%) of the approximation suggested by Gajda [335] was used to modify Equation 10-14 in order to calculate $\alpha(t)$ for the 10MK paste sample:

$$H_u = H_{cem} P_{cem} + 461 P_{slag} + 1800 P_{FA\text{-}CaO} P_{FA} + 1.25 H_{cem} P_{MK} \quad \text{Equation 10-14}$$

$$H_{cem} = 500P_{C3S} + 260P_{C2S} + 866P_{C3A} + 420P_{C4AF} + 624P_{SO3} + 1186P_{FreeCaO} + 850P_{MgO} \quad \text{Equation 10-15}$$

where

H_{cem} = Total heat of hydration of portland cement as describe above (J/gram)

P_i = Mass of i^{th} component-to-total-cement-content ratio.

Scanning Electron Microscopy

After nanoindentation, polished samples were used for energy dispersive x-ray spectroscopy analysis (EDX). SEM and EDX measurements were carried out using a Hitachi S-3500N variable pressure SEM. EDX measurements were collected on polished samples. For the EDX measurements, the electron detector was operated in the back-scattered electron (BSE) mode. Since the samples were not coated to avoid obscuring the EDX spectra, measurements were

performed under variable pressure to minimize the charging effects. EDX measurements were performed in a spot mode with a Princeton Gamma Tech prism light element detector with zero degree tilt. Acceleration voltage was 15.0 kV. The spectra were collected for 200 live seconds. After collecting the EDX spectra, samples were fractured to examine the morphology of hydrated products. Fractured samples were coated in a Hummer 6.2 sputter coater with Au-Pd, which allowed the samples to be examined under high vacuum in the secondary electron (SE) mode.

Results

X-ray Diffraction

When considering the formation of hydration phases, it is important to take into account the mineralogical composition of anhydrous cement. Table 10-3 shows the cement phase composition for reference. This information has already been presented in the Chapter 2.

Table 10-3: Mineralogical Composition of As-Received Cement using QXRD

Cement Phase	Source	CN
C_3S (%)	Rietveld	46.9
C_2S (%)	Rietveld	25.2
C_3A (%)	Rietveld	9.6
C_4AF (%)	Rietveld	8.0
Gypsum	Rietveld	2.8
Hemihydrate	Rietveld	1.8
Anhydrite	Rietveld	0.5
Calcite	Rietveld	2.0
Portlandite	Rietveld	2.5
Quartz	Rietveld	0.8

Addition of mineral admixtures was expected to affect both the chemical composition and the morphology of the hydration products. First, addition of mineral admixtures stimulates cement hydration due to the filler effect. Since mineral admixtures are not as reactive as cement, there is more space available for the cement hydration products. Additionally, mineral admixtures, due to their small particle size, can serve as nucleation sites that promote precipitation of hydration

products [336]. C-S-H is the main product formed during cement hydration, and its chemistry is expected to change with addition of different mineral admixtures. SCMs containing high amounts of silica will significantly reduce the Ca/Si ratio, and Al will be incorporated into the C-S-H from alumina-containing SCMs [62]. X-ray diffraction coupled with Rietveld refinement (QXRD) was used to determine changes, if any, in the type and amount of hydration products with additions of mineral admixtures. First, a control mixture with no mineral or chemical admixtures was examined at 1, 3 and 7 days to establish reference points (Figure 10-3 and Table 10-4).

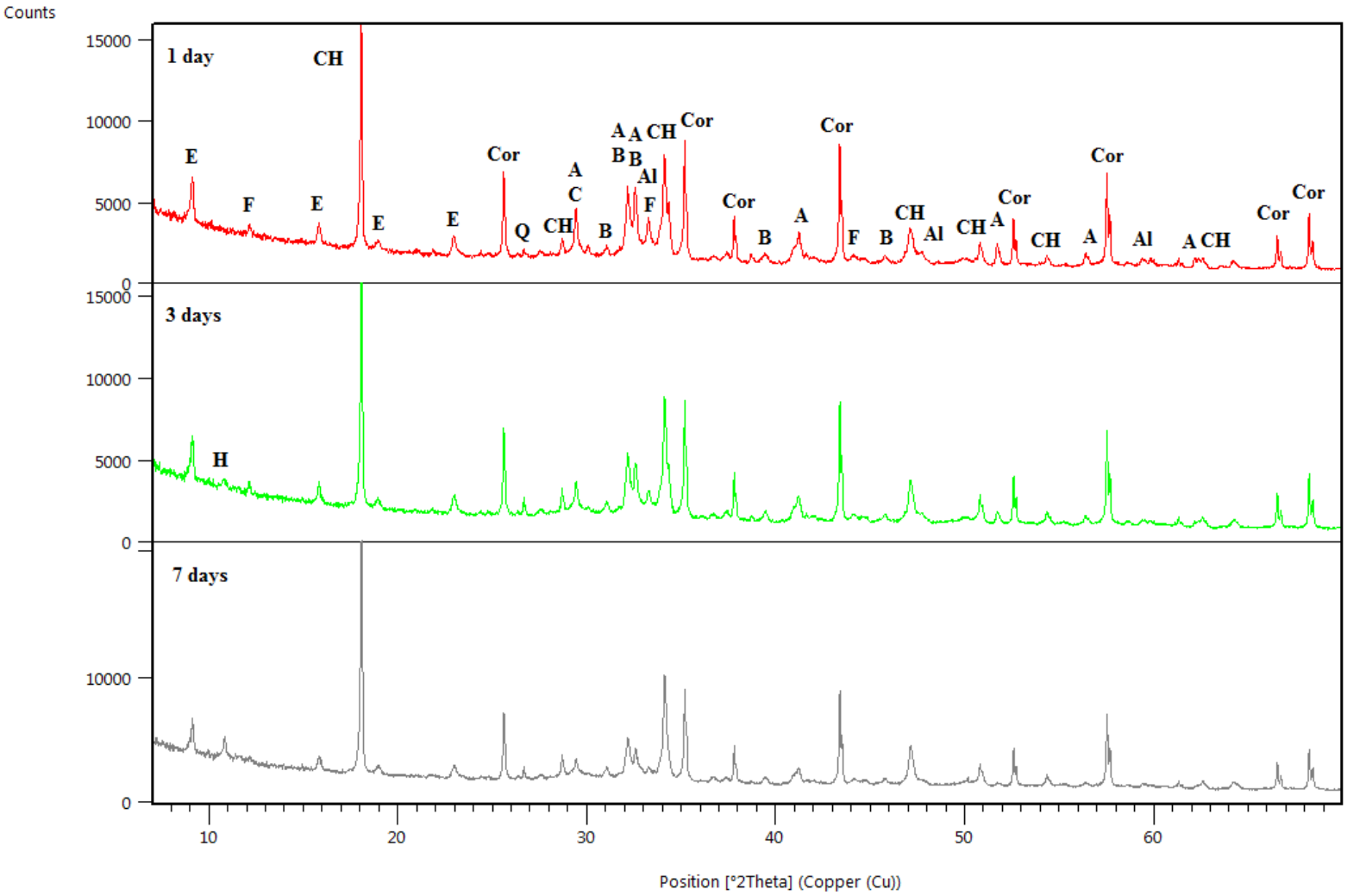

Figure 10-3: X-ray Diffraction Patterns for the Hydrated CN Control Paste with No Mineral or Chemical Admixtures. E – ettringite, F – C_4AF, CH – portlandite, Cor – corundum used as internal standard, Q – quartz, A – alite, B – belite, C – calcite, Al - C_3A, H – hemicarboaluminate

Table 10-4: Phase Quantification for Hydrated CN (No Admixtures)

Phase	**ICSD #**	**1 day**	**3 days**	**7 days**
Alite	94742	10.0	6.0	2.7
Belite	81096	15.0	14.8	14.6
C_3A	1841	5.0	3.3	2.1
C_4AF	9197	4.8	3.8	3.2
Portlandite	15471	8.6	10.9	12.5
Quartz	41414	0.4	0.6	0.6
Calcite	80869	1.3	0.6	0.5
Ettringite	155395	9.6	9.0	7.8
Hemicarboaluminate	263124	0.0	0.5	1.6
Monocarboaluminate	59327	0.0	0.0	0.3
0.8-Carboaluminate	263123	0.0	0.0	0.3
Tobermorite 9Å	87689	0.7	0.7	0.8
Amorphous/Unidentified		44.7	49.8	53.0

As expected, the results show a progressive decrease in the amount of all major clinker phases with time due to hydration, with alite and C_3A having the highest content reduction as expected. Their reactivity is known to be significantly higher during early ages than that of belite and C_4AF [16]. The ferrite phase, however, appears to have been much more reactive than belite, which showed hardly any decrease in content from 1 to 7 days. This is not surprising, as recently Wang at al. [337] demonstrated that in some cements the ferrite phase can be much more reactive than was previously believed, although not as reactive as C_3A.

As for the hydration phases, the amount of portlandite increased with age, as did the amorphous content, which was in line with decreasing alite amounts. At 3 days, hemicarboaluminate appeared. According to the mill certificate, the cement used in this project contained a limestone addition below 5%, which is permitted by ASTM C150. XRD examination of this cement revealed the presence of 2.0% calcite (Table 10-3), which is consistent with the reported limestone addition at the cement plant. Limestone powder has been reported to react with C_3A during cement hydration to form hemicarboaluminate ($C_4A\underline{C}_{0.5}H_{12}$), and with C_3A and CH to form monocarboaluminate ($C_4A\underline{C}H_{11}$), as shown by [336]:

$$C_3A + C\underline{C} + 11\ H \rightarrow C_4A\underline{C}H_{11}$$

$$C_3A + 0.5\ C\underline{C} + 0.5\ CH + 11.5\ H \rightarrow C_4A\underline{C}_{0.5}H_{12}$$

Both hemi- and monocarboaluminate were present in this sample at 3 and 7 days (Table 10-4). As for sulfate-containing hydration phases, only ettringite was observed in this sample. The absence of monosulfoaluminate, at early age, confirms the observations from isothermal calorimetry that the cement was properly sulfated.

Since all the mixtures with SCMs contained AE, WR, and SP1 or SP2, their phase development was compared to the control mixture containing no mineral admixtures, but with all the corresponding chemical admixtures (A1 and A2). Table 10-5 lists the Rietveld refinement results for the A2 paste prepared using the mix design with the lower admixture amount listed in Table 10-1 at 1, 3 and 7 days. Table 10-5also shows the results for the A2 paste at 7 days prepared using the mix design with the higher admixture content, which had a higher dosage of WR and SP2, but the same AE dose. Again, only ettringite was observed in all samples indicating that addition of AE, WR, and SP2 did not significantly shift the sulfate balance at the temperature that these measurements were performed (23°C). Comparing the results for CN (Table 10-4) and A2 (Table 10-5) with Table 10-1 mix design, no significant differences were observed in the type or amounts of phases identified by the Rietveld analysis at 1, 3, and 7 days. Comparing the two mix designs (Table 10-1 and Table 10-2) for A2 at 7 days (Table 10-5), the biggest differences are in the amounts of ettringite and hemicarboaluminate formed, which are lower in the mixture with higher WR and SP2 dosages, although the amounts of C_3A in both pastes are similar. This could be due to incorporation of superplasticizer molecules into C-A-H and formation of "organo-mineral phases" as has been suggested by Plank et al. [338] and Habbaba et al. [339].

Table 10-5: Phase Quantification for Portland Cement-A2 (Two addition levels)

Phase	**ICSD #**	**2.5 ml AE/ 110 ml WR/110 ml SP2**			**2.5 ml AE/ 200 ml WR/170 ml SP2**
		1 day	**3 day**	**7 days**	**7 days**
Alite	94742	10.0	4.4	2.3	3.5
Belite	81096	16.9	15.3	14.1	16.0
C_3A	1841	5.2	3.0	1.5	1.2
C_4AF	9197	4.4	3.5	3.2	2.9
Portlandite	15471	9.2	11.6	12.5	12.4
Quartz	41414	0.5	0.4	0.5	0.6
Calcite	80869	1.1	0.7	0.4	0.3
Ettringite	155395	10	9.4	8.3	6.0
Tobermorite 9Å	87689	1.6	0.7	0.8	1.7
Hemicarboaluminate	263124	0.0	0.8	2.4	0.7
Monocarboaluminate	59327	0.0	0.0	0.4	0.0
0.8-Carboaluminate	263123	0.0	0.0	0.1	0.0
Amorphous/Unidentified		41.0	50.1	53.8	54.8

Similar to the results found for the CN and A2 pastes, no significant differences were observed between CN (Table 10-4) and A1 pastes (Table 10-6) at all ages. The differences between the two mixtures of A1 paste at 7 days were less than with the increase in A2 (Table 10-5). The amount of C_3A was the same as well as the amount of hemicarboaluminate. The amount of ettringite was slightly lower at the higher A1 dosage; however, formation of "organo-mineral phases" in this case appears less likely than with the increase in A2 dosage.

Table 10-6: Phase Quantification for Portland Cement-A1 (Two addition levels)

Phase	**ICSD**	**2.5 ml AE/ 110 ml WR/155 ml SP1**			**2.5 ml AE/ 200 ml WR/170 ml SP1**
		1 day	**3 days**	**7 days**	**7 days**
Alite	94742	11.8	4.4	2.0	3.4
Belite	81096	16.6	15.2	13.9	14.3
C_3A	1841	5.4	2.9	1.6	1.5
C_4AF	9197	4.6	3.3	3.0	1.6
Portlandite	15471	9.1	11.4	12.9	14.3
Quartz	41414	0.5	0.8	0.8	0.4
Calcite	80869	1.4	1.1	1.0	0.4
Ettringite	155395	9.2	9.1	8.6	7.7
Tobermorite 9Å	87689	1.9	0.6	1.0	0.0
Hemicarboaluminate	263124	0.0	1.2	2.8	2.8
Monocarboaluminate	59327	0.0	0.0	0.4	0.0
0.8-Carboaluminate	263123	0.0	0.0	0.2	0.0
Amorphous/unidentified		39.7	50.1	51.8	53.7

Table 10-7 presents QXRD results for the 21% fly ash sample. Generally, the hydration products are very similar to those of the A2 samples, except for the presence of magnetite and mullite. Mullite was the largest crystalline phase present in the as-received fly ash; both mullite and magnetite are not reactive [16] and can be identified in the hydrated sample. The progress of pozzolanic reaction is typically measured through CH consumption [16], [200]. Only a 1% decrease in CH content was observed with 21% cement replacement by fly ash at 7 days. Although the reaction of fly ash is expected to be slow at early ages, higher CH consumption (approximately 5.5% determined by TGA analysis) has been reported in the literature for class F fly ash of similar composition [336]. Low fly ash reactivity is confirmed by its notably lower 7-day compressive strength compared to the control mixture. It is also to be remembered that this particular fly ash had a lower amorphous content from previous measurements.

Table 10-7: Phase quantification for 21FA+A2 Sample

Phase	**ICSD#**	**2.5 ml AE/ 110 ml WR/110 ml SP2**			**2.5 ml AE/ 200 ml WR/170 ml SP2**
		1 day	**3 days**	**7 days**	**7 days**
Alite	94742	7.5	3.5	1.0	1.4
Belite	81096	12.7	12.5	12.2	10.5
C_3A	1841	4.1	2.3	0.9	1.0
C_4AF	9197	3.5	2.4	2.2	1.6
Portlandite	15471	7.2	9.1	9.9	11.4
Quartz	41414	2.1	2.2	2.1	1.8
Calcite	80869	1.0	0.9	0.5	0.8
Ettringite	155395	9.6	8.0	6.1	5.5
Tobermorite 9Å	87689	0.9	1.0	1.7	1.3
Hemicarboaluminate	263124	0.0	1.3	3.7	3.0
Monocarboaluminate	59327	0.0	0.0	0.2	0.0
0.8-Carboaluminate	263123	0.0	0.0	0.1	0.0
Magnetite	49549	0.2	0.2	0.2	0.2
Mullite	23867	3.0	2.9	2.7	2.3
Amorphous/Unidentified		48.0	53.6	56.5	58.8

For silica fume specimens, the same hydration phases were detected as in its corresponding control sample A2, with the exception of the presence of moissanite (SiC) coming from the silica fume (Table 10-8). This is consistent with findings by Lothenbach et al. [340] who only identified the presence of ettringite, hemicarboaluminate, monocarboaluminate, and CH at 7 days in a paste sample with silica fume. Though the level of cement replacement in the 10SF was less than in the 21FA, CH content in the 10SF+A2 sample was lower than in the 21FA+A2 sample, pointing to a higher degree of pozzolanic reaction in the former. This is confirmed by the strength results where the 10SF samples had compressive strengths that were comparable to those of the control mixture with SP2 at 7 days.

Table 10-8: Phase quantification for 10SF+A2 sample

Phase	**ICSD #**	**2.5 ml AE/ 110 ml WR/110 ml SP2**			**2.5 ml AE/ 200 ml WR/170 ml SP2**
		1 day	**3 days**	**7 days**	**7 days**
Alite	94742	9.4	4.4	2.3	2.2
Belite	81096	13.9	13.7	12.9	13.1
C_3A	1841	4.3	2.5	1.6	1.2
C_4AF	9197	4.1	2.9	2.4	2.1
Portlandite	15471	7.4	9.4	9.2	10.6
Quartz	41414	0.5	0.5	0.5	0.5
Calcite	80869	1.2	1.2	0.8	0.2
Ettringite	155395	10.0	8.7	7.9	6.5
Tobermorite 9Å	87689	0.9	1.1	0.6	1.5
Hemicarboaluminate	263124	0.0	1.0	1.5	1.8
Monocarboaluminate	59327	0.0	0.0	0.3	0.0
0.8-Carboaluminate	263123	0.0	0.0	0.1	0.0
Moissanite	164975	0.1	0.1	0.1	0.0
Amorphous/Unidentified		48.1	54.5	59.7	60.4

The effect of incorporating blast furnace slag on phase evolution is presented in Table 10-9. When considering phase quantification results in Table 10-9, it is necessary to keep in mind that only 48% cement was contained in this mixture. 52% slag addition undoubtedly increased the consumption of alite, C_3A, and C_4AF as can be seen in Table 10-11. However, when belite content at 7 days was recalculated based on the amount of cement in the 52Slag paste (48%), a value of approximately 12% was obtained, which was comparable to the rest of mixtures. Therefore, it appears that slag addition did not have an accelerating effect on belite hydration.

Compressive strength of the 52% slag mortar was similar to that of 21% fly ash, which is remarkable considering a significantly higher cement replacement level. This indicates higher reactivity of slag compared to the fly ash. It has already been remarked by Lothenbach et al. [62] that although the reactivity of slag is slow at early ages, it reacts at a faster rate than fly ash. Very low amounts of CH were measured in the 52SL+A2 sample. This is in agreement with Boháč et al. [341] who also reported significantly lower amounts of CH in the 50% slag mixture with OPC

at 1 day. When the CH amount, reported in Table 10-9 for the overall paste sample, is corrected for the amount of cement in the mixture, CH is approximately equal to 9%, which is still lower than that of the fly ash (12.7%), confirming higher slag reactivity. Therefore, slag is expected to outperform fly ash in terms of its rate of compressive strength gain.

Table 10-9: Phase quantification for 52SL+A2 sample

Phase	**ICSD #**	**2.5 mL AE/ 110 ml WR/110 ml SP2**			**2.5 ml AE/ 200 ml WR/170 ml SP2**
		1 day	**3 days**	**7 days**	**7 days**
Alite	94742	4.3	0.7	0.1	0.1
Belite	81096	7.8	6.3	6.0	6.0
C_3A	1841	1.8	0.6	0.0	0.0
C_4AF	9197	1.7	0.8	0.0	0.3
Portlandite	15471	4.0	4.5	4.2	4.0
Quartz	41414	1.0	0.9	0.8	0.9
Calcite	80869	0.9	0.8	0.6	0.0
Ettringite	155395	6.1	4.9	3.1	1.1
Monosulfoaluminate	100138	0.0	0.0	0.0	1.7
Tobermorite 9Å	87689	0.2	0.4	2.8	1.3
Hemicarboaluminate	263124	0.7	3.9	3.8	2.9
Melilite	158175	0.2	0.1	0.3	0.3
Amorphous/Unidentified		71.3	76.2	78.3	81.8

It is worth noting that the 52% slag mixture with the higher WR and SP2 amounts showed the presence of monosulfoaluminate. Based on the chemical oxide analysis, the slag contained 14.25% alumina, while the cement had only 5.2% alumina. The increase in the alumina content changes the SO_3/Al_2O_3 ratio of the mixture. The SO_3/Al_2O_3 molar ratios were calculated to be 0.9, 0.16, and 0.5 for the cement, slag, and 52SLmixtures, respectively, based on the elemental oxide composition of the as-received materials. This potentially resulted in increased formation of monosulfoaluminates since the sulfate content of the slag was minimal. Ettringite formation and stability requires a higher SO_3/Al_2O_3 ratio and, therefore, a lower ratio could lead to ettringite decomposition and formation of monosulfoaluminate, as was identified by XRD (Table 10-9).

Isothermal calorimetry performed on pastes with 52% slag and no chemical admixtures (Figure 10-4) showed that the sulfate depletion point in the slag paste occurred approximately 3.5 hours earlier than in the CN, and its intensity relative to the main hydration peak was significantly higher. This indicates increased aluminate reaction due to decreased sulfate content of the mixture. Additionally, the alumina portion of the slag has been reported to react faster than the silica [342]. All this leads to formation of monosulfoaluminate, making this 52% slag mixture susceptible to sulfate attack.

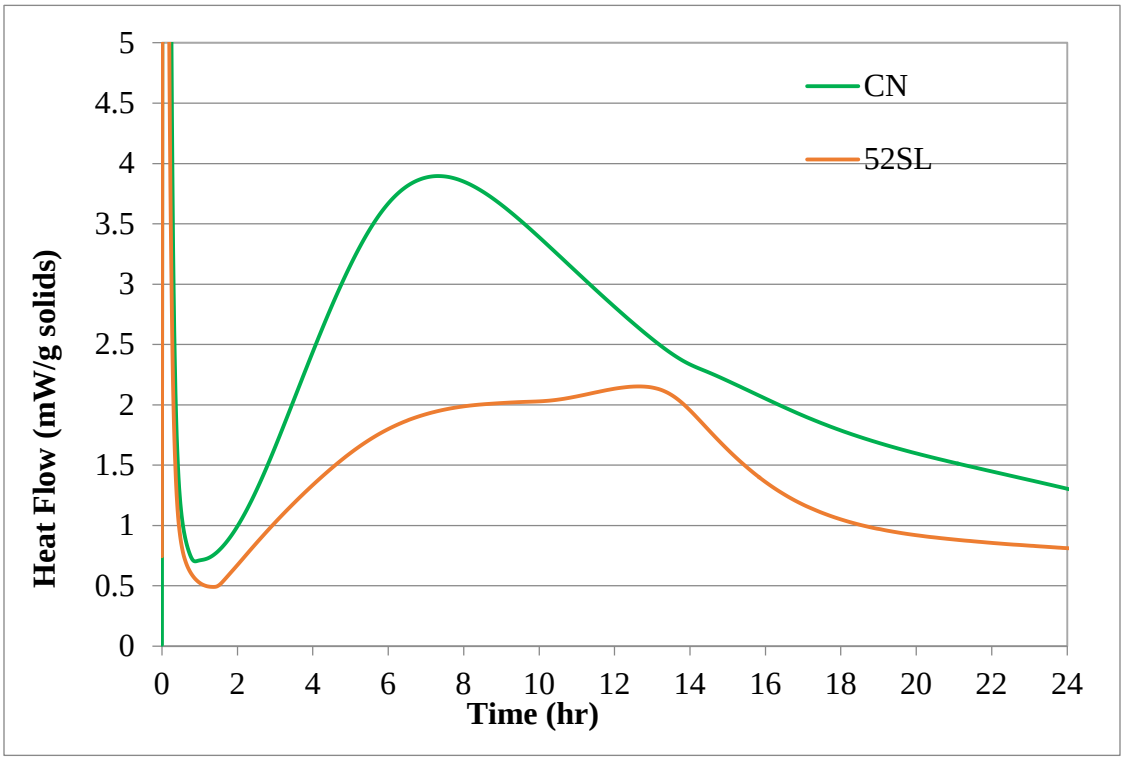

Figure 10-4: Heat Flow for CN and SL Normalized by Mass of Cementitious Materials

There are a number of publications detailing the hydration products in the OPC/MK systems. Antoni et al. [171] predicted, through thermodynamic modeling, the presence of the following phases at 80% degree of hydration for cement with substitutions of 10% metakaolin and 5% limestone: monocarboaluminate, hemicarboaluminate, ettringite, portlandite, OH-hydrotalcite, C-S-H, calcite, and unhydrated OPC. The formula used by the authors for C-S-H was $C_{1.67}A_{0.27}SH_x$. The calculations were performed for hydration under isothermal conditions at 20°C. The authors also provided actual collected XRD patterns at various ages, including blends containing 30% metakaolin at 7 days. In the sample containing 30%MK and 15% limestone (LS),

they identified the following phases at 7 days: strätlingite, ettringite, hemicarboaluminate, monocarboaluminate, C_4AF, and CH. In the 30% MK with no LS, strätlingite, hemicarboaluminate, monocarboaluminate, and C_4AF disappeared, and the presence of monosulfoaluminate was detected. Similarly, Snellings et al. [343] examined a blend of 30%MK and calcite-free OPC at 7 days. They also identified ettringite, monosulfoaluminate, and CH.

It is interesting to note the occurrence of a broad diffuse peak in the 30% MK sample with no LS occurring in the 9-10° 2θ range in the XRD patterns published by Antoni et al. [171]. A similar shape can be seen in this region of patterns in Snelling's paper. In both cases, the authors identified it as a combination of ettringite and monosulfoaluminate only. Cassagnabère et al. [344] also observed a broad peak following ettringite and attributed it to C_4AH_{13}, which has no known crystal structure. It should be noted that the samples in the study by Cassagnabère et al. [344] were cured under variable temperature conditions with the highest temperature reaching 55°C. Boháč et al. [341] also published XRD data for OPC/MK mixes. The only peaks identified in the 7-11° 2θ range were those of ettringite and hemicarboaluminate; however, x-ray diffraction scans were taken only up to 24 hours.

In the current study (Table 10-10), no monocarboaluminate was identified in the 10MK sample, as opposed to the results reported by Antoni et al. [171], most likely due to significantly lower $CaCO_3$ content of the as-received cement (2.1%). Neither Antoni et al. [171] nor Snellings et al. [343] attempted to quantify hydration phases, therefore, our results can only be compared qualitatively. In addition to hemicarboaluminate, CH, ettringite, and monosulfoaluminate, C_4AF was also identified; however, strätlingite was not present in the 10MK sample, which is more in line with Antoni's results for the 30%MK with no LS sample.

Table 10-10: Phase Quantification for 10MK+A1 Sample

Phase	**ICSD #**	**2.5ml AE/ 110 ml WR/155 ml SP1**			**2.5 ml AE/ 200 ml WR/170 ml SP1**
		1 day	**3 days**	**7 days**	**7 days**
Alite	94742	8.6	2.8	1.4	2.2
Belite	81096	15.4	14.5	13.3	12.6
C_3A	1841	4.1	1.8	1.3	0.9
C_4AF	9197	4.0	2.3	1.7	1.7
Portlandite	15471	8.2	9.5	8.0	8.3
Quartz	41414	0.5	0.5	0.4	0.6
Calcite	80869	1.2	1.0	0.9	1.5
Ettringite	155395	9.2	7.6	6.6	8.3
Tobermorite 9Å	87689	0.4	0.6	1.5	3.3
Hemicarboaluminate	263124	0.0	3.5	4.0	2.8
Amorphous/Unidentified		48.4	56.0	61.1	61.2

Brykov et al. [345] found with the use of ^{27}SI-MAS NMR that, starting at 7 days, additions of MK at 10 and 30% reduced the degree of cement hydration. This is contrary to the clinker phase consumption observed in this study (Table 10-11). Addition of MK had no significant effect on the degree of alite reaction compared to the A1 sample. Hydration of C_3A was slightly improved by addition of MK, and the degree of reaction of the ferrite was slightly lower.

Recently, there has been some discussion in the literature regarding the early-age reactivity of the ferrite phase. The traditional view that C_4AF hydration proceeds very slowly at early ages [16] has been questioned by Wang et al. [337] who observed rapid early-age reactions for C_4AF in industrial clinkers. However, Choudhary et al. [346] showed minimal participation of C_4AF in the hydration reactions at 7 days. Minimal ferrite consumption (CN paste) was observed in this study, which is more in agreement with Mindess et al. [16] and Choudhary et al. [346]. Addition of A2 had no effect on its reactivity; however, addition of A1 significantly increased ferrite consumption. Addition of mineral admixtures also increased ferrite consumption, except in the case of metakaolin, when compared to the A1 sample. Wu and Young [89] reported acceleration of the alite hydration by SF. Cheng-yi and Feldman [90] concluded that in addition to C_3S, SF

accelerated C_3A hydration. No significant acceleration in the hydration of these phases with addition of SF was observed in this study at 7 days.

Table 10-11: Consumption of Individual Clinker Phases at 7 Days

		Sample						
Phase	**Age (days)**	**CN**	**A2**	**21FA +A2**	**10SF + A2**	**52SL+ A2**	**A1**	**10MK + A1**
Alite	1	0.68	0.68	0.67	0.67	0.60	0.63	0.70
	3	0.81	0.86	0.84	0.85	0.94	0.86	0.90
	7	0.92	0.93	0.96	0.92	0.99	0.94	0.95
C_3A	1	0.23	0.20	0.11	0.26	0.18	0.16	0.29
	3	0.49	0.54	0.50	0.57	0.73	0.55	0.69
	7	0.68	0.77	0.80	0.73	1	0.75	0.78
C_4AF	1	0.11	0.18	0.09	0.15	0.08	0.15	0.18
	3	0.30	0.35	0.37	0.40	0.57	0.39	0.53
	7	0.41	0.41	0.43	0.51	1	0.44	0.65

To summarize, the main hydration phases identified in the control sample, up to 7 days of hydration, were CH, ettringite, and hemicarboaluminate, although it should be noted that formation of hemicarboaluminate only begins at 3 days. The presence of hemicarboaluminate is attributed to the reaction of C_3A and CH with limestone, which was present in the cement used in this study. The same main hydration phases were observed in the samples with chemical admixtures and no mineral admixtures. The absence of monosulfoaluminate indicated that addition of AE, WR, and SP1 or SP2 did not significantly shift the sulfate balance at the temperature that these measurements were performed (23°C). Generally, there were no significant differences in phase consumption with addition of chemical admixtures compared to the control mixture (CN). This supports the assumption made in section 2.3.1 for Equation 10-14 that chemical admixtures do not affect the ultimate heat of hydration.

Addition of mineral admixtures did not change the main hydration products, with the exception of the 52SL + A2 mixture with higher admixture dosages (Table 10-2 mix design), which showed the presence of monosulfoaluminate. Generally, no significant effect on phase consumption was observed with addition of mineral admixtures, except in the case of 52SL. Cement replacement with 52% slag initially (at 1 day) decreased alite and C_4AF consumption; however, at 3 and 7 days, consumption of all phases was increased compared to SP2.

Nitrogen Adsorption

In comparing porosity of cement pastes, both the total pore volume and the pore size distribution are important. Mehta and Monteiro [19] generally divide concrete porosity into macropores (larger than 50 nm) and micropores (less than 50 nm), while Mindess et al. [16] suggest a more detailed classification, where pores are divided into macropores (larger than 50 nm), large mesopores (10-50 nm), small mesopores (2.5-10 nm) and micropores (0.5-2.5 nm). Since nitrogen adsorption can only measure pores sizes from approximately 1.5 nm to 40 nm [347], prediction of concrete properties is limited to those controlled by the pore sizes in this region.

Figure 10-5 through Figure 10-9 present nitrogen sorption isotherms for all the mixtures. As discussed in section 2.3, isotherms can provide information not only on the total volume of nitrogen adsorbed, but also on the presence of ink-bottle pores.

Figure 10-5 shows the nitrogen adsorption isotherms for the CN paste with no chemical and mineral admixtures, and A1 paste with AE, WR, and SP1 at the dosages listed in Table 10-1. Addition of chemical admixtures slightly lowered the adsorption and desorption isotherms compared to CN sample; however, the width of the hysteresis loop and the total adsorbed volume were not affected. Therefore, it appears that addition of SP1 in combination with AE and WR does not increase bottlenecking at the age of 7 days.

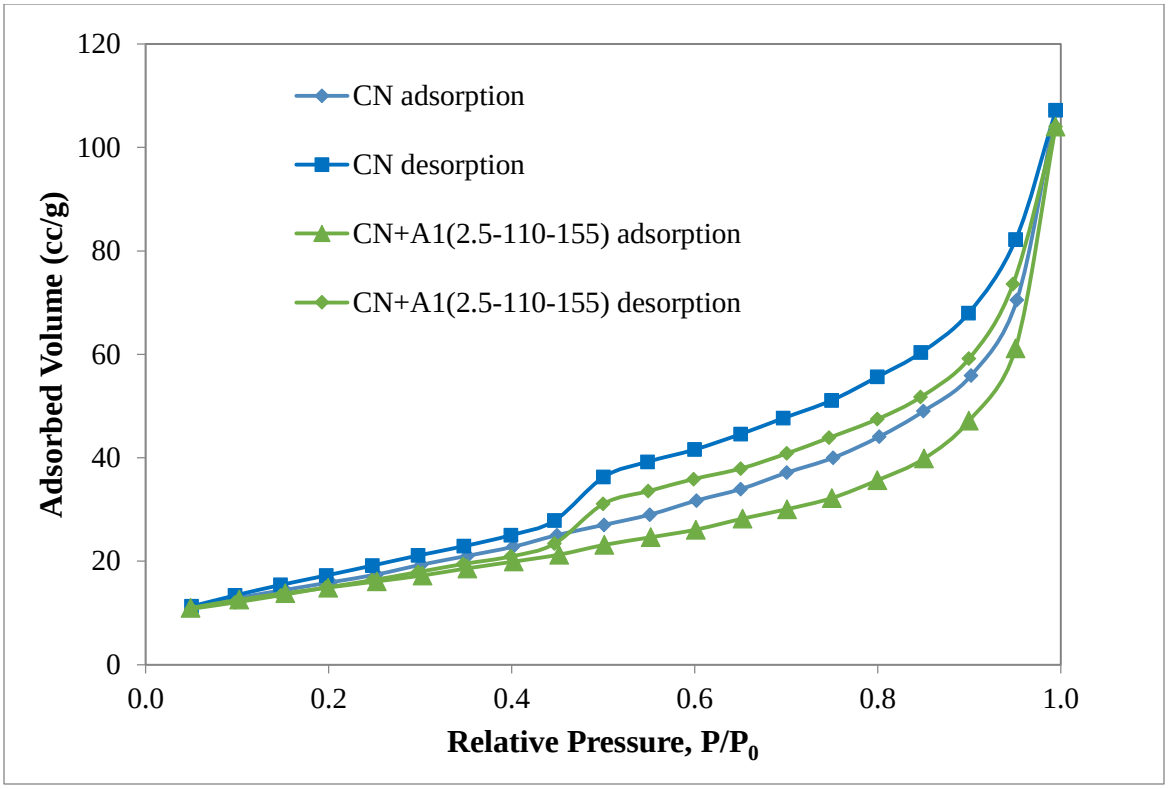

Figure 10-5: Nitrogen Adsorption Isotherms for CN Paste at 7 Days

Figure 10-6 shows the effect of fly ash addition and the effect of increasing WR and SP2 in a 21FA + A2 mixture on nitrogen adsorption. With addition of 21FA+A2 (Table 10-1 mix design), the isotherm shifted downward compared to the CN control and the slope decreased as well. Increasing WR and SP2 dosages in the 21% fly ash mixture (Table 10-2 mix design dosages) shifted the isotherm upward, and increased the total volume and slope of the linear portion of the isotherm. It appears that cement replacement with fly ash increased nitrogen-accessible porosity, and reduced the surface area of hydration products, as fly ash is not reactive at early ages. Increased chemical admixture addition in the 21FA mixture somewhat reduced total porosity and surface area. Since the width of the hysteresis loop remained the same for all the mixtures, addition of fly ash did not appear to increase bottlenecking in the pore system.

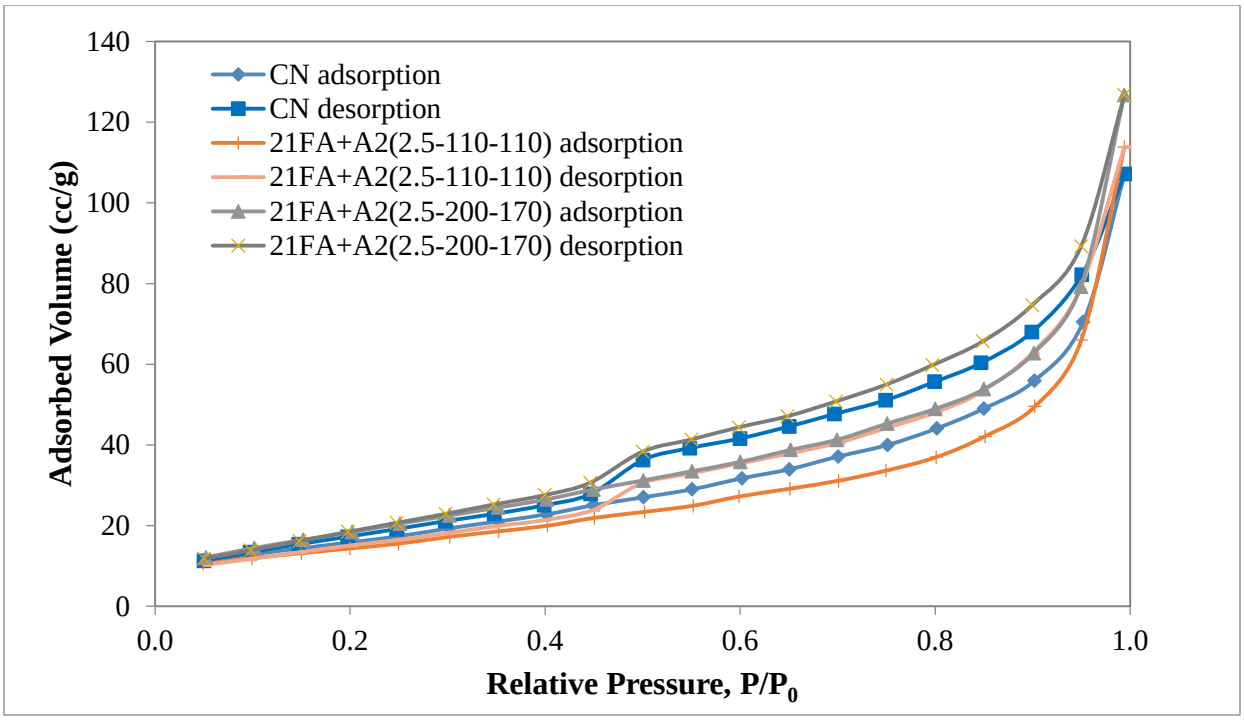

Figure 10-6: NA Isotherms for CN and 21FA at Low and High Chemical Dosages (7 Days)

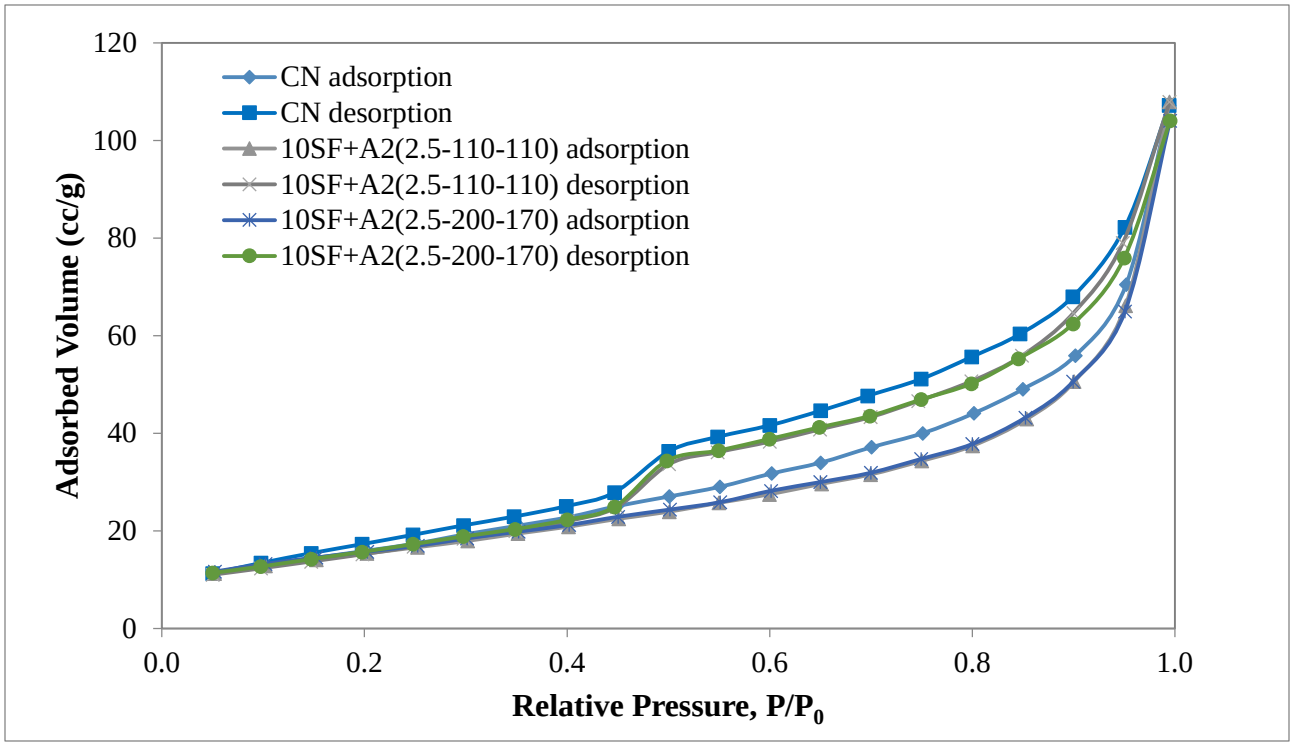

Figure 10-7: NA Isotherms for CN and 10SF at Low and High Chemical Dosages (7 Days)

Cement replacement with 52% slag resulted in an increased total volume of adsorbed nitrogen compared to the CN control paste (Figure 10-8). Additionally, there was a notable increase in the width of the hysteresis loop. This indicates that addition of slag likely produced ink-bottle pores. Similar to silica fume mixes, an increase in the dosages of WR and SP2 for a 52SL mixture resulted in an almost identical isotherm.

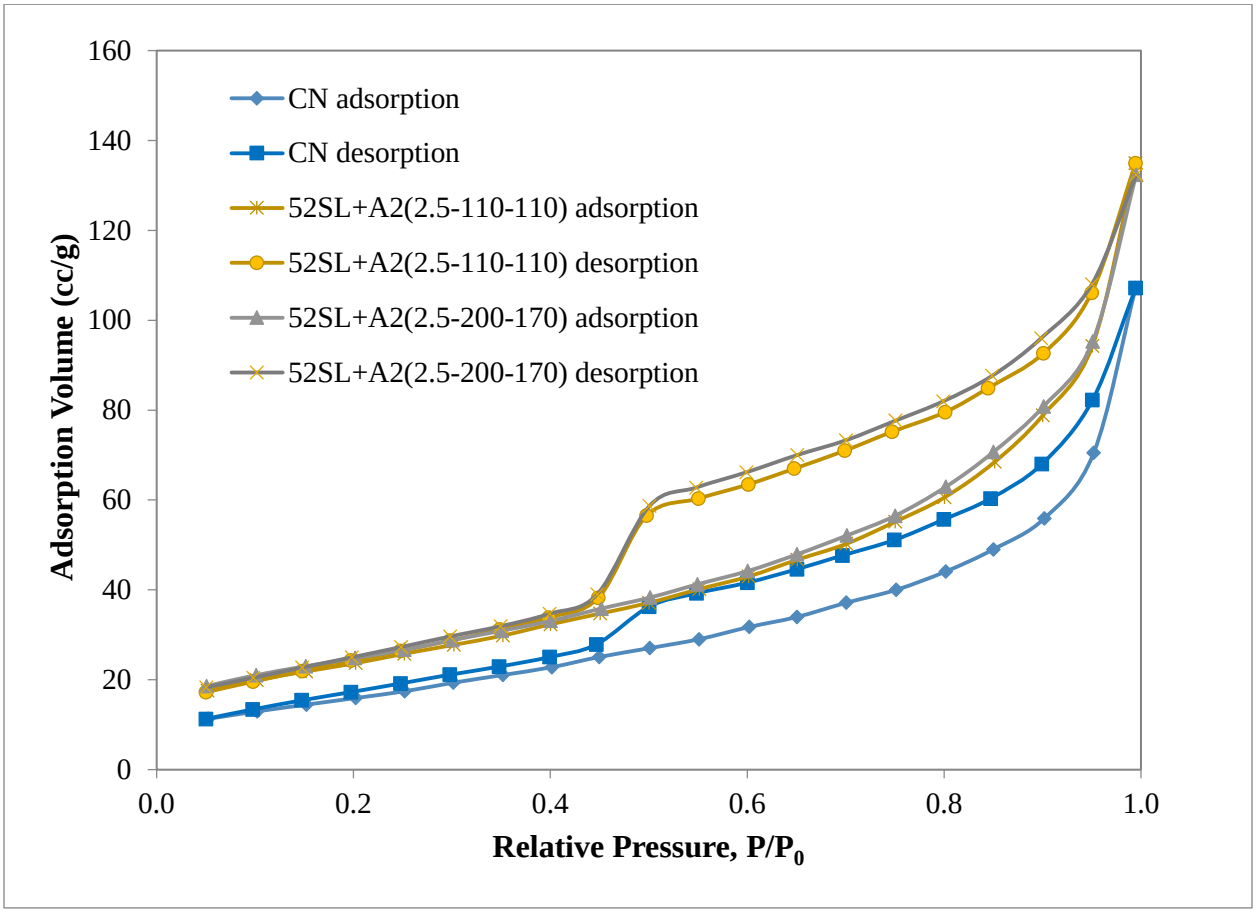

Figure 10-8: NA Isotherms for CN and 52SL at Low and High Chemical Admixture (7 Days)

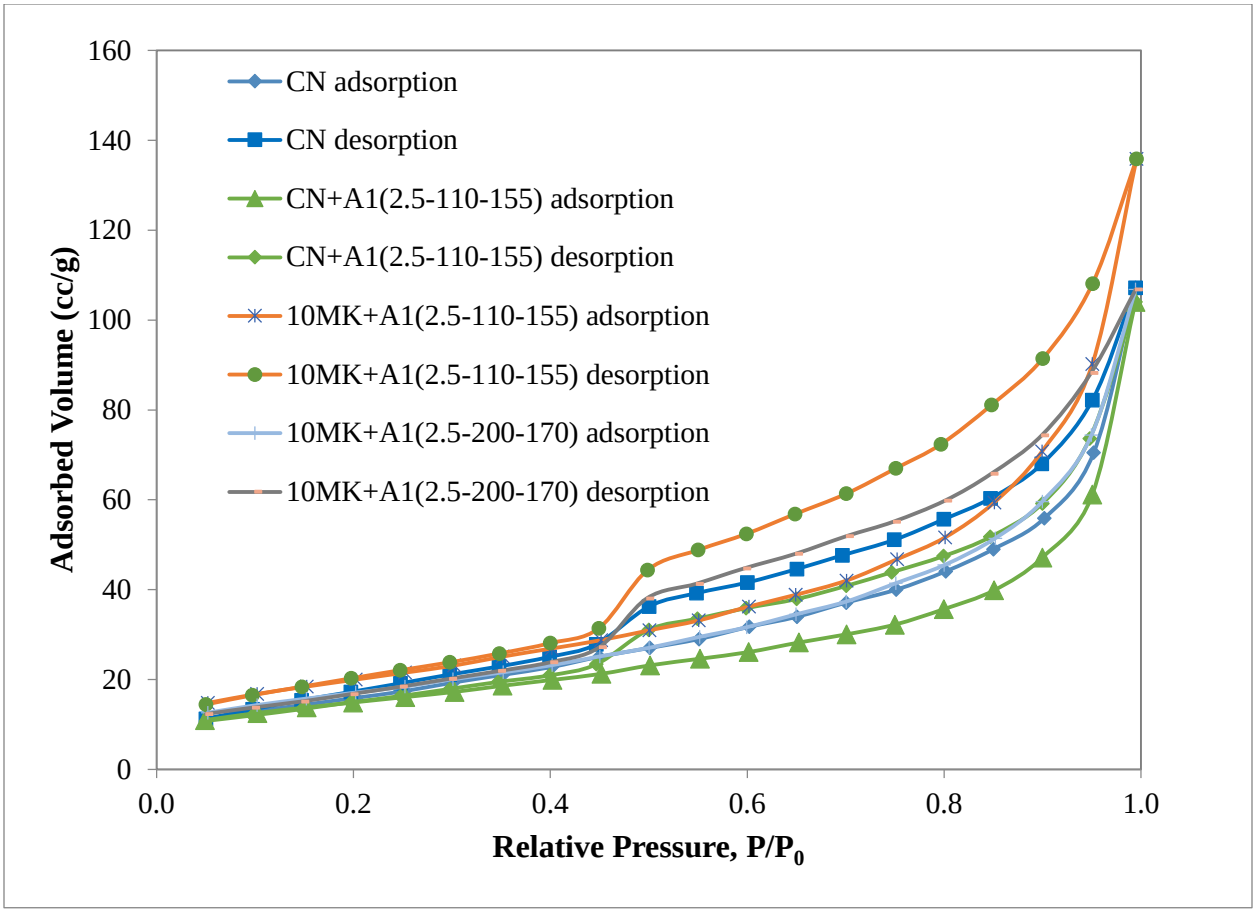

Figure 10-9: NA Isotherms for CN and 10MK at Low and High Chemical Dosages (7 Days)

Addition of chemical and mineral admixtures is known to affect the surface area of paste samples [313]. As can be seen in Table 10-12, addition of chemical admixtures (SP1) decreased the BET specific surface area (SSA) compared to the CN sample with no admixtures. Addition of mineral admixtures had a variable effect on SSA. It was lower compared to the CN paste for 21FA +A2 and 10SF+A2 pastes, and higher in 52SL+A2 and 10MK+A1 pastes. Richardson [348] showed that C-S-H morphology changes with a change in C/S ratio. Specifically, he observed that C-S-H morphology changes from fibrils to foils with slag addition and decrease in the C/S ratio.

When comparing SSA values for Table 10-1 and Table 10-2 mix designs, SSA values of the 10SF+A2 and 52SL+A2 pastes remained unchanged, likely indicating that increasing WR and SP2 dosages did not provide improved dispersion or affect the reactivity of these SCMs. Heinz et al. [104] reported increased reactivity of fly ash in the presence of triethanolamine (TEA), which was present in the WR used in this project. Therefore, an increase in the WR dosage may explain

the increase in the BET surface area of the 21FA+A2 mixture at high WR and SP2 dosages. The surface area of 10MK+A1 decreased with increased WR and SP1 dosages, indicating that initial dosages may not have provided adequate dispersion.

Table 10-12: BET Surface Areas at 7 Days

Mixture	**Degree of Hydration**	**5-point BET Surface Area (m^2/g)**	
	Mix designs from Table 10-1	**Mix designs from Table 10-1**	**Mix designs from Table 10-2**
CN	0.75	63.20	-
21FA	0.79	54.71	74.37
10SF	0.68	56.39	57.40
52SL	0.46	86.37	88.92
SP1	0.72	53.35	-
10MK	0.68	72.18	62.71

In addition to the BET surface area, BJH pore size distributions were determined for all paste samples and are presented in Figure 10-10 through Figure 10-14 as plots of D_v as a function of pore diameter. Dv is the change in the pore volume as a function of the change in pore diameter. The effect of chemical and mineral admixtures on pore size distribution is of great interest, as pores of different size ranges will have an impact on different concrete properties. Since nitrogen sorption can measure porosity in the 1.5-40 nm range, and it is not affected by connectivity of pores when the adsorption branch is used [156], it can provide information regarding the effect of chemical and mineral admixtures on the pore ranges that are responsible for shrinkage (>2.5 nm diameter at all RH; 2.5 to 10 nm at RH 50-80%) and creep (>2.5 nm) [16]. Juenger and Jennings [347] observed that an increase in the nitrogen pore volume and surface area corresponded to an increase in drying shrinkage. Jennings et al. [349] also state that creep is affected by gel porosity. Only a small fraction of the pore range influencing strength (10 nm to 1 mm) and permeability (10 nm to 10 μm) [16] can be accessed by nitrogen sorption, so no definitive conclusions regarding these properties can be drawn from the nitrogen adsorption data.

In the case of the A1 paste, the pore size distribution was lower than that of the CN sample with no mineral or chemical admixtures (Figure 10-10). Juenger and Jennings [347] have previously proposed that an increase in the low density to high density (LD/HD) C-S-H ratio corresponds to an increase in drying shrinkage. It should be noted that in their study, the drying shrinkage included an autogenous shrinkage component. Micropores in general are responsible for creep and shrinkage [16], [349], [350], so a decrease in the micropore volume observed with A1 addition may result in decreased autogenous and drying shrinkage, as well as decreased creep.

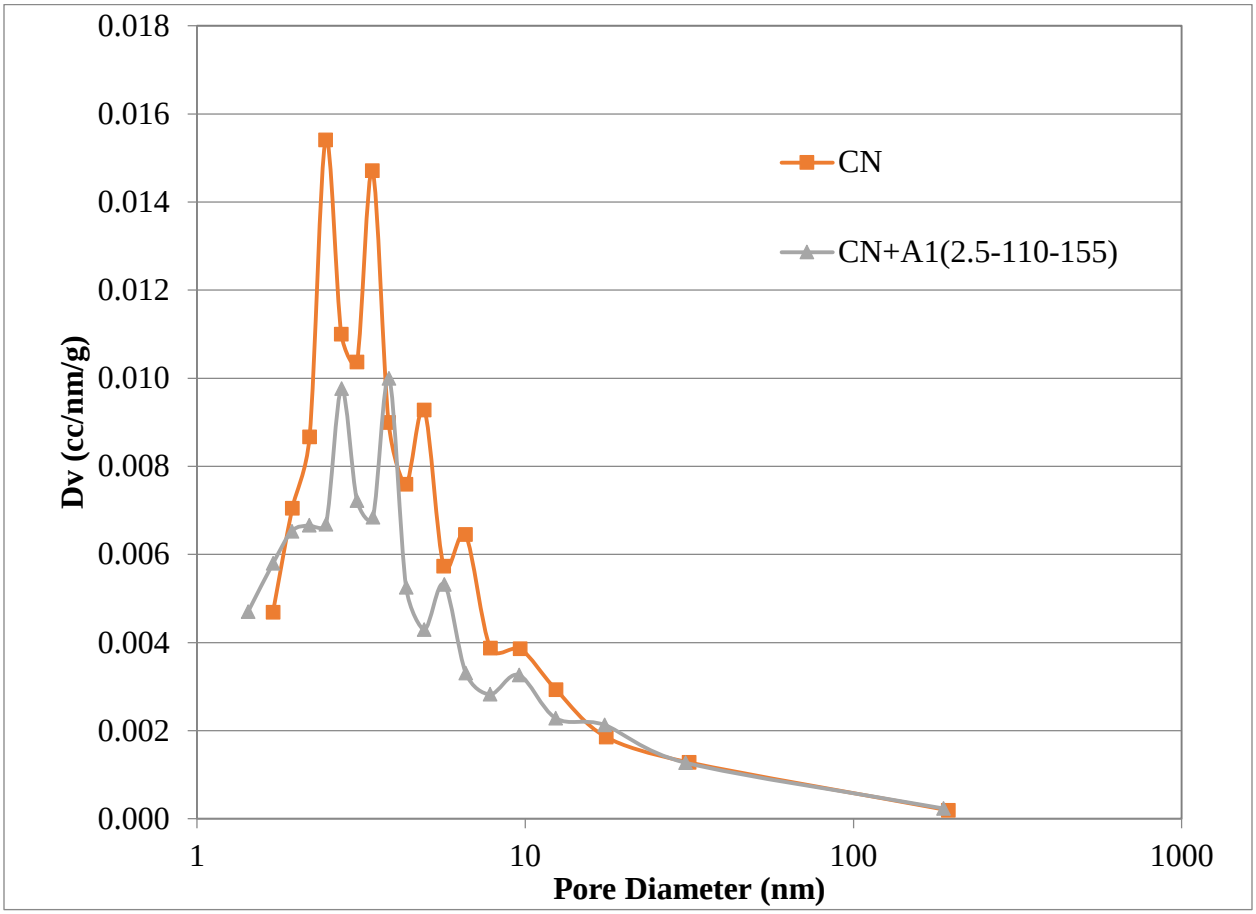

Figure 10-10: BJH Pore Size Distribution for the CN and A1 Paste at 7 Days

The use of fly ash as a cement replacement did not produce any significant changes in the pore size distribution above 10 nm (Figure 10-11). The 21FA+A2 mixture with the lower amounts of chemical admixtures (Table 10-1) had the lowest porosity, which can be explained by the lower amount of C-S-H compared to the CN mixture. An increase in the porosity of the 21FA+A2 with

increasing the dosages of WR and SP2 (Table 10-2 mix design) was likely due to an increase in the LD/HD ratio on increasing the SP2 dosage.

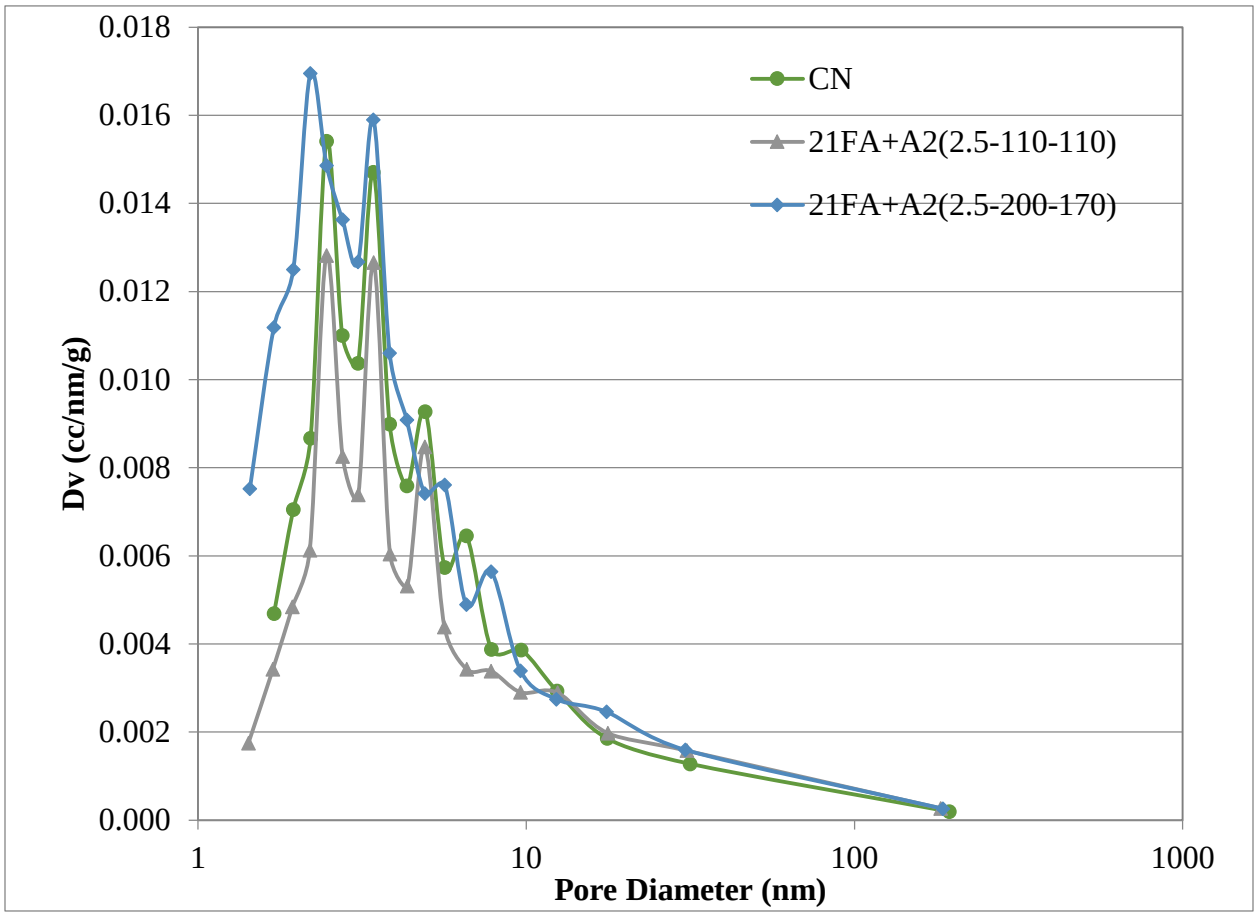

Figure 10-11: BJH Pore Size Distribution for CN and 21FA at 7 Days

The pore size distribution of the 10SF+A2 samples was very similar regardless of admixture dosage (Figure 10-12). The porosity of the 10SF samples was lower than that of the CN paste at all pore sizes, which was expected, as addition of SF is known to result in pore refinement.

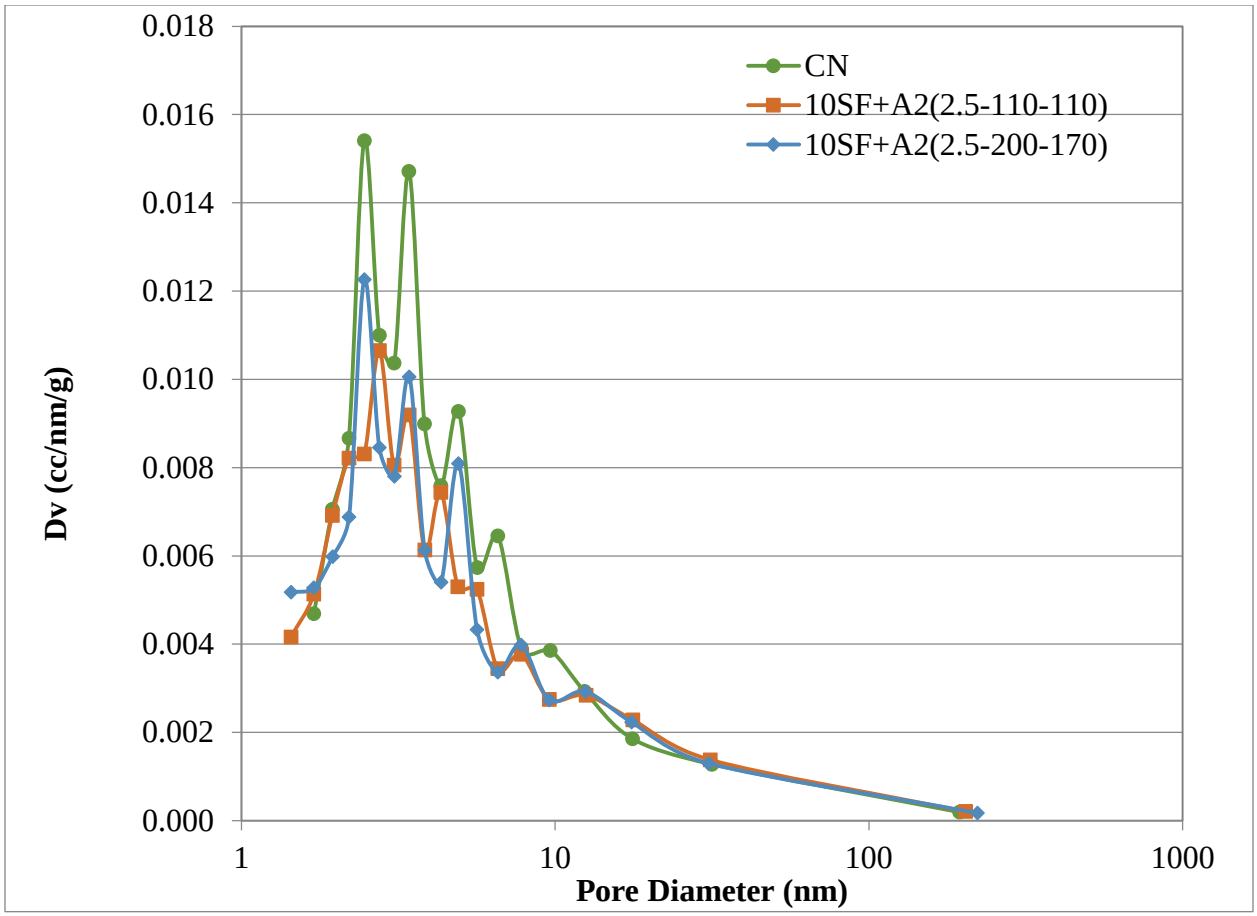

Figure 10-12: BJH Pore Size Distribution for CN and 10SF at 7 Days

As was observed with silica fume, the pore size distribution of the 52SL+A2 samples was very similar regardless of the chemical admixture dosage (Figure 10-13). Cement replacement with 52% slag resulted in a slight increase in the pore volume in the micropore range compared to the CN sample. An increase in the small- and medium-sized capillary pores was even more notable. Based on these results, 52SL+A2 samples could be expected to experience higher shrinkage and creep as well as increased permeability compared to CN samples [16].

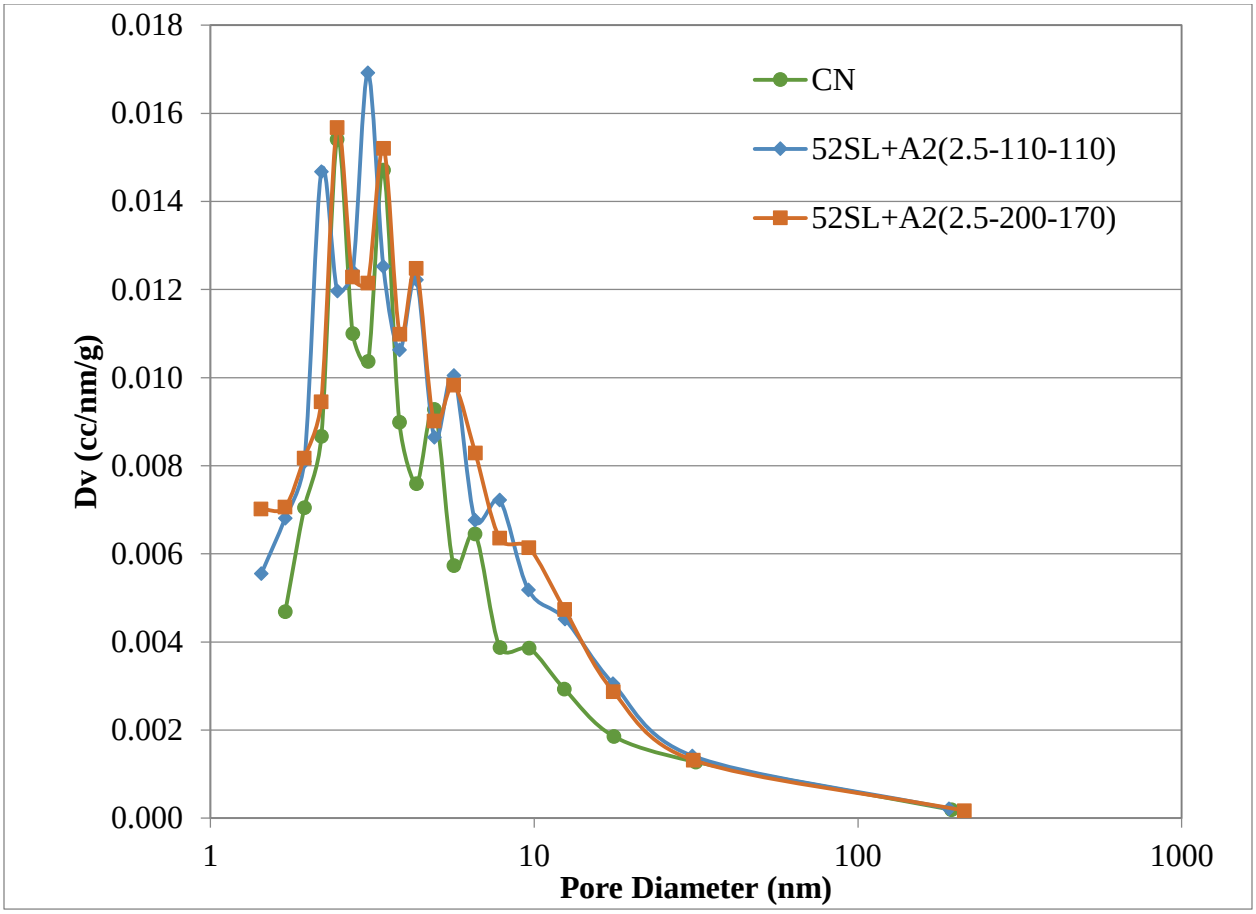

Figure 10-13: BJH Pore Size Distribution for CN and 52SL at 7 Days

10MK+A1 samples generally had similar porosity compared to the CN sample in the micropore range (Figure 10-14). Similar to 52SL+A2 samples, 10MK+A1 samples with high WR and SP1 dosages (Table 10-2 mix design) showed differences in pore size distribution above 10 nm. The difference increased with metakaolin addition, but decreased with increasing dosage of WR and SP1.

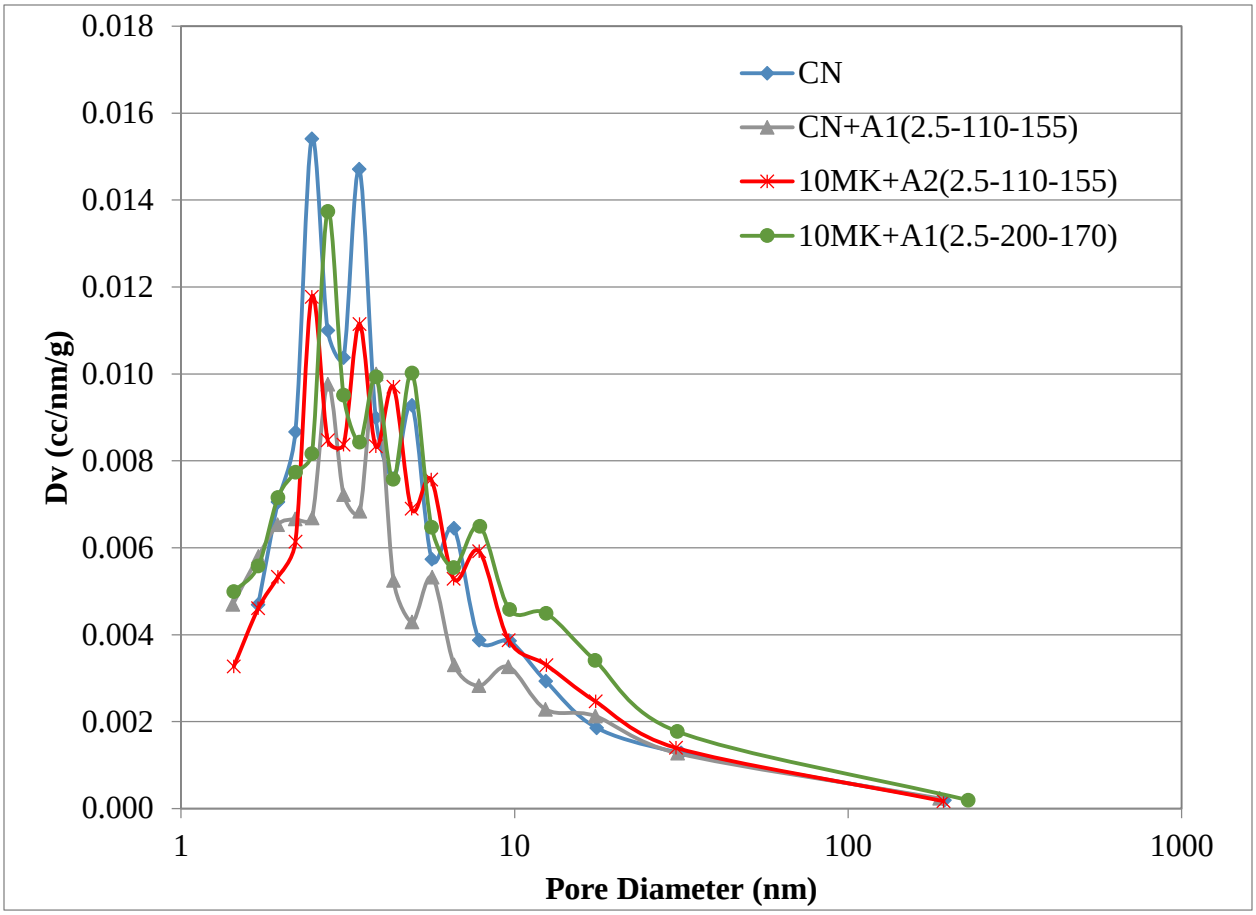

Figure 10-14: BJH Pore Size Distribution for CN and 10MK at 7 Days

In his CM-II model, Jennings [351] distinguishes two types of C-S-H pores: small gel pores (SGP) representing the space within C-S-H particles and large gel pores (LGP) between the C-S-H particles. He estimates the size of SGPs to be below 3 nm, and the size of LGPs to be in the range of 3-12 nm. A recent NMR study reported 10 nm pores between C-S-H particles [352]. Others [353] report clustering of pore sizes around the following average values: 1.8, 7, 50 and 600 nm. The authors attributed 1.8 nm pores to the pores inside C-S-H (SGP pores proposed by Jennings [351]) and 7 nm pores to the pores between C-S-H particles. Reconciling these studies, as well as the pore size classification proposed by Mindess et al. [16], pore size distributions of the samples analyzed in this study were compared for the following pore ranges: <3nm (SGP pores), 3-10 nm (LGP pores) and >10 nm (fraction of capillary pores measured by N_2 sorption).

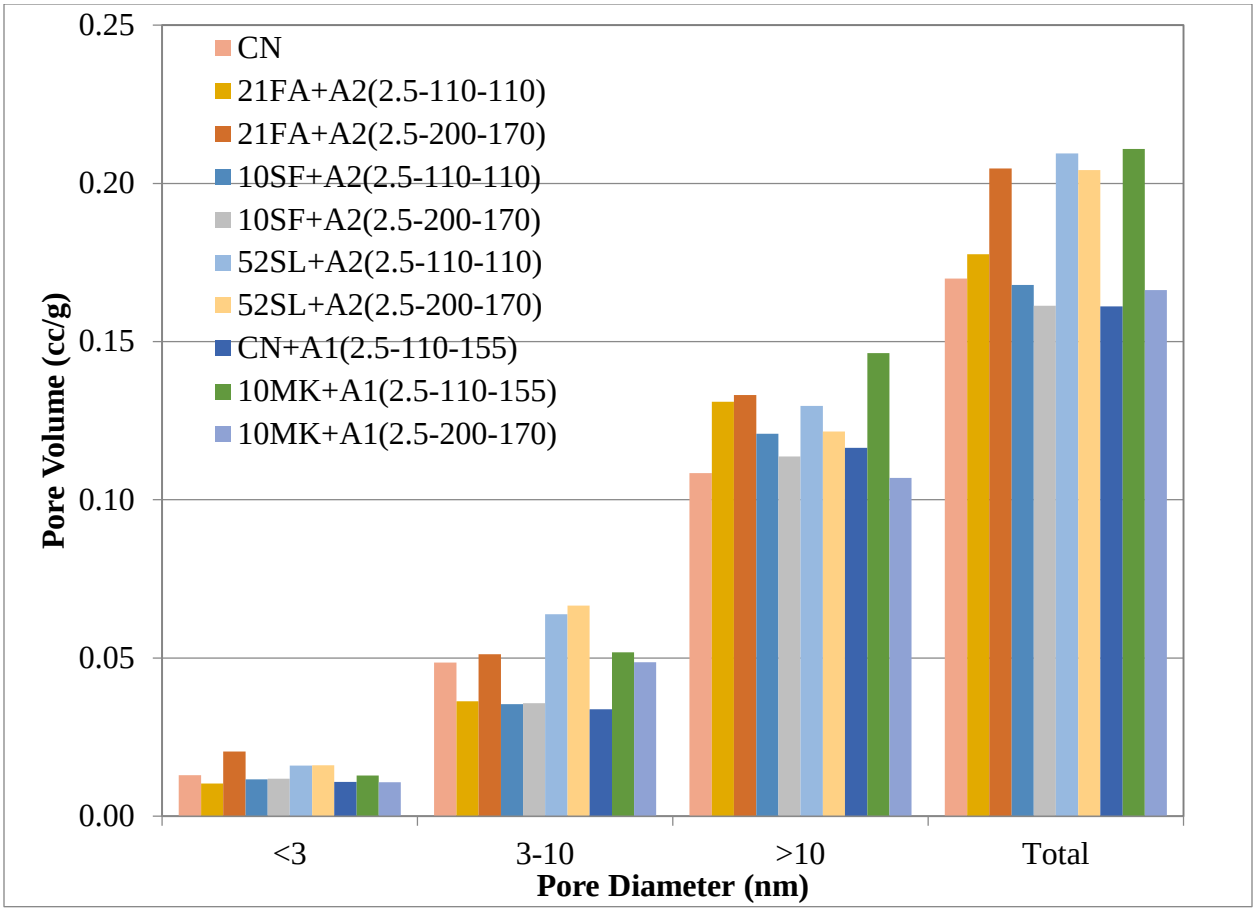

Figure 10-15: BJH Pore Volumes for each Paste Sample at 7 Days

Figure 10-5 shows the pore volumes for these ranges as well as the total pore volumes measured. Addition of SP1 together with WR and AE (A1) had no significant effect on the volume of pores < 3 nm or > 10nm; however, the volume of pores in the 3-10 nm range was decreased (compare CN with CN+A1). Generally, addition of mineral admixtures did not have a significant effect on SGPs. As can be seen from Figure 10-15, the SGP pore volumes for all samples were comparable to that of CN paste, except for 21FA+A2 mixture at the high WR and SP2 dosage (Table 10-2 mix design), where increasing the dosage of WR and SP2 approximately doubled the volume of pores < 3 nm compared to the 21FA mixture with lower dosages. As for the volume of LGPs, it was reduced compared to CN by addition of FA at low WR and SP2 dosages, and by SF regardless of the chemical admixture dosage. At high WR and SP2 dosages, addition of FA resulted in a similar volume of LGPs as that of the CN paste. Addition of slag increased the volume of LGPs regardless of chemical admixture dosages. Addition of MK resulted in similar LGP pore

volumes to that of the CN sample; however, it was notably higher compared to the A1 sample. Generally, slag addition resulted in the highest pore volume in the 3-10 nm

Comparing the mineral admixtures in this group, FA at low chemical admixture dosage and SF at both high and low chemical admixture dosages had the lowest LGP volumes. The 52SL+A2 mixture had a significantly higher LGP volume, almost double that of the 10SF mixture. Metakaolin addition had no effect on SGP volume; however, the LGP volume for the 10MK+A1 mixture increased regardless of chemical admixture dosage (Table 10-1 or Table 10-2 mix designs) compared to the A1 sample. Correspondingly, the LGP/SGP ratio increased as well suggesting that this mixture may be more prone to shrinkage. For the fraction of capillary porosity that was assessed by nitrogen adsorption, the 10MK+A1 sample with the low admixture dosage (Table 10-1 mix design) had the highest pore volume, which indicates that this mixture may be more susceptible to shrinkage.

The degree of hydration for samples prepared using Table 10-1 mix designs was generally comparable, except for the 52SL+A2 paste, for which it was significantly lower. Due to the lower degree of hydration, this mixture was likely to exhibit higher creep compared to the other samples. Although the high LGP/SGP ratio of 52SL+A2 indicates higher potential for shrinkage, its higher creep may be able to relax shrinkage stresses more compared to the other mixtures at this age, thus reducing the shrinkage cracking potential of 52SL+A2 mixture.

[redacted] Nanoindentation

[redacted]Sample Selection for Nanoindentation

Three mixtures were selected for nanoindentation and examination with SEM: 52SL+A2, 10MK+A1, and A1. The 52SL+A2 mixture showed the lowest compressive strength at 7 days, and the 10MK+A1 had the highest (Table 10-13). Additionally, 52SL+A2 bars immersed in sodium sulfate solution showed the highest expansion as can be seen in Figure 10-16. A1 was chosen as a point of comparison since both A2 and A1 had similar 7-day compressive strengths. A1 was selected over A2 because the A1 admixture had a higher concentration of polyacrylates. The 10MK with A1 mixture was selected because, despite its high compressive strength and moderate sulfate durability, preliminary cracking frame tests showed a higher cracking potential for this mixture.

Table 10-13: Compressive Strength of Mortar Cubes at 7 Days (Table 10-1 Mix Design)

Sample	A2	21FA+A2	10SF+A2	52SL+A2	A1	10MK+A1
Compressive strength (psi)	5420	4210	5130	3960	5800	6000

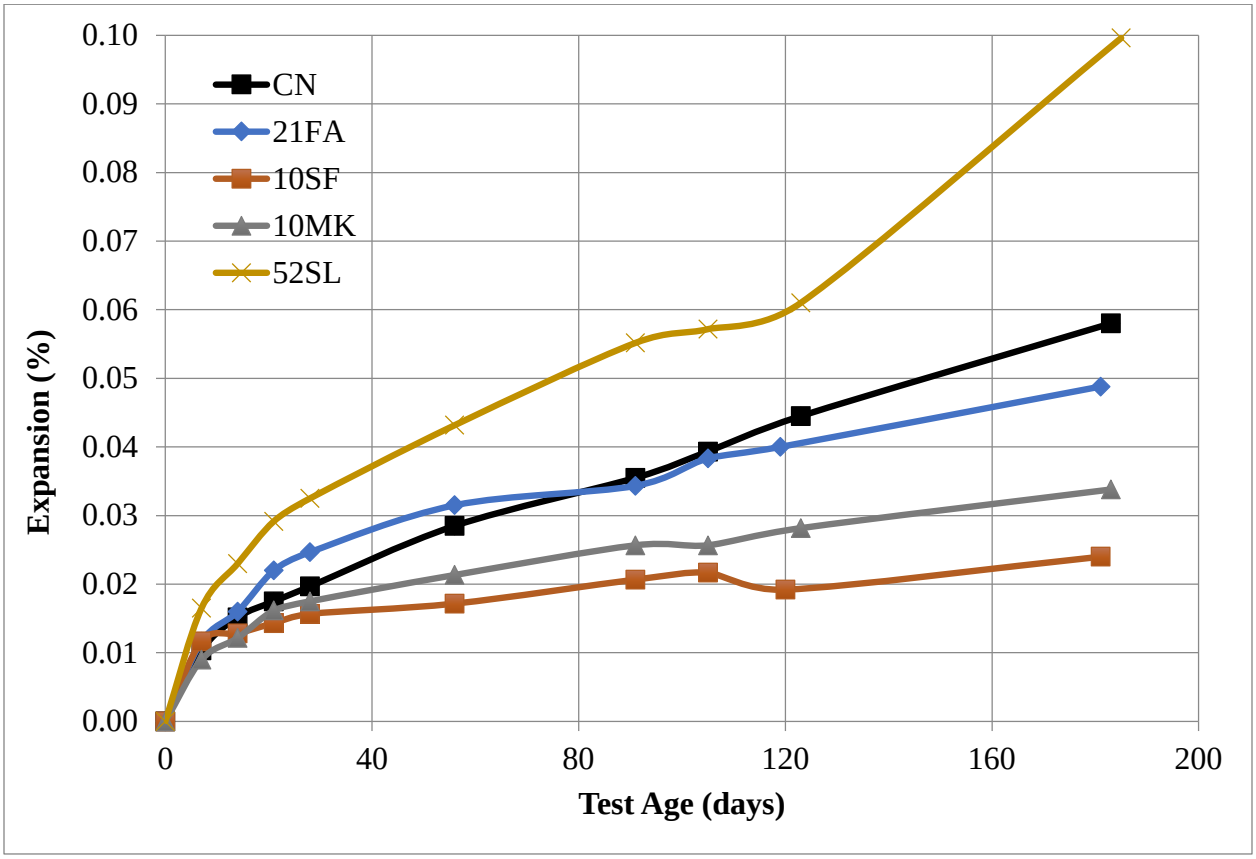

Figure 10-16: Expansion in 5% Sodium Sulfate Solution

Nanoindentation Results

The results obtained from grid indentation were used to calculate the average elastic modulus (*E*), hardness (*H*), and average maximum depth of penetration (h_{max}) for each sample (Table 10-14 and Table 10-15), as well as the probability distribution plots of elastic moduli (Figure 10-17-Figure 10-20). First, the average *E*, *H*, and h_{max} were calculated based on the data obtained from all the indents, which included both the hydration products and the unhydrated clinker phases, and are shown in Table 10-14. The average maximum penetration depths were very

similar and indicate that the majority of the indents were made in the C-S-H phase [332]. However, large differences can be observed between the average elastic moduli and average hardness values for these samples. The A1 sample had the highest elastic modulus, followed by the 52SL+A2 sample, and the 10MK+A1 sample had the lowest. The average hardness of the 10MK+A1 sample was also significantly lower than that of the other samples.

Table 10-14: Average Nanoindentation Values

Sample	**Average E (GPa)**	**Average H (GPa)**	**Average h_{max} (nm)**
10MK+A1	19.7	0.5	323
A1	30.1	1.2	294
52SL+A2	23.0	1.4	323

Figure 10-17 shows the probability distribution plot for the elastic moduli of the samples. It can be seen that the lower elastic modulus was due to a fewer number of indentation points with high elastic moduli (above 40 GPa). The elastic modulus of individual clinker phases is known to be significantly higher than that of hydration products [354]. The lower average elastic modulus of the 10MK sample may have been due to the lower fraction of anhydrous clinker phases.

Although Table 10-11 shows the degree of hydration of individual clinker phases, it cannot be used to compare the degree of hydration of these cementitious systems as a whole. The degree of hydration values, $\alpha(t)$, for 52SL+A2 and A1 pastes were calculated using Equations 10-13, 10-14, and 10-16. The $\alpha(t)$ of the A1 sample was 0.72, while the 52SL+A2 sample was 0.46. For the 10MK+A1 paste, Equation 10-15 was used instead of Equation 10-14, and $\alpha(t)$ for the 10MK+A1 sample was determined to be 0.68.

Despite a large difference in the degree of hydration of the 10MK+A1 and 52SL+A2 samples, their average elastic moduli were similar. Conversely, there is a large difference in the *E* values for the 10MK+A1 and A1 samples in spite of their similar degree of hydration. This indicates that the average *E* values in Table 10-14 are heavily influenced by the presence of unhydrated clinker phases, and may not be the best way to evaluate the mechanical properties of the hydrated paste.

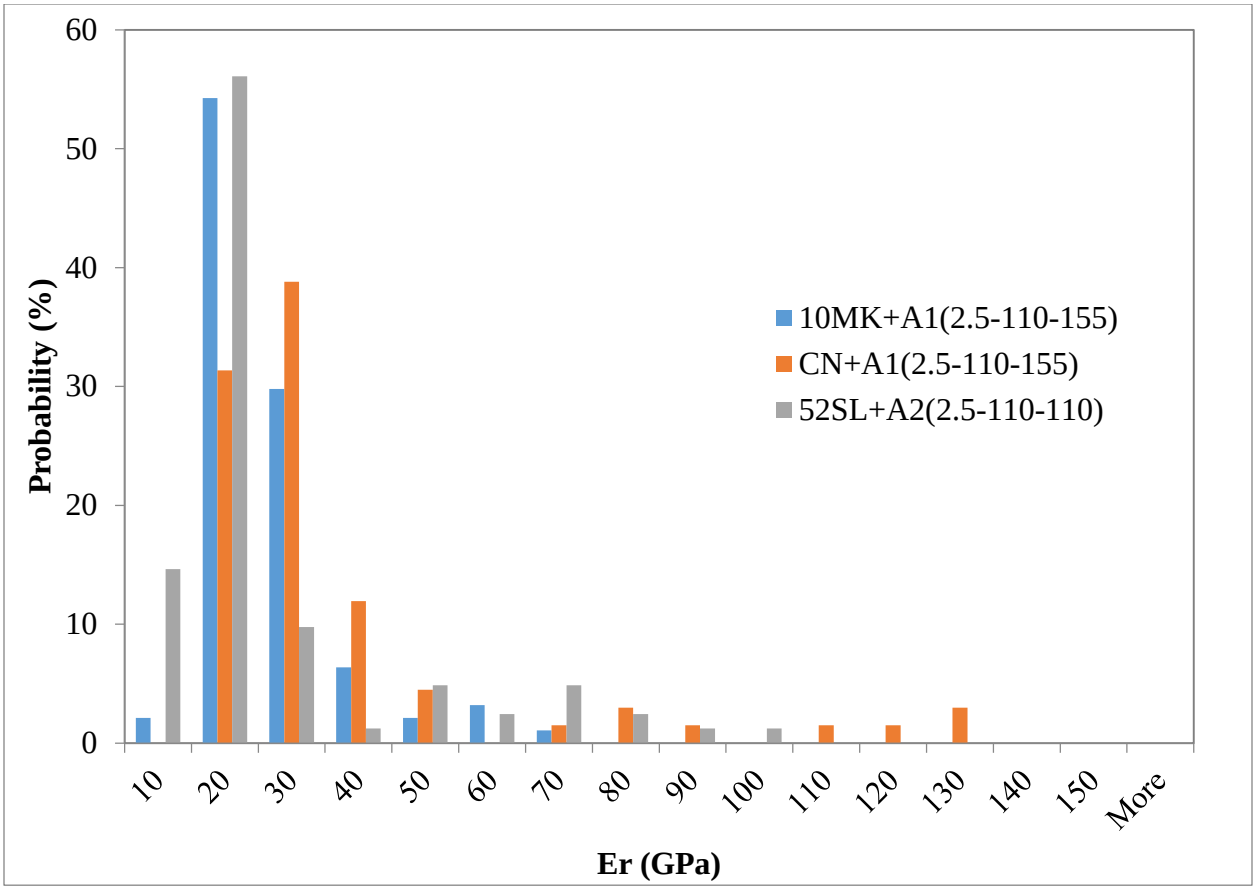

Figure 10-17: Probability Distribution of the Indentation Moduli at 7 Days

Addition of chemical and mineral admixtures is known to change the composition and morphology of the hydration products. In order to evaluate the influence of metakaolin and slag addition on the average mechanical properties of the hydration products, and eliminate the effect of the large difference in the degree of hydration, the average *E*, *H*, and, h_{max} values were recalculated, excluding indents with *E* greater than 40 GPa (Table 10-15). A number of *E* and *H* values for C-S-H and CH have been reported in the literature by [329], [355]–[358]. Němeček et al. [359] reported a modulus of approximately 44 GPa for unreacted metakaolin and 26 GPa for unreacted slag. Therefore, 40 GPa was selected as a cutoff point to ensure that all the possible C-S-H packing arrangements were included in the adjusted average values, but the unreacted metakaolin, if any was be present in the 10MK sample, was excluded. Since the expected value for the unreacted slag modulus was between those reported for LD and HD C-S-H, it could not be excluded. However, based on Figure 10-20 it appears that a minimal number of indents were made

in the unreacted slag particles, and they were not expected to have a significant effect on the values calculated for the 52SL+A2 sample in Table 10-15. The adjusted average E values in Table 10-15 correlate much better with compressive strength results listed in Table 10-13 than those for the nanoindentation values listed in Table 10-14. Although three points are not enough for a definitive trend, compressive strength appeared to increase with an increase in average elastic modulus computed for values below 40 GPa.

Table 10-15: Nanoproperties after Excluding Indentations with E Greater than 40 GPa

Sample	**Average E (GPa)**	**Average H (GPa)**	**Average h_{max} (nm)**
10MK+A1	21.6	0.5	327
A1	19.7	0.5	323
52SL+A2	14.7	0.5	370

Further analysis of nanoindentation data was carried out by plotting the probability distributions of the elastic moduli (below 40 GPa) for each sample as depicted in Figure 10-18 through Figure 10-20. This time the bin size of 2 GPa was selected as opposed to 10 GPa in Figure 10-17 to provide better resolution. The three main peaks observed in the CN+A1 sample (Figure 10-18) can be attributed to very porous (VP) C-S-H gel (first peak at 16 GPa), outer product (OP) C-S-H (second peak at 22 GPa), and inner product (IP) C-S-H (third peak at 26 GPa). These values are in general agreement with those reported by Hu et al. [329], who identify *E* of VP C-S-H as 13.6 GPa, *E* of OP C-S-H as 20.8 GPa, and *E* of IP C-S-H as 31.0 GPa . Values for OP and IP C-S-H, as reported in the literature, range from 20 to 31 GPa [356]; for CH, values vary from 29.05 GPa [355] to 48 GPa [356], with Monteiro and Chang [360] reporting a range of 39.77-44.89 GPa. It is likely that the peak at 38 GPa ,shown in Figures 10-18 and 10-19, belong to the CH phase, although Hughes and Trtik [355] identified a modulus of 46.07 GPa for C-S-H mixed with clinker.

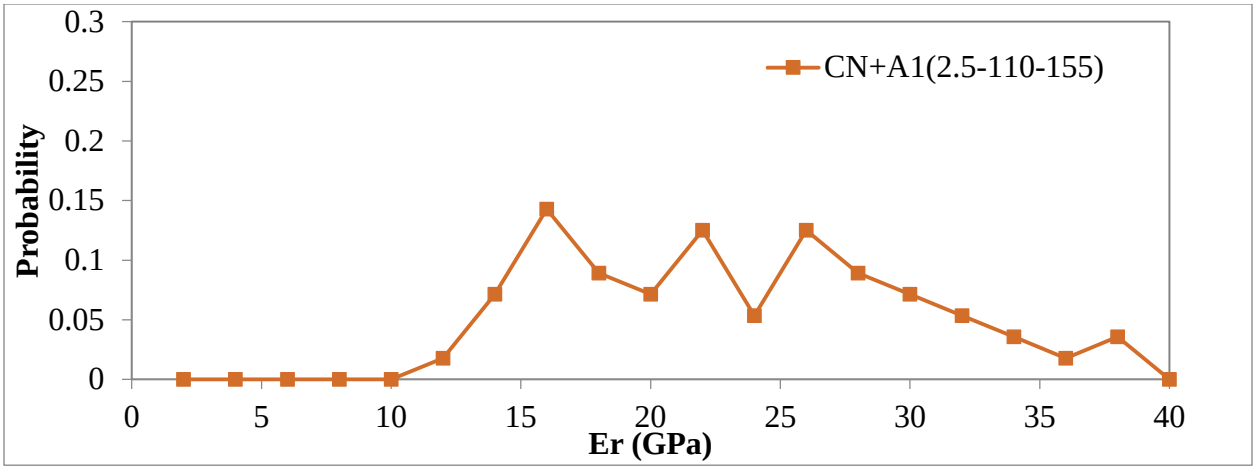

Figure 10-18: Probability Distribution for the Indentation Modulus of CN+A1 Sample

The probability plot for the 10MK+A1 sample (Figure 10-19) is significantly different from that of A1. The first peak at 14 GPa, which can be attributed to VP C-S-H, has notably lower probability than in the A1 sample. The second peak, likely due to OP C-S-H, is showing a higher probability than in the A1 sample. Therefore, the amount of OP C-S-H and the amount of large gel pores (LGP) described in the CM-II model by Jennings [351] between the C-S-H particles is expected to be higher for the 10 MK+A1 sample compared to A1. The amount of IP C-S-H appears to be lower than in the A1 as well as the amount of CH, which is in agreement with the XRD results presented in

Table 10-6 and Table 10-10. Additionally, since the indents with E below 10 GPa are typically attributed to porosity [361], porosity of 10MK+A1 is also expected to be higher than that of the A1 sample.

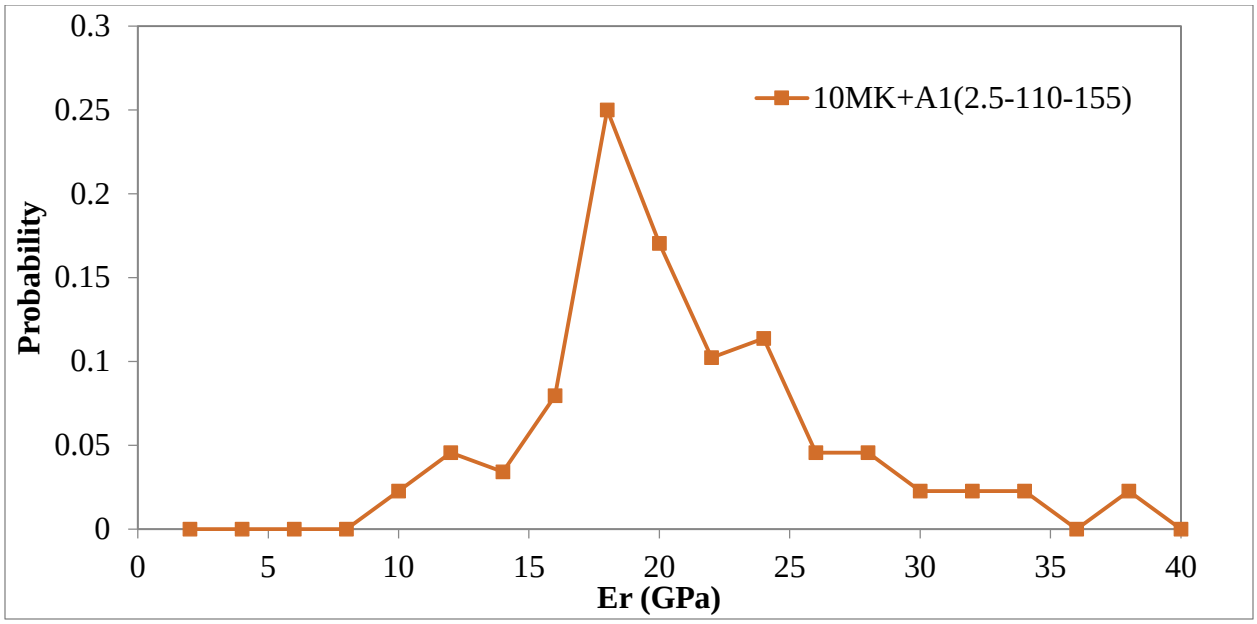

Figure 10-19: Probability Distribution for the Indentation Modulus of 10MK Sample

For 52SL sample (Figure 10-20), the probability distribution also indicates a higher amount of porosity than in the A1 sample, a predominance of VP C-S-H, and notably lower quantities of OP C-S-H than in the other two samples. The peak at 28 GPa can be attributed to IP C-S-H, but its amount appears to be lower than in 10 MK and CN+A1 samples. There are no indents with elastic moduli in the range of 35-40 GPa that could possibly be attributed to CH.. The absence of clear indication of CH presence by nanoindentation is not surprising, as Rietveld refinement identified minimal amounts of CH compared to the other samples (Table 10-9).

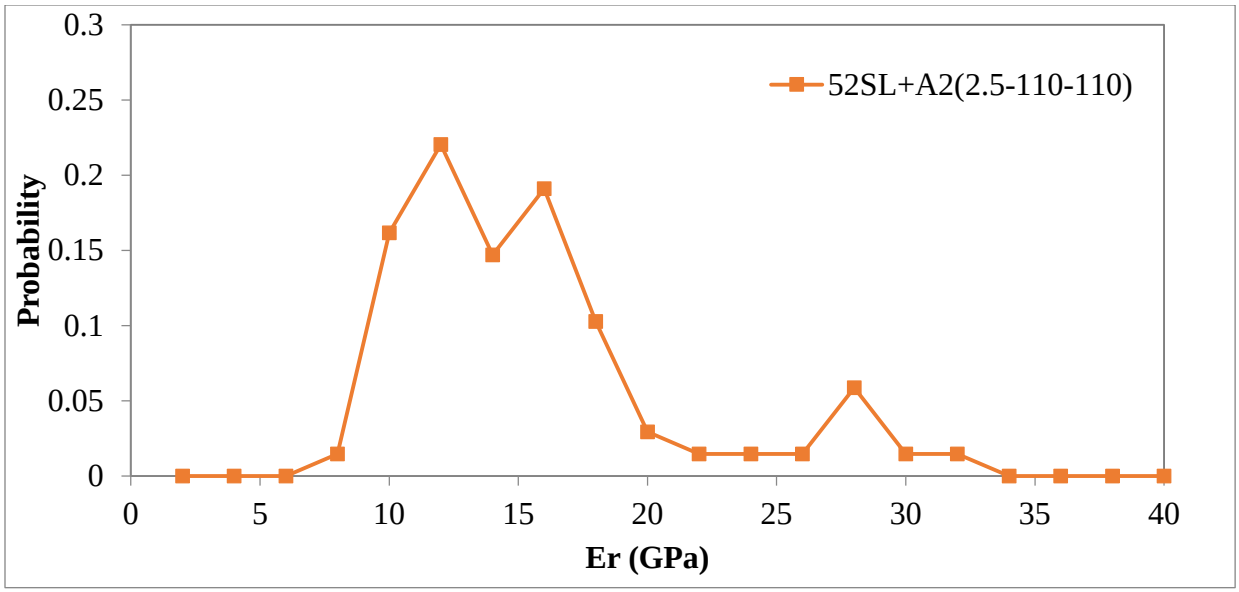

Figure 10-20: Probability Distribution for the Indentation Modulus of 52SL Sample

The probability distributions showed different trends than the average moduli listed in Table 10-14. This was most likely due to the inclusion of the indents of the unhydrated clinker phases, which have significantly higher E values, in the average moduli listed in Table 10-13. This is in contrast to the E ranges shown in Figure 10-18 through Figure 10-20, where the E values are limited to those of hydration phases only and, therefore, these results correspond well with those shown in Table 10-14. Based on these figures, it appears that the 52SL sample had the lowest average elastic modulus in the C-S-H region, while the moduli for 10MK and A1 samples were comparable, with A1 being slightly higher.

Porosity measurements confirm the trends observed in Figure 10-18 through Figure 10-20 as suggested by Sakulich and Li [362]. There is good agreement between BET surface areas (Table 10-12) and the adjusted average elastic moduli (Table 10-15), which show that as the BET surface area increased, the average E decreased. BET surface area values are generally attributed to the surface area of C-S-H. According to Jennings [363], LD C-S-H has a more open morphology and forms only during the early hydration period, while HD C-S-H forms later on and is not accessible by nitrogen. The higher BET surface areas, therefore, would imply a higher fraction of LD C-S-H, which is in agreement with the hypothesis proposed by He et al. [361].

Pelisser et al. [357] investigated the effect of C/S ratio on elastic modulus and hardness of C-S-H. They reported that as the C/S ratio increases, both E and H decrease, although the decrease in H is much more drastic. At 2 mN applied load, the authors reported that E decreased from 26.6 GPa for C/S=0.7 to 19.3 GPa for C/S=2.1, while H decreased from 1.08 to 0.19. However, several other investigators reported no correlation between chemical composition of hydrates determined by EDX and elastic modulus obtained by nanoindentation [359], [362]. This discrepancy between Pelisser's findings and findings of other researchers is likely due to the fact that Pelisser et al. [357] conducted measurements on pure synthetic C-S-H samples, while Němeček [359] and Sakulich and Li [362] utilized composite hydrated samples. Sakulich and Li [362] explain their lack of correlation between EDX and *E* by the fact that the volume from which the x-rays are generated during the EDX examination is greater than the volume probed by nanoindentation. The authors state "chemical composition has less of an effect on modulus than other parameters, such as porosity of C–S–H or the efficiency of packing of the individual C–S–H grains". He et al. [361] suggest that the differences in elastic moduli plots for pastes with different mineral admixtures are due to the "volume fractions of HD C-S-H gel in C-S-H gel." Although they disagree that E is affected by porosity, the change in the HD C-S-H fraction also implies a change in porosity, although in a specific pore size region. As can be seen from Figure 10-15,cement replacement with slag and MK did not have a significant effect on the pore volume of SGPs compared to the CN+A1 sample, but large differences can be observed in the 3-10 nm range, which correlate well with the adjusted modulus results from nanoindentation in Table 10-14. The fraction of LGP pores in the slag sample was significantly higher, corresponding to a lower fraction of HD C-S-H, and a notably lower adjusted modulus. The LGP fraction for 10MK+A1 was slightly higher and its modulus was slightly lower than that of the A1 sample, which is in agreement with He et al. [361].

Scanning Electron Microscopy

The same mixtures that were tested for nanoindentation were examined with scanning electron microscopy (SEM). SEM was initially performed on flat polished samples in the backscatter (BSE) mode for collecting EDX spectra. Figure 10-21 provides an example of a flat polished sample used for EDX measurements. It is important to point out that because of the interaction volume from which x-rays are generated during EDX measurements, the obtained spectra are likely to include elements from both C-S-H and the surrounding phases, even with the use of flat samples [362], [364]. Additionally, since C-S-H is amorphous and does not have a

well-defined chemical formula, a variety of Ca/Si ratios can be obtained for the same paste sample, due to hydrating portland cement clinker phases and reactions with mineral admixtures [171], [348], [365].

Figure 10-21: Example of a Flat Polished Sample under Low Magnification

Since CN+A1 did not contain any mineral admixtures, its average Ca/Si atomic ratio was 1.1. Figure 10-22 shows a representative spectrum for the A1 sample.

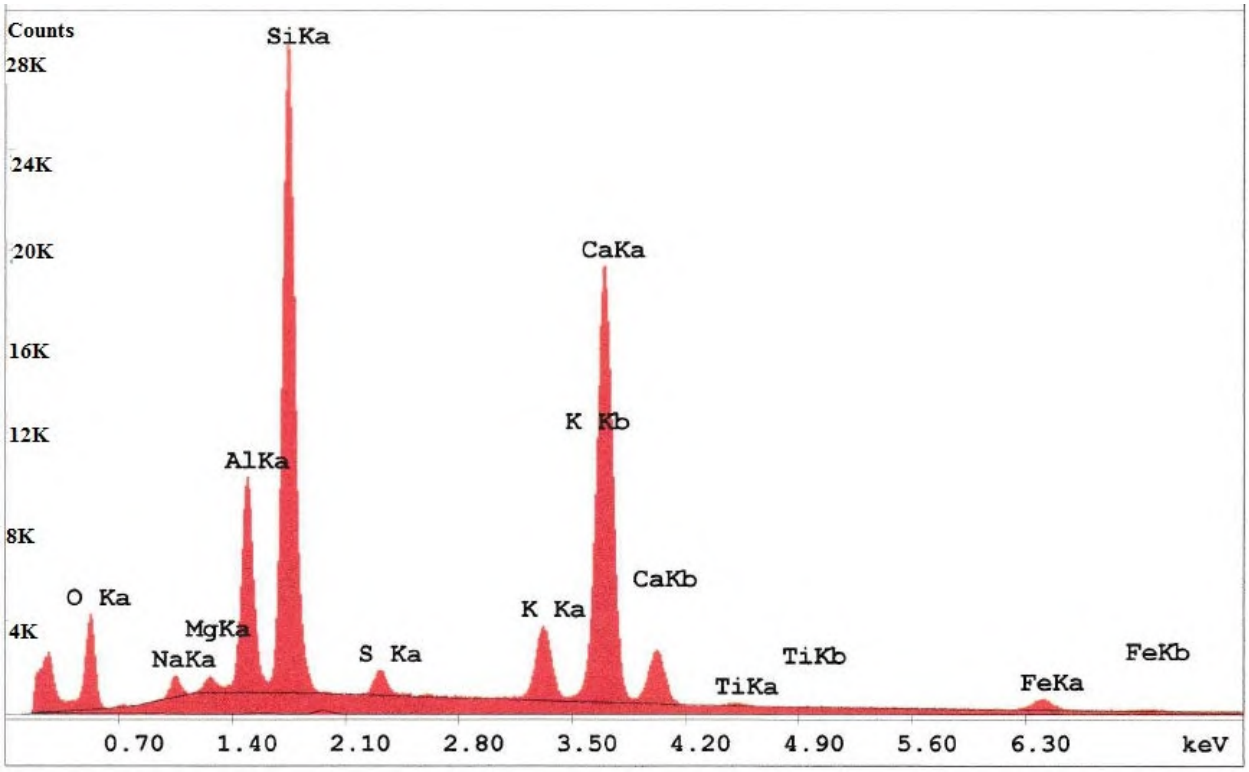

Figure 10-22: EDX Spectrum for CN+A1 Paste at 7 Days

The 10MK sample had generally higher Ca/Si ratios and higher incorporation of Al (Figure 10-23). This was expected since metakaolin has high reactivity [16], [68] and high alumina content [64]–[67].

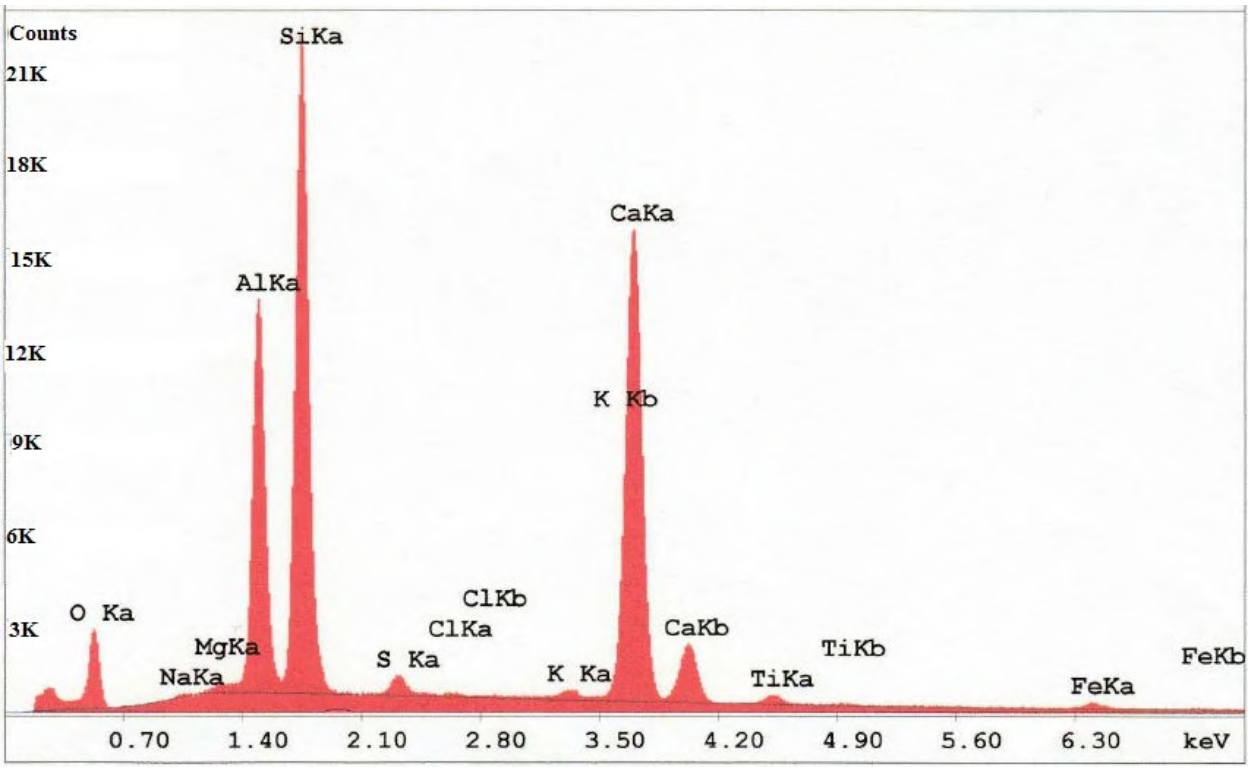

Figure 10-23: EDX Spectrum for 10MK Paste at 7 Days

Incorporation of Al in the 52SL C-S-H was lower compared to the 10MK+A1 sample (Figure 10-24). Slag has much lower reactivity [16] and lower alumina content [44], so the lower incorporation of Al into C-S-H is not surprising.

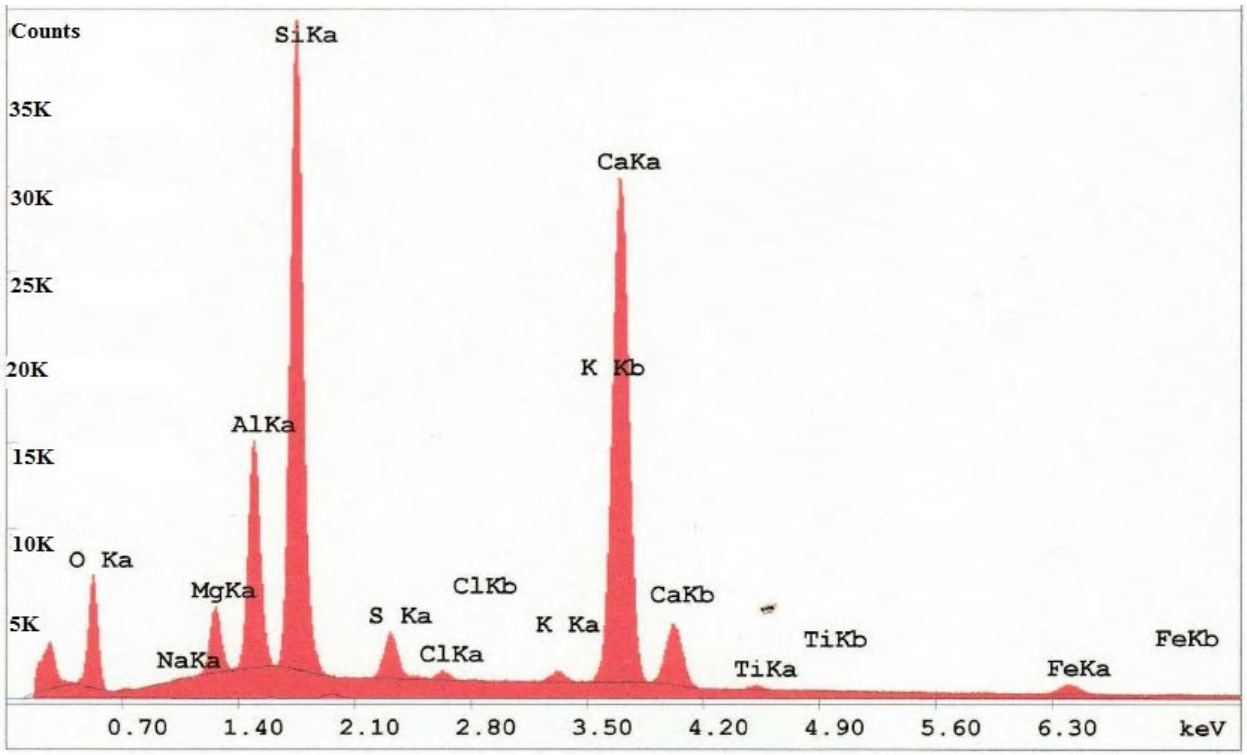

Figure 10-24: EDX Spectrum for 52Slag Paste at 7 Days

In general, the fractured surface of the A1 paste appeared to be dense (Figure 10-25 and Figure 10-26). Two C-S-H morphologies were observed: a denser one as shown in the zoomed-in view in Figure 10-26, and a less dense one as shown in Figure 10-27. It is difficult to say how they relate to the VP, OP, and IP C-S-H identified by nanoindentation. Most likely, they represent OP (Figure 10-26) and VP C-S-H (Figure 10-27). Since a fractured surface sample is obtained by breaking the paste along a plane of weakness, it is likely that the IP C-S-H may not be exposed by this method.

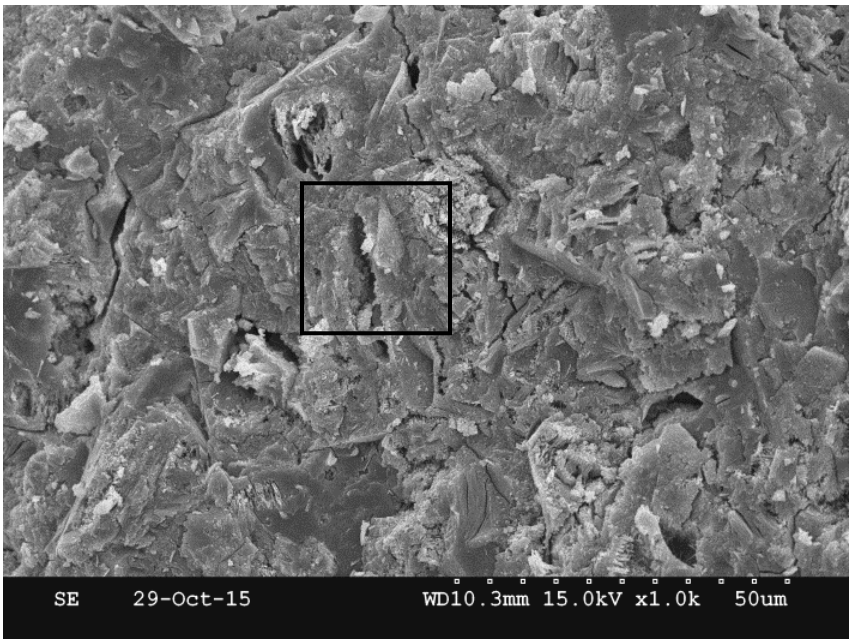

Figure 10-25: Secondary Electron Image of the A1 Sample at 7 Days, Fractured Surface

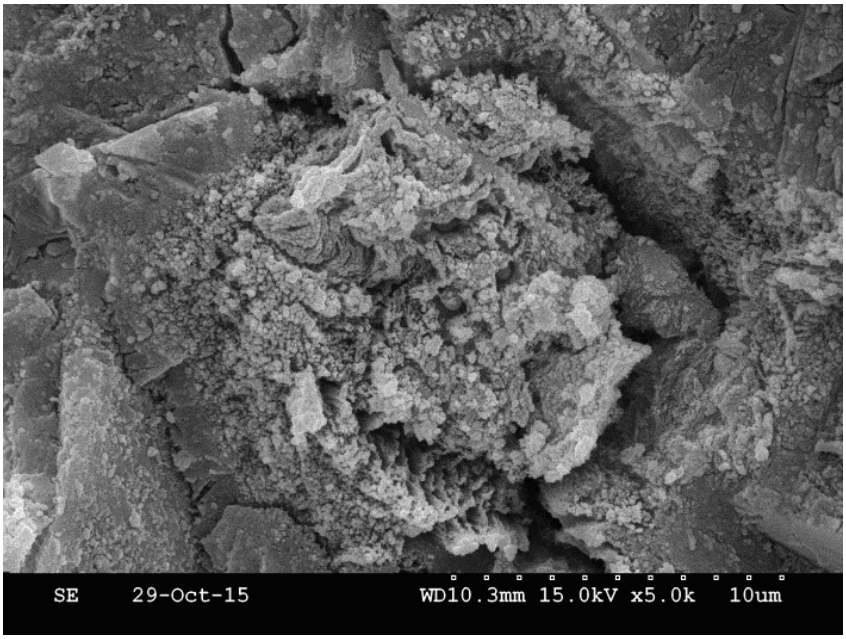

Figure 10-26: Secondary Electron Image of the A1 Sample at 7 Days, Fractured Surface, zoomed-in view of the denser C-S-H

Figure 10-27: Secondary Electron Image of the A1 Sample at 7 Days, Fractured Surface, zoomed-in view of the less dense C-S-H

The fractured surface of the 10MK+A1 sample also appeared dense, with minimal visible porosity (Figure 10-28). Mainly one type of C-S-H was observed (Figure 10-29), which corresponds well to the PDF obtained through nanoindentation (Figure 10-19), where one main peak was observed, likely corresponding to OP C-S-H.

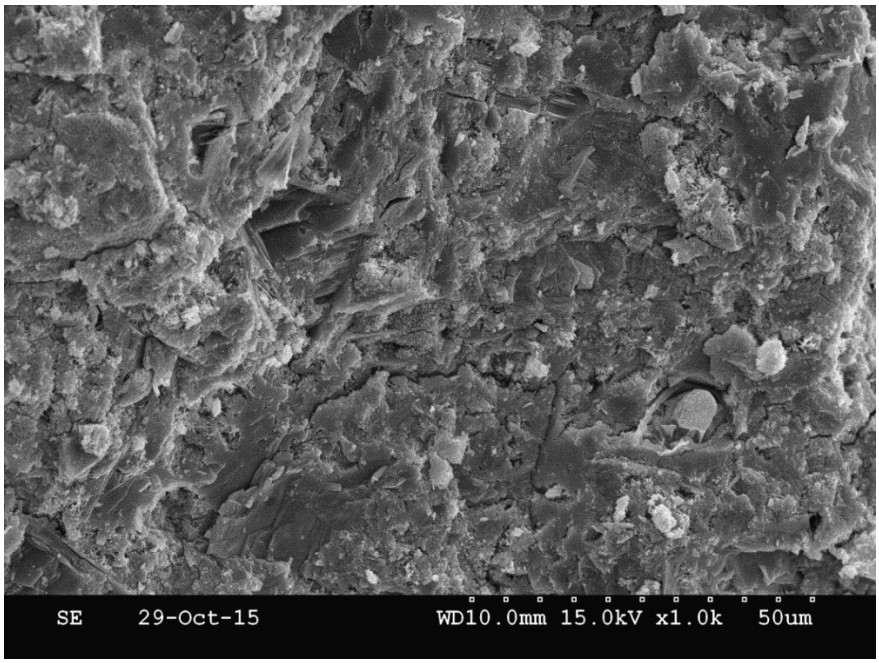

Figure 10-28: Secondary Electron Image of the 10MK+A1 Sample at 7 Days, Fractured Surface

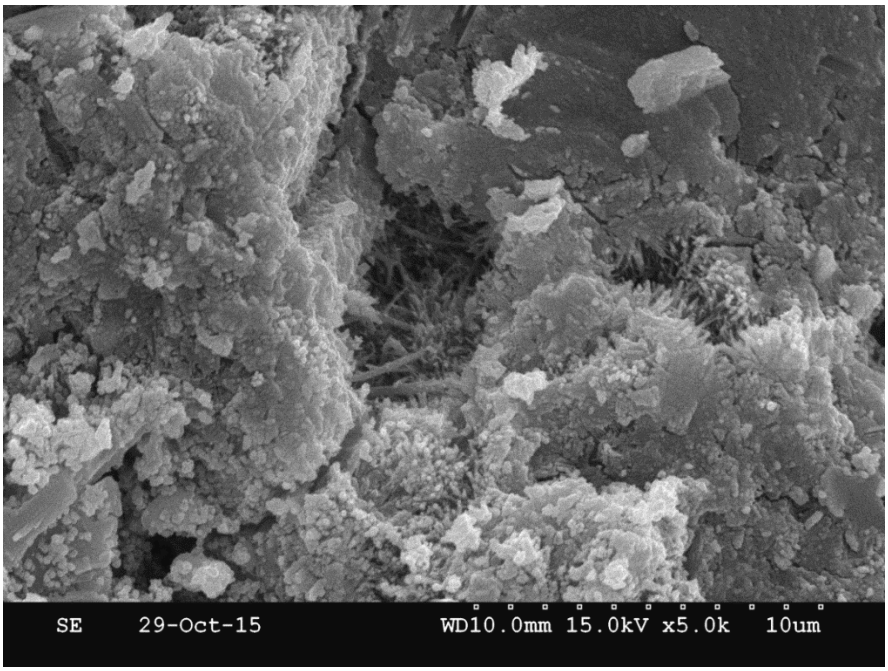

Figure 10-29: Secondary Electron Image of the 10MK+A1 Sample at 7 Days, Fractured Surface, zoomed-in view

SEM examination of the fractured surface of the 7-day paste with 52% cement replacement by slag revealed a number of unhydrated slag particles (Figure 10-30). Kumar et al. [366] showed the presence of unhydrated slag particles in 1-day pastes for mechanically activated slag. Since the slag used in this project was not activated, persistence of unhydrated slag at 7 days is not surprising. Based on isothermal calorimetry, the degree of hydration of this mixture was calculated according to Equations 10-13 and 10-14 to be equal to 0.46. Considering that all the major cement phases were almost fully hydrated (Table 10-11), this indicates that the degree of reaction of slag itself was low at 7 days. Therefore, it is not surprising that the 52% slag mixture had the lowest compressive strength at 7 days. Both fine and denser C-S-H were observed (Figure 10-31). Also, in contrast to the A1 and 10MK+A1 samples, the 52SL+A2 paste had considerable visible porosity, which would increase permeability at early ages, leading to reduced durability in sulfate environments. This porosity cannot be compared to the results of nitrogen adsorption as the pores observed in the SEM were μm-size pores and would not have been captured by nitrogen adsorption.

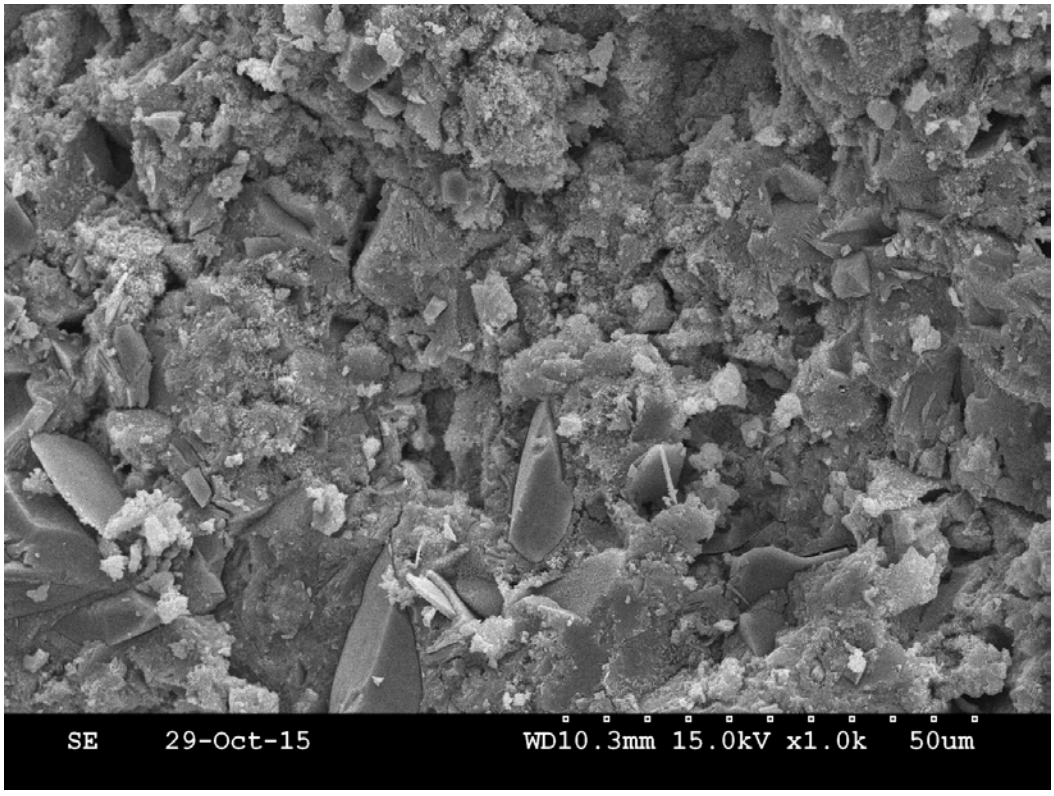

Figure 10-30: Secondary Electron Image of the 52SL+A2 Sample at 7 Days, Fractured Surface

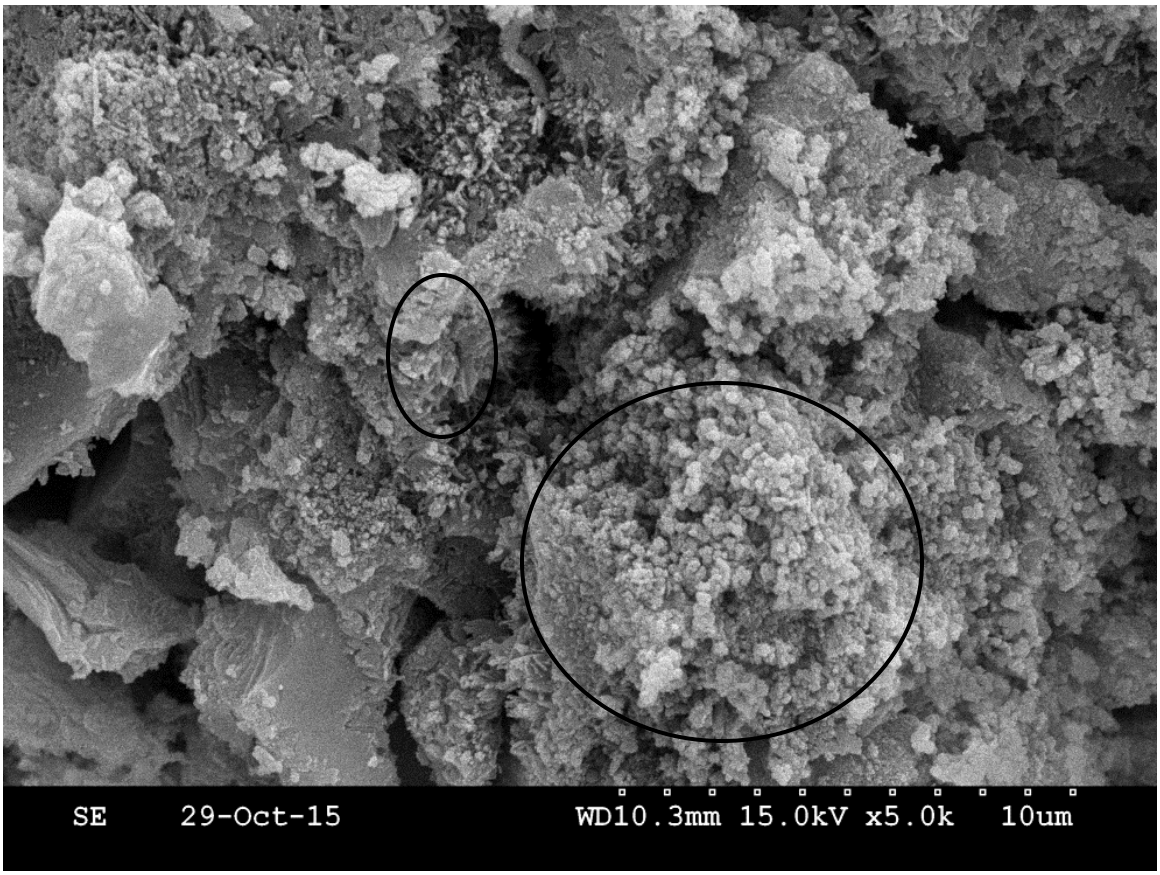

Figure 10-31: Secondary Electron Image of the 52SL+A2 Sample at 7 Days, Fractured Surface showing 2 types of C-S-H

Conclusions

Generally, addition of chemical and mineral admixtures did not change the main hydration products for mixtures cured at 23°C. No significant differences in phase consumption were observed with addition of chemical or mineral admixtures compared to the control mixture (CN), except in the case of the 52SL+A2 sample, which increased consumption of all phases beyond the age of 1 day.

Despite the similarity in phase consumption and the hydration products formed for CN and A1 samples with no mineral admixtures, nitrogen adsorption indicated an effect of superplasticizer on the morphology of the hydrated microstructure. Addition of A1 decreased SGP and LGP porosity, compared to the CN sample, with no chemical or mineral admixtures.

As for mineral admixtures, their addition generally did not have a significant effect on SGP volume. The volume of LGPs was reduced, compared to CN, by the addition of FA at low A2 dosage, and SF regardless of the chemical admixture dosage. At high WR and SP2 dosages, addition of FA resulted in a similar volume of LGPs to that of the CN paste. Addition of slag increased the volume of LGPs, while addition of MK resulted in similar LGP pore volumes to that of the CN sample; however, it was notably higher compared to the A1 sample.

Results of nanoindentation performed on 52SL+A2, 10MK+A1, and A1 samples showed good agreement with porosity results, specifically the LGP pore volume. As the LGP volume increased, the adjusted average E decreased. SEM observations confirmed the presence of different C-S-H morphologies identified by nanoindentation.

The results presented in this chapter indicate that phase quantification by QXRD of hydrated pastes may not be sufficient to assess the impact of chemical or mineral admixtures on the hydrating cementitious system. A multi-technique approach that provides information on both the amount of hydration products and their morphology is preferable.

[redacted] Effect of Chemical Admixtures Dosage on Microstructure of Cement Pastes

[redacted] Introduction

Hydrated cement paste, described as a 'nano-colloid' [367], has a high internal surface area (200 m^2/g for a D-dried mature paste measured using water vapor sorption) as a consequence of the presence of porosity contained in the nanostructure of the hydration product, C-S-H (Calcium Silicate Hydrate) [156]. The porosity and the complex pore structure of the paste spans many orders of magnitude (the classifications being listed in Table A-1) and these pore size ranges influence different properties of the paste [156]. Gas sorption techniques are used to investigate the pore structure of hydrated cement paste specimens primarily in a pore size range of 2-60 nm [368][313]. Relevant material properties affected by pore sizes in this range include drying shrinkage and creep [369].

The gas sorption procedure for studying the pore structure of porous materials is based on quantifying the volume of gas (referred to as the adsorbate) that is physically adsorbed by the porous material whilst the partial pressures of the adsorbate in the analysis cell are varied from near vacuum to 1 atm [156]. When the volume adsorbed is plotted against the relative pressure at a constant temperature, the curve that is obtained from this measurement is referred to as a sorption isotherm [156]. Various gases might be used for this purpose, but typically water vapor and nitrogen are the preferred adsorbates for cement-based systems [369]. Differences arising from the use of either of these gases as an adsorbate, which might influence the results, are discussed in section 11.1.1.

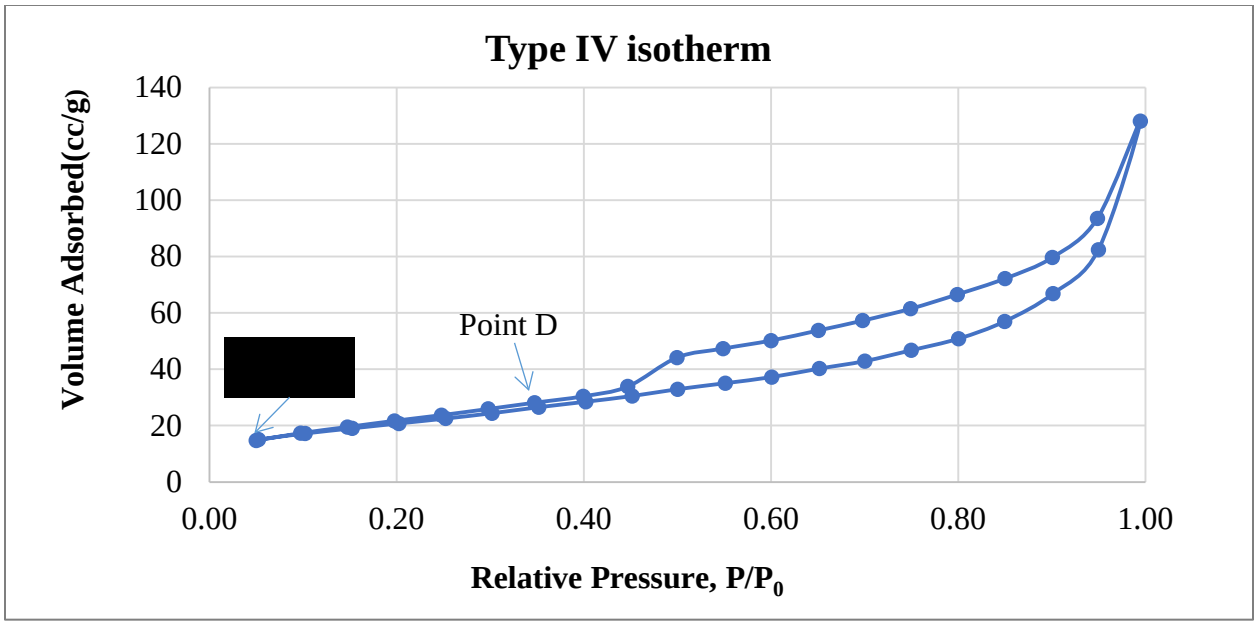

Figure 11-1: A Typical Type IV Isotherm for Cement Based Systems with Milestones

Sorption isotherms obtained from cement-based porous systems display a noticeable hysteresis, classified as a Type IV isotherm according to IUPAC (International Union of Pure and Applied Chemistry) classification [156]. The distinctive hysteresis is the result of the desorption branch not following the same path as the adsorption branch, and is characteristic of porous materials having both meso and macropores [156], which is a consequence of the presence of ink-bottle pores [370].

Points of interest in a type IV hysteresis are indicated in Figure 11-1. These include a knee (point B) which indicates the transition between the adsorption of a monomolecular layer and multilayer adsorption [156]. The start of the hysteresis and capillary condensation is indicated by point D. The BET surface area parameter gives some indication of the surface area of the nitrogen-accessible gel pores. This method is adopted for Type II and IV isotherms, which have a distinct transition from monomolecular layer to multilayer adsorption indicated by the relatively linear portion of the isotherm between partial pressures of 0.05 and 0.35 [156].

More recently, research [371] has suggested that different portions of the isotherm indicate entry of adsorbate into C-S-H with distinct textures: these being high density C-S-H up to 0.25

(P/Po), Low Density C-S-H between 0.25 and 0.8 partial pressure, and capillary porosity constituting the pore volume over 0.8 (P/Po).

BJH pore size distribution is the other parameter that could be used to discern differences induced in pore structure due to the additions of chemical admixtures and supplementary cementitious materials (SCMs). The differences are discussed in the next two sections.

BET Specific Surface Area and BJH pore size distribution determination

One of the distinctive characteristics of the microstructure of a hydrated cement paste is the relatively large internal surface area present. Given that this surface area is derived primarily from gel pores present in the main hydration product, calcium silicate hydrate (C-S-H), the value of specific surface area derived from sorption measurements is indicative of the extent of the hydration reaction at early ages; that is, for early hydration ages, the specific surface area exhibits a monotonic increase with the degree of hydration [370]. This might not be true for later-age hydration when the structure of C-S-H becomes more interwoven [370].

There have been differences in surface area values reported using different adsorbates such as water vapor and nitrogen; the obvious inference from the data being that water vapor penetrates a larger fraction of pores (or all of the porosity including some interlayer spaces) than nitrogen. This was partly attributed to the difference in sizes of the respective molecules, but others [370] suggest that the most significant factor might be the governing kinetics of "activated diffusion." Nitrogen sorption is conducted at a very low temperature (77K), whereas WV (Water Vapor) sorption is conducted at room temperature. The lower temperature impedes or prevents the movement of the adsorbate through the narrower entrances present in the pore structure.

It has been argued that BET SSA values obtained from water vapor adsorption constitutes a 'truer' surface area than that which is derived using nitrogen [369]. For the qualitative analysis of paste morphology, the focus shifts from true surface area to the ability of the method to discern differences in the features being probed [372]. Further, when experimental procedures, such as drying techniques, are the same for samples being compared, nitrogen sorption might reveal more information about induced changes in paste microstructure than other techniques [347].

An additional parameter that influences surface area measurements is the drying technique used for the samples. Porosity and surface area measurements require that the samples be dried,

and several drying techniques have been adopted to remove adsorbed water. The drying technique affects measured SSAs, with oven-dried specimens producing the lowest values and solvent-replacement (using Methanol or Isopropanol) specimens reporting the highest SSAs [373]. It is opined that oven drying at high temperatures for extended period can damage the microstructure and additionally remove some interlayer water [373]. Beaudoin [310] suggests that oven drying for 3 hours at 105°C might be a better alternative to preserve the microstructure and hence this procedure was adopted in this study. Since the surface area is also dependent on the w/c ratio, a constant w/c ratio of 0.485 was maintained in the current study.

A popular technique used to quantify specific surface area is nitrogen physisorption. The surface area analysis and pore size distribution analysis can be performed using the software such as Autosorb ASWin version 1.5x. This software uses the theory developed by Brunauer, Emmett, and Teller (BET) to measure surface area corresponding to the formation of a single monolayer of adsorbate. The assumptions of this theory being [156] [374]:

- The adsorbent has a homogenous surface
- The adsorbate molecules adsorb onto the surface in multiple layers
- At saturation, the number of layers are infinite

These and other assumptions are used to obtain the following relationship given in linear form [156]:

$$V = \frac{V_m \cdot C \cdot P}{(P_0 - P) \cdot [1 + (C-1) \cdot P / P_0]} \qquad \text{Equation 11-1}$$

Where V = volume of adsorbed gas at pressure P (m^3/g)

V_m = volume of gas adsorbed when the entire surface is covered by a monolayer (m^3/g)

C = BET constant

P = pressure (N/m^2)

P_0 = saturation vapor pressure (N/m^2)

For multipoint BET analysis, a plot of $P/ [P_0 V [1+(C-1)P/P_0]]$ and P/P_0 is obtained at relative pressures between 0.05 and 0.35, which represent the region of near complete

monomolecular layer formation. From the slope and intercept, V_m is obtained using (Equation 11-2):

$$V_m=\frac{1}{s+i} \qquad \text{Equation 11-2}$$

Where s =slope,

i =intercept

It is important to note that any negative value obtained for *C* is physically meaningless, as it would imply a repulsive force between the surface of the adsorbate and the adsorbent surface [374]. *C* is given by:

$$C=\frac{s}{i}+1 \qquad \text{Equation 11-3}$$

Once V_m is known, the specific surface area (*S*) in m^2/g can be calculated using (Equation 11-4):

$$S=\frac{V_m \cdot N_A A_m}{V_M}\cdot 10^{-20} \qquad \text{Equation 11-4}$$

Where N_A = Avogadro constant (6.023 X 10^{23} molecules/mol)

A_m = average area occupied by one molecule (m^2)

V_M = molar volume (m^3/mol)

The pore size distribution determined from the Barrett, Joyner and Halenda (BJH) method is based on the assumption that adsorbate molecules of a certain thickness form on the adsorbate molecules, and that this thickness increases with an increase in relative pressure. Earlier studies have adopted this method for pore diameters from 2 nm to 80 nm [313] and 2 nm to 60 nm [313]. The adsorption branch of the isotherm is used for all of the analyses during the course of this study because the desorption branch is likely to incorporate artifacts [375].

Preparation of specimen and testing procedure

The preparation procedure consisted of mixing the pastes listed in Table 11-1 at a w/c ratio of 0.485. The specimens were all cured for a specified period of 168 hours at room temperature, 23°C. For the samples incorporating a water reducer, the admixture was mixed with the mix water to form a solution. The mixing protocol involved mixing this solution containing the water reducer

(and air-entraining agent) with cement for about 2 minutes, followed by the delayed addition of a superplasticizer (if included in the mix design), and remixing for an additional 1 minute.

Two types of PC-based (Poly Carboxylate) superplasticizers most commonly used in Florida, SP1 and SP2, were used during the course of the study. Table 11-2 shows a comparison between the dosage of the admixture used and the maximum dosages prescribed by the manufacturer. At the end of curing, drying was accomplished by placing the samples at 105°C in an outgassing station for 3 hours under vacuum [310].

Table 11-1: Mix Designs of Specimens with Varying Chemical Admixture Types and Dosages

Mix Design	Cement (g)	AE** (g)	WR (g)	SP2(g)	SP1(g)	Water (g)
CN	40	-	-	-	-	19.40
AE (2.5 mL)+WR (174 mL)	40	0.2(2.5)	0.08(174)	-	-	19.09
AE (2.5 mL)+WR (522 mL)	40	0.2(2.5)	0.24(522)	-	-	19.09
AE (2.5 mL)+SP2 (186 mL)	40	0.2(2.5)	-	0.08(186)	-	19.09
AE (2.5 mL)+SP2 (556 mL)	40	0.2(2.5)	-	0.24(556)	-	19.09
AE (2.5 mL)+SP1 (149 mL)	40	0.2(2.5)	-	-	0.064(149)	19.09
AE (2.5 mL)+SP1 (650 mL)	40	0.2(2.5)	-	-	0.28(650)	19.09

*Parentheses Enclose the Admixture Dosages in ml/100kg of cement
**Air entraining agent is added in solution

Table 11-2: Comparative Dosage of Admixtures

Mix Design	Dosage of Admixture (ml/100kg)	*D/DMAX
AE (2.5 mL)+WR (174 mL)	174	0.27
AE (2.5 mL)+WR (522 mL)	522	0.83
AE (2.5 mL)+SP2 (186 mL)	186	0.31
AE (2.5 mL)+SP2 (556 mL)	556	0.94
AE (2.5 mL)+SP1 (149 mL)	149	0.23
AE (2.5 mL)+SP1 (650 mL)	650	1.00

*Ratio of adopted dosage to maximum manufacturer dosage

Seven different paste-admixture mixtures were used in this study, and they are listed below with their designations and descriptions:

1. CN= portland cement paste with no chemical admixtures
2. AE (2.5 mL)+WR (174 mL)= portland cement paste with a Type A/D admixture at 173.95 ml/100 kg of cement

3. AE (2.5 mL)+WR (522 mL)= portland cement paste with a Type A/D admixture at 521.79 ml/100 kg of cement
4. AE (2.5 mL)+SP2 (186 mL)= = portland cement paste with a Type F/I admixture at 185.19 ml/100 kg of cement
5. AE (2.5 mL)+SP2 (556 mL)= portland cement paste with a Type F/I admixture at 555.53 ml/100 kg of cement
6. AE (2.5 mL)+SP2 (149 mL)= portland cement paste with Type F/I admixture at 148.50 ml/100 kg of cement
7. AE (2.5 mL)+SP1 (650 mL)=portland cement paste with a Type F/I admixture at 651.74 ml/100 kg Cement

Results and Discussion

Interpretation of results

The effects of different chemical admixtures on measured SSAs are depicted in Figure 11-4. The results indicate that for the three chemical admixtures studied here, an increase in the accessible porosity was obtained with the higher dosed sample relative to the sample at the lower dosage. Further for WR and SP2, the lower dosage samples had lower surface areas relative to the control. In the instance of pastes dosed with SP1, the surface area decreased for both dosages compared to the control.

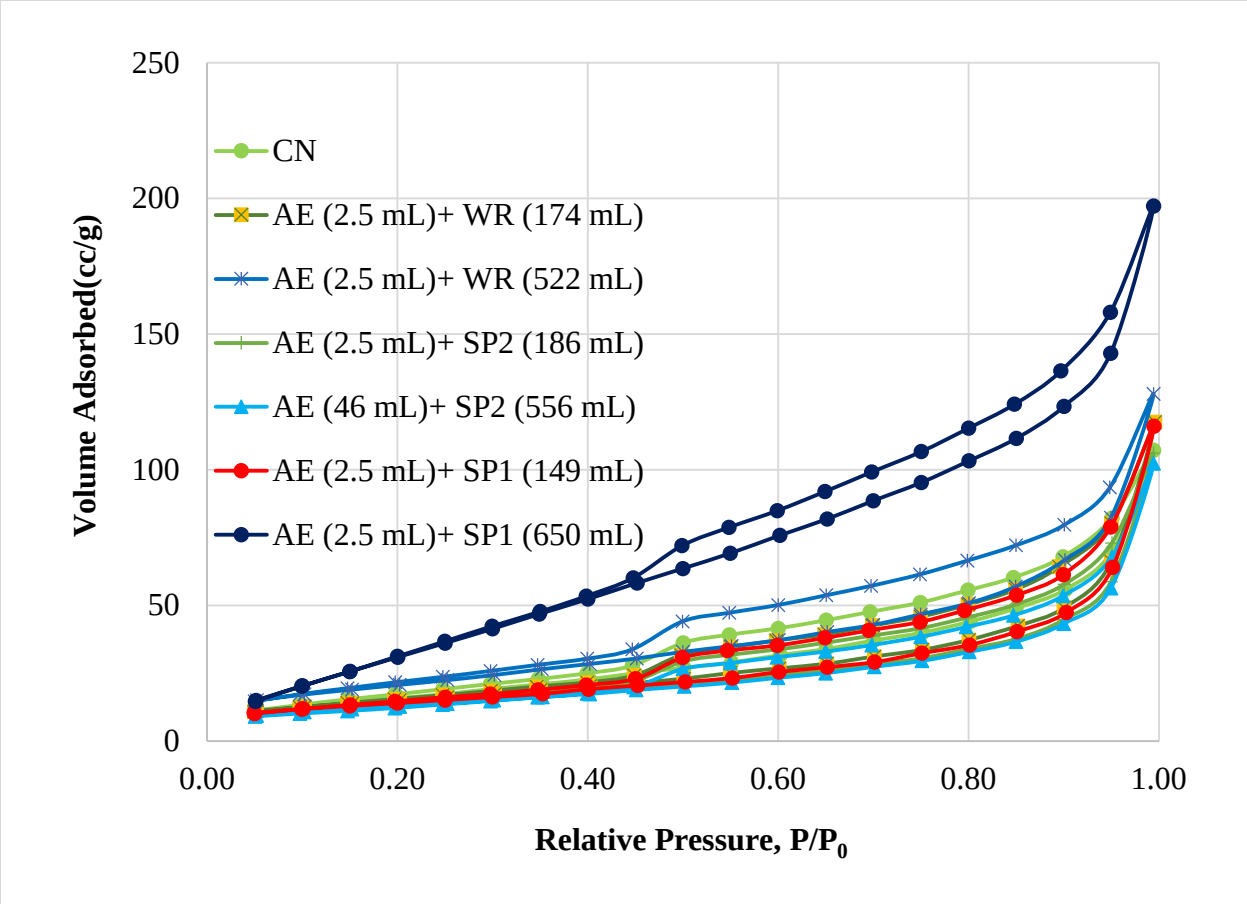

Figure 11-2: Isotherms for the 7 Pastes

The results from nitrogen sorption testing on cementitious systems from different studies reported wide variation in specific surface areas. Some causes of these inconsistencies were discussed in the previous section on BET surface area determination. As noted before, differences in pore structure of the tested pastes were likely manifested in two studied parameters: BJH pore size distributions and the BET specific surface areas. As was observed previously for nitrogen sorption, both of these parameters are expected to be a function of the accessibility of nitrogen to the gel pores in C-S-H.

The Jennings-Tennis Model (J-T) for C-S-H [376] rationalizes these experimental observations by proposing the existence of two types of C-S-H, Low Density (LD) C-S-H and High Density (HD) C-S-H, the only difference between the two products being the packing arrangement of the constituent globules [376]. While water vapor is assumed to enter all of the

pore space and some interlayer space, nitrogen is limited to, for the most part, LD C-S-H spaces [376]. The J-T model assumes that primarily LD C-S-H pores are more accessible during nitrogen adsorption experiments [313][376]. This would imply the following:

1. For pastes with the same material composition and similar degree of hydration, (Figure 11-3 and Table 11-3), differences in pore size distributions are indicative of the relative accessibility of nitrogen to C-S-H pores and, by extension, suggestive of the differences in the relative amount of accessible LD C-S-H present, and in the LD/HD C-S-H ratio [313].

Table 11-3: Degree of Hydration of Pastes

MIX DESIGN	Degree of Hydration (from calorimetry)
CN	0.772*
AE (2.5 mL)+WR (174 mL)	0.779
AE (2.5 mL)+WR (522 mL)	0.794
AE (2.5 mL)+SP2 (186 mL)	0.801
AE (2.5 mL)+SP2 (556 mL)	0.798
AE (2.5 mL)+SP1 (149 mL)	0.788
AE (2.5 mL)+SP1 (650 mL)	0.790

*estimated using XRD and isothermal calorimetry Data (Appendix A)

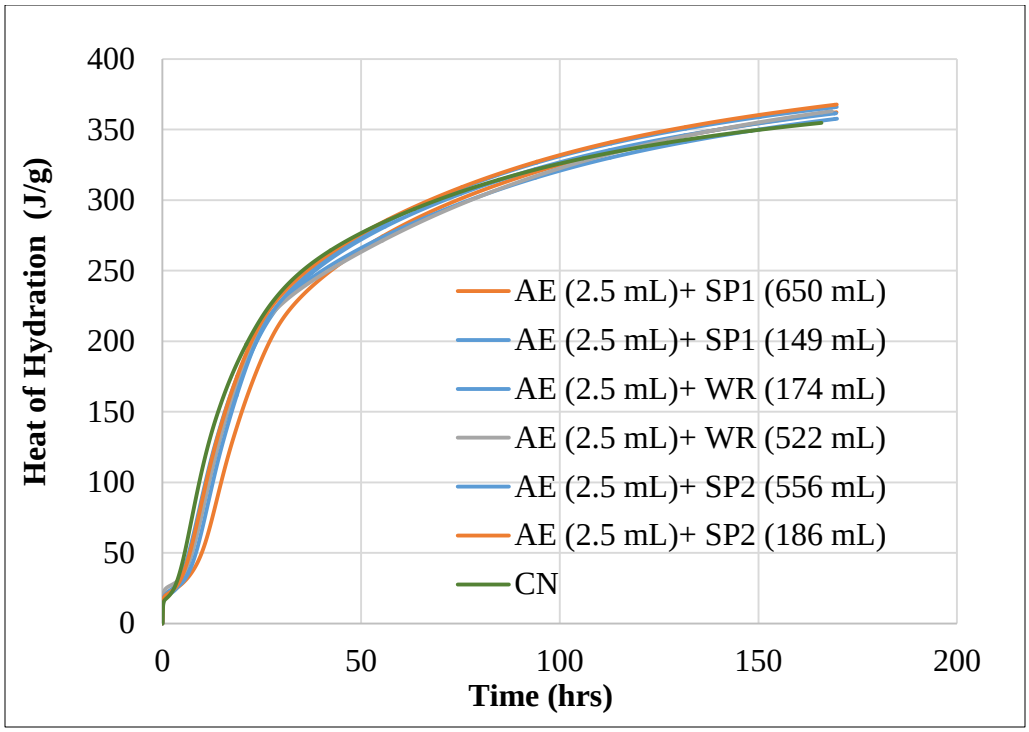

Figure 11-3: Heat of Hydration Curves for Pastes at 23°C at 7 Days

2. Following from (1), it becomes important to determine the degree of hydration in the analysis in order to verify whether the values of the determined parameters (BET surface area and BJH PSD) represent a difference in aging or differences in the intrinsic pore structure. This determination is done using both isothermal calorimetry and data from quantitative XRD for anhydrous phases. The method is described briefly in the section A.1 titled “Determination of degree of hydration.”

Table 11-4 shows the BET surface area obtained for the tested pastes. The results are arranged in the order of decreasing surface area. For a particular paste under study, an increase in the surface area would appear to suggest a monotonic increase in the degree of hydration. BET surface areas measured using nitrogen sorption are indicative of the amount of hydration product formed. C-S-H typically accounts for over 90% of this measured product [369]. This trend can be indicated by porosity contained in the specified sizes; that is, those that are of the same order of magnitude as the gel pores. These and other implications of changes in the pore structure of C-S-H are discussed in 11.3.2.

Table 11-4: BET Surface Area for Pastes incorporating Chemical Admixtures

Mixture ID	BET Surface Area(m^2/g)
AE (2.5 mL)+SP1 (650 mL)	153.70
AE (2.5 mL)+WR (522 mL)	76.69
CN	61.44
AE (2.5 mL)+WR (174 mL)	54.29
AE (2.5 mL)+SP1 (149 mL)	50.32
AE (2.5 mL)+SP2 (186 mL)	49.36
AE (2.5 mL)+SP2 (556 mL)	47.00

The pore size distribution plots obtained for each admixture (low and high dosage) are compared with the control sample in Figure 11-4 to Figure 11-6. The results indicate that for these 3 admixtures, an increase in the accessible porosity was obtained with the higher dosed sample relative to the sample at lower dosage. Further for WR and SP1, the lower dosage samples had lower surface areas, and the PSD curves shifted downward relative to the control. In the instance of pastes dosed with SP2, both the surface areas decreased and the PSD curve was lower than the control.

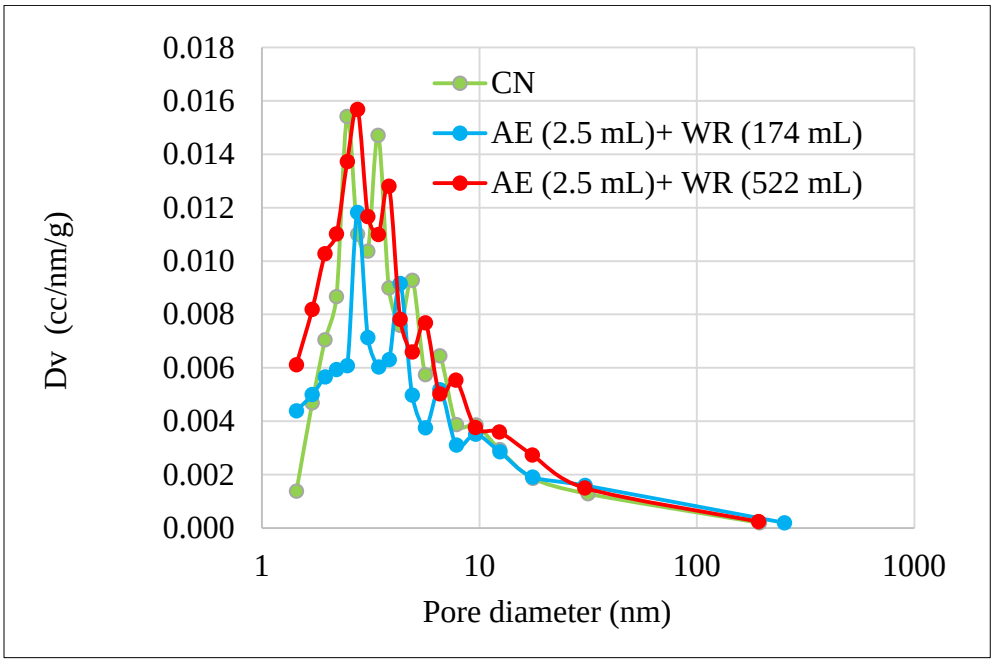

Figure 11-4: Pore Size Distribution Comparison for AE (2.5 mL)+WR (174 mL), AE (2.5 mL)+WR (522 mL), and Control

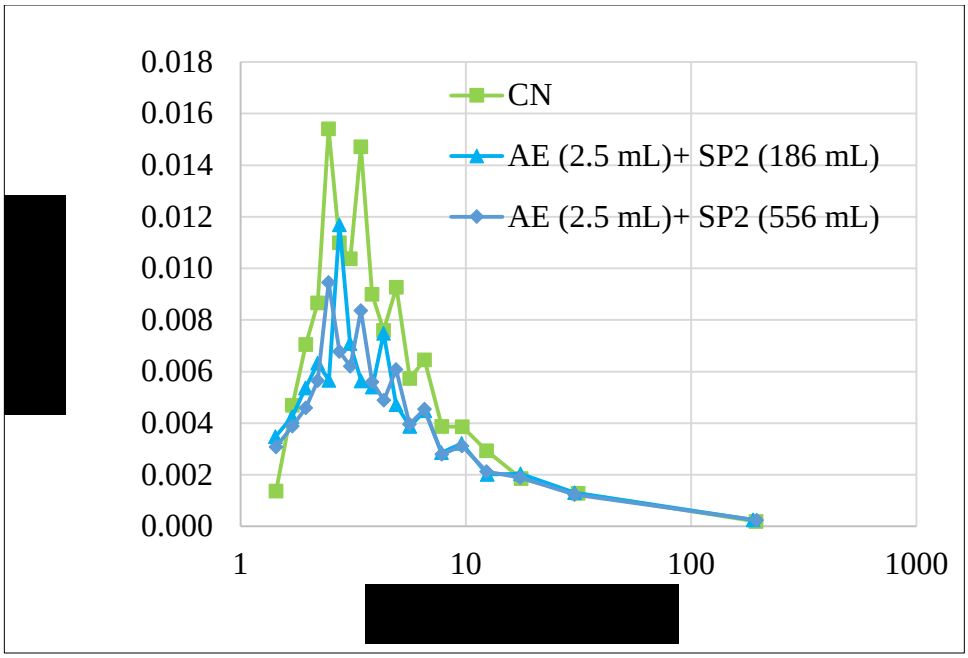

Figure 11-5: Pore Size Distribution Comparison for AE (2.5 mL)+SP2 (186 mL), AE (2.5 mL)+SP2 (556 mL), and Control

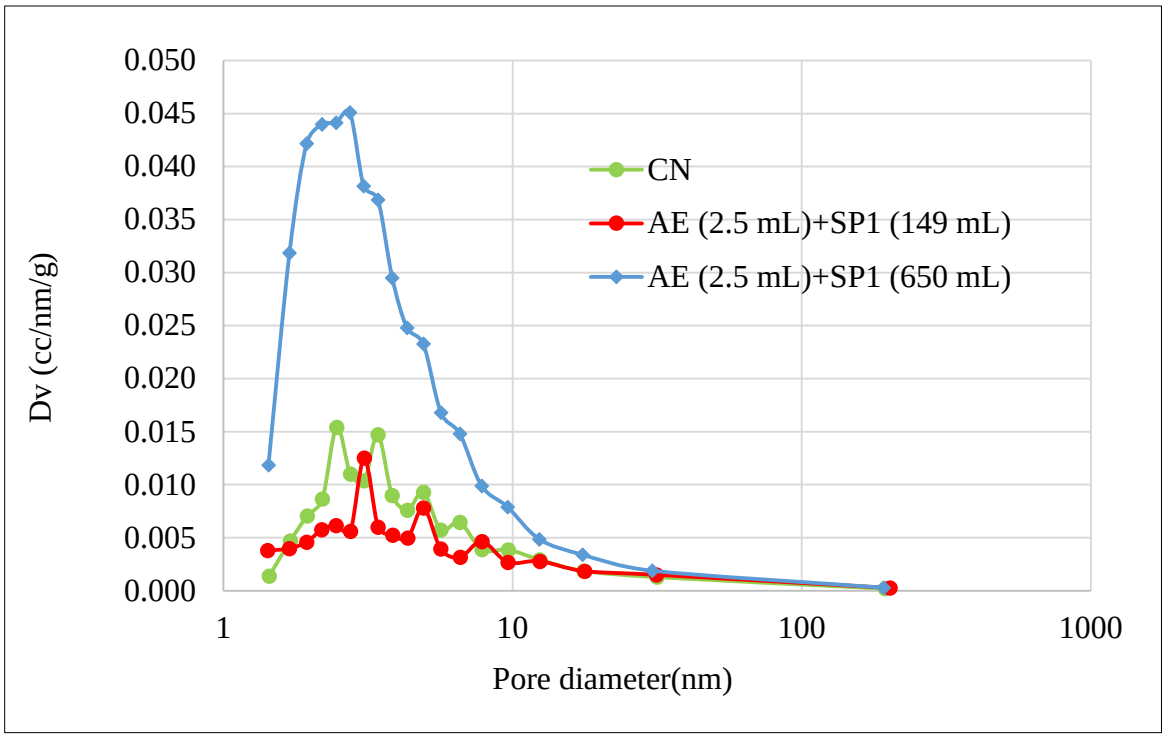

Figure 11-6: Pore Size Distribution Comparison for AE (2.5 mL)+SP1 (149 mL), AE (2.5 mL)+SP1 (650 mL), and Control

Possible effects of admixture additions on properties

Since the calorimetry testing indicated that the pastes at each dosage had similar degrees of hydration (Table 11-3), their differences in pore size distributions can be attributed to the morphology of the hydration product. The implications of the following observations are discussed in the following paragraphs.

Researchers divide the shrinkage obtained on drying a sample from RH 100% to 11% (as a part of the standard drying procedure [376]) into reversible and irreversible components [313]. The irreversible component is that which is not recovered on rehydration [347] after drying. The irreversible shrinkage occurs for the most part on drying between RH of 100 and 40% [377]. It is the component of drying that appears to exhibit a dependence on the amount of LD C-S-H present in the system [313] [347] [377].

Multiple studies [347], [377], [378] have hinted to a correlation between the specific surface area and the irreversible drying shrinkage component. Furthermore, these studies also point to a relationship between irreversible drying shrinkage and the fraction of porosity contained in the mesopore range; that is, in the range of 2-50 nm. This observation is supported by Garci [378] who found that the addition of sugar as a retarder, whilst increasing the SSA, did not appear to manifest in higher drying shrinkage than the corresponding control sample. Thus a higher surface area, which is indicative of higher access to C-S-H pores in the mesopore spectrum [347] [377], may be indicative of susceptibility to drying shrinkage. In this study, both these trends appear to occur simultaneously, indicating the likely dependence of both on the amount of LD C-S-H present. Thus it could be concluded that pastes AE (2.5 mL)+SP1 (650 mL) and AE (2.5 mL)+WR (522 mL) were more susceptible to dimensional change, when subjected to low humidities, than the other pastes in this series, since they both appear to have more porosity in the mesopore range [347]. The mesopore fractions, for pastes tested in this study, are shown in Table 11-5.

Table 11-5: Fraction of Porosity in the Mesopore Range for Pastes

MIX	Fraction of Mesoporosity (2-50nm)
CN	0.1226
AE (2.5 mL)+WR (174 mL)	0.1147
AE (2.5 mL)+WR (522 mL)	0.1428
AE (2.5 mL)+SP2 (186 mL)	0.1016
AE (2.5 mL)+SP2 (556 mL)	0.1045
AE (2.5 mL)+SP1 (149 mL)	0.0893
AE (2.5 mL)+SP1 (650 mL)	0.2801

The packing density has been found to have an effect on the creep modulus, as observed from nanoindentation testing conducted on cement pastes in previous studies [379]. C-S-H pastes with a higher fraction of HD C-S-H could have a higher creep modulus [379] and exhibit a lower creep strain. Thus cement pastes with higher fractions of LD C-S-H might be more susceptible to creep strain than corresponding pastes, at the same degree of hydration, since a higher HD C-S-H fraction increases the fraction of the restraining phase.

Conclusion

Nitrogen sorption was conducted in order to investigate the effect of chemical admixtures on the microstructure and morphology of 7 cement pastes dosed with variable dosages of 3 different chemical admixtures. For confirmation of the extent of reaction at 7 days, results from quantitative XRD and isothermal calorimetry (Figure 11-3) were used. Since the degrees of hydration of the high- and low-dosage specimens were found to be similar, the changes in pore size distribution, accessible surface area, and pore volume contained in various fractions could be attributed to the effects of admixture type and dosage. The use of chemical admixtures was found to affect the pore size distributions and the microstructure of the tested pastes. In some instances (as in the case of SP1-7X) the effect was quite remarkable. At high dosages, the effect of admixture addition on the pore size distribution manifested in an increase in the surface area and the fraction of pores in the mesopore range. Applying the rationale from the Jennings-Tennis model [372], if this effect can be seen at similar degrees of hydration between specimens, then this could be

interpreted as indicating an increase in the amount of Low Density C-S-H, which could possibly have consequences for the shrinkage and creep behavior of the paste. The use of SP2, however, was found to have the opposite effect, although conclusive verification of this effect requires further testing.

Summary, Conclusions, and Recommendations

Based on the research conducted in this study, the following can be concluded:

1. Based on the observed heat flow and total heat trends using isothermal calorimetry, it can be concluded that addition of FA or SL results in a slight retardation of the main hydration peak, which indicates a possible delay in setting time with cement replacement by FA or SL. This finding was also confirmed by setting time measurements on cement pastes. No delay in setting time is noted with additions of SF or MK. Setting time measurements on pastes indicate that SF had similar setting behavior to CN, while 10MK had a slightly shorter setting time. Since both SL and MK shifted the sulfate depletion point and increased the magnitude of the aluminate peak, these mixtures may become undersulfated at higher temperatures or in combination with other mineral or chemical admixtures that also accelerate sulfate depletion.

2. From the heat flow measurements, the slope of the total heat curve, beyond 6 days, was highest for MK and SL mixtures, it is therefore expected that their contribution to heat generation will continue to rise beyond 7 days. This, together with the increase in the aluminate reaction with slag and MK addition, can lead to higher temperatures in concrete mixtures under adiabatic conditions.

3. The compressive strength was lowest for the 52SL mixture at all ages up to 7 days, and highest for the control mixture. The 10MK sample had about the same compressive strength at 7 days as the control. While the 10MK and 8SF mixtures had about the same 1-day strength, the 10MK mixture strength was higher after 24 hours and its compressive strength exceeded that of the 8SF mix at 7 days. The strength of the 21FA mixture was between that of the 52Slag and control mixtures at 1 day, and only slightly higher than that of the 52SL by 7 days.

4. Addition of chemical admixtures is likely to result in setting time delays as indicated by initial retardation of cement hydration. The largest setting time retardation was with SP1 addition and the addition of AE resulted in no retardation. WR, SP1, and SP2 affected the sulfate depletion point; combining WR, SP1 or SP2 with SL or MK can further upset the sulfate balance, causing an increase in the temperature sensitivity of the hydrating system. It should be noted that trends obtained from internal and external mixing were not always the same, especially in the case of chemical admixtures. Therefore, caution should be taken with respect to drawing conclusions on concrete compressive strength from isothermal calorimetry tests.

5. The use of factorial design was successful in identifying admixture combinations that have a non-additive effect on heat evolution. Separate tests on ternary combinations confirmed the interaction of fly ash and slag, fly ash and metakaolin, fly ash and silica fume, slag and metakaolin, and fly ash and WR.

6. In general, incorporation of metakaolin, at a replacement level of 10%, results in the highest 7-day compressive strength among all mixtures studied here. Additionally at 10% replacement level, FA and SF had similar setting time to the control paste while incorporating slag increased the setting time. Metakaolin had the opposite effect of decreasing the setting time when compared to the control mixture.

7. The effect of increasing the superplasticizer dosage, within the range studied here, showed modest increase in setting time of mortar (retardation) for all binary mixtures and the control. The effect was not as pronounced for the control and FA mixtures. As for strength evolution, increasing superplasticizer dosage increased the 28-day strength for all binary mixtures. However, early-age strength measurements showed variation depending on the binary system studied. For example, the control mixture showed an increase in 1 and 7-day strength while for 10SF and 21FA, the 1- and 7-day strength was not improved by increasing SP dosage.

8. Sulfate durability studies on binary and ternary mixtures indicate that silica fume outperformed all mixtures studied here. While all mixtures showed expansion at 0.10% or below at 180 days of exposure to 5 w/o sodium sulfate solution, using high alumina slag (14.35%) did not offer any beneficial contribution towards enhancing the sulfate durability of cementitious mixtures using a Type I/II portland cement.

9. Semi-adiabatic calorimetry was used together with hydration parameters for several binary systems to predict the temperature rise in a 1 m^3 wall. The findings indicate that adiabatic temperature rise was highest for the binary slag system at 52SL. The lowest adiabatic temperature rise was for 21FA binary system. Semi-adiabatic calorimetry testing of several concrete mixtures incorporating silica fume, blast furnace slag, and Class F fly ash indicate that SL delays setting and strength evolution and generates the highest adiabatic temperature rise. Modeling concrete temperatures and imposing the modeled temperature profiles during testing in the cracking frame identified the higher cracking risk of silica fume mixtures and the need to further study blast

furnace slag mixtures with additional measurements to identify effects of variable slag composition on cracking potential.

10. Generally, addition of chemical and mineral admixtures did not change the main hydration products for mixtures cured at 23C. However, nitrogen adsorption indicates an effect of superplasticizer on the morphology of the hydrated microstructure; additions of SP1 decreased SGP and LGP porosity at low dosage and compared to the control mixture with no chemical and mineral admixtures. Increasing SP1 dosage, to the upper range of the recommended manufacturer dosage, results in an increase in the pores fraction in the mesopore range. The same effect was noted for higher dosages of WR admixture. For mineral admixtures, additions of slag increased the volume of LGPs while FA and SF reduced it.

11. Results from nanoindentation measurements performed on 52Slag, 10MK, and SP1 samples show good agreement with porosity results, specifically LGP pore volume; as the LGP volume increased, the adjusted average E decreased. SEM observations confirmed the presence of different C-S-H morphologies identified by nanoindentation.

12. The findings indicate that studying phase content of the hydration products by QXRD may not be sufficient to assess the impact of chemical or mineral admixtures on the hydrating cementitious system and a multi-technique approach that provides information on not only the amount of hydration products but also their morphology is preferable.

13. Scanning electron microscopy measurements indicate that C-S-H in 10 MK has higher alumina content than 52SL. This is not surprising as MK has higher alumina content.

14. Plastic viscosity of fresh pastes is largely unaffected by addition of mineral admixtures, but is reduced by chemical admixtures. The yield stress, on the other hand, is affected by both mineral and chemical admixtures. Chemical admixtures consistently reduced yield stress, while additions of mineral admixtures had a variable effect. In the absence of chemical admixtures, yield stress was increased by addition of mineral admixtures with particle sizes finer than that of cement (SF, MK), while admixtures with similar particle sizes to cement (SL and FA) did not have a significant effect. Addition of fly ash reduced yield stresses in the mixtures containing metakaolin or silica fume, while it had no effect on the yield stress of cement-slag mixtures.

Recommendations for future work:

1. Initiate a study to identify the limit of alumina content in slag cement that renders concrete mixtures durable in an aggressive sulfate environment.
2. Assess the effect of slag chemical composition on the cracking potential in concrete mixtures for mass structural applications.

References

[1] F. Jackson, “The durability of concrete in service,” *ACI J. Proc.*, vol. 43, no. 165, pp. 165–180, 1946.

[2] ASTM C125-15b, “Standard Terminology Relating to Concrete and Concrete Aggregates,” *ASTM Int.*, pp. 1–8, 2015.

[3] L. Tuthill, R. Adams, S. N. Bailey, and R. W. Smith, “A case of abnormally slow hardening concrete for tunnel lining,” *J. Am. Concr. Inst.*, vol. 57, pp. 1091–1110, 1961.

[4] L. Roberts and P. Taylor, “Understanding Cement-SCM-Admixture Interaction Issues,” *Concr. Int.*, vol. 29, no. 01, pp. 33–41, 2007.

[5] J. W. Bullard, H. M. Jennings, R. A. Livingston, A. Nonat, G. W. Scherer, J. S. Schweitzer, K. L. Scrivener, and J. J. Thomas, “Mechanisms of cement hydration,” *Cem. Concr. Res.*, vol. 41, no. 12, pp. 1208–1223, 2011.

[6] K. L. Scrivener, P. Juilland, and P. J. M. Monteiro, “Advances in understanding hydration of Portland cement,” *Cem. Concr. Res.*, vol. 78, pp. 38–56, 2015.

[7] C. Jolicoeur and M.-A. Simard, “Chemical admixture-cement interactions: Phenomenology and physico-chemical concepts,” *Cem. Concr. Compos.*, vol. 20, no. 2–3, pp. 87–101, Jan. 1998.

[8] I. Odler, “Hydration, Setting and Hardening of Portland Cement,” in *Lea’s Chemistry of Cement and Concrete*, 4th ed., P. C. Hewlett, Ed. New York, NY: Arnold, 1998, pp. 241–297.

[9] W. Lerch, “The influence of gypsum on the hydration and properties of Portland cement pastes,” 1946.

[10] C. Bedard and N. Mailvaganam, “The Use of Chemical Admixtures in Concrete. Part I: Admixture-Cement Compatibility,” *J. Perform. Constr. Facil.*, vol. 19, no. 4, pp. 263–267, 2005.

[11] L. Meyer and W. Perenchio, “Theory of Concrete Slump Loss Related to the Use of Chemical Admixtures,” *Concr. Int.*, vol. 1, no. 1, pp. 36–63, 1979.

[12] J. Cheung, a. Jeknavorian, L. Roberts, and D. Silva, “Impact of admixtures on the hydration kinetics of Portland cement,” *Cem. Concr. Res.*, vol. 41, no. 12, pp. 1289–1309, Dec. 2011.

[13] T. Chappex, “The role of aluminium from supplementary cementitious materials in controlling alkali-silica reaction,” Ecole Polytechnique Federale De Lausanne, 2012.

[14] B. R. Bickmore, K. L. Nagy, A. K. Gray, and a. R. Brinkerhoff, “The effect of $Al(OH)_4^-$ on the dissolution rate of quartz,” *Geochim. Cosmochim. Acta*, vol. 70, no. 2, pp. 290–305, Jan. 2006.

[15] G. Azimi, V. G. Papangelakis, and J. E. Dutrizac, “Modelling of calcium sulphate solubility in concentrated multi-component sulphate solutions,” *Fluid Phase Equilib.*, vol. 260, no. 2, pp. 300–315, Nov. 2007.

[16] S. Mindess, J. F. Young, and D. Darwin, *Concrete*, 2nd ed. Upper Saddle River, NJ: Prentice Hall, 2003.

[17] ASTM C494 / C494M-15a, “Standard Specification for Chemical Admixtures for Concrete,” West Conshohocken, PA: ASTM International, 2015.

[18] ASTM Standard C260/C260M 2010a, “Standard Specification for Air-Entraining Admixtures for Concrete,” West Conshohocken, PA: ASTM International, 2010.

[19] P. K. Mehta and P. J. M. Monteiro, *Concrete: Microstructure, Properties and Materials*, 3rd ed. New York, NY: McGraw-Hill, 2006.

[20] W. L. Dolch, “Air-Entraining Admixtures,” in *Concrete Admixtures Handbook: Properties, Science and Technology*, 2nd ed., V. S. Ramachandran, Ed. Park Ridge, NJ: Noyes Publications, 1995, pp. 518–557.

[21] T. Zhang, S. Shang, F. Yin, A. Aishah, A. Salmiah, and T. Ooi, “Adsorptive behavior of surfactants on surface of Portland cement,” *Cem. Concr. Res.*, vol. 31, no. 7, pp. 1009–1015, Jul. 2001.

[22] F. Merlin, H. Guitouni, H. Mouhoubi, S. Mariot, F. Vallée, and H. Van Damme, “Adsorption and heterocoagulation of nonionic surfactants and latex particles on cement hydrates.,” *J. Colloid Interface Sci.*, vol. 281, no. 1, pp. 1–10, Jan. 2005.

[23] H. Uchikawa, S. Hanehara, T. Shirasaka, and D. Sawaki, “Effect of admixture on hydration of cement, adsorptive behavior of admixture and fluidity and setting of fresh cement paste,” *Cem. Concr. Res.*, vol. 22, no. 6, pp. 1115–1129, 1992.

[24] J. Plank and C. Winter, “Competitive adsorption between superplasticizer and retarder molecules on mineral binder surface,” *Cem. Concr. Res.*, vol. 38, no. 5, pp. 599–605, May 2008.

[25] D. Bentz, “Curing with shrinkage-reducing admixtures,” *Concr. Int.*, vol. 27, no. 10, pp. 55–60, 2005.

[26] K. Folliard and N. Berke, “Properties of high-performance concrete containing shrinkage-reducing admixture,” *Cem. Concr. Res.*, vol. 27, no. 9, pp. 1357–1364, 1997.

[27] G. Sant, “The Influence of Temperature on Autogenous Volume Changes in Cementitious Materials Containing Shrinkage Reducing Admixtures,” *Cem. Concr. Compos.*, vol. 34, no. 7, pp. 855–865, Aug. 2012.

[28] R. Rixom and N. Mailvaganam, *Chemical Admixtures for Concrete*, 3rd ed. New York, NY: Routledge, 1999.

[29] ACI Committee 231, *ACI 231R-10: Early-Age Cracking: Causes, Measurement, and Mitigation*. Farmington Hills, MI: American Concrete Institute, 2010.

[30] F. Rajabipour, G. Sant, and J. Weiss, “Interactions between shrinkage reducing admixtures (SRA) and cement paste’s pore solution,” *Cem. Concr. Res.*, vol. 38, no. 5, pp. 606–615, May 2008.

[31] D. P. Bentz, “A review of early-age properties of cement-based materials,” *Cem. Concr. Res.*, vol. 38, no. 2, pp. 196–204, Feb. 2008.

[32] D. P. Bentz, M. R. Geiker, and K. K. Hansen, “Shrinkage-reducing admixtures and early-age desiccation in cement pastes and mortars,” *Cem. Concr. Res.*, vol. 31, no. 7, pp. 1075–1085, Jul. 2001.

[33] D. Bentz, K. Hansen, H. Madsen, F. Vallée, and E. Griesel, “Drying/Hydration in Cement Pastes during Curing,” *Mater. Struct.*, vol. 34, pp. 557–565, 2001.

[34] R. Valckenborg, L. Pel, K. Hazrati, K. Kopinga, and J. Marchand, “Pore water distribution in mortar during drying as determined by NMR,” *Mater. Struct.*, vol. 34, pp. 599–604, 2001.

[35] G. Sant, B. Lothenbach, P. Juilland, G. Le Saout, J. Weiss, and K. Scrivener, “The origin of early age expansions induced in cementitious materials containing shrinkage reducing admixtures,” *Cem. Concr. Res.*, vol. 41, no. 3, pp. 218–229, Mar. 2011.

[36] J. Brooks, M. Johari, and M. Mazloom, “Effect of admixtures on the setting times of high-strength concrete,” *Cem. Concr. Compos.*, vol. 22, no. 4, pp. 293–301, 2000.

[37] S. Hanehara and K. Yamada, “Interaction between Cement and Chemical Admixture from the Point of Cement Hydration, Absorption Behaviour of Admixture, and Paste Rheology,” *Cem. Concr. Res.*, vol. 29, no. 8, pp. 1159–1165, Aug. 1999.

[38] T. R. Naik, Y. Chun, and R. N. Kraus, “Reducing Shrinkage Cracking of Structural Concrete Through the Use of Admixtures,” Madison, WI, 2006.

[39] A. B. Ribeiro, A. Gonçalves, and A. Carrajola, “Effect of Shrinkage Reduction Admixtures on the Pore Structure Properties of Mortars,” *Mater. Struct.*, vol. 39, no. 2, pp. 179–187, Apr. 2006.

[40] G. Sant, A. Eberhardt, D. Bentz, and J. Weiss, “Influence of Shrinkage-Reducing Admixtures on Moisture Absorption in Cementitious Materials at Early Ages,” *J. Mater. Civ. Eng.*, vol. 22, no. 3, pp. 277–287, 2010.

[41] T. Mohammed and H. Hamada, “Durability of Concrete Made with Different Water-Reducing Chemical Admixtures in Tidal Environment,” *ACI Mater. J.*, vol. 100, no. 3, pp. 194–202, 2003.

[42] M. A. Nagi, P. A. Okamoto, R. L. Kozikowski, and K. Hover, “Evaluating Air-Entraining Admixtures for Highway Concrete, NCHRP Report 578,” Transportation Research Board, Washington, D.C., 2007.

[43] R. M. Edmeades and P. C. Hewlett, “Cement Admixtures,” in *Lea’s Chemistry of Cement and Concrete*, 4th ed., P. C. Hewlett, Ed. New York, NY, 1998, pp. 837–901.

[44] A. M. Neville, *Properties of Concrete*, 4th ed. Harlow, England: Pearson Education

Limited, 2006.

[45] L. Du and K. J. Folliard, “Mechanisms of Air Entrainment in Concrete,” *Cem. Concr. Res.*, vol. 35, no. 8, pp. 1463–1471, Aug. 2005.

[46] C. Bedard and N. Mailvaganam, “The Use of Chemical Admixtures in Concrete. Part II: Admixture-Admixture Compatibility and Practical Problems,” *J. Perform. Constr. Facil.*, vol. 20, no. 1, pp. 2–6, 2006.

[47] ACI Committee 212, *ACI 212.3R-91: Chemical Admixtures for Concrete*. Detroit, MI: American Concrete Institute, 1991.

[48] B. S. H. Gebler and P. Klieger, “Effect of Fly Ash on the Air-Void Stability of Concrete,” *ACI Spec. Publ.*, vol. 79, pp. 103–142, 1983.

[49] ASTM C 125, “Standard Terminology Relating to Concrete and Concrete Aggregates,” in *Annual Book of ASTM Standards, V. 04.02*, ASTM International, 2011.

[50] T. J. VanDam, K. R. Peterson, L. L. Sutter, A. Panguluri, and J. Sytsma, “Guidelines for Early-Opening to Traffic Portland Cement Concrete for Pavement Rehabilitation, NCHRP Report 540,” Washington, DC, 2005.

[51] D. Ravina and I. Soroka, “Research on Concrete in Hot Environments at the National Building Research Institute, Haifa, Israel,” *Spec. Publ.*, vol. 139, pp. 107–130, 1993.

[52] P. Sandberg and L. Roberts, “Studies of cement-admixture interactions related to aluminate hydration control by isothermal calorimetry,” in *Seventh CANMET/ACI International Conference on Superplasticizers and Other Chemical Admixtures in Concrete*, 2003, pp. 529–542.

[53] H. Wang, C. Qi, H. Farzam, and J. I. M. Turici, “Interaction of Materials Used in Concrete,” *Concr. Int.*, vol. 28, no. 4, pp. 47–52, 2006.

[54] V. Ramachandran, “Accelerators,” in *Concrete Admixtures Handbook: Properties, Science and Technology*, 2nd ed., V. Ramachandran, Ed. Park Ridge, NJ: Noyes Publications, 1995, pp. 185–285.

[55] M. C. G. Juenger, P. J. M. Monteiro, E. M. Gartner, and G. P. Denbeaux, “A Soft X-ray

Microscope Investigation into the Effects of Calcium Chloride on Tricalcium Silicate Hydration," *Cem. Concr. Res.*, vol. 35, no. 1, pp. 19–25, Jan. 2005.

[56] J. Thomas, A. Allen, and H. Jennings, "Hydration kinetics and microstructure development of normal and $CaCl_2$-accelerated tricalcium silicate pastes," *J. Phys. Chem.*, vol. 113, no. 46, pp. 19836–19844, 2009.

[57] J. J. Shideler, "Calcium Chloride in Concrete," in *ACI Annual Convention*, 1952, no. 48, pp. 537–559.

[58] B. Hope and D. Manning, "Creep of Concrete Influenced by Accelerators," *ACI J. Proc.*, vol. 68, no. 5, pp. 361–365, 1971.

[59] S. Sohoni, R. Sridhar, and G. Mandal, "The Effect of Grinding Aids on the Fine Grinding of Limestone, Quartz and Portland Cement Clinker," *Powder Technol.*, vol. 67, no. 3, pp. 277–286, Sep. 1991.

[60] V. Ramachandran, "Influence of triethanolamine on the hydration characteristics of tricalcium silicate," *J. Appl. Chem. Biotechnol.*, vol. 22, no. 11, pp. 1125–1138, 1972.

[61] V. Rahhal and R. Talero, "Early hydration of portland cement with crystalline mineral additions," *Cem. Concr. Res.*, vol. 35, no. 7, pp. 1285–1291, Jul. 2005.

[62] B. Lothenbach, K. Scrivener, and R. D. Hooton, "Supplementary cementitious materials," *Cem. Concr. Res.*, vol. 41, no. 12, pp. 1244–1256, Dec. 2011.

[63] A. Leemann, B. Lothenbach, and C. Thalmann, "Influence of superplasticizers on pore solution composition and on expansion of concrete due to alkali-silica reaction," *Constr. Build. Mater.*, vol. 25, no. 1, pp. 344–350, Jan. 2011.

[64] A. Shvarzman, K. Kovler, G. . Grader, and G. . Shter, "The effect of dehydroxylation/ amorphization degree on pozzolanic activity of kaolinite," *Cem. Concr. Res.*, vol. 33, no. 3, pp. 405–416, Mar. 2003.

[65] C. Bich, J. Ambroise, and J. Péra, "Influence of degree of dehydroxylation on the pozzolanic activity of metakaolin," *Appl. Clay Sci.*, vol. 44, no. 3–4, pp. 194–200, May 2009.

[66] G. Kakali, T. Perraki, S. Tsivilis, and E. Badogiannis, "Thermal treatment of kaolin: the

effect of mineralogy on the pozzolanic activity," *Appl. Clay Sci.*, vol. 20, no. 1–2, pp. 73–80, Sep. 2001.

[67] T. Ramlochan, M. Thomas, and K. Gruber, "The effect of metakaolin on alkali–silica reaction in concrete," *Cem. Concr. Res.*, vol. 30, no. 3, pp. 339–344, Mar. 2000.

[68] J. Cabrera and M. F. Rojas, "Mechanism of hydration of the metakaolin–lime–water system," *Cem. Concr. Res.*, vol. 31, no. 2, pp. 177–182, Feb. 2001.

[69] M. F. Rojas and J. Cabrera, "The effect of temperature on the hydration rate and stability of the hydration phases of metakaolin–lime–water systems," *Cem. Concr. Res.*, vol. 32, no. 1, pp. 133–138, Jan. 2002.

[70] J. Ambroise, S. Maximilien, and J. Pera, "Properties of metakaolin blended cements," *Adv. Cem. Based Mater.*, vol. 1, no. 4, pp. 161–168, 1994.

[71] M. Murat, "Hydration reaction and hardening of calcined clays and related minerals. I. Preliminary investigation on metakaolinite," *Cem. Concr. Res.*, vol. 13, no. 2, pp. 259–266, 1983.

[72] G. Batis, P. Pantazopoulou, S. Tsivilis, and E. Badogiannis, "The effect of metakaolin on the corrosion behavior of cement mortars," *Cem. Concr. Compos.*, vol. 27, no. 1, pp. 125–130, Jan. 2005.

[73] C.-S. Poon, L. Lam, S. . Kou, Y.-L. Wong, and R. Wong, "Rate of pozzolanic reaction of metakaolin in high-performance cement pastes," *Cem. Concr. Res.*, vol. 31, no. 9, pp. 1301–1306, Sep. 2001.

[74] H.-S. Kim, S.-H. Lee, and H.-Y. Moon, "Strength properties and durability aspects of high strength concrete using Korean metakaolin," *Constr. Build. Mater.*, vol. 21, no. 6, pp. 1229–1237, Jun. 2007.

[75] X. Qian and Z. Li, "The relationships between stress and strain for high-performance concrete with metakaolin," *Cem. Concr. Res.*, vol. 31, no. 11, pp. 1607–1611, Nov. 2001.

[76] S. Wild and J. M. Khatib, "Portlandite Consumption in Metakaolin Cement Pastes and Mortars," *Cem. Concr. Res.*, vol. 27, no. 1, pp. 137–146, 1997.

[77] N. J. Coleman and C. L. Page, “Aspects of the Pore Solution Chemistry of the Hydrated Cement Pastes Containing Metakaolin,” *Cem. Concr. Res.*, vol. 27, no. 1, pp. 147–154, 1997.

[78] W. Aquino, D. A. Lange, and J. Olek, “The influence of metakaolin and silica fume on the chemistry of alkali - silica reaction products,” *Cem. Concr. Compos.*, vol. 23, pp. 485–493, 2001.

[79] N. M. Al-Akhras, “Durability of metakaolin concrete to sulfate attack,” *Cem. Concr. Res.*, vol. 36, no. 9, pp. 1727–1734, Sep. 2006.

[80] L. Courard, A. Darimont, M. Schouterden, F. Ferauche, X. Willem, and R. Degeimbre, “Durability of mortars modified with metakaolin,” *Cem. Concr. Res.*, vol. 33, no. 9, pp. 1473–1479, 2003.

[81] M. Frías, M. I. S. De Rojas, and J. Cabrera, “The Effect that the Pozzolanic Reaction of Metakaolin has on the Heat Evolution in Metakaolin-Cement Mortars,” *Cem. Concr. Res.*, vol. 30, no. 2, pp. 209–216, 2000.

[82] F. Lagier and K. E. Kurtis, “Influence of Portland Cement Composition on Early Age Reactions with Metakaolin,” *Cem. Concr. Res.*, vol. 37, no. 10, pp. 1411–1417, Oct. 2007.

[83] J. Khatib and S. Wild, “Pore size distribution of metakaolin paste,” *Cem. Concr. Res.*, vol. 26, no. 10, pp. 1545–1553, 1996.

[84] J. J. T. Ding and Z. Li, “Effects of metakaolin and silica fume on properties of concrete,” *ACI Mater. J.*, vol. 99, no. 99, pp. 393–398, 2002.

[85] J. Brooks and M. Johari, “Effect of metakaolin on creep and shrinkage of concrete,” *Cem. Concr. Compos.*, vol. 23, pp. 495–502, 2001.

[86] P. J. P. P. Gleize, M. Cyr, and G. Escadeillas, “Effects of Metakaolin on Autogenous Shrinkage of Cement Pastes,” *Cem. Concr. Compos.*, vol. 29, no. 2, pp. 80–87, Feb. 2007.

[87] A. Asbridge, C. Page, and M. Page, “Effects of metakaolin, water/binder ratio and interfacial transition zones on the microhardness of cement mortars,” *Cem. Concr. Res.*, vol. 32, no. 9, pp. 1365–1369, Sep. 2002.

[88] V. Lilkov, E. Dimitrova, and O. Petrov, “Hydration process of cement containing fly ash and silica fume: the first 24 hours,” *Cem. Concr. Res.*, vol. 27, no. 4, pp. 577–588, 1997.

[89] Z. Wu and J. Young, “The hydration of tricalcium silicate in the presence of colloidal silica,” *J. Mater. Sci.*, vol. 19, no. 11, pp. 3477–3486, 1984.

[90] R. F. Feldman and H. Cheng-yi, “Properties of Portland cement-silica fume pastes II. Mechanical properties,” *Cem. Concr. Res.*, vol. 15, no. 6, pp. 943–952, 1985.

[91] B. W. Langan, K. Weng, and M. A. Ward, “Effect of silica fume and fly ash on heat of hydration of Portland cement,” *Cem. Concr. Res.*, vol. 32, pp. 1045–1051, 2002.

[92] E.-H. Kadri and R. Duval, “Hydration heat kinetics of concrete with silica fume,” *Constr. Build. Mater.*, vol. 23, no. 11, pp. 3388–3392, Nov. 2009.

[93] J. Zelić, D. Rušić, D. Veža, and R. Krstulović, “The role of silica fume in the kinetics and mechanisms during the early stage of cement hydration,” *Cem. Concr. Res.*, vol. 30, no. 10, pp. 1655–1662, 2000.

[94] J. A. Larbi, A. L. A. Fraay, and J. M. J. M. Bijen, “The chemistry of the pore fluid of silica fume-blended cement systems,” *Cem. Concr. Res.*, vol. 20, no. 4, pp. 506–516, 1990.

[95] M. Mazloom, A. Ramezanianpour, and J. J. Brooks, “Effect of silica fume on mechanical properties of high-strength concrete,” *Cem. Concr. Compos.*, vol. 26, no. 4, pp. 347–357, May 2004.

[96] J. M. R. Dotto, A. G. d. Abreu, D. C. C. Dal Molin, and I. L. Müller, “Influence of silica fume addition on concretes physical properties and on corrosion behaviour of reinforcement bars,” *Cem. Concr. Compos.*, vol. 26, no. 1, pp. 31–39, Jan. 2004.

[97] M. F. . Zain, M. Safiuddin, and H. Mahmud, “Development of high performance concrete using silica fume at relatively high water–binder ratios,” *Cem. Concr. Res.*, vol. 30, no. 9, pp. 1501–1505, Sep. 2000.

[98] S. Bhanja and B. Sengupta, “Influence of silica fume on the tensile strength of concrete,” *Cem. Concr. Res.*, vol. 35, no. 4, pp. 743–747, Apr. 2005.

[99] Z. Shui, R. Zhang, W. Chen, and D. Xuan, “Effects of mineral admixtures on the thermal

expansion properties of hardened cement paste," *Constr. Build. Mater.*, vol. 24, no. 9, pp. 1761–1767, Sep. 2010.

[100] E. Schulson, I. Swainson, and T. Holden, "Internal stress within hardened cement paste induced through thermal mismatch: Calcium hydroxide versus calcium silicate hydrate," *Cem. Concr. Res.*, vol. 31, pp. 1785–1791, 2001.

[101] R. D. Hooton, "Influence of silica fume replacement of cement on physical properties and resistance to sulfate attack, freezing and thawing, and alkali-silica reactivity," *ACI Mater. J.*, vol. 90, no. 2, pp. 143–151, 1993.

[102] M. Alexander and B. Magee, "Durability performance of concrete containing condensed silica fume," *Cem. Concr. Res.*, vol. 29, no. 6, pp. 917–922, 1999.

[103] ASTM C 618, "Standard Specification for Coal Fly Ash and Raw or Calcined Natural Pozzolan for Use in Concrete," in *Annual Book of ASTM Standards, V. 04.02*, ASTM International, 2012.

[104] D. Heinz, M. Göbel, H. Hilbig, L. Urbonas, and G. Bujauskaite, "Effect of TEA on fly ash solubility and early age strength of mortar," *Cem. Concr. Res.*, vol. 40, no. 3, pp. 392–397, Mar. 2010.

[105] R. Siddique and M. I. Khan, *Supplementary Cementing Materials*, vol. 37. Berlin, Germany: Springer Berlin Heidelberg, 2011.

[106] K. Pedersen, a Jensen, M. Skjothrasmussen, and K. Damjohansen, "A review of the interference of carbon containing fly ash with air entrainment in concrete," *Prog. Energy Combust. Sci.*, vol. 34, no. 2, pp. 135–154, Apr. 2008.

[107] Y. W. Chan, C. Y. Liu, and Y. S. Lu, "Effects of Slag and Fly Ash on the Autogenous Shrinkage of High-Performance Concrete," in *Autogenous Shrinkage of Concrete*, E. Tazawa, Ed. New York, NY: E & FN Spon, 2004, pp. 221–229.

[108] P. J. Tikalsky and R. L. Carrasquillo, "Influence of fly Ash on the Sulfate Resistance concrete," *ACI Mater. J.*, vol. 89, no. 1, pp. 69–75, 1991.

[109] P. Mehta, "Effect of fly ash composition on sulfate resistance of cement," *ACI J. Proc.*, vol.

83, no. 83, pp. 994–1000, 1986.

[110] Y.-S. Choi, J.-G. Kim, and K.-M. Lee, “Corrosion behavior of steel bar embedded in fly ash concrete,” *Corros. Sci.*, vol. 48, no. 7, pp. 1733–1745, Jul. 2006.

[111] ASTM C989/C989M-14, “Standard Specification for Slag Cement for Use in Concrete and Mortars,” West Conshohocken, PA: ASTM International, 2014.

[112] G. Osborne, “Durability of Portland blast-furnace slag cement concrete,” *Cem. Concr. Compos.*, vol. 21, pp. 11–21, 1999.

[113] P. R. Lohtia and R. C. Joshi, “Mineral Admixtures,” in *Concrete Admixtures Handbook: Properties, Science and Technology*, 2nd ed., V. Ramachandran, Ed. Park Ridge, NJ: Noyes Publications, 1995, pp. 657–739.

[114] P. J. Wainwright and N. Rey, “The influence of ground granulated blastfurnace slag (GGBS) additions and time delay on the bleeding of concrete,” *Cem. Concr. Compos.*, vol. 22, pp. 253–257, 2000.

[115] J. M. Khatib and J. J. Hibbert, “Selected engineering properties of concrete incorporating slag and metakaolin,” *Constr. Build. Mater.*, vol. 19, no. 6, pp. 460–472, Jul. 2005.

[116] A. Darquennes, S. Staquet, M.-P. Delplancke-Ogletree, and B. Espion, “Effect of autogenous deformation on the cracking risk of slag cement concretes,” *Cem. Concr. Compos.*, vol. 33, no. 3, pp. 368–379, Mar. 2011.

[117] Z. Giergiczny, M. a. Glinicki, M. Sokołowski, and M. Zielinski, “Air void system and frost-salt scaling of concrete containing slag-blended cement,” *Constr. Build. Mater.*, vol. 23, no. 6, pp. 2451–2456, Jun. 2009.

[118] S. N. Lim and T. H. Wee, “Autogenous Shrinkage of Ground-Granulated Blast- Furnace Slag Concrete,” *ACI Mater. J.*, no. 97, pp. 587–593, 2001.

[119] P. A. M. Basheer, P. R. V. Gilleece, A. E. Long, and W. J. Mc Carter, “Monitoring Electrical Resistance of Concretes Containing Alternative Cementitious Materials to Assess Their Resistance to Chloride Penetration,” *Cem. Concr. Compos.*, vol. 24, no. 5, pp. 437–449, Oct. 2002.

[120] Z. Li and Z. Ding, “Property improvement of Portland cement by incorporating with metakaolin and slag,” *Cem. Concr. Res.*, vol. 33, no. 4, pp. 579–584, Apr. 2003.

[121] M. I. Khan and C. J. Lynsdale, “Strength, permeability, and carbonation of high-performance concrete,” *Cem. Concr. Res.*, vol. 32, no. 1, pp. 123–131, Jan. 2002.

[122] M. Codina, C. Cau-dit-Coumes, P. Le Bescop, J. Verdier, and J. P. Ollivier, “Design and characterization of low-heat and low-alkalinity cements,” *Cem. Concr. Res.*, vol. 38, no. 4, pp. 437–448, Apr. 2008.

[123] E. Güneyisi, M. Gesoğlu, and E. Özbay, “Strength and drying shrinkage properties of self-compacting concretes incorporating multi-system blended mineral admixtures,” *Constr. Build. Mater.*, vol. 24, no. 10, pp. 1878–1887, Oct. 2010.

[124] M. Jones, R. Dhir, and B. Magee, “Concrete containing ternary blended binders: resistance to chloride ingress and carbonation,” *Cem. Concr. Res.*, vol. 27, no. 6, pp. 825–831, 1997.

[125] M. Gesoğlu, E. Güneyisi, and E. Özbay, “Properties of self-compacting concretes made with binary, ternary, and quaternary cementitious blends of fly ash, blast furnace slag, and silica fume,” *Constr. Build. Mater.*, vol. 23, no. 5, pp. 1847–1854, May 2009.

[126] N. Bouzoubaâ, A. Bilodeau, V. Sivasundaram, B. Fournier, and D. M. Golden, “Development of Ternary Blends for High- Performance Concrete,” no. 101, pp. 19–29, 2004.

[127] R. Bleszynski and R. Hooton, “Durability of ternary blend concrete with silica fume and blast-furnace slag: laboratory and outdoor exposure site studies,” *ACI Mater. J.*, vol. 99, pp. 499–508, 2002.

[128] M. D. A. Thomas, M. H. Shehata, S. G. Shashiprakash, D. S. Hopkins, and K. Cail, “Use of ternary cementitious systems containing silica fume and fly ash in concrete,” *Cem. Concr. Res.*, vol. 29, pp. 1207–1214, 1999.

[129] T. K. Erdem and Ö. Kirca, “Use of binary and ternary blends in high strength concrete,” *Constr. Build. Mater.*, vol. 22, pp. 1477–1483, 2008.

[130] ASTM Standard C114 2011b, *Standard Test Method for Chemical Analysis of Hydraulic*

Cement. West Conshohocken, Pa.: ASTM International, 2012.

[131] ASTM Standard C150 2012, *Standard Specification for Portland Cement*. West Conshohocken, Pa.: ASTM International, 2012.

[132] ASTM Standard C188 2009, *Standard Test Method for Density of Hydraulic Cement*. West Conshohocken, Pa.: ASTM International, 2012.

[133] A. Buchwald, R. Tatarin, and D. Stephan, "Reaction progress of alkaline-activated metakaolin-ground granulated blast furnace slag blends," *J. Mater. Sci.*, vol. 44, no. 20, pp. 5609–5617, Aug. 2009.

[134] F. Curcio, B. . DeAngelis, and S. Pagliolico, "Metakaolin as a pozzolanic microfiller for high-performance mortars," *Cem. Concr. Res.*, vol. 28, no. 6, pp. 803–809, Jun. 1998.

[135] ASTM Standard C618 2012, *Standard Specification for Coal Fly Ash and Raw or Calcined Natural Pozzolan for Use in Concrete*. West Conshohocken, Pa.: ASTM International, 2012.

[136] P. E. Stutzman, "Powder Diffraction Analysis of Hydraulic Cements: ASTM Rietveld Round Robin Results on Precision," *ICDD Adv. X-Ray Anal.*, vol. 48, no. 1, pp. 33–38, 2005.

[137] J. . Escalante, L. . Gómez, K. . Johal, G. Mendoza, H. Mancha, and J. Méndez, "Reactivity of Blast-Furnace Slag in Portland Cement Blends Hydrated under Different Conditions," *Cem. Concr. Res.*, vol. 31, no. 10, pp. 1403–1409, Oct. 2001.

[138] P. E. Stutzman, "Guide for X-Ray Powder Diffraction Analysis of Portland Cement and Clinker," Gaithersburg, M.D., 1996.

[139] Y. Leng, *Materials Characterization: Introduction to Microscopic and Spectroscopic Methods*, 2nd ed. Singapore: Wiley-VCH, 2013.

[140] A. Maqsood and K. Iqbal, "Materials Characterization by Non-Destructive Methods," *J. Pakistan Mater. Soc.*, vol. 4, no. 1, pp. 31–38, 2010.

[141] ASTM Standard C1365 2006 (2011), *Standard Test Method for Determination of the Proportion of Phases in Portland Cement and Portland-Cement Clinker Using X-Ray*

Powder Diffraction Analysis. West Conshohocken, Pa.: ASTM International, 2012.

[142] D. Bish and R. J. Reynolds, "Sample Preparation for X-Ray Diffraction," in *Modern Powder Diffraction*, D. Bish and J. Post, Eds. Washington, DC: The Mineralogical Society of America, 1989, pp. 73–99.

[143] W. A. Gutteridge, "On the Dissolution of the Interstitial Phases in Portland Cement," *Cem. Concr. Res.*, vol. 9, no. 3, pp. 319–324, 1979.

[144] H. F. W. Taylor, *Cement Chemistry*, 2nd ed. London, UK: Thomas Telford Publishing, 1997.

[145] P. C. Hewlett, Ed., *Lea's Chemistry of Cement and Concrete*, 4th ed. New York, NY: Arnold, 1998.

[146] J. C. Taylor, I. Hinczak, and C. E. Matulis, "Rietveld Full-Profile Quantification of Portland Cement Clinker: The Importance of Including a Full Crystallography of the Major Phase Polymorphs," *Powder Diffr.*, vol. 15, no. 1, pp. 7–18, 2000.

[147] M. Courtial, M.-N. de Noirfontaine, F. Dunstetter, G. Gasecki, and M. Signes-Frehel, "Polymorphism of tricalcium silicate in Portland cement: a fast visual identification of structure and superstructure.," *Powder Diffr.*, vol. 18, no. 1, pp. 7–15, 2003.

[148] H. P. Klug and L. . Alexander, *X-ray Diffraction Procedures: For Polycrystalline and Amorphous Materials*, 2nd ed. Hoboken, NJ: J. Wiley & Sons, 1974.

[149] I. C. Madsen, N. V. Y. Scarlett, and A. Kern, "Description and survey of methodologies for the determination of amorphous content via X-ray powder diffraction," *Zeitschrift für Krist.*, vol. 226, no. 12, pp. 944–955, Dec. 2011.

[150] ASTM Standard C204 2011, *Standard Test Method for Fineness of Hydraulic Cement by Air Permeability Apparatus*. West Conshohocken, Pa.: ASTM International, 2012.

[151] "Why switch from Blaine to PSD?," *Malvern.com.* .

[152] A. Jillavenkatesa, S. J. Dapkunas, and L. Lum, *Particle Size Characterization*. National Institute of Science and Technology (NIST), Special Publication 960-1, 2001.

[153] HORIBA Instruments, *LA-950 Instructional Manual*. Irvine, CA, 2001.

[154] HORIBA Instruments, “A Guidebook to Particle Size Analysis,” 2012. .

[155] H. Azari, *Statistical Modeling of Cement Heat of Hydration Using Phase and Fineness Variables*. National Cooperative Highway Research Program, Transportation Research Board of the National Academies, NCHRP Web-only Document 167, 2010.

[156] K. K. Aligizaki, *Pore Structure of Cement-Based Materials: Testing, Interpretation and Requirements*. New York, NY: Taylor & Francis, 2006.

[157] J. Yajun and J. H. Cahyadi, “Effects of densified silica fume on microstructure and compressive strength of blended cement pastes,” *Cem. Concr. Res.*, vol. 33, no. 10, pp. 1543–1548, Oct. 2003.

[158] A. Quennoz and K. L. Scrivener, “Interactions between alite and C3A-gypsum hydrations in model cements,” *Cem. Concr. Res.*, vol. 44, pp. 46–54, Feb. 2013.

[159] V. Kocaba, “Development and Evaluation of Methods to Follow Microstructural Development of Cementitious Systems Including Slags,” Ecole Polytechnique Federale de Lausanne, 2009.

[160] K. L. Scrivener and A. Nonat, “Hydration of cementitious materials, present and future,” *Cem. Concr. Res.*, vol. 41, no. 7, pp. 651–665, Jul. 2011.

[161] P. Lawrence, M. Cyr, and E. Ringot, “Mineral Admixtures in Mortars. Effect of Inert Materials on Short-term Hydration,” *Cem. Concr. Res.*, vol. 33, no. 12, pp. 1939–1947, Dec. 2003.

[162] D. P. Bentz, “Powder Additions to Mitigate Retardation in High-Volume Fly Ash Mixtures,” *ACI Mater. J.*, vol. 107, no. 5, pp. 508–514, 2010.

[163] G. Baert, S. Hoste, G. Schutter, and N. Belie, “Reactivity of fly ash in cement paste studied by means of thermogravimetry and isothermal calorimetry,” *J. Therm. Anal. Calorim.*, vol. 94, no. 2, pp. 485–492, Sep. 2008.

[164] K. A. Riding, J. J. L. Poole, K. J. Folliard, M. C. G. G. Juenger, and A. K. Schindler, “Modeling hydration of cementitious systems,” *ACI Mater. J.*, vol. 109, no. 2, pp. 225–234, 2012.

[165] ASTM Standard C1702 2009a, “Standard Test Method for Measurement of Heat of Hydration of Hydraulic Cementitious Materials Using Isothermal Conduction Calorimetry,” West Conshohocken, PA: ASTM International, 2012.

[166] A. C. . Muller, K. L. Scrivener, A. M. Gajewicz, and P. J. McDonald, “Use of bench-top NMR to measure the density, composition and desorption isotherm of C-S-H in cement paste,” *Microporous Mesoporous Mater.*, vol. 178, pp. 99–103, 2013.

[167] S. Dittrich, J. Neubauer, and F. Goetz-Neunhoeffer, “The influence of fly ash on the hydration of OPC within the first 44 h - A quantitative in situ XRD and heat flow calorimetry study,” *Cem. Concr. Res.*, vol. 56, pp. 129–138, Feb. 2014.

[168] A. K. Schindler and K. J. Folliard, “Heat of Hydration Models for Cementitious Materials,” *ACI Mater. J.*, vol. 102, pp. 24–33, 2005.

[169] B. G. M. Gapinski and J. Scanlon, “Silica Fume,” 2006. .

[170] R. Siddique and J. Klaus, “Influence of metakaolin on the properties of mortar and concrete: A review,” *Appl. Clay Sci.*, vol. 43, no. 3–4, pp. 392–400, Mar. 2009.

[171] M. Antoni, J. Rossen, F. Martirena, and K. Scrivener, “Cement substitution by a combination of metakaolin and limestone,” *Cem. Concr. Res.*, vol. 42, no. 12, pp. 1579–1589, Dec. 2012.

[172] X. Feng, E. J. Garboczi, D. P. Bentz, P. E. Stutzman, and T. O. Mason, “Estimation of the Degree of Hydration of Blended Cement Pastes by a Scanning Electron Microscope Point-Counting Procedure,” *Cem. Concr. Res.*, vol. 34, no. 10, pp. 1787–1793, Oct. 2004.

[173] F. Brunet, T. Charpentier, C. N. Chao, H. Peycelon, and A. Nonat, “Characterization by Solid-State NMR and Selective Dissolution Techniques of Anhydrous and Hydrated CEM V Cement Pastes,” *Cem. Concr. Res.*, vol. 40, no. 2, pp. 208–219, Feb. 2010.

[174] W.R.Grace, “WRDA 60 Material Safety Data Sheet,” 2008.

[175] M. M. Collepardi, “Water Reducers/Retarders,” in *Concrete Admixtures Handbook: Properties, Science and Technology*, 2nd ed., V. Ramachandran, Ed. Park Ridge, NJ: Noyes Publications, 1995.

[176] M. Bishop and A. R. Barron, “Cement Hydration Inhibition with Sucrose, Tartaric Acid, and Lignosulfonate: Analytical and Spectroscopic Study,” *Ind. Eng. Chem. Res.*, vol. 45, no. 21, pp. 7042–7049, Oct. 2006.

[177] M. C. Juenger and H. M. Jennings, “New insights into the effects of sugar on the hydration and microstructure of cement pastes,” *Cem. Concr. Res.*, vol. 32, no. 3, pp. 393–399, 2002.

[178] N. L. Thomas and J. D. Birchall, “The retarding action of sugars on cement hydration,” *Cem. Concr. Res.*, vol. 13, no. 6, pp. 830–842, Nov. 1983.

[179] V. Peterson and M. Juenger, “Hydration of tricalcium silicate: effects of $CaCl_2$ and sucrose on reaction kinetics and product formation,” *Chem. Mater.*, vol. 18, no. 24, pp. 5798–5804, 2006.

[180] W.R.Grace, “ADVA 120 Material Safety Data Sheet,” 2008.

[181] A. Zingg, F. Winnefeld, L. Holzer, J. Pakusch, S. Becker, R. Figi, and L. Gauckler, “Interaction of polycarboxylate-based superplasticizers with cements containing different C3A amounts,” *Cem. Concr. Compos.*, vol. 31, no. 3, pp. 153–162, Mar. 2009.

[182] F. Winnefeld, S. Becker, J. Pakusch, and T. Götz, “Effects of the molecular architecture of comb-shaped superplasticizers on their performance in cementitious systems,” *Cem. Concr. Compos.*, vol. 29, no. 4, pp. 251–262, Apr. 2007.

[183] B. Lothenbach, F. Winnefeld, and R. Figi, “The influence of superplasticizers on the hydration of Portland cement,” *Proc. 12th Ina. Congr. Chem. Cem.*, pp. 9–12, 2007.

[184] H. Vikan, H. Justnes, F. Winnefeld, and R. Figi, “Correlating cement characteristics with rheology of paste,” *Cem. Concr. Res.*, vol. 37, no. 11, pp. 1502–1511, Nov. 2007.

[185] B. Ma and H. Wang, “Rheological properties of self-compacting concrete paste containing chemical admixtures,” *J. Wuhan Univ. Technol. Sci. Ed.*, vol. 28, no. 2, pp. 291–297, Apr. 2013.

[186] “DAREX AEA EH Air-Entraining Admixture,” 2007. .

[187] D. C. Montgomery, *Design and Analysis of Experiments*, 6th ed. Hoboken, NJ: John Wiley & Sons, Inc., 2005.

[188] M. Sonebi, L. Svermova, and P. J. M. Bartos, “Factorial Design of Cement Slurries Containing Limestone Powder for Self-Consolidating Slurry-Infiltrated Fiber Concrete,” *ACI Mater. J.*, vol. 101, no. 2, pp. 136–145, 2005.

[189] A. Ghezal and K. H. Khayat, “Optimizing Self-Consolidating Concrete with Limestone Filler by using Statistical Factorial Design Methods,” *ACI Mater. J.*, vol. 99, no. 3, pp. 264–272, 2003.

[190] K. H. Khayat, A. Ghezal, and M. S. Hadriche, “Factorial design models for proportioning self- consolidating concrete,” *Mater. Struct.*, vol. 32, no. November, pp. 679–686, 1999.

[191] K. Soudki, E. F. El-Salakawy, and N. Elkum, “Full factorial optimization of concrete mix design for hot climates,” *J. Mater. Civ. Eng.*, vol. 13, no. 6, pp. 427–433, 2001.

[192] R. Patel, K. Hossain, and M. Shehata, “Development of statistical models for mixture design of high-volume fly ash self-consolidating concrete,” *ACI Mater. J.*, vol. 101, no. 4, pp. 294–302, 2004.

[193] L. Ferrara, Y.-D. Park, and S. P. Shah, “A method for mix-design of fiber-reinforced self-compacting concrete,” *Cem. Concr. Res.*, vol. 37, no. 6, pp. 957–971, Jun. 2007.

[194] C. B. Srinivasan, N. L. Narasimhan, and S. V. Ilango, “Development of rapid-set high-strength cement using statistical experimental design,” *Cem. Concr. Res.*, vol. 33, no. 9, pp. 1287–1292, Sep. 2003.

[195] M. Sonebi, “Factorial design modelling of mix proportion parameters of underwater composite cement grouts,” *Cem. Concr. Res.*, vol. 31, no. 11, pp. 1553–1560, Nov. 2001.

[196] A. a. Abouhussien and A. a. a. Hassan, “Optimizing the durability and service life of self-consolidating concrete containing metakaolin using statistical analysis,” *Constr. Build. Mater.*, vol. 76, pp. 297–306, Feb. 2015.

[197] G. Rishi and B. Nemkumar, “Plastic Shrinkage Cracking Prediction in Cement-Based Materials Using Factorial Design,” *J. Mater. Civ. Eng.*, p. 04014244, Nov. 2014.

[198] S. L. Correia, T. Partala, F. C. Loch, and a. M. Segadães, “Factorial design used to model the compressive strength of mortars containing recycled rubber,” *Compos. Struct.*, vol. 92,

no. 9, pp. 2047–2051, Aug. 2010.

[199] O. Burciaga-Díaz, J. I. Escalante-García, R. Arellano-Aguilar, and A. Gorokhovsky, “Statistical analysis of strength development as a function of various parameters on activated metakaolin/slag cements,” *J. Am. Ceram. Soc.*, vol. 93, no. 2, pp. 541–547, 2010.

[200] M. Whittaker, M. Zajac, M. Ben Haha, F. Bullerjahn, and L. Black, “The role of the alumina content of slag, plus the presence of additional sulfate on the hydration and microstructure of Portland cement-slag blends,” *Cem. Concr. Res.*, vol. 66, pp. 91–101, Dec. 2014.

[201] R. Talero and V. Rahhal, “Calorimetric Comparison of Portland Cements containing Silica Fume and Metakaolin Is Silica Fume, like Metakaolin, characterized by Pozzolanic Activity that is more Specific than Generic?,” *J. Therm.*, vol. 96, no. 2, pp. 383–393, 2009.

[202] A. Fraay, J. Bijen, and Y. De Haan, “The reaction of fly ash in concrete a critical examination,” *Cem. Concr. Res.*, vol. 19, no. 2, pp. 235–246, 1989.

[203] S. Diamond, “Effects of Microsilica (Silica Fume) on Pore-Solution Chemistry of Cement Pastes,” *J. Am. Ceram. Soc.*, vol. 66, no. 5, pp. C–82–C–84, May 1983.

[204] H. Pietersen, “Reactivity of fly ash at high pH,” Delft University of Technology, 1993.

[205] J. Lamond, JF; Pielert, “Hydraulic Cements-Physical Properties,” in *Significance of Test and Properties of Concrete and Concrete-Making Materials*, 2006, p. 439.

[206] C. C. F. Ferraris, K. K. H. Obla, and R. Hill, “The influence of mineral admixtures on the rheology of cement paste and concrete,” *Cem. Concr. Res.*, vol. 31, no. 2, pp. 245–255, Feb. 2001.

[207] R. Pileggi, A. Betioli, F. Cardoso, and V. John, “Extended rheological characterization of cement pastes: squeeze flow plus rotational rheometry,” in *Proceedings of the 12th International Congress on the Chemistry of Cement*, 2007.

[208] E. Brito-de La Fuente, L. Choplin, and P. A. Tanguy, “Mixing with Helical Ribbon Impellers : Effect of Highly Shear Thinning Behaviour and Impeller Geometry,” *Chem. Eng. Res. Des.*, vol. 75, no. 1, pp. 45–52, 1997.

[209] P. Banfill and D. Kitching, “Use of a Controlled Stress Rheometer to Study the Yield Stress

of Oilwell Cement Slurries," in *International Conference on rheology of Fresh Cement and COncrete*, 1990.

[210] J. E. Wallevik, "Relationship between the Bingham parameters and slump," *Cem. Concr. Res.*, vol. 36, no. 7, pp. 1214–1221, Jul. 2006.

[211] M. A. Blankson and S. Erdem, "Comparison of the effect of organic and inorganic corrosion inhibitors on the rheology of self-compacting concrete," *Constr. Build. Mater.*, vol. 77, pp. 59–65, Feb. 2015.

[212] P. Banfill, "Rheology of fresh cement and concrete," *Rheol. Rev.*, vol. 2006, pp. 61–130, 2006.

[213] V. Hackley and C. Ferraris, *Guide to rheological nomenclature: Measurements in ceramic particulate systems*. Gaithersburg, MD: National Institute of Standards and Technology (NIST), Special Publication 946, 2001.

[214] N. Dzuy and D. Boger, "Yield stress measurement for concentrated suspensions," *J. Rheol. (N. Y. N. Y).*, vol. 27, no. 4, pp. 321–349, 1983.

[215] ASTM C305, "Standard practice for mechanical mixing of hydraulic cement pastes and mortars of plastic consistency," *ASTM Int.*, pp. 1–3, 2014.

[216] C. Ferraris, "Measurement of the rheological properties of cement paste: a new approach," in *International RILEM Symposium on the Role of Admixtures in High Performance Concrete*, 1999, pp. 333–342.

[217] J. Hot, "Influence des polymères de type superplastifiants et agents entraineurs d ' air sur la viscosité macroscopique des matériaux cimentaires," Université Paris-Est, 2013.

[218] E. P. Koehler and D. W. Fowler, "Development of a Portable Rheometer for Fresh Portland Cement Concrete," Washington, DC, 2004.

[219] A. K. H. Kwan and Y. Li, "Effects of fly ash microsphere on rheology, adhesiveness and strength of mortar," *Constr. Build. Mater.*, vol. 42, pp. 137–145, May 2013.

[220] C. K. Park, M. H. Noh, and T. H. Park, "Rheological properties of cementitious materials containing mineral admixtures," *Cem. Concr. Res.*, vol. 35, no. 5, pp. 842–849, 2005.

[221] L. Rudzinski, “The effect of fly ashes on the rheological behaviour of cement pastes,” *Matériaux Constr.*, vol. 17, no. 5, pp. 369–373, 1984.

[222] A. A. Ramezanianpour, *Cement Replacement Materials*. Berlin, Germany: Springer Berlin Heidelberg, 2014.

[223] X. Zhang and J. Han, “The effect of ultra-fine admixture on the rheological property of cement paste,” *Cem. Concr. Res.*, vol. 30, no. 5, pp. 827–830, May 2000.

[224] M. Palacios, F. Puertas, P. Bowen, and Y. F. Houst, “Effect of PCs superplasticizers on the rheological properties and hydration process of slag-blended cement pastes,” *J. Mater. Sci.*, vol. 44, no. 10, pp. 2714–2723, Mar. 2009.

[225] Y. Shi, I. Matsui, and N. Feng, “Effect of compound mineral powders on workability and rheological property of HPC,” *Cem. Concr. Res.*, vol. 32, no. 1, pp. 71–78, Jan. 2002.

[226] H. Uchikawa, S. Hanehara, and D. Sawaki, “The role of steric repulsive force in the dispersion of cement particles in fresh paste prepared with organic admixture,” *Cem. Concr. Res.*, vol. 27, no. 1, pp. 37–50, 1997.

[227] D. P. Bentz, “Blending different fineness cements to engineer the properties of cement-based materials,” *Mag. Concr. Res.*, vol. 62, no. 5, pp. 327–338, Jan. 2010.

[228] S. K. Agarwal, I. Masood, and S. K. Malhotra, “Compatibility of superplasticizers with different cements,” *Constr. Build. Mater.*, vol. 14, no. July 1999, pp. 253–259, 2000.

[229] D. P. Bentz, G. Sant, and J. Weiss, “Early-Age Properties of Cement-Based Materials. I: Influence of Cement Fineness,” *J. Mater. Civ. Eng.*, vol. 20, no. July, pp. 502–508, 2008.

[230] E. Amankwah, M. Bediako, and C. Kankam, “Influence of calcined clay pozzolana on strength characteristics of Portland cement concrete,” *Int. J. Mater. Sci. Appl.*, vol. 3, no. 6, pp. 410–419, 2015.

[231] ASTM C807, “Standard Test Method for Time of Setting of Hydraulic Cement Mortar by Modified,” *ASTM Int.*, pp. 1–3, 2013.

[232] ASTM C109, “Standard test method for compressive strength of hydraulic cement mortars (Using 2-in. or cube specimens),” *Am. Soc. Test. Mater.*, vol. i, pp. 1–10, 2002.

[233] ASTM C305-14, “Standard practice for mechanical mixing of hydraulic cement pastes and mortars of plastic consistency,” in *ASTM International*, West Conshohocken, PA: ASTM International, 2014, pp. 1–3.

[234] J. J. Brooks and M. A. M. Johari, “Effect of metakaolin on creep and shrinkage of concrete,” *Cem. Concr. Compos.*, vol. 23, no. 6, pp. 495–502, 2001.

[235] Y. Kocak and S. Nas, “The effect of using fly ash on the strength and hydration characteristics of blended cements,” *Constr. Build. Mater.*, vol. 73, pp. 25–32, Dec. 2014.

[236] S. Kourounis, S. Tsivilis, P. E. Tsakiridis, G. D. Papadimitriou, and Z. Tsibouki, “Properties and hydration of blended cements with mineral alunite,” *Constr. Build. Mater.*, vol. 37, no. 2, pp. 815–822, 2007.

[237] C. S. Poon, S. C. Kou, and L. Lam, “Compressive Strength, Chloride Diffusivity and Pore Structure of High Performance Metakaolin and Silica Fume Concrete,” *Constr. Build. Mater.*, vol. 20, pp. 858–865, 2006.

[238] S. Wild, J. M. Khatib, and A. Jones, “Relative Strength, Pozzolanic Activity and Cement Hydration in Superplasticised Metakaolin Concrete,” *Cem. Concr. Res.*, vol. 26, no. 10, pp. 1537–1544, 1996.

[239] E.-H. Kadri, S. Kenai, K. Ezziane, R. Siddique, and G. De Schutter, “Influence of metakaolin and silica fume on the heat of hydration and compressive strength development of mortar,” *Appl. Clay Sci.*, vol. 53, no. 4, pp. 704–708, 2011.

[240] H. a. Toutanji and Tahar El-Korchi, “The influence of SF on the compressive strength of cement paste and mortar,” *Cem. Concr. Res.*, vol. 25, no. 7, pp. 1591–1602, 1995.

[241] G. A. Rao, “Investigations on the performance of silica fume-incorporated cement pastes and mortars,” *Cem. Concr. Res.*, vol. 33, no. 11, pp. 1765–1770, Nov. 2003.

[242] H. A. Mohamed, “Effect of fly ash and silica fume on compressive strength of self-compacting concrete under different curing conditions,” *Ain Shams Eng. J.*, vol. 2, no. 2, pp. 79–86, 2011.

[243] Y. Fan, S. Yin, Z. Wen, and J. Zhong, “Activation of fly ash and its effects on cement

properties 1,” *Cem. Concr. Res.*, vol. 29, no. December 1997, pp. 467–472, 1999.

[244] J. Liu, Y. Zhang, R. Liu, and B. Zhang, “Effect of fly ash and silica fume on hydration rate of cement pastes and strength of mortars,” *J. Wuhan Univ. Technol. Sci. Ed.*, vol. 29, pp. 1225–1228, 2014.

[245] C. S. Poon, L. Lam, and Y. L. Wong, “A study on high strength concrete prepared with large volumes of low calcium fly ash,” *Cem. Concr. Res.*, vol. 30, pp. 447–455, 2000.

[246] G. Menéndez, V. Bonavetti, and E. F. Irassar, “Strength development of ternary blended cement with limestone filler and blast-furnace slag,” *Cem. Concr. Compos.*, vol. 25, pp. 61–67, 2003.

[247] C. M. Aldea, F. Young, K. Wang, and S. P. Shah, “Effects of Curing Conditions on Properties of Concrete using Slag Replacement,” *Cem. Concr. Res.*, vol. 30, pp. 465–472, 2000.

[248] D. M. Roy, P. Arjunan, and M. R. Silsbee, “Effect of silica fume, metakaolin, and low-calcium fly ash on chemical resistance of concrete,” *Cem. Concr. Res.*, vol. 31, no. 12, pp. 1809–1813, Dec. 2001.

[249] W. Wongkeo, P. Thongsanitgarn, and A. Chaipanich, “Compressive strength and drying shrinkage of fly ash-bottom ash-silica fume multi-blended cement mortars,” *Mater. Des.*, vol. 36, pp. 655–662, 2012.

[250] M. Gesoğlu, E. Güneyisi, and E. Özbay, “Properties of self-compacting concretes made with binary, ternary, and quaternary cementitious blends of fly ash, blast furnace slag, and silica fume,” *Constr. Build. Mater.*, vol. 23, pp. 1847–1854, 2009.

[251] ASTM C308, “Standard practice for mechanical mixing of hydraulic cement pastes and mortars of plastic consistency,” *ASTM Int.*, pp. 1–3, 2014.

[252] S. Alsadey, “Effect of Superplasticizer on Fresh and Hardened Properties of Concrete,” *J. Agric. Sci. Eng.*, vol. 1, no. 2, pp. 70–74, 2015.

[253] M. Heikal, M. S. Morsy, and I. Aiad, “Effect of polycarboxylate superplasticizer on hydration characteristics of cement pastes containing silica fume,” *Ceram. - Silikaty*, vol.

50, no. 1, pp. 5–14, 2006.

[254] ASTM C187, “Standard Test Method for Amount of Water Required for Normal Consistency of Hydraulic Cement Paste,” *ASTM Int.*, pp. 13–15, 2011.

[255] F. Puertas, H. Santos, M. Palacios, and S. Martínez-Ramírez, “Polycarboxylate superplasticiser admixtures: effect on hydration, microstructure and rheological behaviour in cement pastes,” *Adv. Cem. Res.*, vol. 17, no. 2, pp. 77–89, 2005.

[256] K. Yamada and T. Takahashi, “Effects of the chemical structure on the properties of polycarboxylate-type superplasticizer,” *Cem. Concr. Res.*, vol. 30, no. 2, pp. 197–207, Feb. 2000.

[257] L. Z. Xiao, Z. J. Li, and X. S. Wei, “Selection of superplasticizer in concrete mix design by measuring the early electrical resistivities of pastes,” *Cem. Concr. Compos.*, vol. 29, no. 5, pp. 350–356, 2007.

[258] M. Toledano-Prados, M. Lorenzo-Pesqueira, B. González-Fonteboa, and S. Seara-Paz, “Effect of polycarboxylate superplasticizers on large amounts of fly ash cements,” *Constr. Build. Mater.*, vol. 48, pp. 628–635, 2013.

[259] J. G. Jang, N. K. Lee, and H. K. Lee, “Fresh and hardened properties of alkali-activated fly ash/slag pastes with superplasticizers,” *Constr. Build. Mater.*, vol. 50, pp. 169–176, 2014.

[260] ASTM C191, “Standard Test Method for Time of Setting of Hydraulic Cement by Vicat Needle,” *ASTM Int.*, pp. 1–8, 2013.

[261] “ASTM C1012/C1012M-15 Standard Test Method for Length Change of Hydraulic-Cement Mortars Exposed to a Sulfate Solution,” West Conshohocken, PA: ASTM International, 2012.

[262] ASTM C157/C157M, “Standard Test Method for Length Change of Hardened Hydraulic-Cement Mortar and Concrete,” *ASTM Int.*, pp. 1–7, 2014.

[263] ASTM C1017/C1017M, “Standard Specification for Chemical Admixtures for Use in Producing Flowing Concrete,” *ASTM Int.*, pp. 1–9, 2013.

[264] A. C. / C1157M-11, “Standard Performance Specification for Hydraulic Cement,” *ASTM Int.*, pp. 1–5, 2011.

[265] A. Mardani-Aghabaglou, G. İnan Sezer, and K. Ramyar, “Comparison of fly ash, silica fume and metakaolin from mechanical properties and durability performance of mortar mixtures view point,” *Constr. Build. Mater.*, vol. 70, pp. 17–25, 2014.

[266] J. M. Khatib and S. Wild, “Sulphate Resistance of Metakaolin Mortar,” *Cem. Concr. Res.*, vol. 28, no. 1, pp. 83–92, 1998.

[267] R. D. Hooton, “Influence of silica fume replacement of cement on physical properties and resistance to sulfate attack, freezing and thawing, and alkali-silica reactivity,” *ACI Mater. J.*, vol. 90, no. 2, pp. 143–151, 1993.

[268] W. Kunther, B. Lothenbach, and J. Skibsted, “Influence of the Ca/Si ratio of the C–S–H phase on the interaction with sulfate ions and its impact on the ettringite crystallization pressure,” *Cem. Concr. Res.*, vol. 69, pp. 37–49, 2015.

[269] M. D. Cohen and a Bentur, “Durability of Portland Cement - Silica Fume Pastes in Magnesium Sulfate and Sodium Sulfate Solutions,” *ACI Mater. J.*, vol. 85, no. 3, pp. 148–157, 1988.

[270] S. Kandasamy and M. H. Shehata, “Durability of ternary blends containing high calcium fly ash and slag against sodium sulphate attack,” *Constr. Build. Mater.*, vol. 53, pp. 267–272, 2014.

[271] N. Ghafoori, M. Najimi, H. Diawara, and M. S. Islam, “Effects of Class F Fly Ash on Sulfate Resistance of Type V Portland Cement Concretes under Continuous and Interrupted Sulfate Exposures,” *Constr. Build. Mater.*, vol. 78, pp. 85–91, 2015.

[272] R. S. Gollop and H. F. W. Taylor, “Microstructural and Microanalytical Studies of sulfate Attack. V. Comparison of Different Slag Blends,” *Cem. Concr. Res.*, vol. 26, no. 7, pp. 1029–1044, 1996.

[273] S. O. Ekolu and A. Ngwenya, “Sulphate resistance of concrete made with moderately high alumina slag,” in *Proceedings of the First International Conference on Construction Materials and Structures*, 2014, pp. 797–805.

[274] G. J. Osborne, “Durability of Portland blast-furnace slag cement concrete,” *Cem. Concr. Compos.*, vol. 21, no. 1, pp. 11–21, 1999.

[275] C. Yu, W. Sun, and K. Scrivener, “Degradation mechanism of slag blended mortars immersed in sodium sulfate solution,” *Cem. Concr. Res.*, vol. 72, pp. 37–47, 2015.

[276] M. M. López, Y. Pineda, and O. Gutiérrez, “Evaluation of Durability and Mechanical Properties of the Cement Mortar Added with Slag Blast Furnace,” *Procedia Mater. Sci.*, vol. 9, pp. 367–376, 2015.

[277] S. Ogawa, H. Hyodo, H. Hirao, K. Yamada, A. Matsui, and D. Hooton, “Sulfate Resistance Improvement of Blended Cement Based on Ground Granulated Blast Furnace Slag,” *3rd ACF Int. Conf.*, pp. 499–506, 2008.

[278] S. Ogawa, T. Nozaki, K. Yamada, H. Hirao, and R. D. Hooton, “Improvement on Sulfate Resistance of Blended Cement with High Alumina Slag,” *Cem. Concr. Res.*, vol. 42, no. 2, pp. 244–251, 2012.

[279] D. Buidens, “Effects of Mix Design Using Chloride-Based Accelerator on Concrete Pavement Cracking Potential,” Univeristy of South Florida, Tampa, FL, Master’s Thesis, 2014.

[280] A. Zayed, K. Riding, C. C. Ferraro, A. Bien-Aime, N. Shanahan, D. Buidens, T. Meagher, V. Tran, J. D. Henika, J. M. Paris, C. M. Tibbetts, and B. E. Watts, “Long-Life Slab Replacement Concrete,” 2015.

[281] K. A. Riding, “Early Age Concrete Thermal Stress Measurement and Modeling,” *PhD Diss.*, no. University of Texas, Austin, 2007.

[282] K. A. Riding, J. L. Poole, A. K. Schindler, M. C. G. Juenger, and K. J. Folliard, “Quantification of Effects of Fly Ash Type on Concrete Early-Age Cracking,” *ACI Mater. J.*, vol. 105, no. 2, pp. 149–155, 2008.

[283] P. Mukherjee and M. Thomas, “The Effect of Slag on Thermal Cracking in Concrete,” no. 1. 1994.

[284] Y. Wei and W. Hansen, “Early-age strain-stress relationship and cracking behavior of slag cement mixtures subject to constant uniaxial restraint,” *Constr. Build. Mater.*, vol. 49, pp. 635–642, 2013.

[285] R. Springenschmid, R. Breitenbucher, and W. Kussmann, “Cracking Tendency of Concretes with Blastfurnace Slag Cements due to Outflow of Heat of Hydration,” *Concr. Precast. Plant Technol.*, vol. 53, pp. 817–821, 1987.

[286] B. G. Kim, K. M. Lee, and H. K. Lee, “Autogenous shrinkage of high-performance concrete containing fly ash,” *Magazine of Concrete Research*, vol. 55, no. 6. pp. 507–515, 2003.

[287] B. E. Byard, A. K. Schindler, R. W. Barnes, and A. Rao, “Cracking Tendency of Bridge Deck Concrete,” *Transp. Res. Rec. J. Transp. Res. Board*, vol. 2164, no. -1, pp. 122–131, 2010.

[288] S. Slatnick, K. a. Riding, K. J. Folliard, M. C. G. Juenger, and A. K. Schindler, “Evaluation of autogenous deformation of concrete at early ages,” *ACI Mater. J.*, vol. 108, no. 1, pp. 21–28, 2011.

[289] O. M. Jensen and P. F. Hansen, “Autogenous deformation and RH-change in perspective,” *Cem. Concr. Res.*, vol. 31, no. 12, pp. 1859–1865, 2001.

[290] J. A. Whigham, “Evaluation of Restraint Stresses and Cracking in Early-Age Concrete with the Rigid Cracking Frame,” Auburn University, Auburn, AL, Master’s thesis, 2005.

[291] E. Güneyisi, M. Gesoğlu, and K. Mermerdaş, “Improving Strength, Drying Shrinkage, and Pore Structure of Concrete using Metakaolin,” *Mater. Struct.*, vol. 41, pp. 937–949, 2008.

[292] E. E. Holt, “Early Age Autogenous Shrinkage of Concrete,” *VTT Publ.*, no. 446, pp. 2–184, 2001.

[293] D. Jansen, F. Goetz-Neunhoeffer, C. Stabler, and J. Neubauer, “A remastered external standard method applied to the quantification of early OPC hydration,” *Cem. Concr. Res.*, vol. 41, no. 6, pp. 602–608, Jun. 2011.

[294] D. Jansen, S. T. Bergold, F. Goetz-Neunhoeffer, and J. Neubauer, “The hydration of alite: A time-resolved quantitative XRD approach using the G-factor method compared with heat

release," *J. Appl. Crystallogr.*, vol. 44, pp. 895–901, 2011.

[295] D. Jansen, C. Stabler, F. Goetz-Neunhoeffer, S. Dittrich, and J. Neubauer, "Does Ordinary Portland Cement Contain Amorphous Phase? A Quantitative Study Using an External Standard Method," *Powder Diffr.*, vol. 26, no. 01, pp. 31–38, Mar. 2012.

[296] J. P. Cline, R. B. Von Dreele, R. Winburn, P. W. Stephens, and J. J. Filliben, "Addressing the amorphous content issue in quantitative phase analysis: the certification of NIST standard reference material 676a," *Acta Crystallogr. A.*, vol. 67, no. Pt 4, pp. 357–67, Jul. 2011.

[297] A. G. De La Torre, S. Bruque, and M. A. G. Aranda, "Rietveld quantitative amorphous content analysis," *J. Appl. Crystallogr.*, vol. 34, pp. 196–202, 2001.

[298] R. Snellings, A. Bazzoni, and K. Scrivener, "The existence of amorphous phase in Portland cements: Physical factors affecting Rietveld quantitative phase analysis," *Cem. Concr. Res.*, vol. 59, pp. 139–146, 2014.

[299] T. Westphal, T. Füllmann, and H. Pöllmann, "Rietveld quantification of amorphous portions with an internal standard—Mathematical consequences of the experimental approach," *Powder Diffr.*, vol. 24, no. September, pp. 239–243, 2009.

[300] E. Robens, B. Benzler, G. Buchel, H. Reichert, and K. Schumacher, "Investigation of characterizing methods for the microstructure of cement," *Cem. Concr. Res.*, vol. 32, pp. 87–90, 2002.

[301] F. Rouquerol, J. Rouquerol, K. S. W. Sing, G. Maurin, and P. Llewellyn, "Introduction," in *Adsorption by Powders and Porous Solids: Principles, Methodology and Applications*, 2nd ed., J. Rouquerol, F. Rouquerol, P. Llewellyn, G. Maurin, and K. S. W. Sing, Eds. Oxford, UK: Academic Press, 2014, pp. 1–24.

[302] S. Naumov, "Hysteresis Phenomena in Mesoporous Materials," Universität Leipzig, 2009.

[303] E. Bodor, J. Skalny, S. Brunauer, J. Massy, and M. Yudenfreund, "Pore structures of hydrated calcium silicates and Portland cements by nitrogen adsorption," *J. Colloid Interface Sci.*, vol. 34, no. 4, pp. 560–570, 1970.

[304] M. Thommes, B. Smarsly, M. Groenewolt, P. I. Ravikovitch, and A. V Neimark, “Adsorption hysteresis of nitrogen and argon in pore networks and characterization of novel micro- and mesoporous silicas,” *Langmuir*, vol. 22, no. 2, pp. 756–64, Jan. 2006.

[305] Y. Zeng, C. Fan, D. D. Do, and D. Nicholson, “Evaporation from an Ink-Bottle Pore: Mechanisms of Adsorption and Desorption,” *Ind. Eng. Chem. Res.*, p. 140312125108002, Mar. 2014.

[306] K. S. W. Sing, F. Rouquerol, J. Rouquerol, and P. Llewellyn, “Assessment of Mesoporosity,” in *Adsorption by Powders and Porous Solids: Principles, Methodology and Applications*, 2nd ed., J. Rouquerol, F. Rouquerol, P. Llewellyn, G. Maurin, and K. S. W. Sing, Eds. Oxford, UK: Academic Press, 2014, pp. 269–302.

[307] R. Mikhail, L. E. Copeland, and S. Brunauer, “Pore structures and surface areas of hardened Portland cement pastes by nitrogen adsorption,” *Can. J. Chem.*, vol. 42, pp. 426–438, 1964.

[308] A. Korpa and R. Trettin, “The influence of different drying methods on cement paste microstructures as reflected by gas adsorption: Comparison between freeze-drying (F-drying), D-drying, P-drying and oven-drying methods,” *Cem. Concr. Res.*, vol. 36, no. 4, pp. 634–649, Apr. 2006.

[309] R. Detwiler, L. Powers, U. Jakobsen, W. U. Ahmed, K. L. Scrivener, and K. O. Kjellsen, “Preparing specimens for microscopy,” *Concr. Int.*, vol. 23, no. 11, pp. 51–58, 2001.

[310] J. Beaudoin, “A discussion on,‘ The use of nitrogen adsorption to assess the microstructure of cement paste’ by MCG Juenger and HM Jennings,” *Cem. Concr. Res.*, vol. 32, pp. 831–832, 2002.

[311] E. P. Barrett, L. G. Joyner, and P. P. Halenda, “The Determination of Pore Volume and Area Distributions in Porous Substances. I. Computations from Nitrogen Isotherms,” *J. Am. Ceram. Soc.*, vol. 73, 1951.

[312] I. Maruyama, Y. Nishioka, G. Igarashi, and K. Matsui, “Microstructural and bulk property changes in hardened cement paste during the first drying process,” *Cem. Concr. Res.*, vol. 58, pp. 20–34, 2014.

[313] M. C. G. Juenger and H. M. Jennings, “The use of nitrogen adsorption to assess the

microstructure of cement paste," *Cem. Concr. Res.*, vol. 31, no. 6, pp. 883–892, May 2001.

[314] J. M. Justice, "Evaluation of Metakaolins for Use as Supplementary Cementitious Materials," 2005.

[315] G. W. Scherer, "Drying, Shrinkage, and Cracking of Cementitious Materials," *Transp. Porous Media*, 2015.

[316] J. C. Groen, L. A. A. Peffer, and J. Pérez-Ramírez, "Pore size determination in modified micro- and mesoporous materials. Pitfalls and limitations in gas adsorption data analysis," *Microporous Mesoporous Mater.*, vol. 60, pp. 1–17, 2003.

[317] S. Brunauer, P. H. Emmett, and E. Teller, "Adsorption of Gases in Multimolecular Layers," *J. Am. Chem. Soc.*, vol. 60, no. 1, pp. 309–319, 1938.

[318] G. J. G. Gluth and B. Hillemeier, "Pore structure and permeability of hardened calcium aluminate cement pastes of low w/c ratio," *Mater. Struct.*, vol. 46, no. 9, pp. 1497–1506, Dec. 2012.

[319] W. Kurdowski, *Cement and Concrete Chemistry*. Dordrecht: Springer Netherlands, 2014.

[320] G. Constantinides, K. S. Ravi Chandran, F.-J. Ulm, and K. J. Van Vliet, "Grid indentation analysis of composite microstructure and mechanics: Principles and validation," *Mater. Sci. Eng. A*, vol. 430, no. 1–2, pp. 189–202, 2006.

[321] Hysitron Inc, *TriboIndenter Users Manual*. Minneapolis, MN: Hysitron Inc., 2001.

[322] W. C. Oliver and G. M. Pharr, "An Improved Technique for Determining Hardness and Elastic-Modulus Using Load and Displacement Sensing Indentation Experiments," *J. Mater. Res.*, vol. 7, no. 6, pp. 1564–1583, 1992.

[323] J. J. Chen, L. Sorelli, M. Vandamme, F.-J. Ulm, and G. Chanvillard, "A Coupled Nanoindentation/SEM-EDS Study on Low Water/Cement Ratio Portland Cement Paste: Evidence for C-S-H/Ca(OH)2 Nanocomposites," *J. Am. Ceram. Soc.*, vol. 1493, pp. 1484–1493, Feb. 2010.

[324] M. Miller, C. Bobko, M. Vandamme, and F.-J. Ulm, "Surface roughness criteria for cement

paste nanoindentation," *Cem. Concr. Res.*, vol. 38, no. 4, pp. 467–476, Apr. 2008.

[325] P. Mondal, S. P. Shah, L. D. Marks, and J. J. Gaitero, "Comparative Study of the Effects of Microsilica and Nanosilica in Concrete," *Transp. Res. Rec. J. Transp. Res. Board*, vol. 2141, no. -1, pp. 6–9, 2010.

[326] L. Sorelli, G. Constantinides, F.-J. Ulm, and F. Toutlemonde, "The nano-mechanical signature of Ultra High Performance Concrete by statistical nanoindentation techniques," *Cem. Concr. Res.*, vol. 38, no. 12, pp. 1447–1456, Dec. 2008.

[327] N. X. Randall, M. Vandamme, and F.-J. Ulm, "Nanoindentation analysis as a two-dimensional tool for mapping the mechanical properties of complex surfaces," *J. Mater. Res.*, vol. 24, pp. 679–690, 2009.

[328] P. Trtik, B. Münch, and P. Lura, "A critical examination of statistical nanoindentation on model materials and hardened cement pastes based on virtual experiments," *Cem. Concr. Compos.*, vol. 31, no. 10, pp. 705–714, Nov. 2009.

[329] C. Hu, Y. Han, Y. Gao, Y. Zhang, and Z. Li, "Property investigation of calcium-silicate-hydrate (C-S-H) gel in cementitious composites," *Mater. Charact.*, vol. 95, pp. 129–139, 2014.

[330] G. Constantinides and F. J. Ulm, "The nanogranular nature of C-S-H," *J. Mech. Phys. Solids*, vol. 55, no. 1, pp. 64–90, 2007.

[331] C. Hu, Y. Gao, B. Chen, Y. Zhang, and Z. Li, "Estimation of the poroelastic properties of calcium-silicate-hydrate (C-S-H) gel," *Mater. Des.*, vol. 92, pp. 107–113, 2016.

[332] F.-J. Ulm, M. Vandamme, H. M. Jennings, J. Vanzo, M. Bentivegna, K. J. Krakowiak, G. Constantinides, C. P. Bobko, and K. J. Van Vliet, "Does microstructure matter for statistical nanoindentation techniques?," *Cem. Concr. Compos.*, vol. 32, no. 1, pp. 92–99, Jan. 2010.

[333] M. Vandamme, "The Nanogranular Origin of Concrete Creep : A Nanoindentation Investigation of Microstructure and Fundamental Properties of Calcium-Silicate-Hydrates," 2008.

[334] K. J. Folliard, M. Juenger, A. Schindler, K. A. Riding, J. L. Poole, L. Kallivokas, S. Slatnick,

J. Whigham, and J. L. Meadows, “Prediction Model for Concrete Behavior - Final Report,” Austin, TX, 2008.

[335] J. Gajda, *Mass Concrete for Buildings and Bridges*. Skokie, IL: Portland Cement Association, 2007.

[336] K. De Weerdt, M. Ben Haha, G. Le Saout, K. O. Kjellsen, H. Justnes, and B. Lothenbach, “Hydration mechanisms of ternary Portland cements containing limestone powder and fly ash,” *Cem. Concr. Res.*, vol. 41, no. 3, pp. 279–291, 2011.

[337] H. Wang, D. De Leon, and H. Farzam, “C4AF Reactivity—Chemistry and Hydration of Industrial Cement,” *ACI Mater. J.*, vol. 111, no. 2, pp. 201–210, 2014.

[338] J. Plank, D. Zhimin, H. Keller, F. V. Hössle, and W. Seidl, “Fundamental mechanisms for polycarboxylate intercalation into C3A hydrate phases and the role of sulfate present in cement,” *Cem. Concr. Res.*, vol. 40, no. 1, pp. 45–57, Jan. 2010.

[339] a. Habbaba, Z. Dai, and J. Plank, “Formation of organo-mineral phases at early addition of superplasticizers: The role of alkali sulfates and C3A content,” *Cem. Concr. Res.*, vol. 59, pp. 112–117, May 2014.

[340] B. Lothenbach, D. Rentsch, and E. Wieland, “Hydration of a silica fume blended low-alkali shotcrete cement,” *Phys. Chem. Earth*, vol. 70–71, pp. 3–16, 2014.

[341] M. Boháč, M. Palou, R. Novotný, J. Másilko, D. Všianský, and T. Staněk, “Investigation on early hydration of ternary Portland cement-blast-furnace slag–metakaolin blends,” *Constr. Build. Mater.*, vol. 64, pp. 333–341, Aug. 2014.

[342] S. Stephant and A. Nonat, “Influence of the Slag Content on the Hydration of Blended Cement,” in *Proceedings of the 1st International Conference on Concrete Sustainability (ICCS13)*, 2015, pp. 447–452.

[343] R. Snellings, a. Salze, and K. L. Scrivener, “Use of X-ray diffraction to quantify amorphous supplementary cementitious materials in anhydrous and hydrated blended cements,” *Cem. Concr. Res.*, vol. 64, pp. 89–98, 2014.

[344] F. Cassagnabère, G. Escadeillas, and M. Mouret, “Study of the reactivity of

cement/metakaolin binders at early age for specific use in steam cured precast concrete," *Constr. Build. Mater.*, vol. 23, no. 2, pp. 775–784, 2009.

[345] A. Brykov, S. Krasnobaeva, and M. Mokeev, "Hydration of Portland Cement in the Presence of Highly Reactive Metakaolin," no. May, pp. 391–400, 2015.

[346] H. K. Choudhary, A. V. Anupama, R. Kumar, M. E. Panzi, S. Matteppanavar, B. N. Sherikar, and B. Sahoo, "Observation of phase transformations in cement during hydration," *Constr. Build. Mater.*, vol. 101, pp. 122–129, 2015.

[347] M. C. Garci Juenger and H. M. Jennings, "Examining the relationship between the microstructure of calcium silicate hydrate and drying shrinkage of cement pastes," *Cem. Concr. Res.*, vol. 32, no. 2, pp. 289–296, Feb. 2002.

[348] I. G. Richardson, "Tobermorite/jennite- and tobermorite/calcium hydroxide-based models for the structure of C-S-H: applicability to hardened pastes of tricalcium silicate, β-dicalcium silicate, Portland cement, and blends of Portland cement with blast-furnace slag, metakaol," *Cem. Concr. Res.*, vol. 34, no. 9, pp. 1733–1777, 2004.

[349] H. M. Jennings, J. W. Bullard, J. J. Thomas, J. E. Andrade, J. J. Chen, and G. W. Scherer, "Characterization and Modeling of Pores and Surfaces in Cement Paste: Correlations to Processing and Properties," *J. Adv. Concr. Technol.*, vol. 6, no. 1, pp. 5–29, 2008.

[350] R. Kumar and B. Bhattacharjee, "Porosity, pore size distribution and in situ strength of concrete," *Cem. Concr. Res.*, vol. 33, pp. 155–164, 2003.

[351] H. M. Jennings, "Refinements to colloid model of C-S-H in cement: CM-II," *Cem. Concr. Res.*, vol. 38, no. 3, pp. 275–289, Mar. 2008.

[352] A. Valori, P. J. McDonald, and K. L. Scrivener, "The morphology of C–S–H: Lessons from 1H nuclear magnetic resonance relaxometry," *Cem. Concr. Res.*, vol. 49, pp. 65–81, Jul. 2013.

[353] J. P. Korb, L. Monteilhet, P. J. McDonald, and J. Mitchell, "Microstructure and texture of hydrated cement-based materials: A proton field cycling relaxometry approach," *Cem. Concr. Res.*, vol. 37, no. 3, pp. 295–302, 2007.

[354] K. Velez, S. Maximilien, D. Damidot, G. Fantozzi, and F. Sorrentino, “Determination by nanoindentation of elastic modulus and hardness of pure constituents of Portland cement clinker,” *Cem. Concr. Res.*, vol. 31, no. 4, pp. 555–561, Apr. 2001.

[355] J. J. Hughes and P. Trtik, “Micro-mechanical properties of cement paste measured by depth-sensing nanoindentation: a preliminary correlation of physical properties with phase type,” *Mater. Charact.*, vol. 53, no. 2–4, pp. 223–231, Nov. 2004.

[356] G. Constantinides and F.-J. Ulm, “The effect of two types of C-S-H on the elasticity of cement-based materials: Results from nanoindentation and micromechanical modeling,” *Cem. Concr. Res.*, vol. 34, no. 1, pp. 67–80, Jan. 2004.

[357] F. Pelisser, P. J. P. Gleize, and A. Mikowski, “Effect of the Ca/Si molar ratio on the micro/nanomechanical properties of synthetic C-S-H measured by nanoindentation,” *J. Phys. Chem. C*, vol. 116, no. 32, pp. 17219–17227, 2012.

[358] C. Hu and Z. Li, “Property investigation of individual phases in cementitious composites containing silica fume and fly ash,” *Cem. Concr. Compos.*, Dec. 2014.

[359] J. Němeček, V. Šmilauer, and L. Kopecký, “Nanoindentation characteristics of alkali-activated aluminosilicate materials,” *Cem. Concr. Compos.*, vol. 33, no. 2, pp. 163–170, 2011.

[360] P. J. M. Monteiro and C. T. Chang, “The elastic moduli of calcium hydroxide,” *Cem. Concr. Res.*, vol. 25, no. 8, pp. 1605–1609, 1995.

[361] Z. He, C. Qian, Y. Zhang, F. Zhao, and Y. Hu, “Nanoindentation characteristics of cement with different mineral admixtures,” *Sci. China Technol. Sci.*, vol. 56, no. 5, pp. 1119–1123, 2013.

[362] A. R. Sakulich and V. C. Li, “Nanoscale characterization of engineered cementitious composites (ECC),” *Cem. Concr. Res.*, vol. 41, no. 2, pp. 169–175, 2011.

[363] H. M. Jennings, “A model for the microstructure of calcium silicate hydrate in cement paste,” *Cem. Concr. Res.*, vol. 30, pp. 101–116, 2000.

[364] J. E. Rossen, “Stability of C-A-S-H in pastes of alite and cement blended with

supplementary cementitious materials," 2014.

[365] I. G. Richardson, "The nature of C-S-H in hardened cements," *Cem. Concr. Res.*, vol. 29, no. July, pp. 1131–1147, 1999.

[366] S. Kumar, R. Kumar, a. Bandopadhyay, T. C. Alex, B. Ravi Kumar, S. K. Das, and S. P. Mehrotra, "Mechanical activation of granulated blast furnace slag and its effect on the properties and structure of portland slag cement," *Cem. Concr. Compos.*, vol. 30, pp. 679–685, 2008.

[367] F. Ridi, E. Fratini, R. Alfani, and P. Baglioni, "Influence of acrylic superplasticizer and cellulose-ether on the kinetics of tricalcium silicate hydration reaction.," *J. Colloid Interface Sci.*, vol. 395, pp. 68–74, Apr. 2013.

[368] D. K. Panesar and J. Francis, "Influence of limestone and slag on the pore structure of cement paste based on mercury intrusion porosimetry and water vapour sorption measurements," *Constr. Build. Mater.*, vol. 52, pp. 52–58, 2014.

[369] H. M. . Jennings and J. J. Thomas, "7.6.1 Introduction," in *The Science of Concrete Monograph*, 2006.

[370] I. Odler, "The BET-specific surface area of hydrated Portland cement and related materials," *Cem. Concr. Res.*, vol. 33, no. 12, pp. 2049–2056, Dec. 2003.

[371] E. Strekalova, R. J.-M. Pellenq, and F.-J. Ulm, "C-S-H Texture From Sorption Isotherms," *Concrete Sustainability Hub@MIT Research Profile Letter*, no. July, 2012.

[372] P. D. Tennis and H. M. Jennings, "Model for two types of calcium silicate hydrate in the microstructure of Portland cement pastes," *Cem. Concr. Res.*, vol. 30, pp. 855–863, 2000.

[373] J. Zhang and G. W. Scherer, "Comparison of methods for arresting hydration of cement," *Cem. Concr. Res.*, vol. 41, no. 10, pp. 1024–1036, Oct. 2011.

[374] M. F. De Lange, T. J. H. Vlugt, J. Gascon, and F. Kapteijn, "Adsorptive characterization of porous solids: Error analysis guides the way," *Microporous Mesoporous Mater.*, vol. 200, pp. 199–215, 2014.

[375] J. Kaufmann, R. Loser, and A. Leemann, "Analysis of cement-bonded materials by multi-

cycle mercury intrusion and nitrogen sorption," *J. Colloid Interface Sci.*, vol. 336, no. 2, pp. 730–737, 2009.

[376] H. M. . Jennings and J. J. Thomas, "7.6.5 Surface Area of Two C-S-H Morphologies," in *The Science of Concrete Monograph*, 2006.

[377] H. M. Jennings, "Colloid model of C-S-H and implications to the problem of creep and shrinkage," *Mater. Struct.*, vol. 37, no. 265, pp. 59–70, 2003.

[378] M. Garci, "Quantifying Microstructural Variations in Cement Pastes: Implications on Drying Shrinkage," Northwestern University, 1999.

[379] M. Vandamme and F.-J. Ulm, "Nanogranular origin of concrete creep.," *Proc. Natl. Acad. Sci. U. S. A.*, vol. 106, no. 26, pp. 10552–10557, 2009.

[380] D. Jansen, F. Goetz-Neunhoeffer, B. Lothenbach, and J. Neubauer, "The Early Hydration of Ordinary Portland Cement (OPC): An Approach Comparing Measured Heat Flow with Calculated Heat Flow from QXRD," *Cem. Concr. Res.*, vol. 42, no. 1, pp. 134–138, 2012.

[381] D. P. Bentz, "A three-dimensional cement hydration and microstructure program: I. Hydration rate, heat of hydration, and chemical shrinkage," Building and Fire Research Laboratory, National Institute of Standards and Technology, Gaithersburg, MD, 1995.

[382] H. M. . Jennings and J. J. Thomas, "7.2 The Pore System and Classification of Pores," in *The Science of Concrete Monograph*, 2006.

Appendix A. Determination of Degree of Hydration

Determination of degree of hydration for samples incorporating chemical admixtures was done in the specified method. This approach is adapted from various studies [380] [381].

$$\alpha_t = \frac{H_t}{H_u} \qquad \text{Equation A-1}$$

Where α_t = degree of hydration at time,'t'

H_t = cumulative heat released by cementitious system at time't' in J/g

H_u = ultimate cumulative heat in J/g

Also

$$H_u = \sum H_P \cdot P_{P/SCM} \qquad \text{Equation A-2}$$

Where $P_{P/SCM}$ is the weight fraction of the SCM in the cement phase.

Equation A-3 takes the following form, based on enthalpies [381]:

$$H_u = 517 \cdot P_{C3S} + 262 \cdot P_{C2S} + 725 \cdot P_{C3A} + 1144 \cdot P_{C4AF} \qquad \text{Equation A-3}$$

Using XRD data and Equation A-7 for CN cement used in this study we get:

$$H_u(J/g) = 517 \cdot 0.465 + 262 \cdot 0.231 + 725 \cdot 0.09 + 1144 \cdot 0.075 = 458.26$$

This result is used to obtain the degree of hydration by using Equation A-5 and the 7-day HOH from isothermal calorimetry at 23°C.

Table A-1: The Pore Sizes found in Cement/Concrete and Their Effects on Mechanical and Physical Properties (Image: Courtesy Jennings and Thomas [382])

Type of Pore	Description	Size	Water	Technique[a]	Properties
Capillary Pores	Large	10 μm – 50 nm	Evaporable Bulk water	SEM, OM	Permeability, strength
	Medium	50 – 10 nm	Evaporable Moderate menisci	SEM	Permeability, strength, shrinkage (high RH)
Gel Pores	Small	10-2.5 nm	Evaporable Strong menisci	Adsorption/ MIP/IS	Shrinkage (to 50% RH)
	Micropores	2.5-0.5 nm	Non-evaporable -No menisci -Intermolecular interactions	Adsorption/ MIP/IS	Shrinkage, creep (35-11% RH)
Interlayer Spaces	Structural	< 0.5 nm	Non-evaporable -Ionic/covalent bond	Adsorption/ Thermal	Shrinkage, creep (< 11% RH)
Other Features	ITZ	20-50 μm	Bulk Water	SEM/OM	Permeability, strength
	Microcracks	50 - > 200 μm	Bulk Water	SEM/OM	Permeability, strength

[a] SEM: scanning electron microscopy; OM: optical microscopy; IS: impedance spectroscopy.

Table A-2: Enthalpies of Cement Phases and Phase Fractions determined from XRD [381]

Phase	Enthalpy (J/g)	Phase Fraction from XRD
C_3S	517	46.5
C_2S	262	23.1
C_3A	725	9
C_4AF	1144	7.5